Synthesis of Bioactive Nitrogen Heterocycles and Functionalized Nanomaterials for Biological and Catalytic Applications

Submitted in fulfilment of the requirements of the Degree of Doctor of Technology: Chemistry in the Faculty of Appllied Sciences at Durban University of Technology

Anand Krishnan

June and 2014 in which the dissertation/thesis is submitted

	Prof. R M Gengan		29-08-2014
Promoter:	. . . . .	Date:	. . . . .
	Prof. A A Chuturgoon		29-08-2014
Joint Promoter:	. . . . .	Date:	. . . . .

Declaration

I, Anand Krishnan, hereby declare that this dissertation entitled **"Synthesis of Bioactive Nitrogen Heterocycles And Functionalized Nanomaterials For Biological And Catalytic Applications",** submitted to the Durban University of Technology, in fulfilment of the requirements for the Degree of Doctor of Technology, Chemistry, in the Faculty of Applied Sciences, is the result of my own work and that all sources used or quoted have been indicated and acknowledged by means of complete references.

Student : ……. (Anand Krishnan) Date: …….

Promoter : …… (Professor R M Gengan) Date: ……

Joint Promoter: ……. (Professor A A Chuturgoon) Date: ……..

Department of Chemistry

Durban University of Technology

June 2014

Dedicated To

My Beloved family

Acknowledgements

அகர முதல எழுத்தெல்லாம் ஆதி
பகவன் முதற்றே உலகு - கடவுள் வாழ்த்து (திருக்குறள்)

Just as the letter 'A' (அ) is the head of the alphabet, God is the Head of the world - The Praise of God (Thirukkural)

My sincere gratitude and appreciation to:

- My Guru Professor R M Gengan, for the opportunity to join in his research group and his family and for his constant encouragement, motivation and valuable suggestions and inspiration throughout this study, holding me strong in all the places I faltered. I admire his spirit, creativity and desire for excellence which has always inspired me.
- Professor P S Mohan from Bharathiar University, Professor K Sellathai from Madurai Kamaraj University and Assistant Professor C Satheesh Kumar from University of Madras for their constant encouragement.
- Professor A Chuturgoon, Dr. A Phulukdaree and Professor Sunil Singh for their guidance and assistance in all aspects of biological studies.
- My cousin, Assistant Professor P Pitchai for his support and help.
- Professor K G Moodley, Mr. Jimmy Chetty, Mrs Lutchmee Moodley and Dr. Thishana Singh for their encouragement and support throughout this study.
- Mr Dilip Jagjiven from UKZN for his assistance with all NMR experiments.
- My colleagues Talent Makhanya, Nirvashini Bipath, Sandisiwe Zondo and S'busiso Nkosi for their limitless care and precious discussion to pursue this work.
- My colleagues M Sureshkumar and T Muthu for their immense assistance with editing and compiling this dissertation.
- My friends, Dr. S Anandakumar, Dr. P Elumalai, A Selvasharma, P Devraj, T Saravanan, G Ramesh and K Sivanandhan for their valuable assistance.
- My parents S Krishnan and K Senthamarai for the many sacrifices they made for me to accomplish all my academic studies. Thanks also go to my sister, Athilakshmi Palanivelrajan, and my brothers, Murali Anand and Dev Anand, who formed part of my vision.
- My South African family, Shirley, Trinisha and Kerena for their love and care during this study period.
- The Durban University of Technology for providing funding during my post-graduate studies.

ABSTRACT

Aromatic heterocycles are highly important structural units found in a large number of biologically active natural compounds, pharmaceuticals and catalytic compounds. They have a crucial role in organic syntheses, which results in the generation of high value products. Among heterocycles, those containing nitrogen are the most indispensable structural motifs and are widely used against dreaded diseases such as Malaria, TB, HIV/AIDS and Cancer. The inclusion of highly electronegative atoms such as fluorine in these organic molecules render them very reactive towards proteins. Furthermore these molecules exhibit strong interactions with surfaces of quantum range particles of elemental gold. Various approaches for the synthesis of novel gold nanoparticles linked to potent bioactive molecules are documented and their application as drug delivery systems are of immense value to human health. Also many chemical and physical methods are available for the synthesis of gold, silver and palladium nanoparticles however these methods are usually laborious and produce toxic by-products. The green approach is to use plant extracts to synthesise various size and shape nanoparticles which could be used in biological and catalytic systems.

A simple one-pot two component and three component reaction using formyl quinoline, 2-aminothiophenol, thiosemicarbazone and trifluoromethylbenzaldehyde as a reactant to synthesise quinoline, pyridine and pyran based bioactive small molecules; these products are a quinoline type bearing a benzothiazole moiety, quinoline thio semicarbazone ligand, fluorine substituted dihydro pyridine, fluorine substituted dihydropyran and fluorine substituted pyridine derivatives. In total, fifteen compounds were synthesized eleven of which were novel; all compounds were characterized by spectroscopic techniques. *In vitro* anti-bacterial activities of the synthesized compounds were investigated against a representative panel of pathogenic strains. Compounds 6, 7, 8, 11 and 13 exhibited excellent anti-bacterial activity compared with first line drugs. Potent p53–MDM2 interaction inhibitors 2-thio-1,2-dihydroquinoline-3-carbaldehyde thiosemicarbazone and fluorine substituted new pyridine scaffold were successfully identified by structure-based design.

An efficient one-pot four component route to the synthesis of trifluorinated pyrrolophenanthroline and fluoroquinoline pyrrolophenanthrolines was designed. In this reaction 1-butyl-2,3-dimethylimidazolium tetrafluoroborate ionic liquid (DMTIL) was used as a reaction medium; no catalyst was required. The structure of the pyrrolophenanthrolines was deduced by IR and NMR analysis. These compounds were studied with Bovine Serum

Albumin (BSA) through molecular docking. Hydrophopic, electrostatic and hydrogen bonding interaction played a crucial role in the binding to sub domain of BSA. Interaction studies of DMTIL with BSA by emission, absorption, synchronous fluorescence, circular dichroism (CD) and three dimensional emission (3D) spectroscopic techniques were under taken. The results from emission titration experiments revealed the existence of a strong interaction between BSA and DMTIL ionic liquid. It showed that compounds with lesser number of hydrogen bonds are found to be more active which is attributed to hydrophobic interaction and electrostatic interaction which also played a vital role in DMTIL binding to sub domain IB of BSA.

A novel copper-loaded boron nitride nanosheet (Cu/BN) catalyst was prepared and fully characterized. It was used as an efficient and chemoselective catalysts for the synthesis of α-aminophosphonates by the Kabachnik-Fields reaction; twenty one α-aminophosphonates were synthesised. The enhanced catalytic activity and product yield was attributed to the increase of surface acidity. Overall, this methodology offered competitive advantages such as recyclability of the catalyst without further purification or without using additives or cofactors, low catalyst loading, broad substrate applicability and high yields. The application of this new nanocatalyst in organic synthesis will provide a novel pathway for the synthesis of pharmaceutically important compounds.

Gold nanoparticle surfaces were modified with self-assembled monolayers of important thiol and disulfide bioactive molecules since considerable interest is due to their potential application as anti-cancer agents. Herein, a carbazole was conjugated to lipoic acid by using an amide coupling catalyst HBTU and DIEA reaction. The structure of the carbazole thio octanic acid (CTN) was identified by IR and NMR. CTN was attached to the gold nanoparticles surface and the capping behaviour was characterized by UV-vis spectroscopy, TEM, DLS and FTIR. The cytotoxicity of CTNAuNPs on A549 cell lines was determined using the MTT assay. The results suggest CTN and CTNAuNPs possess anti-proliferative properties in the cancerous A549 cells.

Furthermore a dual thiol ligand was synthesized by using equimolar 4-aminothiophenol (4-ATP) and amino oxadiazole thiol (AXT). This dual ligand was attached to the gold nanoparticles surface (DTAu) and the capping behaviour was characterized by UV-vis spectroscopy, TEM, DLS and FTIR. The cytotoxicity of DTAu on A549 cell lines was

determined using the MTT assay. The results suggest dual ligands (4-ATP, AXT) and DTAu possess anti-proliferative properties in the cancerous A549 cells.

South African indigenous plants and agroforestry waste were also used in the synthesis of silver, gold and palladium nanoparticles (NPs). Green protocols such as the use of environmentally benign solvents and non-hazardous reagents were an added advantage to physical and chemical means. Furthermore these reactions were rapid and the size and shape of the NPs could be manipulated by choosing the correct medium. The formulation of natural medicinal compounds capped onto NPs was assessed for their anti-cancer activity, in A549 lung cancer line, and catalytic reduction of dyes and nitrobenzene derivatives were studied. These NPs displayed:

- Significant cytotoxicity to lung cancer cells with minimal effect on normal healthy cells.
- Outstanding catalytic reduction of pharmaceutical and textile waste effluents such as dyes and nitro aromatic compounds.

In addition, palladium nanoparticles containing capped Moringa *olifera* compounds were used effectively in the Suzuki coupling reaction of iodobenzene and phenylboronic acid. The reaction was rapid and was conducted in an aqueous medium.

General Remarks

The chemical structures appearing in each chapter are given numbers, which apply only to the respective chapters, whereas, the reference numbers are common to all chapters. Each chapter contains separate experimental section.

The following abbreviations are used in the text:

°C	- centigrade
µl	- microlitre
µM	- micrometre
4-ATP	- 4-aminothiophenol
AgNPs	- silver nanoparticles
alc	- alcoholic
anhy	- anhydrous
aq	- aqueous
AuNPs	- gold nanoparticles
AXT	- 5-(4-aminophenyl)-1,3,4-oxadiazole-2-thiol
BN	- boron nitride
BSA	- bovine serum albumin
calcd	- calculated
$CDCl_3$	- chloroform
cm	- centimetre
conc	- concentration
CTAB	- cetyl trimethyl ammonium bromide

CTN	- carbazole thiooctanic acid
CTNAuNPs	- carbazole thiooctanic acid capped gold nanoparticles
DIEA	- N,N-diisopropylethylamine
dil	- diluted
DMAP	- 4-dimethylaminopyridine
DMF	- dimethyl formamide
DMSO	- dimethylsulfoxide
DNA	- deoxy ribo nucleic acid
DSC	- differential scanning calorimeter
DTAu	- dual thiol gold nanoparticles
EDS	- energy dispersive X-ray spectroscopy
EtOAc	- ethyl acetate
GC	- gas chromatography
gla	- glacial
h	- hour(s)
HBTU	- o-(benzotriazol-1-yl)-N,N,N’,N’-tetramethyluronium hexafluorophosphate
IR	- infra red
ml	- millilitre
mm	- millimetre
mp	- melting point
ms	- mass spectrum

MW	- microwave
nm	- nanometre
NMR	- nuclear magnetic resonance
PDB	- protein data bank
PE	- petroleum ether
Phen	- phenanthroline
$POCl_3$	- phosphoryl chloride
PTSA	- p-toluene sulfonic acid
SDS	- sodium-n-dodecyl sulphate
SEM	- scanning electron microscope
TEA	- triethylamine
TEM	- transmission electron microscope
THF	- tetrahydrofuran
TLC	- thin layer chromatography
UV-vis	- ultraviolet visible
XRD	- X-ray diffraction
XRPD	- X-ray powder diffraction

The purity of the products was tested by TLC using glass coated with silica gel G and the mixture of petroleum ether/ ethyl acetate, methanol and ethanol were used as the developing solvents. UV chamber and a chamber containing iodine vapour were used to locate the spots. Columns packed with activated silica gel (60-120 mesh) were used to purify the crude products. The solvents and reagents used for the synthesis were of reagent grade and were purified/dried by standard methods. Petroleum ether used was of boiling range 60-80°C.

Melting points were determined by using Stuart SMP10 apparatus (Bibby Scientific, UK) and were uncorrected. IR spectra were recorded using KBr on a Varian FTIR-800 spectrophotometre (Agilent Technology, United States).

Particle analyses were done on JEOL 1010 TEM using Megaview III camera and iTEM software (Jeol, Japan), Philips PW 1050 diffractometer for X-ray diffraction, PANalytical, Netherlands, Malvern Zetasizer Nano ZS for DLS (Malvern Instruments Ltd, UK) and Zeiss EVO 60 ESEM (Bruker, Germany). Mass spectra were recorded on Shimadzu LC20AT mass spectrometer (Shimadzu, Japan).

NMR spectra were recorded in $CDCl_3$/DMSO-d_6 on a Bruker Avance (TOPSPIN) - 400, 600 (Bruker, Germany) using tetramethylsilane (TMS) as internal standard. In general for all compounds $CDCl_3$ is used as a solvent, wherever DMSO-d_6 has been used, it is mentioned in the experimental part. The chemical shifts were expressed in ppm. The following abbreviations are used in the NMR spectral data.

s	- singlet
d	- doublet
t	- triplet
q	- quartet
m	- multiplet
dd	- doublet of doublet
brs	- broad singlet
J	- coupling constant

CONTENTS

Chapter 1

Introduction

1.1. Introduction

Highly skilled organic chemists are venturing deeper into the unknown! When reading this statement, Retinal **1**, an organic compound, converts visible light into nerve impulses. As this dissertation is physically lifted, sugar molecules in the muscles causes chemical reactions. During this process, gaps between the brain cells are being bridged by neuro-transmitter amines such as serotonin **2.** This allows nerve impulses to travel around the brain. Although these processes occur in the human body, they are not fully understood. To date, no one, however brilliant, understands the detailed mechanism that occurs in the human mind and body. As a result, there is an opportunity to venture into the unknown[1].

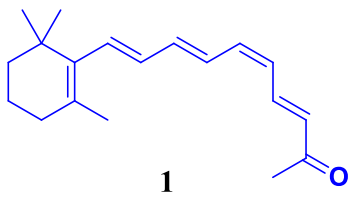

1

11-*cis*-retinal
absorbs light when we see

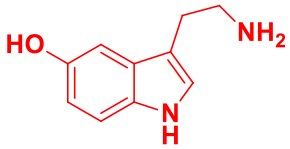

2

serotonin
human neurotransmitter

Figure 1. Representative example of a light absorbing and human neuro-transmitter

Organic chemistry research is a dynamic field mainly concerned with developing and applying new methods for making molecules, understanding their reactivity and enhancing knowledge in other research fields. The application of organic chemistry research and education programs into an integrated trans disciplinary program is important for good research. In 2012, two biologists, Professor Robert J Lefkowitz and Professor Brian Kobika, were awarded the Nobel Prize for Chemistry. They unveiled the signalling mechanism of G protein-coupled receptors (GPCRs). These proteins belong to one of the largest families of human proteins. They are involved in many physiological activities and therefore are targets of a number of drugs. Determination of the molecular structures of this class of receptors helps researchers to understand the actual mechanism of different cellular processes. Also life saving and more effective drugs can be designed.

Recently, nano and organic chemists have captured the high-resolution images of a molecule as it breaks and reforms chemical bonds. Using a high resolution atomic force microscope, these scientists have taken the first atom-by-atom picture which shows how a

molecule's structure changes during a reaction. In the past, scientists have obtained this type of information from spectroscopic analysis. This great achievement was only realised through interdisciplinary collaboration between organic chemists and nanotechnologists[2].

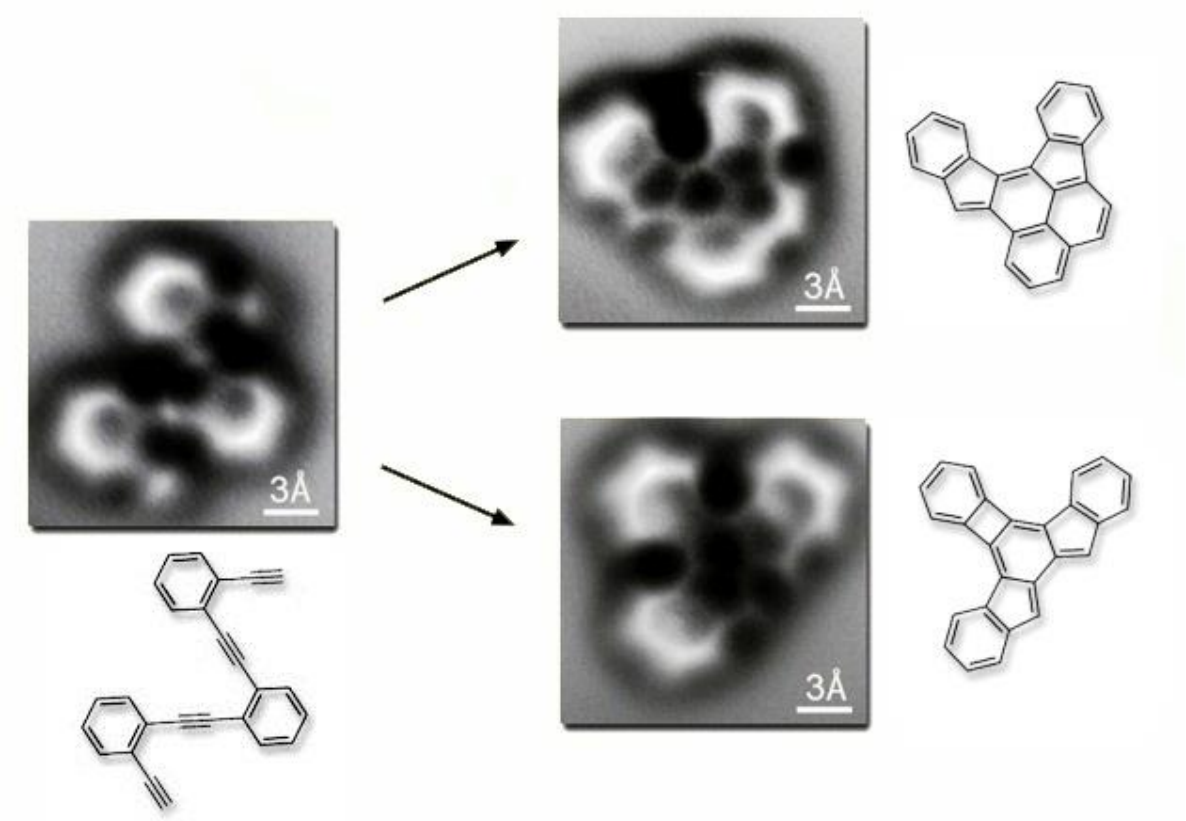

Figure 2. Direct imaging of covalent bond structure in single-molecule chemical reactions.

During the 20th century, total synthesis of complex natural product was the main theme of organic chemistry[3]. Fundamental information into reactivity and selectivity principles were obtained by these synthetic projects. Nowadays, synthetic chemists can construct molecules which are complex. However, a change in the perception defining organic synthesis as an art, is needed. In 1975, a key issue was addressed by Hendrickson. He defined an "ideal synthesis" as one which[4]:

"...Creates a complex molecule... In a sequence of only construction reactions involving no intermediary refunctionalizations, and leading directly to the target, not only its skeleton but also its correctly placed functionality."

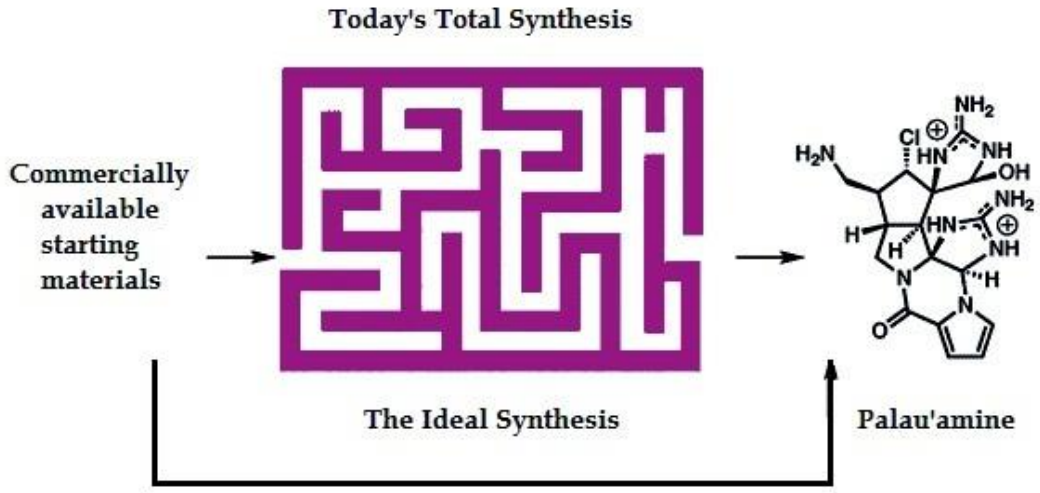

Figure 3. A schematic diagram showing a pathway of ideal synthesis

Aromatic heterocycles are highly important structural units in a vast number of biological active natural compounds, pharmaceuticals and materials. They are also important intermediates in organic synthesis, often providing access to other highly desirable structures. Thus, there is a compelling need to develop novel and more general methods for the synthesis of heterocycles. Functionalized heterocycles are excellent scaffolds for preparing diversity-oriented compounds for medicinal and pharmaceutical applications[5]. This is due to their ability to mimic the structure of peptides and their protein binding potential. Among the heterocycles, the nitrogen based ones such as quinoline and carbazole derivatives are one of the most indispensable structural motifs. These are wide spread in nature and are key structural component in several families of bioactive compounds[6]. Several alkaloids isolated from natural resources or prepared synthetically are important for medicinal and biomedical use.

Fluorine, a small and highly electronegative atom, has a huge impact in medicinal chemistry. The presence of fluorine in a therapeutic or diagnostic small molecule enhances many pharmacokinetic and physicochemical properties. These include improved metabolic stability and enhanced membrane permeation. Increased binding affinity of fluorinated drug candidates enhance interaction with biomolecules. Other properties are an increased blood brain barrier (BBB) permeability which is important in CNS active drugs[7]. Therefore fluorinated drugs are exploited for therapeutic applications.

Ionic liquids (ILs) are organic nitrogen-containing heterocyclic cations with inorganic anions or organic salts with low melting points. These are being used for many fields of chemistry and industry, due to their potential as ‘‘Green’’ recycle alternatives to the traditional organic solvents. They possess a wide liquid range, in some cases in excess of 400°C. Their very favourable properties, such as high polarity, negligible vapour pressure, high ionic conductivity and thermal stability, make them effective in catalysis. Recently, hydrated ILs have been identified as an ideal medium for long-term DNA and protein storage. Hence, understanding the binding characteristics and molecular mechanism of interactions of ILs with DNA and protein is of paramount importance.

The power of chemistry lies in being able to create new forms of matter and/or nanostructures. Both the covalent and non-covalent bond are essential in fabricating nanostructures. By understanding the kinetics and thermodynamics of many fundamental chemical processes, nanosized molecules and nanomaterials can be produced, thereby leading to discoveries of new phenomena. **Figure 4** shows some synthetic nanosized molecules size-dependent properties of quantum dots and organic nanoparticles. Nanomaterial have gained focus due to their potential applications in drug delivery, sensing, imaging and chemotherapy; drug delivery includes polymeric nanoparticles, dendrimers, liposomes and quantum dots[8].

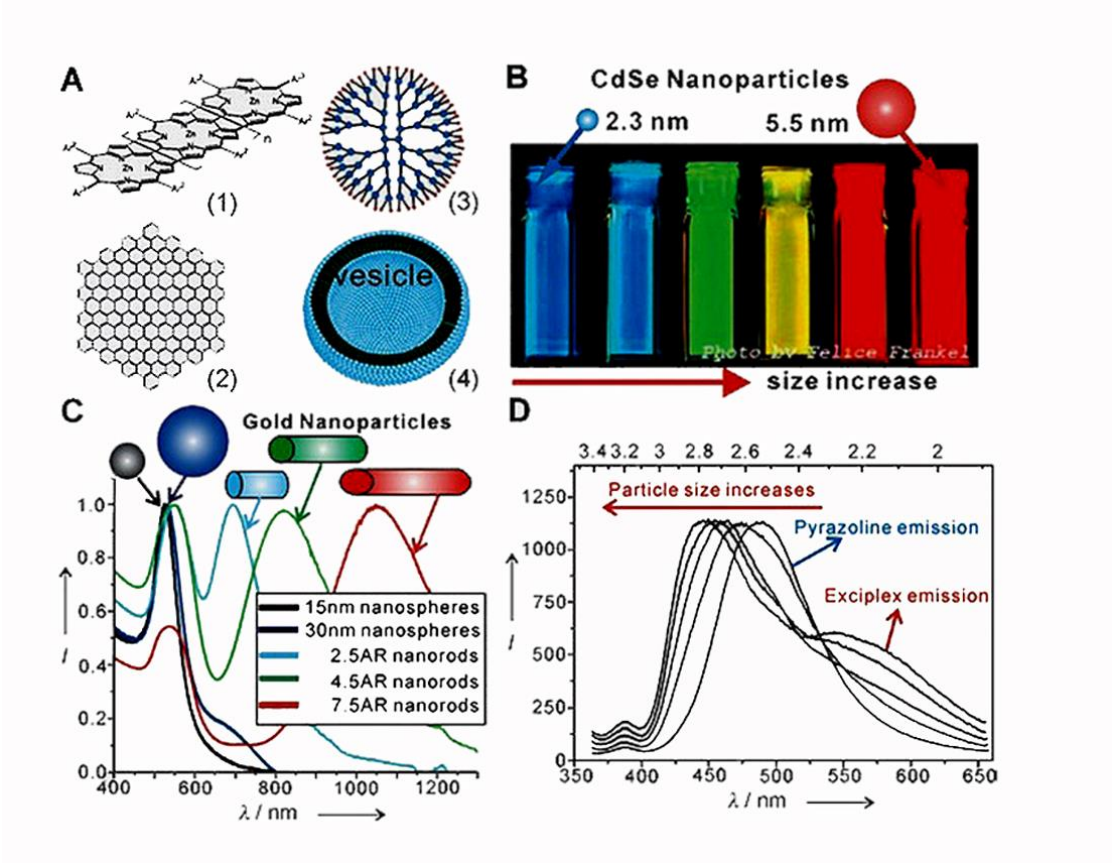

Figure 4. **A**) Examples of nanosized molecules and assemblies: 1) fused porphyrins 2) molecular graphene 3) dendrimers 4) a self-assembled vesicle. **B**) Fluorescence emission of CdSe quantum dots with different sizes. **C**) Absorption spectra of gold nanoparticles with various sizes and shapes. **D**) Fluorescence emission spectra of organic nanoparticles with different sizes[9].

Metal nanoparticles are recently being widely explored. In particular, design of drug functional gold nanomaterial is of interest because of a variety of potential applications ranging from chemistry to biological sciences. Silver, gold and palladium nanoparticles have unique optical, thermal, hetero and homogeneous catalytic properties[10]. After the discovery of carbon nanotubes (CNT) it was suggested that carbon is not a unique element being able to form nanotubes; boron nitride (BN) appears as a potential material for this class in view of the structural similarity of graphite and bulk BN[11]. Hexagonal boron nitride (h-BN) is well known as one important ceramic material with outstanding thermal and electrical properties. Furthermore, it has excellent chemical stability, good resistance to corrosion, low density and high melting point. Boron nitride

nanotubes are a good alternative to carbon nanotubes and other kinds of inorganic materials, because of their improved chemical properties. They possess good heterogeneous catalytic activity and theoretically guarantee better stability and compatibility for safe drug delivery and targeting carriers[12].

1.2. Synthesis and Utility of Nitrogen Heterocycle System

Heterocyclic compounds are cyclic compounds in which one or more of the ring carbons are replaced by another atom. The non-carbon atoms in such rings are referred to as "heteroatoms". Heterocycles form the largest class of organic compounds. The majority of pharmaceutical products that mimic natural products with biological activity are heterocycles. Therefore, researchers are designing and producing better pharmaceuticals, pesticides, insecticides, rodenticides and weedicides by following natural models. Other important practical applications of these compounds are used as additives and modifiers in a wide variety of industries including cosmetics, reprography, information storage, plastics, solvents, anti-oxidants and vulcanization accelerators. Hence, heterocyclic chemistry is an inexhaustible resource of novel compounds. Many combinations of carbon, hydrogen and heteroatoms can be designed, providing compounds with the most diverse physical, chemical and biological properties[13]. Among the approximately 20 million chemical compounds identified by the end of the second millennium, more than two-thirds are fully or partially aromatic and approximately one-half are heteroaromatic[14]. Heterocyclic compounds, especially nitrogen heterocycles, are the most important class of compounds in the pharmaceutical and agrochemical industries, in which heterocycles comprising around 60% are covered as a drug substances. 5-membered N-heterocycles such as pyrroles, indoles and carbazoles are important structural motifs and are present in an extensive number of biologically active compounds[15]. The 5-membered N-heterocycles are of exceptional interest in the pharmaceutical industry, as they appear in the core structure of several drugs. Six membered heterocycles such as substituted pyridines exhibit a broad range of biological activity. They are used to modulate hypertension, angina pectoris act as Ca^{2+} channel blockers and are anti-diabetic, hepatoprotective and show anti-tumor properties[16]. The fused quinoline moiety is also present in an extensive number of naturally occurring sources and are biologically active[17]. In addition, pyridine derivatives are also used as organic bases and organo catalysts in organic synthesis. Six membered aromatic rings containing two nitrogen atoms, such as phthalazinones,

quinazolinones, pyrimidines and pyrimidinones possess a broad spectrum of biological activities and are therefore of interest as target compounds in pharmaceutical and medicinal chemistry[18]. Six membered rings containing three nitrogen atoms, like 1,3,5-triazines are used as a templates in supramolecular chemistry and dendrimer synthesis, due to their unlike C3 symmetric core structure[19]. Seven and higher membered nitrogen containing compounds, e.g. benzodiazepines, show interesting anti-cancer properties and inhibit HIV-1 reverse transcriptase[20].

The following few sections cover the review of the nitrogen heterocyclic compounds as a core area of research. Several quinoline derivatives isolated from natural resources or prepared synthetically are significant with respect to medicinal chemistry and biomedical use. Compounds containing pyridine, quinoline, carbazole and indole motif are most widely used as anti-malarials[21], anti-bacterials[22], anti-fungals[23] and anti-cancer[24] agents. Furthermore, quinoline derivatives are used in the synthesis of fungicides, virucides, biocides, rubber chemicals and flavouring agents[25].

Kimpe De N *et al.*,[26] reported the high-yielding, asymmetric synthesis of novel 4-formyl-1-(2- and 3-haloalkyl) azetidin-2-ones **3**. It was developed as a valuable starting material for the synthesis of different enantiomerically enriched bicycles azetidin-2-ones **4**. These include preparation of morpholine, and 1,4-diazepane annulled β-lactam derivatives.

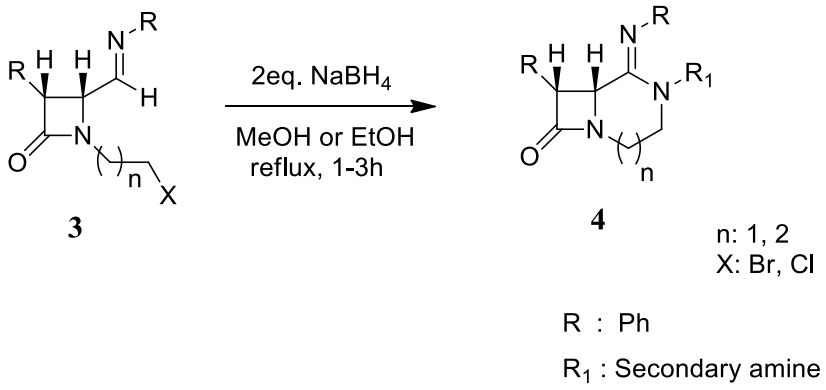

Li Z *et al.*,[27] reported the iodine-mediated intramolecular cyclization of enamines **5.** This leads to various 3H-indole derivatives **6** containing multifunctional groups. Transition metal-free reaction conditions are used and yields are good.

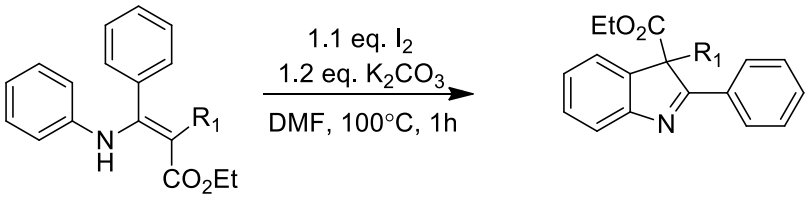

5 **6**

R_1 : alkyl, Bn. CO_2Et, *p*-NO_2-C_6H_4

Chauhan *et al*.,[28] reported the synthesis of 2, 3-dihydro/spiroquinazolin-4(1H)-ones **10** via. three-component cyclocondensation reaction of isatoic anhydride **7**, amines **8** and Isonicotinaldehyde **9**.

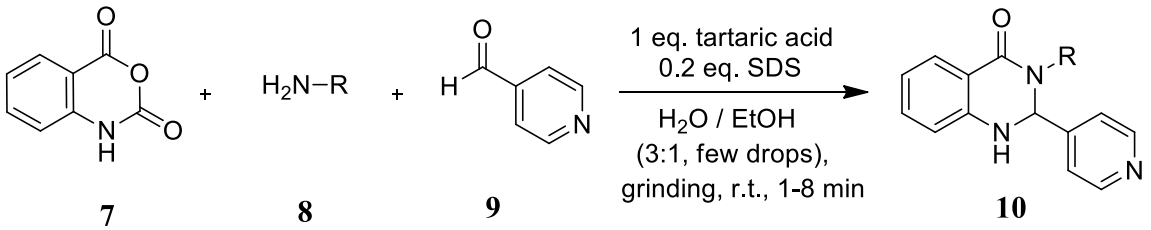

7 **8** **9** **10**

R: Alkyl, Ph. H

Perumal *et al*.,[29] reported an environmentally friendly method for the cyclization of 2-aminochalcones **11** to 2-aryl-2,3-dihydroquinolin-4(1H)-ones **12** on the surface of silica gel impregnated with indium(III)chloride. They used microwave irradiation without a solvent.

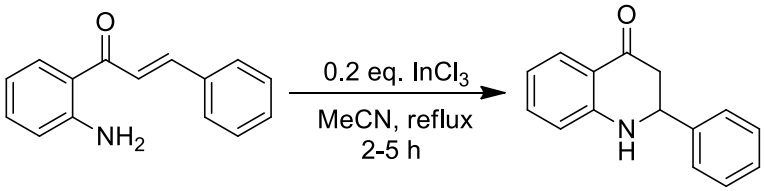

11 **12**

Chuchi Tang *et al*.,[30] reported an efficient procedure for the stereo controlled construction of 2H-thiopyrano [2, 3-b] quinoline **15** starting from simple compounds. The domino Michael/Aldol reactions between 2-mercapto benzaldehydes **13** and 3-Phenylprop-2-enal **14**, promoted by chiral diphenylprolinol TMS ether, proceeded with excellent on chemo- and enantioselectivity. A synthetically useful and pharmaceutically valuable 2H-thiopyrano[2,3-b]quinolines in high yields with 90-99% ee was obtained.

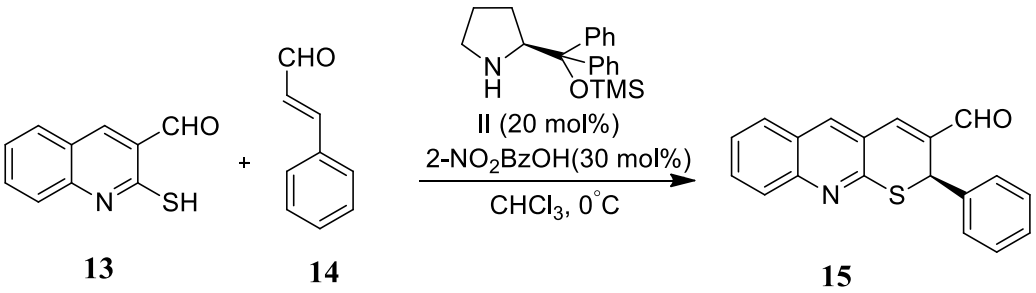

13 14 15

Ramrao A. Mane *et al.*,[31] reported a one-pot water-mediated synthesis via. 2-chloro-3-formyl quinoline **16** and phenyl hydrazine **17** for pyrazolo[3,4-b] quinolines **18**. They used microwave energy irradiation. This route is convenient, eco-friendly and can be scaled up easily.

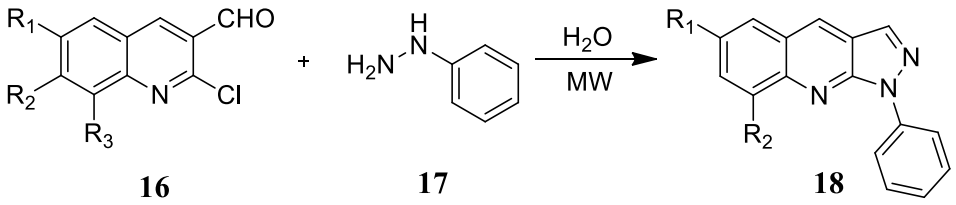

16 17 18

R_1 = H, R_2 = H, R_3 = H, Me
R_1 = OMe, R_2 = H, R_3 = H, Me
R1 = Me, R2 = H, R_3 = H, Me
R_1 = H, R_2 = Et, R_3 = H, Me

Sikha S Dave *et al.*,[32] reported the synthesis of diversely substituted chalcones **20** derived from 2-chloro-3-formylquinoline **16**, with appropriately substituted 2-hydroxyl acetophenones **19** via. Claisen Condensation. All derivatives showed promising potent pfLDH activity.

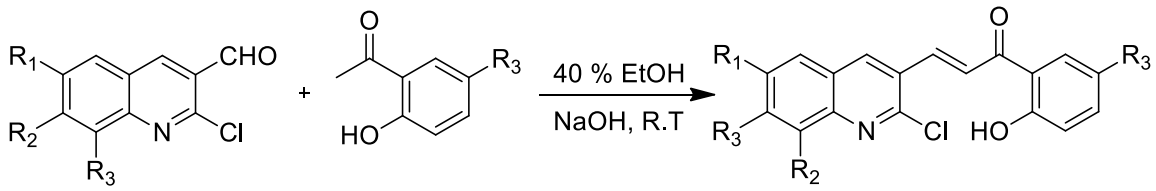

16 19 20

R_1 = H, R_2 = H, R_3 = H, Me
R_1 = OMe, R_2 = H, R_3 = H, Me
R1 = Me, R2 = H, R_3 = H, Me
R_1 = H, R_2 = Et, R_3 = H, Me

1.2.1. Multi- Component Reactions (MCRs)

Among the known strategies of drug discovery, high throughput screening is one that serve most efficient to the pharmaceutical industry. To guarantee the success on acquiring lead compounds via. this kind of screening tactic, sources of large amount of molecular libraries are important preconditions. With the advent of multi- resistant strains of bacteria, viruses and cancer cells, the search for new drugs is paramount[33]. Although the use of monoclonal anti-bodies as drugs is on the rise, the majority of new drugs are still- and are likely to continue to be small molecules. A key step in the drug discovery process is the generation of novel chemical entities that can serve as potential drug candidates[34-36]. Successful drug development relies on high efficiency and low cost and short cycles of design make test and therefore requires short and efficient synthetic sequences for lead discovery. Multi-component reactions (MCRs) are a one-pot process that involves the reaction of at least three components to form a single product that incorporates essentially all the atoms of the starting materials. These reactions are atom economic, step efficient and have high exploratory power with regard to chemical space and are therefore ideally suited for the generation of libraries of compounds[37].

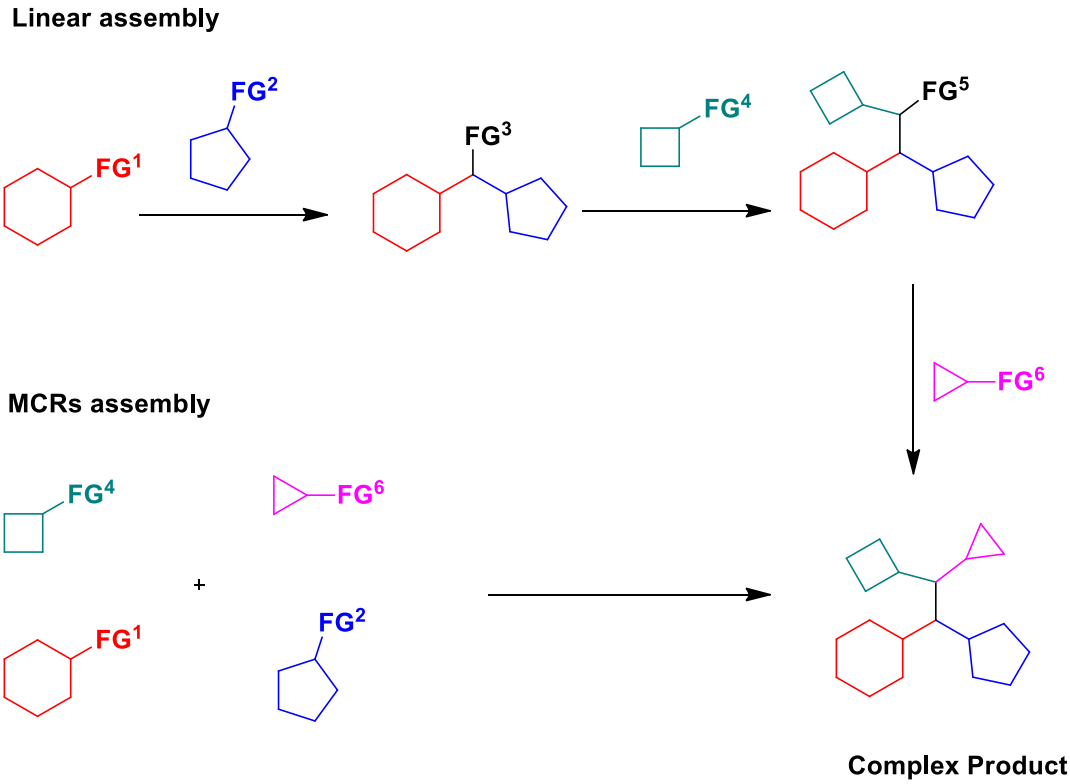

Scheme 1. Traditional linear synthesis (3 steps) vs. multi-component assembly (1 step)

Zhen Yang *et al.*,[38] reported a novel functionalized quinolines via. Ugi and Pd-catalyzed intramolecular arylation reactions. To prepare this interesting ring system, the authors made use of an Ugi-Heck MCRs aryl-aryl coupling which occurs in a second step.

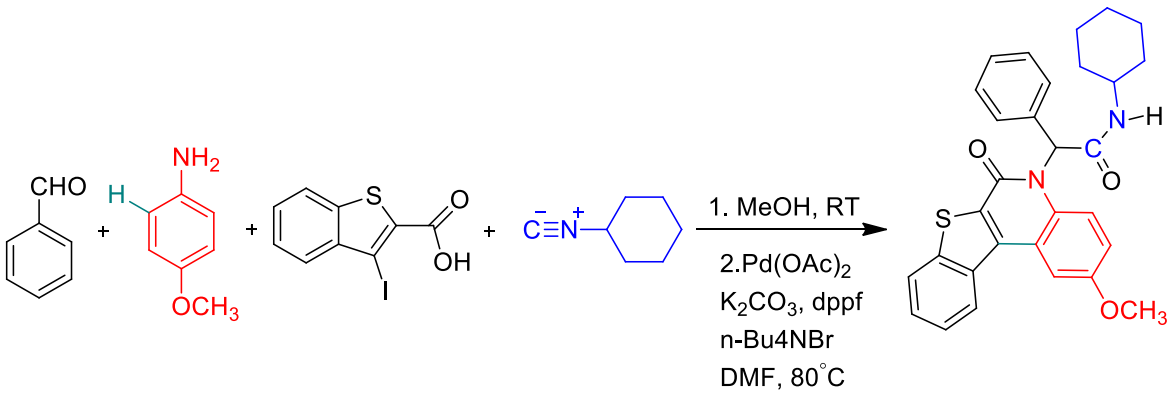

21 **22** **23** **24** **25**

The second most important iso cyanide-based MCR is the Ugi four component reaction. This elegant four-component reaction between cyclcohexyl isocyanide **24**, 3-iodobenzo[b]thiophene-2-carboxylic acid **23**, benzaldehyde **21** and p-toluidine **22**, afford dipeptide-like structures **25**. Song Cao *et al.*,[39] prepared pseudopeptides bearing a

difluoromethyl **30.** A Ugi reaction using aniline **27**, trimethylacetonitrile **29,** 4-fluorobenzaldehyde **26** and 2, 2-difluoro-2-(phenylthio) acetic acid **28** as one component is used to prepare **31**.

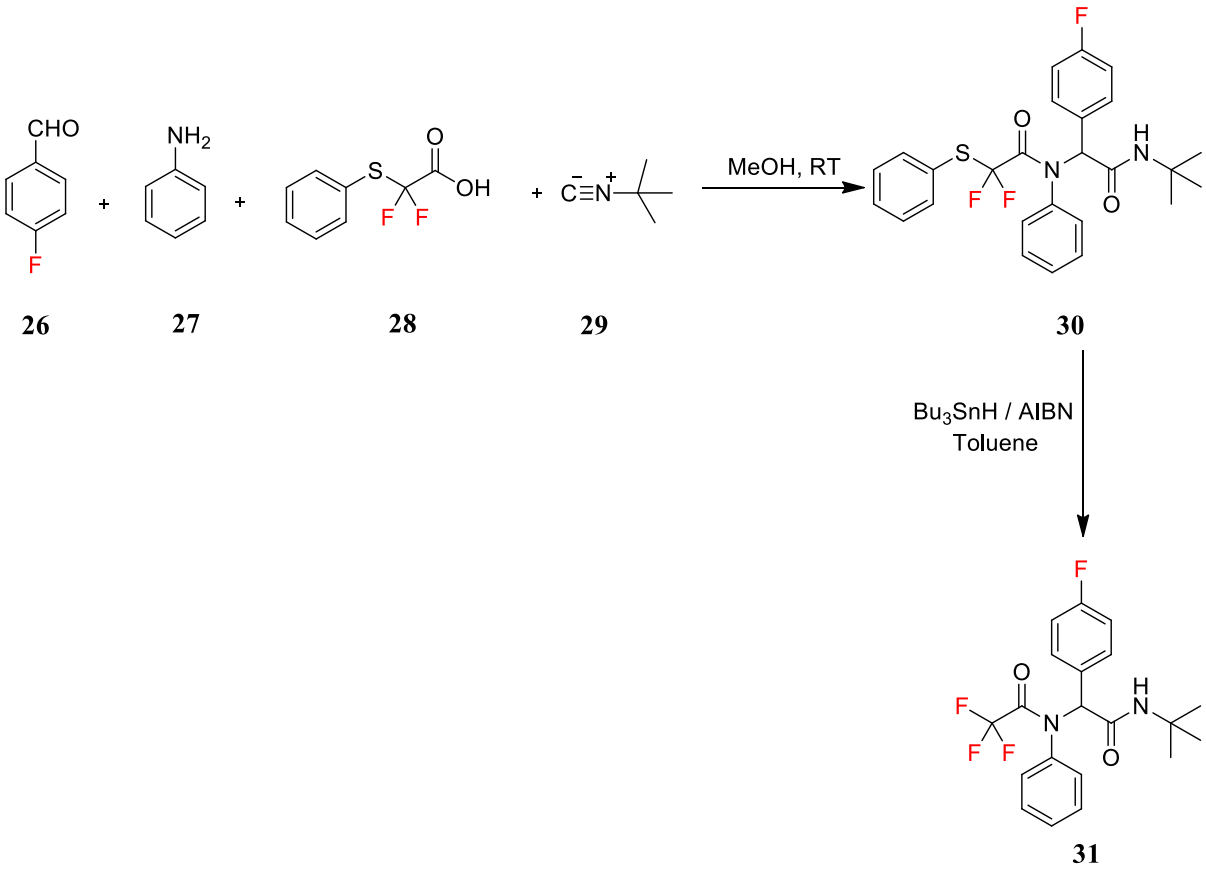

26 **27** **28** **29** **30** **31**

Non-isocyanide-based multi-component reactions usually involve an activated carbonyl species. Biginelli reaction discovered, in 1891, used p-tolualdehyde **32**, (thio) ureas **33** and ethyl acetoacetate **34** to **s**ynthesize dihydro pyrimidinones **35.** The products of the Biginelli reaction are widely used in the pharmaceutical industry as calcium channel blockers[40], anti-hypertensive agents and alpha-1-a-antagonists.

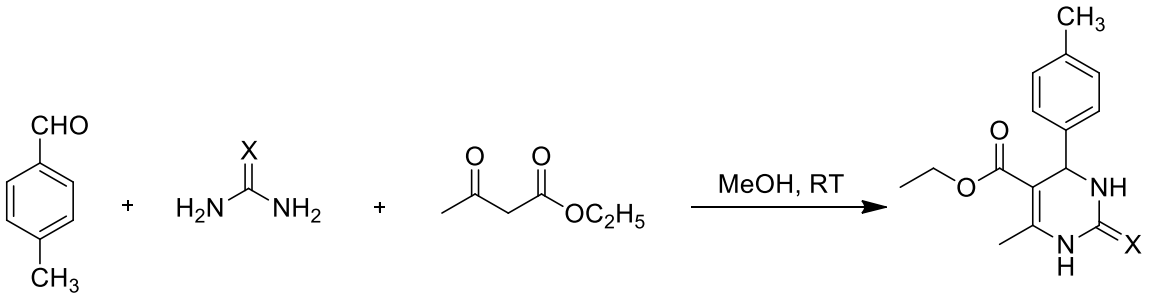

32 **33** **34** **35**

X = O, S

1.3. Fluorine Substituted Heterocyclic Nitrogen Systems

The incorporation of fluorine atom(s) within organic molecule enhances their biopotency, bioavailability, metabolic stability and lipophilicity[41]. It has shown to modulate the stereo electronic parameters of organic molecules[42,43], alters the electronic environment, but also influences the p-value of neighboring Bronsted acid/base centers, polarity, and influences lipophilicity. Organo fluorine interactions with protein residues is used to enhance protein-ligand binding affinity and selectivity[44] and hence synthesis of bioactive compounds for the treatment of infectious diseases[45,46] are being undertaken.

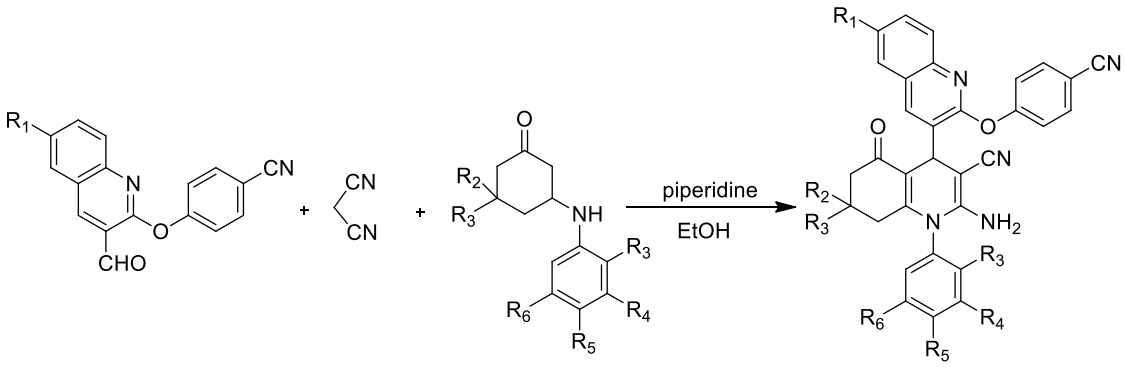

36 **37** **38** **39**

R_1 = H, CH_3. Cl, OCH_3 R_2 = H, CH_3
R_3 = R_5 = R_6 = H, F R_4 = H, F, CF_3

Manish P. Patel *et al.*,[47] reported a one-pot three component cyclocondensation of betaaryloxyquinoline-3-carbaldehydes **36**, malononitrile **37** and beta enaminones **38**. They used a catalytic amount of piperidine. *In vitro* anti-microbial activity and anti-tuberculosis activity were evaluated against Mycobacterium tuberculosis H37Rv.

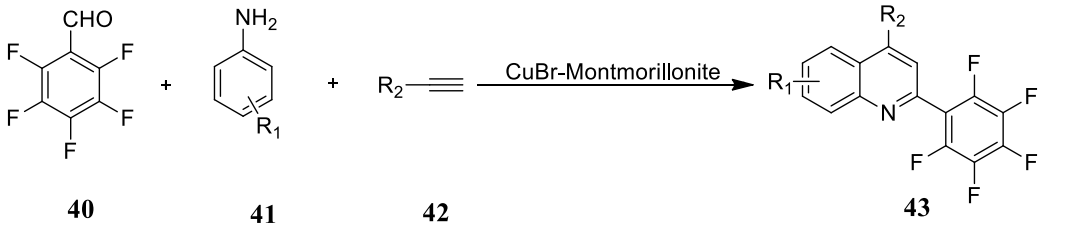

40 41 42 43

R1 = H, *p*-OMe, *p*-NO_2, P-Me;
R2 = Ph, CH_2OH, CH_2OAc

Microwave irradiation was used for the synthesis of 2-pentafluorophenylquinoline derivatives **43** by Zhang and co-workers[48]. This was a one pot reaction of pentafluorobenzaldehyde **40**, aromatic anilines **41** and alkynes **42** on the surface of montmorillonitle clay impregnated with a catalytic amount of CuBr under solvent-free conditions. Improved yields and enhanced reaction rates were recorded.

1.4. Organic Nitrogen-Containing Heterocylic Cations and Inorganic Fluorine Anions (Ionic Liquids)

In recent years, interest in ionic liquids has grown rapidly. Fluorine containing heterocycles is a class of organofluoro molten salts. The synthesis and properties of quaternary alkyl substituted ammonium, imidazolium, triazolium and pyridinium salts with fluorine containing anions have unique applications in biological and catalysis field[49].

Prajapati *et al.*,[50] reported an eco-friendly method for the synthesis of phenyl substituted quinolines **46** via. Meyer-Schuster rearrangement of 2-aminoaryl ketones **44** and phenylacetylenes **45** in the presence of a catalytic amount of zinc trifluoromethane sulfonate in the ionic liquid 1-butyl-3-methylimidazolium hexafluorophosphate [hmim] PF_6.

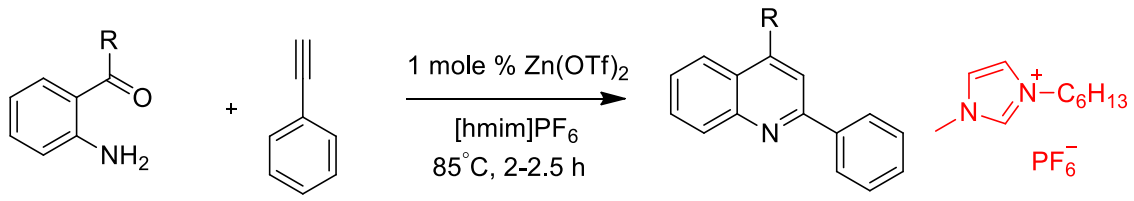

44 45 46

R: Ar, Me

Zhu *et al.,*[51] reported the interactions of bovine serum albumin (BSA) with two alkyl imidazolium based ionic liquids, 1-butyl-3-methylimidazolium tetrafluoroborate ([bmim]BF4) and 1-butyl-3-methylimidazolium hexafluorophosphate [bmim] PF_6, in buffer solutions at pH~7.0. These were analysed by isothermal titration calorimetry (ITC) and circular dichroism (CD); spectra showed that the two ionic liquids changed the secondary structure of BSA.

1.5. Gold–Sulfur Nanoparticles

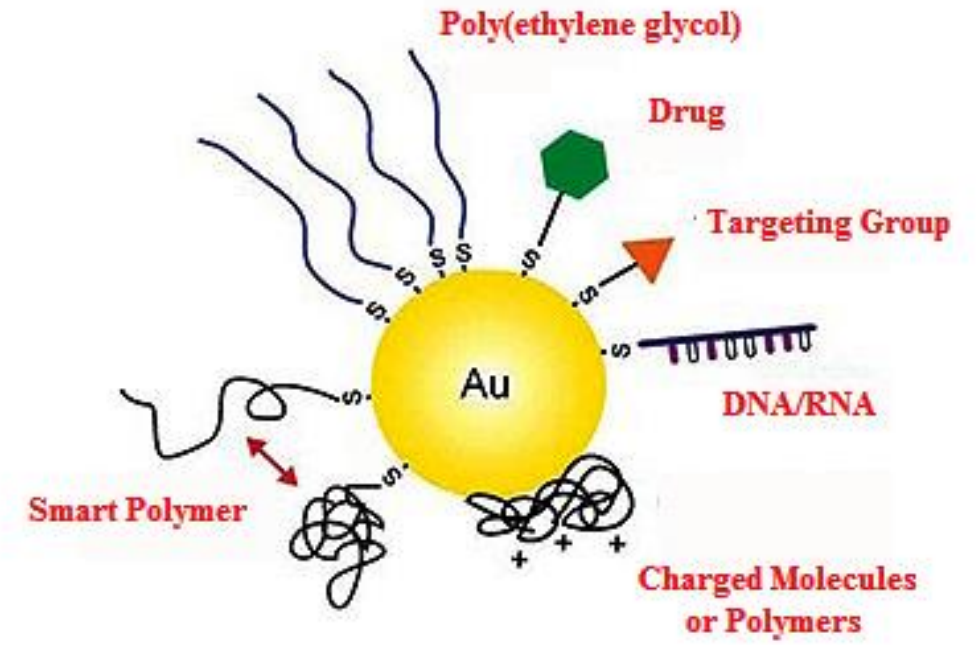

Figure 5. Gold nanoparticle

The covalent bond between gold and sulfur stabilizes nanostructures and transmits electronic interactions between gold and sulfur containing molecules[52]. These interactions are mediated through the sulfhydryl (SH) functional group in thiols (RSH). A wide variety of studies in molecular biology, inorganic chemistry, surface science and materials science are undertaken. Potential applications include in site specific bioconjugate labelling and sensing[53], drug delivery and medical therapy[54], molecular recognition and molecular

electronics[55]. The interplay between experiment and theory has aided in developing the understanding of the gold sulfur nano interface.

1.5.1. Bioactive Thiolated Molecules-Conjugated Gold Nanoparticles

Self-assembly of organothiols (OTs) and thiolated biomolecules is used extensively for AuNPs surface modification. This improves functionality, biocompatibilities, and target specificities[56-60].

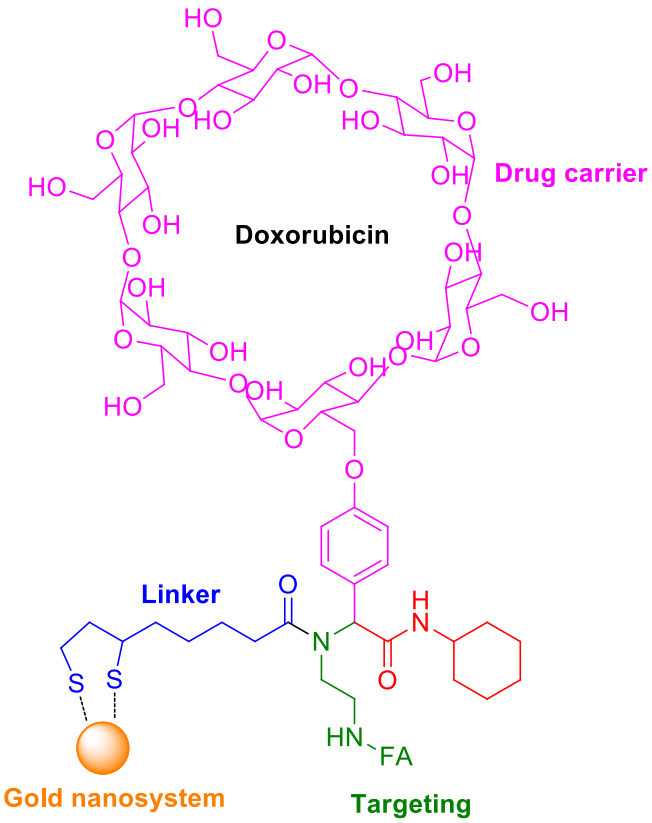

Figure 6. Bioactive thiolated molecule conjugated gold nanoparticle.

Bing Yan *et al.*,[61] reported that multi-functionalized nanoparticles are important for nano biomedical applications. However, synthesis are tedious and time consuming. Hence, multi-component reactions on nanostructures is a good way to prepare nanomaterials. Gold nano organothiol system, illustrated in the scheme, was made. This shows enhanced cancer cell targeting and killing.

Surinder P. Singha *et al.*,[62] reported 11-mercaptoundecanoic acid modified gold nanoparticles (~7 nm). These were conjugated with chloroquine to assess their potential

application in cancer therapeutics. The anti-cancer activity of chloroquine-gold nanoparticle conjugates (GNP-ChlQ) was demonstrated in MCF-7 breast cancer cells.

1.6. Metal-Loaded Boron nitride

Elemental palladium, nickel and rhodium have a high affinity for hydrogen and form hydrides in reaction with hydrogen. They are used in hydrogen storage technology and as catalysts for hydrogenation due to their high hydrogen solubility, diffusivity, and corrosion resistance[63]. Boron nitride (BN) is a catalyst support. It is a benign powder possessing a hexagonally shaped crystal structure composed of continuous boron-nitrogen bonds. The numerous lone pairs on the nitrogen atoms can co-ordinate with Pd metal and suppress catalyst activity for hydrogenation and coupling reactions[64].

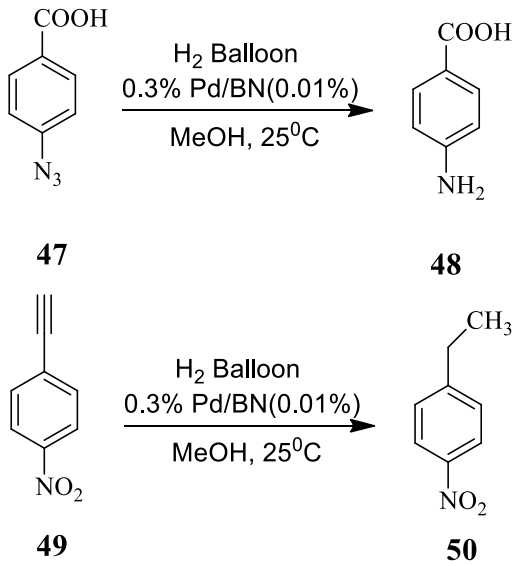

Hironao Sajiki *et al*.,[65] reported a hydrogenation catalyzed heterogeneous reaction by Pd on boron nitride (Pd/BN) in methanol. Hydrogenation product of azides **47** and alkynes **49** in the presence of other reducible functionalities such as benzyl ethers, aryl halides, aryl ketones and nitro groups were obtained. Also, the semi hydrogenation of alkynes could be achieved without the reduction of other coexisting reducible functionalities.

1.7. Biomolecules Functionalized Nanoparticles

Living organisms have high potential for nanoparticles[66] production. Hence, green synthetic methods using biological extracts have gained importance in nanoparticle synthesis[67]. However, the mechanism of involvement of biomolecules is not well understood. Plants, algae, diatoms, heterotrophic human cell lines and some biocompatible agents are reported to synthesize greener nanoparticles. Metals such as cobalt, copper, silver, gold, bimetallic alloys, silica, palladium, platinum, iridium and magnetite are used. However, the use of phototrophic and heterotrophic eukaryotes and biocompatible agents for the synthesis of nanomaterials is yet to be fully explored[68].

Yunzhi Fu *et al*.,[69] reported the biosynthesis of silver nanoparticles using aqueous aloe leaf extract. Their results suggest that nanoparticles can be used as effective growth inhibitors against the test microorganisms. Greater bactericidal activity was observed for silver nanoparticles. The *Escherichia coli*, a gram negative bacterium, was reported as more efficient for gold and silver nanoparticles synthesis than *S. aureus*, a gram positive bacterium.

Mata *et al*.,[70] reported the bio reduction of Au(III) to Au(0) using biomass of the brown alga *Fucus vesiculosus*. Bioreduction with *F. vesiculosus* could be an alternative and environmentally friendly process. It can be used for recovering gold from dilute hydrometallurgical solutions and leachates of electronic scraps and for the synthesis of gold nanoparticles of different size and shape.

Venkataraman *et al*.,[71] reported the synthesis of biomolecules functionalized gold nanoparticles using edible mushroom *Pleurotus florida* by photo-irradiation method. The mixture containing aqueous gold ions and mushroom extract was kept in sunlight.

Sharma *et al*.,[72] reported on metal nanoparticles having catalytic activities. However, they are difficult to recover after downstream processing of chemical reactions. Therefore, plant-based nanoparticles have enormous advantages.

Also, an increased awareness towards green chemistry has necessitated the development of simple, cost-effective and eco-friendly procedures.

1.8. The Objectives and Scope of Study

The present work pertains to the synthesis of:

i) pharmacologically active planar quinoline bearing benzothiazole, quinoline thiosemicarbazone, fluorinated dihydropyridine and dihydropyran derivatives via. a one-pot reaction approach and evaluation of their antibacterial activities and inter molecular interaction with MDM2 human protein by molecular docking.

ii) fluorinated pyrrolophenanthroline derivatives using ionic liquids, as catalyst. BSA protein binding and detailed physicochemical and spectroscopic analysis with supporting molecular docking studies.

iii) copper-loaded boron nitride (Cu/BN) nanomaterials as an innovative support for the Kabachnik-Fields reaction involving the condensation of amines, aldehydes and diethyl phosphite species. This facile method is a good choice for the synthesis of α-aminophosphonates. The Cu/BN was recyclable for a minimum of four cycles making it highly effective.

iv) gold nano surfaces capped with anchor sulfur organic groups, such as thiols and disulfides; these are the proto type components of supramolecular systems. Two novel systems were used for the synthesis of gold capped small bioactive molecules and their cytotoxicity elucidated.

v) silver, gold and palladium nanoparticles (NPs) by using South African indigenous medicinal plants via. simple green chemistry approach. Aqueous extracts of leaf and flower were used as a natural reducing agent. The application of NPs as anti-cancer agents and catalytic reduction of dyes and nitrobenzene derivatives were undertaken

Chapter 2, describes the synthesis of quinoline, pyridine and pyran based bioactive small molecules; these were of a quinoline type bearing a benzothiazole moiety, quinoline thio semicarbazone ligand, fluorine substituted dihydro pyridine, fluorine substituted dihydropyran and fluorine substituted pyridine derivatives. In total, fifteen compounds were synthesized via. a one-pot reaction. Eleven compounds were novel. All compounds were characterized by straight forward consideration of spectroscopic techniques. A good number of analogues have shown considerable *in vitro* anti-bacterial activity against two gram-negative bacteria, *Escherichia coli* (ATCC 25922) and *Pseudomonas aeruginosa* (ATCC 27853) and one gram-positive bacterium, *Staphylococcus aureus* (ATCC 29213).

All the compounds showed the minimum inhibitory concentration 256 µg/ml against *Escherichia coli* and *Pseudomonas aeruginosa* except for compound **13** which showed activity at 128 µg/ml MIC. The binding interaction of the compounds through molecular docking with p53−MDM2 tumor suppressor protein is also discussed.

Chapter 3, discusses an efficient one-pot four component route to the synthesis of tri fluorinated pyrrolophenanthroline and fluoroquinoline pyrrolophenanthrolines. In this reaction 1-butyl-2,3-dimethylimidazolium tetrafluoroborate ionic liquid (DMTIL) was used as a reaction medium; no catalyst was required. This structure of the pyrrolophenanthroline were deduced by IR and NMR analysis. Compounds were studied with Bovine Serum Albumin (BSA) through molecular docking. Hydrophopic, electrostatic and hydrogen bonding interaction played a crucial role in the binding to sub domain of BSA. Interaction studies of DMTIL with BSA by emission, absorption, synchronous fluorescence, circular dichroism (CD) and three dimensional emission (3D) spectroscopic techniques is discussed. The results from emission titration experiments revealed the existence of a strong interaction between BSA and DMTIL ionic liquid. It showed that compounds with lesser number of hydrogen bonds are found to be more active which is attributed to hydrophobic interaction and electrostatic interaction which also played a vital role in DMTIL binding to sub domain IB of BSA.

Chapter 4, describes preparation of copper-loaded boron nitride (Cu/BN) and used as an efficient and chemoselective catalysts for the synthesis of α-aminophosphonates by the Kabachnik-Fields reaction; 21 α-aminophosphonates were synthesised. The enhanced catalytic activity and product yield could be attributed to the increase of surface acidity. Overall, this methodology offers competitive advantages such as recyclability of the catalyst without further purification or without using additives or cofactors, low catalyst loading, broad substrate applicability and high yields. The application of this new nanocatalyst in organic synthesis will provide a novel pathway for the synthesis of pharmaceutically pertinent compounds.

Chapter 5, describes modified gold surfaces with self-assembled monolayers of thiol and disulfide bearing bioactive small molecules; this received considerable interest due to their potential application as anti-cancer agents. In this study a carbazole was conjugated to lipoic acid by using an amide coupling catalyst HBTU and DIEA reaction. The structure of the carbazole thio octanic acid (CTN) was identified by IR and NMR. CTN was

attached to the gold nanoparticles surface and the capping behaviour was characterized by UV-vis spectroscopy, TEM, DLS and FTIR. The cytotoxicity of CTNAuNPs on A549 cell lines was determined using the MTT assay. The results suggest CTN and CTNAuNPs posses anti-proliferative properties in the cancerous A549 cells.

Furthermore this chapter includes the thiol dual ligand capped gold nanoparticle synthesis, characterization and their cytotoxic evaluation in A549 lung cancer cells. DTAu was synthesized by equimolar 4-aminothiophenol (4-ATP) and amino oxadiazole thiol (AXT). This dual ligand was attached to the gold nanoparticles surface and the capping behaviour was characterized by UV-vis spectroscopy, TEM, DLS and FTIR. The cytotoxicity of DTAu on A549 cell lines was determined using the MTT assay. The results suggest dual ligands (4-ATP, AXT) and DTAu posses anti-proliferative properties in the cancerous A549 cells.

Chapter 6, communicates the role of South African indigenous plants and agroforestry waste in the synthesis of silver, gold and palladium nanoparticles (NPs). Green protocols are presented such as environmentally benign solvents, non-hazardous and highly rapid synthesis of NPs. The formulation of natural medicinal compounds capped onto nanoparticles (NPs) are assessed for their anti-cancer activity and catalytic reduction of dyes and nitrobenzene derivatives. In addition, the palladium nanoparticles were used effectively in the Suzuki coupling reaction carbon-carbon formation in water.

Reference

(1) *Organic Chemistry*; Clayden, J., Greeves, N., Warren, S., Eds.; Oxford Press: UK, **2010**.

(2) De Oteyza, D. G.; Gorman, P.; Chen, Y. C.; Wickenburg, S.; Riss, A.; Mowbray, D. J.; Etkin, G.; Pedramrazi, Z.; Tsai, H. Z.; Rubio, A.; Crommie, M. F.; Fischer, F. R. *Science*. **2013**, 340, 1434.

(3) (a) *The Logic of Chemical Synthesis*; Corey, E. J., Cheng, X. M., Eds.; John Wiley: New York, **1989**. (b) *Classics in Total Synthesis: Targets, Strategies, Methods*; Nicolaou, K. C., Sorensen, E. J., Eds.; VCH: Weinheim: New York, **1996**. (c) *Classics in Total Synthesis II: More Targets, Strategies, Methods*; Nicolaou, K. C., Snyder, S. A., Eds.; Wiley-VCH: Weinheim, **2003**. (d) *Molecules That Changed the World: A Brief History of the Art and Science of Synthesis and Its Impact on Society*; Nicolaou, K. C., Montagnon, T., Eds.; Wiley: New York, **2008**.

(4) Hendrickson, J. B. *J. Am. Chem. Soc*. **1975**, 97, 5784.

(5) Dolle, R. E.; Nelson, K. H. Jr. *J. Comp. Chem*. **1999**, 1, 235.

(6) Nordell, P.; Lincoln, P. *J. Am. Chem. Soc.* **2005**, 127, 9670.

(7) *Biomedicinal Aspects of Fluorine Chemistry*; Elliot, A. J., Filler, R., Kobayashi, Y., Eds.; Elsevier Biomedical Press: Amsterdam, **1982**.

(8) *Advanced Drug Delivery Reviews*. Tamara, M., Lorna, R. R.,Vitaly P., In Press; **2013**.

(9) Kostarelos, K. *Nanomedicine.* **2006**, 1, 1.

(10) Yuki, Y.; Yoshinari, S.; Tsuyoshi, Y.; Saori, N.; Yasunari, M.; Hironao, S. *Chem. Cat. Chem.* **2013,** 5, 2360.

(11) Sousa, A.; Sousa, E. M. B. *J. Non-Crystalline. Solids*. **2006**, 352, 3451.

(12) Xiao, D.; Xi, L.; Yang, W.; Fu, H.; Shuai, Z.; Fang, Y.; Yao, J. *J. Am. Chem. Soc.* **2003**, 125, 6740.

(13) (a) *Comprehensive Heterocyclic Chemistry II*; Katritzky, A. R., Ress, C. W., Scriven, E. F. V., Eds.; Pergamon: Oxford, U.K, **1996**, 1. (b) *Comprehensive Heterocyclic Chemistry III*; Katritzky, A. R., Ramsden, C. A., Scriven, E. F. V., Taylor, R. J. K., Eds.; Pergamon: Oxford, U.K, **2008**, 1. (c) Martins, M. A. P.; Cunico, W.; Pereira, C. M. P.; Flores, A. F. C.; Bonacorso, H. G.; Zanatta, N. *Curr. Org. Synth*. **2004**, 1, 39. (d) Drunhinin, S. V.; Balenkova, E. S.; Nenajdenko,

V. G. *Tetrahedron*. **2007**, 63, 7753. (e) Martins, M. A. P.; Frizzo, C. P.; Moreira, D. N.; Zanatta, N.; Bonacorso, H. G. *Chem. Rev*. **2008**, 104, 2015.

(14) Balaban, A. T.; Oniciu, D. C.; Katrizky, A. R. *Chem. Rev*. **2004**, 104, 2777.

(15) (a) Torok, B.; Abid, M.; London, G.; Esquibel, G. K. S. *Angew. Chem. Int. Ed*. **2005**, 44, 3086. (b) Estevez, V.; Villacampa, M.; Menendez, J. C. *Chem. Soc. Rev*. **2010**, 39, 4402. (c) Sheikh, K. D.; Banerjee, P. P.; Jagadeesh, S.; Grindrod, S. C.; Zhang, C.; Paige, M.; Brown, M. C. *J. Med. Chem*. **2010**, 53, 2376.

(16) (a) Kumar, R.; Mittal, A.; Ramachandran, U. *Bioorg. Med. Chem. Lett*. **2007**, 17, 4613. (b) Boecker, R. H.; Guengerich, F. P. *J. Med. Chem*. **1986**, 29, 1596. (c) Humphries, P. S.; Almaden, J. V.; Barnum, S. T.; Carlson, T. J.; Do QQ, T.; Fraser, J. D.; Hess, M.; Kim, Y. H.; Ogilvie, K. M.; Sun, S. *Bioorg. Med. Chem. Lett*. **2006**, 16, 6116. (d) Son, J. K.; Zhao, L. X.; Thapa, P.; Karki, R.; Na, Y.; Jahng, Y.; Jeong, T. C.; Jeong, B. S.; Lee, C. S.; Lee, E. S. *Eur. J. Med. Chem*. **2008**, 43, 675.

(17) (a) Solmon, V. R.; Haq, W.; Srivastava, K.; Puri, S. K.; Katti, S. B. *J. Med. Chem*. **2007**, 50, 394. (b) Chauhan, P. M. S.; Srivastava, S. K. *Curr. Med. Chem*. **2001**, 8, 1535. (c) Michael, J. P. *Nat. Pro. Rep*. **2004**, 21, 650. (d) Michael, J. P. *Nat. Pro. Rep*. **2007**, 24, 223. (e) Kim, J. I.; Shim, I. S.; Lee, J. K. *J. Am. Chem. Soc*. **2005**, 127, 1614.

(18) (a) Achterrathtuckermann, U.; Weischer, C. H.; Szelenyi, I. *Pharmacology*. **1988**, 36, 265. (b) Druker, B. J.; Tamura, S.; Buchdunger, E.; Ohno, S.; Segal, G. M.; Fanning, S.; Zimmermann, J.; Lydon, N. B. *Nat. Med*. **1996**, 2, 561. (c) Kappe, C. O. *Eur. J. Med. Chem*. **2000**, 35, 1043. (d) Lee, Y.; Shacter, E. *J. Biol. Chem*. **1999**, 274, 19792. (e) McNeely, W.; Wisemann, L. R. *Drugs*. **1998**, 56, 91. (f) Normann, M. H.; Rigdon, G. L.; Navas, F.; Cooper, B. R. *J. Med. Chem*. **1994**, 37, 2552. (g) Ralevic, V.; Burnstock, S. G. *Pharmacol. Rev*. **1998**, 50, 413. (h) Studer, A.; Hadida, S.; Ferrito, R.; Kim, S. Y.; Jegger, P.; Wipf, P.; Curran, D. P. *Science*. **1997**, 275, 823. (i) Wolfe, J. F.; Rathman, T. L.; Sleevi, M. C.; Campbell, J. A.; Greenwood, T. D. *J. Med. Chem*. **1990**, 33, 161. (j) Yamaguchi, M.; Kamei, K.; Koga, T.; Akima, M.; Kuroki, T.; Ohi, N. *J. Med. Chem*. **1993**, 36, 4052.

(19) (a) McCallien, D. W.; Sanders, J. K. M. *J. Am. Chem. Soc*. **1995**, 117, 6611. (b) Chouai, A.; Simanek, E. E. *J. Org. Chem*. **2008**, 73, 2357.

(20) (a) Wang, J.; Shen, Y.; Hu, W.; Hsieh, M.; Lin, F.; Hsu, M. K.; Hsu, M. H. *J. Med. Chem*. **2006**. 49, 1442. (b) DeCorte, B. L. *J. Med. Chem*. **2005**, 48, 1689.

(21) Roma, G.; Braccia, M. D.; Grossi, G.; Mattioli, F.; Ghia, H. *Eur. J. Med. Chem.* **2000**, 35, 1021.

(22) Benkovic, S. J.; Baker, S. J.; Alley, M. R. K.; Youn, H. W.; Yong, K. Z.; Tsutomu, A.; Weimin, M.; Justin, B.; Ravi, R. P. T.; Mark, W.; Lyn Sue, K.; Ali, T.; Lucy, S. *J. Med. Chem.* **2005**, 48, 7468.

(23) Vargas, M. L. Y.; Castelli, M. V.; Kouznetsov, V. V.; Urbina, G. J. M.; Lopez, S. N.; Sortino, M.; Enriz, R. D.; Ribas, J. C.; Zacchino, S. *Bioorg. Med. Chem.* **2003**, 11, 1531.

(24) Bailly, C. *Biochemistry*. **1999**, 38, 7719.

(25) *Comprehensive Heterocyclic Chemistry II*; Jones, G., Kartrizky, A. R., Rees, C. W., Scriven, E.F., Eds.; Pergamon: Oxford, **1996**, 5, 167.

(26) Van Brabandt, W.; Vanwalleghem, M.; Dhooghe, M.; De Kimpe, N. *J. Org. Chem.* **2006**, 71, 7083.

(27) He, Z.; Li, H.; Li, Z. *J. Org. Chem*. **2010**, 75, 4296.

(28) Sharma, R.; Pandey, A. K.; Chauhan, P. M. S. *Synlett*. **2012**, 2209.

(29) Kumar, K. H.; Muralidharan, D.; Perumal, P. T. *Synthesis*. **2004**, 63.

(30) Lulu, W.; Youming, W.; Haibin, S.; Liangfu T.; Zhenghong, Z.; Chuchi, T. *Asian. J. Chemistry*. **2013**, 8, 2204.

(31) Mali, J. R.; Pratap, U. R.; Dhanaji, V.; Jawale, D. V.; Ramrao, A. *Tetrahedron Letters*. **2010**, 51, 3980.

(32) Shika, S. D.; Ajay, M. G.; Anjali, M. R.; Mukund, S. C.; Chavoun, P. M. S.; Kumkum, S. *Ind. J. Chem*. **2009**, 48, 1780.

(33) Coates,A.; Hu, Y.; Bax, H. R.; Page, C. *Nat. Rev. Drug Discovery*. **2002**, 1, 895.

(34) Kirkpatrick, P. *Nat. Rev. Drug Discovery*. **2002**, 1, 97.

(35) Szakacs, G.; Paterson, J. K.; Ludwig, J. A.; BoothGenthe, C.;Gottesman, G. M. *Nat. Rev. Drug Discovery*. **2006**, 5, 219.

(36) Keser, G. M.; Makara, G. M. *Drug Discovery Today*. **2006**,11,741.

(37) Orru, R. V. A.; De Greef, M. *Synthesis*. **2003**,1471.

(38) Zhibo, M.; Zheng, X.; Tuoping, L.; Kui, L.; Zhibin, X.; J iahua, C.; Zhen, Y. *J.Comb. Chem*. **2006**, 8, 696.

(39) Jingjing, W.; Hui, L.; Song, C. *Beilstein. J. Org. Chem.* **2011**, 7, 1070.

(40) Rovnyak, G. C.; Atwal, K. S.; Hedberg, A.; Kimball,S. D.; Moreland, S.; Gougoutas, J. Z.; O'Reilly, B. C.; Schwartz, J.; Malley, M. F. *J. Med. Chem*. **1992**, 35, 3254.

(41) Saeed, A.; Shaheen, U.; Hameed, A.; Kazmi, F. *J. Fluorine Chem*. **2010**, 131, 333.

(42) Smart, B. E. *J. Fluorine Chemistry*. **2001**, 109, 1, 3.

(43) Bonacorso, H. G.; Wentz, A. P.; Lourega, R. V. *J. Fluorine Chemistry*. **2006**, 127, 8, 1066.

(44) Olsen, J. A.; Banner, D. W.; Seiler, P. *Chem Bio Chem*. **2004**, 5, 5, 666.

(45) Abdel R, R. M.; Al Footy, K. O.; Aqlan, F. M. *Inter. J. ChemTech. Research.* **2011**, 3, 1, 423.

(46) Abdel, R,; Makki, R. M,; Bawazir, M. S. I. T. *J. Chemistry*. **2011**, 8, 1, 405.

(47) Harshad, G. K.; Manish, P. P. *E. J. Med. Chem.* **2013,** 63, 675.

(48) Zhang, J. M.; Yang, W.; Song, L. P.; Cai, X.; Zhu, S. Z. *Tet. Lett*. **2004**, 45, 5771.

(49) Dongbin, Z.; Min, W.; Yuan, K.; Enze, M. *Catalysis. Today.* **2002**,74,157.

(50) Sarma, R.; Prajapati, D. *Synlett.* **2008**, 3001.

(51) Lan, Y. Z.; Guang, Q. L.; Fu, Y. Z. *J. Biophy. Chem*. **2011**, 2, 146.

(52) Dubois, L. H.; Nuzzo, R. G. *Annu. Rev. Phys. Chem*. **1992**, 43, 437.

(53) *Cryo-EM Part A: Sample Preparation and Data Collection*. *Methods in Enzymology*; Ackerson, C. J., Powell, R. D., Hainfeld, J. F., Eds.; Elsevier, **2010**, 481.

(54) Bowman, M. C. *J. Am. Chem. Soc.* **2008**, 103, 6896.

(55) Demers, L. M. *Science.* **2002**, 296, 1836.

(56) Kang, B.; Mackey, M. A.; El Sayed, M. A. *J. Am. Chem. Soc*. **2010**, 132, 1517.

(57) Daniel, M. C.; Astruc, D. *Chem. Rev*. **2004**, 104, 293.

(58) Huang, X.; El Sayed, I. H.; Qian, W.; El Sayed, M. A. *J. Am. Chem. Soc*. **2006**, 128, 2115.

(59) Kim, B.; Han, G.; Toley, B. J.; Kim, C. K.; Rotello, V. M.; Forbes, N. S. *Nat. Nano*. **2010**, 5, 465.

(60) Gong. *J. Chem. Rev*. **2012**, 112, 2987.

(61) Hongyu, Z.; Gaoxing, S.; Peifu, J.; Bing, Y. *Asian. J. Chemistry*. **2012**, 18, 18, 5501.

(62) Prachi, J.; Soumyananda, C.; Jaime, E.; Ramirez Vick, Z. A.; Ansari.; Virendra, S.; Pinak, C.; Surinder, S. P. *Colloids. Surfaces Biointerfaces.B.* **2012**, 95, 195.

(63) Zhang, L. P.; Wu, P.; Sullivan, M. B. *J. Phys. Chem*. **2011**, 115, 4289.

(64) Yuki, Y.; Tsuyoshi, Y.; Saori, N.; Yoshinari, S.; Yasunari, M.; Hironao, S. *Adv. Synth. Cata*. **2012**, 354, 1264.

(65) Yuki, Y.; Tsuyoshi, Y.; Saori ,N.; Yoshinari, S.; Yasunari, M.; Hironao, S. *Adv. Synth. Cata*. **2012**, 354, 7, 1264.

(66) Sastry, M.; Ahmad, A.; Khan, M. I.; Kumar, R. *Current Science*. **2003**, 85, 170.

(67) Noruzi, M.; Zare, D.; Davoodi, D. *Molecular. Biomolecular. Spectroscopy*. **2012**, 94, 84.

(68) Kannan, B. N.; Natarajan, S. *Adv . Colloid. Inter. Science*. **2011**, 169, 59.

(69) Yongqiang, Z.; Xinfeng, C.; Yucang, Z.; Xinghua, X.; Yunzhi, F. *Colloids. BioSurfaces. B*. **2013**, 423, 63.

(70) Mata, Y. N.; Torres, E.; Blazquez, M. L.; Ballester, A.; Gonzalez, F.; Munoz, J. A. *J. Hazard. Mater*. **2009**, 166, 612.

(71) Ravishankar, B.; Sharanabasava, V. G.; Raghunandan, D.; Ullas, S.; Ganesh, S.; Venkataraman, A. *J. Photochemistry. Photobiology. Biology. B.* **2013**, 125, 63.

(72) Sharma, N. C.; Sahi, S. V.; Nath, S.; Parsons, J. G.; Gardea, T. J. L.; Pal, T. *Environ. Sci. Technol.* **2007**, 41, 5137.

Chapter 2

One pot synthesis, anti-bacterial and molecular docking studies of new quinoline and fluorinated pyridine, pyran nucleus

CHAPTER II

One pot synthesis, anti-bacterial and molecular docking studies of new quinoline and fluorinated pyridine, pyran nucleus

2.1. Abstract

A new class of bioactive small molecules was synthesized; these were a quinoline type bearing a benzothiazole moiety, fluorine substituted dihydro pyridine, fluorine substituted dihydro pyran and fluorine substituted pyridine derivatives. In total, fifteen compounds were synthesized, eleven of which were novel. These compounds were fully characterised by spectroscopic techniques, i.e. IR, ^{1}H-NMR, ^{13}C-NMR, ^{19}F-NMR and MS. Compounds **1**, **2**, **3** and **4** were synthesized previously by known protocols established in our laboratory. Three novel planar compounds **6**, **7** and **8** were synthesized efficiently with 2-aminothiophenol and 3-formylquinoline-2-one, 3-formylquinoline-2-thione and tetrazoloquinoline respectively, by aerobic oxidative cyclization. Of these three compounds, **6** was selected as a representative and analysed for its crystal structure by XRD.

While extensive work has been carried out with thiosemicarbazone scaffold, there is no reported literature on compounds derived from 2-thio-1,2-dihydro-quinoline-3-carbaldehyde; we synthesized novel compounds **11** and **13** by using thiosemicarbazide and 4-methyl- 3-thiosemicarbazide, respectively. Compounds **18**, **21**, **23** and **25** are novel poly functional fluorine substituted dihydro pyridine and dihydro pyran quinolines which were synthesized via. a one-pot multi-component reaction. Compounds **18** and **21** were synthesized by a practical and efficient procedure through a unique four-component reaction of trifluoromethylbenzaldehyde, malononitrile, 2-fluoroaniline and acetylene dicarboxylate in the presence of triethylamine as a base promoter and catalyst. Compounds **23** and **25** were synthesized by refluxing trifluoromethylbenzaldehyde, malononitrile, activated phenol or dimedone in the presence of PTSA or DMAP as a catalyst.

Compound **28** was synthesized from fusaric acid and phenylhydrazine whilst compound **30** was synthesized from fusaric acid and pentafluoro phenylhydrazine, in the presence of the coupling reagents HBTU and DIEA, respectively.

The synthesized compounds were evaluated *in vitro* for anti-bacterial activity against two gram-negative bacteria, *Escherichia coli* (ATCC 25922) and *Pseudomonas aeruginosa* (ATCC 27853) and one gram-positive bacterium, *Staphylococcus aureus*

(ATCC 29213). Standard anti-biotics were used as positive control. An examination of the data revealed that all compounds, that were tested, indicated no inhibitory effect against *staphylococcus*. However, all the compounds showed the minimum inhibitory concentration of 256 µg/ml against *Escherichia coli* and *Pseudomonas aeruginosa* except for **13** which showed activity at 128 µg/ml MIC.

Molecular docking experiments were carried out against p53−MDM2 tumor suppressor protein using Surflex-Dock GeomX programme of Sybyl software on Dell T-1500 work station to confirm the mechanism of action of active compounds among the series. The p53−MDM2 interaction is a valuable target to develop effective anti-tumor agents. In this study we discovered potent p53–MDM2 inhibition by 2-thio-1,2-dihydroquinoline-3-carbaldehyde thiosemicarbazone and fluorine substituted new pyridine derivatives as identified by structure-based design.

2.2. Introduction

Heterocyclic compounds have fascinating chemical behaviour as well as pharmacological properties which are beneficial to mankind. In particular quinolines are ubiquitous heterocycles in nature. Quinoline alkaloids are mainly isolated from Rutaceae and Solanaceae plant species and they show significant biological activities which include vasoconstrictive, anti-diuretic, anti-arrhythmic, spamolytic, sedative, hypothermal effects[1], anti-tumaral, anti-pyretic, anti-platelet, cytotoxic activities and also photosensitization for DNA damage and mutation[2]. Due to such a wide range of biological activities, increased attention is directed to the synthesis of quinoline derivatives and alkaloids.

It is known that the chloroquinoline moiety serves as a backbone of many natural products and analogues. A wide range of heterocycles can be generated from the quinoline type of compounds. However quinoline are not only good synthetic intermediates but also act as good pharmacophores. Owing to their relevant biological activities including anti-microbial[3], anti-malarial[4], anti-cancer and cytotoxic activities[5], the synthesis of novel chloroquinoline and others compounds are promising research areas of study.

The 2-chloro-3-formylquinolines are versatile precursors which serve as good building blocks for more complex organic structures. Acccording to literature, this precursor is prepared from an amine derivative leading to acetanilides followed by a double formylation reaction via. a Vilsmeier Haack reaction. These reaction sequences are presented below.

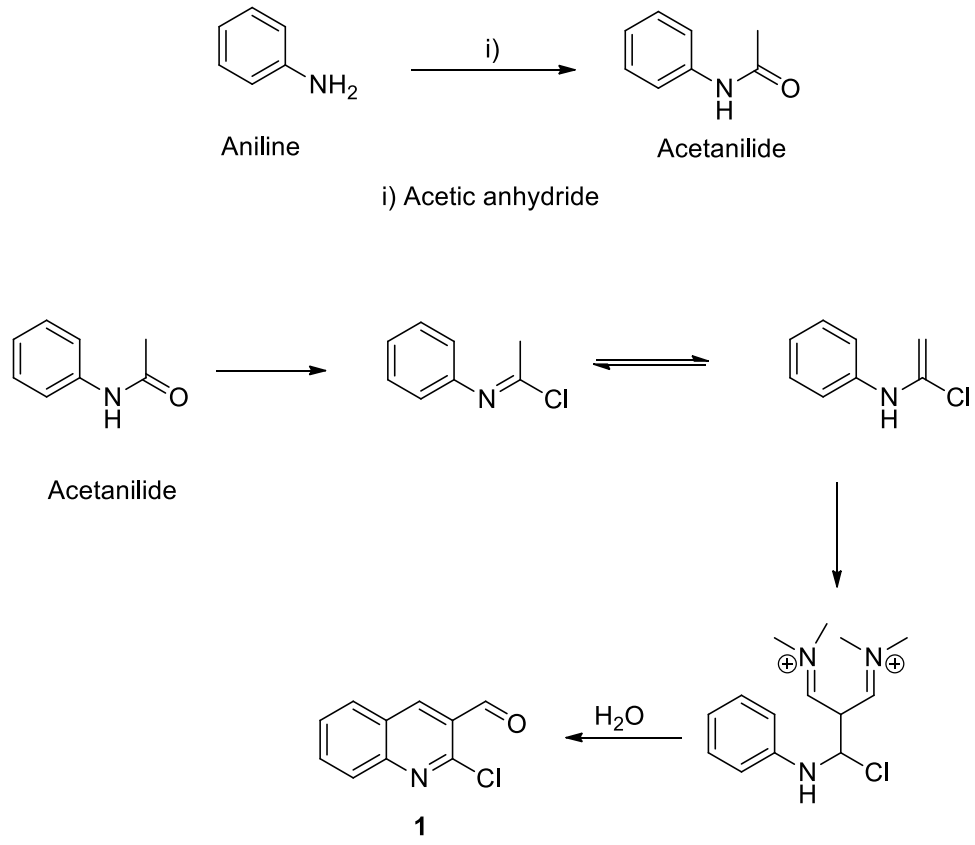

Scheme 1. A reaction outline for formation of 2-chloro-3-formylquinoline

The mole ratio of acetanilide, DMF and $POCl_3$ is 1:2.5:7, respectively and the temperature of 96°C is standardized as the optimum condition to get maximum yield. Yields are generally good especially with anilides carrying electron donating groups. Acetanilides containing an electron withdrawing groups such as NO_2 and Cl produces low yield of the final product. Hence to increase the yield, many attempts were made which included microwave induced Vilsmeier reaction and formylation in the presence of micelles. The micelles act as a kind of mini reactor and are produced either using cetyltrimethyl ammonium bromide (CTAB), sodium n-dodecyl sulphate (SDS) or Triton-X-100 under Vilsmeier condition, in acetonitrile. In this methodology the yields are increased even though acetanilide bearing electron withdrawing groups are present.

Over the last few decades, drug resistance to the commonly used anti-biotics has become a serious problem. Therefore, the synthesis of compounds that could be used for the effective treatment of infectious diseases without side effects is an urgent biomedical

issue[6]. Various heterocyclic compounds have shown anti-microbial potential and quinoline is one of the most promising heterocyclic nuclei having prominent anti-bacterial activity. Realizing the medicinal importance of quinoline compounds, it was considered worthwhile to incorporate this moiety. It was therefore thought interesting to synthesize these quinoline compounds with an object of determining whether such compounds could enhance their anti-bacterial activity.

Although many quinoline and quinolones have been synthesized and reported, the most notable ones being developed, or used, in veterinary medicine worldwide include, amifloxacin, benofloxacin, ciprofloxacin, danofloxacin, difofloxacin, norfloxacin and sarafloxacin. Other major quinolones in human medicine include enoxacin, ofloxacin and tosufloxacin. These fluoroquinolones show good oral bioavailability in all monogastric species. A large volume of distribution and low binding to plasma proteins allows them to cross membranes and reach the most remote parts of the body at concentrations above the minimum inhibitory concentrations (MIC's) of most pathogens[7].

Molecular docking is a typical computational approach of modern drug discovery; it serves as a rapid method for the theoretical prediction of binding mode of the "drug like candidates" with active site of the known macromolecular structure. Despite its complexity in molecular docking algorithm and scoring function, accuracy is the only standalone solution of this approach leading to drug discovery. One of the techniques used is Glide; it is an esteemed docking panel which operates with the help of funnel type modules locating the binding geometry of the small molecule with protein active site. Glide is conserved as the top search algorithm in the docking community and was used in this study. The 3D coordinates of X-ray crystal structure of human mdm2 (PDB ID: 3VZV) is complexed from the Protein data bank. To perform docking, the most crucial aspect is to prepare the protein is such way that it can be read by the algorithm and subsequently to match with the parameter existing in the protein preparation wizard. The band of operations executed in preparing the protein are assigned bond orders, adding hydrogen, treating metals, deleting water molecules, removing co-crystal ligand, treating disulfide bonds, adjusting bond order, building missing heavy atoms, formal charges and alleviating potential steric clashes. OPLS-2005 force field is employed for energy minimization at quantum level 0.3 Å RMSD; cut off is taken as threshold valve to diagnose the protein refinement strategies.

2.3. Experimental

2.3.1. General

Melting points were determined by using a Stuart SMP10 Melting Point Apparatus and were uncorrected. IR spectra were recorded on Varian 800 FTIR using KBr pellets and the absorption frequencies are expressed in reciprocal centimeters (cm^{-1}). NMR spectra were taken on BRUKER TOPSPIN 400 MHz and 600 MHz spectrometer using TMS as an internal reference. The chemical shifts were expressed in parts per million (ppm). The mass spectra were determined on a GC mass spectrometer. Elemental analyses were performed on Perkin Elmer Analyzer. CrysAlisPRO (Oxford Diffraction, 2009) Empirical absorption correction using spherical harmonics, implemented in SCALE3 ABSPACK scaling algorithm.

2.3.2. Synthesis and Spectroscopic Data of Organic Compounds

2.3.2.1. Synthesis of 2-chloro-3-formylquinoline (1)

An accurate mass of acetanilide (6.08 g, 45 mmol) was dissolved in DMF (10.4 ml, 135 mmol). The solution was cooled to 0-5°C. Then $POCl_3$ (52 ml, 540 mmol) was added dropwise and the mixture was stirred at 90-100°C for 24 hours. The progress of the reaction was monitored by TLC. The reaction mixture was poured into 500 g of crushed ice; the precipitate was neutralized with dil NaOH and filtered. The crude mixture was separated by column chromatography using petroleum ether: EtOAc mixture (95:5) v/v as the eluent. A white solid was obtained. The yield was 90 %.

2.3.2.2. Synthesis of 2-oxo-1, 2-dihydroquinoline-3-carbaldehyde (2)

A suspension of 2-chloro-3-formylquinoline **1** (4.7 g, 25 mmol) in 50 % acetic acid (150ml) was heated under reflux for six hours. The completion of the reaction was checked by TLC. Upon cooling the reaction mixture, a solid product precipitated out which was filtered, washed with distilled water and dried. The yield was 92 %.

2.3.2.3. Synthesis of 2-thio-1, 2-dihydroquinoline-3-carbaldehyde (3)

To a solution of 2-chloro-3-formylquinoline **1** (4.7 g, 25 mmol) in dry DMF (25 ml), sodium sulphide (2.4 g, 26 mmol) was added and the mixture stirred for two hours at room temperature. On completion of the reaction, monitored by TLC; the reaction mixture was poured into 500 g of crushed ice. The resulting residue was filtered off, washed with distilled water and dried. The yield was 85 %.

2.3.2.4. Synthesis of 2-azide-1, 2-dihydroquinoline-3-carbaldehyde (4)

To a solution of 2-chloro-3-formylquinoline **1** (4.7 g, 25 mmol) in absolute ethanol (25ml), *p*-toluenesulphonic acid (PTSA) (0.17 g, 1 mmol) and sodium azide (1.6 g, 26 mmol) were added. The reaction mixture was heated under reflux for seven hours. After completion of the reaction, monitored by TLC; the reaction mixture was poured into 500 g of crushed ice. The resulting residue was filtered to afford the desired product. The yield was 80 %.

2.3.2.5. Synthesis of 3-(benzo[d]thiazol-2-yl)quinolin-2(1H)-one (6)

Equimolar quantities of 2-oxo-1,2-dihydroquinoline-3-carbaldehyde **2** (1.038 g, 6 mmol) and 2-aminothiophenol (0.64 ml, 6 mmol) were dissolved in 50 ml ethanol. A few drops of glacial acetic acid was added. The solution was refluxed for six hours to produce a pale yellow solid. The solid was filtered and then recrystallized in DMSO to produce the target compound as pale-yellow crystals, (94 % yield). mp: 347°C; IR (KBr, cm^{-1}): 3358, 2874, 1685, 1577, 1332; ^{1}H-NMR (600 MHz, DMSO-d_6): δ (ppm) 12.41 (brs, 1H), 9.1 (s, 1H), 8.0 (d,1H), 7.47 (t, 1H), 7.31 (t, 1H), 7.45 (d, 1H), 8.14 (d, 1H), 7.65 (t, 1H), 7.57 (t, 1H), 8.08 (d, 1H); ^{13}C-NMR (600 MHz, DMSO-d_6): δ (ppm) 115.88, 119.40, 122.43, 122.79, 123.17, 123.66, 125.41, 126.75, 130.07, 132.63, 136.75, 139.07, 139.59; Anal Calcd. $C_{16}H_{10}N_2OS$ (278.33): C, 69.04; H, 3.62; N, 10.06; O, 5.75; S, 11.52 %. Found: C, 69.05; H, 3.696; N, 10.23; S, 11.45

2.3.2.6. Synthesis of 3-(benzo[d]thiazol-2-yl)quinoline-2(1H)-thione (7)

Equimolar quantities of 3-formylquinoline-2(1H)-thione **3** (1.134 g, 6 mmol) and 2-aminothiophenol (0.64 ml, 6 mmol) were dissolved in 50 ml ethanol. A few drops of glacial acetic acid was added. The solution was refluxed for six hours to produce a yellow solid, (84 % yield). mp: 254°C; IR (KBr, cm^{-1}): 3358, 2345.17, 1685, 1577, 1332, 1241.77, 1157.88, 1057.82, 930.54, 750.811; ^{1}H-NMR (400 MHz, DMSO-d_6): δ (ppm) 9.4 (s, 1H), 8.8 (s, 1H), 7.4-7.8 (dd, 1H), 7.4-7.14 (m, 2H), 7.15-7.10 (m, 1H), 7.09-6.92 (d, 2H), 6.8 (d, 2H); ^{13}C-NMR (400 MHz, DMSO-d_6): δ (ppm) 181.07, 156.84, 151.35, 137.72, 134.18, 133.15, 132.62, 129.35, 127.90, 124.78, 122.25, 119.62, 119.34, 116.17, 40.40, 40.11, 39.90, 39.69, 39.48, 39.28, 39.07, 38.86.

2.3.2.7. Synthesis of 2-(2-azidoquinolin-3-yl)benzo[d]thiazole (8)

Equimolar quantities of 4-formyltetrazolo[1,5-a]quinoline (1.188 g , 6 mmol) and 2-aminothiophenol (0.64 ml, 6 mmol) were dissolved in 50 ml ethanol. A few drops of glacial acetic acid was added. The solution was refluxed for six hours to produce a yellow solid, (90 % yield). mp: 268°C; IR (KBr, cm^{-1}): 3489.44, 2848.40, 1667.88, 1556.87, 1384.47, 1319.70, 1150.77, 979.53, 749.89; ^{1}H-NMR (400 MHz, DMSO-d_6): δ (ppm) 9.3 (s, 1H), 8.10 (s, 1H), 7.9-8.00 (d, 2H), (d, 1H), 7.47-7.78 (dd, 4H), 7.4 (t, 1H); ^{13}C-NMR (400 MHz, DMSO-d_6): δ (ppm) 161.37, 160.69, 152.18, 139.59, 139.70, 136.75, 132.63, 130.07, 126.75, 125.41, 123.17, 122.79, 199.40, 115.88, 40.72, 40.60, 40.46, 40.32, 40.04, 39.90, 39.76.

2.3.2.8. Synthesis of (E)-2-((2-thioxo-1,2-dihydroquinolin-3-yl)methylene) hydrazine carbothioamide (11)

Thiosemicarbazide (0.911 g, 0.01 mol), dissolved in warm methanol (50 ml), was added to a methanol solution (50 ml) containing 2-oxo-1,2-dihydroquinoline-3-carbaldehyde (1.73 g, 0.01 mol). The mixture was refluxed for one hour during which period a yellow precipitate was formed. The reaction mixture was then cooled to room temperature and the solid compound was filtered. It was then washed with methanol and dried under vacuum. The crude product was recrystallized with 50 % methanol and chloro form combination to give a yellow powder, (92 % yield). mp: 234°C; IR (KBr, cm^{-1}): 2361.63, 1621.16, 1582.26, 1463.09, 1344.66, 851.05; ^{1}H-NMR (400 MHz, DMSO-d_6,): δ (ppm) 13.98 (s, 1H), 11.92 (s, 1H), 8.88 (s, 1H), 8.42 (s, 2H), 8.38 (s, 1H), 7.96 (d, 2H), 7.86 (t, 1H), 7.76 (d, 1H), 7.35 (t, 1H); ^{13}C-NMR (400 MHz, DMSO-d_6): δ (ppm) 180.00, 178.21, 151.67, 138.82, 138.119, 132.16, 131.88, 131.63, 128.53, 124.70, 122.33, 116.03, 40.04, 39.84, 39.63, 39.42, 39.21, 39.00, 38.79, 24.97, 17.48.

2.3.2.9. Synthesis of (E)-N-methyl-2-((2-thioxo-1,2-dihydroquinolin-3-yl)methylene) hydrazinecarbothioamide (13)

4-methyl-3-thiosemicarbazide (1.05 g, 0.01 mol), dissolved in warm methanol (25 ml), was added to a methanol solution (25 ml) containing 2-oxo-1,2-dihydroquinoline-3-carbaldehyde (1.73 g, 0.01 mol). The mixture was refluxed for one hour during which period a yellow precipitate was formed. The reaction mixture was then cooled to room temperature and the solid compound was filtered. It was then washed with methanol and dried under vacuum. The final product was recrystallized with 50 % methanol and chloro form combination to give a yellow powder, (89 % yield). mp: 255°C; IR (KBr, cm^{-1}):

1943.44, 1704.14, 1623.67, 1489.37, 1383.16; ^{1}H-NMR (400 MHz, DMSO-d_6): δ (ppm) 13.87 (s, 1H); 11.78 (s, 1H); 8.85 (s, 1H,); 8.65-8.61 (s, 2H); 7.78 (s, 1H,); 7.64-7.58 (d, 1H); 7.40 (t, 1H); 3.34 (s, 3H); ^{13}C-NMR (400 MHz, DMSO-d_6): δ (ppm) 180.03, 177.86, 139.47, 139.18, 132.34, 131.64, 131.29, 128.44, 124.74, 122.26, 116.09, 40.08, 39.87, 39.66, 39.45, 39.23, 39.04, 38.83, 30.81, 30.69, 30.65, 24.93, 17.47.

2.3.2.10. Synthesis of Dimethyl 6-amino-5-cyano-1-phenyl-4-(4-(trifluoromethyl) phenyl)-1,4-dihydropyridine-2,3-dicarboxylate (18)

In a round bottom flask, a mixture of 4-trifluoromethyl benzaldehyde (0.27 ml, 2.0 mmol), malononitrile (0.144 g, 2.0 mmol) and triethylamine (0.27 ml, 2.0 mmol) in 10 mlethanol was stirred at room for ten minutes. Then a solution of aniline (0.18 ml, 2.0 mmol) and dimethyl acetylenedicarboxylate (0.24 ml, 2.0 mmol) in 10 ml ethanol was added. The whole solution was stirred at room temperature for 24 hours. The precipitate was filtered, washed with cold ethanol to give a white solid, (82 % yield). mp: 202°C; IR (KBr, cm^{-1}): 3466.64, 3378.99, 3228.27, 3058.42, 3009.39, 2955.14, 2904.22, 2844.90, 2181.79, 1749.75, 1653.95, 1579.79, 1418.64, 1066.07, 977.20, 929, 861.79, 888.09, 669.43; ^{1}H-NMR (600 MHz, $CDCl_3$): δ (ppm) 7.51 (s, 2H), 7.31 (s, 1H), 7.59 (d, 2H), 7.60 7.58 (d, 2H), 7.42 (d, 2H), 4.98 (s, 2H), 4.25 (s, 1H), 3.77 (s, 3H), 3.54 (s, 3H); ^{13}C-NMR (600 MHz, $CDCl_3$): δ (ppm) 165.41, 163.27, 149.80, 148.63, 142.27, 134.89, 130.75, 130.20, 130.08, 127.35, 125.94, 125.90, 125.86, 120.13, 104.48, 62.12, 52.66, 52.16, 38.49; ^{19}F-NMR (400 MHz, $CDCl_3$): δ (ppm) 62.403.

2.3.2.11. Synthesis of dimethyl 6-amino-4(4-chlorophenyl)-5-cyano-1-(2-fluorophenyl-1,4-dihydropyridine-2,3-dicarboxylate (21)

In a round bottom flask, a mixture of 4-chloro benzaldehyde (0.281 g, 2.0 mmol), malononitrile (0.144 g, 2.0 mmol) and triethylamine (0.27 ml, 2.0 mmol) in 10 ml ethanol was stirred at room for ten minutes. Then a solution of 2-fluoroaniline (0.19 ml, 2.0 mmol) and dimethyl acetylenedicarboxylate (0.24 ml, 2.0 mmol) in 10 ml ethanol was added. The whole solution was stirred at room temperature for ten hours. The precipitate was filtered and washed with cold ethanol to give a white solid, (94 % yield). mp: 193°C; IR (KBr, cm^{-1}): 3042.26, 2997.41, 2842.88, 2294.13, 1748.59, 1651.43, 1574.59, 1353.78, 1260.06, 1151.59, 1045.11, 971.11, 831.45, 770.61, 673.82; ^{1}H-NMR (600 MHz, $CDCl_3$): δ (ppm) 7.53-7.52 (s, 1H), 7.38-7.34 (s, 5H), 7.29- 7.25 (m,2H), 4.58 (s, 1H), 4.25 (s, 2H), 3.68 (s, 3H), 3.45 (s, 3H); ^{13}C-NMR (600 MHz, $CDCl_3$); δ (ppm) 165.34, 163.24, 149.25, 143.03, 141.40, 133.03, 132.95, 131.86, 128.93, 128.73, 125.10, 122.95, 122.93, 119.92, 117.40,

117.21, 105.92, 63.51, 52.73, 52.12, 38.34; ^{19}F-NMR (400 MHz, $CDCl_3$): δ (ppm) 116.856.

2.3.2.12. Synthesis of 2-amino-7,7-dimethyl-5-oxo-4-(4-(trifluoromethyl)phenyl)-5,6,7, 8-tetrahydro-4H-chromene-3-carbonitrile (23)

Into a mixture of 4-trifluoromethyl benzaldehyde (0.13 ml, 1 mmol) and malononitrile (0.066 g, 1 mmol) in 4 ml of ethanol, was added the catalyst DMAP (0.025 g, 0.2 mmol) and stirred at room temperature. The white solid precipitate was formed immediately. Dimedone (0.14 g, 1 mmol) was added into the reaction mixture and it was kept for stirring under reflux conditions. After sometime, the reaction mixture turned into a clear solution. After completion of the reaction, the solid precipitated out under hot conditions. The reaction mixture was cooled and the precipitate was filtered to give the desired product as a white solid, (94 % yield). mp: 224°C; IR (KBr, cm^{-1}): 3789.81, 3183.50, 3049.04, 2976.39, 2894.04, 2644.04, 2191.70, 2083.57, 1926.78, 1875.17, 1746.53, 1609.49, 9014.83, 8057.35, 661.88; ^{1}H-NMR (400 MHz, DMSO-d_6): δ (ppm) 1.05 (s, 3H), 1.10 (s, 3H), 2.14–2.23 (m, 2), 2.43 (s, 2H), 4.26 (s, 1H), 7.08 (s, 2H), 7.25-7.28 (d, 2H), 7.70–7.85 (d, 2H); ^{13}C-NMR (400 MHz, DMSO-d_6): δ (ppm) 195.69, 162.90, 168.49, 158.90, 128.06, 125.26, 119.41, 111.95, 59.71, 57.39, 49.86, 40.10, 39.89, 30.68, 39.38, 39.27, 39.08, 38.85, 35.56, 31.79, 26.24, 26.88; ^{19}F-NMR (400 MHz, CDCl3): δ (ppm) 60.79.

2.3.2.13. Synthesis of 3-amino-1-(4-(trifluoromethyl)phenyl)-1H-benzo[f]chromene-2-carbonitrile (25)

A mixture containing 4-trifluoromethyl benzaldehyde (0.13 ml, 1 mmol), malononitrile (0.066 g, 1 mmol), β-naphthol (0.144 g, 1 mmol) and *p*-toluenesulfonic acid (PTSA) (0.03 g), in acetonitrile (5 ml), was refluxed for 3 hours. After completion of the reaction, which was monitored by TLC, the mixture was cooled to room temperature and filtered. The crude product was recrystallized from methanol to give a pale yellow solid, (95 % yield). mp: 228°C; IR (KBr, cm^{-1}): 2219.63, 1925.06, 1741.11, 1655.61, 1626.29, 1555.71, 1492.15, 1450.94, 1325.88, 1296.77, 1214.66, 1166.52, 1088.52, 906.86, 846.64, 801.92, 688.49; ^{1}H-NMR (400 MHz, DMSO-d_6): δ (ppm) 5.25 (s, 1H), 7.15-7.43 (s, 2H), 7.19 (s, 1H), 7.60-7.62 (d, 2H), 7.63-7.65 (d, 2H), 7.74-7.79 (m, 3H), 9.07-9.09 (d, 1H); ^{13}C-NMR (400 MHz, DMSO-d_6): δ (ppm) 129.77, 128.05, 126.08, 125.65, 122.21; ^{19}F-NMR (400 MHz, DMSO-d_6): δ (ppm) 62.7733.

2.3.2.14. Synthesis of 5-butyl-N'-phenylpicolinohydrazide (28)

Fusaric acid (0.5 g, 2.75 mmol) was dissolved in DMF (15 ml), THF (5 ml), HBTU (1 g, 3.05 mmol), DIEA (1 ml, 6.00 mmol) and phenylhydrazine (0.3 ml, 2.7 mmol) were added. The reaction mixture was then stirred at room temperature until no more starting material could be detected by TLC analysis. The reaction mixture was poured into 50 ml of distilled water; the mixture was then extracted thrice with ethyl acetate (25 ml). The combined extracts were dried over anhydrous sodium sulfate, filtered and then concentrated to dryness affording the crude product. This crude product was purified by column chromatography (50:50 EtOAc/Hexane) to afford a white solid, (90 % yield). mp: 98°C; IR (KBr, cm^{-1}): 3266.39, 2955.39, 2924.85, 2566.91, 2311.07, 1843.13, 1676.56, 1605.25, 1531.89, 1440.70, 1399.54, 1333.71, 1177.01, 1088.15, 906.47, 858.79, 755.27, 693.27; ^{1}H-NMR (400 MHz, $CDCl_3$): δ (ppm) 0.90 (t, 3H), 1.31((t, 2H), 1.59 (t, 2H), 2.62 (t, 2H), 6.75 (s, 1H), 6.85-7.20 (t, 2H), 7.3-7.4 (t, 3H), 7.65-7.68 (dd, 2H), 8.0-8.01 (d, 1H), 8.4-8.41 (s, 1H), 9.6 (d, 1H); ^{13}C-NMR (400 MHz, $CDCl_3$): δ (ppm) 206.9, 163.5, 147.9, 147.8, 145.9, 142.3, 137.9, 129.16, 122.64, 121.3, 113.88, 32.97, 32.76, 30.92, 22.20, 13.79.

2.3.2.15. Synthesis of 5-butyl-N'-(perfluorophenyl)picolinohydrazide (30)

Fusaric acid (0.5 g, 2.75 mmol) was dissolved in DMF (15 ml) and THF (10 ml), HBTU (1 g, 3.5 mmol), DIEA (1 ml, 6.00 mmol) and pentafluorophenylhydrazine (0.54 g, 2.7 mmol) were added. The reaction mixture was then stirred at room temperature until no more starting material could be detected by TLC analysis. The reaction mixture was poured into 50 ml of distilled water; the mixture was then extracted thrice with ethyl acetate (25 ml). The combined extracts were dried over anhydrous sodium sulfate, filtered and then concentrated to dryness affording the crude product. This crude product was purified by column chromatography (50:50 EtOAc/Hexane) to afford a white solid, (92 % yield). mp: 101°C; IR (KBr, cm^{-1}): 3282.48, 2929.64, 2858.78, 2448.08, 1665.5, 1472.86, 1399.54, 1383.89, 1252.02, 1203.15, 1131.47, 966.014, 857.79, 712.69, 630.85; ^{1}H-NMR (400 MHz, $CDCl_3$): δ (ppm) 0.94 (t, 3H), 1.36 (t, 2H), 1.6 (t, 2H), 2.70 (t, 2H), 6.35 (s, 1H), 7.65-7.68 (dd, 1H), 8.0-8.01 (d, 1H), 8.4-8.41 (s, 1H), 9.6 (d, 1H); ^{13}C-NMR (400 MHz, $CDCl_3$): δ (ppm) 164.34, 148.81, 145.88, 142.35, 137.08, 122.26, 32.99, 32.78, 22.19, 13.79; ^{19}F-NMR (400 MHz, $CDCl_3$): δ (ppm) 155.80, 163.21, 164.70.

2.3.3. General Procedure used for Bacterial Studies

2.3.3.1. Preparation of media

Fresh Nutrient Agar, Oxoid LTD (Hampshire, England) was used according to the manufacturers instruction as follows: 28 g was weighed out into 3 separate one-litre glass bottles. Distilled water was added until the one litre mark of each bottle was reached using a measuring cylinder. The solution was mixed until the powder completely dissolved. Bottles were sterilized by autoclaving for 15 min at 121°C. The agar was then poured into plates to solidify.

2.3.3.2. Preparation of the nutrient broth

Fresh Mueller Hinton Broth (Sigma Aldrich) was made up according to the manufacturers instruction as follows: 23 g of nutrient broth powder was weighed into a one-litre glass bottle. Distilled water was added until the 1 litre mark was reached. The solution was mixed until the powder completely dissolved. This solution was dispensed into Bijou bottles before autoclaving. The Bijou bottles were sterilized by autoclaving for 15 min at 121°C.

2.3.3.3. Microbial Cultures used

The cultures of *Staphylococcus aureus* (ATCC 29213), *Escheriachia coli* (ATCC 25922) and *Pseudomonas aeuginosa* (ATCC 27853) were maintained on nutrient agar slopes at 4°C and subcultured on to blood agar plates for 24 hours before use.

2.3.3.4. Preparation of Reagent: Microplate Alamar Blue Assay (MABA)

An amount of 0.2 g of Resazurin powder was dissolved in 10 ml autoclaved distilled water and the dye solution was vortex rigorously; the solution was immediately covered with aluminium foil to keep away from light as it is light sensitive[8-9].

2.3.3.5. Anti-bacterial activity

The activities of the synthesized compounds were studied by Microplate Alamar Blue Assay (MABA) using 96-wells microplates including positive control (containing standard anti-biotic) and growth control (containing culture broth without testing materials). Three bacteria strains were selected and were diluted in broth. Each microtitre plate well was inoculated with a bacterial suspension containing 1 x 10^6 CFU/ml and incubated at 37°C for 24 hours. Then 20 µl of each concentration of the synthesized compound was added to two neighbour wells except for positive and growth control wells. After adding alamar blue (20 µl) to all of 96 wells, the total volume in each well reached 200 µl. The final concentrations of the tested compound were 256, 128, 64, 32, 16, 8, 4, 2,

1 µg/ml. After incubation, results were recorded as MIC (minimum concentration of each synthesized compound which completely inhibited growth of microorganism). Standard anti-biotics were used as positive control.

2.3.4. The Protocol used for Molecular Docking Studies

2.3.4.1. Preparation of protein structure

The crystal structure of human mdm2 (PDB ID: 3VZV), were retrieved from the Protein Data Bank. After selecting the protein structure, protein preparation wizard of Schrodinger suite was used to prepare the protein structure. All the water molecules were removed from the protein structure, metals were treated and hydrogen atoms were added; all atom force field (OPLS-2005) charges and atom types were assigned. The protein structure energy was minimized.

2.3.4.2. Preparation of ligand and Dockingstudies

Since the structure of the organic compounds are not available in pubchem database, chemsketch was used to draw the structure and all these ligands were prepared for molecular docking studies using ligprep version 2.3[10]. The ligand structure energy was minimized; partial atomic charges were computed using the OPLS-2005 force field by using Schrodinger suite. The prepared protein structure follows up the grid–fashion kinetic docking which commonly holds several physical parameters; there is great significance in prescribing the ligand interaction with the receptor. Grid files generation for protein was accomplished with "Receptor Grid Generation" panel of Glide. The grid box was generated by assigning a common constituency point; from there an actually cubic grid box was extended to touch the bounty of 20 Å in size or in words allocated size for grid generation for protein-ligand docking is 20 Å since our approach is site-specific not generalized. Co-crystal ligand binding pattern with protein is well documented in recent studies. Hence, we attempted to crop the grid box to focus on the centroid of human mdm2 (PDB ID: 3VZV) refined structure and box coordinate X, Y, Z were set at (X=18.341215 Å, Y=-3.662453 Å, Z=0.929674 Å). The foremost process in the hit identification pipeline, docking was performed using Glide of Schrodinger[11].

2.4. Results, Discussion and Conclusion

The synthesis of organic compounds for application in different research areas, such as medicine, used to be a tedious and laborious process; the synthesis was a step-wise reaction of individual steps requiring purification after each process. However recently, much research interest has been generated in the multi-component (MCRs) approach since the desired product could be obtained in a one pot reaction containing the correct substrates. In the initial years much research activity in MCRs was based on understanding the course of reaction and the effect of different catalysts. Subsequently MCRs became a high profile reaction since it could be used to produce important scaffolds for pharmaceutical applications.

Recently, we have embarked on MCRs based projects to achieve synthetic targets in an ideal and expeditious way. Since our organic research focus is on heterocyclic compounds especially quinoline derivatives, we decided to use our current knowledge of simple synthesis and extend it to MCRs. In the synthetic part of this study, we report the synthesis of novel quinoline derivatives by conventional step-wise reaction followed by synthesis of dihydro pyridine and pyran derivatives by MCRs. In the case of MCRs, we decided to focus on poly-functionalised dihydropyridine and dihydropyran type molecules containing a quinoline moiety with the intention of improving the biological activity of the final product. As mentioned earlier in the thesis, quinoline derivatives display a wide range of activities. Furthermore, we wanted to increase our research synthetic activity in terms of a green approach.

Our research plan was to use a simple quinoline derivative as one of the substrates in a MCR, hence we decided to start by synthesizing a chloro formyl quinoline derivative that could be used to obtain other simple novel derivatives.

The first step of this research study was to synthesize 2-chloro-3-formyl quinoline according to the procedure reported by Otto-Meth Cohn *et a1.*,[12]. This reaction proceeds via. the Vilsmeier-Haack reaction; the protocol is well established in our laboratory. This reaction is presented in **Scheme 2** below:

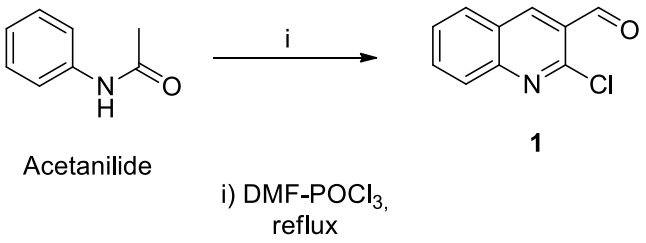

Scheme 2. Synthesis of 2-chloro-3-formyl quinoline from acetanilide

In the second part of the synthesis, we replaced the chloro group in **1** by heteroatoms oxygen, sulphur and nitrogen according to the procedure reported by Singh *et al.*,[13]. For the transformation of **1** to compounds **2**, **3** and **4,** we used 70% acetic acid, sodium sulphide and sodium azide in DMF, respectively; the reaction is presented in **Scheme 3**.

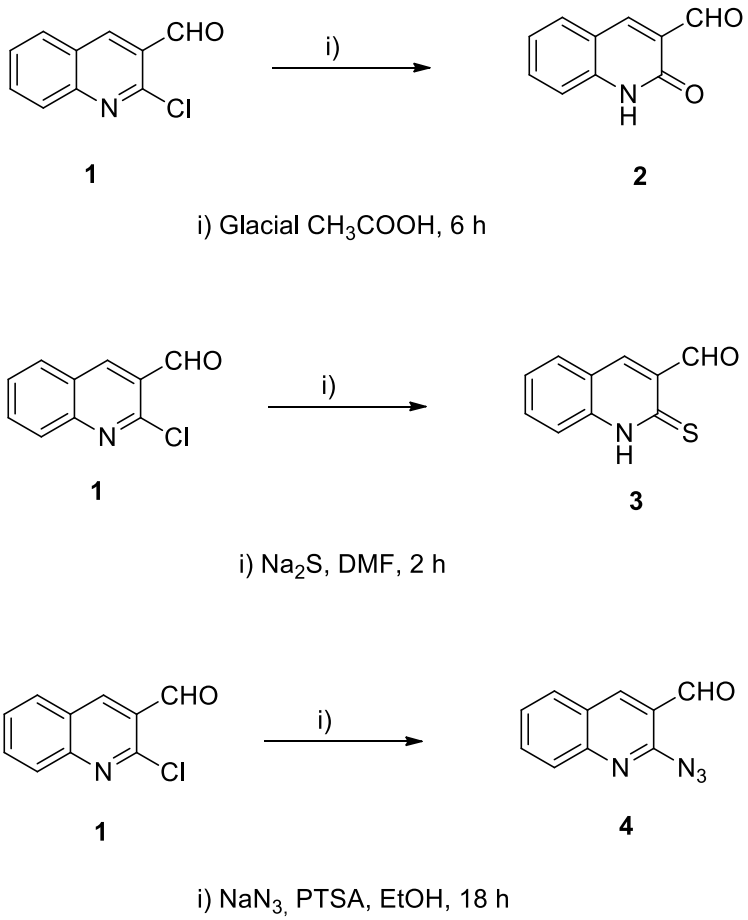

Scheme 3. Synthesis of quinoline nucleus with different substituents

In the third part of the synthesis, we reacted compounds **2**, **3** and **4** with ortho-amino thiophenol, in the presence of glacial acetic acid, to obtain **6**, **7** and **8**, respectively. This reaction is a simple condensation followed by *in situ* aerobic oxidative cyclization. Characterization of these compounds were achieved by IR, ^{1}H-NMR, ^{13}C-NMR, ^{19}F-NMR and MS. Compound 6 was chosen as a model structure; mass spectroscopic and XRD data were obtained. A typical interpretation of data for 6 is presented; the compound's molecular weight was confirmed by GC-MS ; M+• (m/z) 278.11 amu (**Figure 2.5**: page 61). The IR spectra (**Figure 2.1**: page 59): the carbonyl (-CO = 1685) and secondary amine (-NH= 3358) stetching frequency was present. The starting compound functional group SH stretch 2600-2540 cm^{-1} was not observed. The ^{1}H-NMR spectrum (**Figure 2.2**: page 59) of **21** showed a broad singlet signal near δ 12.15 (ppm) due to NH. In the ^{13}C-NMR (**Figure 2.3**: page 60), a signal at 161.37 was due to the carbonyl carbon.

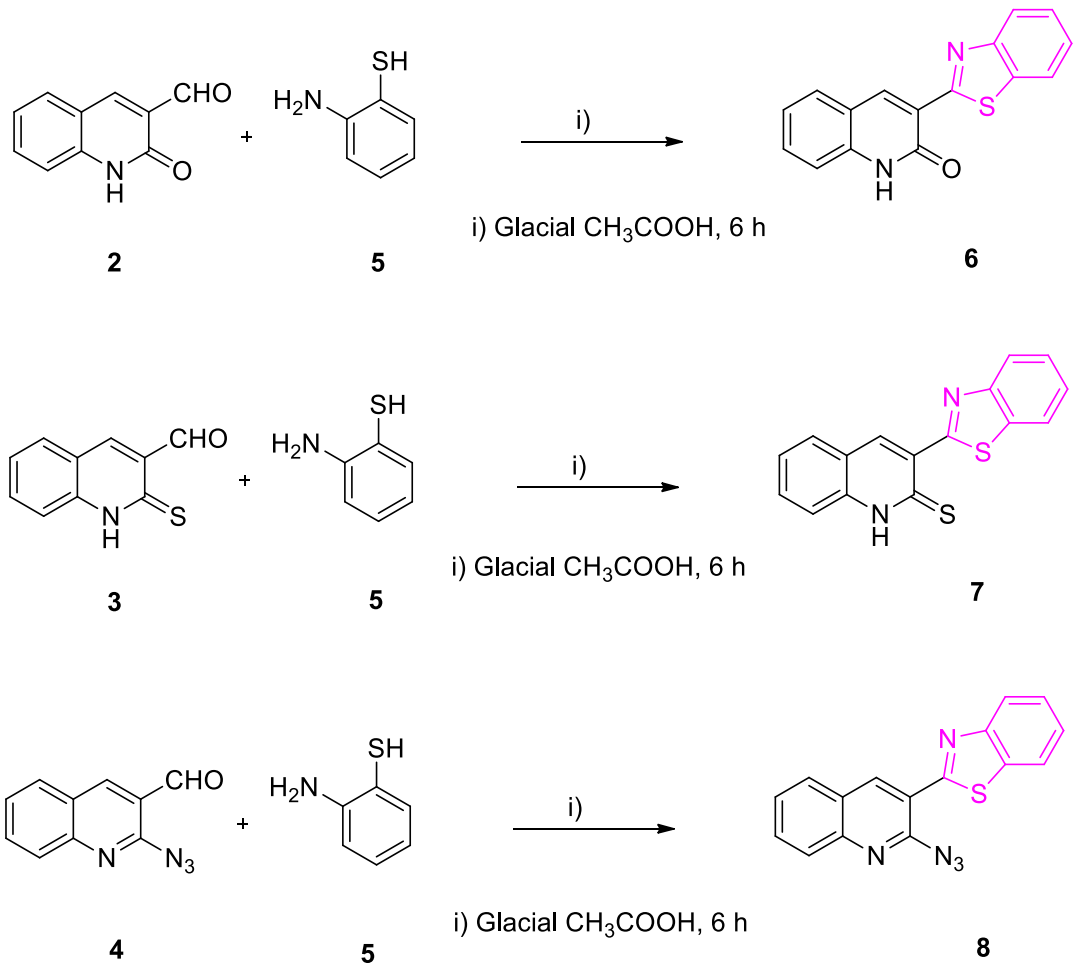

Scheme 4. Synthesis of quinoline bearing benzothiazole

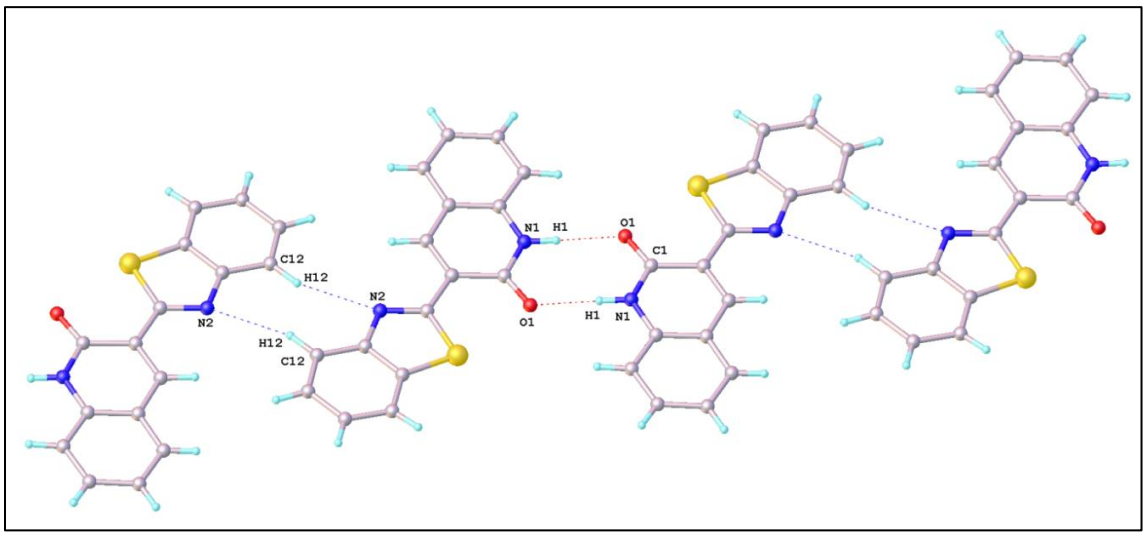

Figure 1. X-ray crystal structure and the packing, viewed down the b axis of **6**. Dashed lines indicate hydrogen bonds.

XRD analysis **Figure 1** showed the quinoline moiety bearing a nitrogen and an oxygen atom approximates to a planar conformation to the benzothiazole. The compound is linked to an adjacent molecule by N−H•••O and C−H•••N hydrogen bonding thereby producing a one-dimensional chain.

With the knowledge gained from literature, a series of reactions were carried out to prepare thiosemicarbazones, hydrazones and semicarbazones. Novel thiosemicarbazone derivatives **11** and **13** were prepared by a simple one step reaction of 2-thio-1,2-dihydroquinoline-3-carbaldehyde **3** with thiosemicarbazide **9** and 4-methyl-3-thio semicarbazide **12** respectively. The IR spectrum of **11** and **13** (**Figure 2.12 and 2.15**; pages 64 and 66) showed strong absorption in the range of 1140 cm^{-1} and 1142 cm^{-1} attributable to C=S. These molecules have three functional groups in position that will enable affective co-ordination with metal salts. The tridentate ligand is indicated in **Figure 2.**

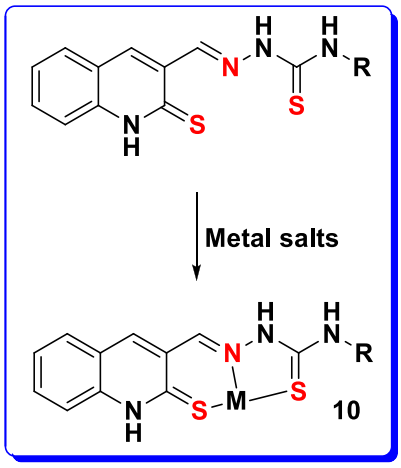

Figure 2. The metal ion in a neutral manner via. SNS donor atoms

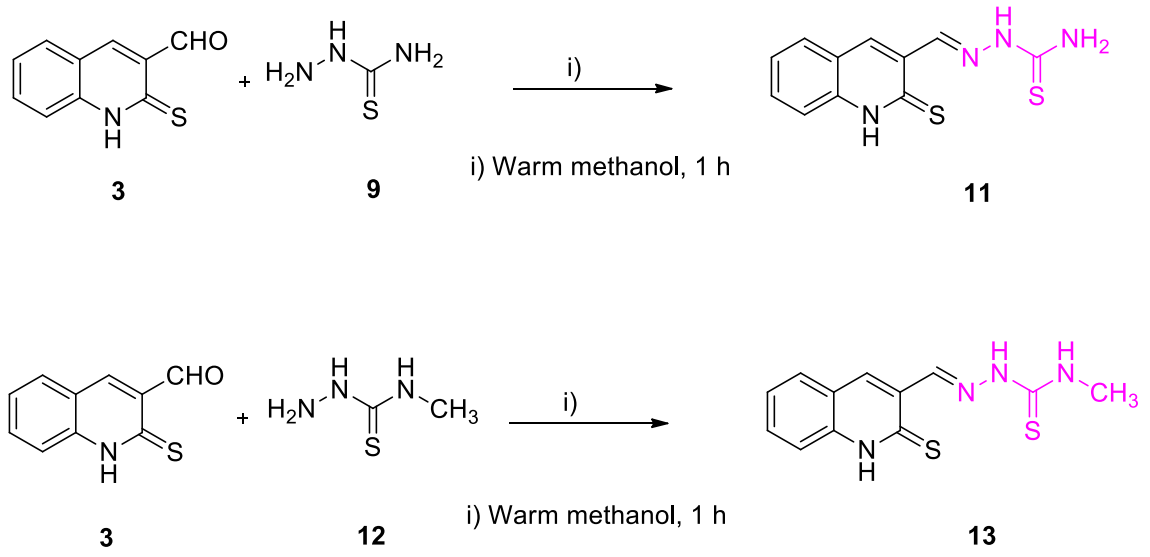

Scheme 5. Synthesis of 2-thio-1,2-dihydroquinoline-3-carbaldehyde thiosemicarbazone and N-methylthiosemicarbazone

The most important part of the synthetic plan was to use the MCR concept to synthesize fluorinated poly-functionalised dihydropyridine and dihydropyran derivatives. The MCRs used for this synthesis is presented in **Scheme 6** Compound **18**, a fluorinated poly functionalized dihydropyridine derivative was synthesized in excellent yields through a one-pot condensation and cyclisation containing four substrates viz. 4-trifluoromethyl benzaldehyde, malononitrile, aniline and dimethyl acetylenedicarboxylate in the presence of a catalytic amount of triethylamine. TLC anlaysis showed a single spot indicating all the substrates were used up in the reaction. After usual work-up, a white solid was obtained in 82 % yield.

Compound **21** was synthesized in a similar way except that 4-chlorobenzaldehyde and 2-fluoro aniline were used; all other reaction conditions were similar. The final product was a white solid, 80 % yield.

The structure of fluorinated poly-functionlised dihydropyrdine **21** was characterized by IR, ^{1}H-NMR, ^{13}C-NMR and ^{19}F-NMR and is in complete agreement with the proposed structure as described. The ^{19}F-NMR spectrum of **21** (**Figure 2.25**: page 71) furnised singlet at 116.856 attributed to the fluorine (C-F) function. In IR spectra (**Figure 2.22**: page 69) the nitrile (-CN = 2182), amine (-NH_2 = 3042) and (C-F = 1353) stetching frequency were present. The ^{1}H-NMR spectrum (**Figure 2.23**: page 70) showed a singlet signal near δ (ppm) 7.25 for NH_2. In the ^{13}C-NMR (**Figure 2.24**: page 70) signals at δ

143.03 (ppm) and δ 125.10 (ppm) were due to the carbonyl carbon and nitrile carbon, respectively.

In the synthesis of **23**, 4-trifluoromethylbenzaldehyde, malononitrile and dimedone were refluxed in DMAP. This product was a white solid produced in 94 % yield.

The structure of fluorine substituted dihydropyran **23** was characterized by IR, ^{1}H-NMR, ^{13}C-NMR and ^{19}F-NMR analysis and are in complete agreement with the proposed structure as described. The ^{19}F-NMR spectrum of **23** (**Figure 2.29**: page 73) furnished a singlet at δ 60.79 (ppm) attributed to the fluorine (-CF_3) function. The IR spectra (**Figure 2.26**: page 72) the nitrile (-CN = 2182) and amine (-NH_2 = 3042) stetching frequency were present. The ^{1}H-NMR spectrum (**Figure 2.27**:page 72) of **21** showed a singlet signal near δ 4.25 (ppm) due to NH_2. In ^{13}C-NMR (**Figure 2.28**:page 73) signals at 162.90 and 125.26 were due to the carbonyl carbon and nitrile carbon, respectively.

In the synthesis of **25**, 4-trifluoromethylbenzaldehyde, malononitrile and 2-naphthol were used in the presence of PTSA. The product was a white solid produced in 95 % yield.

The structure of **25** was characterized by IR, ^{1}H-NMR, ^{13}C-NMR and ^{19}F-NMR analysis and are in complete agreement with the proposed structure as described. The ^{19}F-NMR spectrum of **25** (**Figure 2.38**: page 76) furnished singlet at 62.77 attributed to the fluorine (-CF_3) function. In the IR spectra (**Figure 2.30**: page 74) the nitrile (-CN = 2219) and trifluoromethyl (-CF3 = 1325) stetching frequency were present. The ^{1}H-NMR spectrum (**Figure 2.31**: page 74) of **25** showed a singlet signal near δ 7.15-7.43 (ppm) due to NH_2. In ^{13}C-NMR (**Figure 2.32**: page 75) a signal at 125.66 was due to the nitrile carbon.

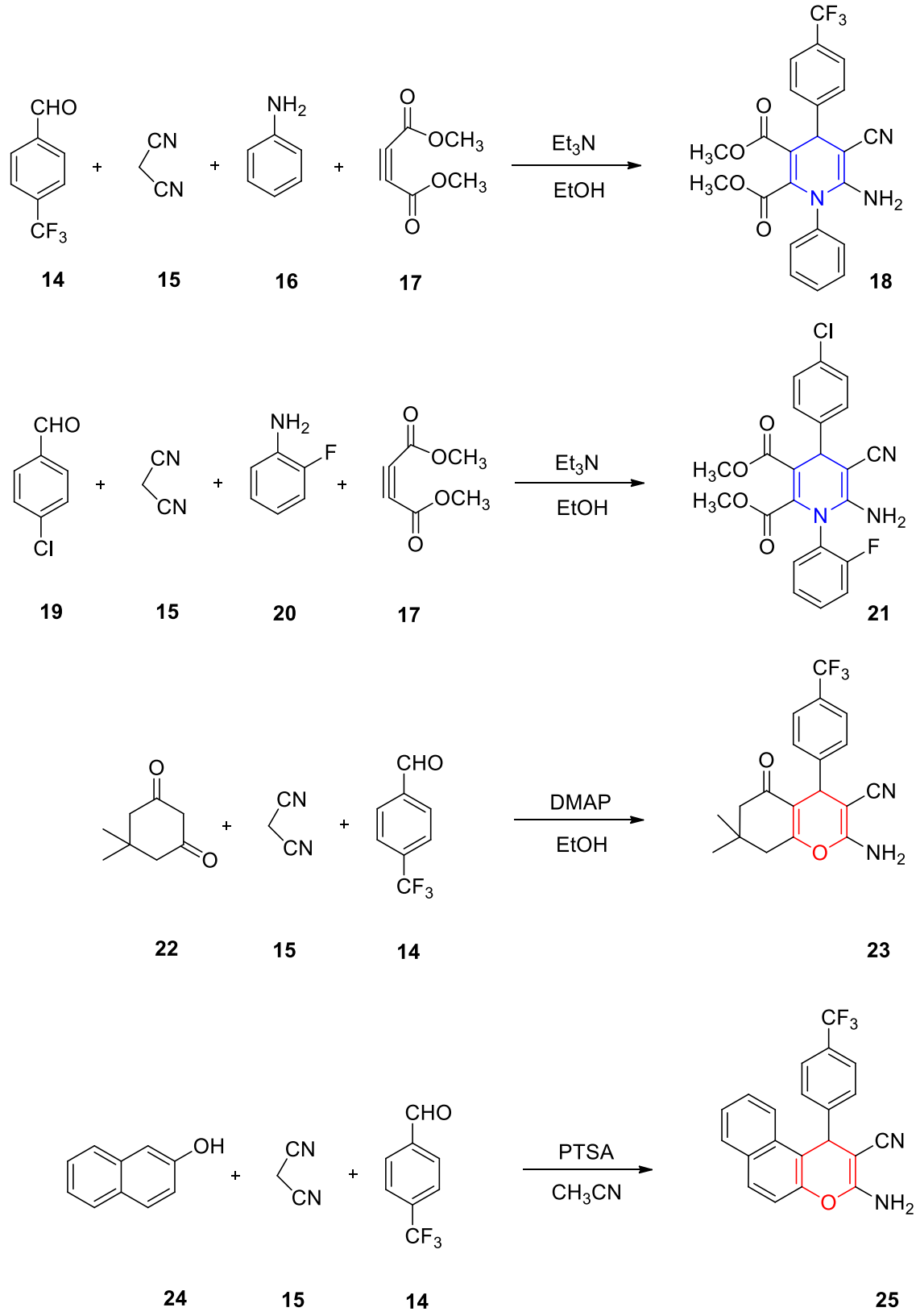

Scheme 6. Synthesis of fluorine substituted pyridine and pyran nucleus

In the final part of the synthetic plan, we synthesized two novel picolinohydrazide derivatives **28** and **30** from fusaric acid; the substrates were phenyl hydrazine and pentafloro phenyl hydrazine **Scheme 7**.

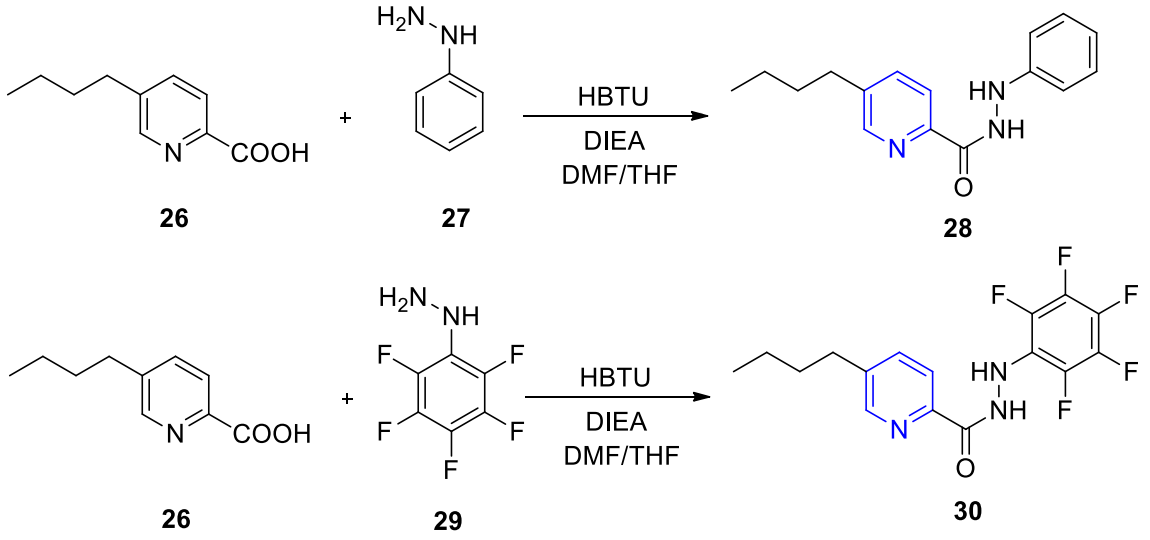

Scheme 7. Synthesis of hydrazides from fusaric acid

The IR, ^{1}H-NMR and ^{13}C-NMR interpretation of data for **28** and **30** are presented in (**Figures 2.34, 2.35 and 2.36**: pages 77 and 78). The ^{1}H-NMR, ^{13}C-NMR and ^{19}F-NMR interpretation of data for **30** are presented in (**Figures 2.39, 2.40 and 2.41**: pages 80 and 81). Also, the compound **30** was confirmed by its X-ray crystal structure **Figure 3**.

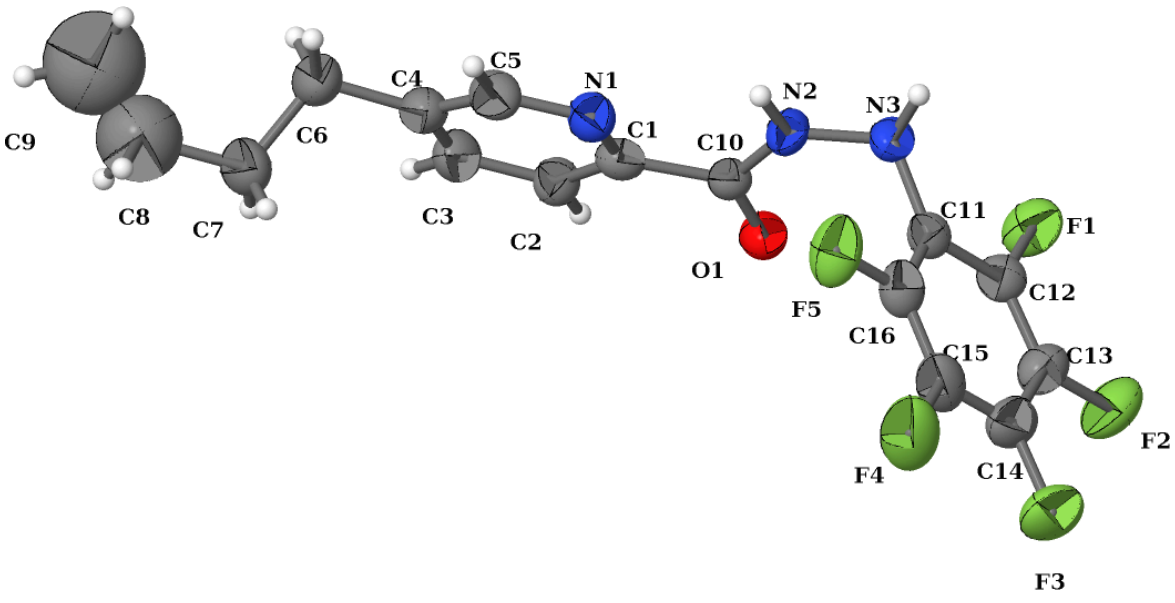

Figure 3. ORTEP views of compound **30**

After having synthesized novel compounds, we selected some of the quinoline derivatives for their bacterial activity. *In vitro* analysis for anti-bacterial activity against two gram-negative bacteria, *Escherichia coli* (ATCC 25922) and *Pseudomonas aeruginosa* (ATCC 27853) and one gram-positive bacterium, *Staphylococcus aureus* (ATCC 29213) were undertaken; the results are presented in **Table 1.** We used **s**tandard anti-biotics, Ciprofloxacin and Nalidixic acid**,** as positive control. An examination of the data revealed that all compounds, that were tested, indicated no inhibitory effect against *staphylococcus.* However, all the compounds showed the minimum inhibitory concentration 256 µg/ml against *Escherichia coli* and *Pseudomonas aeruginosa* except for **13** compound which showed activity at 128 µg/ml MIC.

Table 1. Anti-bacterial activities of quinoline derivatives: Minimum Inhibitory Concentration

Compound	Staphylococcus aureus (µg/ml)	Pseudomonas aeruginosa (µg/ml)	Escherichia coli (µg/ml)
6	ND	256	256
7	ND	256	256
8	ND	256	256
11	ND	ND	ND
13	ND	128	128

KEY: ND indicates not detected

Figure 4 indicates a typical microtitre plate showing the MIC's for the tested compounds against Gram-negative bacteria *Pseudomonas aeruginosa*, whilst **Figure 5** shows a typical microtitre plate showing the MIC's for tested compounds against Gram-negative bacteria *Escherichia coli.* **Figure 6** indicates a typical microtitre plate showing the MIC's for tested compounds against Gram-positive bacteria *Staphylococcus aureus.*

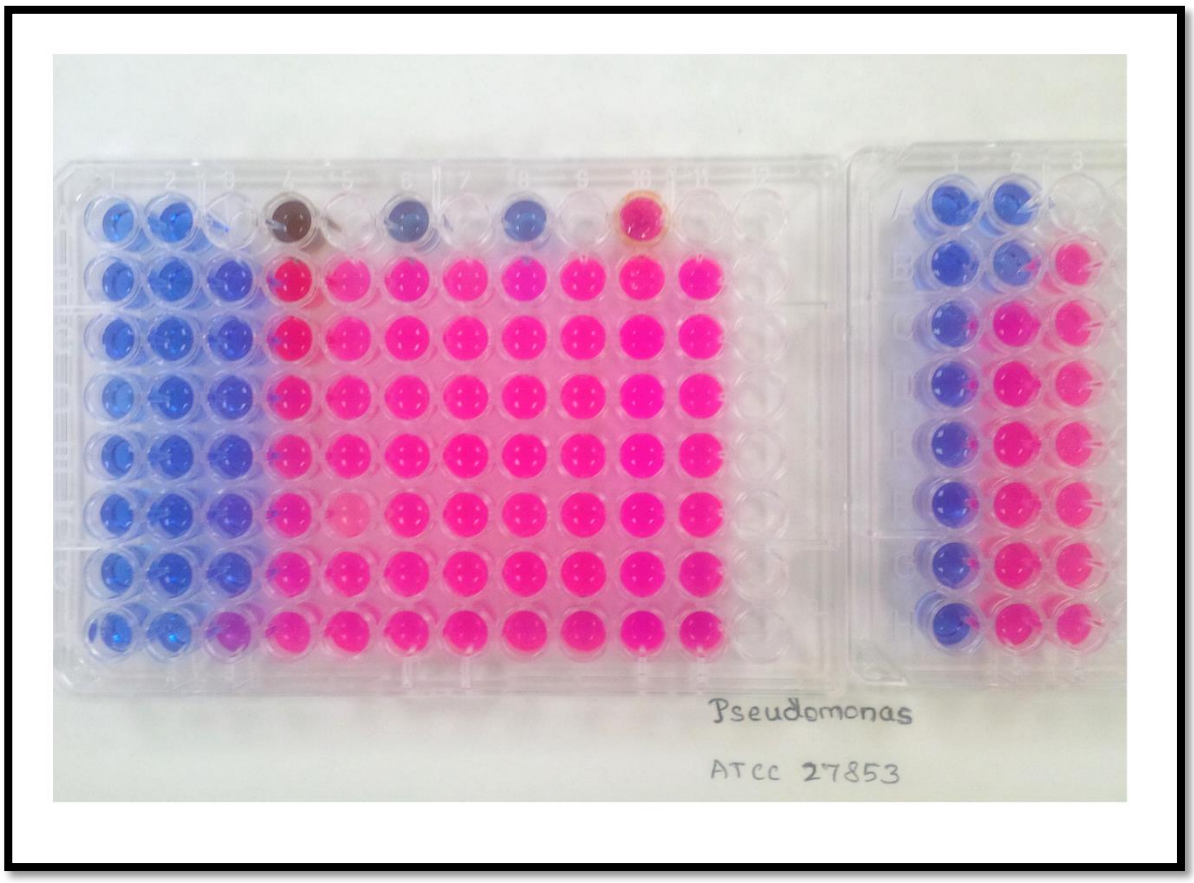

Figure 4. Typical microtitre plate showing the MIC's for tested compounds against Gram-negative bacteria Pseudomonas aeruginosa.

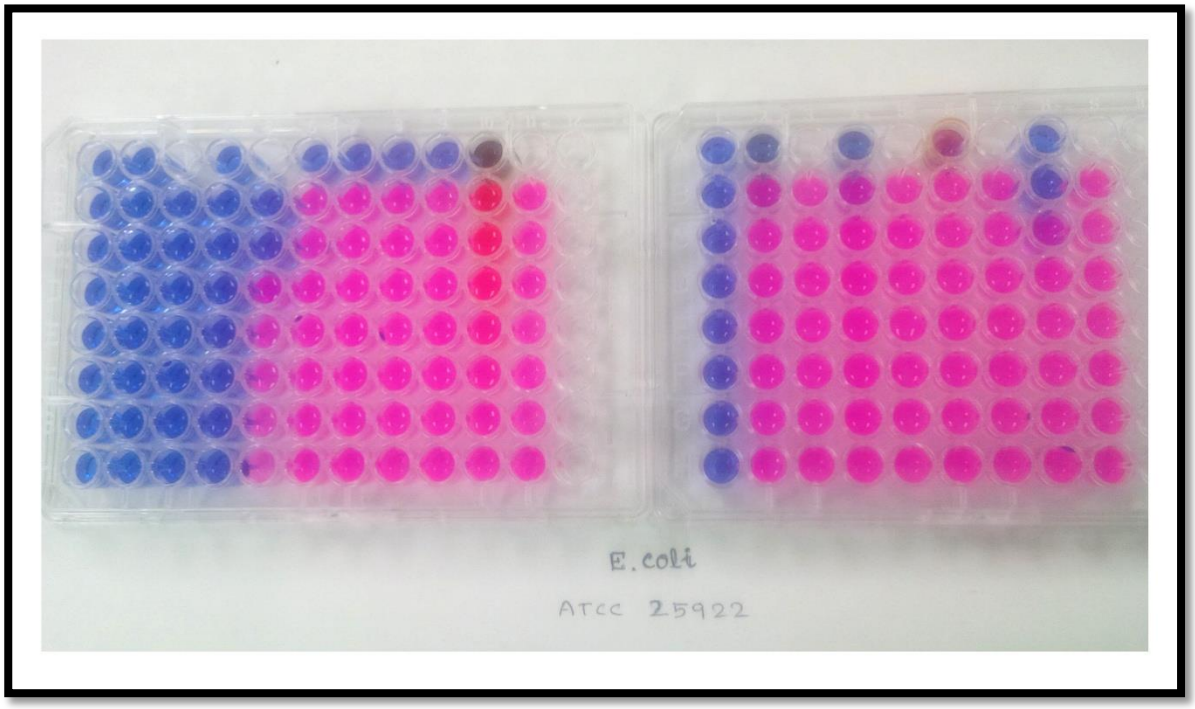

Figure 5. Typical microtitre plate showing the MIC's for tested compounds against Gram-negative bacteria Escherichia coli.

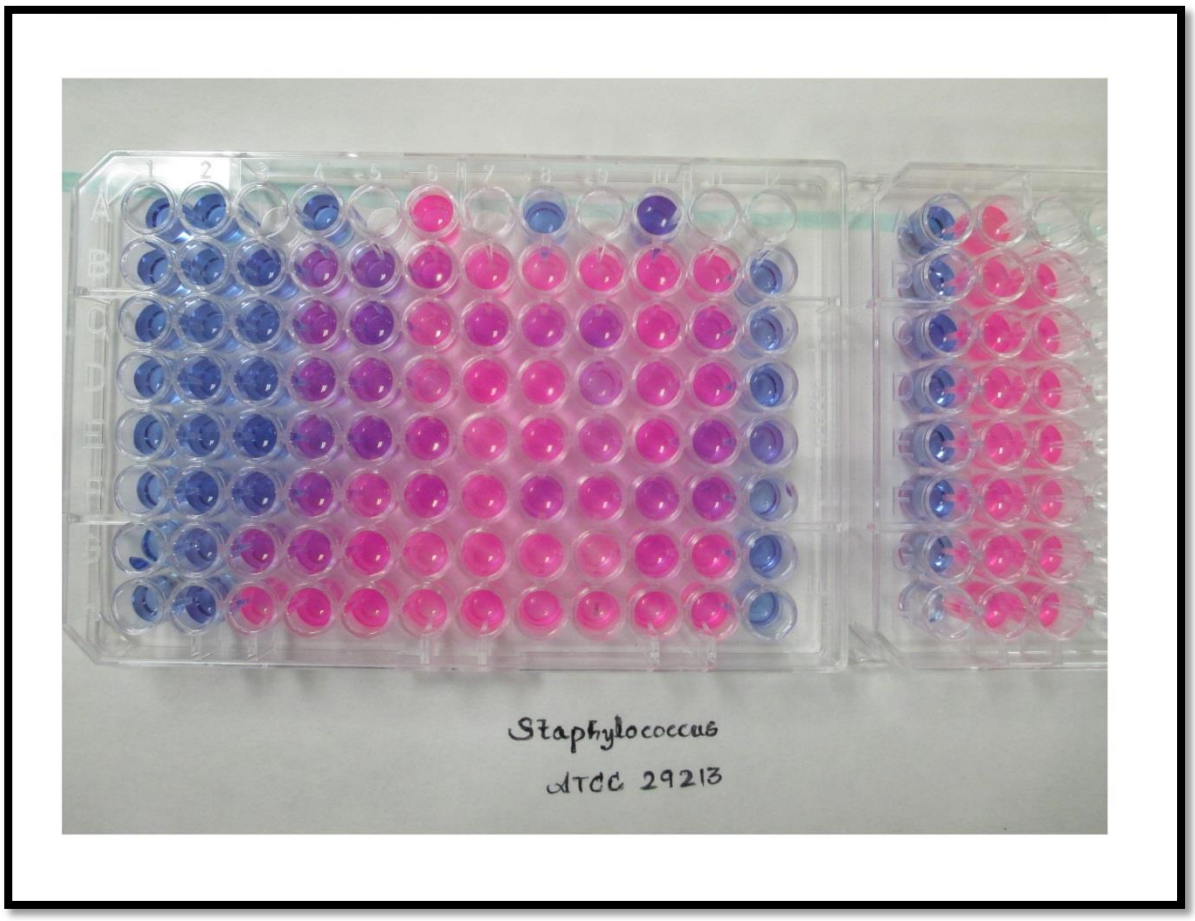

Figure 6. Typical microtitre plate showing the MIC's for tested compounds against Gram-positive bacteria Staphylococcus aureus.

Docking of the human mdm2 protein with our synthesized compounds provided insights into the binding regions. The theoretical conformations of **6, 7, 8, 11, 13, 18, 21, 23, 25, 28** and **30** in the binding cleft furnished valuable details of the interaction with active site of the human mdm2 protein. Only 2-amino-7,7-dimethyl-5-oxo-4-(4-(trifluoro methyl)phenyl)-5,6,7,8-tetrahydro-4H-chromene-3 carbonitrile **23** constituted with least glide score of -7.7509244 Kcal/mol and glide energy -34.14 Kcal/mol **Table 2.** Three hydrogen bonds were formed between the Thr 26, Glu 25 and Tyr 104 atoms. The distances between in the three bonded atoms are 2.18 Å, 1.88 Å, 2.48 Å.

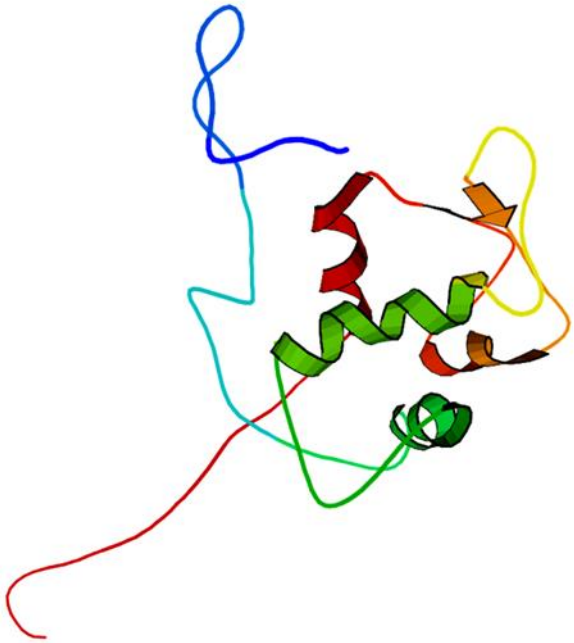

Figure 7. Mdm2 p53 binding protein.

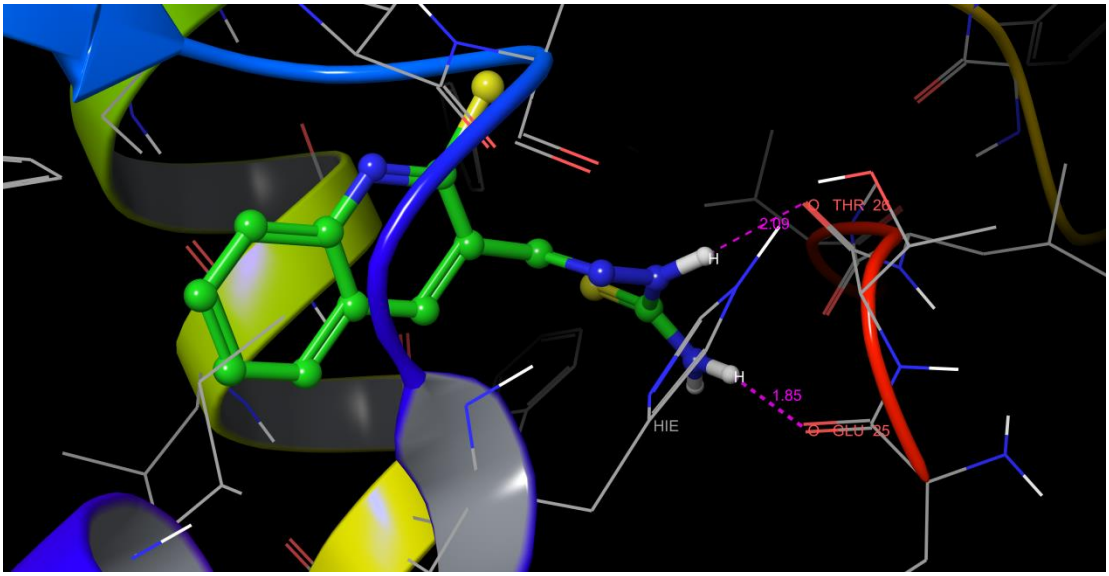

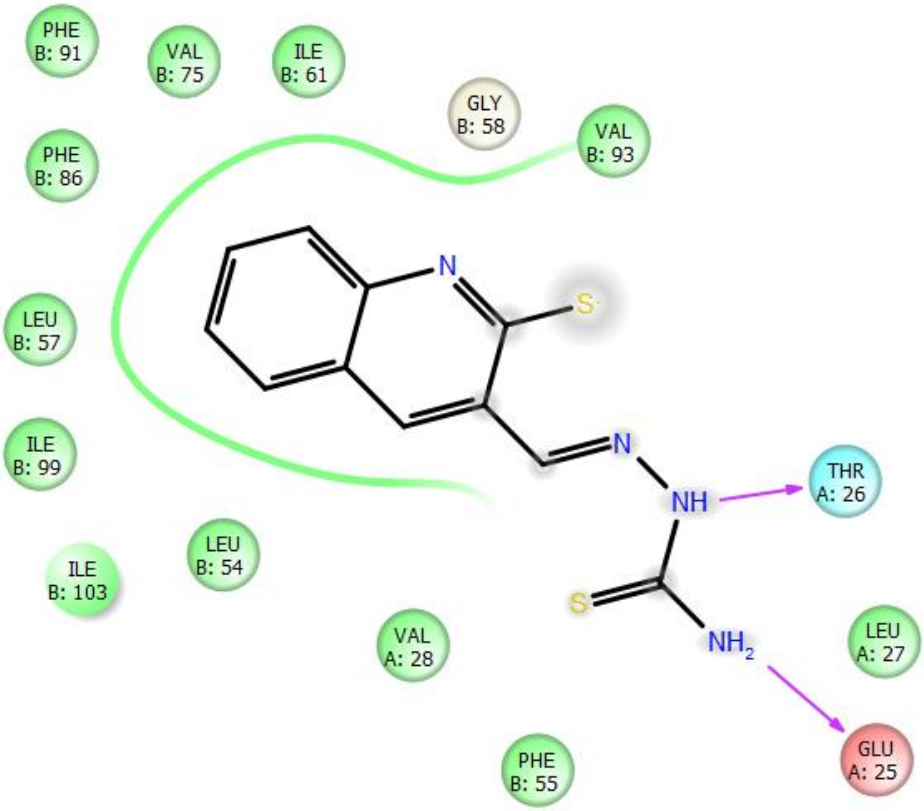

Figure 8. Binding modes and docking of the MDM2 protein with **11.** This shows three hydrogen bonds were formed between the Thr 26, Glu 25, Tyr 104 atoms.

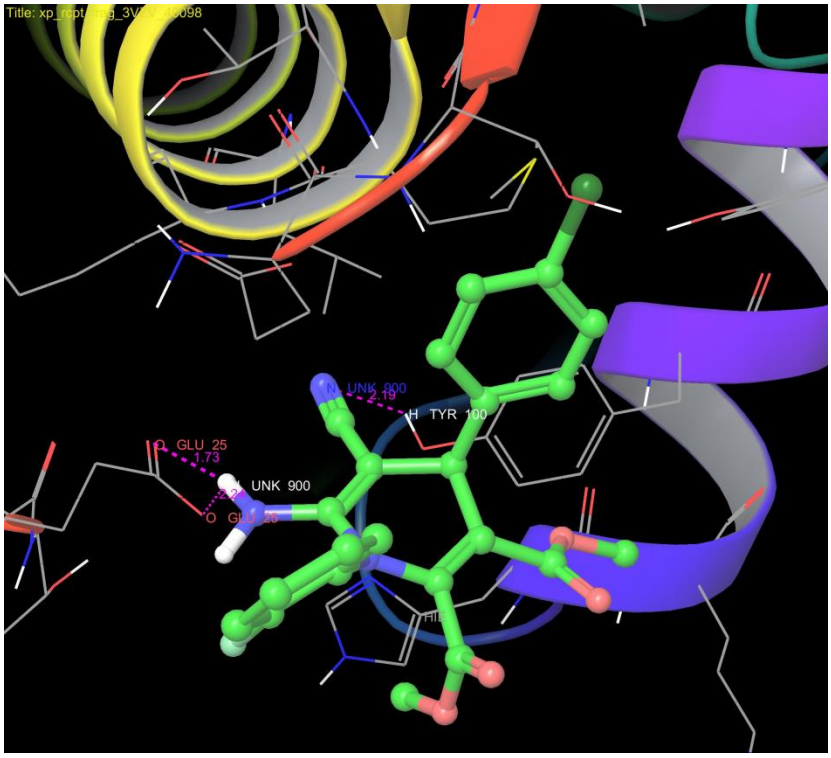

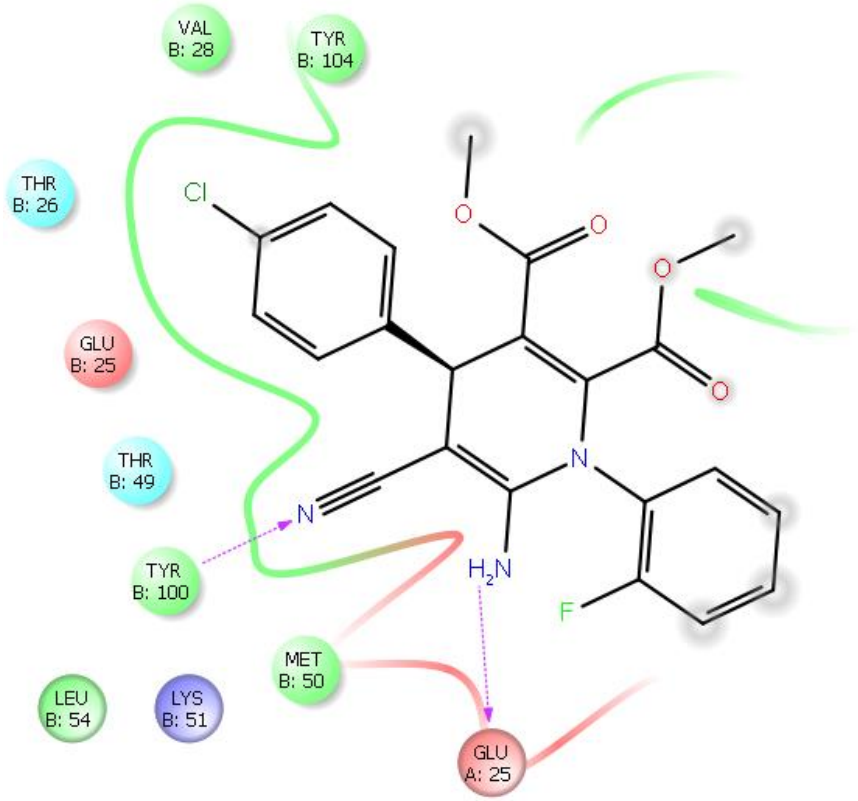

Figure 9. Binding modes and docking of the MDM2 protein with **21**. This shows three hydrogen bonds were formed between the Thr 26, Glu 25, Tyr 104 atoms.

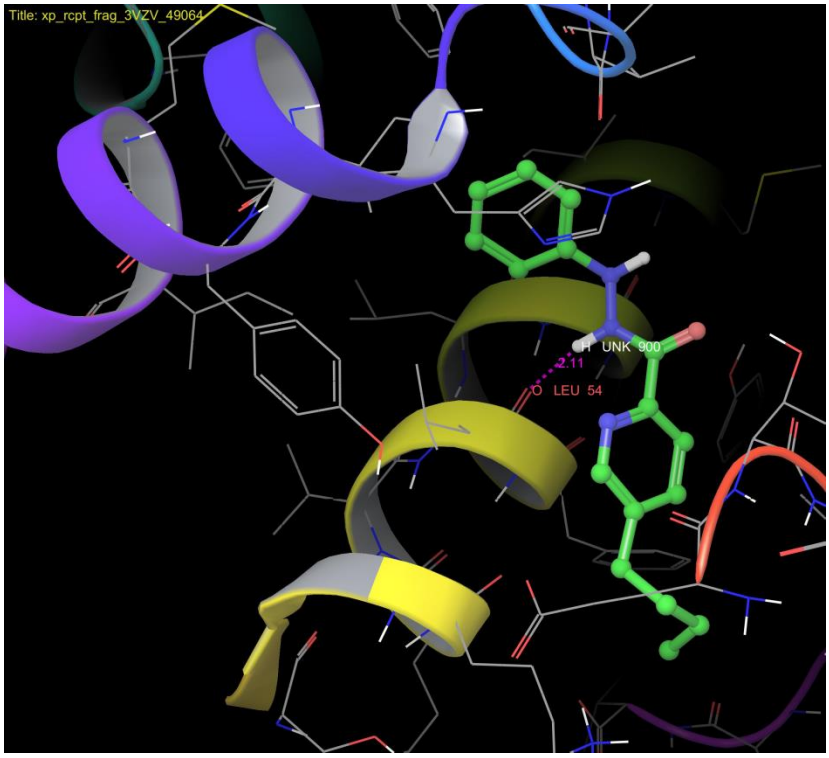

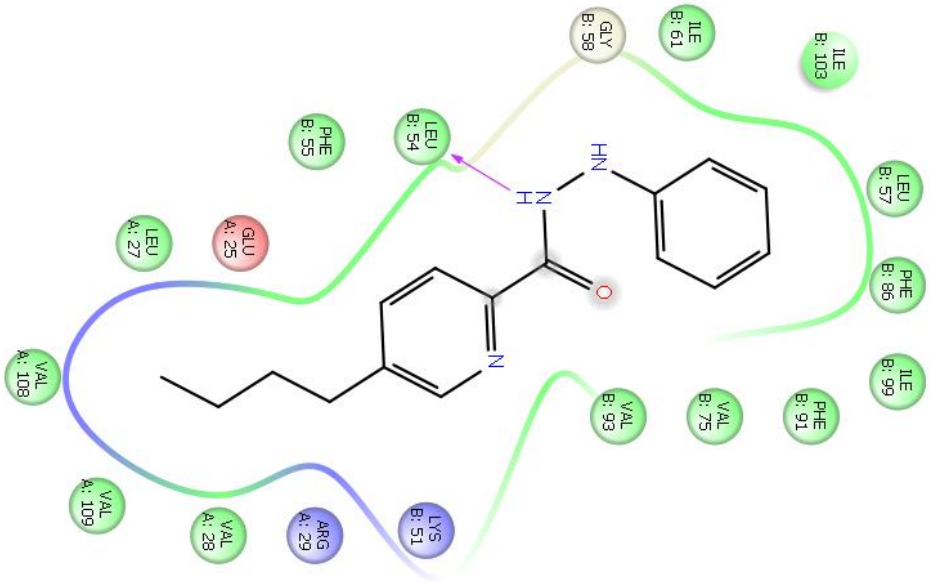

Figure 10. Binding modes and Docking of the MDM2 protein with **28**. This shows three hydrogen bonds were formed between the Thr 26, Glu 25, Tyr 104 atoms.

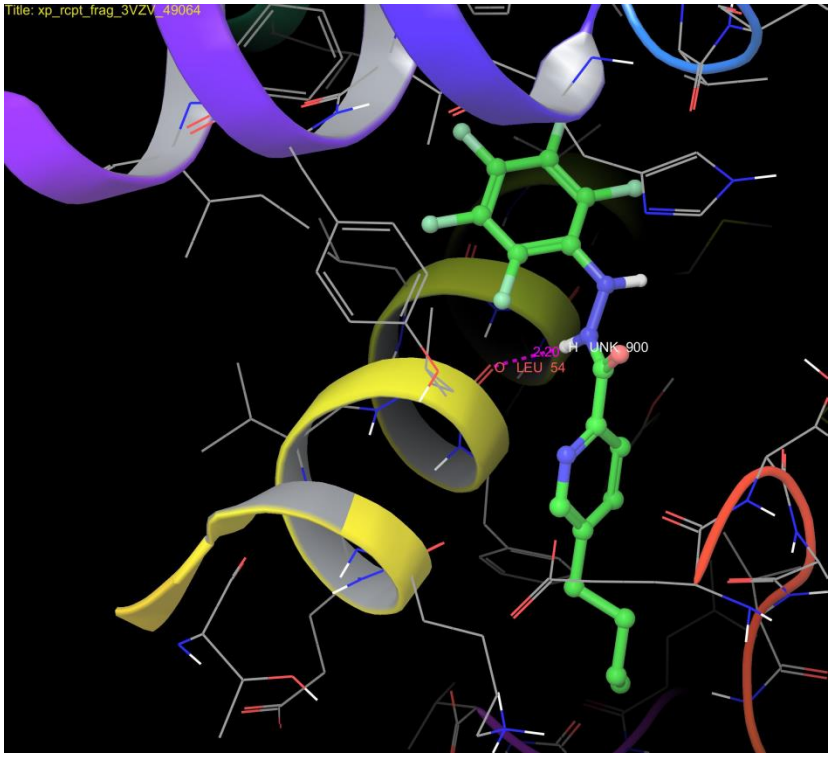

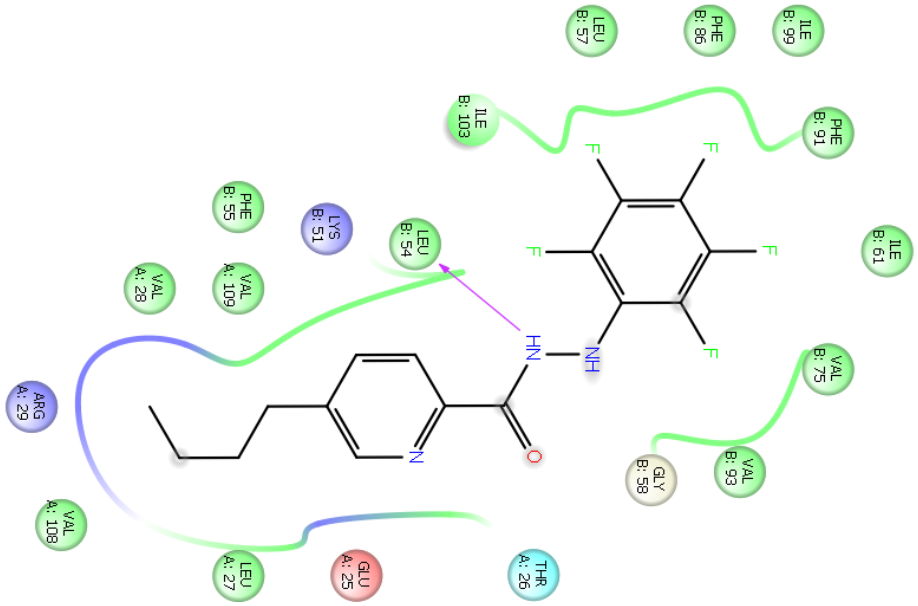

Figure 11. Binding modes and Docking of the MDM2 protein with **30**. This shows three hydrogen bonds were formed between the Thr 26, Glu 25, Tyr 104 atoms.

Table 2. Glide extra-precision (XP) results for 11 compounds with human mdm2 (PDB ID: 3VZV), by use of Schrodinger 9.5.

Code	Glide Score	Glide Energy	No. of H bonds	Interacting Residues	Distance (Å)	Hydrogen bond donor	Hydrogen bond acceptor
23	-7.750919	-34.143351	-	-	-	-	-
11	-7.21025	-31.3582	2	Glu 25 Thr 26	1.85 2.09	Ligand: (H) H Ligand: (H) H	A: GLU 25: (O) O A: THR 26: (O) O
13	-6.84675	-34.945	2	Glu 25	1.84 2.3	Ligand: (H) Ligand: (H)	A: THR 26: (O) O A: THR 26: (O) O
25	-6.651432	-30.923184	-	-	-		-
28	-6.197	-54.176	1	LEU 54	2.11	Ligand: (H)	B: LUE 54: (O) O
30	-5.871	-53.822	1	LEU 54	2.2	Ligand: (H)	B: LUE 54: (O) O
18	-4.324394	-48.218878	-	-	-		-
8	-4.146666	-38.5525	-	-	-		-
7	-3.95436	-30.0365	1	Thr 26	1.98	A: THR 26: (H) HG1	Ligand: (O)
6	-0.95745	-22.2567	1	Arg 29	2.14	Ligand: (N)	A: ARG 29: (H) HH21
21	-0.654346	-25.396569	3	Tyr 100 Glu 25(2)	2.19 1.73 2.24	B: TYR 100: (H) HH Ligand: (H) Ligand: (H)	Ligand: (N) Ligand: (N) A: GLU 25: (O) OE2

This table shows the name of the compounds, Glide score (Kcal/mol), Glide energy (Kcal/mol), Interacting residues, Distance between the protein and ligand (Å), Hydrogen bond donor, Hydrogen bond acceptor. 3k only shows least glide score and energy.

In conclusion, a total of fifteen compounds were synthesized, eleven of which were novel. These compounds were fully characterised by spectroscopic techniques, i.e. IR, ^{1}H-NMR and ^{13}C-NMR, ^{19}F-NMR, MS and Single crystal XRD were used for selected compounds. The anti-bacterial evaluation of selected quinoline derivatives showed a minimum inhibitory concentration 256 µg/ml against *Escherichia coli* and *Pseudomonas aeruginosa* except for **13** compound which showed activity at 128 µg/ml MIC. The docking score of the synthesized compounds could not be correlated with the *in-vitro* anti-cancer activity and conclusion could not be drawn on their exact mechanism of action. So further molecular modification is required in order to arrive at a more accurate structure activity relationship with their anti-cancer activity on breast cancer cell lines or different crystal structure of tyrosine kinase domain could be selected from PDB to study their mechanism of action.

Reference

(1) Hino, K.; Kawashima, K.; Oka, M.; Nagai, Y.; Uno, H.; Matsumoto. *J. Chem Pharm Bull.* **1989** , 37, 110.

(2) (a) Wang, J.; Shen, Y.; Hu, W.; Hsieh, M.; Lin, F.; Hsu, M. K.; Hsu, M. H. *J. Med. Chem*. **2006**, 49, 1442. (b) DeCorte, B. L. *J. Med. Chem*. **2005**, 48, 1689.

(3) Roma, G.; Braccia, M. D.; Grossi, G.; Mattioli, F.; Ghia, H. *Eur. J. Med. Chem.* **2000**, 35, 1021.

(4) Benkovic, S. J.; Baker, S. J.; Alley, M. R. K.; Youn, Hi. W,; Yong, K. Z.; Tsutomu, A.; Weimin, M.; Justin, B.; Ravi, R. P. T.; Mark, W.; Lyn, S. K.; Ali, T.; Lucy, S. *J. Med. Chem.* **2005**, 48, 7468.

(5) Bailly, C. *Biochemistry*. **1999**, 38, 7719.

(6) Ligprep., Eds.; Schrodinger, LLC: New York, **2009**, 2, 3.

(7) Glide., Eds.; Schrodinger, LLC: New York, **2009**, 5, 5.

(8) Alanis, A. J. *Arch. Medi. Research*. **2005**, 36, 697.

(9) Sarkozy, G. *Vet. Med. Zchech*. **2001**, 46, 257.

(10) Schwalbe, *R.*, Eds.; CRC: New York, **2007**, 75.

(11) Fothergill, A. W.; Rinaldi, M. G. *J. Clin. Microbiol*. **1995**, 33, 2660.

(12) a) Otto, M.; Bramha, N.; Brain, T. *J. Chem. Soc. Perkin (I).* **1981**, 2509. b)Otto,M.; Bramha, N.; Brain, T. *J. Chem. Soc. Prekin (I).* **1981**, 1553.

(13) Srivastava.; A; Singh, R. M. *Indian J. Che*. **2005,** 44, 1875.

(14) Pitchai, P.; Mohan, P. S.; Gengan. R. M. *Indian J. Che*. **2009,** 48B ,692.

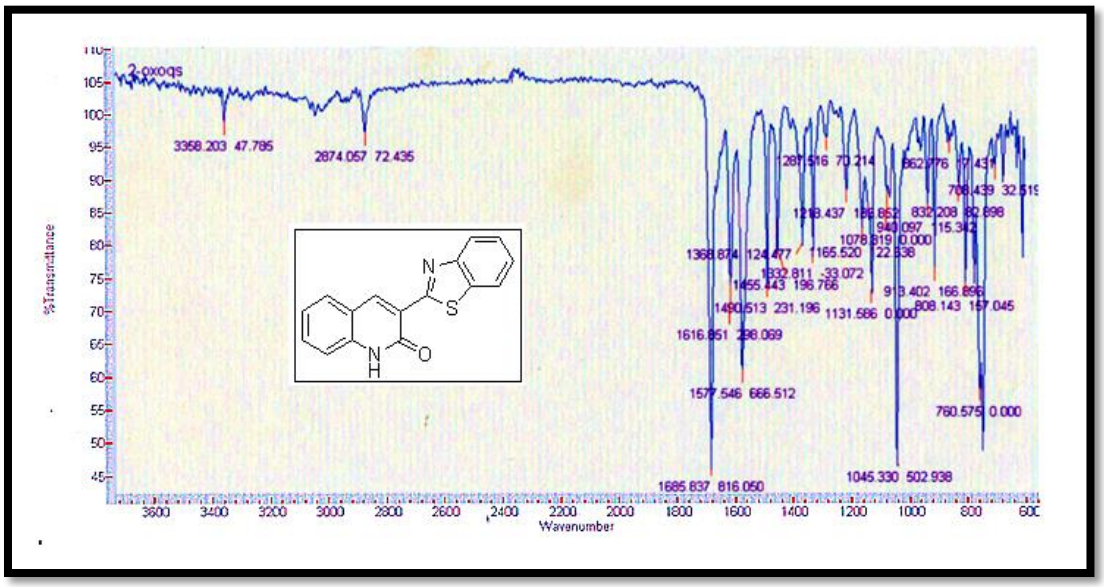

Figure. 2.1 IR Spectrum of **6**

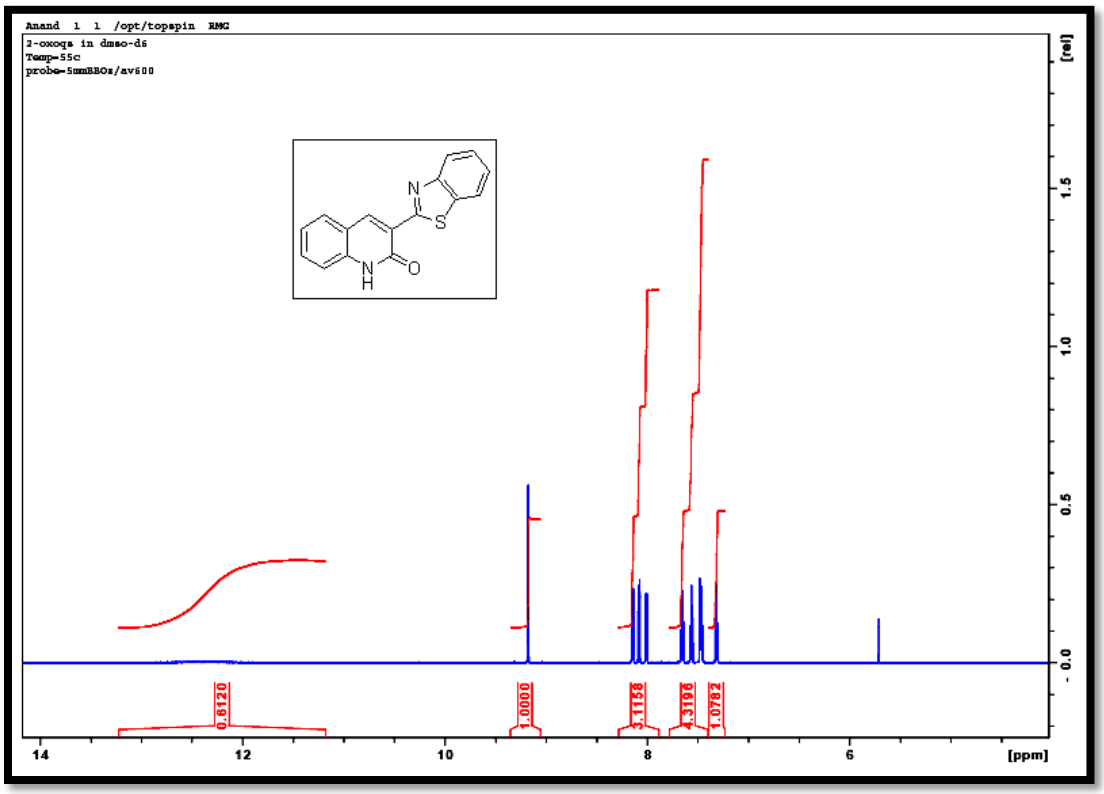

Figure. 2.2 ^{1}H-NMR spectrum of **6**

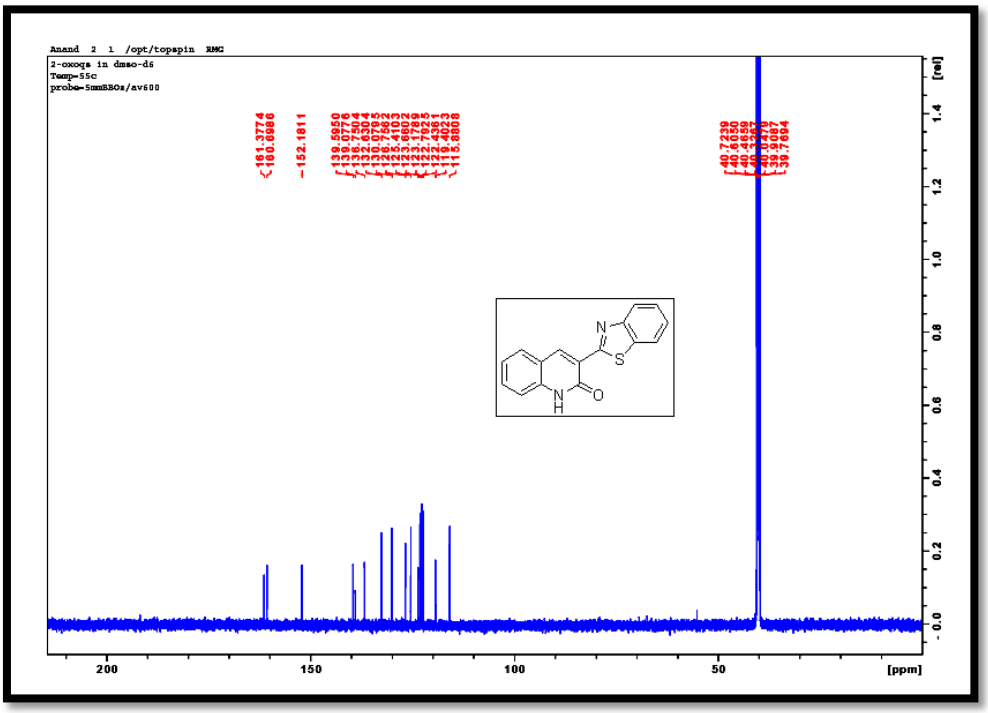

Figure.2.3 ^{13}C-NMR spectrum of **6**

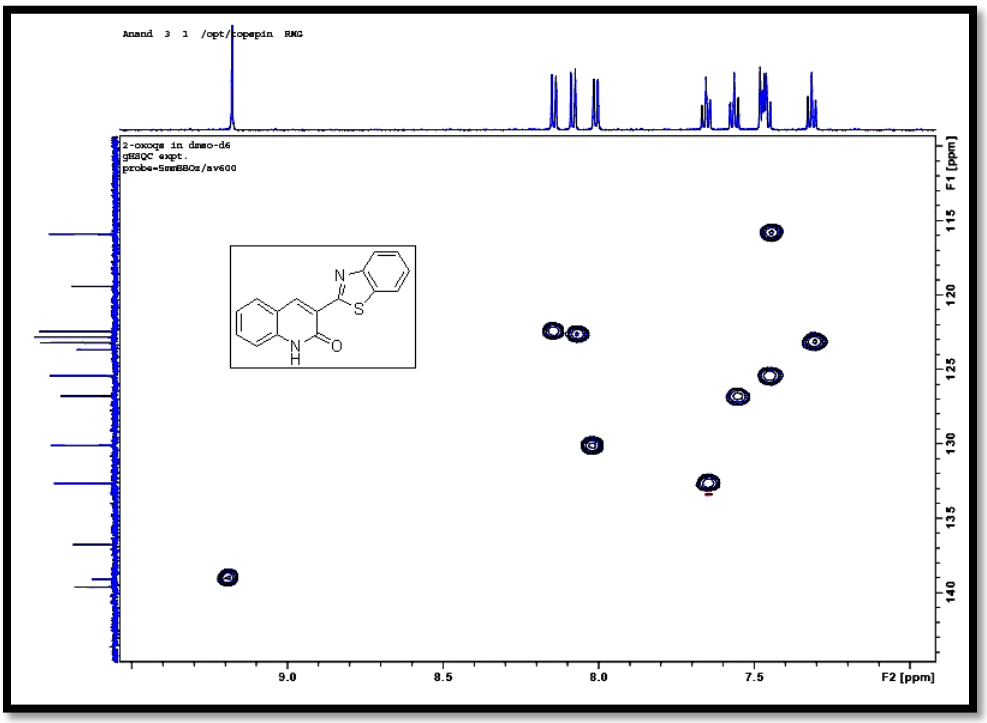

Figure. 2.4 HSQC Spectrum of **6**

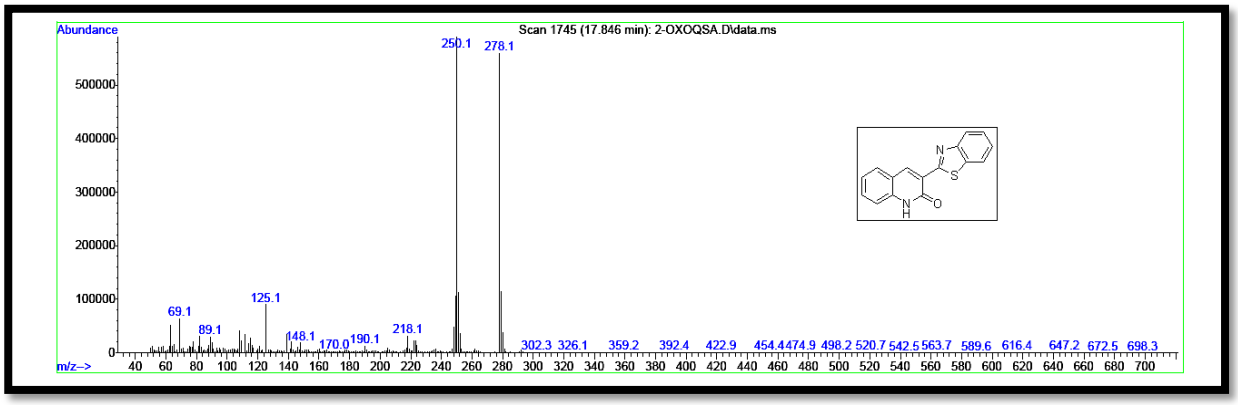

Figure. 2.5 Mass Spectrum of **6**

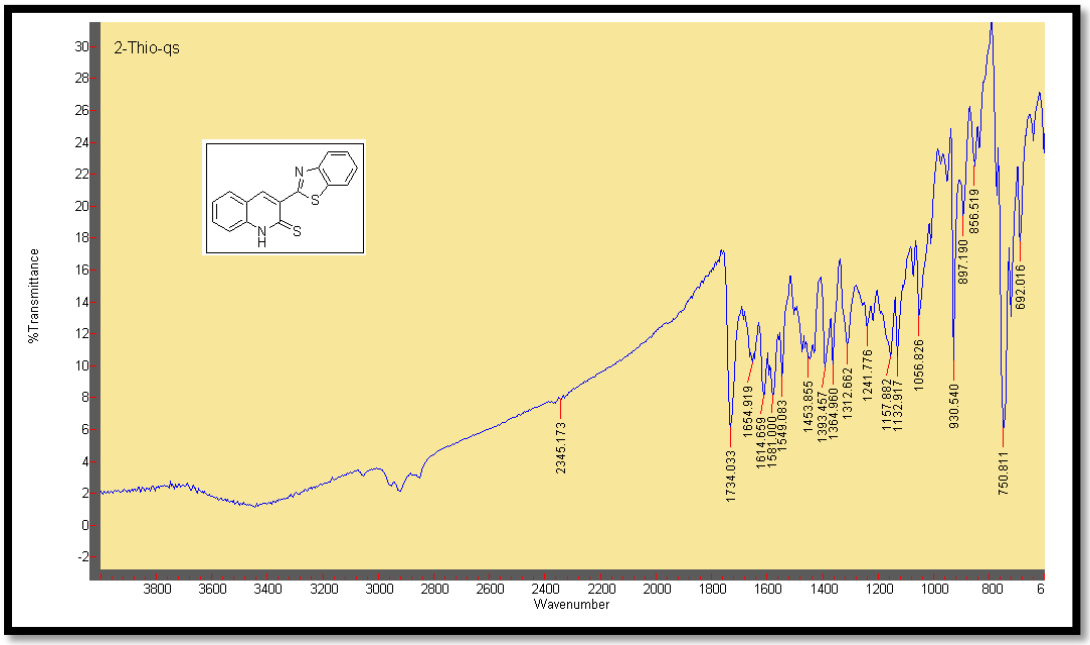

Figure. 2.6 IR Spectrum of **7**

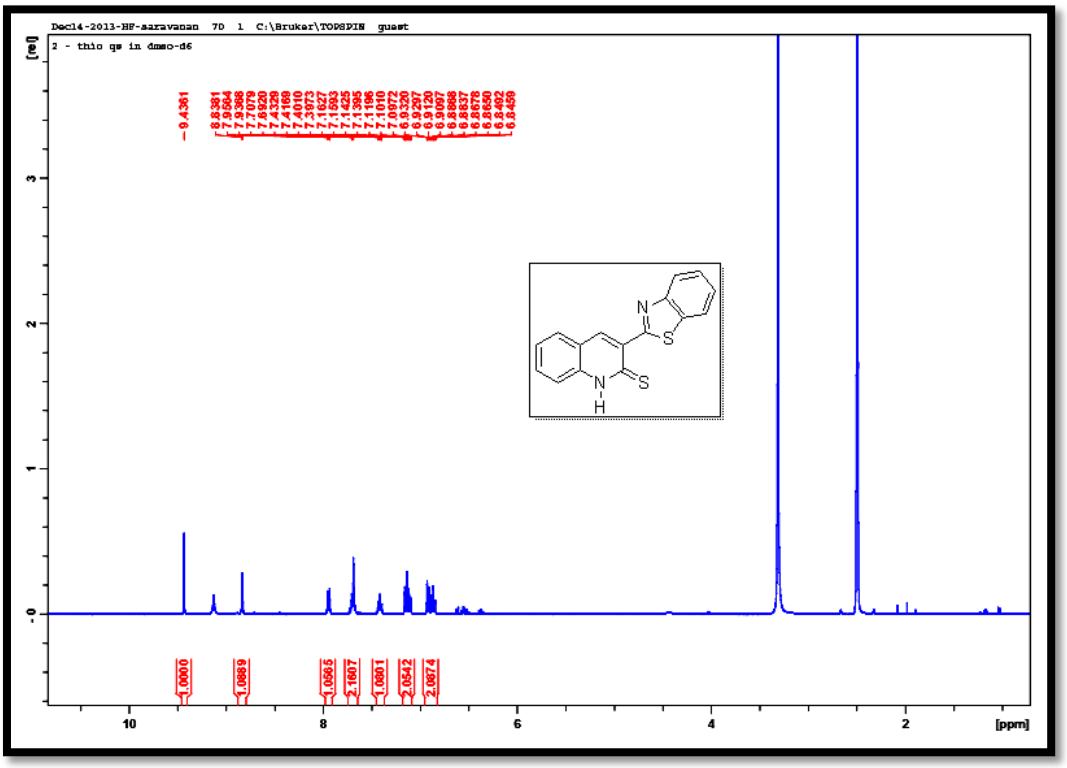

Figure. 2.7 ^{1}H-NMR spectrum of **7**

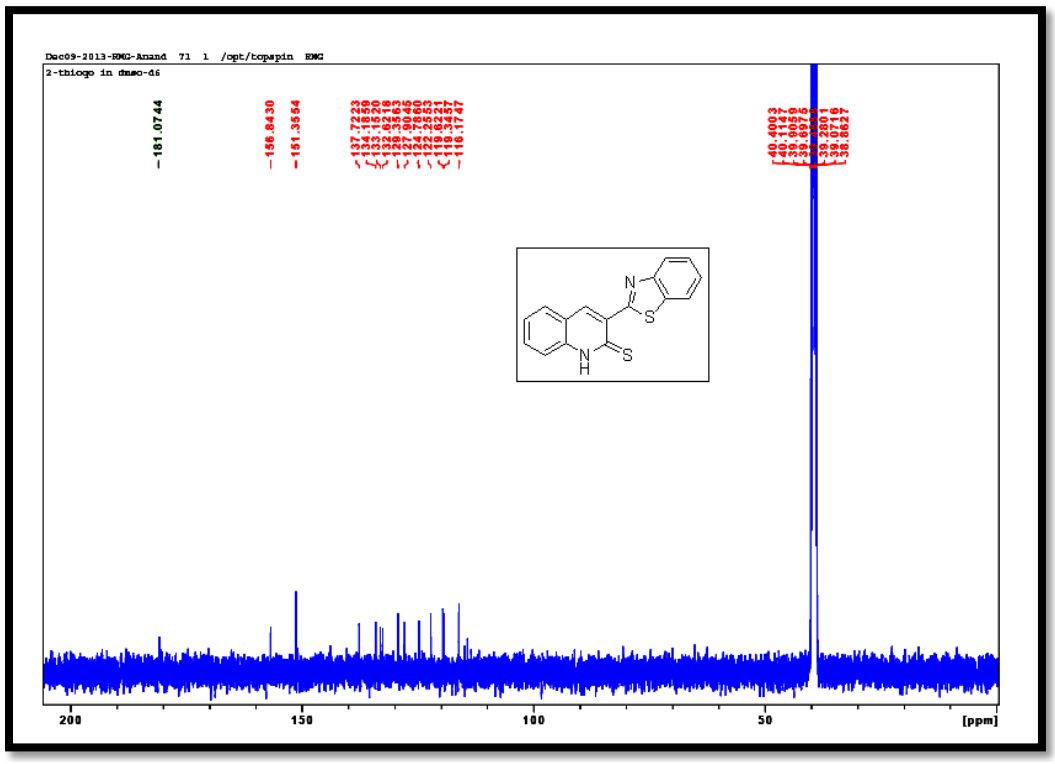

Figure. 2.8 ^{13}C-NMR spectrum of **7**

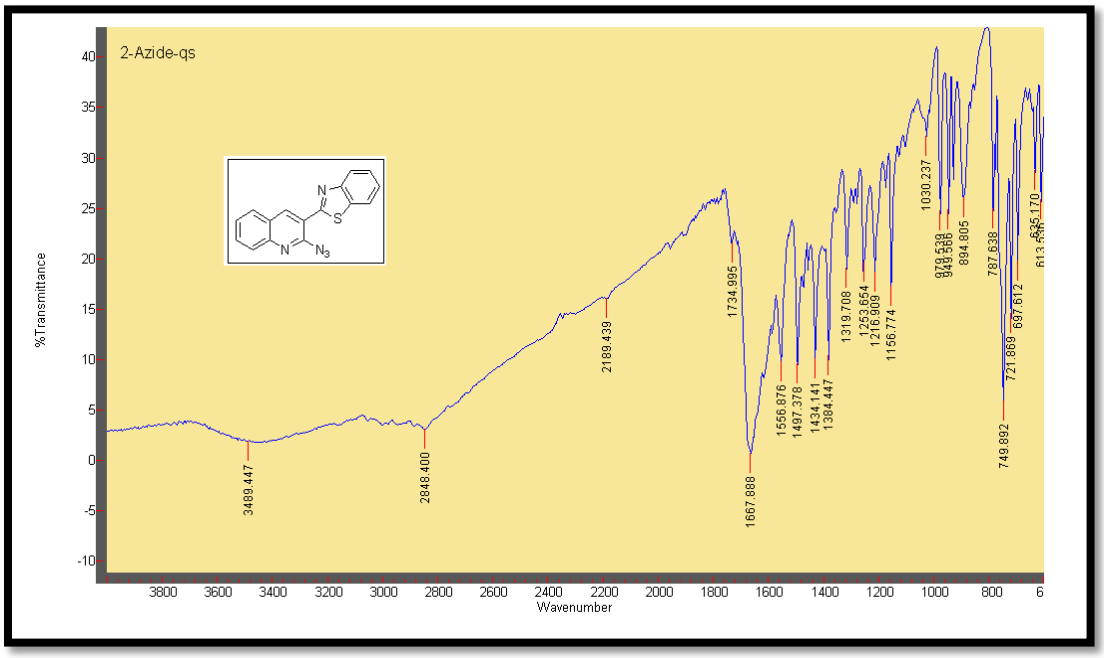

Figure. 2.9 IR Spectrum of **8**

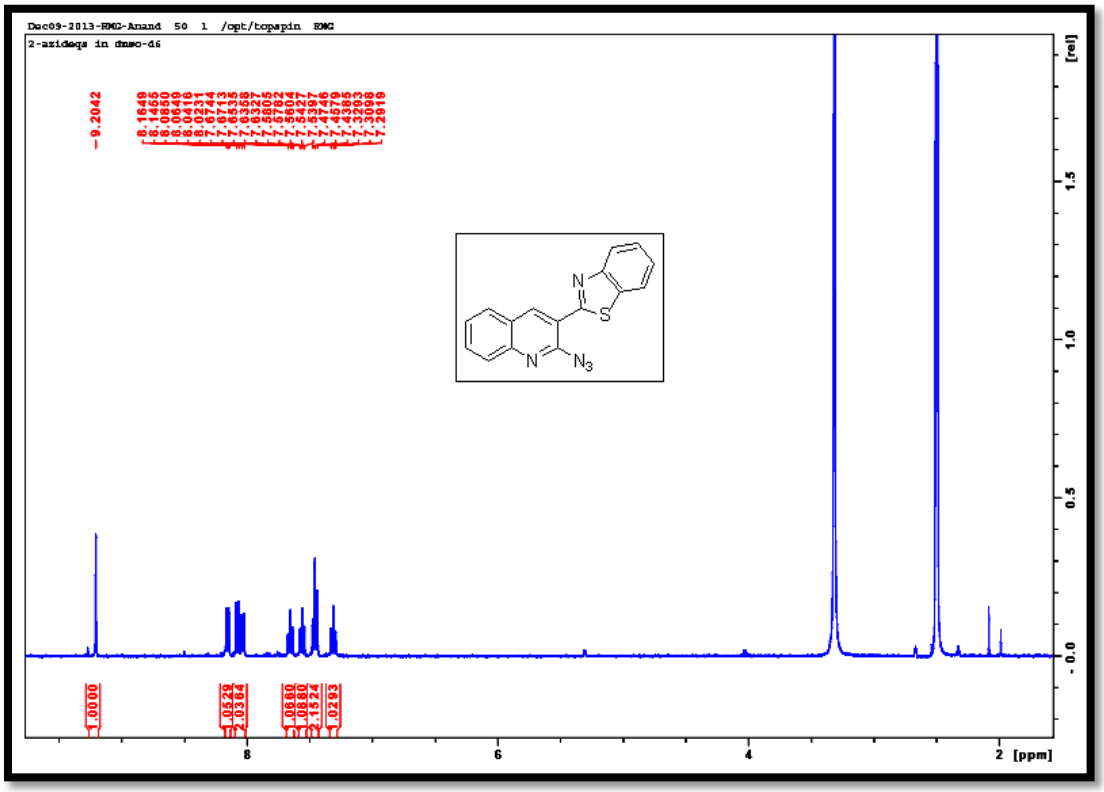

Figure. 2.10 ^{1}H-NMR spectrum of **8**

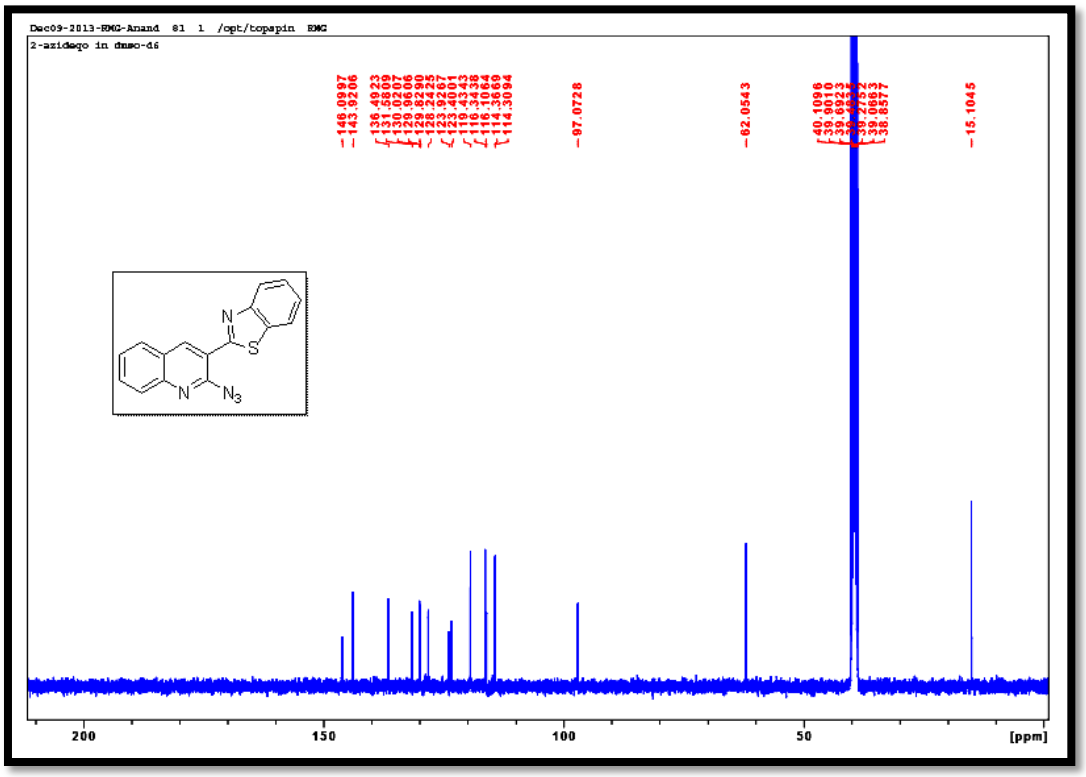

Figure. 2.11 ^{13}C-NMR spectrum of **8**

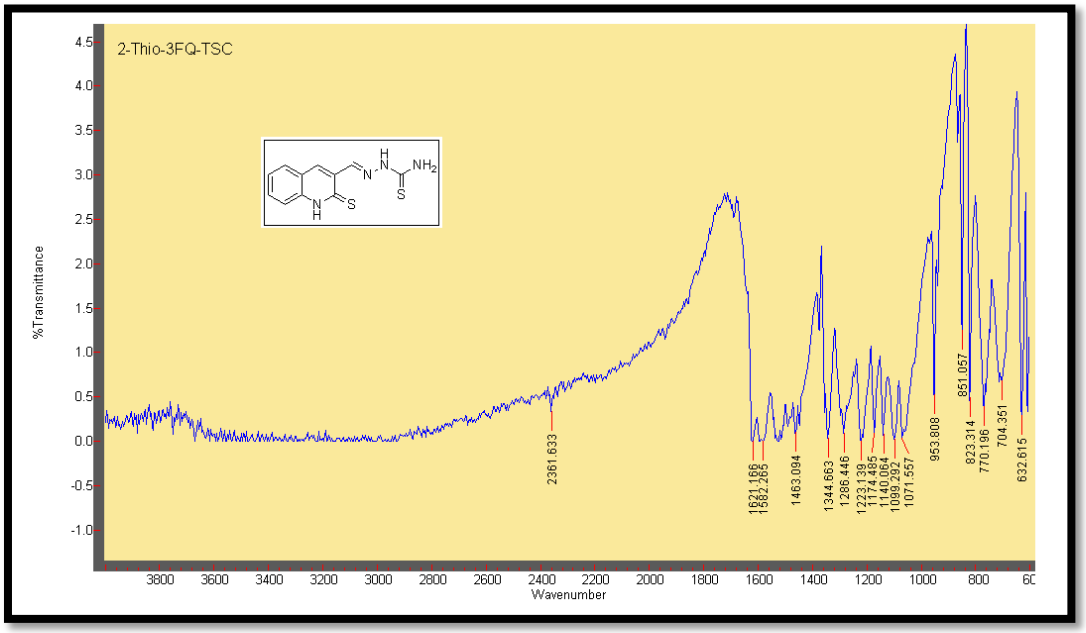

Figure. 2.12 IR Spectrum of **11**

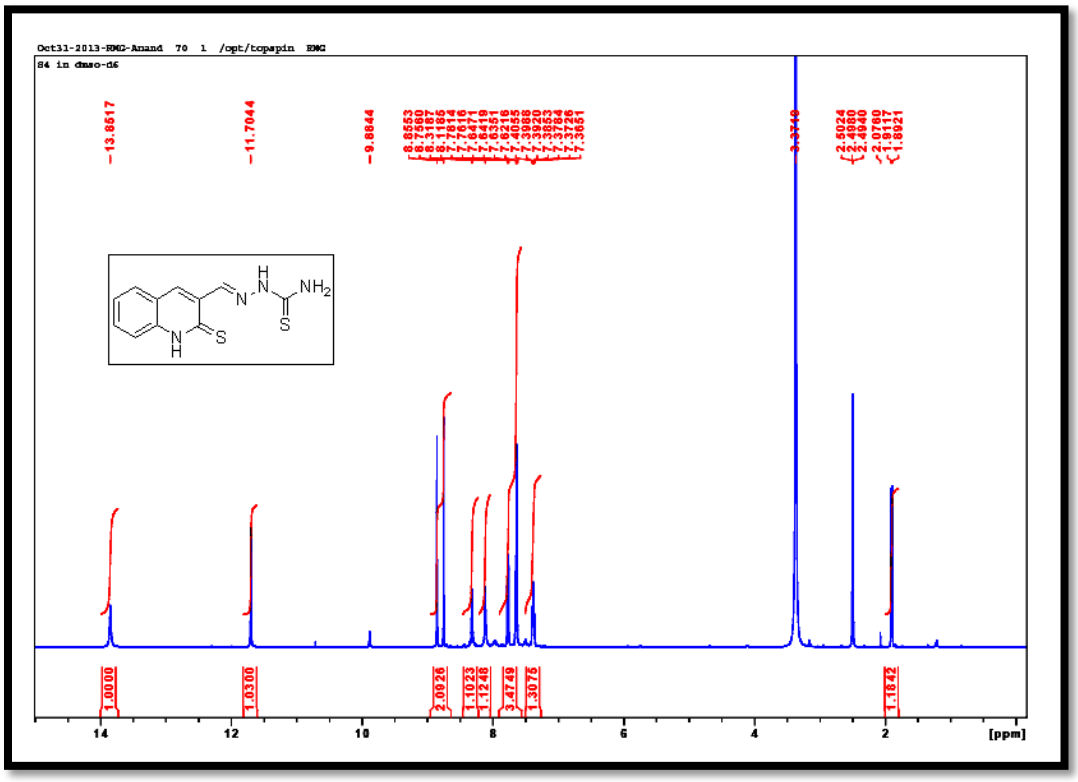

Figure. 2.13 ^{1}H-NMR spectrum of **11**

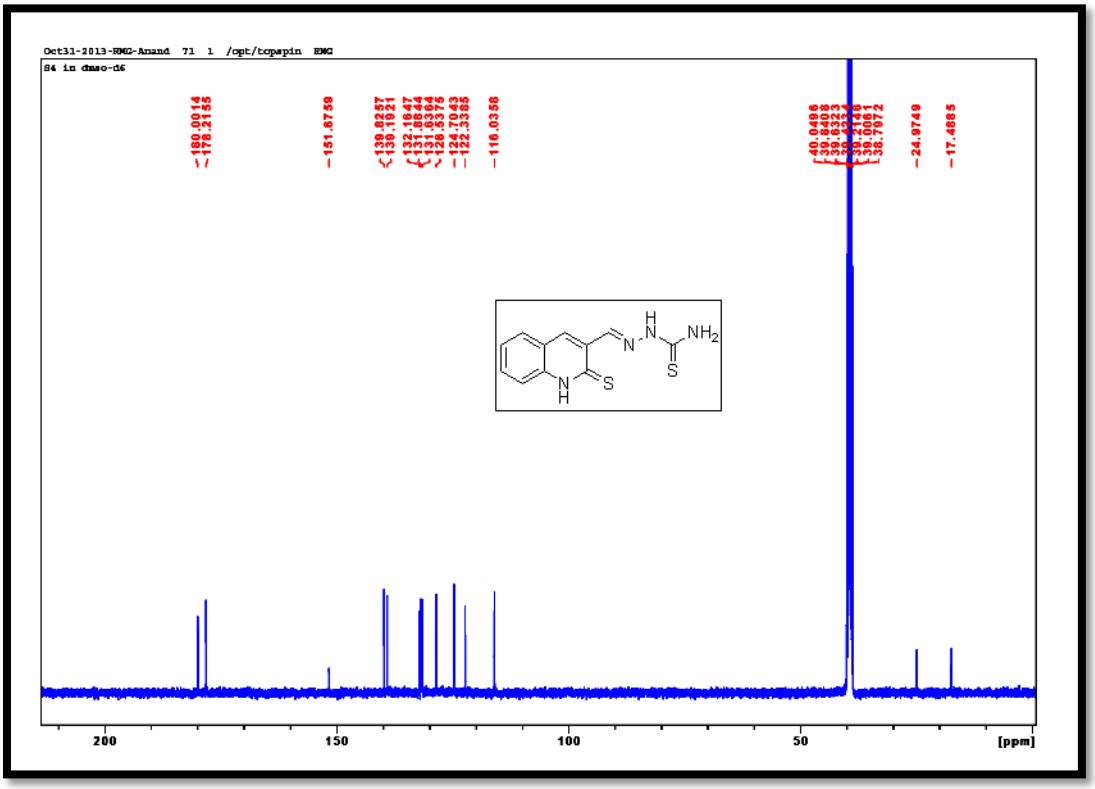

Figure. 2.14 ^{13}C-NMR spectrum of **11**

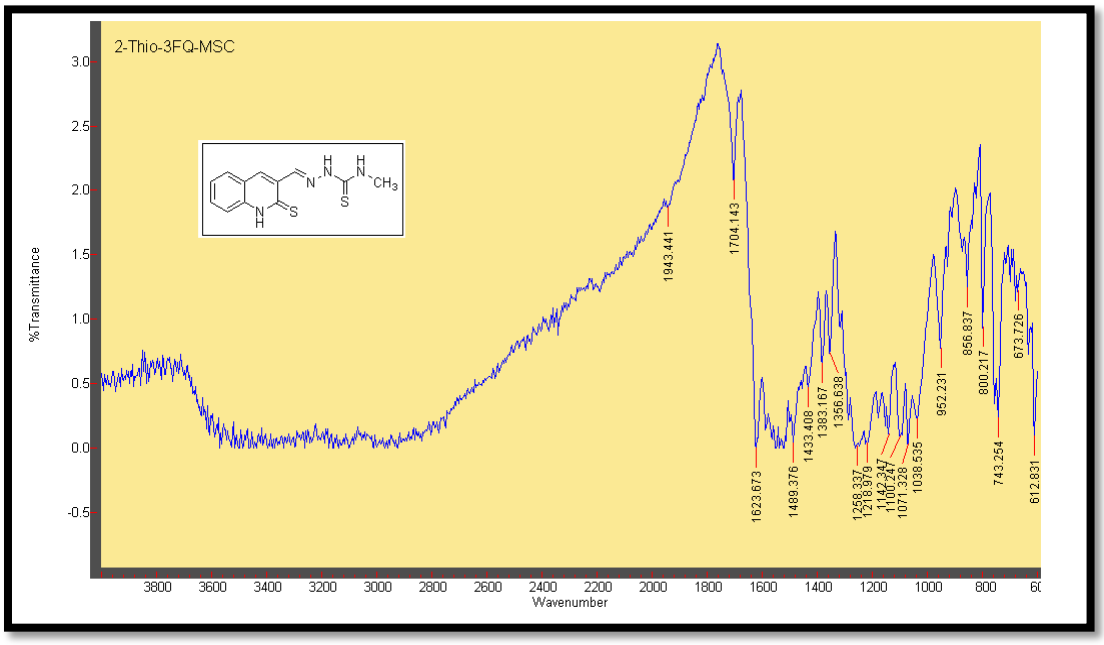

Figure. 2.15 IR Spectrum of **13**

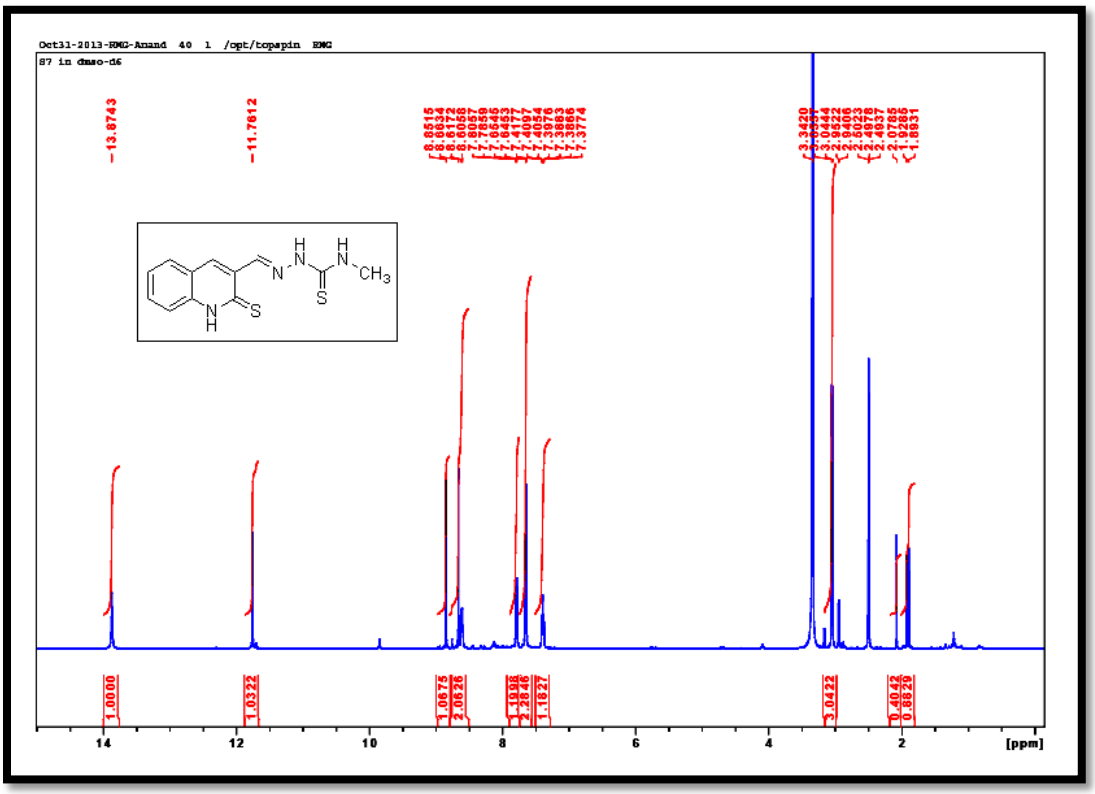

Figure. 2.16 ^{1}H-NMR spectrum of **13**

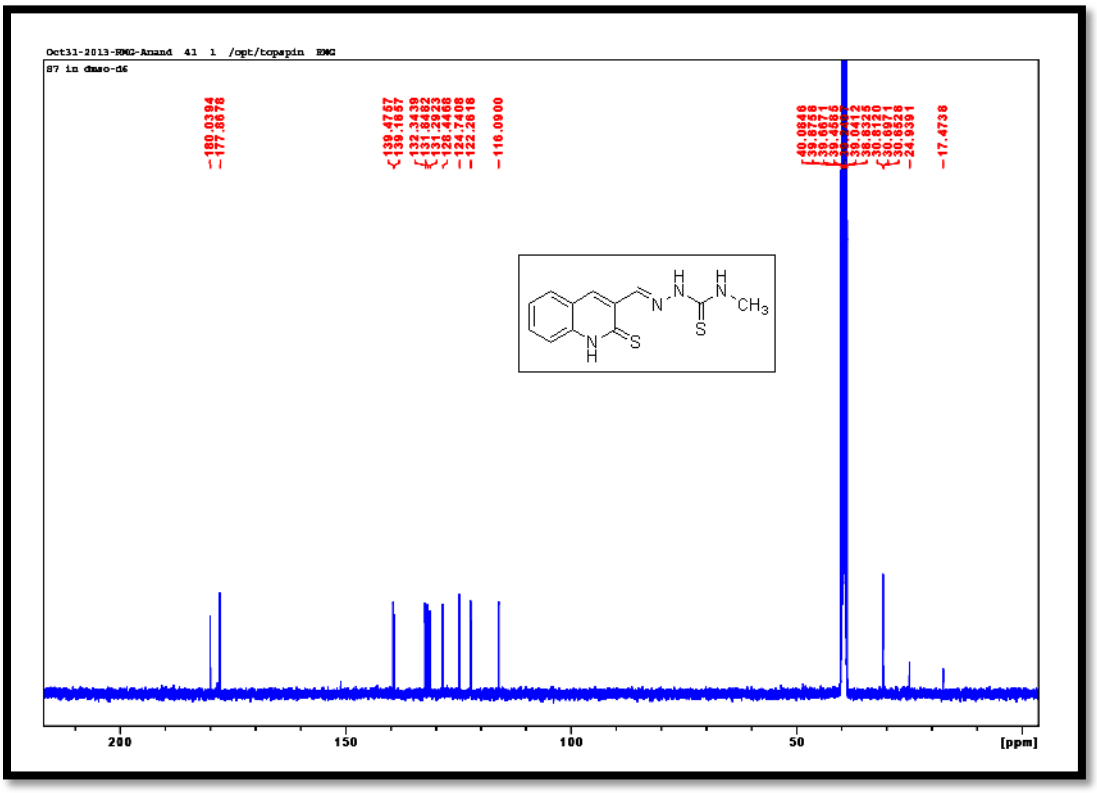

Figure. 2.17 ^{13}C-NMR spectrum of **13**

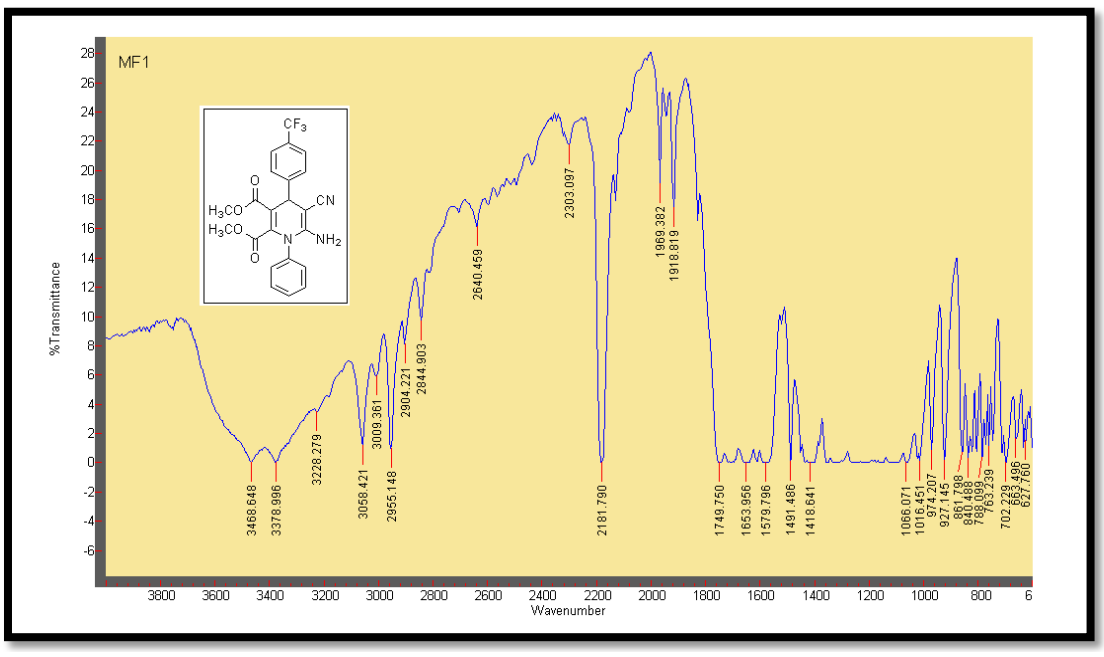

Figure. 2.18 IR Spectrum of **18**

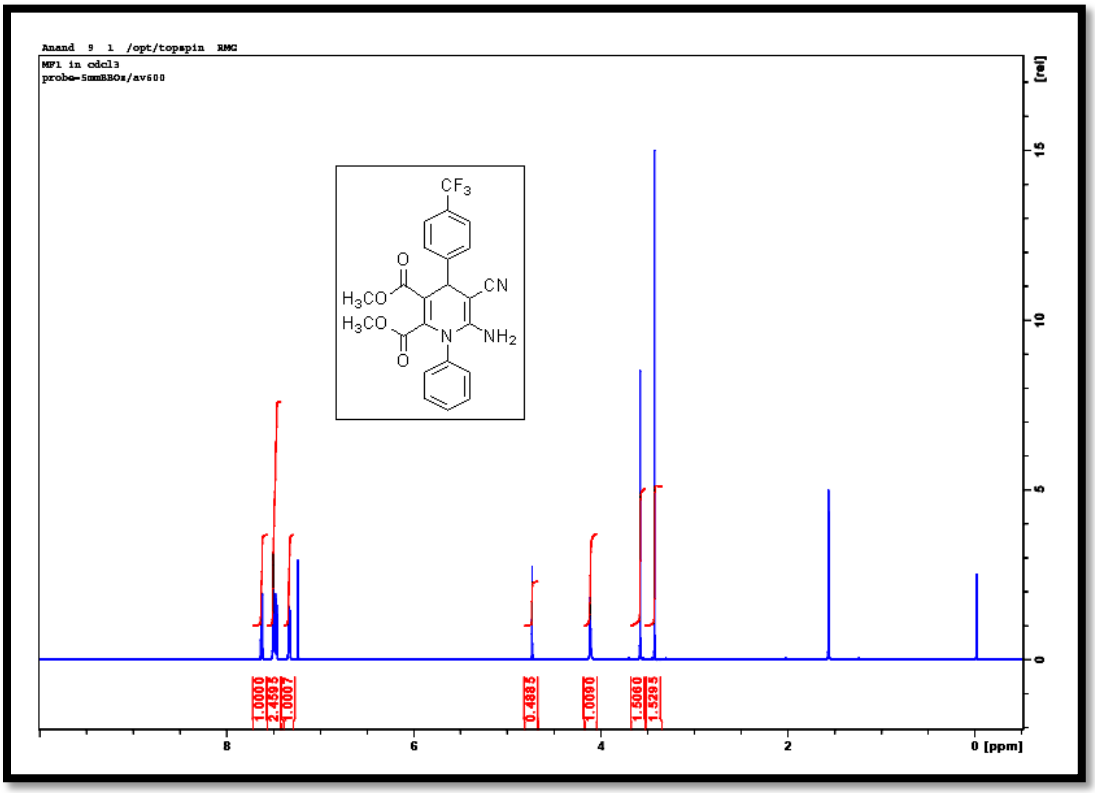

Figure. 2.19 ^{1}H-NMR spectrum of **18**

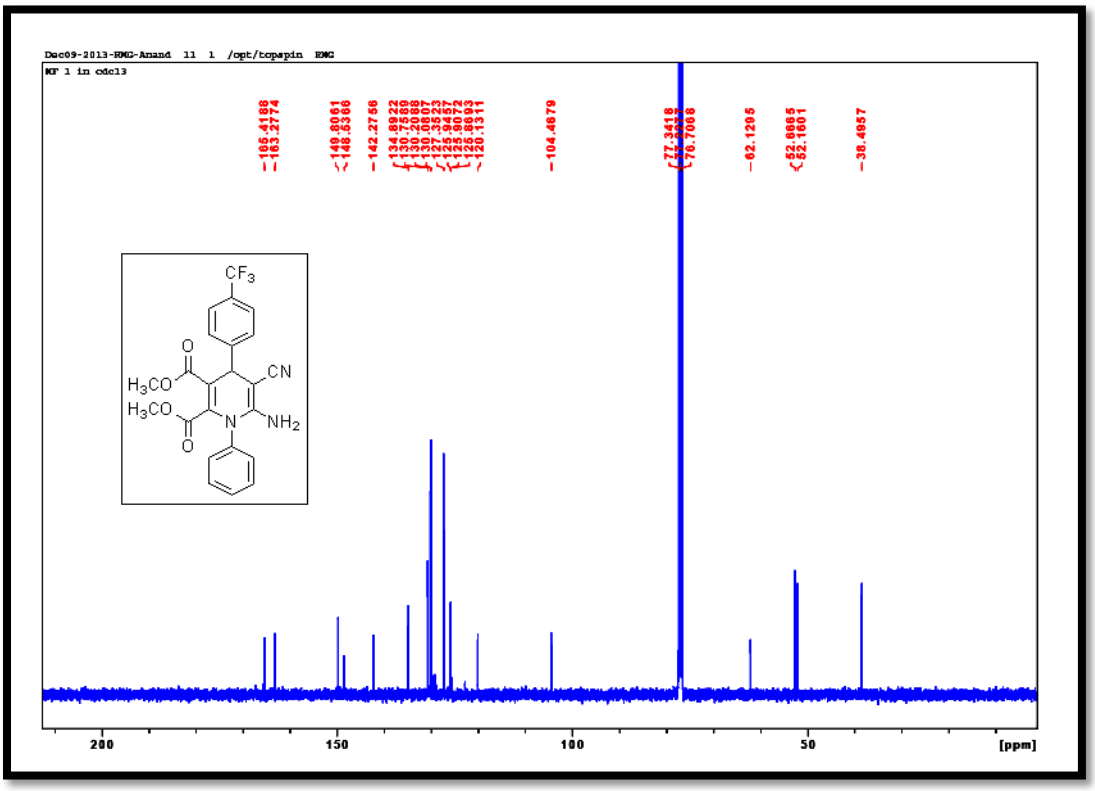

Figure. 2.20 ^{13}C-NMR Spectrum of **18**

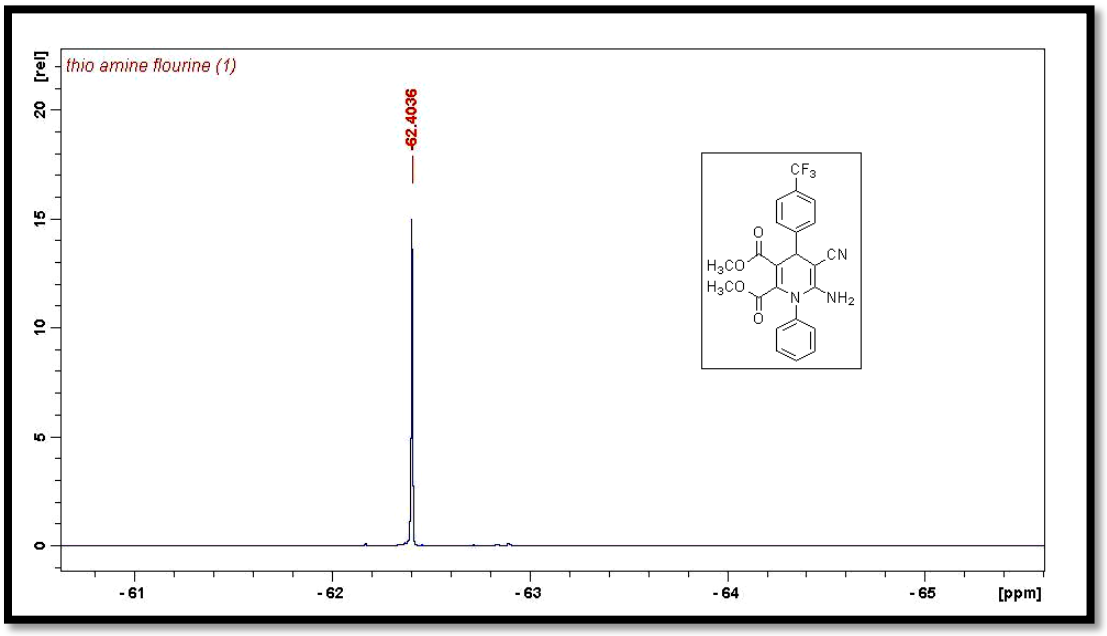

Figure. 2.21 ^{19}F-NMR spectrum of **18**

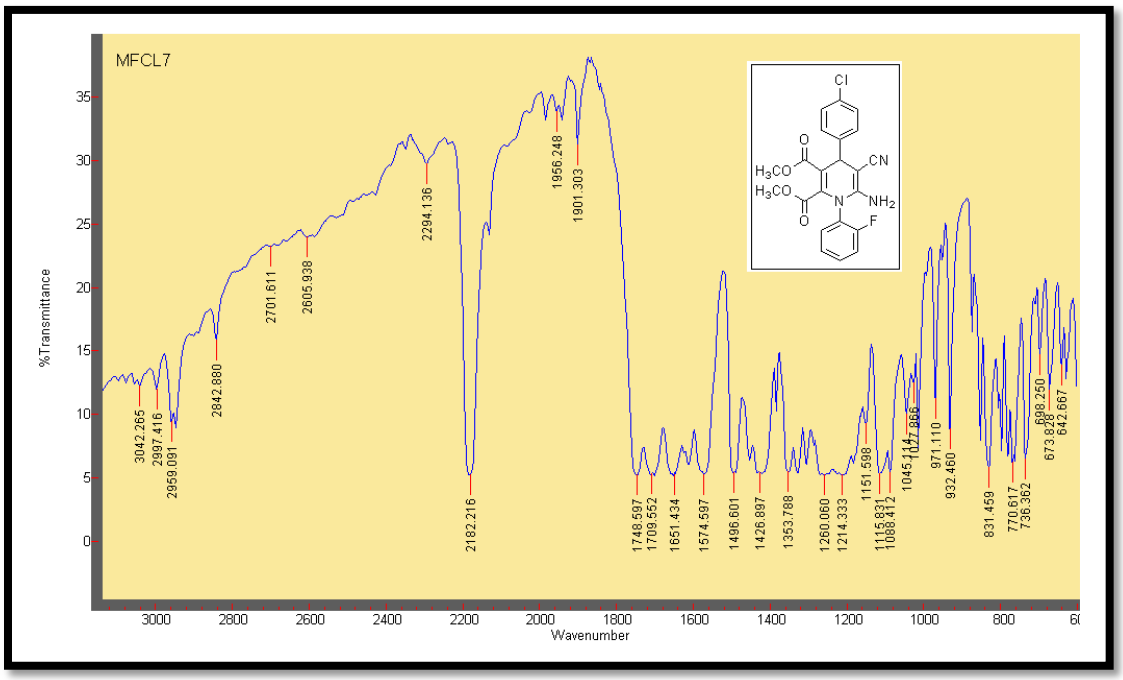

Figure. 2.22 IR Spectrum of **21**

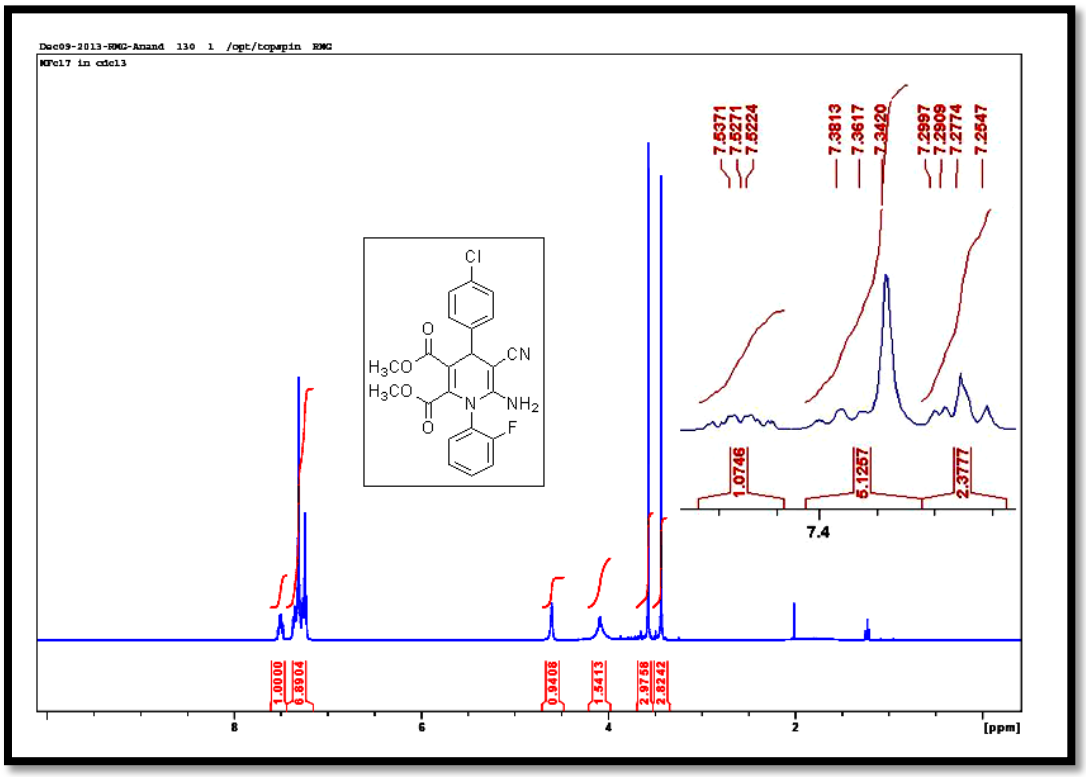

Figure. 2.23 ^{1}H-NMR spectrum of **21**

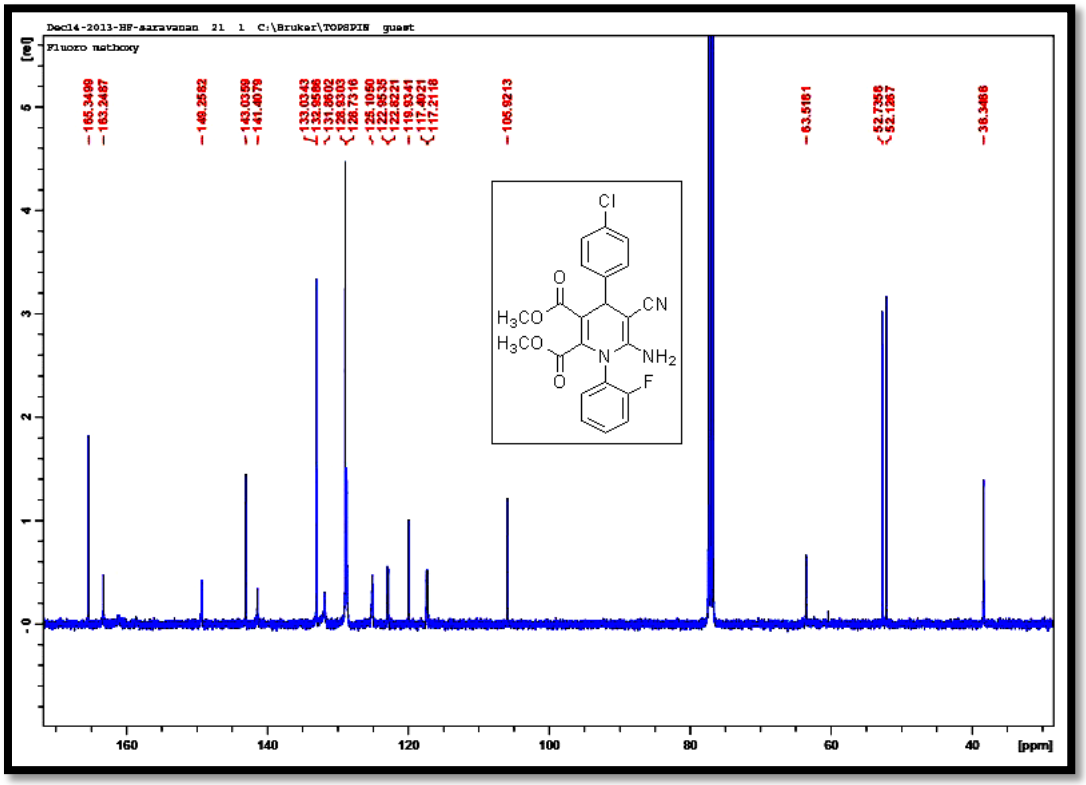

Figure. 2.24 ^{13}C-NMR spectrum of **21**

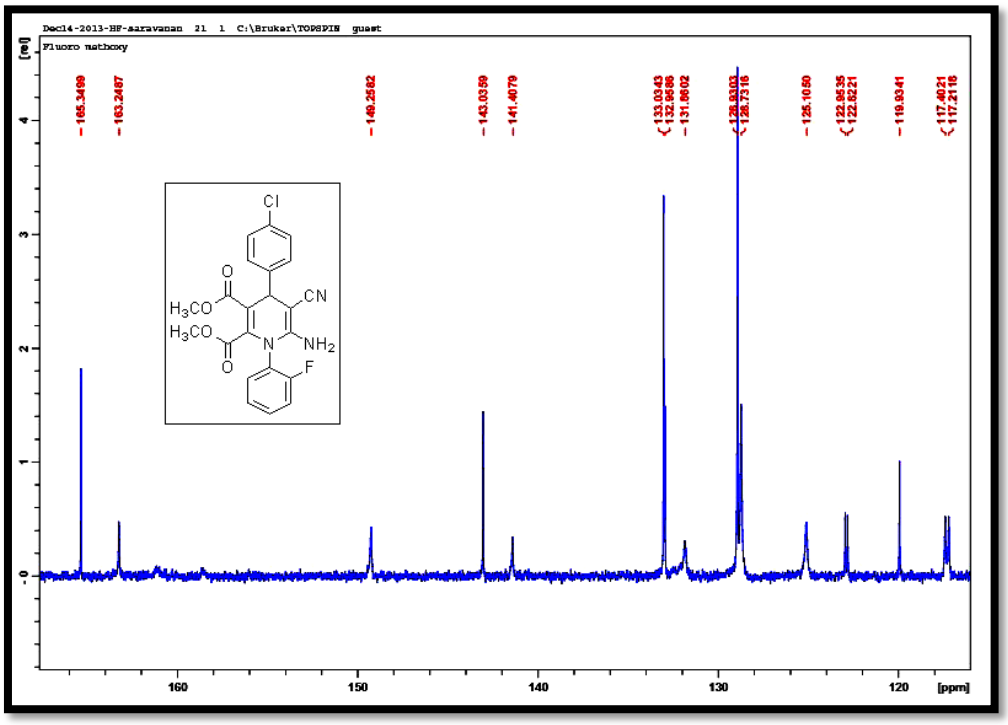

Figure. 2.24a ^{13}C-NMR spectrum of **21**

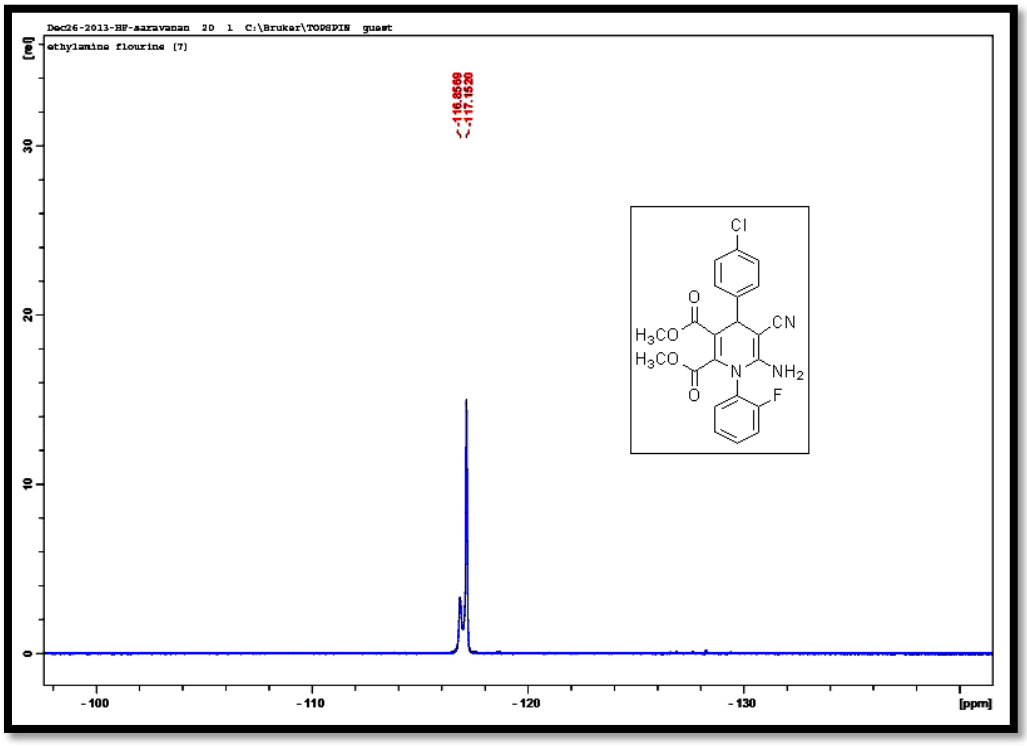

Figure. 2.25 ^{19}F-NMR spectrum of **21**

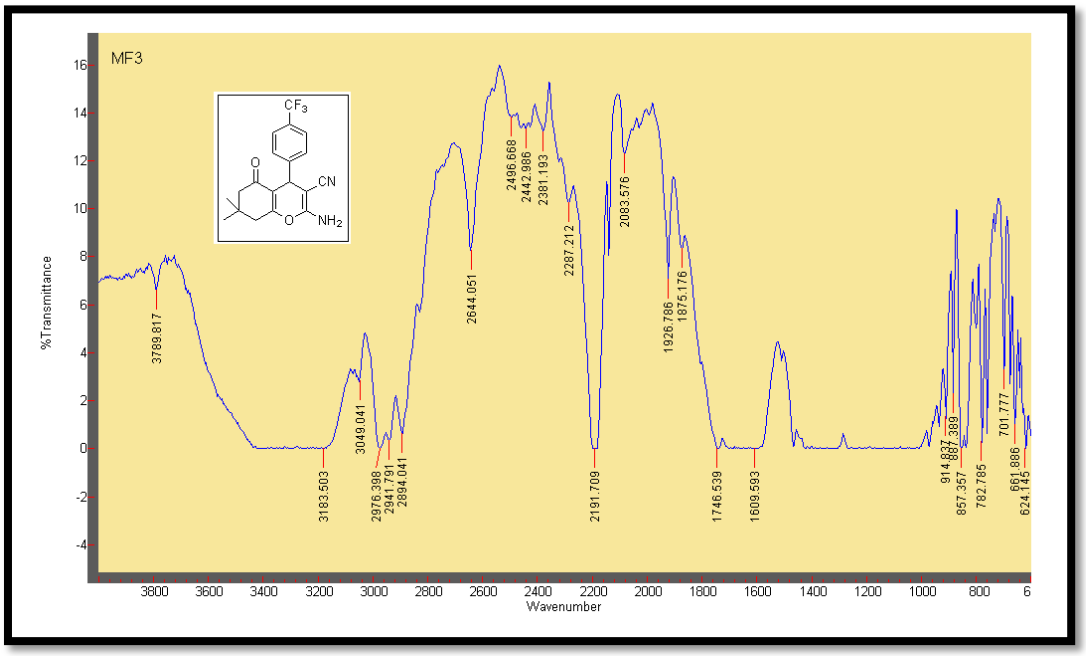

Figure. 2.26 IR Spectrum of **23**

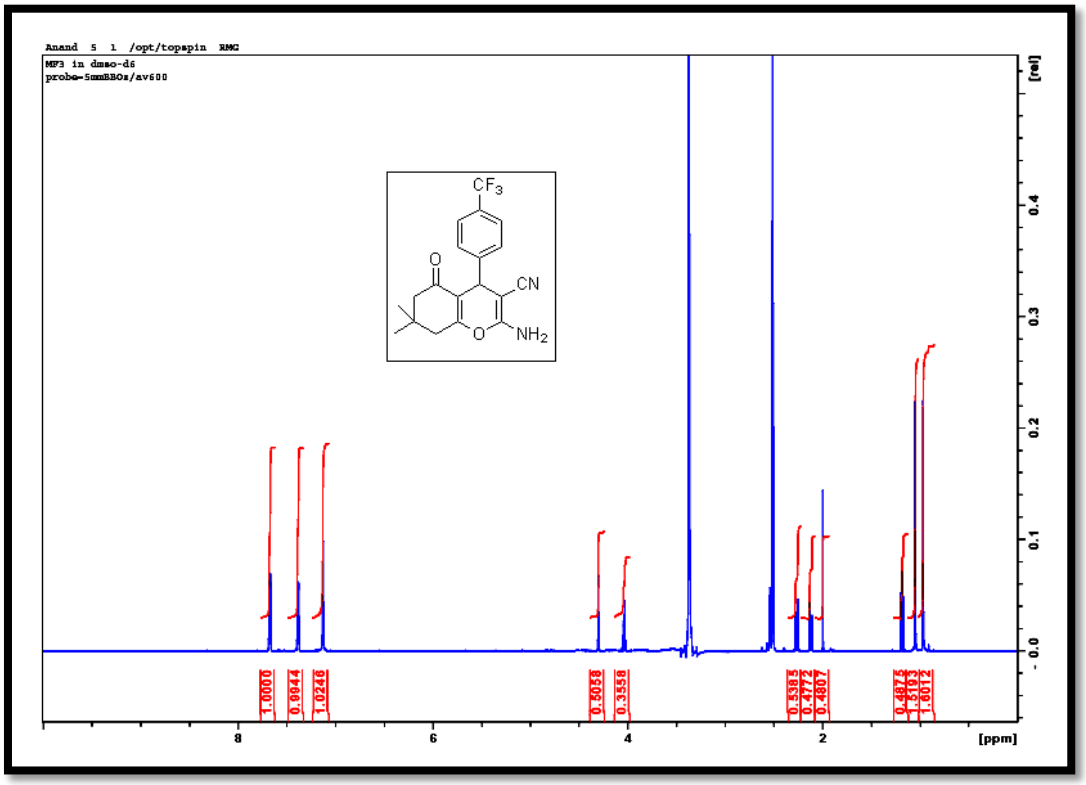

Figure. 2.27 ^{1}H-NMR spectrum of **23**

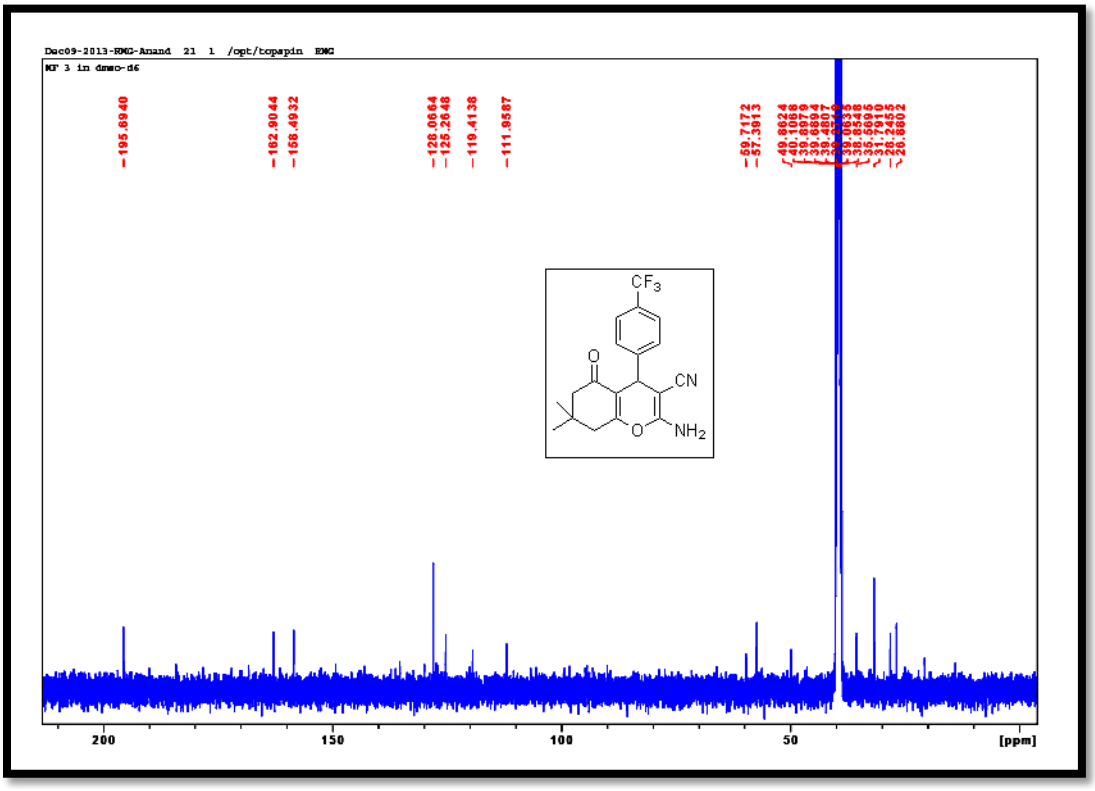

Fig. 2.28 ^{13}C-NMR spectrum of **23**

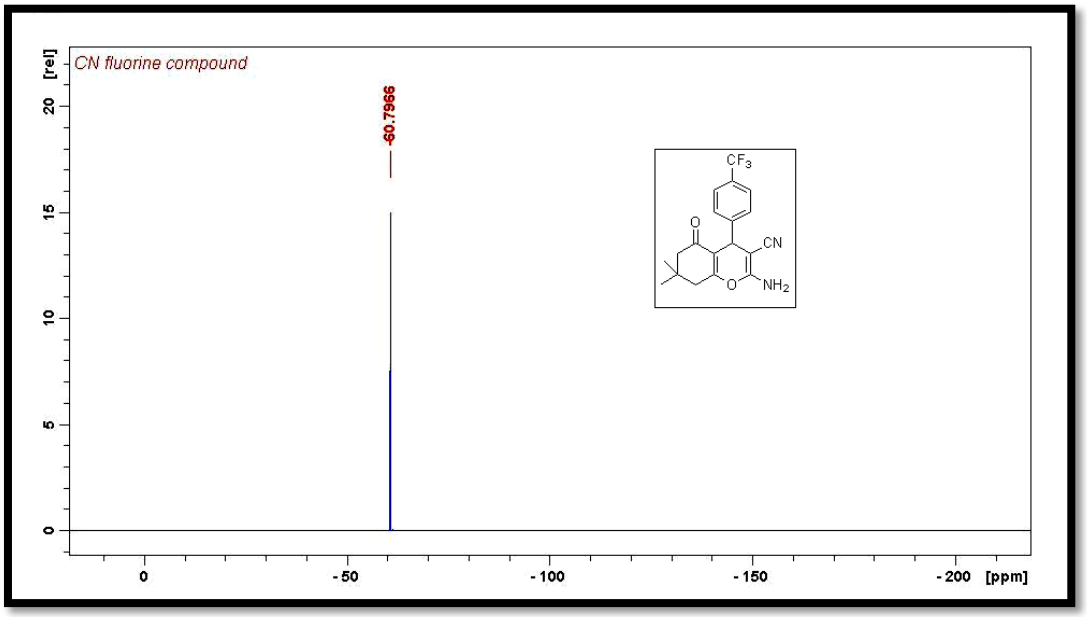

Fig. 2.29 ^{19}F-NMR spectrum of **23**

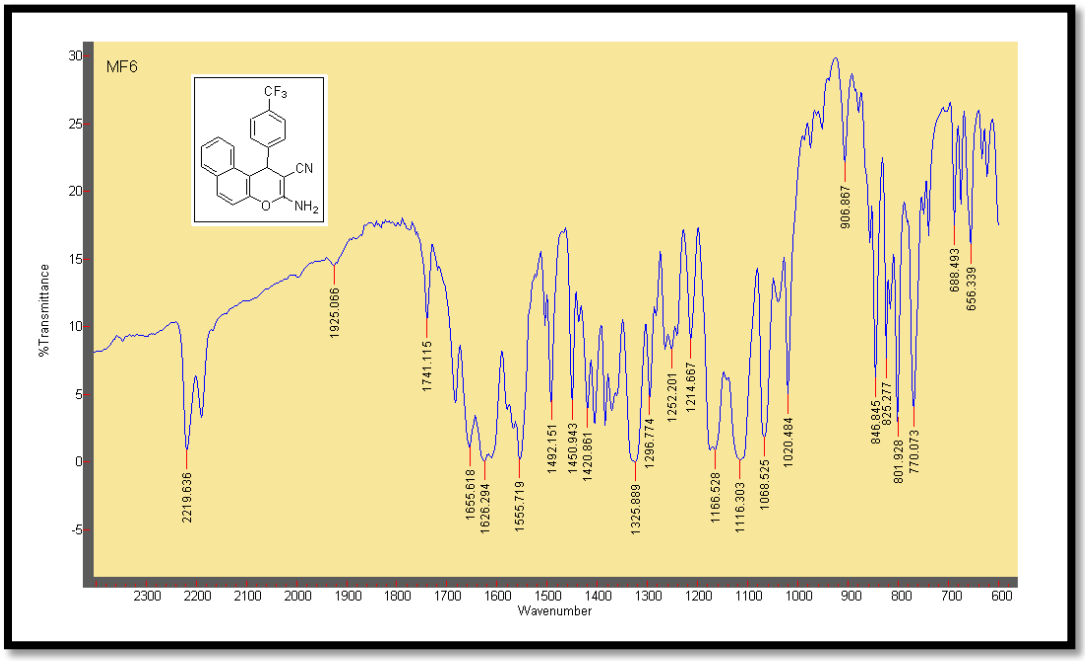

Figure. 2.30 IR Spectrum of **25**

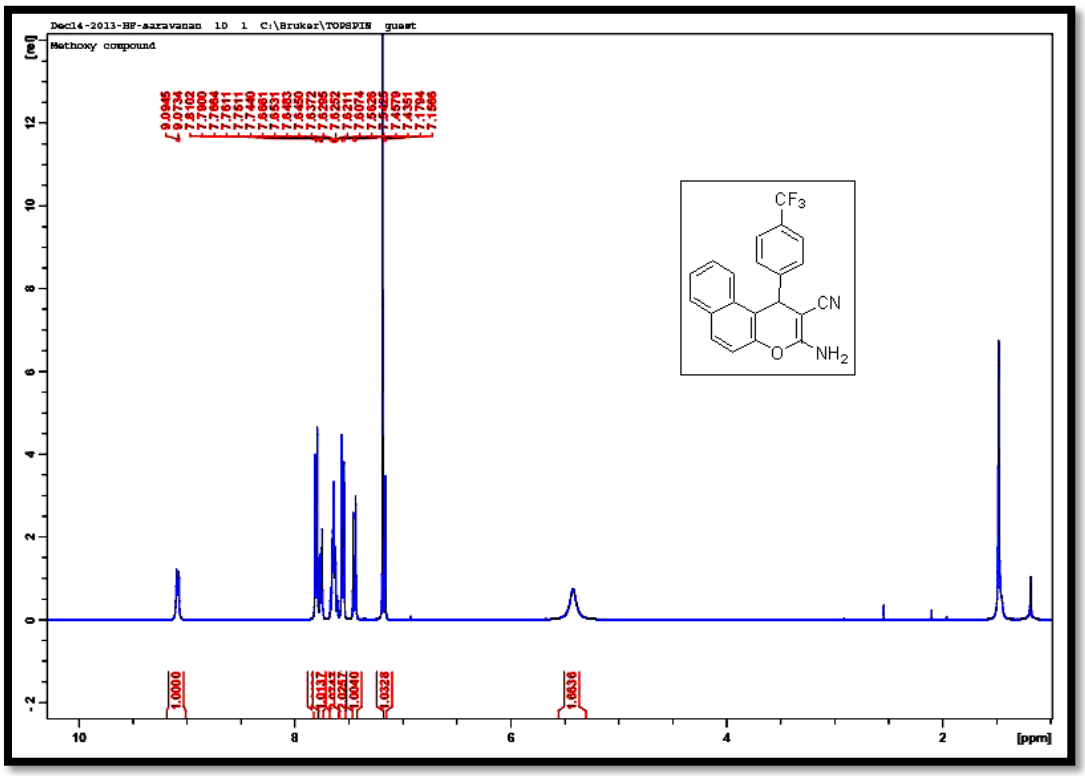

Figure. 2.31 ^{1}H-NMR spectrum of **25**

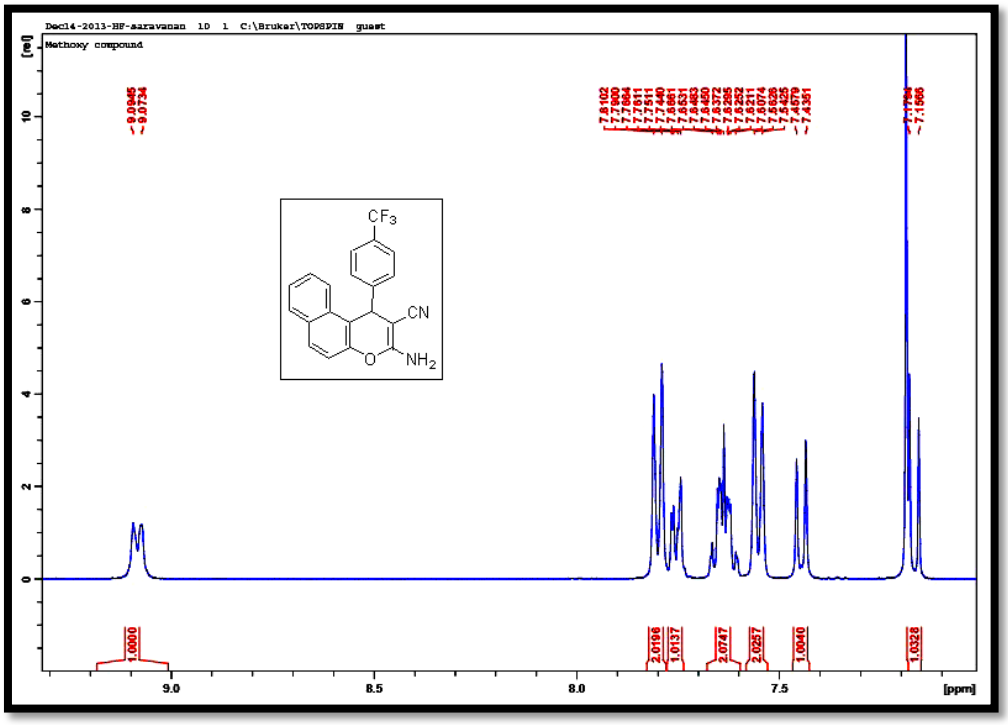

Figure. 2.31a Expanded ^{1}H-NMR spectrum of **25**

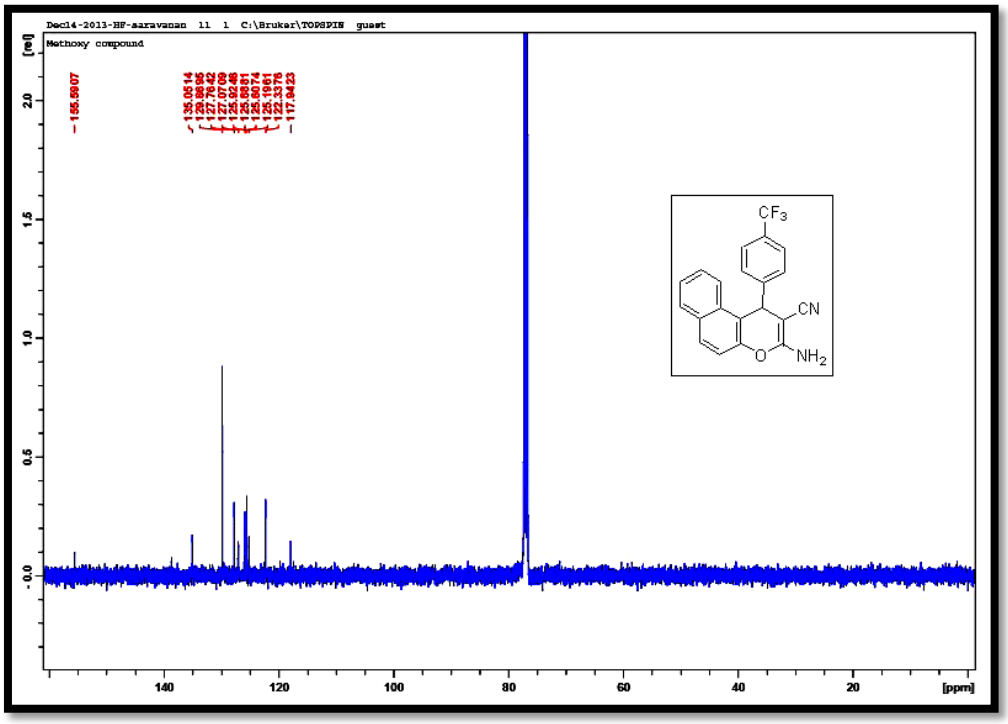

Figure. 2.32 ^{13}C-NMR spectrum of **25**

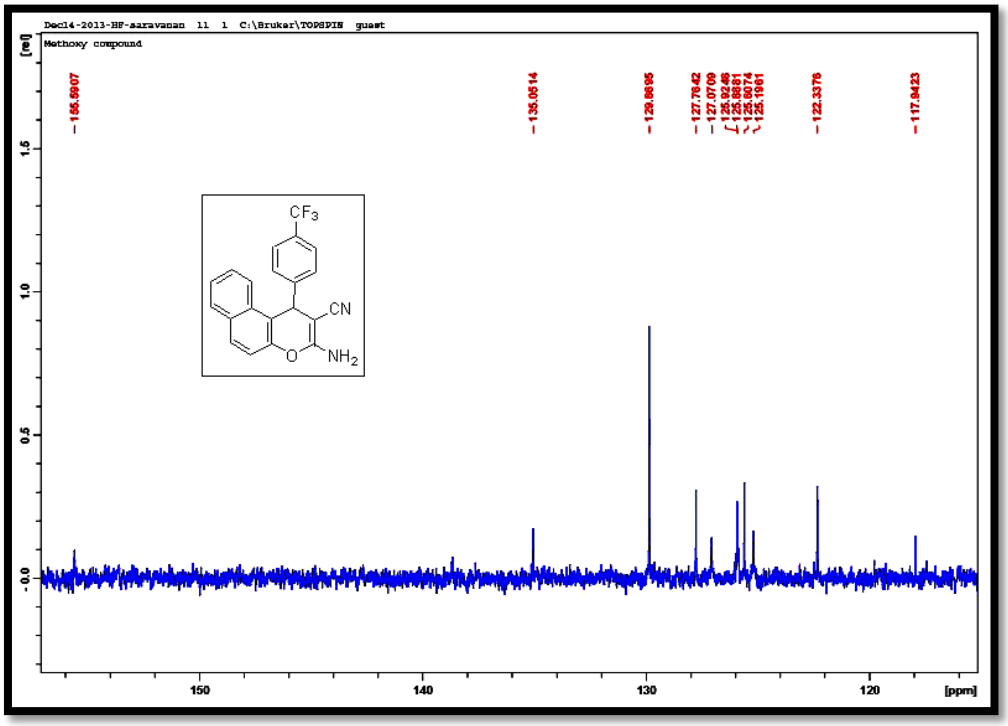

Figure. 2.32a Expanded ^{13}C-NMR spectrum of **25**

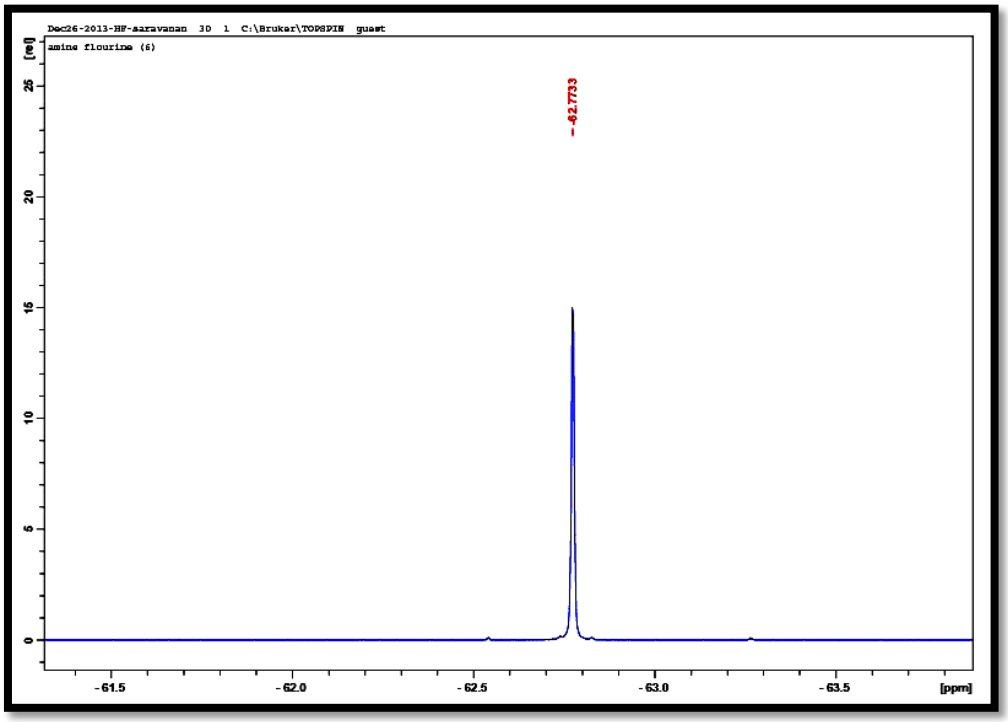

Figure. 2.33 ^{19}F-NMR spectrum of **25**

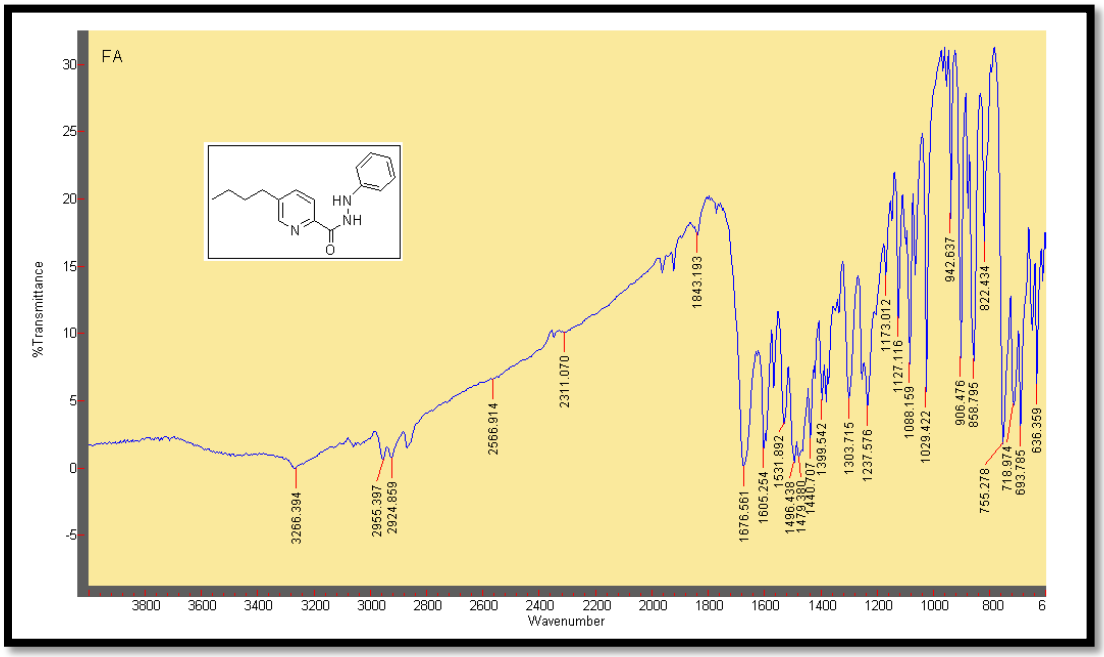

Figure. 2.34 IR Spectrum of **28**

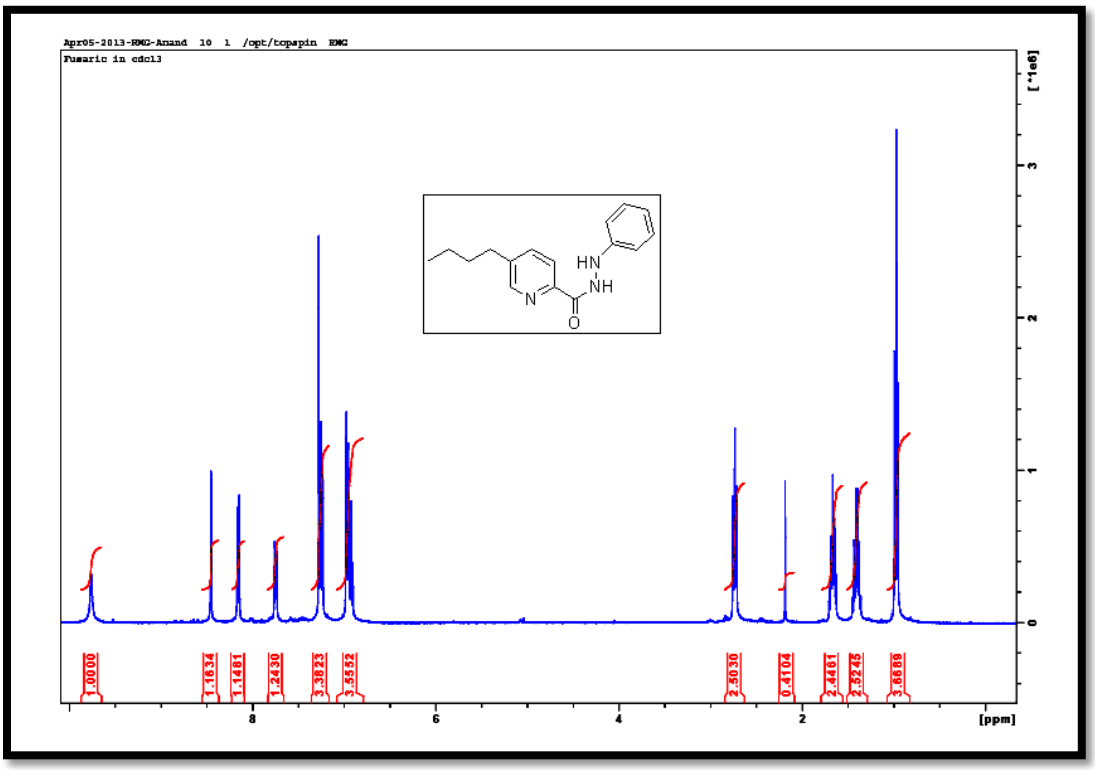

Figure. 2.35 ^{1}H-NMR spectrum of **28**

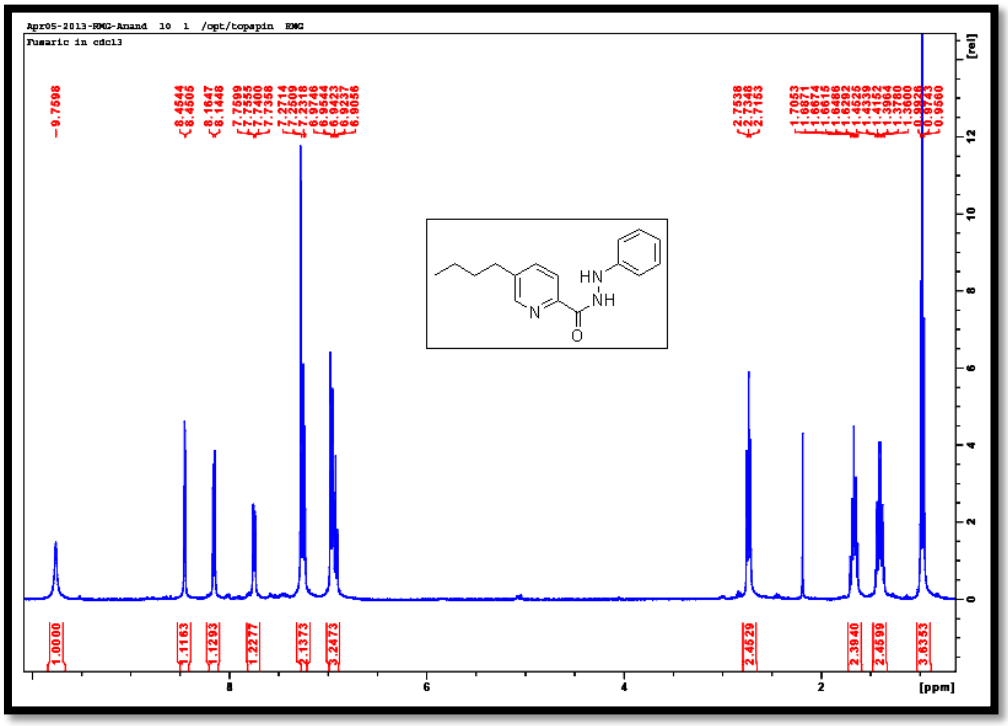

Figure. 2.35a ^{1}H-NMR spectrum of **28**

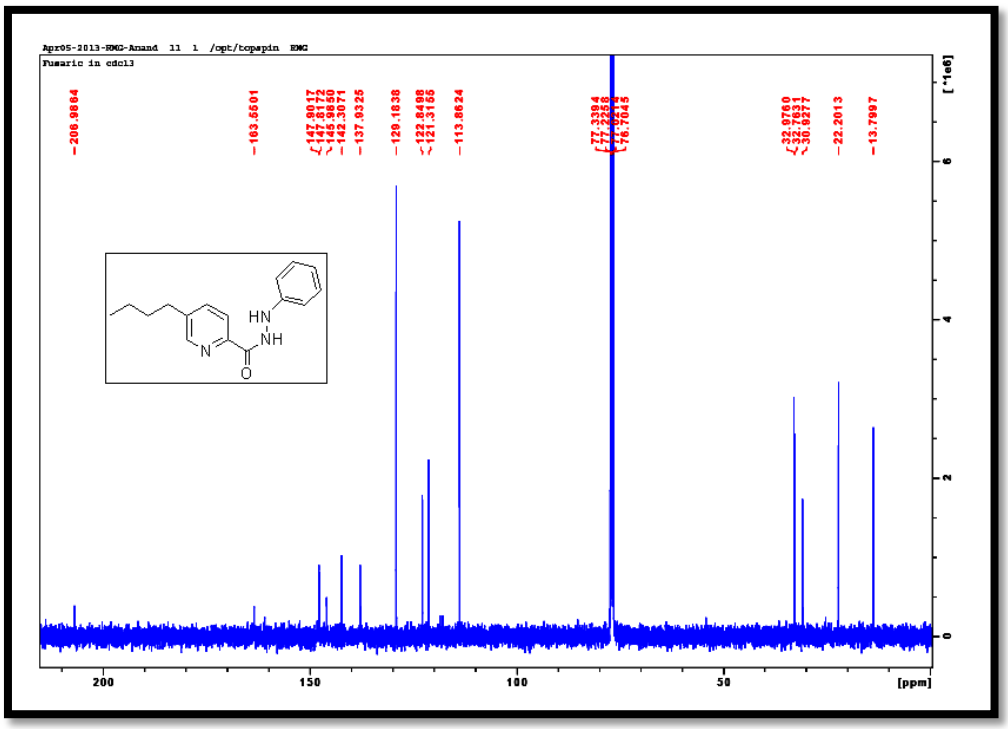

Figure. 2.36 ^{13}C-NMR spectrum of **28**

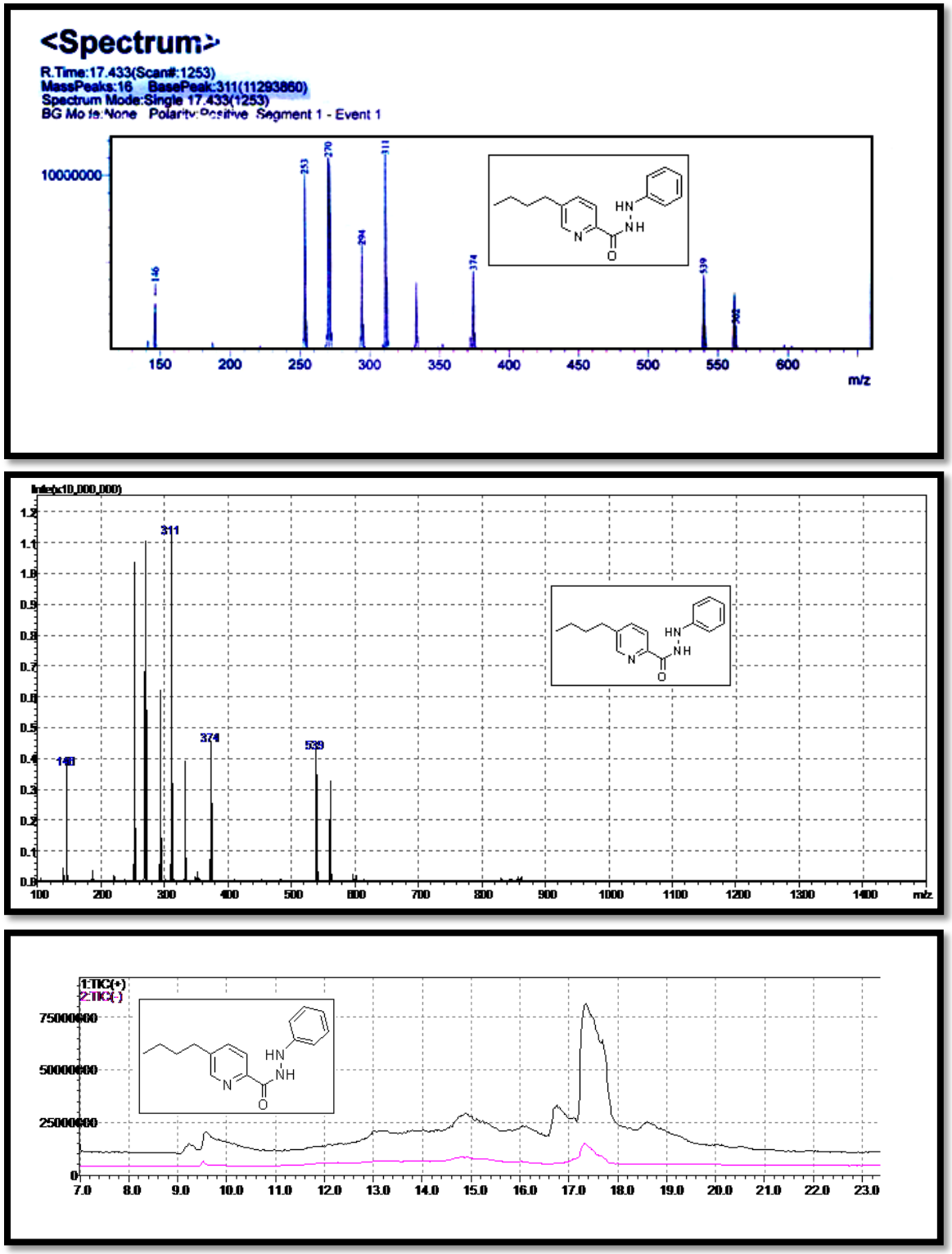

Figure. 2.37 Mass Spectrum of **28**

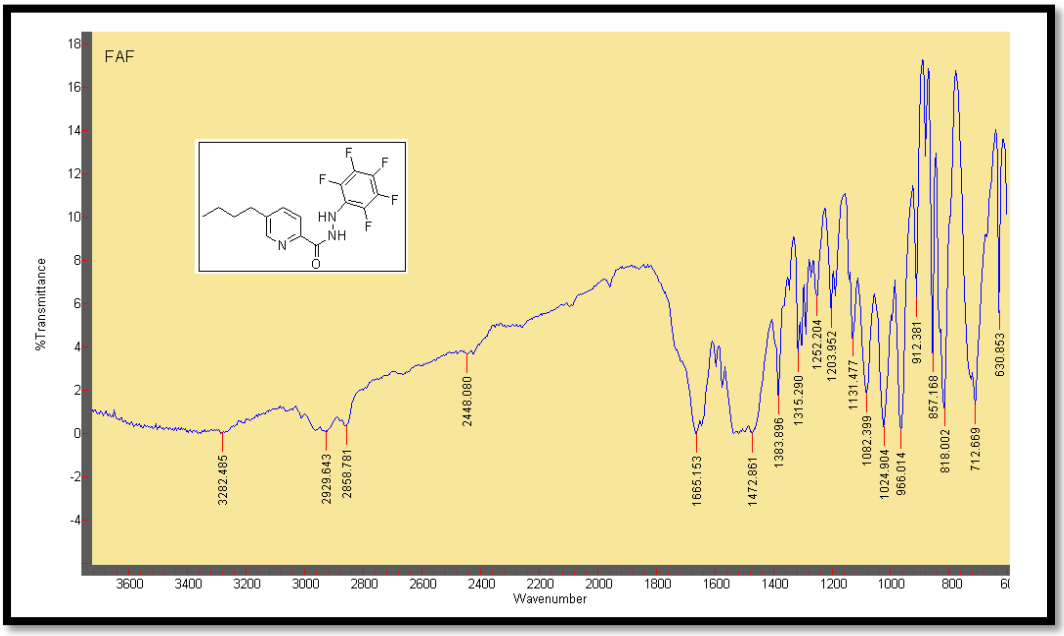

Figure. 2.38 IR Spectrum of **30**

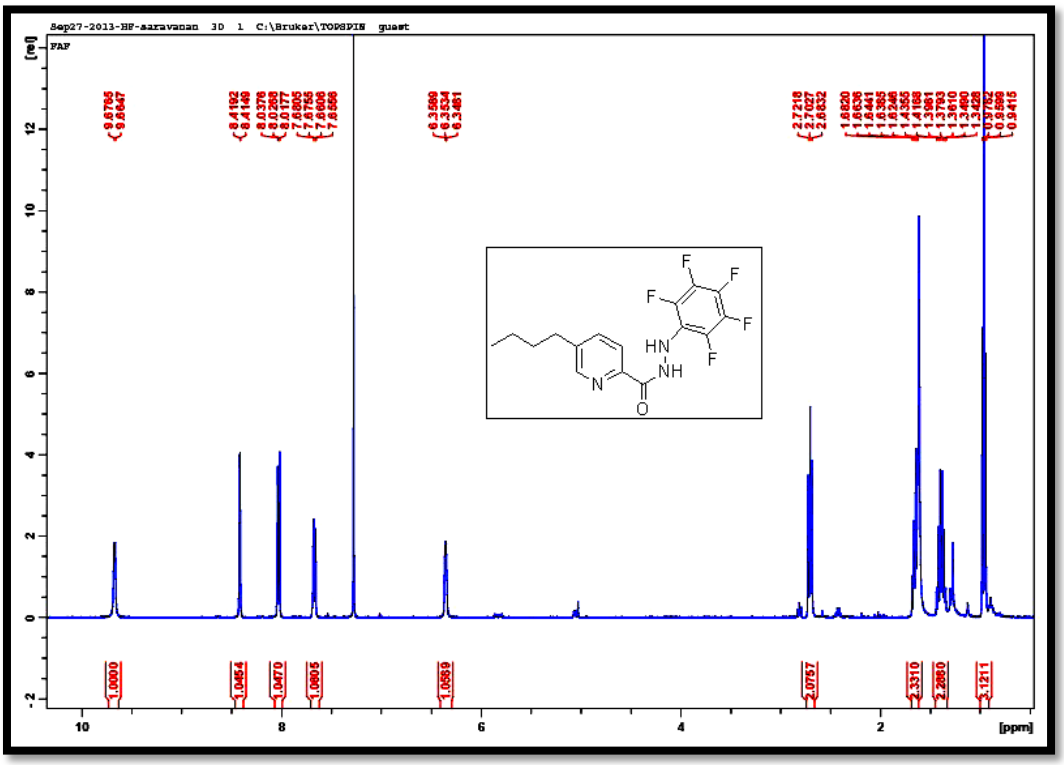

Figure. 2.39 ^{1}H-NMR spectrum of **30**

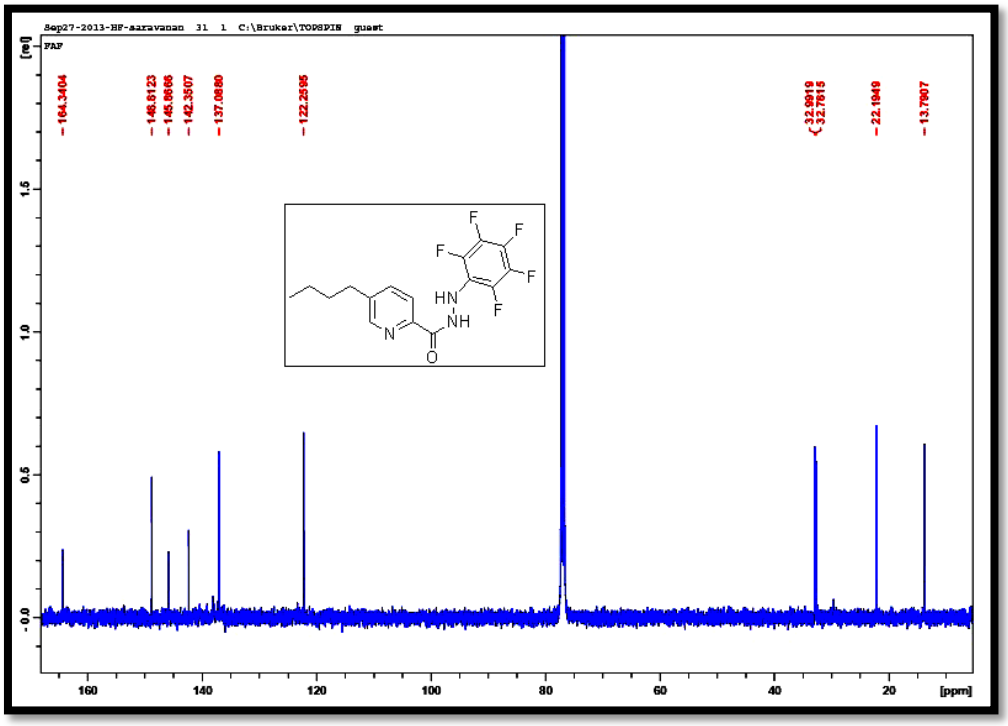

Figure. 2.40 ^{13}C-NMR spectrum of **30**

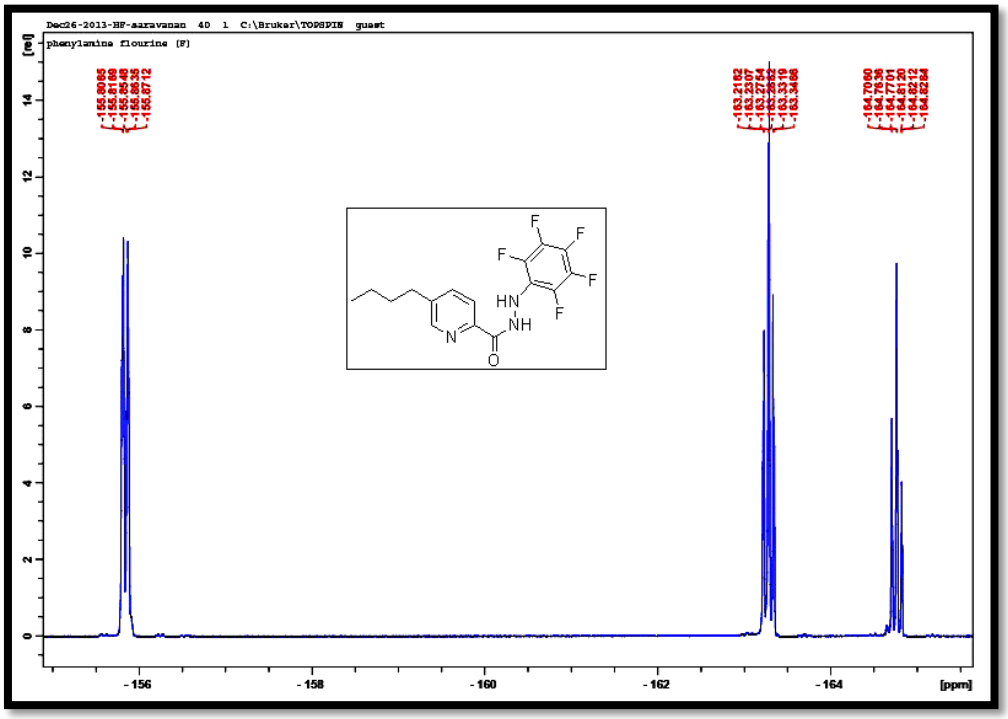

Figure. 2.41 ^{19}F-NMR spectrum of **30**

Chapter 3

A facile synthesis of fluorinated pyrrolphenanthroline in dimethylimidazolium tetrafluoroborate ionic liquid and their strong interaction with bovine serum albumin

CHAPTER III

A facile synthesis of fluorinated pyrrolophenanthroline in dimethylimidazolium tetrafluoroborate ionic liquid and their strong interaction with bovine serum albumin

3.1. Abstract

Synthesis of fluorinated nitrogen heterocyclic is highly essential in organic chemistry because of its wide application as drug for almost all known disease. Therefore in this study two novel fluorinated pyrrolophenanthroline derivatives **5** and **7** were synthesized via a four component isocyanide based multi-component reaction (IMCRs). In this reaction 1-butyl-2,3-dimethylimidazolium tetrafluoroborate ionic liquid (DMTIL) was used as a reaction medium; no catalyst was required. These compounds were fully characterised by spectroscopic techniques, i.e. IR, ^{1}H-NMR, ^{13}C-NMR and ^{19}F-NMR. DMTIL may become a potential hazard to public health especially to researchers who are the one exploring their physiochemical behaviour. Therefore it was necessary to understand their binding mechanism with model proteins. In view of this consideration, the present investigation also deals with the interaction studies of DMTIL with Bovine Serum Albumin (BSA) by emission, absorption, synchronous fluorescence, circular dichoroism (CD) and three dimensional emission (3D) spectroscopic techniques. The results from emission titration experiments revealed the existence of a strong interaction between BSA and DMTIL ionic liquid. The negative free energy change for the interaction of BSA with DMTIL indicates the spontaneity of the complexation process. The binding related emission quenching of BSA by DMTIL was initiated by a static quenching mechanism via ground state complex formation. DMTIL induced secondary structural and micro environmental changes of BSA were established by synchronous emission, three dimensional emission and circular dichroism studies. The autodock based molecular docking suggested that the cationic imidazolium moieties of ILs and two novel trifluoromethyl pyrrolophenanthroline **5** and fluoro quinoline pyrrolophenanthroline **7** enter the sub domains of protein and interact with the hydrophobic residues of domain III of BSA.

3.2. Introduction

Fluorinated nitrogen heterocyclic compounds are important in the pharmaceutical and drug industries[1]. Recently, fluorinated ionic liquids have become a green route for catalytic applications due to their exceptional physicochemical properties, such as their non-volatile nature, water immisciblity, high ionic conductivity, low melting point, and thermal and electrochemical stability. Because of these unique properties, fluorinated ionic liquids have found wide spread use in organic synthesis, i.e. as solvent catalyst, catalyst activator or co-catalyst[2]. Multi-component reactions (MCRs) which use more than three reactant starting materials in a one-pot facile reaction conditions are examples of discovery for rapid identification and optimization of biologically active lead compounds. Isocyanides-based multi-component reactions[3] (IMCRs), for classical organic chemistry, are suitable for building large compound libraries. A large number of fluorinated nitrogen heterocyclic are known to be medicinally important; an example of a quinoline nucleus with fluorinated atom are ciprofloxacin[4] and Nalidixic acid[5]. 1,10-Phenanthroline (phen) is a classic chelating bidentate ligand for transition metal ions. It has played an important role in the development of coordination chemistry and still continues to be of considerable interest as a versatile starting material for organic, inorganic and supramolecular chemistry[6].

Recently, we have embarked on IMCRs projects to achieve synthetic targets in an ideal and expeditious way. Phen is a rigid planar, hydrophobic, electron-poor heteroaromatic system with two or more nitrogen atoms. An increasing interest in the chemistry of phen derivatives has prompted development of more efficient synthetic procedures of this functionalization of the phen nucleus at various ring positions. Of this the symmetric synthetic manipulation at the 2,9-positions to prepare elaborate phen-based structures is the most preferred strategy. Condensed phenanthroline heterocyles are mainly an extension of aromatic scaffold of the phenanthroline moiety. They are traditionally prepared by thermal and/or acid-catalyzed cyclization, super-electrophilic cyclization, photochemical dehydrocyclization, and other approaches[7].

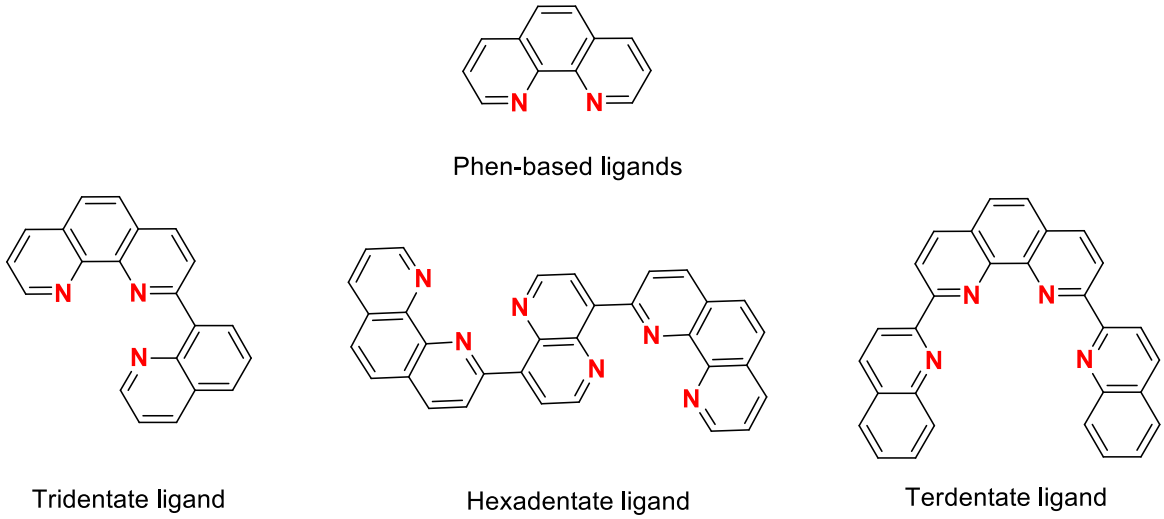

Serum albumins are one of the most abundant proteins present in the blood plasma, which assists in the disposition and transportation of various exogenous and endogenous ligands to specific targets[8-9]. Albumins are the principal bio-macromolecules that are involved in the maintenance of colloid-blood pressure needed for proper distribution of body fluids between intravascular compartments and body tissues[10]. They also act as a plasma carrier by nonspecific binding through several hydrophobic steroid hormones across organ-circulatory interfaces such as the liver, intestine, kidney, and brain[11-12]. BSA is extensively used in biophysical and biochemical studies as a model system for protein folding, aggregation and drug delivery. The primary structure of BSA protein has about 580 amino acid residues which assume the solid equilateral triangular shape with sides ~80 Å and depth ~ 30 Å. BSA proteins are characterized by low tryptophan content and a high content of cystine stabilizing a series of nine loops. The secondary structure of BSA is constituted of ~67% helix content with six turns and 17 disulfide bridges[13-14]. Human and bovine serum albumins display approximately 80% sequence homology and a repeating pattern of disulfides that is strictly conserved.

ILs are gaining extensive attention in protein assays, because ILs not only provide a novel and highly efficient reaction medium but also serve as effective participants in various biological reaction processes. Usually, ILs are employed as neat solvents containing little or no water and emphasis is often placed on protein dynamics and structure due to their relationship to the protein activity, function, and stability. In addition, ILs may be used as co-solvents for water in biphasic systems. The two aqueous phase systems composed of ILs and phosphate are frequently applied for the separation of

proteins[23-25]. Investigations on the interactions between ILs and proteins in aqueous solutions are even more important than those in neat ILs phase. The behaviour of proteins in IL phase have been frequently reported. However, the interactions between proteins and ILs in aqueous media are not well understood and the underlying interpretations are still mostly speculative. Fluorine contains ionic liquids highly charged by electron negativity properties it can enhance the binding properties with protein molecules[26].

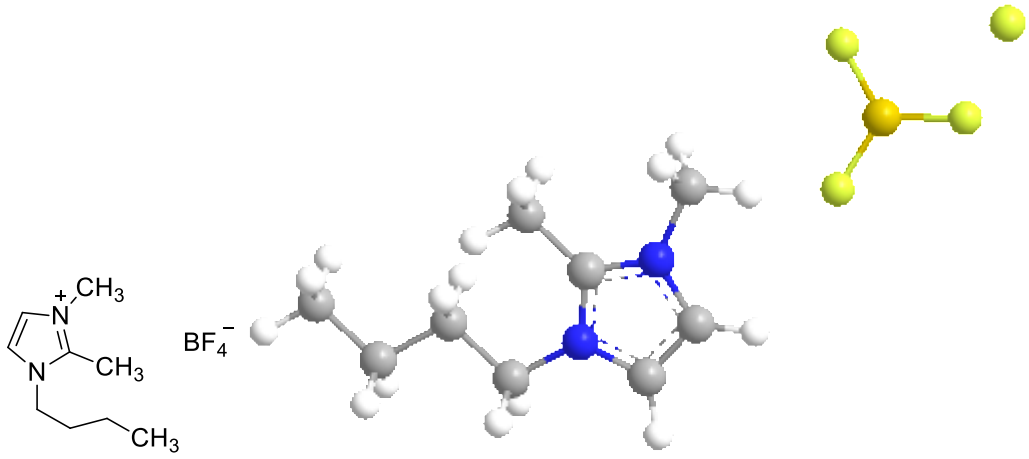

Scheme 1. Structure of 1-butyl-2,3-dimethylimidazoliumtetrafluoroborate (DMTIL)

In this study a novel efficient one-pot four-component region selective synthesis of fluoro pyrrolo phenanthrolines in excellent yields has been developed. The 1,3-dipolar cycloaddition of equimolar trifluoromethylated benzaldehyde or 7-fluoro-3-formyl quinoline with malononitrile and 1,10-phenanthroline under DMT ionic liquids mild conditions without using any catalyst were used.

Also, a comprehensive investigation is performed for the binding properties of 1-butyl-2,3-dimethyl imidazolium tetrafluoroborate **Scheme 1** (DMTIL) to BSA by spectroscopic methods including absorption, emission, three dimensional emission (3D), synchronous emission and circular dichroism. An attempt is also undertaken to unravel the effect of DMTIL binding on the secondary structure of BSA. The probable binding location of DMTIL within BSA is explored by auto dock based molecular docking strategy.

3.3. Experimental

3.3.1. Materials and methods

Melting points were determined by using a Stuart SMP10 Melting Point Apparatus and were uncorrected. IR spectra were recorded on Varian 800 FTIR using KBr pellets and the absorption frequencies are expressed in reciprocal centimeters (cm^{-1}). NMR spectra were taken on BRUKER TOPSPIN 400 MHz and 600 MHz spectrometer using TMS as an internal reference. BSA was purchased from Sigma-Aldrich, South Africa and used without further purification. DMTIL was obtained from Sigma-Aldrich, South Africa and used as received. The stock solution of BSA was prepared by using phosphate buffer solution (PBS) of pH = 7.40. A stock solution of DMTIL was prepared at a concentration of 1.40×10^{-4} mol dm^{-3} and kept protected in dark until further use. All other reagents were of analytical grade and water used in this investigation was doubly distilled over alkaline potassium permanganate using an all glass apparatus.

3.3.2. Synthesis of 11-(Cyclohexylamino)-10-(4-trifluoromethyl)pyrrolo[1,2a][1,10] phenanthroline-9-carbonitrile(**5**)

The reaction vessel containing a mixture of 4-trifluoromethyl benzaldehyde **2** (0.19 g, 1.2 mmol), malononitrile **3** (0.072 g, 1.2 mmol), cyclohexylisocyanide **1** (0.125 ml, 1.0 mmol) and 1,10-phenanthroline **4** (0.18 g, 1.0 mmol) followed by DMTIL (0.024 g, 0.1 mmol) was placed in a preheated oil bath at 40°C for 5 min. The crude product was dissolved in EtOAc and extracted with water. The extract was dried over sodium sulphate and then concentrated to dryness affording the crude product. This crude product was purified by column chromatography 10:90 EtOAc/PE to afford the product as a red solid, (90% yield). mp: 265°C; IR (KBr, cm^{-1}): 3487.57, 3419.36, 2927.11, 2856.65, 2203.86, 1613.511, 1449.93, 1418.80, 1384.45, 1322.04, 1164.29, 1136.34, 1115.83, 1067.13, 1015.36, 840.49, 770.45, 720.85, 669.37; ^{1}H-NMR (400 MHz, $CDCl_3$): δ (ppm) 0.49-0.56 (m, 2H), 0.71–0.77 (m, 3H), 1.07–1.19 (m, 5H), 2.19 (s, 1H), 6.12 (s, 1H), 7.18 (d, 2H), 7.40–7.42 (m, 1H), 7.58–7.61 (d, 1H), 7.80–7.83 (m, 1H), 7.86 (d, 2H), 8.19–8.21 (m, 2H), 8.35–8.38 (dd, 1H), 9.08–9.09 (d, 1H,); ^{13}C-NMR (400 MHz, $CDCl_3$): δ (ppm) 147.77, 136.75, 129.98, 129.61, 129.20, 128.34, 125.69, 125.42, 122.82, 121.21, 118.90, 33.08, 25.34, 24.23; ^{19}F-NMR (400MHz, $CDCl_3$): δ (ppm) 62.58-62.96.

3.3.3. Synthesis of 16-cyclohexyl-13-fluoro-16Hquinolino[3'',2'':4',5']pyrrolo[3',2':4,5]pyrrolo[1,2-a][1,10]phenanthroline-9-carbonitrile(7)

The reaction vessel containing a mixture of 7-fluoro-3-formyl quinoline **6** (0.25 g, 1.2 mmol), malononitrile **3** (0.072 g, 1.2 mmol), cyclohexylisocyanide **1** (0.125 ml, 1.0 mmol) and 1,10-phenanhroline **4** (0.18 g, 1.0 mmol) were dissolved in DCM (3ml) followed by DMTIL (0.024 g, 0.1 mmol). It was placed in a preheated oil bath at 40 °C for 10 hours. The crude product was dissolved in EtOAc and extracted with water after confirmation by TLC. The extract was dried over sodium sulphate and then concentrated to dryness affording the crude product. This crude product was purified by column chromatography 10:90 EtOAc/PE to afford the product as a dark red solid, 95 % yield. mp: 270°C; IR (KBr, cm^{-1}): 2926.766, 2203.53, 1629.47, 1550.90, 1322.64, 1206.22, 841.10, 620.37; ^{1}H-NMR (400MHz, $CDCl_3$): δ (ppm) 0.49-0.56 (m, 2H), 0.71–0.77 (m, 3H), 1.07–1.19 (m, 5H), 2.19 (s, 1H), 7.3-7. (d, 2H), 7.6–7.63 (m, 1H), 7.52–7.7 (d, 1H), 7.85–7.91 (m, 1H), 7.86 (d, 2H), 8.39–8.42 (dd, 2H), 8.4 (s, 1H), 9.11–9.12 (d, 1H,); ^{13}C-NMR (400 MHz, $CDCl_3$): δ (ppm) 206.99, 147.83, 136.75, 129.98, 129.61, 129.20, 128.34, 125.69, 125.42, 122.82, 121.21, 118.90, 33.08, 25.34, 24.23; ^{19}F-NMR (400MHz, $CDCl_3$) δ (ppm) 107.33.

3.3.4. Absorption and emission spectral measurements

Absorption spectral measurements were carried out using JASCO V-630 UV-visible spectrophotometer. Quartz cuvettes of path length 1 cm were used to record the absorption spectra. The emission spectral studies were performed with JASCO FP-6600 spectro fluorometer equipped with a 1 cm quartz cuvette. All the titration experiments were carried out by adding appropriate amount of DMTIL to1 ml of BSA solution in a 5 ml standard flask in sequence and then made up to the mark with phosphate buffer solution. The solution was allowed to equilibrate for 10 minutes before recording the spectra and the homogeneous solution systems were taken in a quartz cuvette (1 cm). The synchronous emission spectra were recorded at $\Delta\lambda$ = 15 nm and $\Delta\lambda$ = 60 nm. 3D emission spectra were performed under the following conditions; the emission was recorded between the wavelength range of 200 nm to 500 nm and the excitation was recorded between the wavelength ranges from 200 nm to 350 nm. The excitation and emission bandwidths for 3D emission spectra were 10 nm and 2 nm, respectively. All the measurements were carried out at room temperature (25^{o}C).

3.3.5. Circular dichroism measurements

Circular dichroism measurements were performed with a JASCO-810 spectro polarimeter using a 0.1 cm path length quartz cell. The CD spectra were recorded in the range of 200-260 nm with 0.1 nm step resolution and averaged over two scans at a speed of 50 nm min^{-1}. All observed spectra were baseline subtracted for buffer solution and the α-helical content was calculated on the basis of change of molar ellipticity value.

3.3.6. Molecular docking studies

Auto dock 4.2 program which utilizes the Lamarckian Genetic Algorithm (LGA) was used to dock DMTIL with the 3D structure of BSA. The crystallographic coordinates of DMTIL was obtained from the PubChem Database. The native structure of BSA (PDB id: 4F5S) was retrieved from the Protein Data Bank and all water molecules were removed with subsequent addition of hydrogen atoms, followed by the calculation of Gasteiger charges, as required for Lamarckian Genetic Algorithm docking compilation. To encompass the entire protein during the docking process, the grid size along the x-, y-, z-axes was set to 126Å, 44Å, 78Å and the grid spacing was set as 1Å. The auto docking parameters used were, Genetic Algorithm (GA) population: 150; maximum number of energy evaluations: 250,000 and GA crossover mode of two points. For each docking simulation, 25 different conformers were generated and for visualization of the docked conformations PyMoL software package was used. The conformation with the lowest binding free energy was used for further analysis.

3.4. Results, discussion and conclusion

Fluorinated nitrogen heterocyclic compounds are highly used as pharmaceutical drugs because of their good affinity to bind biomolecules. Recently, fluorinated ionic liquids have been used as a green route for catalytic applications. This prompted our research interest in terms using a green approach to MCRs. Our work plan was to use a simple fluorinated ionic liquid as one of the reaction medium without catalysis in a MCR. Hence we decided to use simple starting compounds including a phenanthroline derivative. This reaction is presented in **Scheme 2**.

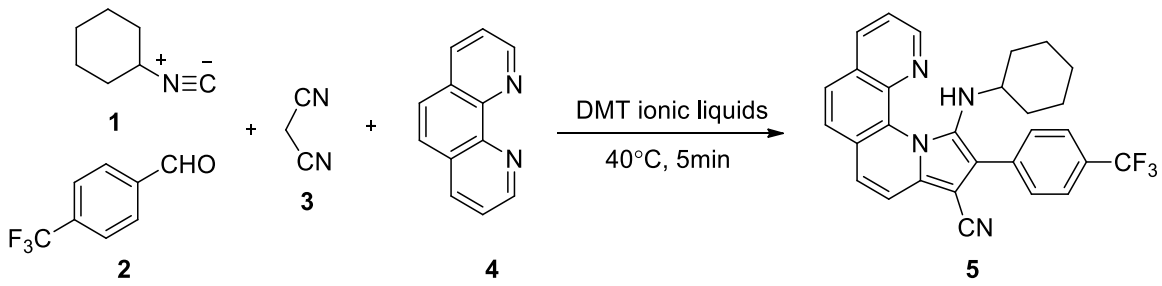

Scheme 2. Synthesis of trifluoromethylated pyrrolophenanthroline **5**

In the first part of the synthesis, we reacted compounds **1**, **3** and **4** with trifluoromethyl benzaldehyde **2**, in the presence of DMTILs, to obtain **5**. This reaction is a simple 1, 3 cycloaddtion via. Condensation, N-cyclization, aromatization and imine-enamine tautomerization. Characterizations of these compounds were achieved by IR, ^{1}H-NMR, ^{13}C-NMR and ^{19}F-NMR. IR spectra of **5** (**Figure 3.1**: page 112) showed nitrile (-CN = 2203.96), trifluoro methyl carbon (-CF_3 = 1322.04) and secondary amine (-NH = 3487.57) stretching frequency were present. The ^{1}H-NMR spectrum (**Figure 3.2**: page 112) of **5** showed a broad singlet signal near δ 6.1 due to NH. The ^{13}C-NMR (**Figure 3.3**: page 113) showed at signals at δ 147.77 and 33.08 the nitrile carbon and fluorine carbon, respectively.

The next research plan was to use the developed reaction protocol with fluoroquinoline as one of the substrates to synthesize a condensed pyrrolophenanthroline quinoline derivative. This reaction is presented in **Scheme 3**.

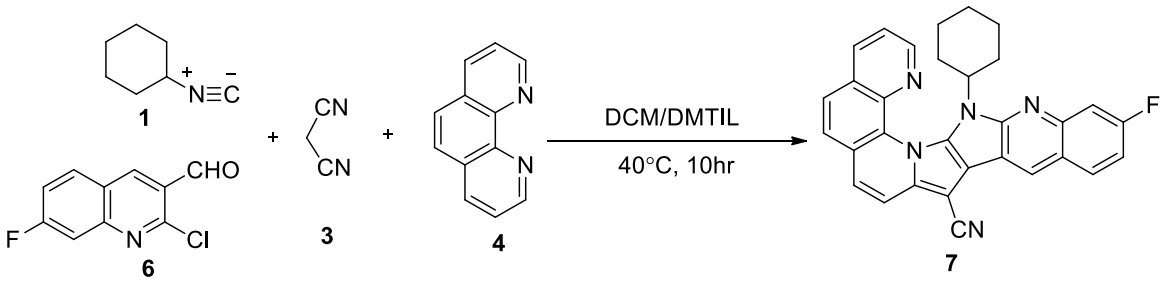

Scheme 3. Synthesis of fluoroquinoline pyrrolophenanthroline **7**

Compounds 1, 3 and 4 was reacted fluoroquinoline, in the presence of DMTILs, to obtain **7**. This reaction is a simple 1,3 cycloaddtion via. condensation, N-cyclization, aromatization, imine-enamine tautomerization followed by nucleophilic substitution.

Characterization of **7** was achieved by IR, ^{1}H-NMR, ^{13}C-NMR and ^{19}F-NMR. IR spectra of **7** (**Figure 3.5**: page 114) showed the nitrile group (-CN = 2203.53) and fluoro carbon (-C-F=1544.63). The secondary amine (-NH) and C-Cl stretching frequency were absent. This suggested that an additional step i.e. a nucleophilic substitution occurred. This was confirmed by the absence of NH signal in the ^{1}H-NMR spectrum (**Figure 3.6**: page 114). The ^{13}C-NMR (**Figure 3.9**: page 116) showed a signal at 147.83 due to the nitrile carbon however the C-Cl signal was absent.

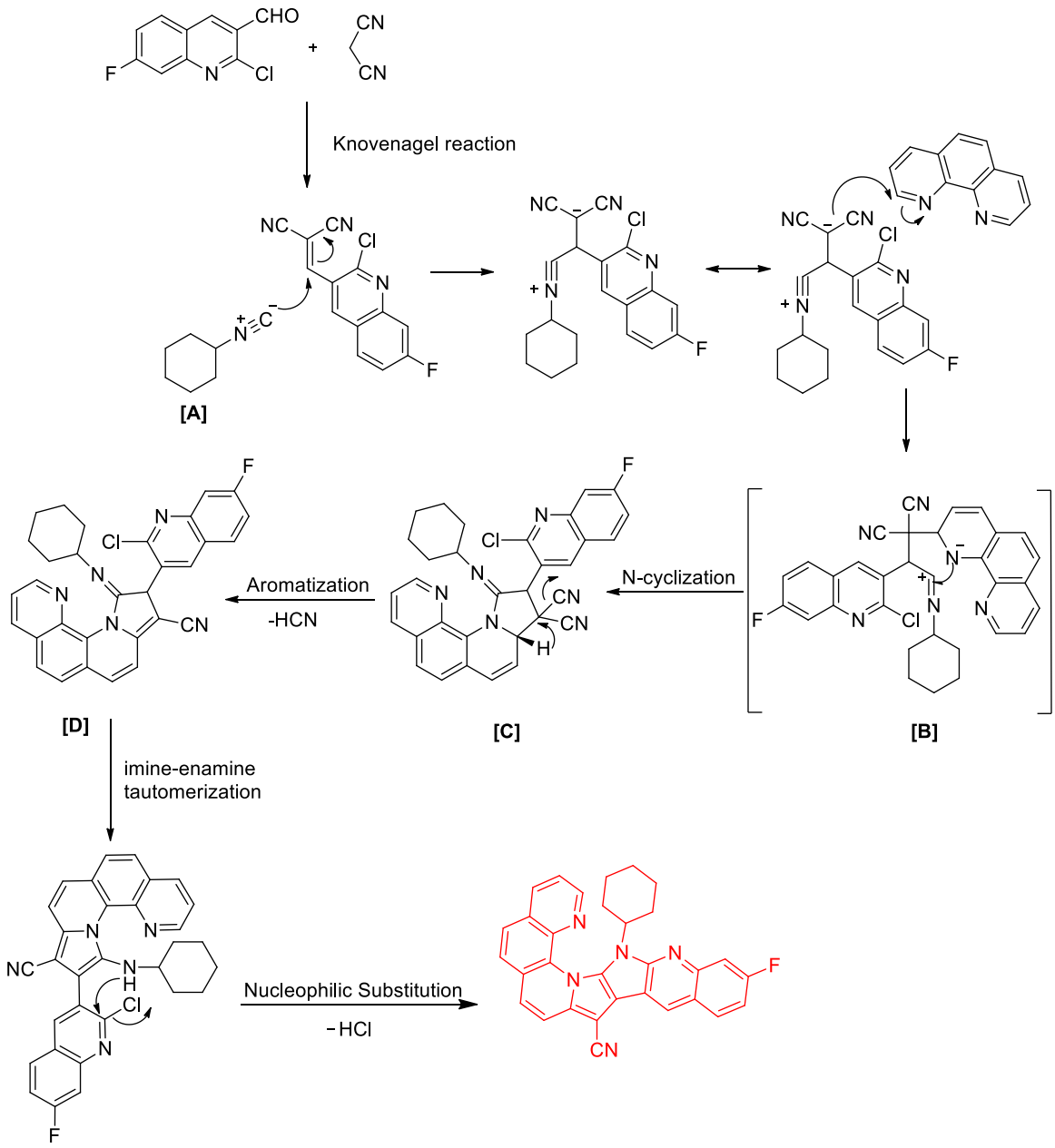

Mechanism 1. Plausible mechanism for the synthesis of **7**

A plausible reaction scenario for the domino cyclocondensation is presented in **Mechanism 1**. The first step is a Knoevenagel condensation between an 7-fluoro-3-formyl quinoline and malononitrile to generate 2-arylidene malononitrile which then reacts with cyclohexyl isocyanide to give a highly reactive zwitter ion intermediate **A**. This is followed by *in situ* trapping with 1,10-phenanthroline to afford the intermediate **B**. Next, **C** and **D** are obtained by N-cyclization and aromatization with loss of HCN. This is followed by an imine-enamine tautomerization. The next step was nucleophilic substitution with loss of HCl to form **7**. The chlorine atom in fluoroquinolines can be displaced by N-nucleophiles under this condition.

The next research plan was to investigate the ability of the ionic liquid to bind with BSA protein via. some conventional spectroscopic techniques.

To elucidate the binding mechanism of DMTIL with BSA. Steady-state emission spectral studies of BSA with varying concentrations of DMTIL was carried out. The resultant emission spectral data of BSA in the presence of DMTL is displayed in **Figure 1** It is evident from **Figure 1** that upon the addition of DMTIL (0 to 43.20×10^{-6} mol dm^{-3}), the emission intensity of BSA decreased gradually with a slight blue shift from 348 nm to 345 nm. From the above observations, it is believed that the slight blue shift in the emission wavelength of BSA was due to the changes in protein conformations and a probable decrease in the polarity around tryptophan residues of BSA. Similar kind of observation has been reported for the interaction of cationic Toludine Blue O with serum proteins[28]. The results from emission spectral studies implied that the binding site of DMTIL on BSA was adjacent to the tryptophan residues of BSA[29].

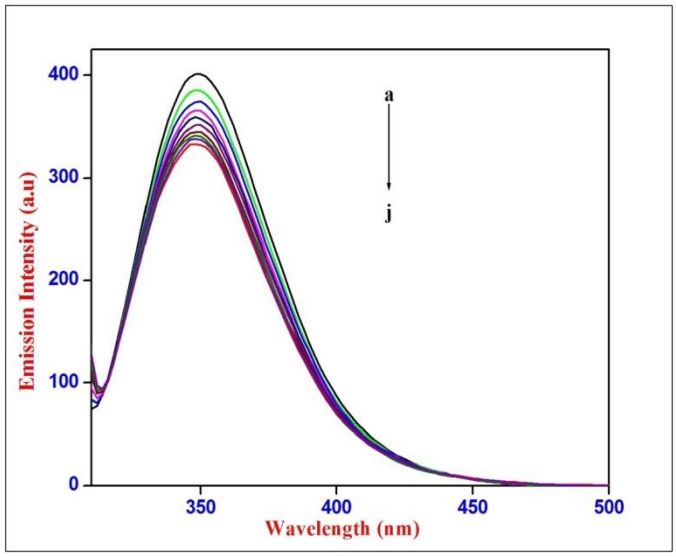

Figure 1. Emission spectra of BSA (2.00×10^{-6}mol dm^{-3})] at various DMTIL concentrations. [DMTIL]: (a) 0, (b) 4.80×10^{-6}, (c) 9.60×10^{-6}, (d) 14.40×10^{-6}, (e) 19.20×10^{-6}, (f) 24.00 x 10^{-6}, (g) 28.80×10^{-6}, (h) 33.60×10^{-6} (i) $38.40\times 10^{-6}$and (j) 43.20×10^{-6} mol dm^{-3}.

To quantify the DMTIL induced emission quenching of BSA, the conventional strategy of treating the quenching data using the Stern–Volmer equation (Eq. (1))[30] was used.

$$\frac{F_0}{F} = 1 + k_{sv}[Q] = 1 + k_q\tau_0[Q] - \quad (1)$$

where, F_0 and F are the emission intensities in the absence and presence of quencher, respectively. K_{sv} is the Stern-Volmer quenching constant, which procedures the efficiency of quenching, k_q is the bimolecular quenching rate constant, τ_0 is the average lifetime of the biomolecule without quencher (τ_0= 10^{-8}s)[24] and [Q] is the concentration of quencher. K_{sv} is determined by slope of a plot of F_0/F versus [Q].

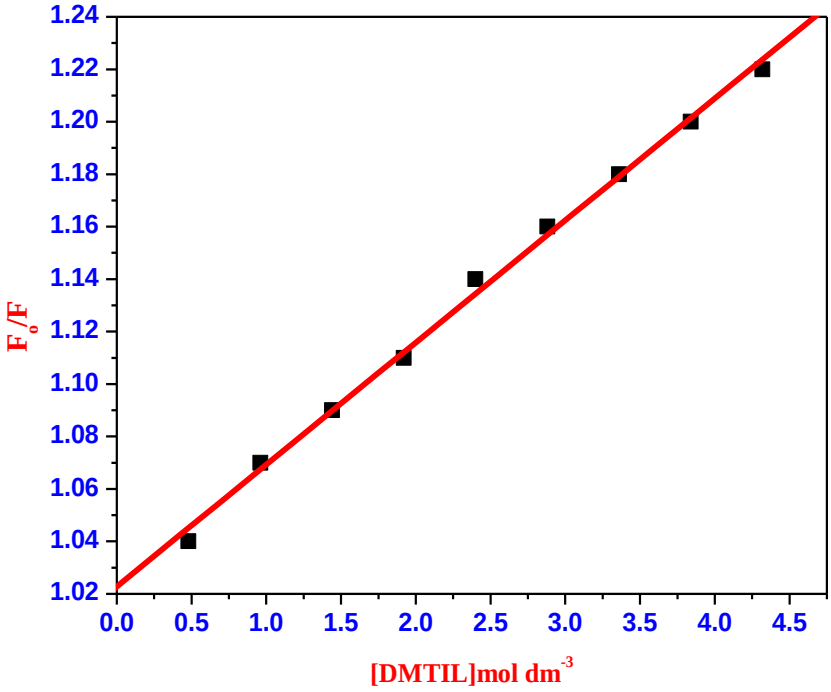

Figure 2. Stern-Volmerplot for BSA with DMTIL (λ_{ex}= 295 nm).

The Stern-Volmer plot for relative emission intensity at 348 nm *vs* DMTIL concentration is shown in **Figure 2** As depicted in **Figure 2** Stern-Volmer plot exhibited a good linearity within the experimental DMTIL concentrations. The value of Stern-Volmer quenching constant K_{sv} obtained from the slope and intercept of the linear plot is shown in **Table 1** The bimolecular quenching constant K_q for BSA-DMTIL system was calculated from the relation $K_q=K_{SV}/\tau_0$ and it was computed as 4.60 x 10^{12} $dm^3\,mol^{-1}s^{-1}$. It has been well established that for a static quenching process, the quenching constant K_q is for greater than the maximum scatter collision quenching constant (2.00 x 10^{10} $dm^3\,mol^{-1}s^{-1}$) [30]. In this case, the obtained higher value of K_q for BSA-DMTIL system suggests that the quenching process is not initiated by collision process but it is primarily due to complex formation viz. static quenching.

For a static quenching process a modified Stern-Volmer equation is used to calculate the affinity constant K_a of the binding between BSA and DMTIL. The possibility of differential accessibilities of the protein residues to the probe can be resolved using Modified Stern-Volmer equation (Eq. (2))[30].

$$\frac{F_0}{\Delta F} = \frac{1}{f_a k_a}\frac{1}{[Q]} + \frac{1}{f_a} \ldots . (2)$$

where, ΔF is the difference in emission intensity in the absence and presence of the quencher concentration [Q], K_a is the effective quenching constant for the accessible fluorophores and f_a is the fraction of available fluorescence. The dependence of $F_0/\Delta F$ on the reciprocal value of the quencher concentration $[Q]^{-1}$ is linear with also per equal to the value of $(f_a K_a)^{-1}$ and the corresponding results depicted in **Figure 3.** The estimated binding constant K_a for BSA-DMTIL is calculated as 3.40×10^4 mol^{-1} dm^3. The obtained result suggests that BSA form a strong complex with DMTIL and the K_a value is found to be in reasonable accord with previously available literature[28-29].

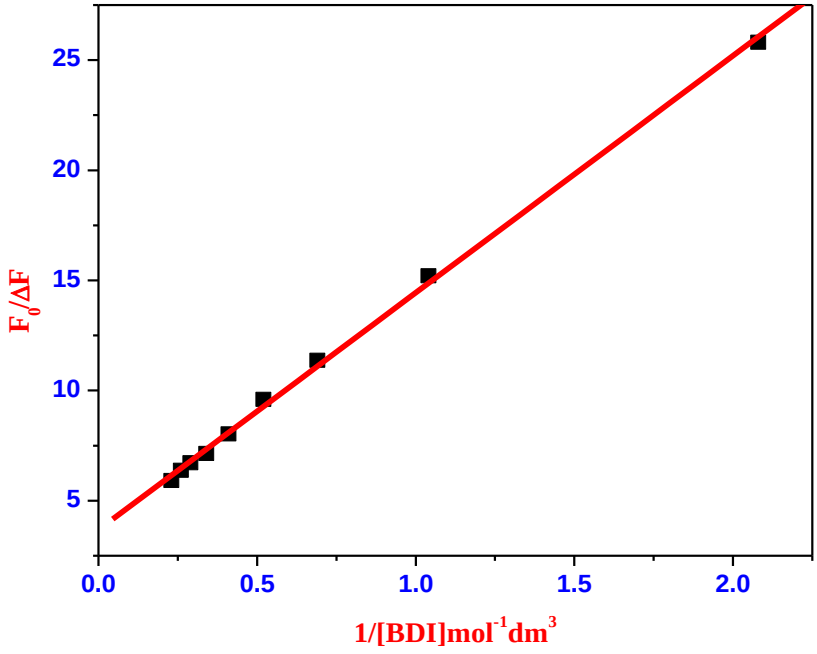

Figure 3. Modified Stern-Volmer plot for BSA-DMTIL complex

Data from emission spectral studies were then utilized to calculate the binding constant and stoichiometry of BSA with DMTIL using the Benesi-Hildebrand equation (Eq. (3)[31].

$$\frac{1}{(F_0 - F)} = \frac{1}{(F_0 - F_1)} + \frac{1}{(F_0 - F_1)K\,[DMTIL]} - \quad (3)$$

Where, F_0 is the emission intensity of BSA in the absence of DMTIL, F is the emission intensity of BSA at intermediate concentration of DMTIL, F_1 is the emission intensity of BSA at infinite concentration of DMTIL and K is the binding constant.

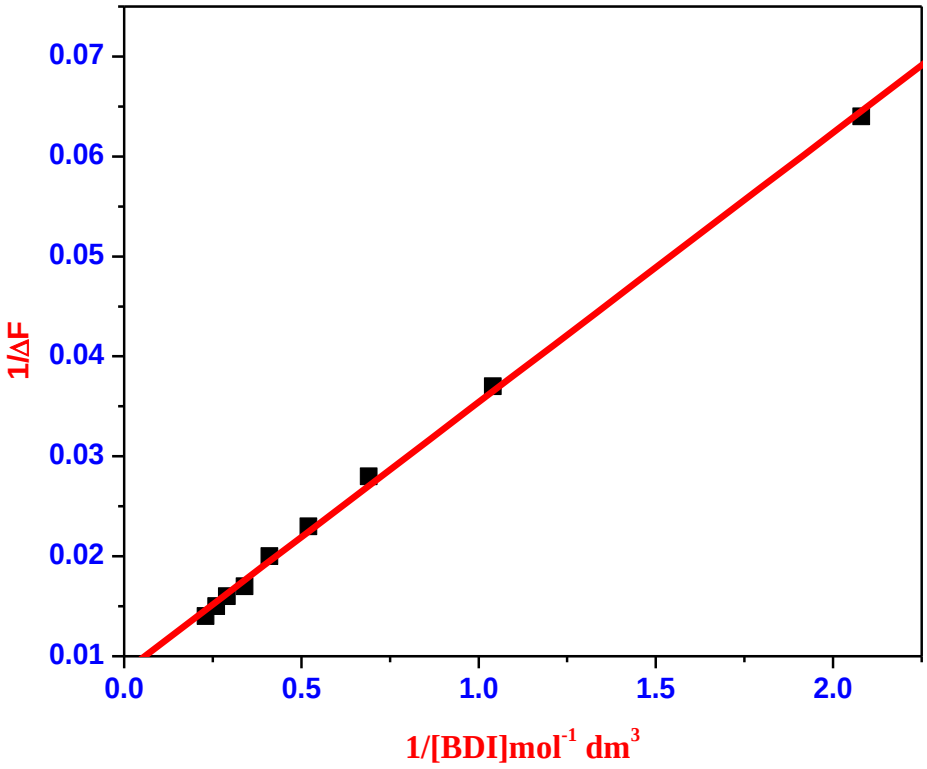

Figure 4. Benesi-Hildebrand plot of 1/[F_0-F] *vs* 1/[DMTIL] for binding of DMTIL with BSA (λ_{ex}= 295 nm).

The double reciprocal plot of BSA with DMTIL is shown in **Figure 4** It can be seen from **Figure 4** the plot of 1/[F_0-F] *vs* 1/[DMTIL] abides by a linear regression indicating the formation of a 1:1 stoichiometry between DMTIL and BSA. It is widely accepted that the linearity in Benesi-Hildebrand plot is indicative of one-to-one complexation and deviation from non-linearity is a scribed to the involvement of 1:2 complexation. It has also been reported earlier by our group that for a system involving one-to-one complexation process a modified Benesi-Hildebrand plot of 1/[F_0-F] *vs* 1/[AZA]^2 would result in a non-linear plot[28]. Thus, in order to establish the existence of 1:1 binding stoichiometry and to exclude the possibility of 1:2 complexation of DMTIL with BSA we have employed a modified Benesi-Hildebrand plot. As shown in the inset of

Figure 4 the plot of 1/[F_0-F] *vs* 1/[DMTIL]^2 showed a deviation from linearity. This clearly suggests the occurrence of one to one complexation between DMTIL and BSA. The binding constant value determined from the ratio of intercept and slope of B-H plot is listed in **Table 1**

The free energy change for the interaction of DMTIL with BSA was estimated by using the following equation (Eq. (4))[10].

$$\Delta G = -RT \ln K \text{----- (4)}$$

where, ΔG is free energy change, R is universal gas constant and T is room temperature (298 K), K is analogous to binding constant value obtained from Benesi-Hildebrand equation respectively. The free energy (ΔG) change for the complexation process of DMTIL and BSA is evaluated as -25.62 kJ mol^{-1}. The negative free energy change value indicates that the complexation process of DMTIL with BSA was spontaneous and it is highly favorable. In general the negative free energy change is indicative of hydrophobic and hydrogen bonding in biomolecular-ligand interactions. Therefore in the present case, it is inferred that hydrophobic and hydrogen bonding played a crucial role in the binding of DMTIL with BSA. However, the role of other possible interactions such as electrostatic, multiple hydrogen bonds, van der waals interactions and steric contacts cannot be ruled out. Moreover, it is well known that Serum albumins possess a net negative charge at physiological pH, whereas DMTIL carries a positive charge in aqueous solution[28-34]. Hence, the binding of DMTIL to BSA might involve electrostatic interactions as well.

The monitoring of BSA-DMTIL binding equilibrium was further extended by subjecting the quenching data to the following equation (Eq (5)), which describes the equilibrium between free and bound molecules when small molecules bind independently to a set of equivalent sites in a macromolecule[35].

$$\log\left[\frac{F_0 - F}{F}\right] = \log K_b + n \log [Q] - (5)$$

where, F_0, F and [Q] are the same as in (Eq. (1)), *n* is the number of binding sites and K_b is the binding constant. Elucidation of binding parameters from emission quenching data on the basis of the afore mentioned equation (Eqn (5)) has been extensively utilized in the literature. The representative double logarithmic plot of log [(F_0-F)/F] *vs* log [Q], shown in **Figure 5** produced a linear plot with a slope value close to

1 (*n*). The average binding number for one DMTIL molecule (*n*) is approximately equal to 1 BSA-DMTIL system (1.09). The results thus obtained, indicates the presence of single class of binding site for DMTIL in BSA. Furthermore, the observed value complement the findings of 1:1 binding stoichiometry in the previous section. The calculated binding parameters of BSA-DMTIL complex is listed in **Table 1** The binding constant value obtained from the double logarithmic plot was found to be in good agreement with literature reports and it indicates a moderately strong binding of DMTIL with BSA[27-29-32].

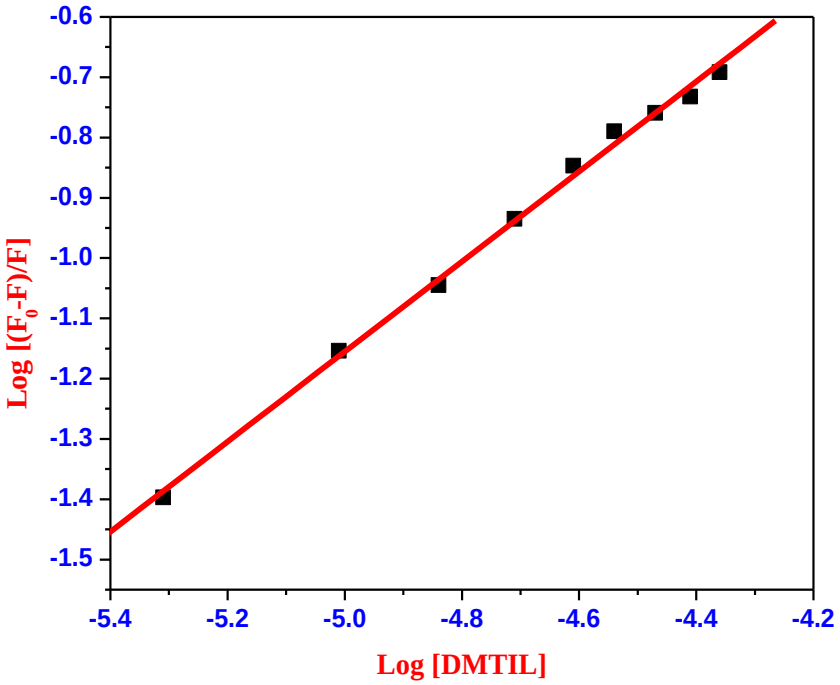

Figure 5. Double logarithmic plot for BSA-DMTIL complex.

Table 1. Binding parameters of BSA-DMTIL complex

Binding Parameters	K_{sv}[a] ($dm^3\ mol^{-1}$)	K_q ($dm^3 mol^{-1}s^{-1}$)	K_a[a] ($dm^3\ mol^{-1}$)	K^a ($dm^3\ mol^{-1}$)	K_b[a] ($dm^3\ mol^{-1}$)	**n**
BSA	**4.60×10^4**	**4.60×10^{12}**	**3.40×10^4**	**3.10×10^4**	**0.63×10^4**	**0.85**

[a] The mean value of three individual experiments with standard deviation (S.D.).

The binding interaction of DMTIL with BSA has been confirmed by emission quenching studies. However, binding induced structural and micro environmental change in BSA needs to be ascertained. Therefore in the present investigation, we have utilized UV-vis absorption, CD, and three dimensional fluorescence spectroscopic techniques to investigate the conformational changes of BSA.

The influence of DMTIL binding interaction on the protein secondary structure has been ascertained by monitoring the far-UV CD spectra of the protein in the presence of increasing concentration of DMTIL and the results are displayed in **Figure 6** As reported in the literature, the CD spectra for BSA monitored in the range 200 nm-260 nm revealed the presence of two bands at 208 nm and 222 nm, which are characteristic of the α-helical structure in proteins. As depicted in **Figure 6** in the presence of DMTIL the far-UV CD spectra of BSA showed appreciable decrease without any shift in the peak positions. This indicates that binding interaction of DMTIL induces some modification in the secondary structural content of BSA. The lowering in the negative ellipticity points toward a decrease in the helical content which dictates unfolding of the peptide strand even more. To get deep insight into the results of far-UV CD spectra of BSA in the presence of DMTIL, the percentage α-helical content of BSA was calculated from (Eq (6)) and (Eq(7))[36].

$$\mathrm{MRE} = \frac{\mathrm{ObservedCD(mdeg)}}{[\mathrm{C_P nl\ x\ 10}]} - (6)$$

$$\alpha - \mathrm{Helix}(\%) = \left[\frac{-\mathrm{MRE}_{208} - 4000}{33000 - 4000}\right] \mathrm{x}\ 100 - (7)$$

where, C_P is the molar concentration of the protein, n is the number of amino acid residues (583 amino acids for BSA) and l is the path length of the cell. Where, MRE 208 is the observed MRE value at 208 nm, 4000 is the MRE of the β-form and random coil conformation cross at 208 nm and 33000 is the MRE value of a pure α-helix at 208 nm.

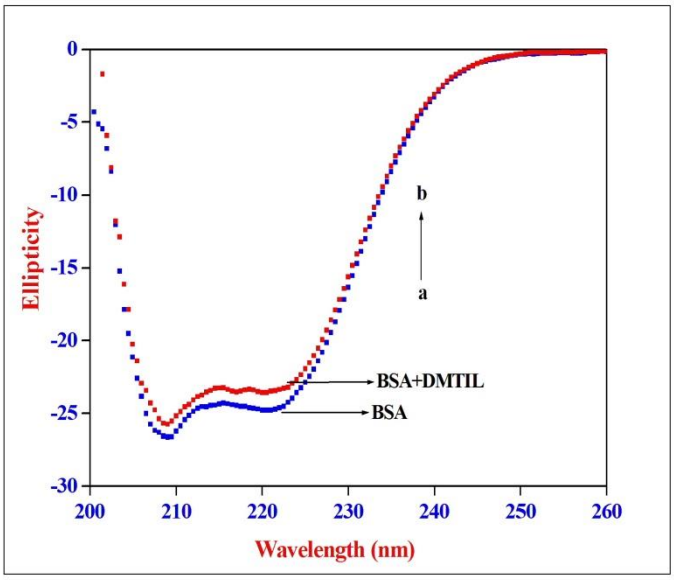

Figure 6. CD spectra of BSA in presence of DMTIL. conditions: [BSA] = 2.0×10^{-6} mol dm^{-3}; [DMTIL] = 2.0×10^{-6} mol dm^{-3}.

According to the (Eq (6)) and (Eq (7)), the estimated α-helicity content of free BSA in PBS buffer (pH = 7.40 and atT= 298 K) was 64.00%, which is in reasonable accord with the reported literature. The percentage α-helix content of BSA in the presence of DMTIL showed a decrease from 64.00 % to 61.29 % (BSA + DMTIL complex). The decrease in the α-helix content suggest that DMTIL altered the secondary structure of protein, which turn induces changes in the atomic arrangement and their hydrogen bonding network. Thus, the results from CD spectral studies enabled us to conclude that the interaction of DMTIL induced partial unfolding of the secondary structure of BSA.

Absorption spectral measurements were used to investigate the behaviour of protein in the presence of ligand and also to explore the structural aspects and micro environmental changes of proteins[42]. The absorption spectra of BSA in the presence of varying concentrations of DMTIL and the resulting spectra are displayed in **Figure 7.** In the absence of DMTIL, BSA exhibits an absorbance maximum at 278 nm which mainly originates from aromatic residues and disulfide bonds in the protein[28]. As shown in **Figure 7** the addition of increasing concentration of DMTIL to BSA resulted in the increase in absorption intensity at 278 nm without any shift in absorption maxima. In the recent past, similar kind of observations in the absorption spectral profile of proteins has been attributed to the interaction of ligand with proteins and complexation induced secondary structural changes in protein[28-32]. Thus, in the present case the DMTIL induced absorption

spectral changes of BSA is solely attributed to the interaction of BSA with DMTIL. In addition, the present set of observations also advocates that the binding of DMTIL induced some molecular micro environmental and conformational changes in BSA. Further, it is well accepted that the dynamic quenching is largely caused by the collision. According to the collisional quenching mechanism, absorption spectrum of BSA would have no change. Whereas, static quenching involves the formation of ground state complex between the protein and ligand, as a result the absorption spectrum of BSA would change[34]. From the absorption spectral analysis of BSA and DMTIL, we come to a conclusion that the increase in absorption spectra is primarily due to the formation of ground state complex between BSA and DMTIL.

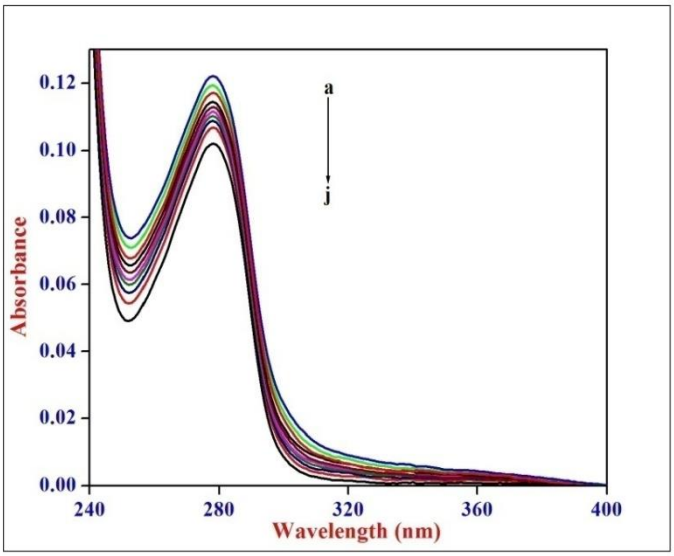

Figure 7. Absorption spectra of BSA (2.00×10^{-6} mol dm^{-3}) at various DMTIL concentrations. [DMTIL]: (a) 0, (b) 4.80×10^{-6}, (c) 9.60×10^{-6}, (d) 14.40×10^{-6}, (e) 19.20×10^{-6}, (f) 24.00×10^{-6}, (g) 28.80×10^{-6}, (h) 33.60×10^{-6} (i) $38.40 \times 10^{-6}$and (j) 43.20×10^{-6} mol dm^{-3}.

The effect of DMTIL on BSA synchronous fluorescence spectra are depicted in **Figure 8(A)** and **Figure 8(B)**. As shown in **Figures 8 (A&B)**, the synchronous emission intensity decreased gradually upon the addition of DMTIL. This observation further substantiates the occurrence of emission quenching in the association process of DMTIL-BSA. It is evident from **Figure 8(A)** that at $\Delta\lambda$=15nm, the maximum emission wavelength corresponding to Tyr residue showed no significant change in the presence DMTIL ionic liquids. However at $\Delta\lambda$=60 nm, the emission maxima is slightly blue shifted from 344 nm

to 341nm. The DMTIL induced blue shift signifies that the microenvironment around the fluorescent aromatic residues of the protein (Trp) in nonpolar hydrophobic environment is changed and it is associated with the decrease in hydrophilicity after interaction with the ionic liquid.

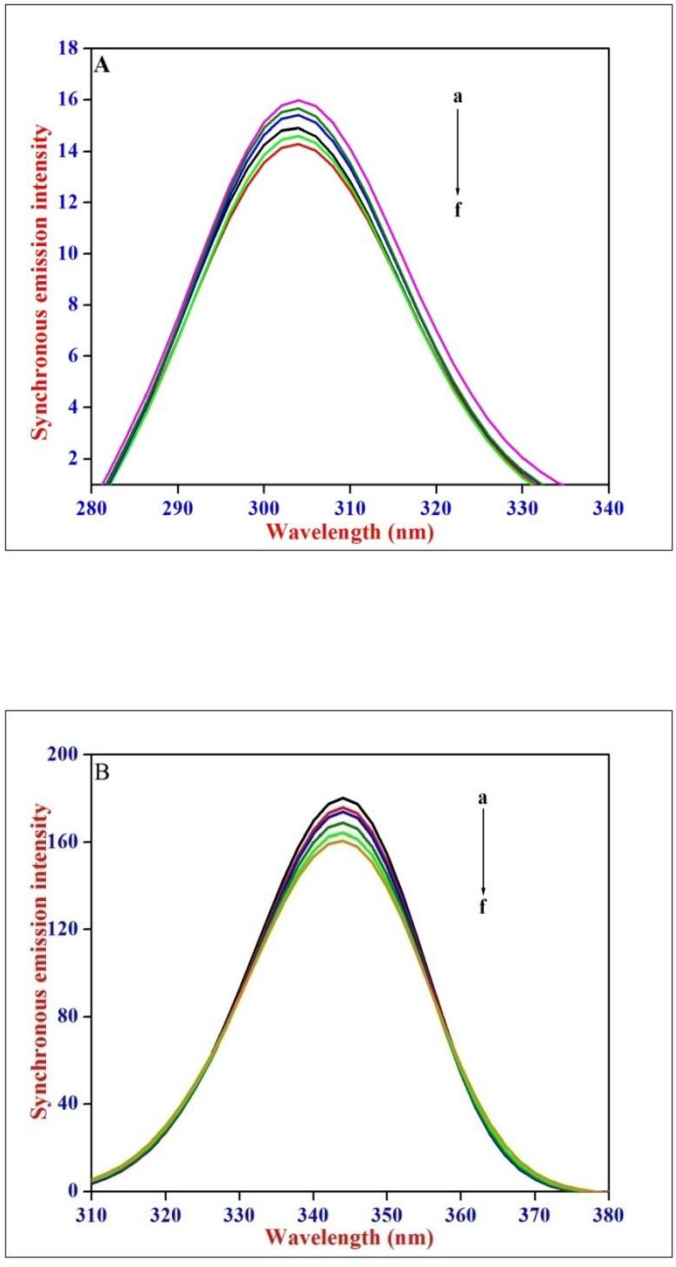

Figure 8. Synchronous emission spectra of **(A)** BSA at Δλ=15 nm and **(B)** BSA at Δλ=60 nm

The DMTIL induced conformational and microenvironmental changes of BSA were investigated by 3D emission spectrum comparing the spectral changes in the absence and presence of DMTIL and the resultant spectral data are shown in **Figures 9 (A&B).** From **Figure 9(A)** it can be noticed that the 3D emission spectrum of BSA exhibits two peaks namely peak 1 and peak 2. Peak 1 is the Rayleigh scattering peak ($\lambda_{em}=\lambda_{ex}$). Peak 2 reveals the spectral behaviour of Trp and Tyr residues of BSA and it is closely related to micro environmental polarity around these residues[40]. As shown in **Figure 9(B)** in the presence of DMTIL, the emission intensity of peak 1 is increased. The possible reason for this phenomenon is that the interaction of DMTIL with BSA could have caused an increase in the diameter of the macromolecule, which in turn resulted in an enhanced scattering effect. The enhancement in Rayleigh scattering peak of serum proteins upon ligand binding is widely reported in literature[28-40]. Further, it is evident from figure that the emission intensity of peak 2 showed a sharp decrease upon the addition of DMTIL to BSA. The observed changes in the emission intensity of peak 1 and peak 2 indicate that the interaction of DMTIL with BSA have induced changes in the secondary structure of BSA. From the above spectral implications, it can be concluded that the interaction of DMTIL with BSA has induced a slight conformational change in the protein structure and this result was in good accord with the absorbance and CD spectral measurements.

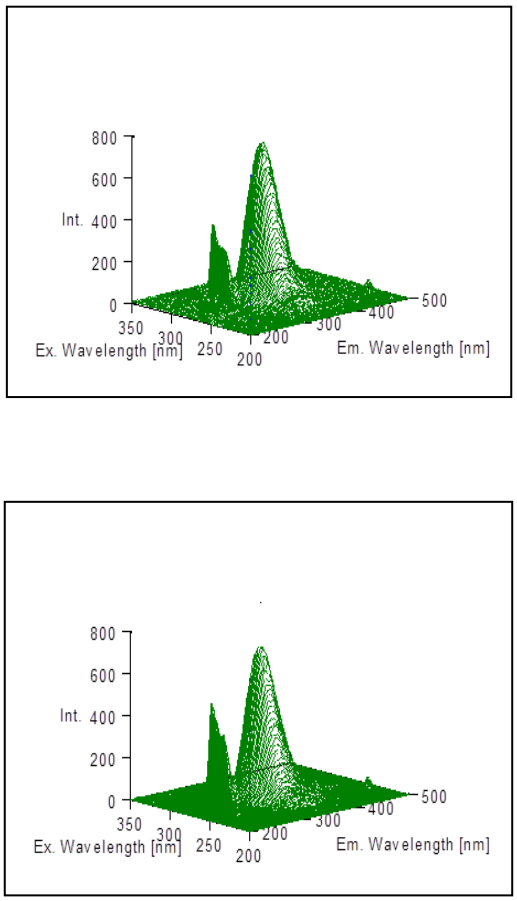

Figure 9. Three dimensional emission spectra of **(A)** BSA-alone and **(B)** BSA-DMTIL.

To understand the binding mechanism of DMTIL with BSA, the knowledge of exact binding location of the ionic liquid within the macromolecule is very crucial and important[41]. Herein, the DMTIL binding site in BSA has been explored on the basis of docking simulation. With a view to get an unbiased result in this respect, AutoDock based blind docking has been employed as the actuating strategy. The strategy of AutoDock based blind docking includes a search over the entire surface of the protein for binding sites (and simultaneously optimizes the conformations of the peptides) whereby indulging in an unbiased result, and hence has rightfully been described as ‘‘very encouraging’’ in a recent review[44] and is also receiving enormous attention from various research groups[42-44]. During the docking process, the lowest binding energy conformer was searched out of 25 different conformers for each docking simulation, and the resultant one was used for further analysis. The best ranked result, which has the lowest free energy for BSA is displayed in **Figure 10** The docking summary of BSA-DMTIL complex listed in **Table 2**

provide a convincing evidence for probable binding location of DMTIL in subdomain IB of BSA. The docked pose displayed in **Figure 10** reveals domain IB of the protein to be the favorable binding site for the drug. The principal hydrophobic binding sites in BSA are located in domains II and III, while domain I, characterized by a net negative charge, generally serve as an appropriate binding site for cationic probe molecules. As is usual in a blind docking simulation protocol, we obtained a number of binding sites and the corresponding binding constants and free energies. Compelling evidence for the probable-binding location of the drug in subdomain IB of BSA was derived from the observation that the binding of DMTIL in the IB region was found to be characterized by a favourable binding energy of -4.61 kcal mol^{-1} and a high inhibition constant (418.89 uM). As shown in **Figure 10** the protein residues in the near vicinity (within 4 Å) of the probe, which shows the presence of both hydrophobic residues (Val-118, Phe-130, Pro-114 and Ala-122), as well as charged/polar residues (Met-119 and Lys-133), which evinces the binding phenomenon to be mainly governed by hydrophobic forces with a significant contribution from electrostatic interactions. This observation is further substantiated by the fact that the Subdomain IB, characterized by a net negative charge, can serve as an appropriate binding site for cationic probe molecules.

The free energy change (ΔG) and binding constant (K_b) values estimated from the computational studies for BSA-DMTIL system was found as -19.30 kJ mol^{-1} and 0.24×10^4 dm^3 mol^{-1} respectively. The ΔG and K_b values evaluated from computational studies showed a deviation from that of the experimentally calculated values for BSA-DMTIL system (ΔG = -25.68 kJ mol^{-1} and $K_b = 3.10 \times 10^4$ dm^3 mol^{-1}). The difference in computational and experimental values can be explained based on the fact that X-ray structure of the protein from crystals is different from that of the aqueous system used in the study, which results in the difference of the microenvironment around the ligand[32]. Similar kind of results was observed in coumaroyl tyramine and naringin binding to HSA[32-39-40]. Thus, from the docking simulation studies it is inferred that the existence of hydrophobic interaction and electrostatic interactions played a vital role in DMTIL binding to sub domain IB of BSA. Thus, the molecular docking studies of BSA- DMTIL complex have provided a good structural basis to correlate the results with that of the emission quenching studies of BSA in the presence of DMTIL.

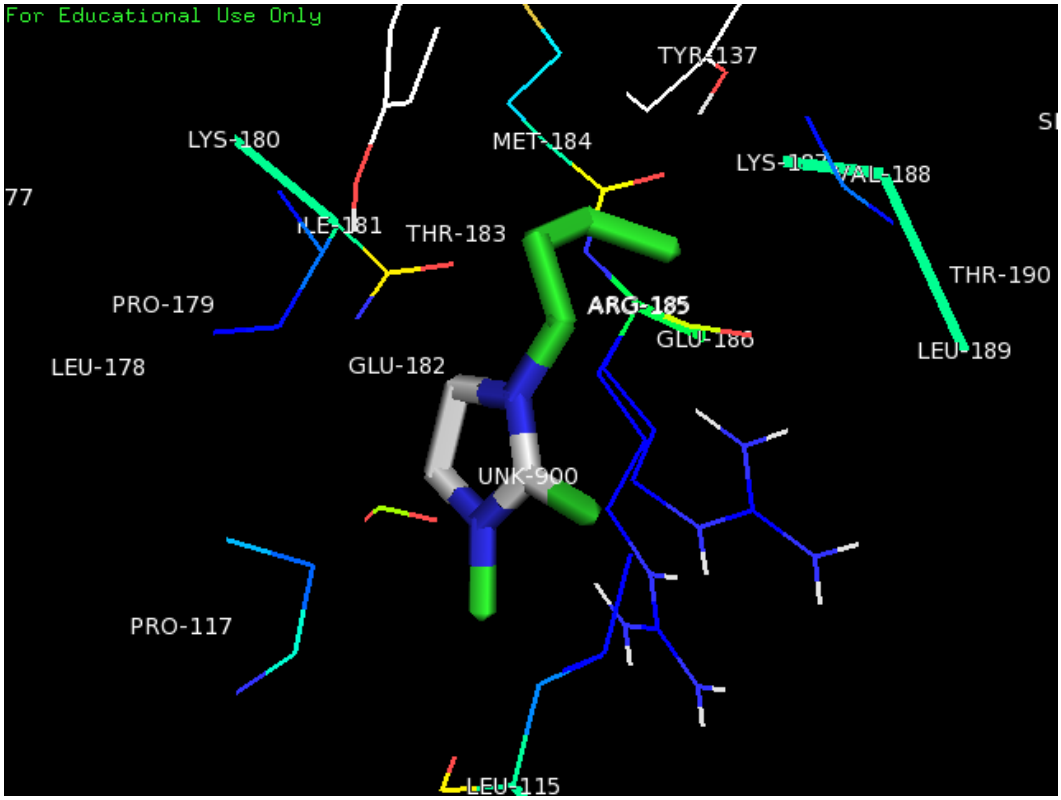

Figure 10. Docked pose of DMTIL with BSA.

Table 2. Docking summary of BSA- DMTIL complex

Rank	Run	Binding Energy	Inhibition Constant (K_i)
1	18	-4.61	418.89 uM
2	24	-4.60	425.84 uM
3	25	-4.51	491.72 uM
4	20	-4.25	767.82 uM
5	19	-4.10	773.17 uM

The present study also focused on an endeavor to explore the important and pertinent issue of binding interaction of prospective organic molecules **5** and **7** with a model transport protein, bovine serum albumin (BSA). The interaction of organic compounds with relevant biological receptors is a field of research which still promises viability for significant exploration. Herein, an attempt is made to unravel the binding location of the drug within the protein by using the AutoDock-based docking.

In order to understand the efficacy of a biologically active drug molecule to function as a therapeutic agent, knowledge of its binding location in the model transport protein environment is very crucial and important. Herein, the drug (**5** and **7**) binding site in BSA has been explored on the basis of docking simulation performed according to the protocol described in experimental section. With a view to evaluating an unbiased result in this respect, the AutoDock-based blind docking has been employed as the actuating strategy. The strategy of AutoDock-based blind docking includes a search over the entire surface of the protein for binding sites (and simultaneously optimizes the conformations of the peptides) whereby indulging in an unbiased result and hence has rightfully been described as ‘‘very encouraging’’ in a recent review and is also receiving enormous attention from various research groups[42-44].

During the docking process, the lowest binding energy conformer was searched out of 25 different conformers for each docking simulation and the resultant one was used for further analysis. The best ranked result, which has the lowest free energy for BSA is displayed in **Figure 11&12**. The docking summary of **5** and **7** with BSA listed in **Table 3** provide a convincing evidence for probable binding location of both **5** and **7** in BSA macromolecule. The docked pose displayed in **Figure 11** reveals domain IB of the protein to be the favorable binding site for **5**. The principal hydrophobic binding sites in BSA are located in domains II and III, while domain I, characterized by a net negative charge, generally serve as an appropriate binding site for cationic probe molecules. As is usual in a blind docking simulation protocol, we obtained a number of binding sites and the corresponding binding constants and free energies. Compelling evidence for the probable-binding location of the drug in subdomain IB of BSA was derived from the observation that the binding of **5** in the IB region was found to be characterized by a favourable binding energy of -9.44 kcal/mol and a high inhibition constant (119.47 nM). As shown in **Figure 11** the protein residues in the near vicinity of the **5** clearly shows the presence of both hydrophobic residues as well as charged/polar residues, which evinces the binding phenomenon to be mainly governed by hydrophobic forces with a significant contribution from electrostatic and hydrogen bonding interactions. This observation is further substantiated by the formation of one hydrogen bond between ASP118 and HN atom of **5**. The H-bond length between ASP118 and HN atom of **5** is 2.049 Å and it showed a considerable binding energy value of -9.44 kcal/mol. Thus, from the docking simulation studies it is inferred that the existence of hydrophobic, electrostatic and hydrogen bonding

interactions played a vital role in **5** binding to sub domain IB of BSA. Thus, the molecular docking studies of BSA- DMTIL complex have provided a good structural basis to correlate the results with that of the emission quenching studies of BSA in the presence of DMTIL.

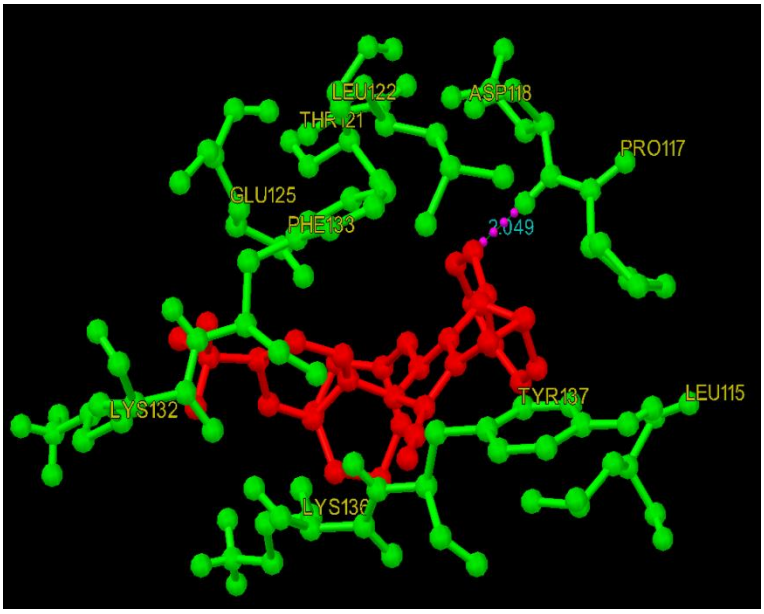

Figure 11. Docked pose of **5** with BSA.

The docking pose of **7** with BSA is displayed in **Figure 12** As evidenced from **Figure 12** it is clear that **7** also binds to BSA in the same subdomain I as that of **5**. This clearly shows that the presence of additional ring in **7** did not bring about significant change in its binding location in BSA. The exact binding location of **7** in subdomain IB of BSA was derived from the observation that the binding of **7** in the IB region was found to be characterized by a high binding energy of -10.31 kcal/mol and a high inhibition constant (27.59 nM). As depicted in **Figure 12** the protein residues in the near vicinity of the **7** is surrounded by both hydrophobic residues as well as charged/polar residues, which clearly indicates that the binding phenomenon is mainly governed by hydrophobic forces with a significant contribution from electrostatic and hydrogen bonding interactions. This observation is further supported by the formation of two hydrogen bonds between ASP 108 and **7** (**5** and O atoms). The bond length of two hydrogen bonds between ASP 108 and **7** are found to be 3.4 Å and 3.6 Å respectively and it showed a considerably high binding

energy value of -10.31 kcal/mol. Thus, from the docking simulation studies it is inferred that the existence of hydrophobic, electrostatic and hydrogen bonding interactions played a crucial role in the binding of **7** to sub domain IB of BSA. Thus, the molecular docking studies of BSA-**7** complex have provided a good structural basis to correlate the biological significance of synthesized compound.

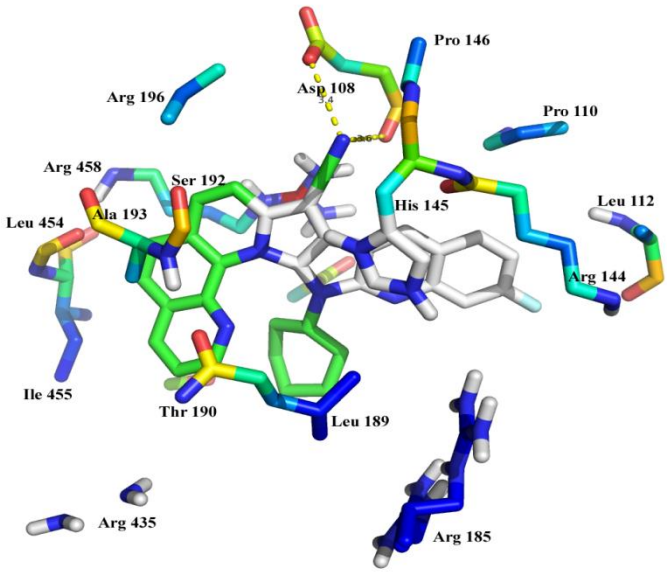

Figure 12. Docked pose of **7** with BSA

Table 3. Docking summary of BSA- synthesized compound **5** and **7** complex

Rank	Run		Binding Energy kcal/mol		Inhibition Constant (K_i)	
	5	**7**	**5**	**7**	**5**	**7**
1	1	4	-9.44	-10.31	119.47 nM	27.59 nM
2	14	9	-8.77	-10.10	372.90 nM	39.73 nM
3	18	14	-8.56	-9.40	493.85 nM	128.49 nM
4	8	20	-8.60	-8.93	846.27 nM	285.05 nM
5	20	13	-7.60	-8.37	2.680 uM	729.17 nM

In conclusion, an easy and rapid method to synthesize fluorine containing pyrrolophenanthrolines with appreciable yield via. green solvent assisted approach was developed. The catalytic application in isocyanide-based multicomponent reaction using DMTIL offered good yield. The trifluoromethylated pyrrolophenanthroline **5** and fluoroquinoline pyrrolophenanthroline **7** BSA complex have provided a good structural basis to correlate the biological significance of synthesized compound **5** and **7**. Docking study of the novel 5 and 7 shows these compounds act as inhibitors. Furthermore, the outcome of this present investigation provides a deep insight into the interaction mechanism of BSA with DMTIL. The emission spectral studies along with high binding constant and free energy values suggested that the interaction between DMTIL and BSA was strong and the binding of DMTIL to BSA is a spontaneous process. The Stern–Volmer analysis of DMTIL induced emission quenching of BSA indicated the existence of static quenching mechanism. The results from CD, synchronous emission, 3D-emission and steady-state absorption spectroscopic studies enabled us to conclude the conformational and micro environmental changes of BSA upon binding with DMTIL. The binding location of DMTIL in BSA has been explored through molecular docking studies which suggested site I as the favourable binding site for DMTIL. The binding studies of ILs such as DMTIL with BSA are of great importance due to their toxic nature. The present study confesses important information regarding the nature of DMTIL binding to BSA and the existence of molecular interactions between them.

References:

(1) Dolle, R.E.; Nelson, K. H. *J. Comb. Chem*. **1999**, 1, 235.

(2) Pereiro, A. B.; Araujo, J. M. M.; Martinho, S.; Filipa, A.; Sara, N.; Ana, M.; Duarte, C. M. M.; Rebelo, L. N.; Marrucho, I. M. *ACS. Sust. Chem. Eng*., **2013**, 1 (4) 427.

(3) Irini, A. Z. *Curr. Opi. Chem. Bio*. **2008**, 3, 12, 324.

(4) Young, L. S.; Berlin, O. G.; Inderlied, C. B. *Am J Med*. **1987,** 82, 23.

(5) Andersson, M. I.; MacGowan., A. P. *J. Antimicro. Chem*. **2003**, 51,

(6) Andrea, B.; Vito, L.; *Coord*.*Chem. Rev*. **2010**, 254, 2096.

(7) Hu, Y. Z.; Xiang, Q.; Thummel, R .P. *Inorg. Chem.* **2002**, 41, 3423.

(8) Genetics and Medicinal Applications; Peters, T. J., Academic Press: San Diego, CA, **1996**.

(9) Site-specific photocleavage of proteins; Kumar, C. V., Buranaprapuk, A. S. Angew. Chem. Int. Eds.; Engl. **1997**.

(10) Singer, S.J.; Nicolson, G.L. *Science.* **1972**, 17, 720.

(11) Partridge, W. M. *J. Am. Physiol.* **1987**, 252, 157.

(12) Banerjee, P.; Pramanik, S.; Sarkar, A.; Bhattacharya, S. C. *J. Phys. Chem.* **2009**, 113 11429.

(13) He, X. M.; Carter, D. C. *Nature.* **1992**, 358, 209.

(14) Albumin Advances in Protein Chemistry**;** Peters, T., Serum Academic Press: New York, **1985.**

(15) Helms, M. K.; Peterson, C. E.; Bhagavan, N. V.; Jameson, D. M. *FEBS. Lett.* **1997**, 408, 67.

(16) El-Kemary, M.; Gil, M. A. *J. Med. Chem.* **2007**, 50, 2896.

(17) Li, Z. Y.; Pei, Y. C.; Wang, H. Y.; Fan, J.; Wang**,** J. J. *Trends Anal. Chem.* **2010**, 29 1336.

(18) Rantwijk, F. V.; Sheldon, R. A. *Chem. Rev.* **2007**, 107, 2757.

(19) Sun, P.; D. W. *Anal. Chim. Acta.* **2010**, 6611.

(20) Moniruzzaman, M.; Nakashima, K.; Kamiya, N.; Masahiro, G. M. *J. Biochem. Eng.* **2010**, 48, 295.

(21) Olivier, B. H.; Magna, L.; Morvan, D. *Applied Catalysis. A* .**2010**, 373, 1.

(22) Zhou, Z. B.; Takeda, M.; Ue, M. *J. Fluorine Chem.* **2003**, 123, 127.

(23) Yu, J.; Shi, F.; Gong, L. Z. *Acc. Chem. Res.* **2011**, 44, 1156.

(24) Domling, A.; Wang, W.; Wang, K. *Chem. Rev.* **2012**, 112, 3083.

(25) Ugi, I.; Steinbruckner, C. *Angew. Chem.* **1960,** 72, 267.

(26) Nair, V.; Rajesh, C.; Vinod, A. U.; Bindu, S; Sreekanth, A. R.; Mathen, J. S.; Balagopal, L. *Acc. Chem. Res.* **2003**, 36, 899.

(27) Papadopoulou, A.; Green, R. J.; Frazier, R. A. *J. Agric. Food Chem.* **2005**, 53, 158.

(28) Selva Sharma, A.; Anandakumar, S.; Ilanchelian**,** M. *J. Lumin.* **2014**, 151, 206.

(29) Tian, J.; Liu, J.; He, W.; Hu, Z.; Yao, X.; Chen, X. *Biomacromolecules.* **2004**, 5, 1956.

(30) Principles of Fluorescence Spectroscopy; Lakowicz, J. R., Third eds.; Springer Science + Business Media, New York, **2006**.

(31) Benesi, H.; Hildebrand, J. *J. Am. Chem. Soc.* **1949**, 71, 2703.

(32) Shanmugaraj, K.; Anandakumar, S.; Ilanchelian, M. *J. Photochemistry. Photobiology B: Biology.* **2014**, 131, 43.

(33) Binding Constants, The Measurements of Molecular Complex Stability: Connors, K. A. Wiley: New York, **1987**.

(34) Hu, Y. J.; Liu, Y.; Xiao, X. H. *Biomacromolecules.* **2009**, 10, 517.

(35) Lissi, E.; Calderon, C.; Campos, A. *Photochem.Photobiol.* **2013**, 89, 413.

(36) Kelly, S. M.; Jess T. J.; Price, N. C. *Biochim. BiophysActa.* **2005**, 1751, 119.

(37) Lloyd, J. B. F.; Evett, I. W. *Anal. Chem.* **1977**, 49, 1710.

(38) Naveenraj, S.; Anandan, S. *J. Photochem. Photobiol. C.* **2013**, 14, 53.

(39) Sarkar, M.; Shankar Paul, S.; Mukherjea,K. K. *J. Lumin.* **2013**, 142,220.

(40) Naik, K. M.; Nandibewoor, S. T. *J. Lumin.* **2013**, 143, 484.

(41) Paul, B. K.; Ray, D. l; Guchhait, N. *Phys. Chem. Chem. Phys.* **2013,** 15, 1275.

(42) Morris, G. M.; Huey, R.; Lindstrom, W.; Sanner, M. F.; Belew, R. K. l; Goodsell, D. S.; Olson, A. J. *J. Comput. Chem.* **2009**, 30, 2785.

(43) Monti, S.; Manet, I.; Manoli F.; Marconi, G. *Phys. Chem.Chem. Phys.* **2008**, 10, 6597.

(44) Campbell, S. J.; Gold, N. D.; Jackson, R. M. Westhead, D. R. *Biol.* **2003**, 13, 389.

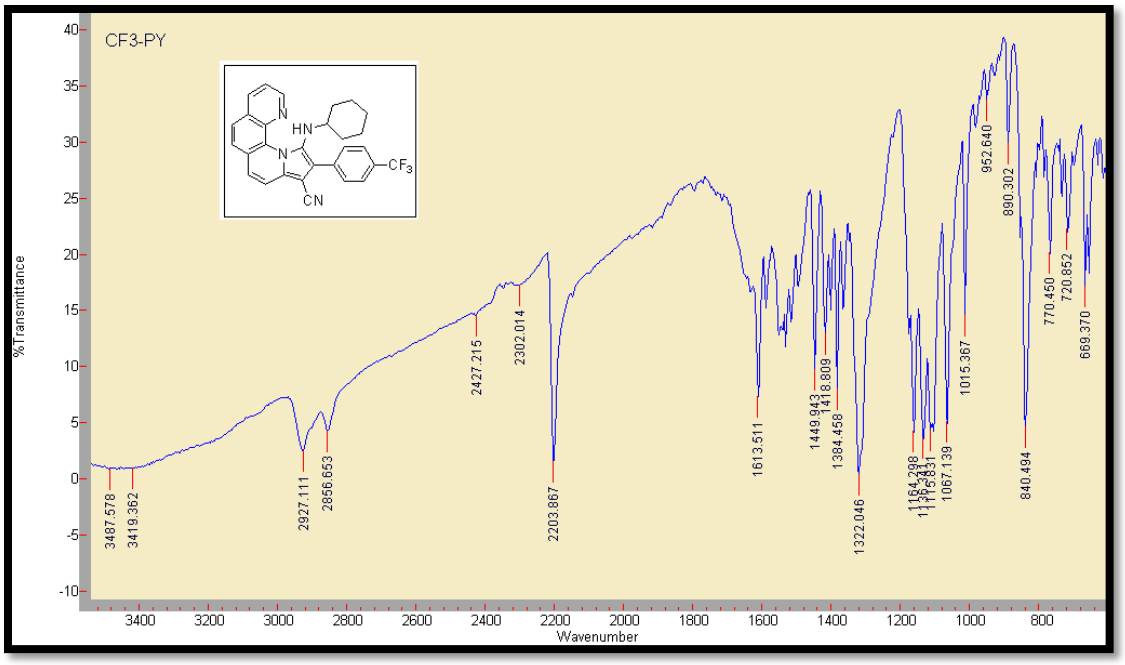

Figure. 3.1 IR Spectrum of **5**

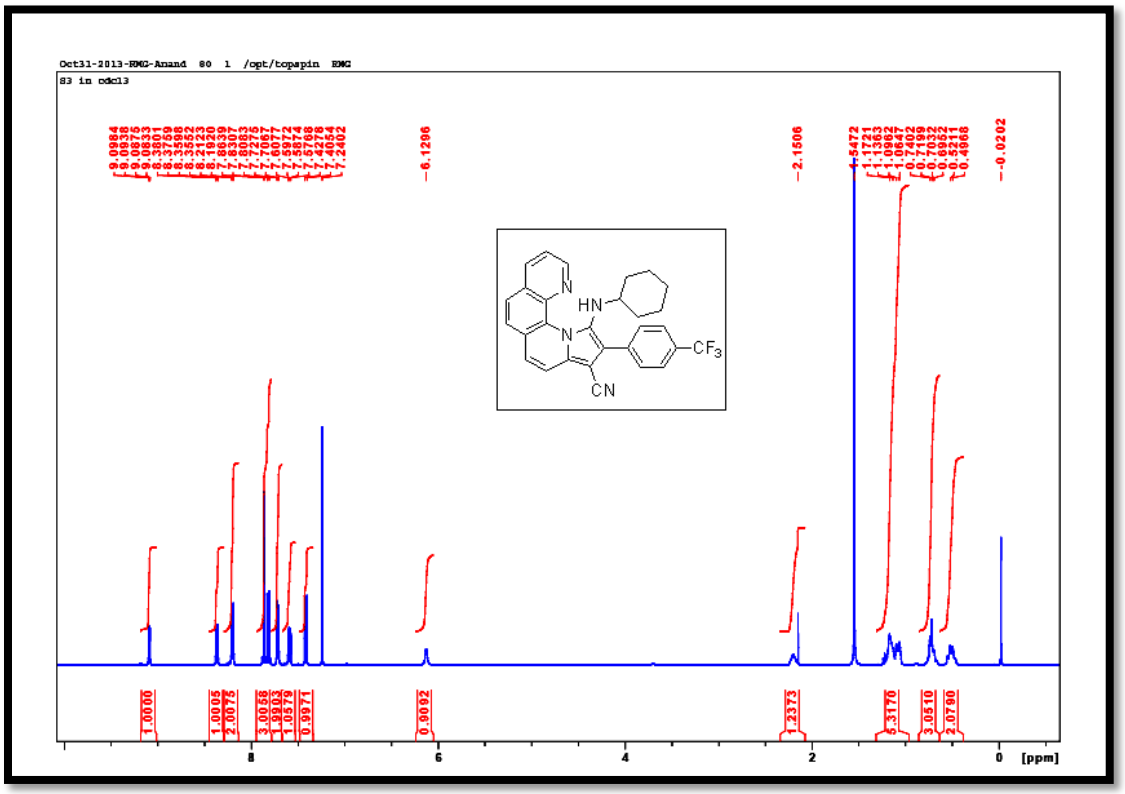

Figure. 3.2 ^{1}H Spectrum of **5**

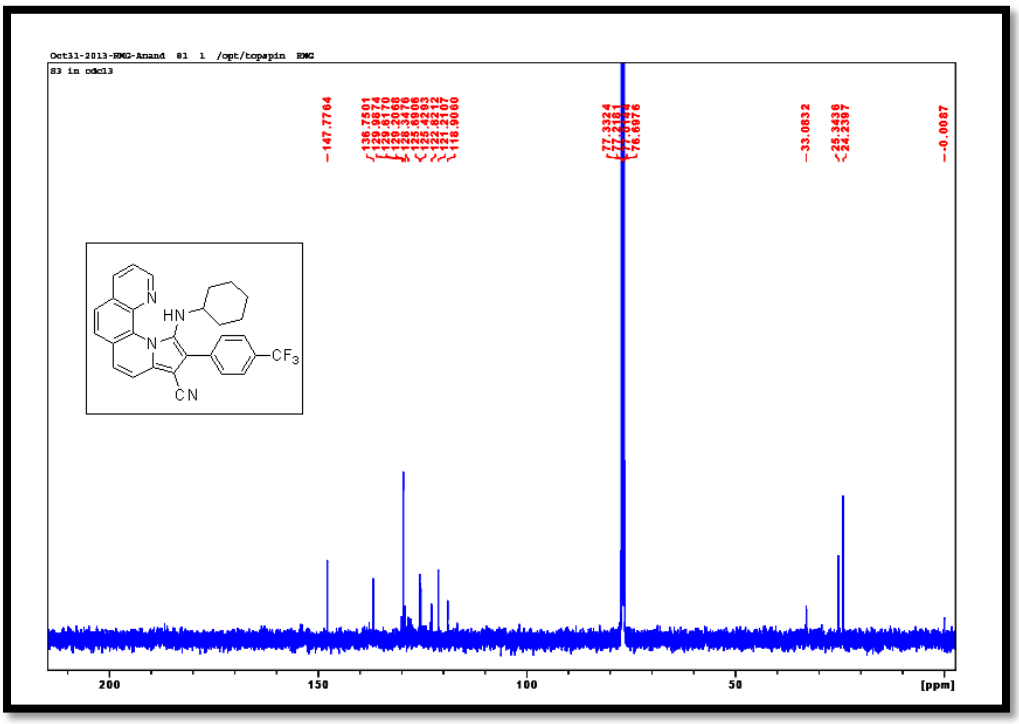

Figure.3.3 ^{13}C Spectrum of **5**

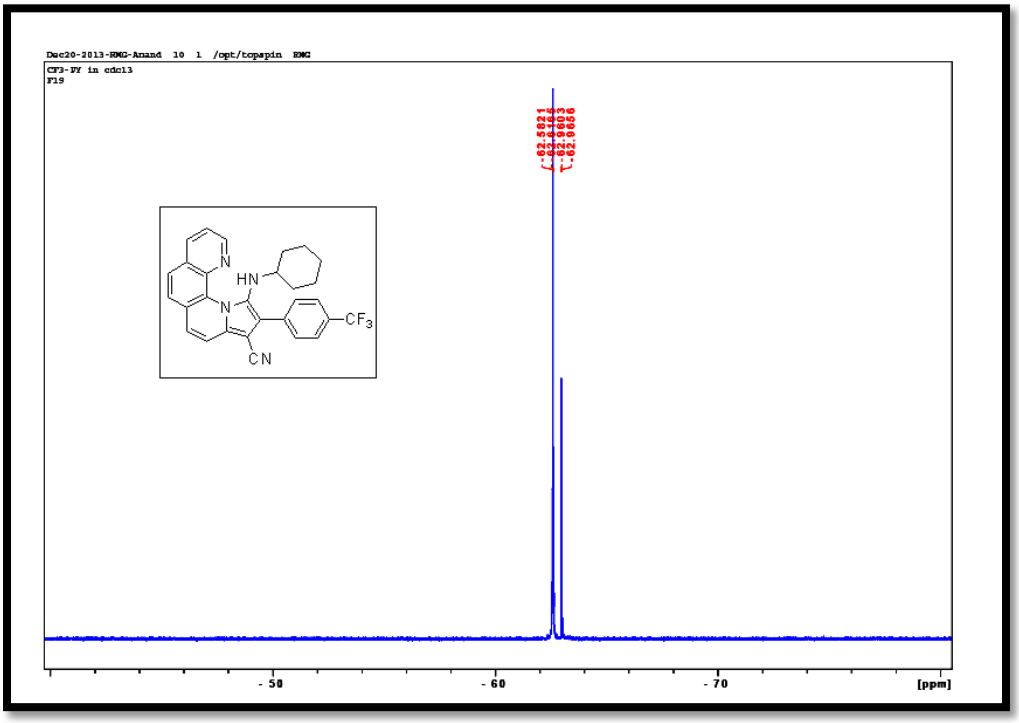

Figure. 3.4 ^{19}F Spectrum of **5**

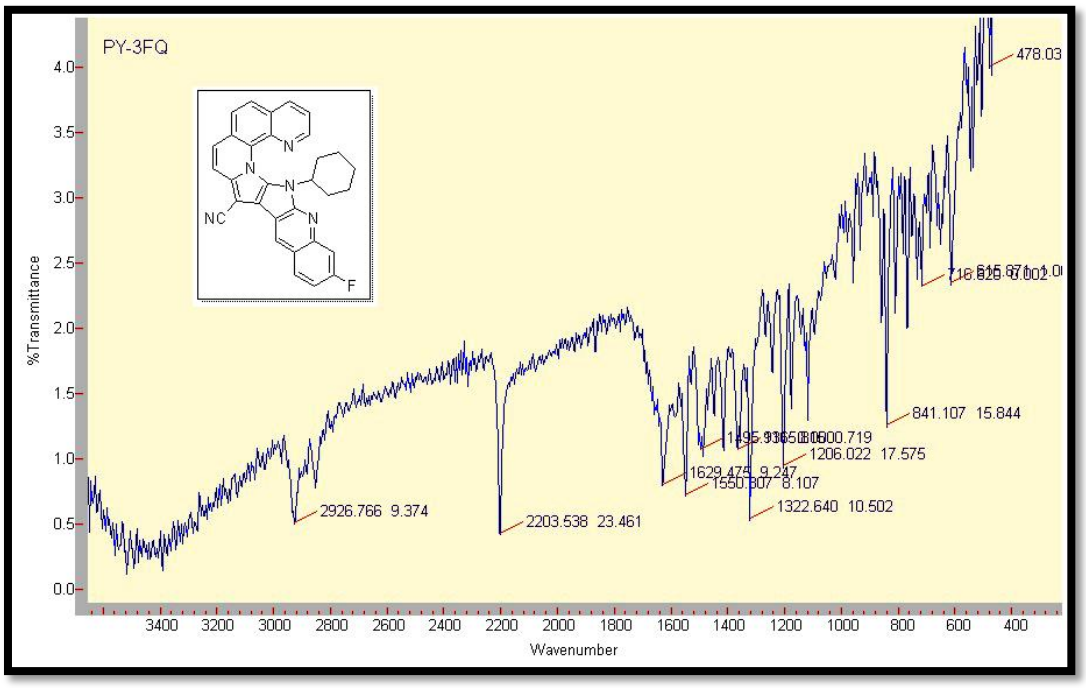

Figure. 3.5 IR Spectrum of **7**

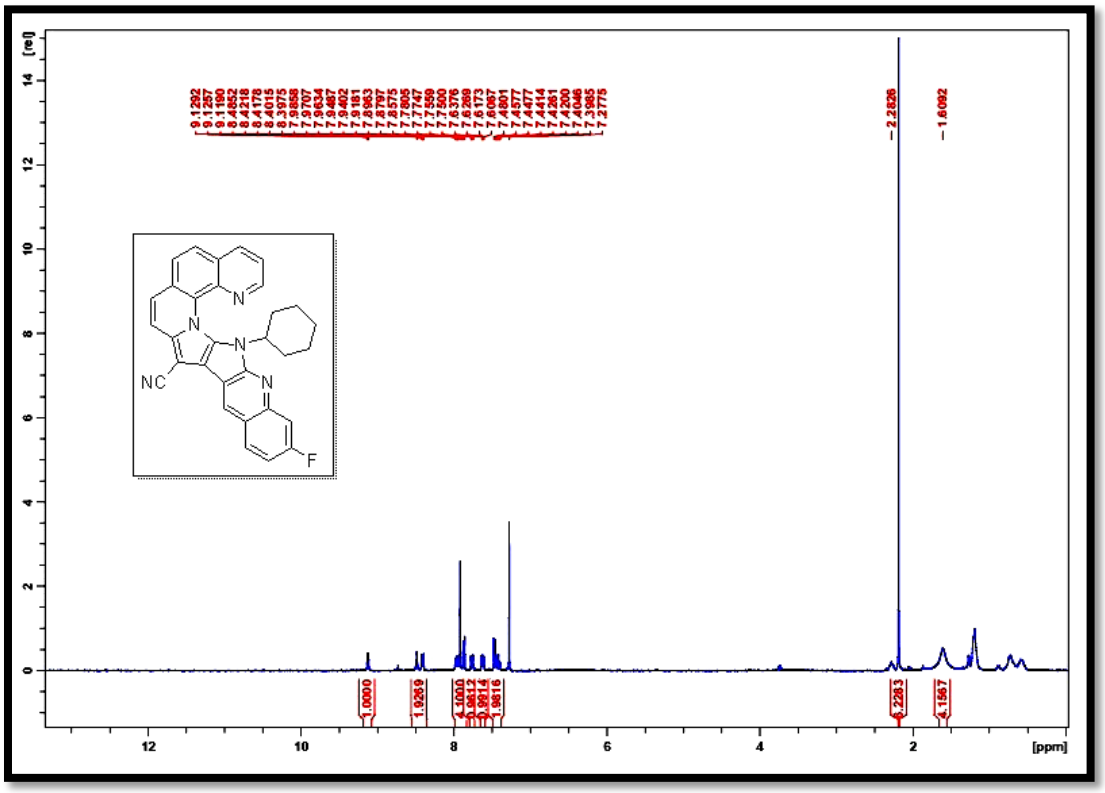

Figure 3.6. ^{1}H Spectrum of **7**

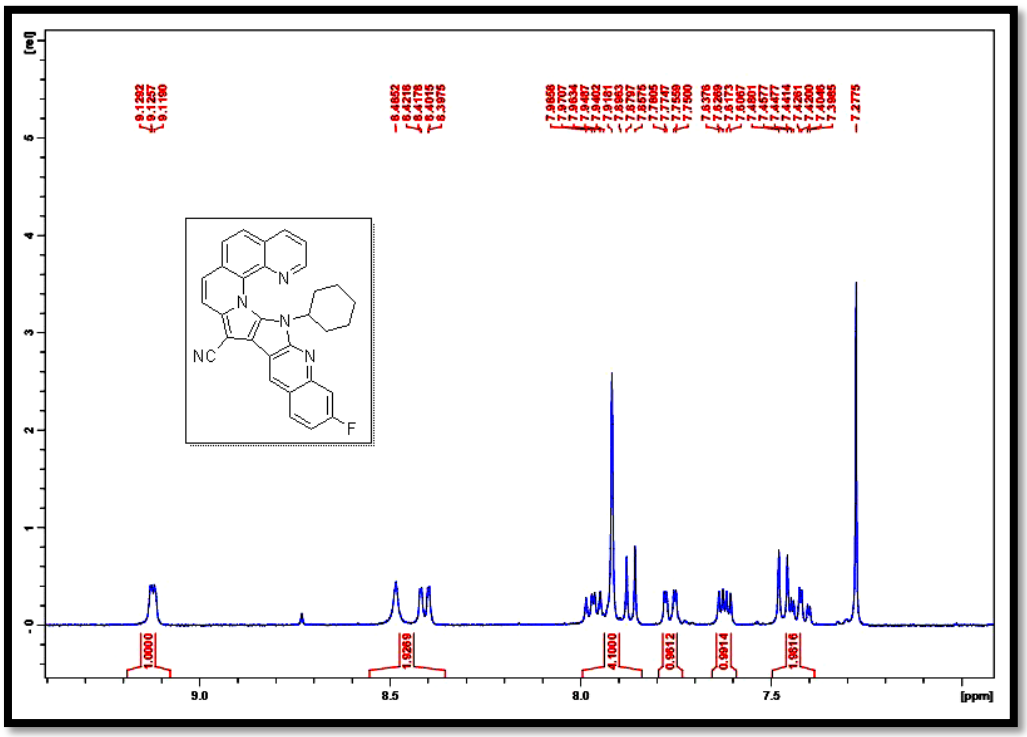

Figure . 3.7 Expanded ^{1}H Spectrum of **7**

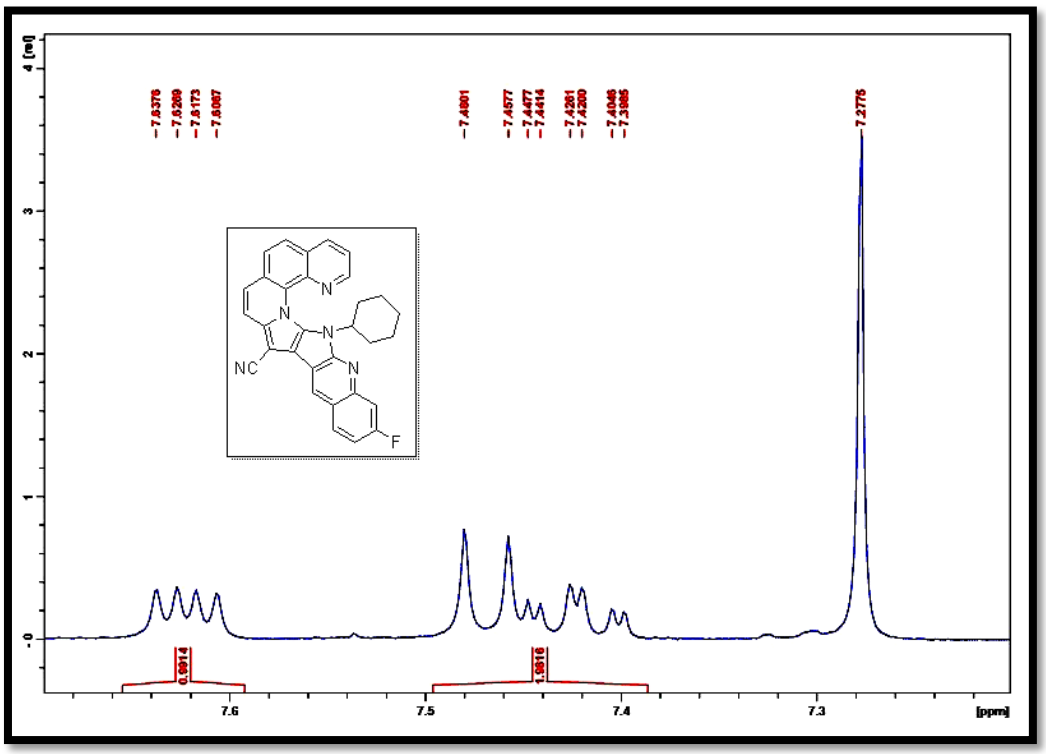

Figure. 3.8 Expanded ^{1}H Spectrum of **7**

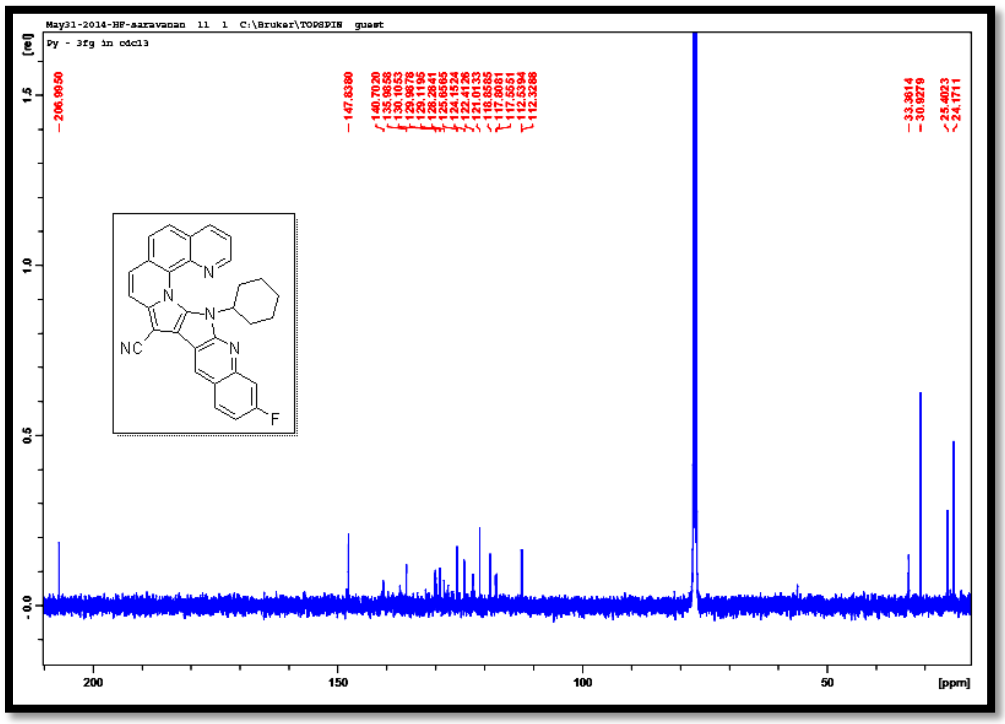

Figure. 3.9 ^{13}C Spectrum of **7**

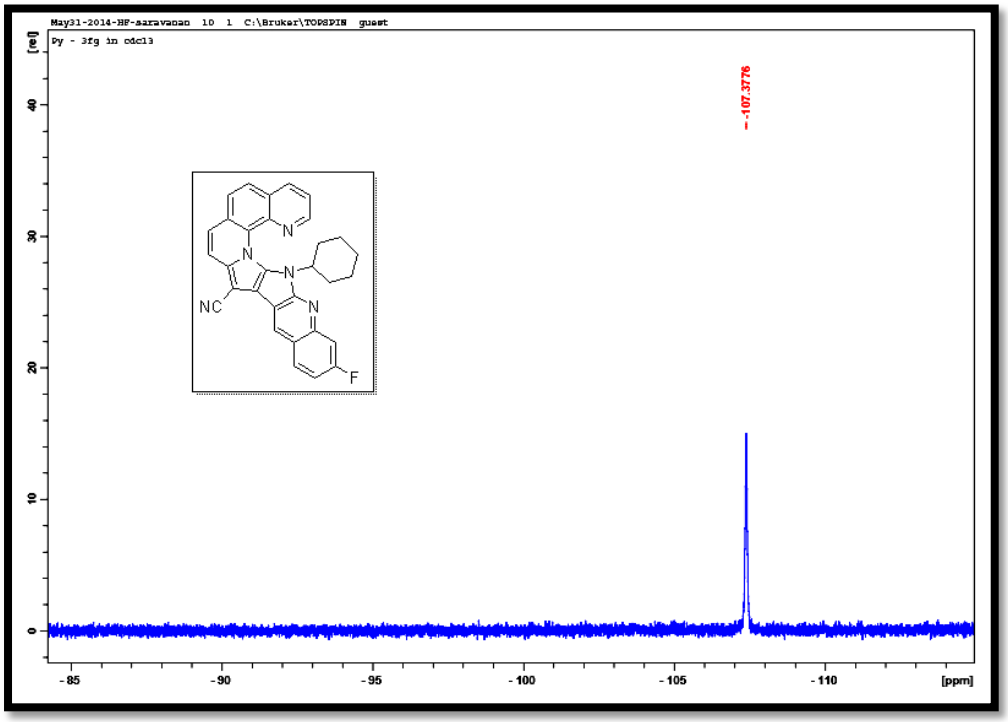

Figure. 3.10 ^{19}F Spectrum of **7**

Chapter 4

Copper boron nitride-catalyzed three component coupling reaction: a convenient synthesis of α-aminophosphonates

CHAPTER IV

Copper boron nitride catalyzed three component coupling reaction: a convenient synthesis of α-aminophosphonates

4.1. Abstract

Various methods are available for the synthesis of α-aminophosphonates; the addition of diethyl phosphite to an imine is most common. This reaction is promoted by catalysts such as BF_3OEt_2, $ZnCl_2$, $MgBr_2$ and Cu-nanoparticles. We report a simple preparative method for a novel copper supported on boron nitride (Cu/BN) catalyst which is subsequently used in a novel one-pot reaction containing an amine, aldehyde and diethyl phosphite. A total of twenty one compounds were synthesized and characterized by IR, ^{1}H-NMR, ^{13}C-NMR and ^{31}P-NMR. The catalyst was prepared by using $Cu(OAc)_2$ and boron nitride in an inert atmosphere and characterized by SEM with EDX and XRD. The effects of solvent and amount of catalyst for the reaction were optimized. Among the solvents, acetonitrile gave the highest yield and was used in all subsequent reactions. The catalyst is found to be a selective and stable solid for a three-component reaction. It could be recovered by simple filtration from the reaction mixture without further treatment and it can be re-used four times with consistent catalytic activity.

4.2. Introduction

Organophosphorus molecules are ubiquitous in nature and find applications in the fields of medicine, agriculture and industry[1–3]. Some organophosphorus compounds are important pesticides[4], bactericides[5–7] and antibiotics[5]. Phosphorus analogues of α-pyrones act as HIV protease inhibitors[8]. α-Aminophosphonic acids constitute important motifs among the organophosphorus compounds in medicinal chemistry due to their obvious structural similarities to α-aminoacids[9,10]. Many natural and synthetic aminophosphonic acids and their ester and peptide derivatives display a wide range of biological activities.

The most common synthetic route to α-aminophosphonic acids is via. chemical manipulation of the corresponding α-aminophosphonates. The hydro phosphonylation of imines is a widely used method for the synthesis of α-aminophosphonates[11]. This is achieved by one of two pathways: (i) in a two-component fashion known as the Pudovik reaction[12] or (ii) by the Kabachnik-Fields reaction which involves an *in situ* formation of imine by condensation of amines with an aldehyde or ketone followed by a hydro

phosphonylation step[13]. The one-pot Kabachnik-Fields reaction is promoted by acidic or basic catalysts, microwave irradiation, or by heating[14]. Several Lewis acid catalysts, such as $InCl_3$[15], base catalysts such as $CaCl_2$ and PPh_3 and other catalysts such as ZnO, TiO_2, tosyl chloride and mesoporous alumino silicate nano cage[16] have also been used to promote this reaction. Boron nitride (BN) is a layered material with a structure similar to graphite. It consists of a planar networks of BN hexagons which are regularly stacked; the continuous boron-nitrogen bonds and many lone pair electrons allows it to coordinate with some metals. We decided to investigate a more feasible and efficient recyclable catalyst which could be applied for the synthesis of α-aminophosphonates.

4.3. Experimental

4.3.1. General

Melting points were determined by using a Stuart SMP10 Melting Point Apparatus and were uncorrected. IR spectra were recorded on Varian Scimitar 1000 FTIR using KBr pellets and the absorption frequencies are expressed in reciprocal centimeters (cm^{-1}). NMR spectra were taken on BRUKER 400 MHz and 600 MHz spectrometer using TMS as an internal reference. The chemical shifts were expressed in parts per million (ppm). A Carl Zeiss Ultra Plus scanning electron microscope with EDX detector was used. X-ray diffraction analyses were conducted with a Philips PW1050 diffractometer set at 1˚/min with a scanning step size of 0.02˚ from 40˚ to 100˚ 2 θ using monochromated CoK_α radiation. Data were captured using a Sietonics 122D automated micro processor linked to the diffractometer.

4.3.2. Preparation of Copper-loaded Boron Nitride catalyst

To a solution of $Cu(OAc)_2$ (28.1 mg, including 9.8 mg of Cu metal; 0.5 wt. % Cu metal vs. BN) in MeOH (50 ml) was added boron nitride (BN) (2.66 g, 0.1 mol) and the suspension was stirred at room temperature for 7 days. The resulting suspension was filtered and the solid was washed with aqueous MeOH and dried under reduced pressure to give the 0.3 % Cu/BN catalyst as a pale green powder of mass 2.55 g (92 % yield).

4.3.3. General procedure for the synthesis of α- aminophosphonates (4a-u)

In a 50 ml round bottom flask, a mixture containing an aldehyde (1 mmol), amine (1 mmol), diethyl phosphite (1 mmol) and Cu/BN (0.25 mg, 0.5 mol % of the substrate) in acetonitrile (6 ml) was refluxed on an oil bath. The progress of the reaction was monitored

by TLC. After completion of the reaction, excess water was added and the organic compound was separated with ethyl acetate (3 × 10 ml) and dried over anhydrous Na_2SO_4. The catalyst was recovered by filtration. Evaporation of the solvent followed by purification on silica gel (eluent ethyl acetate: petroleum ether, 90 %) afforded pure α-aminophosphonates (**Table 1**, entry 4a-4u). The products were characterized by IR, ^{1}H-NMR, ^{13}C-NMR and ^{31}P-NMR.

4.3.3.1. Diethyl (phenyl(phenylamino)methyl)phosphonate (4a)

White solid, (95 % yield). mp: 97-99°C; IR (KBr, cm^{-1}): 3294.34 (N-H), 2982.75 (C-H), 1605.19 (Ar, C-C), 1497.58 (N-H), 1235.98 (P=O), 1059.12 (P-C-O), 751.523 (P-C aliphatic); ^{1}H-NMR (400 MHz, $CDCl_3$): δ (ppm) 1.13 (t, 3H), 1.30 (t, 3H), 3.66–3.75 (m, 1H), 3.91–4.00 (m, 1H), 4.06–4.21 (m, 2H), 4.80 (d, 1H), 4.87 (br, s, 1H), 6.62 (d, 2H), 6.70 (t, 1H), 7.11 (t, 2H), 7.27–7.36 (m, 3H), 7.50 (d, 2H); ^{13}C-NMR (400 MHz, $CDCl_3$): δ (ppm) 146.4180, 145.27, 135.88, 135.85, 128.61, 128.68, 127.95, 127.92, 127.90, 127.85, 118.37, 113.86, 63.39, 63.33, 56.77, 55.27, 16.45; ^{31}P- NMR (400 MHz, $CDCl_3$): δ (ppm) 22.680.

4.3.3.2. Diethyl ((4-chlorophenyl)(phenylamino)methyl)phosphonate (4b)

White solid, (94 % yield). mp: 74-76°C; IR (KBr, cm^{-1}): 3299.232 (N-H), 2984.173 (C-H), 1603.155 (Ar, C-C), 1528.062 (N-H), 1233.475 (P=O), 1047.899 (P-C-O), 748.523 (P-C aliphatic); ^{1}H-NMR (400 MHz, $CDCl_3$): δ (ppm) 1.13 (t, 3H), 1.30 (t, 3H), 3.66–3.75 (m, 1H), 3.91–4.00 (m, 1H), 4.06–4.21 (m, 2H), 4.80 (d, 1H), 4.87 (br, s, 1H), 6.62 (d, 2H), 6.70 (t, 1H), 7.11 (t, 2H), 7.27–7.36 (m, 2H), 7.50 (d, 2H); ^{13}C-NMR (400 MHz, $CDCl_3$): δ (ppm) 146.0667, 145.9214, 134.5802, 134.5504 133.7553, 133.7171, 133.2334, 129.2354, 129.1748, 129.1197, 128.8189, 128.7912, 118.7082, 113.8706, 64.2043, 63.32, 56.31, 54.81, 30.92; ^{31}P-NMR (400 MHz, $CDCl_3$): δ (ppm) 21.1576.

4.3.3.3. Diethyl ((2-nitrophenyl)(phenylamino)methyl)phosphonate (4c)

White solid, (95 % yield). mp: 157-159°C; IR (KBr, cm^{-1}): 3305.42 (N-H), 2984.63 (C-H), 1605.53 (Ar, C-C), 1530.88 (N-H), 1233.65 (P=O), 1020.77 (P-C-O), 756.93 (P-C aliphatic); ^{1}H-NMR (400 MHz, $CDCl_3$): δ (ppm) 1.11 (t, 3H), 1.33 (t, 3H), 3.77–3.88 (m, 1H), 3.92–4.02 (m, 1H), 4.12–4.26 (m, 2H), 5.05 (br, s, 1H), 6.20 (d, 1H), 6.71 (d, 2H), 6.76 (t, 1H), 7.15–7.19 (m, 2H), 7.42–7.46 (m, 1H), 7.57 (t, 1H), 7.76–7.78 (m, 1H), 8.03 (d, 2H); ^{13}C-NMR (400 MHz, $CDCl_3$): δ (ppm) 149.47, 149.42, 145.40, 145.26, 133.63, 133.50, 131.97, 131.95, 129.44, 128.81, 128.77, 128.55, 128.52, 125.27,

125.25, 118.87, 113.59, 63.90, 63.84, 63.43, 63.35, 50.77, 49.27, 16.39, 16.33, 15.97, 15.91; ^{31}P-NMR (400 MHz, $CDCl_3$): δ (ppm) 20.939

4.3.3.4. Diethyl ((4-nitrophenyl)(phenylamino)methyl)phosphonate (4d)

Pale yellow solid, (94 % yield). mp: 178-180°C; IR (KBr, cm^{-1}): 3401.09 (N-H), 2925.56 (C-H), 1603.17 (Ar-C-C), 1521.39 (N-H), 1289.96 (P=O), 1023.02 (P-C-O), 779.84 (P-C aliphatic); ^{1}H-NMR (400 MHz, $CDCl_3$): δ (ppm) 1.22 (t, 3H), 1.31 (t, 3H), 3.86–3.97 (m, 1H), 4.03–4.10 (m, 1H), 4.11–4.26 (m, 2H), 4.88 (d, 1H), 6.56 (d, 2H), 6.71–6.78 (m, 1H), 7.12–7.15 (m, 2H), 7.67–7.72 (m, 2H), 8.18–8.24 (m, 2H); ^{13}C-NMR (400 MHz, $CDCl_3$): δ (ppm) 149.47, 149.42, 145.40, 145.26, 133.63, 133.50, 131.97, 131.95, 129.44, 128.44, 128.77, 128.55, 128.66, 125.27, 125.25, 118.87, 113.59, 63.90, 63.84, 63.43, 63.35, 50.71, 49.21, 16.39, 16.33, 16.97, 16.91; ^{31}P-NMR (400MHz, $CDCl_3$): δ (ppm) 21.427.

4.3.3.5. Diethyl ((4-fluorophenyl)(phenylamino)methyl)phosphonate (4e)

White solid, (94 % yield). mp: 94-96°C; IR (KBr, cm^{-1}): 3108.232 (N-H), 2986.173 (C-H), 1605.160 (Ar, C-C), 1518.30 (N-H), 1387.37 (P=O), 1094.72 (P-C-O), 761.48 (P-C aliphatic); ^{1}H-NMR (400 MHz, $CDCl_3$): δ (ppm) 1.35 (t, 3H), 1.43 (t, 3H), 3.65–3.75 (m, 1H), 3.90–4.10 (m, 1H), 4.08–4.24 (m, 2H), 4.82 (d, 1H), 4.88 (s, 1H), 6.46 (d, 2H), 6.57 (t, 1H), 7.12 (t, 2H), 7.48–7.52 (m, 2H), 7.60 (d, 2H); ^{13}C-NMR (400 MHz, $CDCl_3$): δ (ppm) 163.69, 163.65, 161.24, 161.20, 146.16, 146.01, 132.87, 132.77, 131.63, 131.60, 129.48, 129.43, 129.40, 129.35, 129.21, 129.08, 118.61, 116.30 ,116.08, 115.69, 115.67, 115.48, 115.45, 113.88, 64.16, 64.09, 63.42, 63.35, 63.27, 56.15, 54.64, 30.92, 16.45, 16.39, 16.34, 16.25, 16.20; ^{31}P-NMR (400 MHz, $CDCl_3$): δ (ppm) 22.191.

4.3.3.6. Diethyl ((phenylamino)(p-tolyl)methyl)phosphonate (4f)

White solid, (92 % yield). mp: 74-76°C; IR (KBr, cm^{-1}): 3323.34 (N-H), 2989.15 (C-H), 1604.69 (Ar, C-C), 1524.45 (N-H), 1316.37 (P=O), 1054.72 (P-C-O), 748.55 (P-C aliphatic); ^{1}H-NMR (400 MHz, $CDCl_3$): δ (ppm) 1.53 (t, 3H), 1.55 (t, 3H), 3.64–3.74 (m, 1H), 3.92–4.00 (m, 1H), 4.10–4.25 (m, 2H), 4.85 (d, 1H), 4.85 (s, 1H), 6.45 (d, 2H), 6.56 (t, 1H), 7.15 (t, 2H), 7.42–7.45 (m, 2H), 7.48 (d, 2H); ^{13}C-NMR (400 MHz, $CDCl_3$): δ (ppm) 146.45, 146.30, 137.62, 137.59, 132.70, 132.68, 129.33, 129.30, 129.14, 127.75, 127.69, 118.34, 113.88, 63.29, 63.28, 63.23, 63.21, 56.50, 56.00, 30.92, 21.13, 16.46, 16.40, 16.25, 16.19; ^{31}P-NMR (400 MHz, $CDCl_3$): δ (ppm) 22.657.

4.3.3.7. Diethyl ((2-oxo-1,2-dihydroquinolin-3-yl)(phenylamino)methyl)phosphonate (4g)

White solid, (93 % yield). mp: 206-208°C; IR (KBr, cm^{-1}): 3477.53 (N-H), 3284.32 (N-H), 2904.95 (C-H), 1650.78 (Ar, C-C), 1498.69 (N-H), 1268.57 (P=O), 1031.20 (P-C-O), 750.06 (P-C aliphatic); ^{1}H-NMR (400 MHz, $CDCl_3$): δ (ppm) 1.50 (t, 3H), 1.53 (t, 3H), 3.74–3.84 (m, 1H), 3.93–4.11 (m, 1H), 4.13–4.15 (m, 2H), 4.65 (d, 1H), 4.70 (s, 1H), 12.00 (br, s, 1H, NH), 8.1 (s, 1H), 7.68 (d, 1H), 7.54 (t, 1H), 7.48 (t, 71H), 7.42 (d, 1H,), 7.10 (d, 2H), 6.89 (d, 2H), 6.37 (t, 1H), 6.52 (t, 1H); ^{13}C-NMR (400 MHz, $CDCl_{3,}$): δ (ppm) 161.13, 161.07, 148.98, 146.82, 137.97, 137.21, 137.15, 130.35, 129.51, 128.84, 127.65, 122.08, 118.86, 117.22, 115.01, 113.12, 62.73, 62.66, 62.45, 62.38, 63.23, 63.21, 47.53, 45.98, 40.11, 39.90, 39.89, 39.48, 39.27, 39.06, 38.08, 30.85, 16.27, 16.22, 16.08, 16.03; ^{31}P-NMR (400 MHz, $CDCl_{3,}$): δ (ppm) 22.404.

4.3.3.8. Diethyl (phenyl(m-tolylamino)methyl)phosphonate (4h)

White solid, (82 % yield). mp: 84-86°C; IR (KBr, cm^{-1}): 3296.91 (N-H), 2986.31 (C-H), 1608.15 (Ar, C-C), 1532.47 (N-H), 1236.91 (P=O), 1023.74 (P-C-O), 771.95 (P-C aliphatic); ^{1}H-NMR (400 MHz, $CDCl_3$): δ (ppm) 1.15 (t, 3H), 1.45 (t, 3H), 2.35 (s, 3H), 3.65–3.78 (m, 1H), 3.92–4.00 (m, 1H), 4.08–4.18 (m, 2H), 4.75–4.85 (m, 2H), 6.54 (d, 2H), 7.00 (t, 1H), 7.20–7.28 (m, 4H), 7.45–7.50 (m, 2H); ^{13}C-NMR (400 MHz, $CDCl_3$): δ (ppm) 146.38, 146.24, 138.95, 135.99, 135.97, 132.68, 129.87, 129.03, 128.86, 128.59, 128.56, 127.90, 127.86, 127.81, 119.36, 114.78, 110.79, 63.34, 63.32, 63.27, 63.25, 56.76, 55.28, 29.69, 21.55, 16.45, 16.39, 16.35, 16.21, 16.15; ^{31}P-NMR (400 MHz, $CDCl_3$): δ (ppm) 22.478.

4.3.3.9. Diethyl (((2-nitrophenyl)amino)(phenyl)methyl)phosphonate (4i)

White solid, (71 % yield). mp: 112-114°C; IR (KBr, cm^{-1}): 3464.50 (N-H), 2929.88 (C-H), 1616.98 (Ar, C-C), 1510.78 (N-H), 1215.27 (P=O), 1016.37 (P-C-O), 744.39 (P-C aliphatic); ^{1}H-NMR (400 MHz, $CDCl_3$): δ (ppm) 1.25 (t, 3H), 1.26 (t, 3H), 3.88–3.97 (m, 1H), 4.00–4.10 (m, 1H), 4.12–4.20 (m, 2H), 4.92 (br, s, 1H), 6.57 (d, 2H), 6.71 (d, 1H), 7.38 (t, 1H), 7.40-7.45 (m, 2H), 7.50–7.55 (m, 1H), 7.76–7.78 (m, 1H), 8.03 (d, 1H), 8.35 (t, 1H); ^{13}C-NMR (400 MHz, $CDCl_3$): δ (ppm) 136.08, 134.53, 133.28, 128.89, 128.86, 128.39, 128.36, 127.62, 127.57, 126.67, 116.65, 114.65, 63.80, 63.73, 63.55, 63.48, 56.21, 54.77, 16.39, 16.32, 16.26; ^{31}P-NMR (400 MHz, $CDCl_3$): δ (ppm) 20.085.

4.3.3.10. Diethyl ((4-chlorophenyl)((2-nitrophenyl)amino)methyl)phosphonate (4j)

Yellow solid, (75 % yield). mp: 92-94°C; IR (KBr, cm^{-1}): 3363.59 (N-H), 2984.44 (C-H), 1615.14 (Ar, C-C), 1425.34 (N-H), 1300.50 (P=O), 1031.57 (P-C-O), 785.98 (P-C

aliphatic); ^{1}H-NMR (400 MHz, $CDCl_3$): δ (ppm) 1.25 (t, 3H), 1.26 (t, 3H), 3.88–3.97 (m, 1H), 4.00–4.10 (m, 1H), 4.12–4.20 (m, 2H), 4.92 (br, s, 1H), 6.57 (d, 2H), 6.71 (d, 1H), 6.98 (t, 1H), 7.20-7.25 (m, 2H), 7.30–7.35 (m, 1H), 8.28 (d, 1H), 8.86 (t, 1H); ^{13}C-NMR (400 MHz, $CDCl_3$): δ (ppm) 143.76, 143.62, 136.15, 134.32, 134.28, 133.40, 133.25, 133.21, 129.11, 129.08, 128.92, 128.87, 126.95, 116.95, 114.50, 63,94, 63,87, 63.66, 63.59, 55.71, 54.20, 16.40, 16.35, 16.29; ^{31}P-NMR (400 MHz, $CDCl_3$): δ (ppm) 19.470.

4.3.3.11. Diethyl (furan-2-yl((2-nitrophenyl)amino)methyl)phosphonate (4k)

Brown solid, (79 % yield). mp: 83-85°C; IR (KBr, cm^{-1}): 2878.43, (C-H), 1520.67 (Ar, C-C), 1462.66 (N-H), 1204.88 (P=O), 1139.52 (P-C-O), 795.30 (P-C aliphatic); ^{1}H-NMR (400 MHz, $CDCl_3$): δ (ppm) 1.28 (t, 3H), 1.30 (t, 3H), 3.88–3.97 (m, 1H), 4.00–4.20 (m, 1H), 4.22–4.24 (m, 2H), 4.98 (br, s, 1H), 6.35 (d, 2H), 6.65 (d, 1H), 6.98 (t, 1H), 7.38-7.45 (m, 2H), 8.28 (d, 1H), 8.86 (t, 1H); ^{13}C-NMR (400 MHz, $CDCl_3$): δ (ppm) 147.99, 147.96, 143.72, 143.61, 142.99, 142.96, 136.12, 133.41, 126.89, 119.15, 119.08, 116.96, 114.25, 111.00, 110.97, 63.89, 63.82, 63.79, 63.72, 50.39, 48.81, 16.42, 16.38, 16.33; ^{31}P-NMR (400 MHz, $CDCl_3$): δ (ppm) 17.803.

4.3.3.12. Diethyl (((2-nitrophenyl)amino)(p-tolyl)methyl)phosphonate (4l)

Yellow solid, (75 % yield). mp: 98-100°C; IR (KBr, cm^{-1}): 3295.37 (N-H), 2929.51 (C-H), 1618.40, (Ar, C-C), 1575.36 (N-H), 1396.53 (P=O), 1037.08 (P-C-O), 741.63 (P-C aliphatic); ^{1}H-NMR (400 MHz, $CDCl_3$): δ (ppm) 1.25 (t, 3H), 1.35 (t, 3H), 2.35 (s, 3H), 3.85–3.90 (m, 1H), 3.92–4.00 (m, 1H), 4.08–4.18 (m, 2H), 4.80–4.85 (m, 2H), 6.62 (t, 2H), 7.23 (d, 1H), 7.20–7.28 (m, 4H), 8.25–8.35 (d, 1H); 8.8, 1H); ^{13}C-NMR (400 MHz, $CDCl_3$): δ (ppm) 144.12, 143.98, 138.22, 138.18, 136.07, 133.22, 131.41, 131.37, 129.60, 129.57, 127.49, 127.44, 126.83, 116.56, 114.68, 63.75, 63.68, 63.50, 63.43, 55.98, 54.47, 21.17, 16.40, 16.34, 16.28: ^{31}P-NMR (400 MHz, $CDCl_3$): δ (ppm) 20.279.

4.3.3.13. Diethyl ((4-fluorophenyl)((2-nitrophenyl)amino)methyl)phosphonate (4m)

White solid, (73 % yield). mp: 85-87°C; IR (KBr, cm^{-1}): 3372.08 (N-H), 2983.45 (C-H), 1616.15 (Ar, C-C), 1477.24 (N-H), 1397.61 (P=O), 1008.11 (P-C-O), 706.58 (P-C aliphatic); ^{1}H-NMR (400 MHz, $CDCl_3$): δ (ppm) 1.35 (t, 3H), 1.36 (t, 3H), 3.88–3.97 (m, 1H), 4.00–4.10 (m, 1H), 4.12–4.20 (m, 2H), 4.98 (br, s, 1H), 6.57 (d, 2H), 6.98 (m, 2H), 7.32 (m, 1H), 7.46-7.48 (t, 2H), 8.28 (d, 1H), 8.86 (t, 1H); ^{13}C-NMR (400 MHz, $CDCl_3$): δ (ppm) 163.91, 163.87, 161.45, 161.41, 143.83, 143.69, 136.12, 133.36, 130.36, 130.32, 130.29, 129.32, 129.26, 129.23, 129.18, 126.92, 116.86, 116.03, 116.00, 115.82, 115.79,

114.53, 63.86, 63.79, 63.60, 63.33, 55.56, 54.04, 16.40, 16.34, 16.28: ^{31}P-NMR (400 MHz, $CDCl_3$): δ (ppm) 19.807.

4.3.3.14. Diethyl ((phenylamino)(pyridin-2-yl)methyl)phosphonate (4n)

Yellow solid, (90 % yield). mp: 104-106°C; IR (KBr, cm^{-1}): 3303.93 (N-H), 2978.32 (C-H), 1605.49 (Ar, C-C), 1402.60 (N-H), 1387.10 (C=N), 1262.26 (P=O), 1098.11 (P-C-O), 813.496 (P-C aliphatic); ^{1}H-NMR (400 MHz, $CDCl_3$): δ (ppm) 1.33 (t, 3H), 1.48 (t, 3H), 3.86–3.95 (m, 1H), 4.00–4.10 (m, 1H), 4.21–4.30 (m, 2H), 4.82 (d, 1H), 5.2 (br, s, 1H), 6.62 (m, 3H), 7.10 (t, 2H), 7.27–7.36 (m, 1H), 7.50 (d, 1H), 7.63-7.70 (t, 1H), 8.52-8.54 (s, 1H) ; ^{13}C-NMR (400 MHz ,$CDCl_3$): δ (ppm) 155.69, 148.57, 146.43, 146.31, 137.33, 129.20, 129.08, 123.08, 123.04, 122.99, 122.96, 119.70, 118.59, 114.02, 63.67, 63.59, 63.34, 63.27, 58.30, 56.80, 16.43, 16.37, 16.24, 16.19; ^{31}P-NMR (400 MHz, $CDCl_3$): δ (ppm) 21.128.

4.3.3.15. Diethyl ((2-hydroxyphenyl)(phenylamino)methyl)phosphonate (4o)

White solid, (85 % yield). mp: 262-264°C; IR (KBr, cm^{-1}): 3433.40 (-OH), 3277.92 (N-H), 2920.27 (C-H), 1603.15 (Ar, C-C), 1389.36 (N-H), 1201.01 (P=O), 1194.95 (P-C-O), 806.69 (P-C aliphatic); ^{1}H-NMR (400 MHz, $CDCl_3$): δ (ppm) 1.33 (t, 3H), 1.51 (t, 3H), 3.86–3.95 (m, 1H), 4.12–4.13 (m, 1H), 4.18–4.21 (m, 2H), 4.48 (d, 1H), 5.5 (br, s, 1H), 6.32 (m, 3H), 6.52 (m, 2H), 6.92-7.10 (t, 3H), 7.27–7.36 (s, 1H), 11.50 (br, s, 1H); ^{13}C-NMR (400 MHz, $CDCl_3$): δ (ppm) 206.56, 155.65, 148.12, 148.013, 39.42, 39.21, 39.00, 31.29, 30.64, 28.95, 28.84, 28.64, 28.50, 22.04, 20.71, 16.73, 16. 68, 14.04, 13.90; ^{31}P-NMR (400 MHz, $CDCl_3$): δ (ppm) 20.157.

4.3.3.16. Diethyl ((4-(dimethylamino)phenyl)(phenylamino)methyl)phosphonate (4p)

Pale yellow solid, (79 % yield). mp: 112-114°C; IR (KBr, cm^{-1}): 3292.78 (N-H), 2981.66 (C-H), 1613.155 (Ar, C-C), 1528.062 (N-H), 1233.475 (P=O), 1047.899 (P-C-O), 748.523 (P-C aliphatic); ^{1}H-NMR (400 MHz, $CDCl_3$): δ (ppm) 1.15 (t, 3H), 1.45 (t, 3H), 2.35 (s, 3H), 3.65–3.78 (m, 1H), 3.92–4.00 (m, 1H), 4.08–4.18 (m, 2H), 4.05–4.10 (m, 1H), 4.15-4.20 (br, s 1H), 6.54 (d, 5H), 7.00 (t, 2H), 7.30–7.48 (t, 2H); ^{13}C-NMR (400 MHz, $CDCl_3$): δ (ppm) 1419.91, 146.64, 146.50, 129.26, 129.11, 128.66, 128.63, 118.16, 113.92, 112.88, 63.23, 63.16, 63.14,63.06, 56.11, 54.59, 40.72, 16.50, 16.44, 16.34, 16.28; ^{31}P-NMR (400 MHz, $CDCl_3$): δ (ppm) 23.494.

4.3.3.17. Diethyl (furan-2-yl(phenylamino)methyl)phosphonate (4q)

Brown solid, (90 % yield). mp: 68-70°C; IR (KBr, cm^{-1}): 3035.86 (C-H), 2900.95 (Ar, C-C), 1602.04 (N-H), 1527.95 (P=O), 1392.91 (P-C-O), 673.55 (P-C aliphatic); ^{1}H-

NMR (400 MHz, $CDCl_3$): δ (ppm) 1.38 (t, 3H), 1.40 (t, 3H), 3.88–3.98 (m, 1H), 4.00–4.20 (m, 1H), 4.22–4.24 (m, 3H), 4.98 (s, 1H), 6.35 (d, 2H), 6.65 (t, 3H), 7.20-7.22 (m, 2H), 7.50 (d, 1H); ^{13}C-NMR (400 MHz, $CDCl_3$): δ (ppm) 149.29, 145.99, 145.86, 142.53, 142.50, 129.21, 119.06, 114.10, 110.81, 110.79, 118.90, 108.83, 63.58, 63.51, 63.40, 63.33, 51.12, 49.54, 16.46, 16.41, 16.32, 16.26; ^{31}P-NMR (400 MHz, $CDCl_3$): δ (ppm) 19.944.

4.3.3.18. Diethyl ((4-nitrophenyl)(m-tolylamino)methyl)phosphonate (4r)

Pale yellow solid, (85 % yield). mp: 178-180°C, IR (KBr, cm^{-1}): 3458.09 (N-H), 2979.56 (C-H), 1608.17 (Ar, C-C), 1522.39 (N-H), 1347.96 (P=O), 1052.02 (P-C-O), 753.84 (P-C aliphatic); ^{1}H-NMR (400 MHz, $CDCl_3$): δ (ppm) 1.22 (t, 3H), 1.31 (t, 3H), 2.32(s, 3H), 3.86–3.97 (m, 1H), 4.03–4.10 (m, 1H), 4.11–4.26 (m, 2H), 4.88 (d, 1H), 6.56 (d, 2H), 6.71–6.78 (m, 1H), 7.12–7.15 (m, 2H), 7.67–7.72 (m, 2H), 8.18–8.24 (m, 2H); ^{13}C-NMR (400 MHz, $CDCl_3$): δ (ppm) 147.59, 145.70, 145.56, 144.17, 139.27, 129.22, 128.65, 128.60, 123.99, 123.76, 123.74, 120.08, 114.73, 110.74, 63.80, 63.73, 63.49, 63.43, 56.73, 55.25, 21.53, 16.44, 16.39, 16.27, 16.22; ^{31}P-NMR (400 MHz, $CDCl_3$): δ (ppm) 20.809.

4.3.3.19. Diethyl ((4-fluorophenyl)(m-tolylamino)methyl)phosphonate (4s)

White solid, (90 % yield). mp: 124-126°C; IR (KBr, cm^{-1}): 3303.49 (N-H), 2355.39 (C-H), 1607.56 (Ar, C-C), 1387.43 (N-H), 1238.17 (P=O), 1016.08 (P-C-O), 767.75 (P-C aliphatic); ^{1}H-NMR (400 MHz, $CDCl_3$): δ (ppm) 1.25 (t, 3H), 1.40 (t, 3H), 2.55 (br, s, 1H), 3.68–3.88 (m, 1H), 3.90 (m, 1H), 4.10–4.18 (m, 2H), 4.65 (s, 1H), 6.30 (d, 2H), 6.7 (d, 1H), 7.20 (d, 3H), 7.45–7.50 (t, 2H); ^{13}C-NMR (400 MHz ,$CDCl_3$): δ (ppm) 163.66, 146.17, 146.03, 139.05, 133.76, 129.46, 129.40, 126.38, 129.32, 129.08, 119.56, 115.67, 115.64, 115.45, 115.43, 114.75, 110.77, 63.40, 63.33, 63.29, 63.22, 56.10, 54.59, 21.54, 16.45, 16.40, 16.26, 16; ^{31}P-NMR (400 MHz, $CDCl_3$): δ (ppm) 22.391.

4.3.3.20. Diethyl (furan-2-yl(m-tolylamino)methyl)phosphonate (4t)

Brown solid, (93 % yield). mp: 83-85°C; IR (KBr, cm^{-1}): 2979.10 (Ar, C-C), 1609.04 (N-H), 1527.95 (P=O), 1329.91 (P-C-O), 693.87 (P-C aliphatic); ^{1}H-NMR (400 MHz, $CDCl_3$): δ (ppm) 1.38 (t, 3H), 1.40 (t, 3H), 2.55 (br, s, 1H), 3.88–3.98 (m, 1H), 4.00–4.20 (m, 1H), 4.22–4.24 (m, 3H), 4.98 (s, 1H), 6.35 (d, 2H), 6.65 (t, 3H), 7.35-7.40 (t, 1H), 7.50-7.55 (d, 1H); ^{13}C-NMR (400 MHz, $CDCl_3$): δ (ppm) 148.78, 145.09, 142.61, 139.07, 129.06, 120.76, 115.75, 111.87, 110.84, 110.82, 109.35, 109.28, 63.67, 63.60,

63.49, 63.42, 51.57, 49.97, 21.52, 16.46, 16.40, 16.31, 16.26; ^{31}P-NMR (400 MHz, $CDCl_3$): δ (ppm) 19.640.

4.3.3.21. Diethyl ((4-methoxyphenyl)(phenylamino)methyl)phosphonate (4u)

White solid, (81 % yield). mp: 107-109°C; IR (KBr, cm^{-1}): 3294.01 (N-H), 2985.67 (C-H), 1603.56 (Ar, C-C), 1441.90 (N-H), 1387.91 (P=O), 1032.81 (P-C-O), 887.49 (P-C aliphatic); ^{1}H-NMR (400 MHz, $CDCl_3$): δ (ppm) 1.32 (t, 3H), 1.40 (t, 3H), 3.3-3.45 (m, 1H), 3.6–3.74 (s, 3H), 3.82–4.00 (m, 1H), 4.10–4.25 (m, 2H), 4.85 (s, 1H), 4.85 (s, 1H), 6.55 (t, 3H), 6.88 (d, 2H), 7.2 (t, 2H), 7.42–7.48 (d, 2H); ^{13}C-NMR (400 MHz, $CDCl_3$): δ (ppm) 159.32, 159.29, 146.40, 146.25, 132.54, 129.14, 129.01, 128.95, 127.63, 127,60, 118.38, 114.18, 114.07, 114.05, 113.94, 63.30, 63.23, 56.13, 55.22, 54.62, 30.91, 29.69, 16, 47, 16.41, 16.28, 16.23; ^{31}P-NMR (400 MHz, $CDCl_3$): δ (ppm) 22.874.

4.4. Results, Discussion and Conclusion

With the aim of adding new knowledge via. MCRs, we investigated the Kabachnik-Fields reaction with the intention of introducing a new catalyst which could be selective, efficient and recyclable. Thus we decided to investigate the BN system since it is planar and comprises of a network of B-N atoms with abundant charges **Figure 1**. A recent report by Hironao Sajiki *et al.*,[17] discussed a simple preparative method for a palladium-loaded (Pd/BN) system which is used for chemo selective hydrogenation of alkynes. We decided to load a new metal into BN and investigate its catalytic potential in the Kabachnik-Fields reaction.

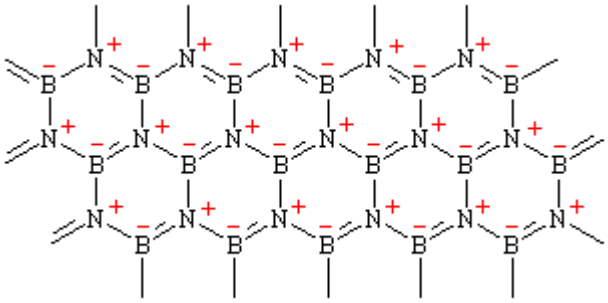

Figure 1. The iso electronic structure of boron nitride (BN)

The first step of this research investigation was to synthesize a Cu-loaded BN material (Cu/BN). We accomplished this by using $Cu(OAc)_2$ and BN in a methanolic solution, under inert atmospheric conditions. The reaction was allowed to run for 7 days

after which the novel material was worked-up to give a pale green powder of 92% yield. **Scheme 1** shows the method used to prepare the Cu/BN material.

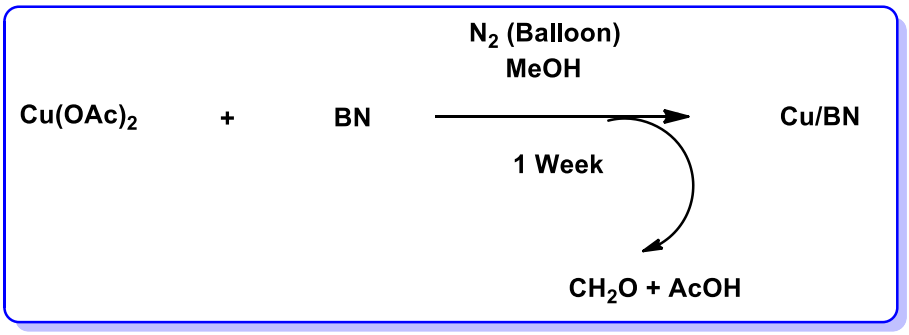

Scheme 1. Preparation of copper-loaded boron nitride catalyst (Cu/BN)

The Cu/BN material was then characterized using the SEM/EDX and powder XRD techniques. The crystalline nature of the Cu/BN and nano size was confirmed by SEM spectroscopy and the EDX pattern **Figure 2**. The particle dimensions of nano material were observed in the 1-10 µm range with plate like particles of boron nitride particle with size 200 nm. EDX pattern for Cu/BN showed signals for copper metal.

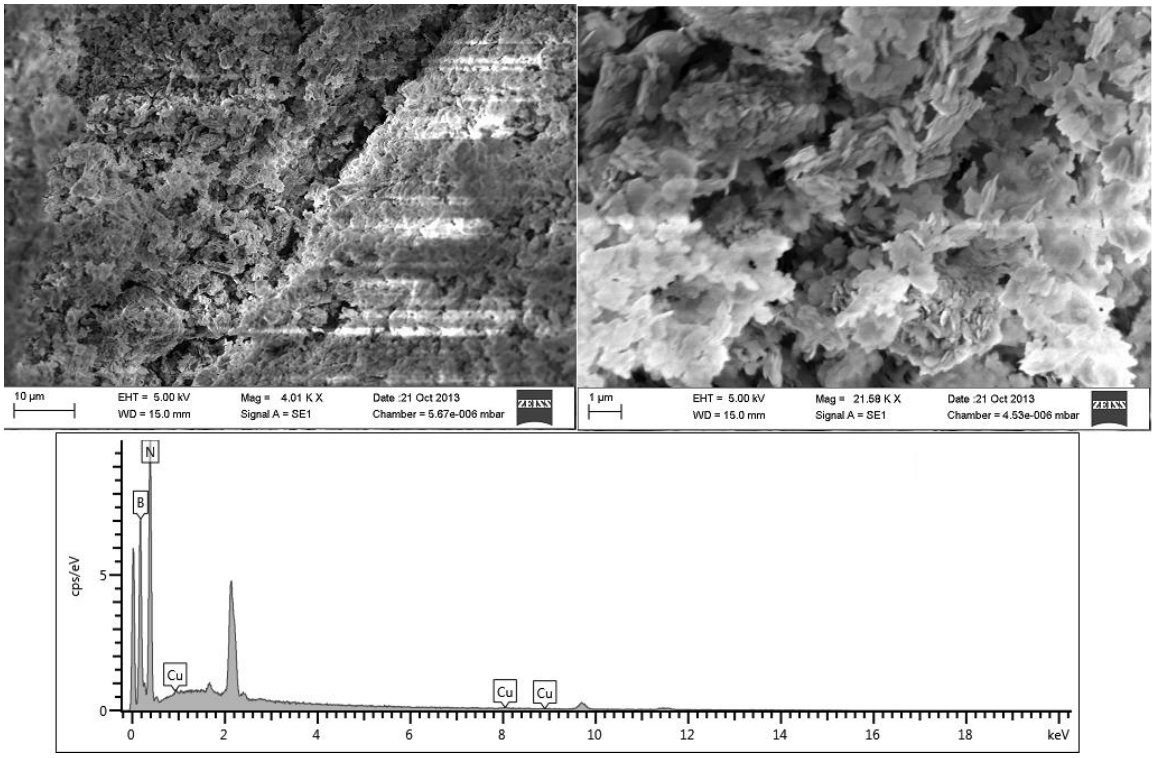

Figure 2. SEM with EDX for copper-loaded boron nitride (Cu/BN)

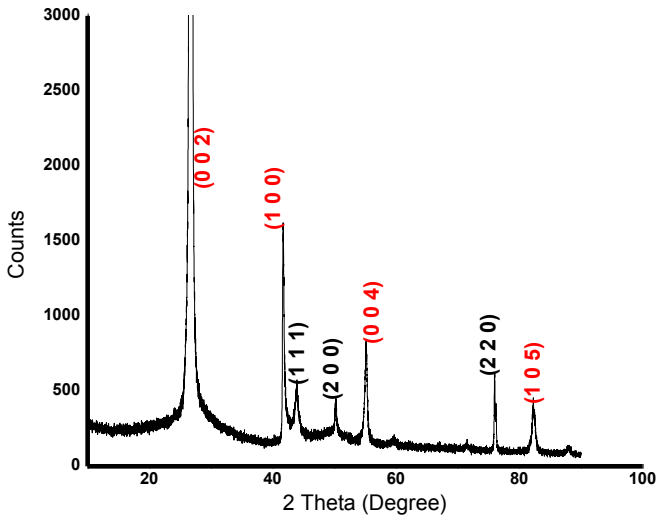

Figure 3. The powder XRD pattern for copper-loaded boron nitride (Cu/BN)

Cu/BN were also subjected to X-ray diffraction analyses. **Figure 3** shows the XRD pattern; the crystalline nature of the Cu/BN was confirmed and the characteristic Bragg's

XRD peaks at 2 θ = 26.75˚, 41.58˚, 50.16˚, 75.86˚ are indexed to the (0 0 2), (1 0 0), (2 0 0), (2 2 0) and Copper 2 θ = 44.58˚, 57.58˚, 83.58˚ are indexed to the (1 1 1), (0 0 4), (1 0 5) crystallographic planes of the boron nitride and copper metal, respectively[18].

The next step in the research investigation was to use the Cu/BN material and assess its catalytic potential in a MCR particularly the Kabachnik-Fields reaction. We chose an equimolar quantity of aniline, benzaldehyde, diethyl phosphite and added Cu/BN followed by the addition of methanol. This mixture was refluxed on an oil bath and the progress of the reaction was monitored hourly for ten hours. After working-up the mixture, the catalyst was filtered and the organic compound was separated via. column chromatography. Pure 4a (yield 75 %) was obtained then characterized by IR, ^{1}H-NMR, ^{13}C-NMR and ^{31}P-NMR.

Thereafter the solvent was optimized **Table 1**. Acetonitrile gave the highest yield (95 %) and this solvent was used in all subsequent reactions.

Table 1. Solvent optimization[a] for the synthesis of **4a.**

Entry	Catalyst	Solvent	Temp (°C)	Time (h)	Yield (%)[b]
1	Cu/BN	Acetonitrile	82	10	95
2	Cu/BN	Toluene	110	10	90
3	Cu/BN	Methanol	65	10	75
4	Cu/BN	Ethanol	78	10	70

[a] Reaction condition (benzaldehyde, 1 mmol; aniline, 1 mmol; diethylphosphite, 1 mmol; Cu/BN 0.25 g, acetonitrile, 6 ml, reflux 82°C)

[b] Isolated Yield.

Using the above optimized protocol, we synthesized **4b-4u**. The general reaction is represented in **Scheme 2** for the synthesis of **4a. Scheme 3** shows the synthesis of **4g**, a novel quinoline derivative.

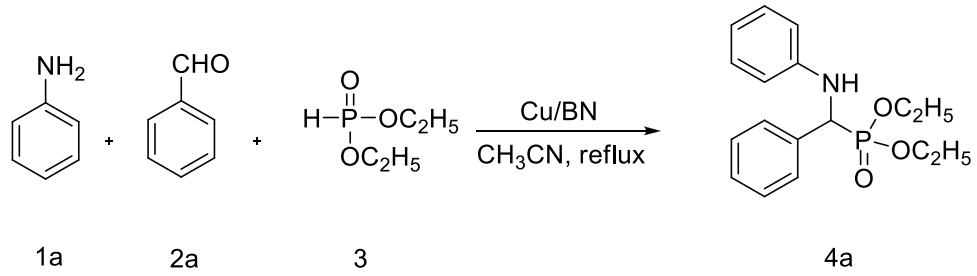

Scheme 2. Synthesis of α-aminophosphonates

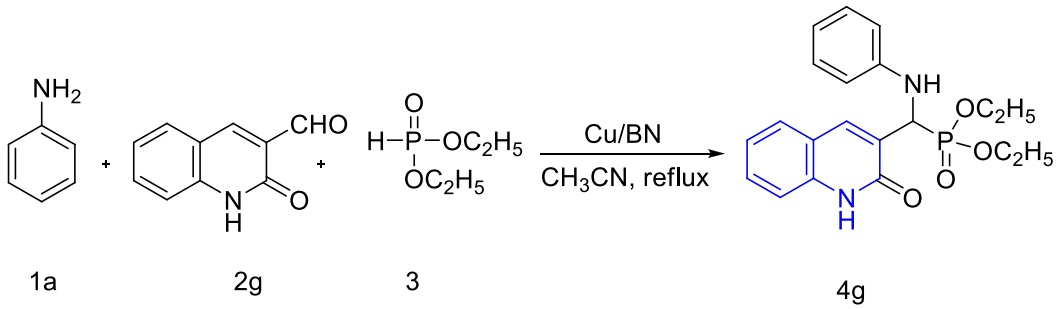

Scheme 3. Synthesis of quinoline based α-aminophosphonates

All the compounds were confirmed by IR, ^{1}H-NMR, ^{13}C-NMR and ^{31}P-NMR. **Figure 4** shows the X-ray crystal structure of compound **4h**.

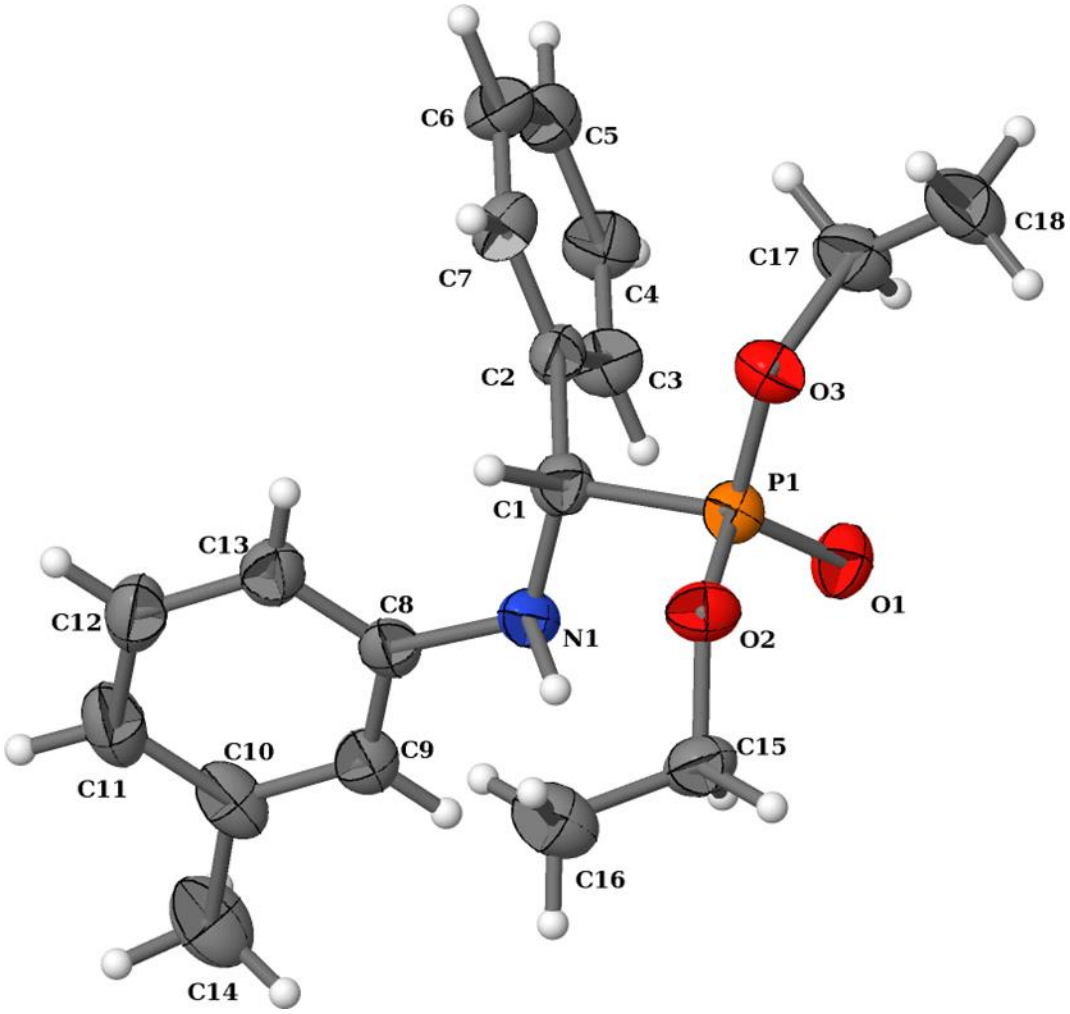

Figure 4. ORTEP views of compound **4h**.

A proposed mechanism for the Kabachnik-Fields reaction catalyzed by Cu/BN is represented in **Scheme 4**.

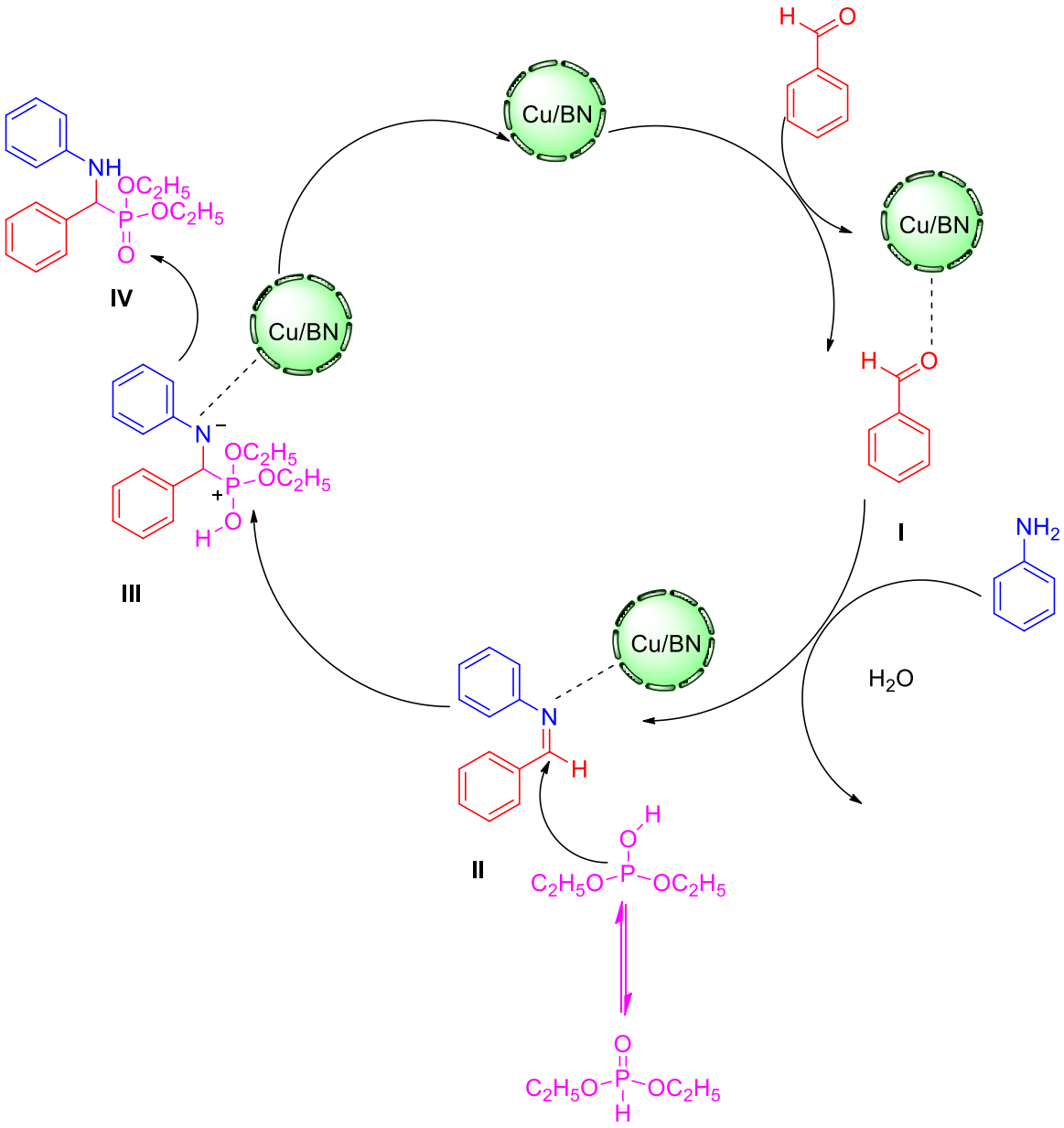

Scheme 4. Plausible "imine" mechanism for the formation of α-aminophosphonates

Table 2 shows the twenty one α-aminophosphonates (**4a-u**) synthesized, the melting point and % yield.

We also compared the % yield of a model reaction i.e. synthesis of **4a** with literature values **Table 3**. We found that the % yield was higher than literature values.

Table 2. Synthesis of α- aminophosphonates (**4a-u**)

Entry	Aldehyde	Amine	Time (h)	Product	Melting Point (°C)	Yield (%)
a			10	4a	97-99	95
b	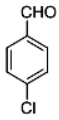		10	4b	74-76	94
c			10	4c	157-159	95
d	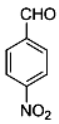		10	4d	178-180	94
e	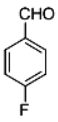		10	4e	94-96	94
f	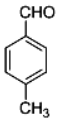		10	4f	74-76	92
g	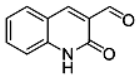		10	4g	206-208	93
h		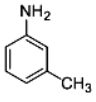	10	4h	84-86	82
i			10	4i	112-114	71
j	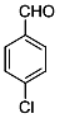		10	4j	92-94	75

Entry	Aldehyde	Amine	Time (h)	Product	Melting Point (°C)	Yield %
k	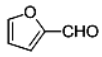		10	4k	83-85	79
l	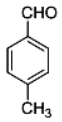		10	4l	98-100	75
m	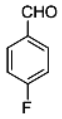		10	4m	85-87	73
n	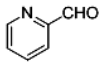		10	4n	104-106	90
o			10	4o	262-264	85
p	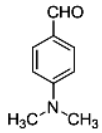		10	4p	112-114	79
q	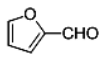		10	4q	68-70	90
r	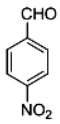		10	4r	99-101	85
s	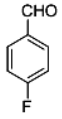		10	4s	124-126	90
t	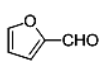		10	4t	83-85	93
u	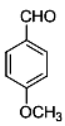		10	4u	107-109	81

Table 3. shows reaction time and percentage yield of **4a** with different catalysts and reaction conditions.

Entry	Catalyst used	Reaction condition	Reaction Time	% Yield	Reference
1	β-Cyclodextrin	H_2O Reflux	24 h	61	19
2	$YbCl_3$	CH_3CN/RT	24 h	93	20
3	$TaCl_5$-SiO_2	CH_2Cl_2/RT	22 h	92	21
4	$In(OTf)_3$	THF/Reflux	21 h	79	22
5	$InCl_3$	THF/RT	11 h	92	23
6	ZnO	Solvent-free/RT	9 h	90	24
7	$BiCl_3$	CH_3CN/Reflux	6 h	92	25
8	Silica sulfuric acid	CH_3CN/RT	5 h	87	26
9	$Mg(ClO_4)_2$	Solvent-free/80˚C	5 h	95	27
10	$CaCl_2$	Solvent-free/ 60˚C	3 h	96	28
11	Cu/BN	CH_3CN/Reflux	10 h	95	**Present work**

Key : RT= Room temperature.

To determine the re-usability of Cu/BN, the filtered Cu/BN material was used in the model reaction to form **4a**. **Figure 5** shows a graphical representation. It was found that the catalyst could be used more than four times. This indicated an efficient and effective catalyst was prepared and could be used for the Kabachnik-Fields reaction. As mentioned earlier, comparing literature **Table 3** it was also found that the Cu/BN catalyst gave high yield of **4a**.

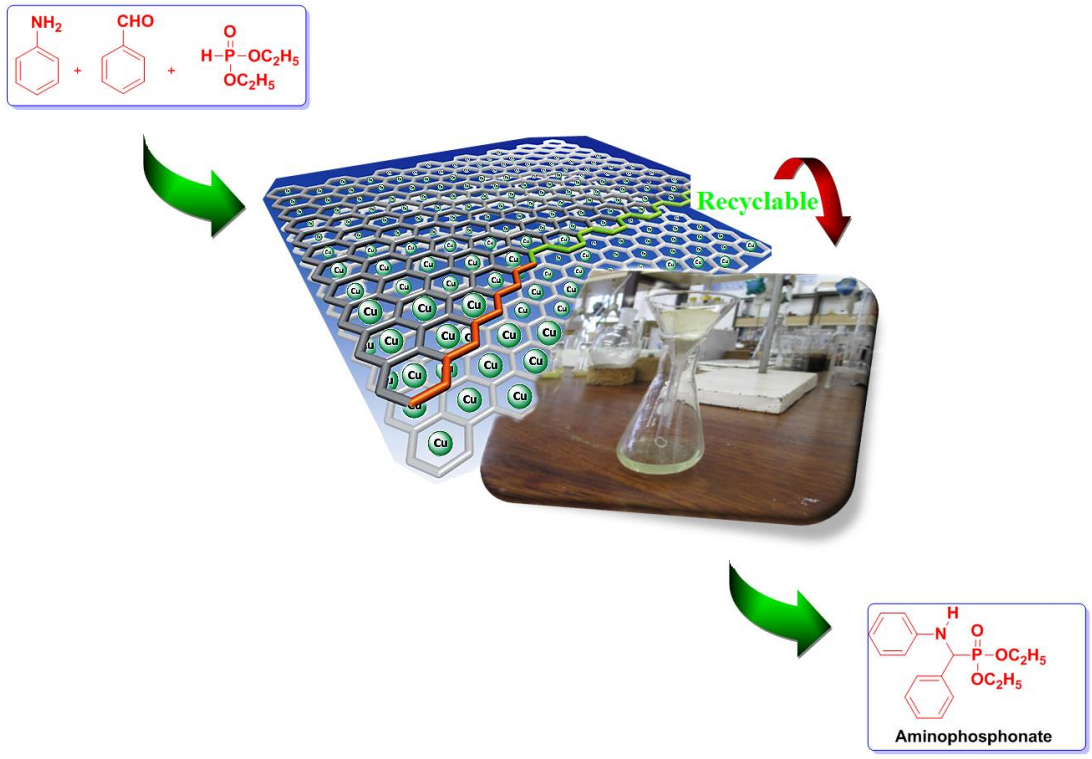

Figure 5. Graphical picture of the reusability of copper-loaded boron nitride (Cu/BN)

Table 5. Reusability of the Catalyst [a]

Run	1	2	3	4	5
Yield (%)[b]	95	93	91	90	88

a Reaction conditions: benzaldehyde (1 mmol), aniline (1 mmol), diethylphosphite (1 mmol), (0.25 mg, 15 mol % of Cu/BN), acetonitrile 6.0 ml, Reflux, 82°C.

b Isolated yield.

In conclusion, we have demonstrated that the Kabachnik-Fields reaction via. a three-component one-pot reaction was catalyzed by the novel copper-loaded boron nitride catalyst. Twenty one compounds were synthesized and characterized. The catalyst can be used more than four times. The yield of the products are good. The reaction proceeds with high efficiency to give the corresponding amino phosphates which are extremely useful in the construction of biologically important compounds. Cleaner conversion, higher yield and the simplicity of operation are some of the advantages of the protocol.

Reference

(1) *The Chemistry of Organophosphorus Compounds;* Breuer, E., Eds.; John Wiley: New York, USA, **1996**.

(2) Srinivasulu, K.; Anilkumar, M.; Nagaraju, C.; Reddy, C. S. *ARKIVOC*. **2007**, 14, 100.

(3) Prakasha, T. K.; Day, R. O.; Holmes, R. R. *J. Am. Che. Society.* **1994**, 116, 8095.

(4) *The Chemistry of Organophosphorus Pesticides*; Fest, C., Schmidt, K. J. Eds.; Springer. **1982**, 12, 1111.

(5) *The Chemistry of Organophosphorus Pesticides*; Fest, C., Schmidt, K. J. Eds.; Experientia, **1976**, 32.

(6) Manne, P. N.; Deshmukh, S. D.; Rao, N. G. V.; Dodale, H. G.; Tikar, S. N. *Pestology.* **2000**, 34, 65.

(7) Hendlin, D.; Stapley, E. O.; Jackson et al, M. *Science.* **1969**, 166, 122.

(8) Polozov, A. M.; Cremer, S. E. *J. Org. metal. Chem.* **2002**, 646, 153.

(9) *Aminophosphonic and Amino-phosphinic Acids Chemistry and Biological Activity;* Kukhar, V. P., Hudson, H. R., Eds.; John Wiley: New York, USA, **2000**.

(10) Huang, J.; Chen, R. *Heteroatom Chemistry.* **2000**, 11, 480.

(11) Rai, V.; Namboothiri, I. N. N. *Tetrahedron Asymmetry.* **2008**, 19, 2335.

(12) Pudovik, A. N. *DokladyAkademii Nauk.* **1952**, 85, 349.

(13) Wiemer, D. F. *Tetrahedran.* **1997**, 53, 16609.

(14) Ranu B. C.; Hajra, A. *Green Chem.* **2002**, 4, 551.

(15) Ranu, B. C.; Hajra, A.; Jana, U. *Organic Letters.* **1999**, 1, 1141.

(16) Hou Gao, J.; Zhang, H. *Applied. Orga. Chemistry.* **2011**, 25, 47.

(17) Yuki Y.; Tsuyoshi Y.; Saori N.; Yoshinari S.; Yasunari M.; Hironao, S. *Advanced. Synthesis.Catalysis*. **2012**, 354, 7, 1264.

(18) Tiago, H. F.; Paulo, R. O.; Raquel, G. S.; Edésia, M. B. S. *J. Bio. Nano bio*. **2011**, 2, 426.

(19) Hou, J.; Gao, J.; Zhang, H. *Applied. Organ. Chem.* **2011.** 25, 47.

(20) Xu, F.; Luo, Y. Q.; Wu, J. T.; Shen, Q.; Chen, H. *Heteroatom Chemistry***. 2006,** 17, 389.

(21) Chandrasekhar, S.; Prakash, S. J.; Jagadeshwar, V.; Narsihmulu, C. *Tetrahedron Letters.* **2001**, 42, 5561.

(22) Ghosh, R.; Maiti, S.; Chakraborty, A.; Maiti, D. K. *J. Molecular Catalysis A.* **2004**, 210, 53.

(23) Ranu, B. C.; Hajra, A.; Jana, U. *Organic Letters.* **1999**, 1, 1141.

(24) Hou, J.; Gao, J.; Zhang, H. *Applied.Org. metal. Chem.* **2011**, 25, 47.

(25) Zhan, Z. P.; Li, J. P. *Synthetic Communications.* **2005**, 35, 2501.

(26) Bhattacharya, A. K.; Ranan, K. C. *Tetrahedron Letters.* **2008**, 49, 2598.

(27) Bhagat, S.; Chakraborti, A. K. *J. Org. Chem.* **2007**, 72, 1263.

(28) Tian, Y. P.; Xu, F.; Wang, Y.; Tang, J. J. *J. Chem. Res*. **2009**, 2, 78.

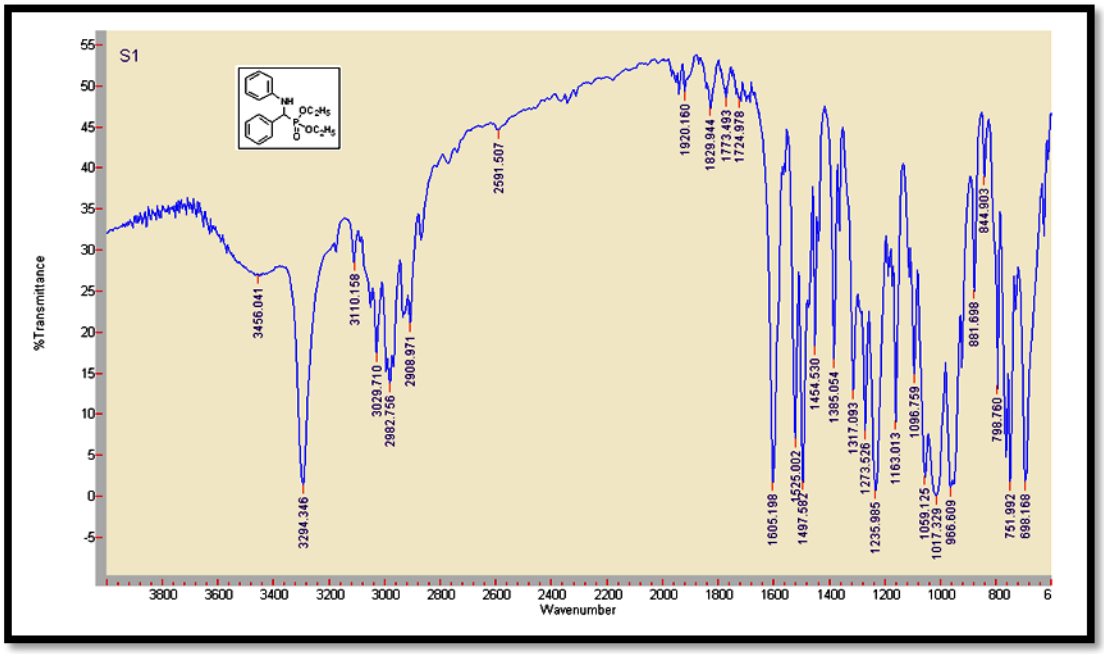

Figure. 4.1 IR Spectrum of **4a**

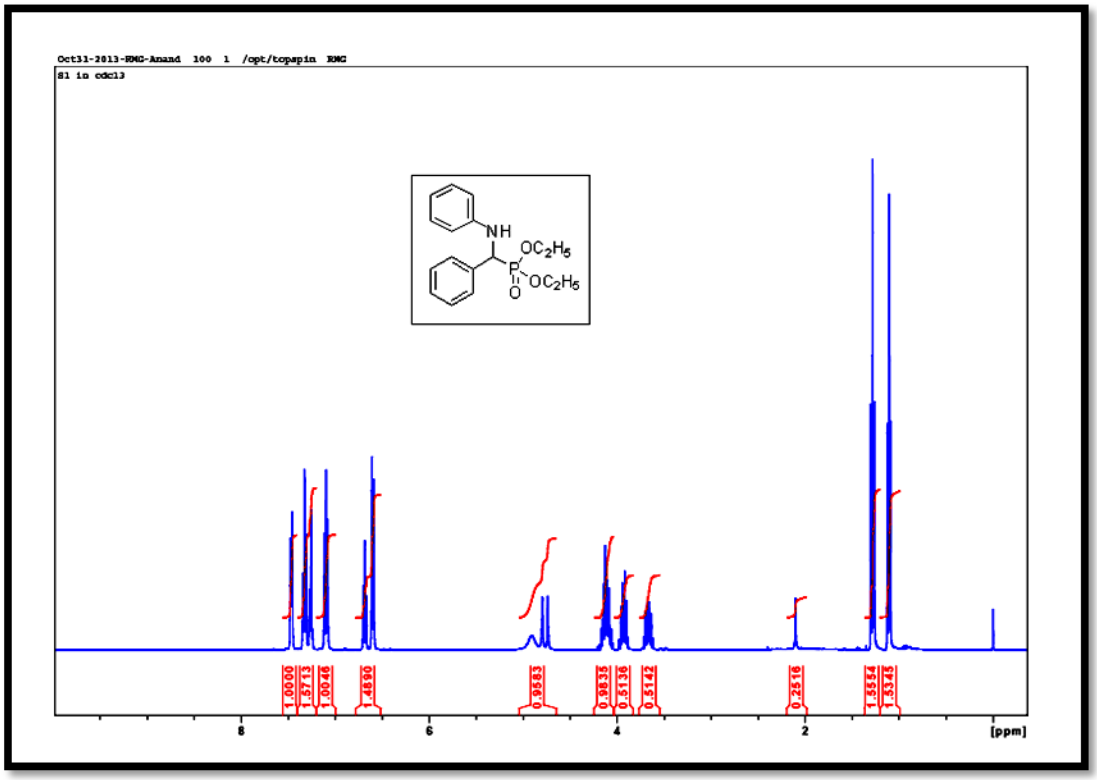

Figure. 4.2 ^{1}H-NMR spectrum of **4a**

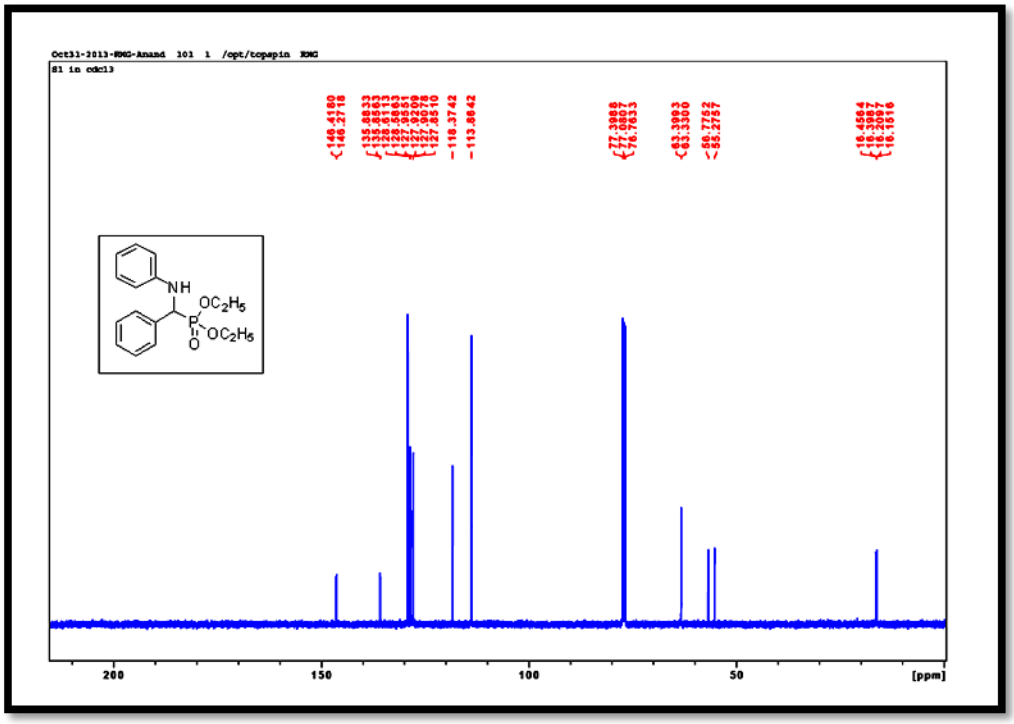

Figure. 4.3 ^{13}C-NMR spectrum of **4a**

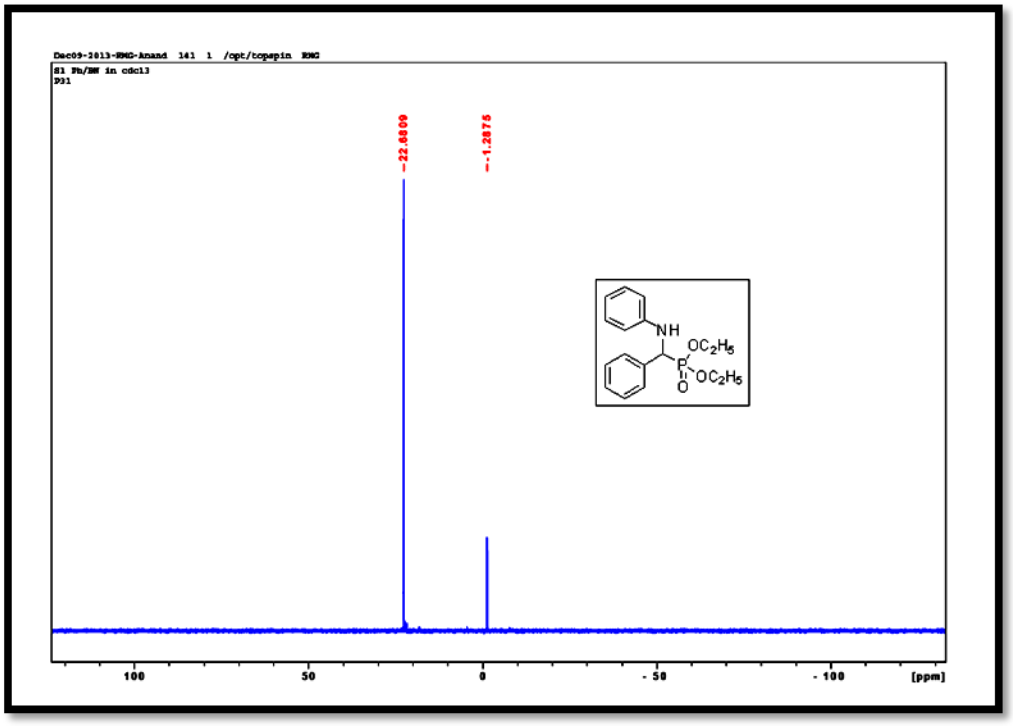

Figure. 4.4 ^{31}P-NMR spectrum of **4a**

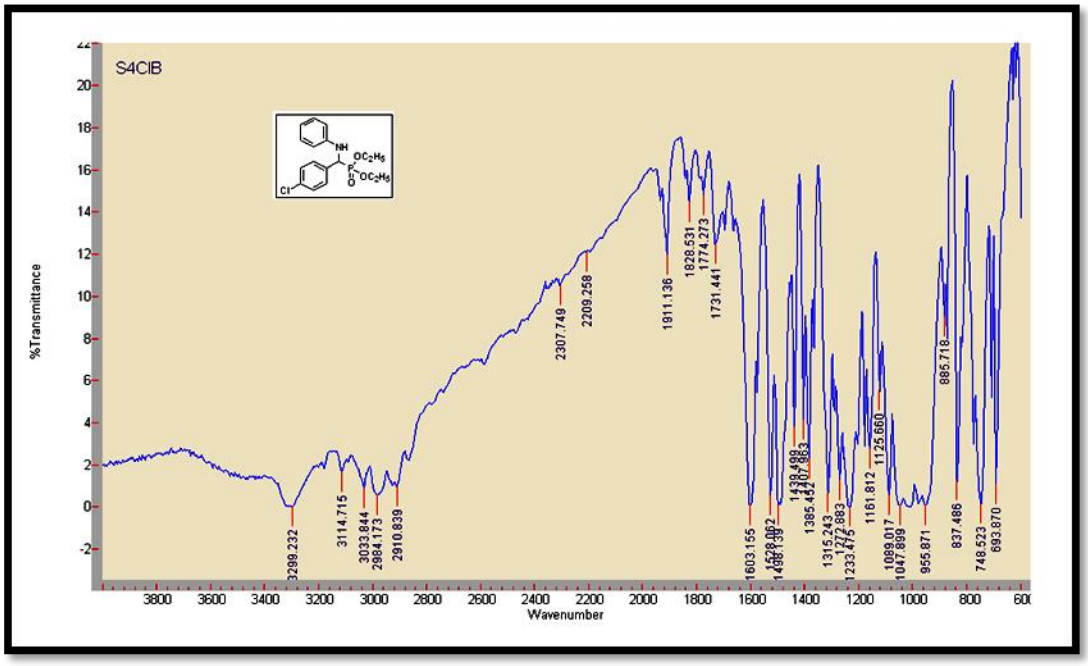

Figure. 4.5 IR Spectrum of **4b**

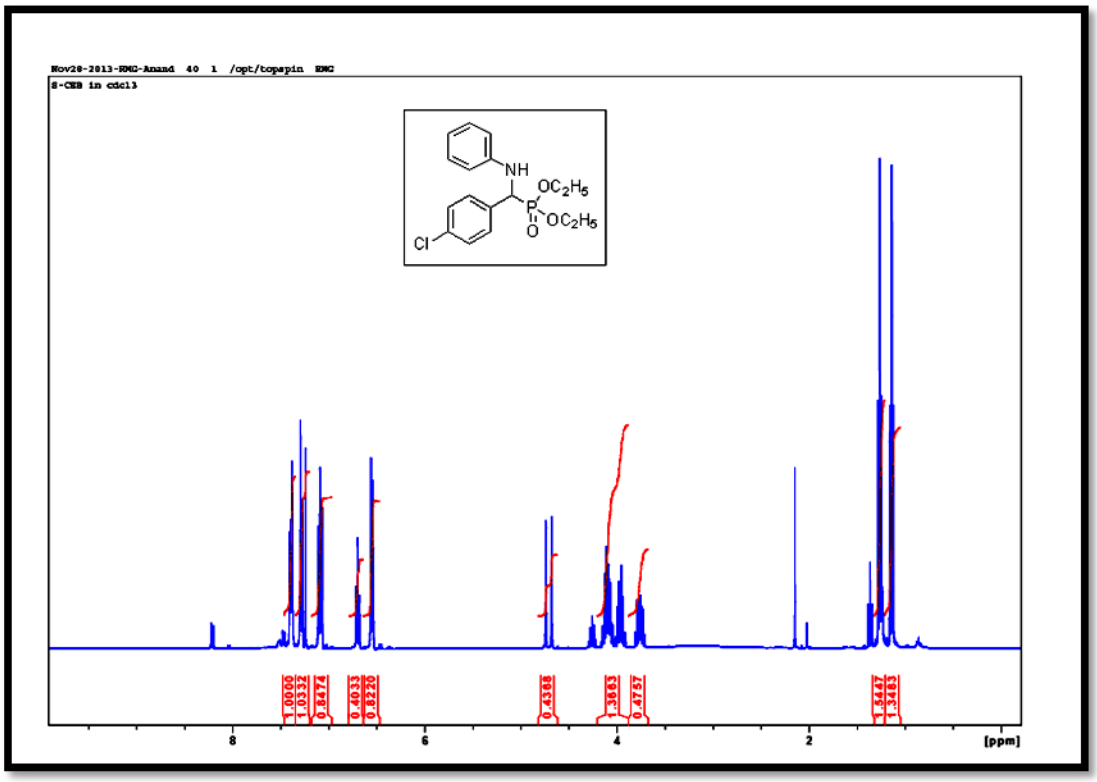

Figure. 4.6 ^{1}H-NMR spectrum of **4b**

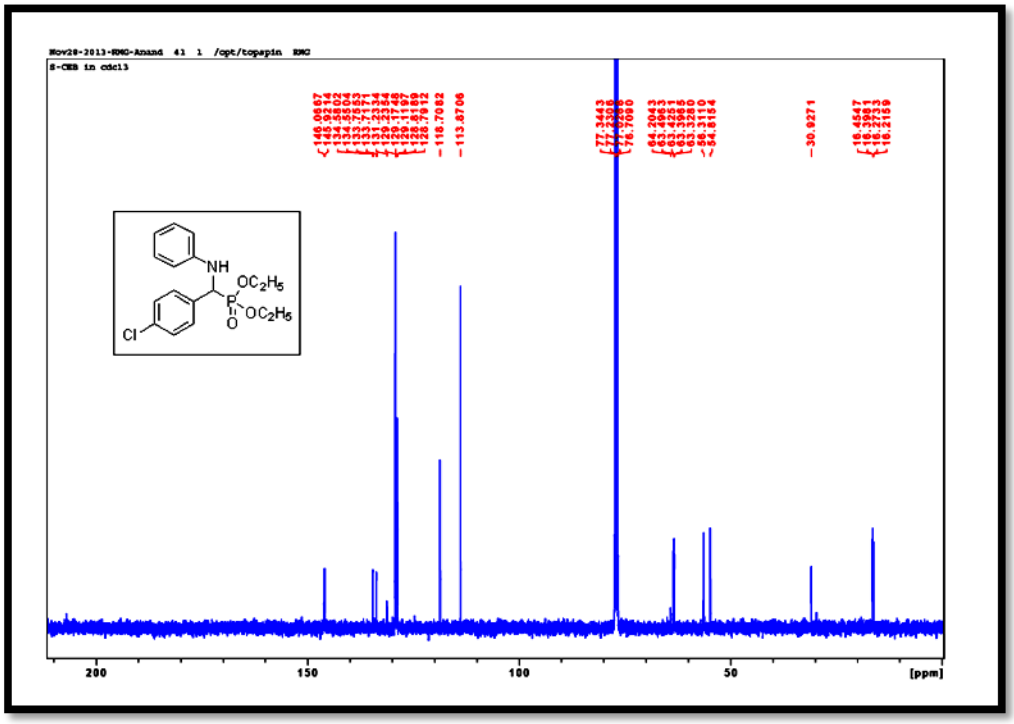

Figure. 4.7 ^{13}C-NMR spectrum of **4b**

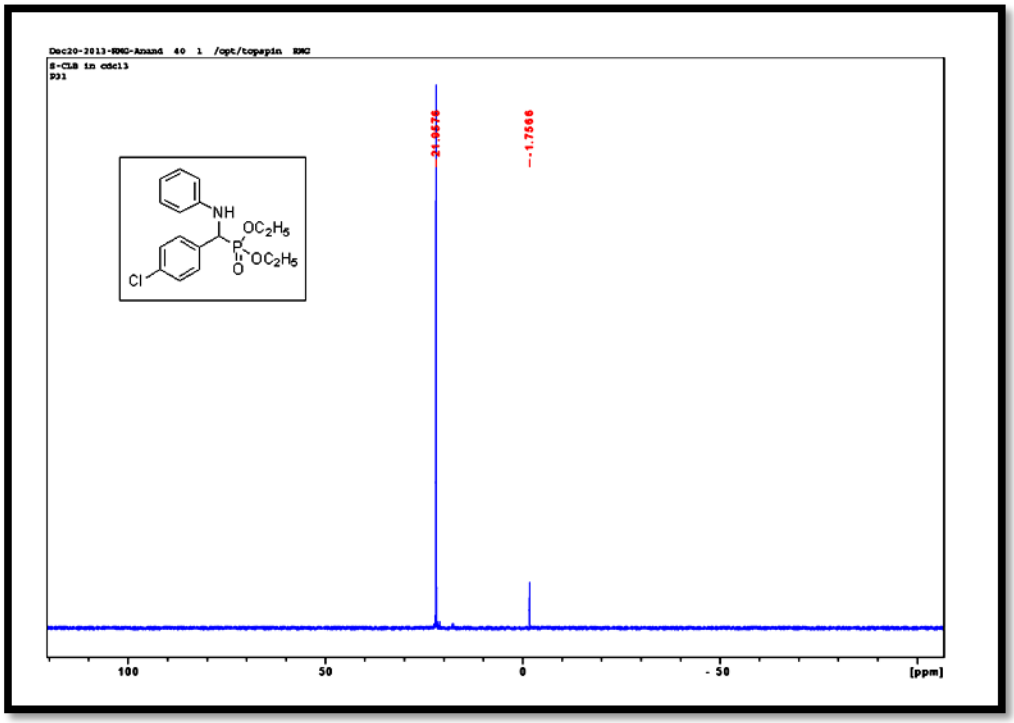

Figure. 4.8 ^{31}P-NMR spectrum of **4b**

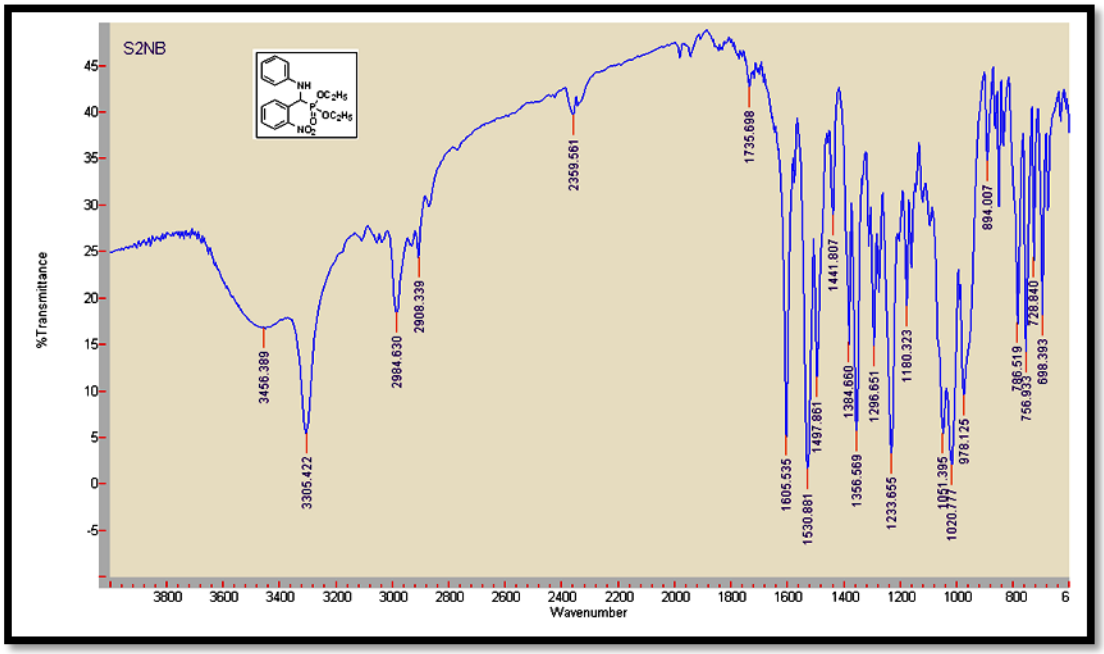

Figure. 4.9 IR Spectrum of **4c**

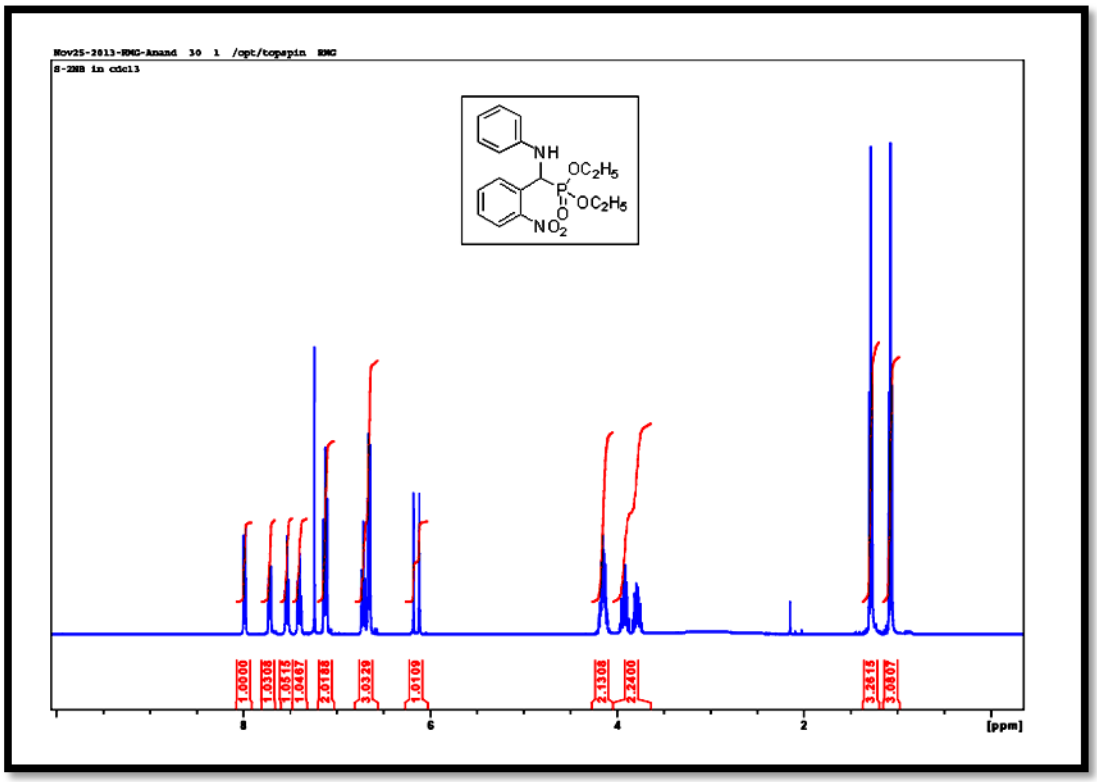

Figure. 4.10 ^{1}H-NMR spectrum of **4c**

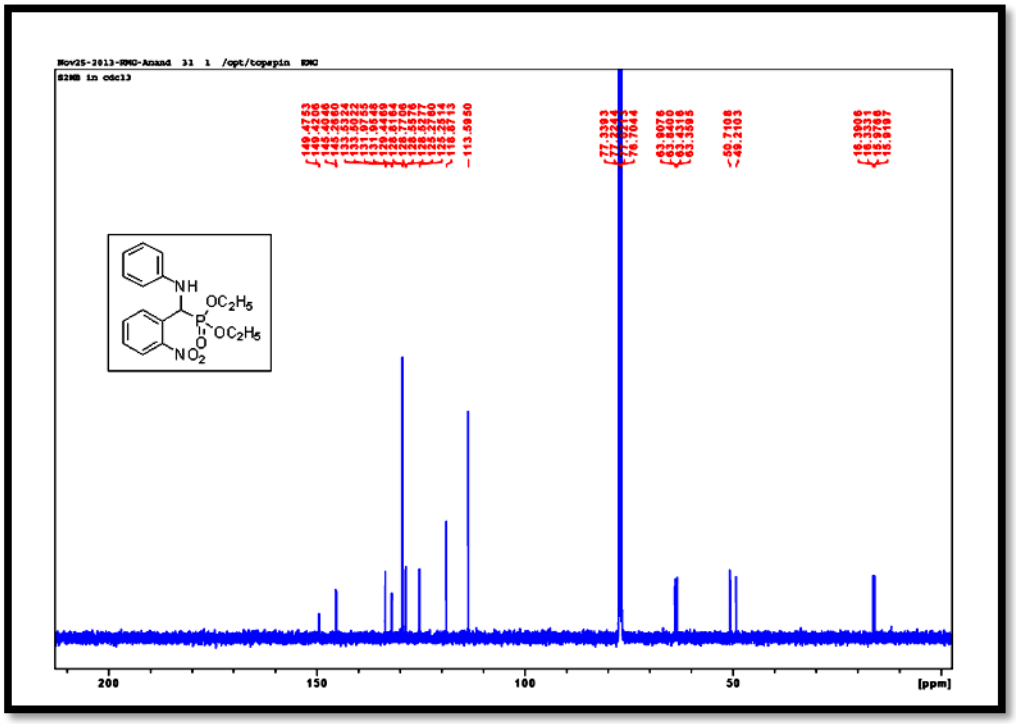

Figure. 4.11 ^{13}C-NMR spectrum of **4c**

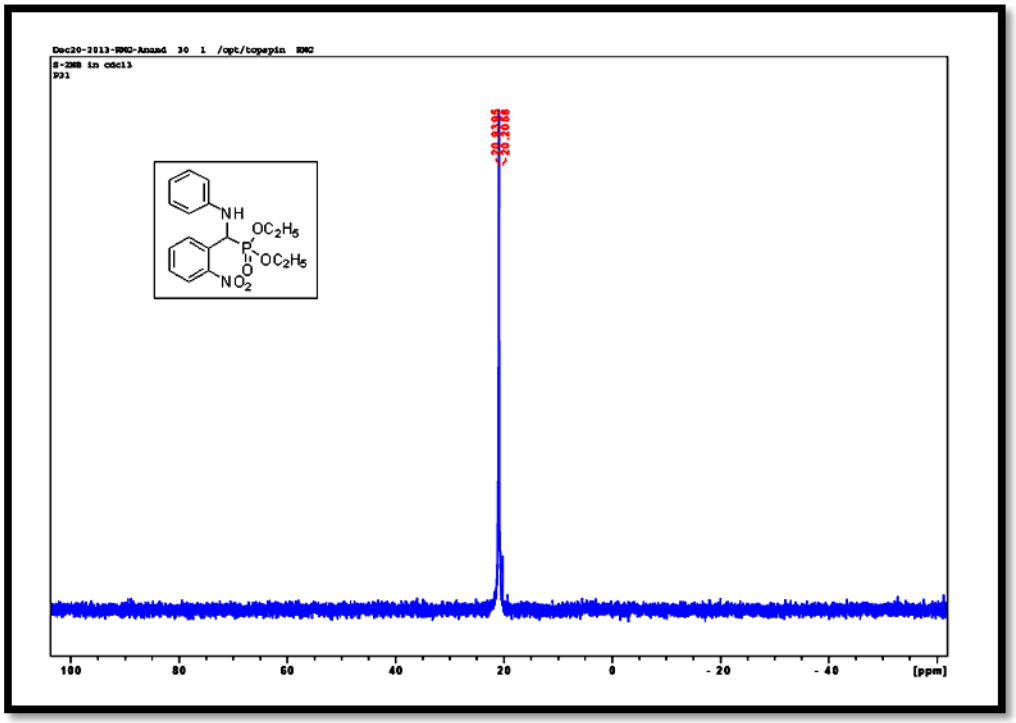

Figure. 4.12 ^{31}P-NMR spectrum of **4c**

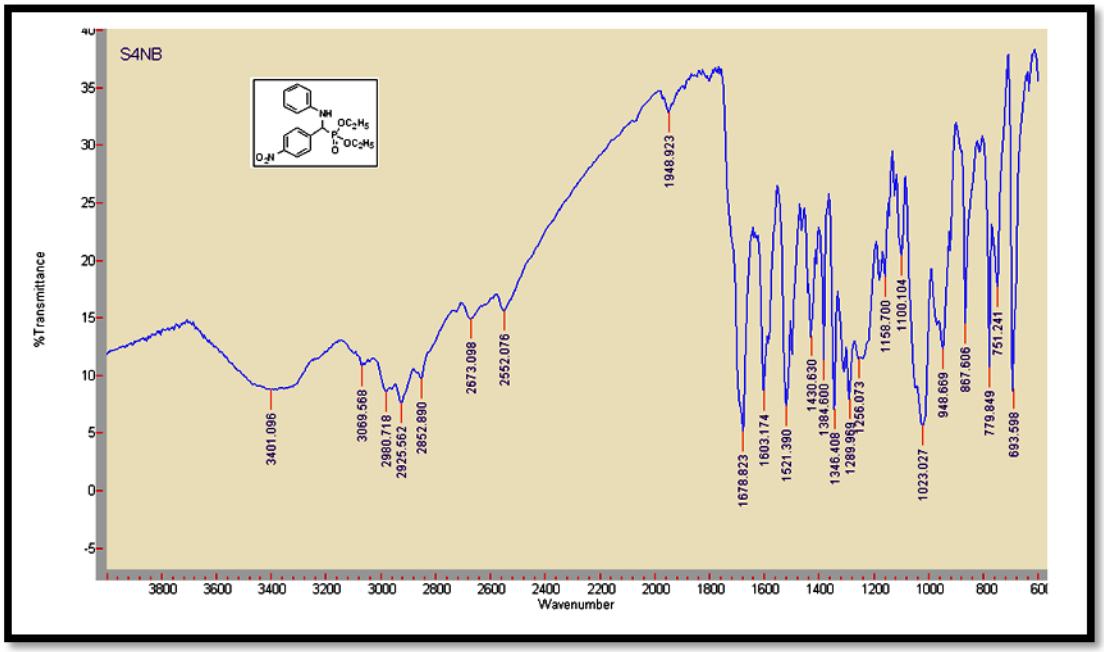

Figure. 4.13 IR Spectrum of **4d**

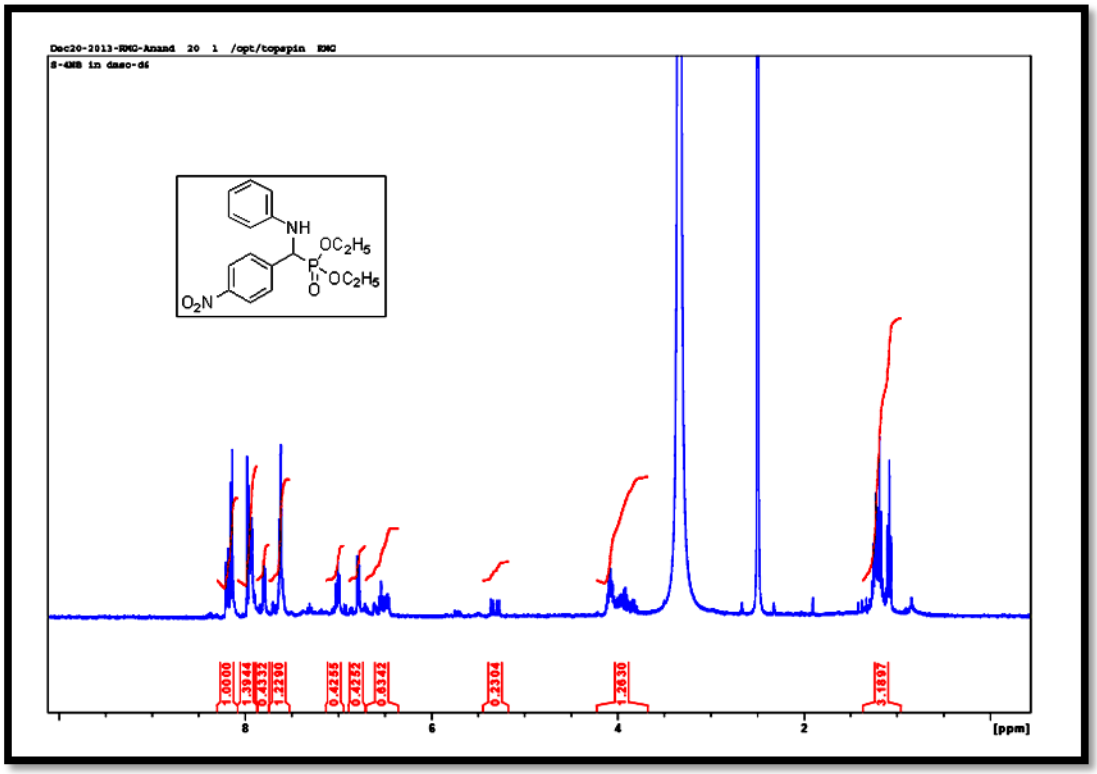

Figure. 4.14 ^{1}H-NMR spectrum of **4d**

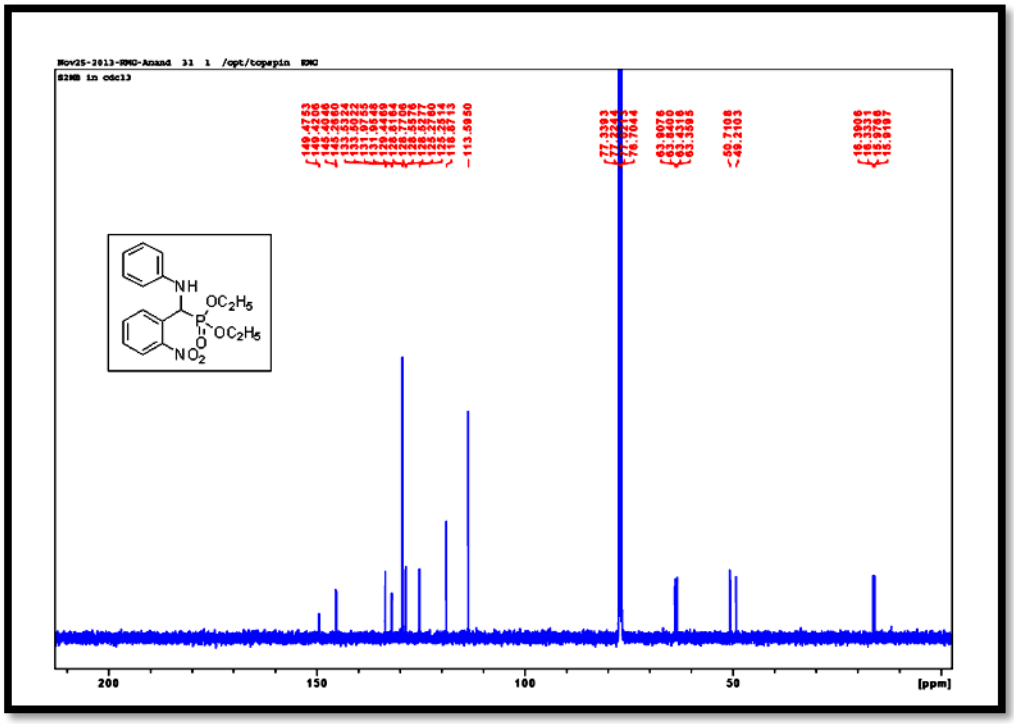

Figure. 4.15 ^{13}C-NMR spectrum of **4d**

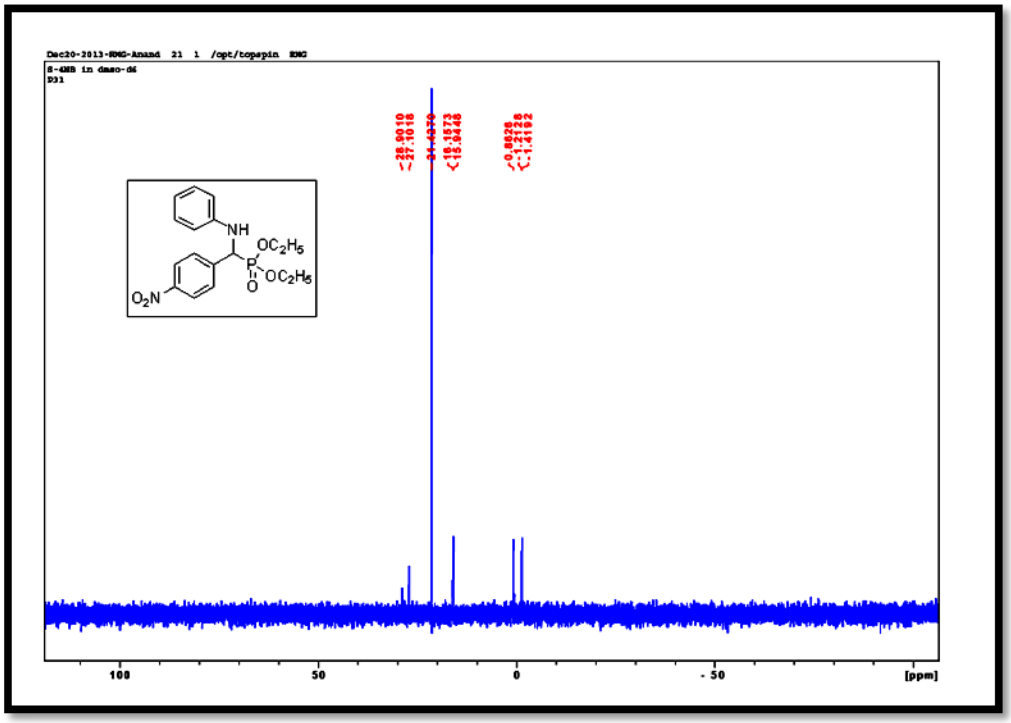

Figure. 4.16 ^{31}P-NMR spectrum of **4d**

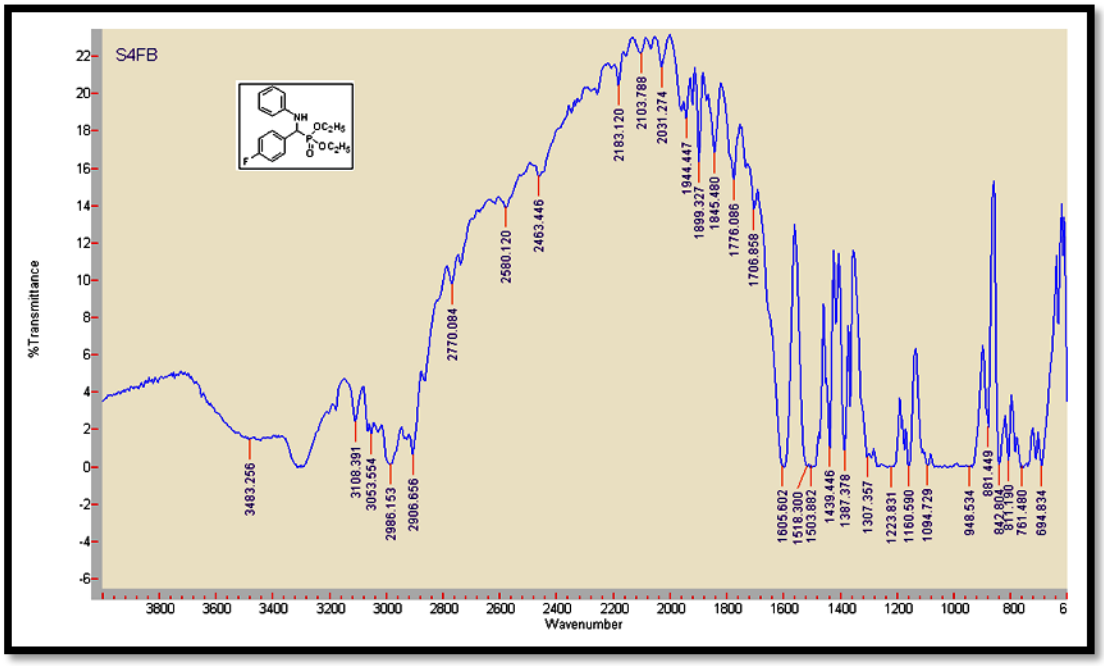

Figure. 4.17 IR Spectrum of **4e**

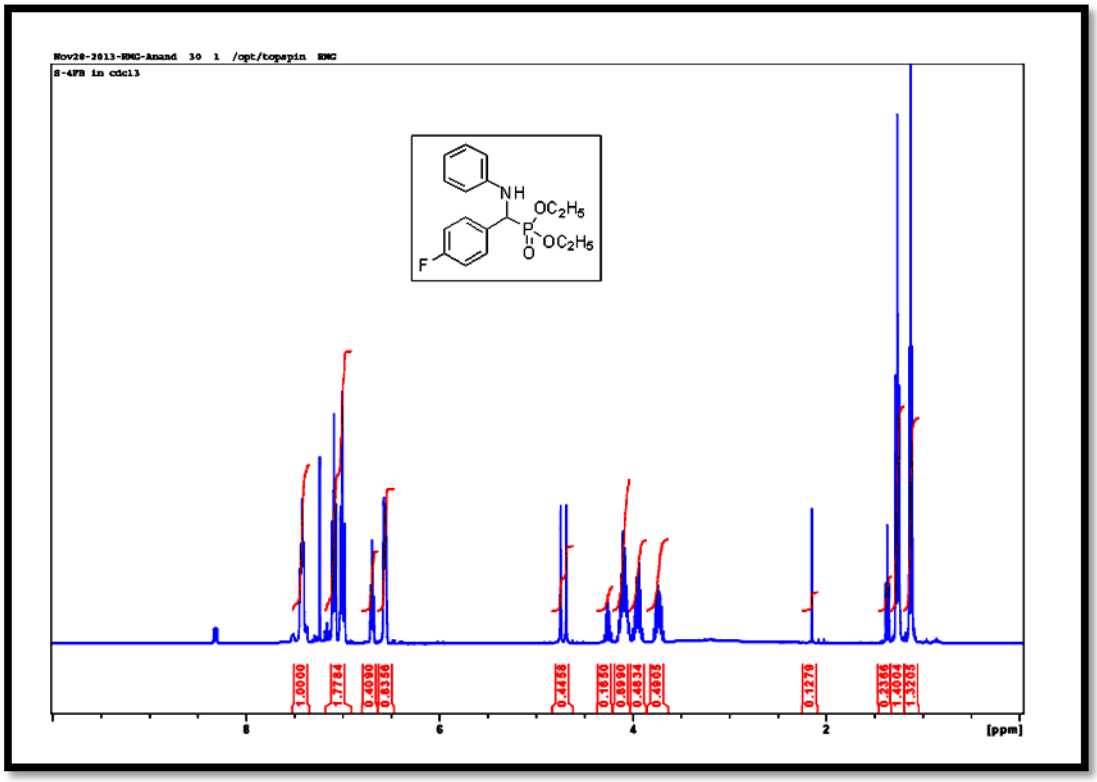

Figure. 4.18 ^{1}H-NMR spectrum of **4e**

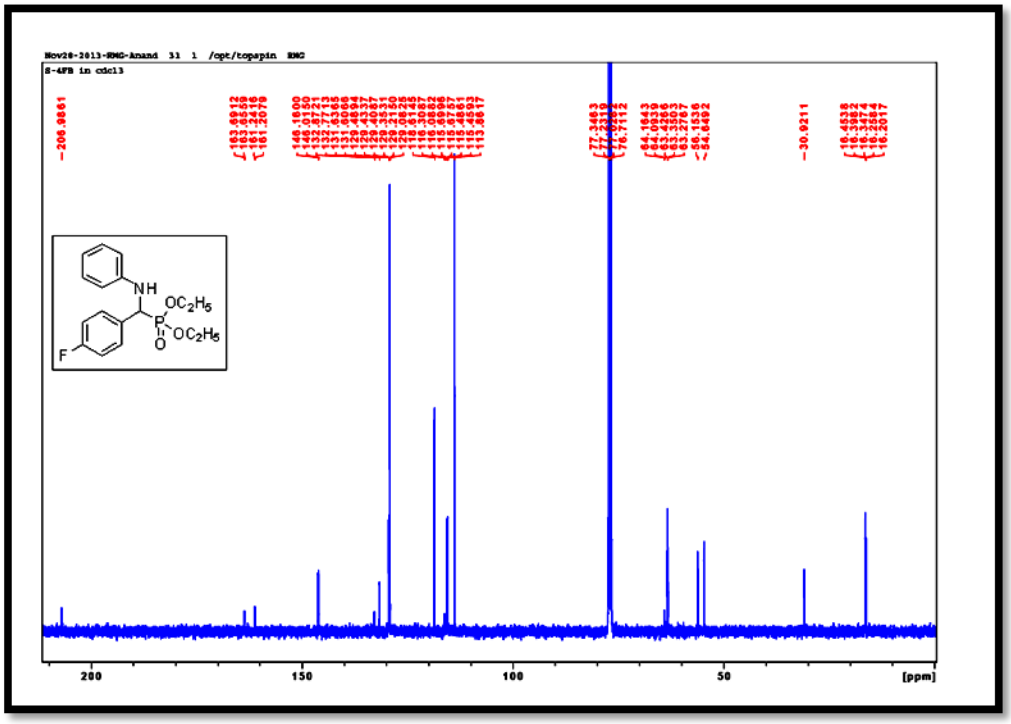

Figure. 4.19 ^{13}C-NMR spectrum of **4e**

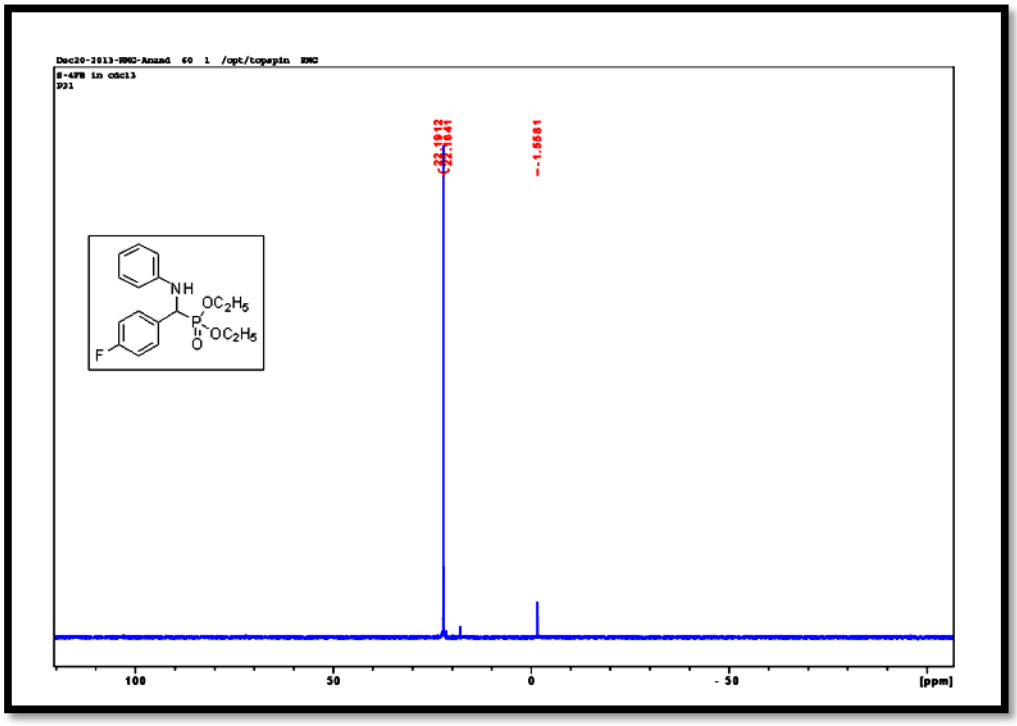

Figure. 4.20 ^{31}P-NMR spectrum of **4e**

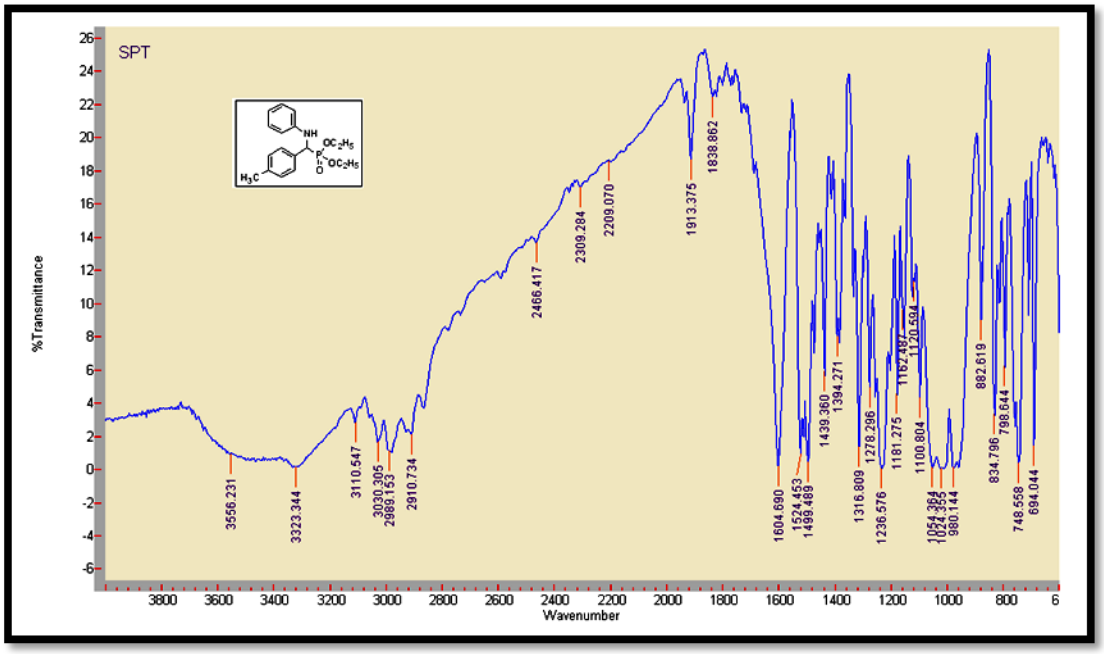

Figure. 4.21 IR Spectrum of **4f**

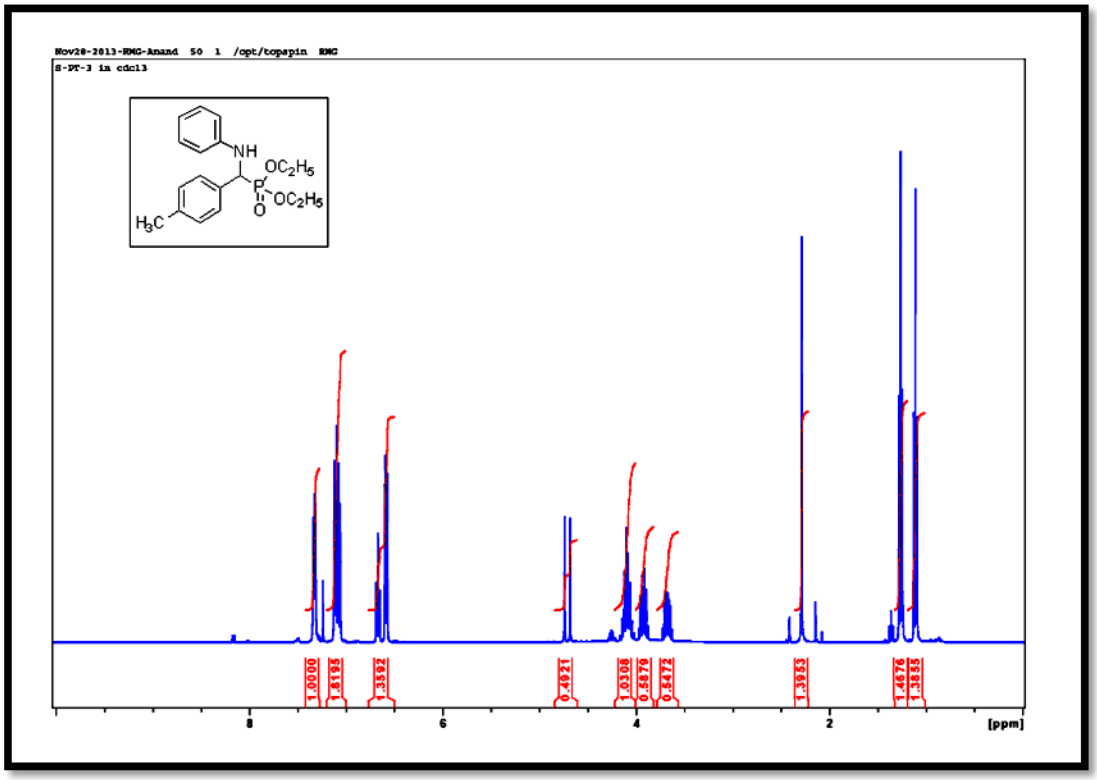

Figure. 4.22 ^{1}H-NMR spectrum of **4f**

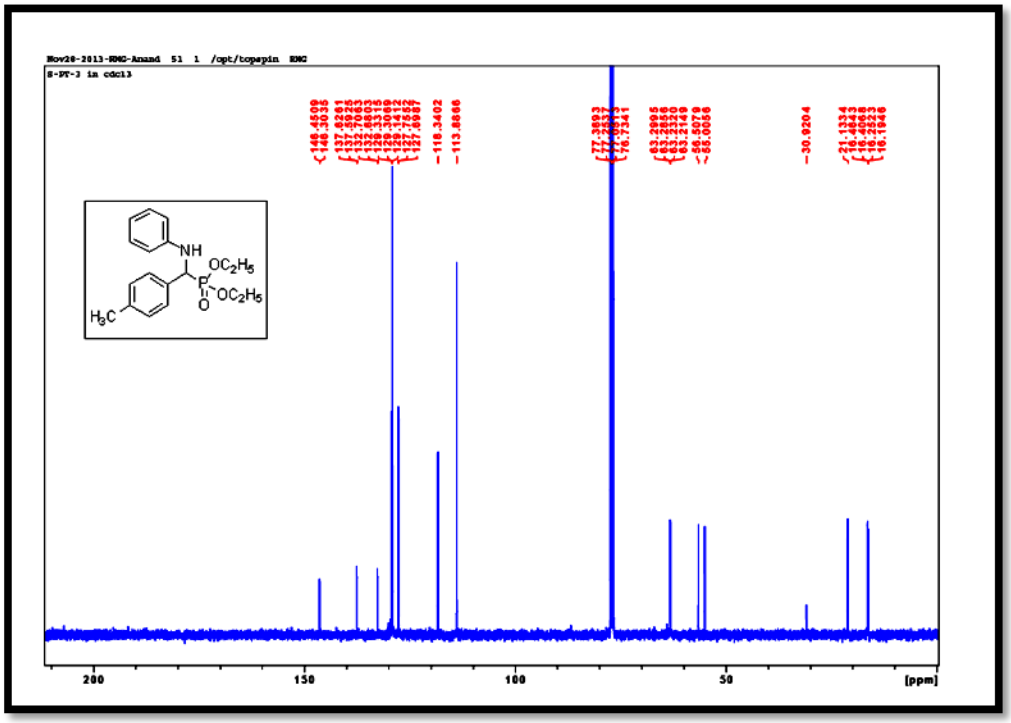

Figure. 4.23 ^{13}C-NMR spectrum of **4f**

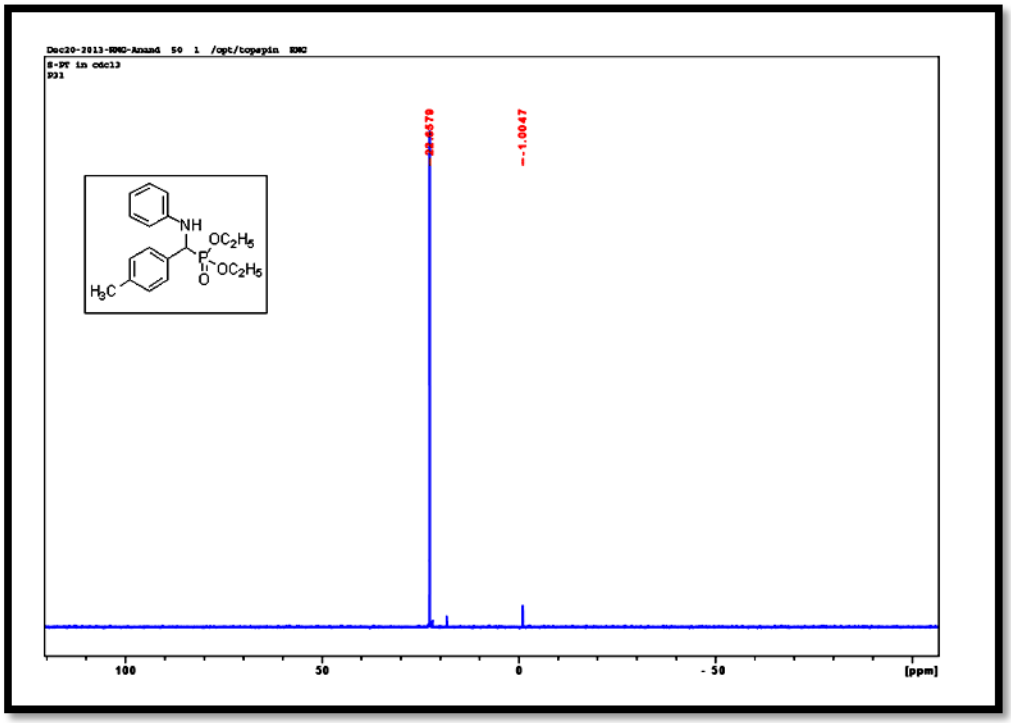

Figure. 4.24 ^{31}P-NMR spectrum of **4f**

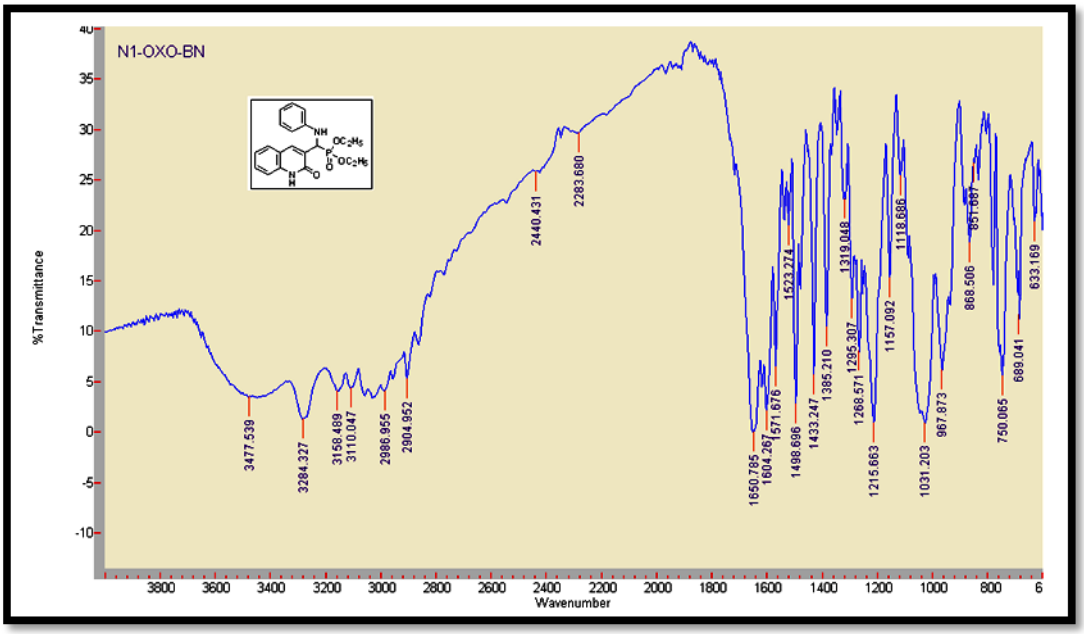

Figure. 4.25 IR Spectrum of **4g**

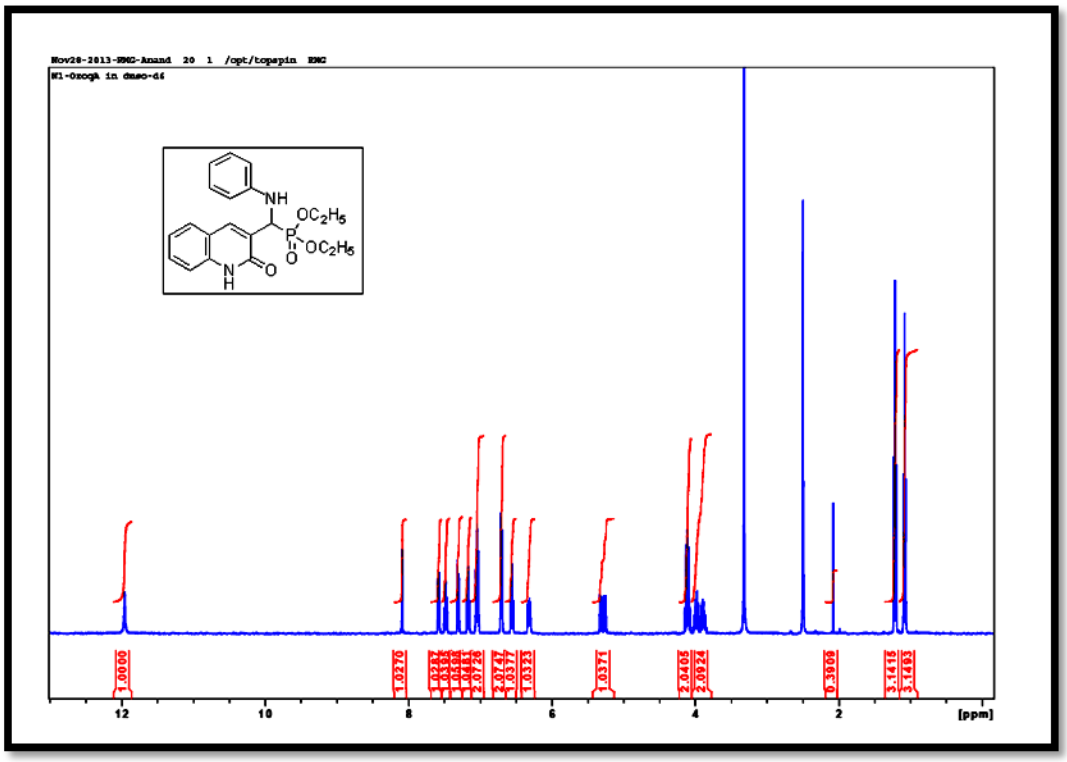

Figure. 4.26 ^{1}H-NMR spectrum of **4g**

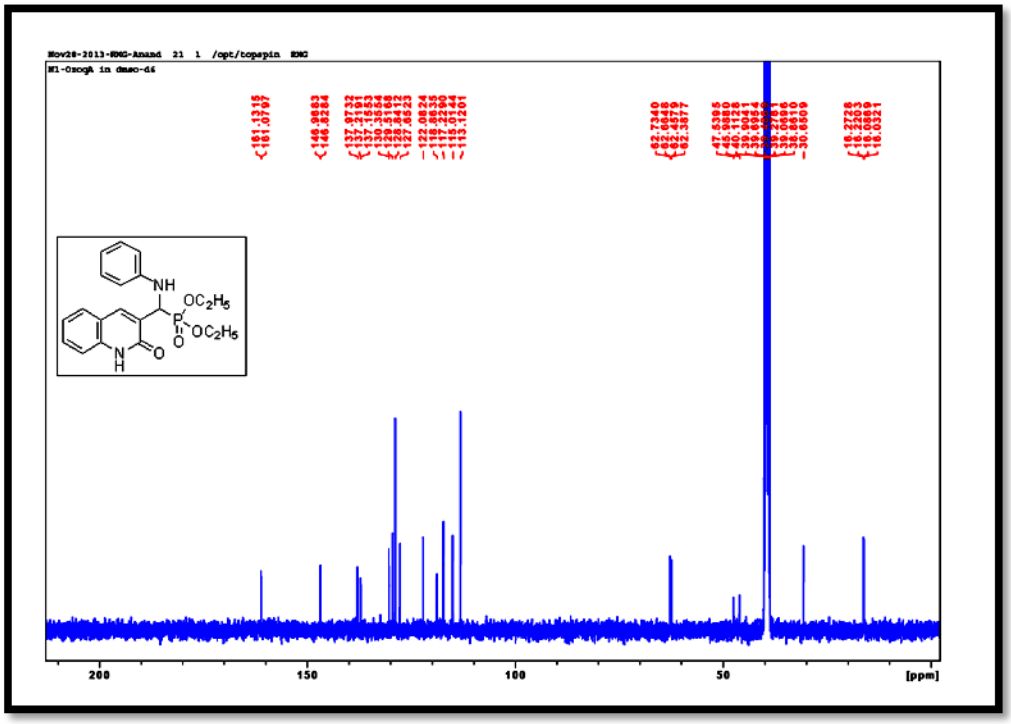

Figure. 4.27 ^{13}C-NMR spectrum of **4g**

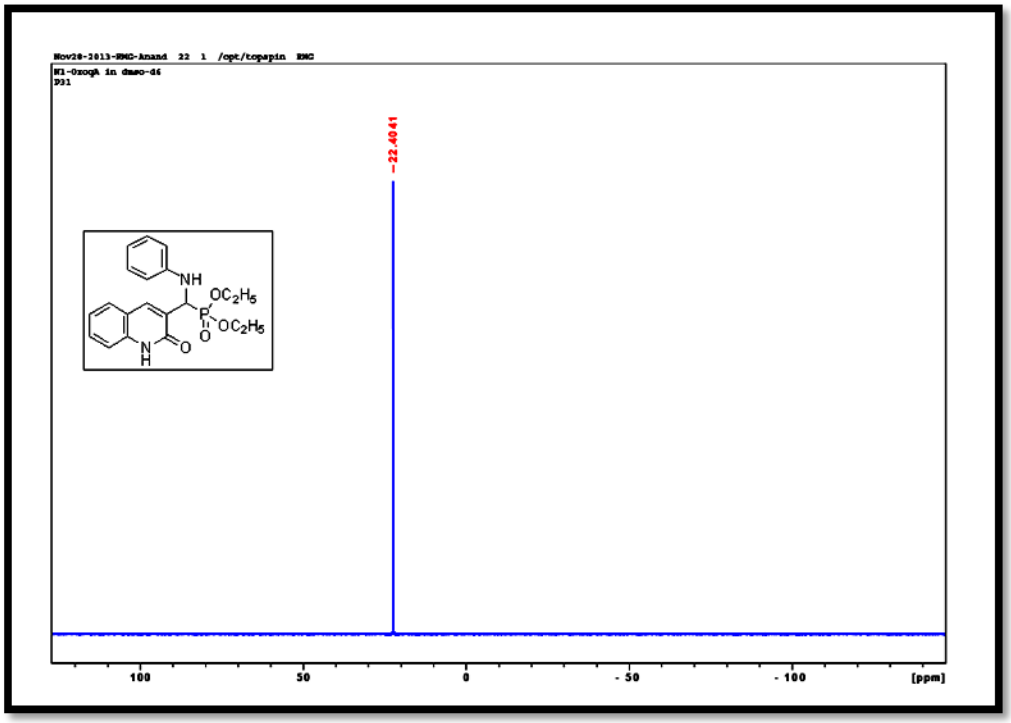

Figure. 4.28 ^{31}P-NMR spectrum of **4g**

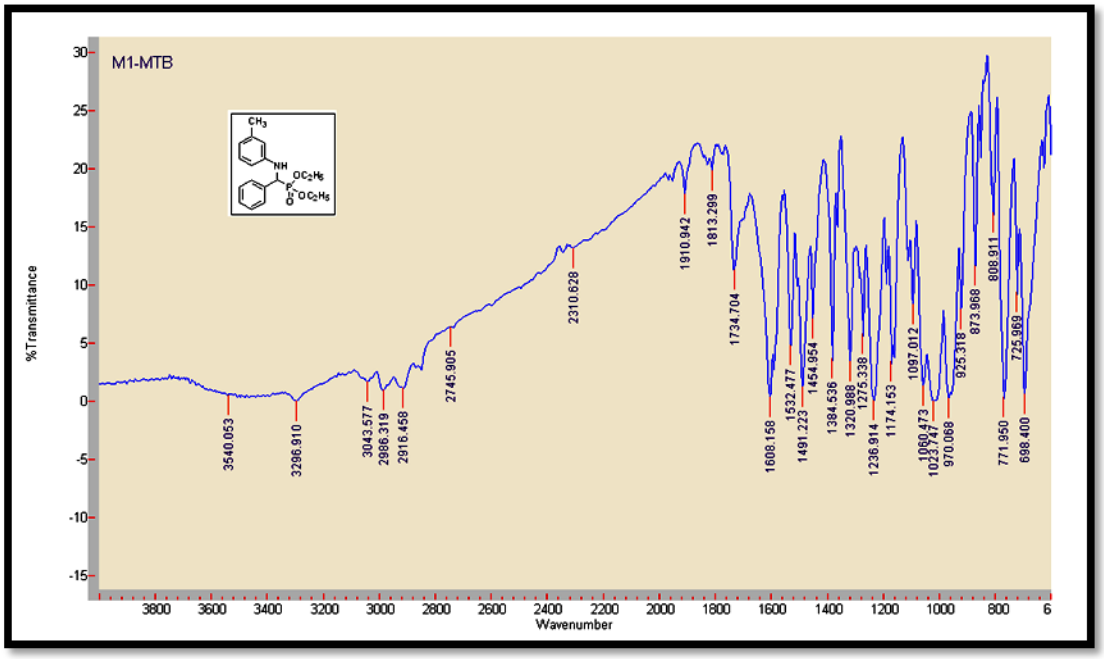

Figure. 4.29 IR Spectrum of **4h**

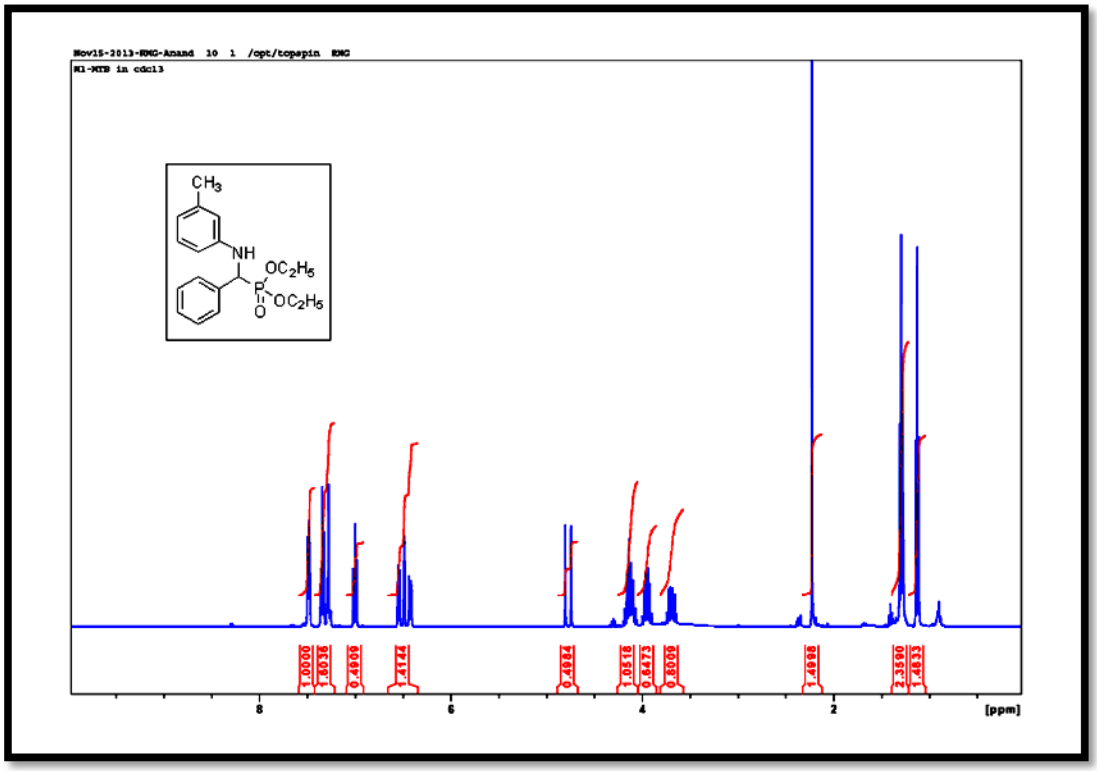

Figure. 4.30 ^{1}H-NMR spectrum of **4h**

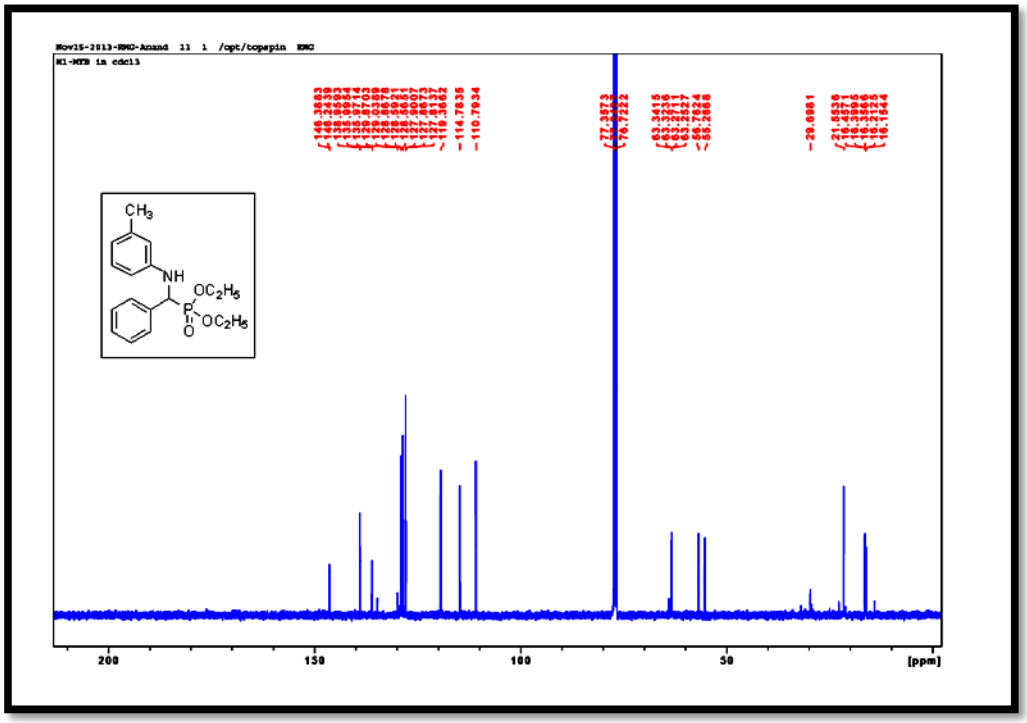

Figure. 4.31 ^{13}C-NMR spectrum of **4h**

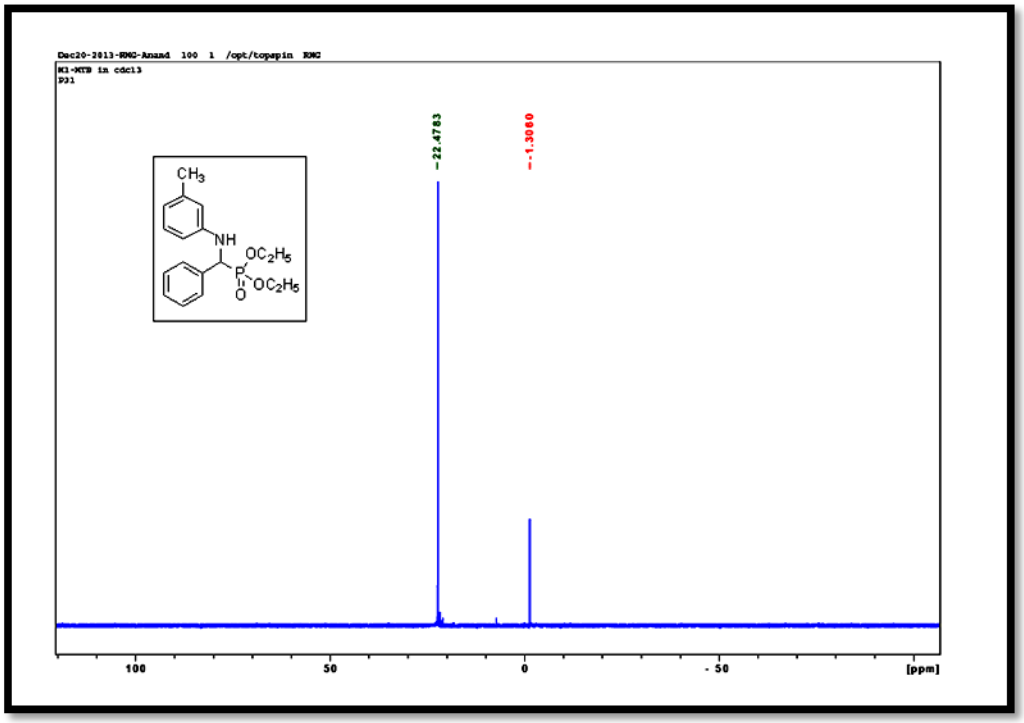

Figure. 4.32 ^{31}P-NMR spectrum of **4h**

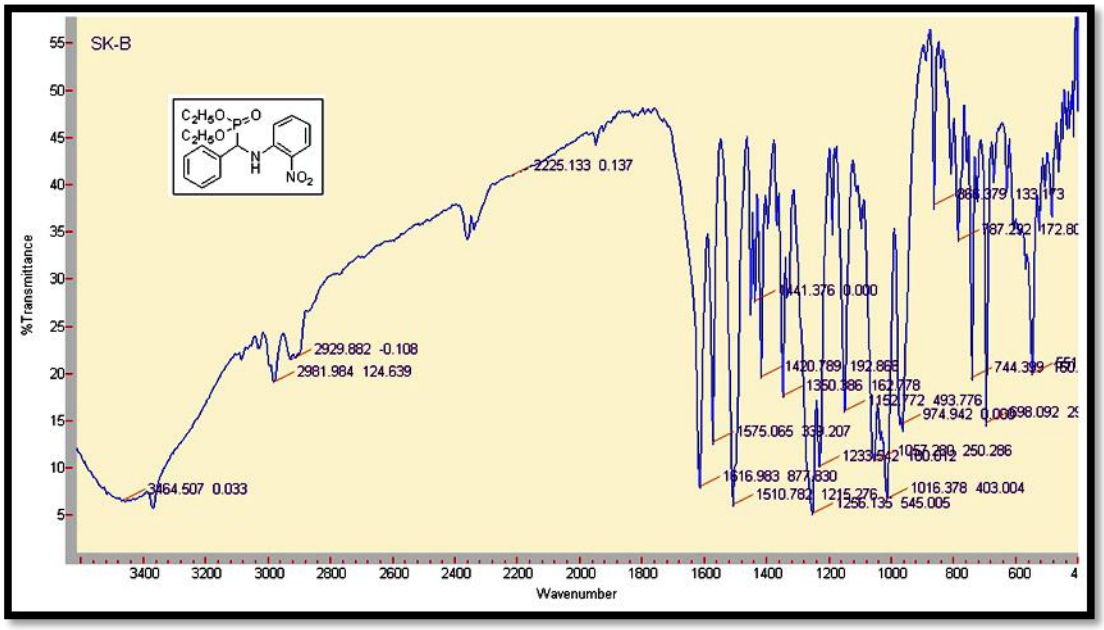

Figure. 4.33 IR Spectrum of **4i**

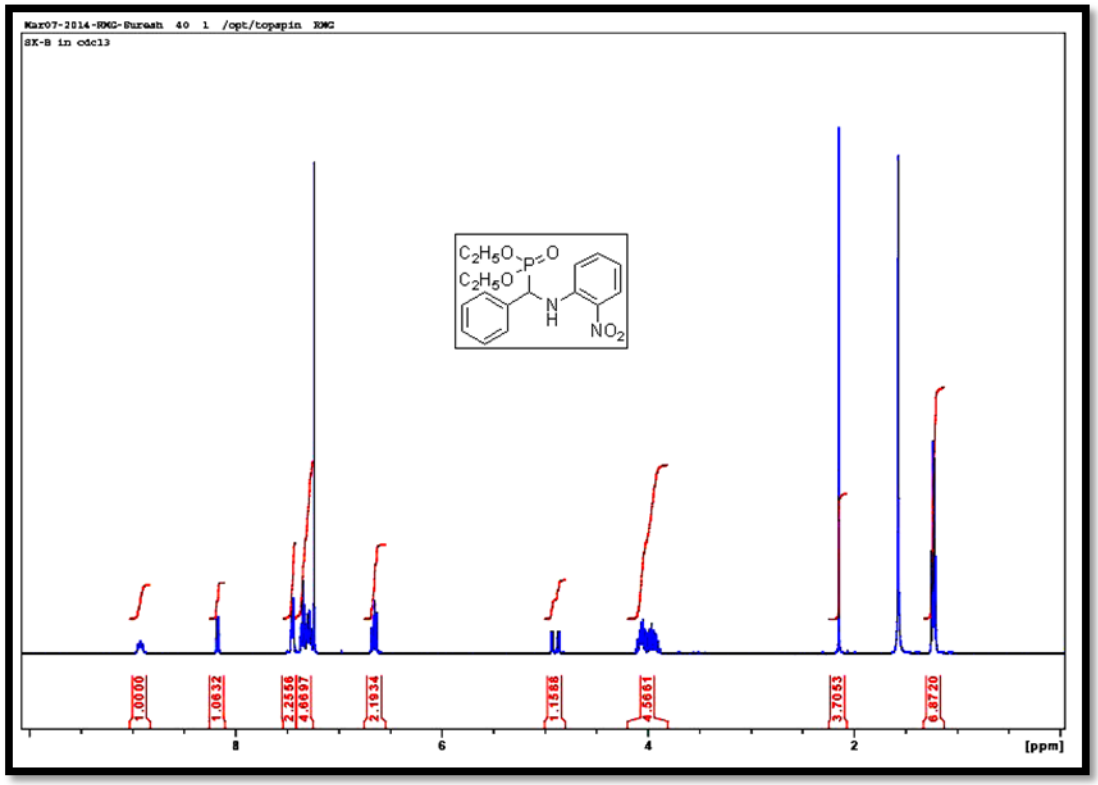

Figure. 4.34 ^{1}H-NMR spectrum of **4i**

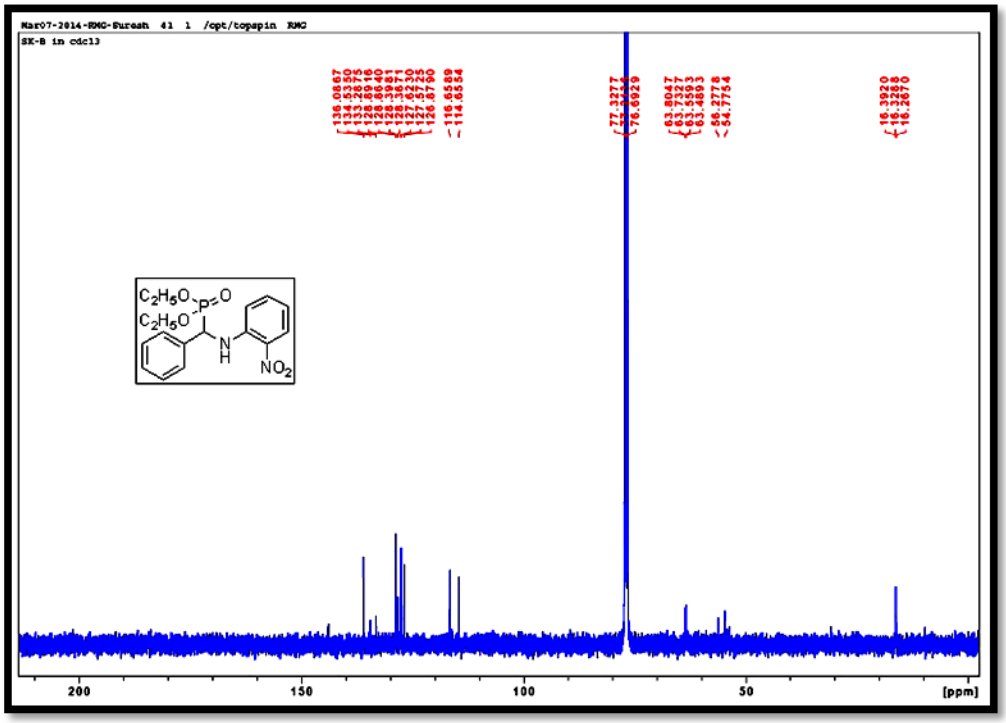

Figure. 4.35 ^{13}C-NMR spectrum of **4i**

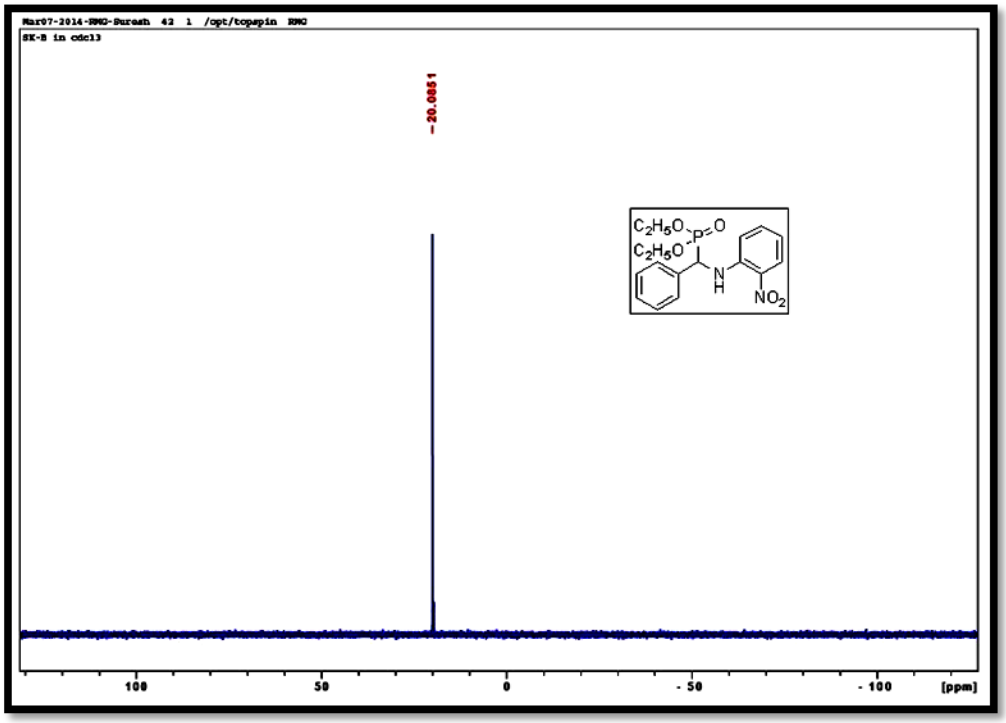

Figure. 4.36 ^{31}P-NMR spectrum of **4i**

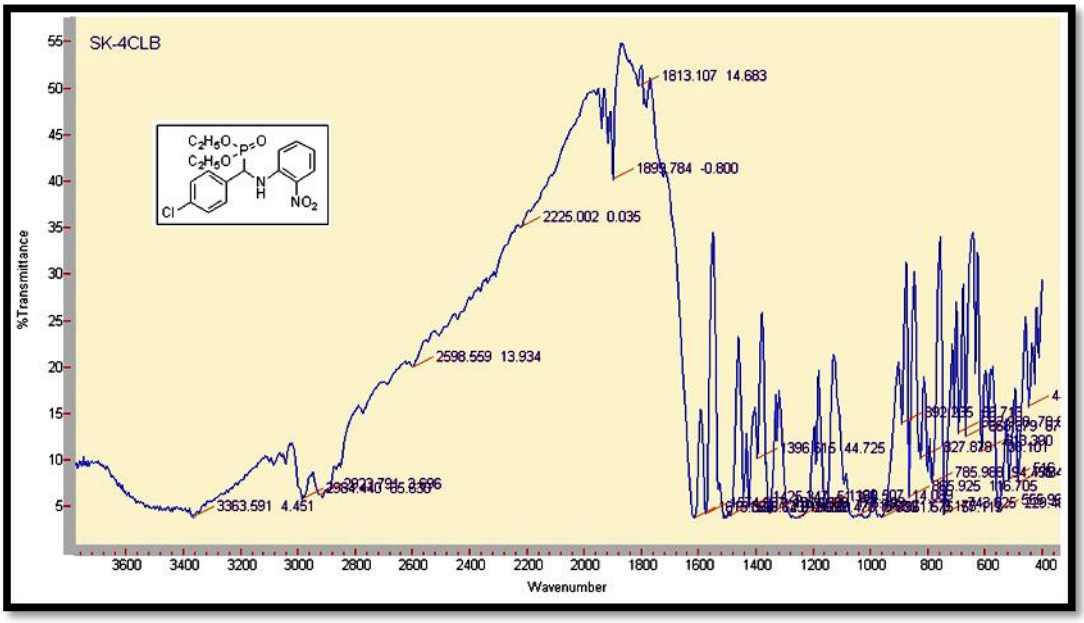

Figure. 4.37 IR Spectrum of **4j**

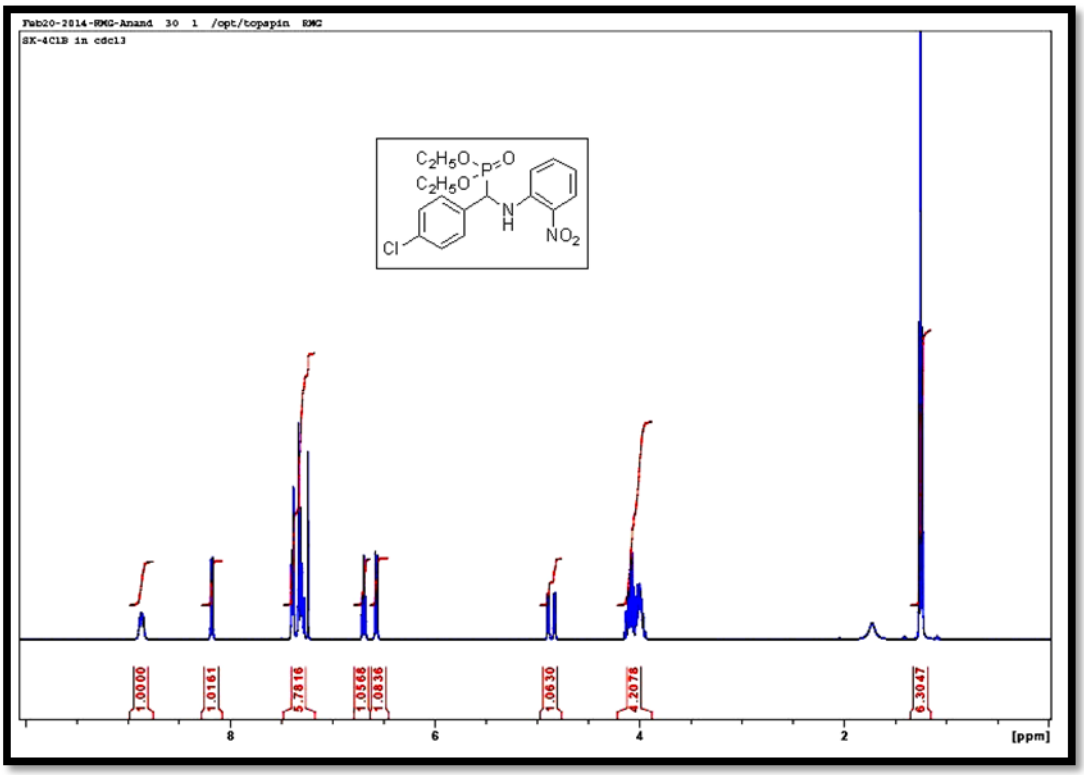

Figure. 4.38 ^{1}H-NMR spectrum of **4j**

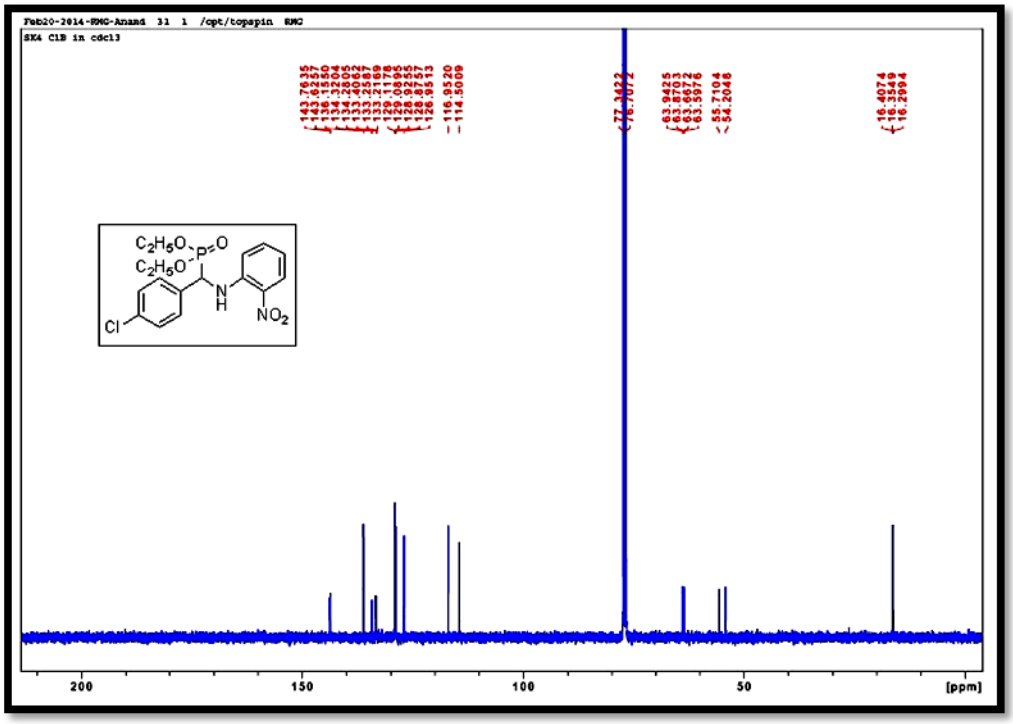

Figure. 4.39 ^{13}C-NMR spectrum of **4j**

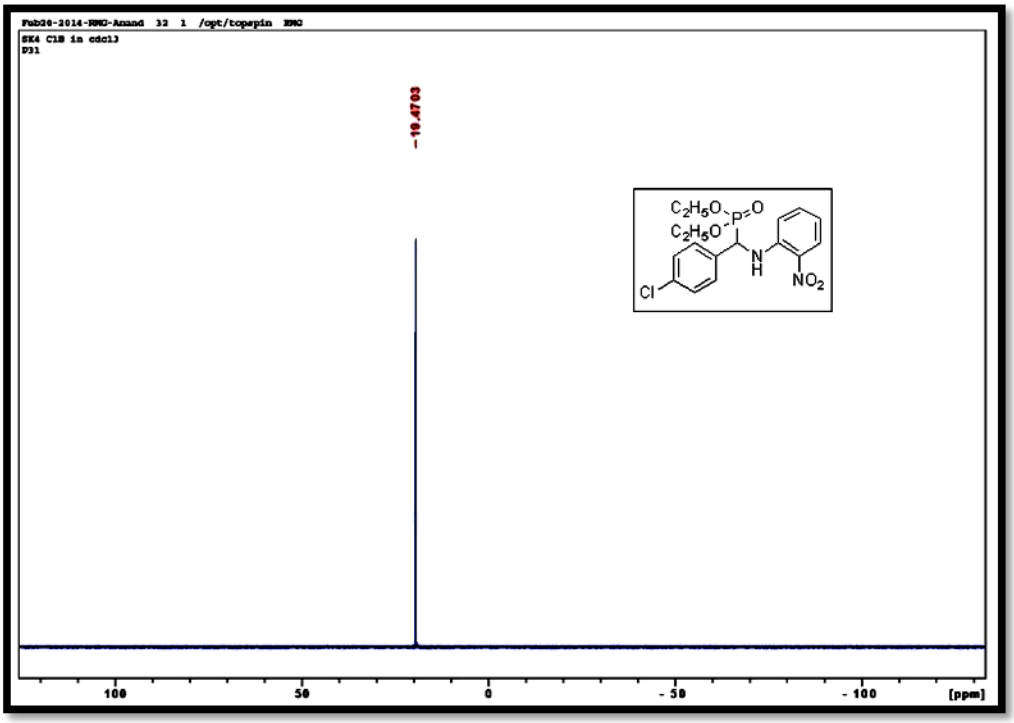

Figure. 4.40 ^{31}P-NMR spectrum of **4j**

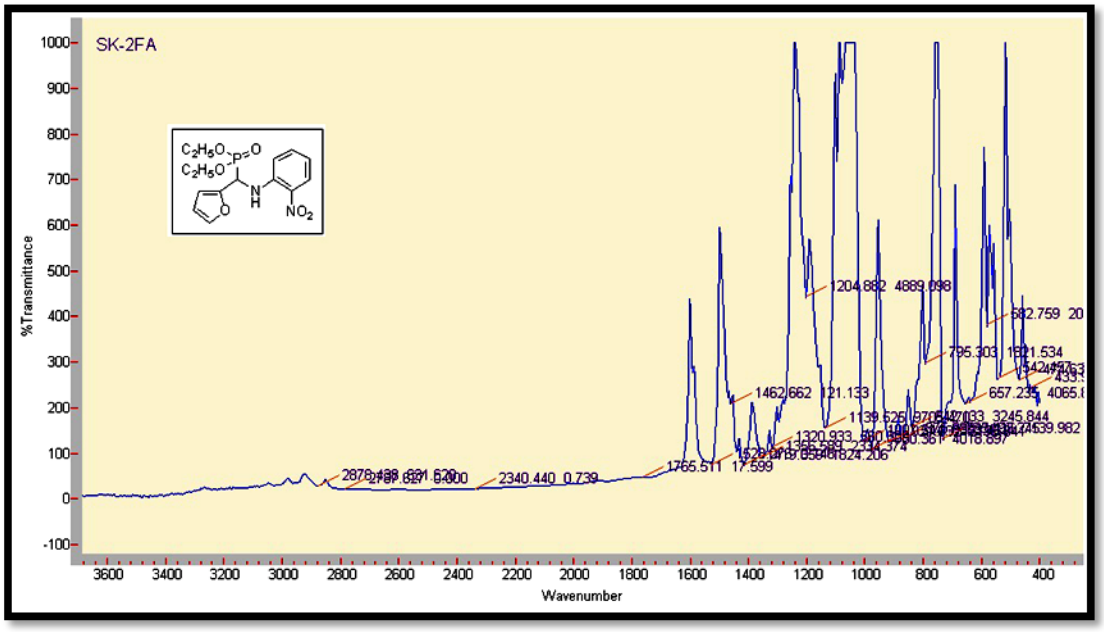

Figure. 4.41 IR Spectrum of **4k**

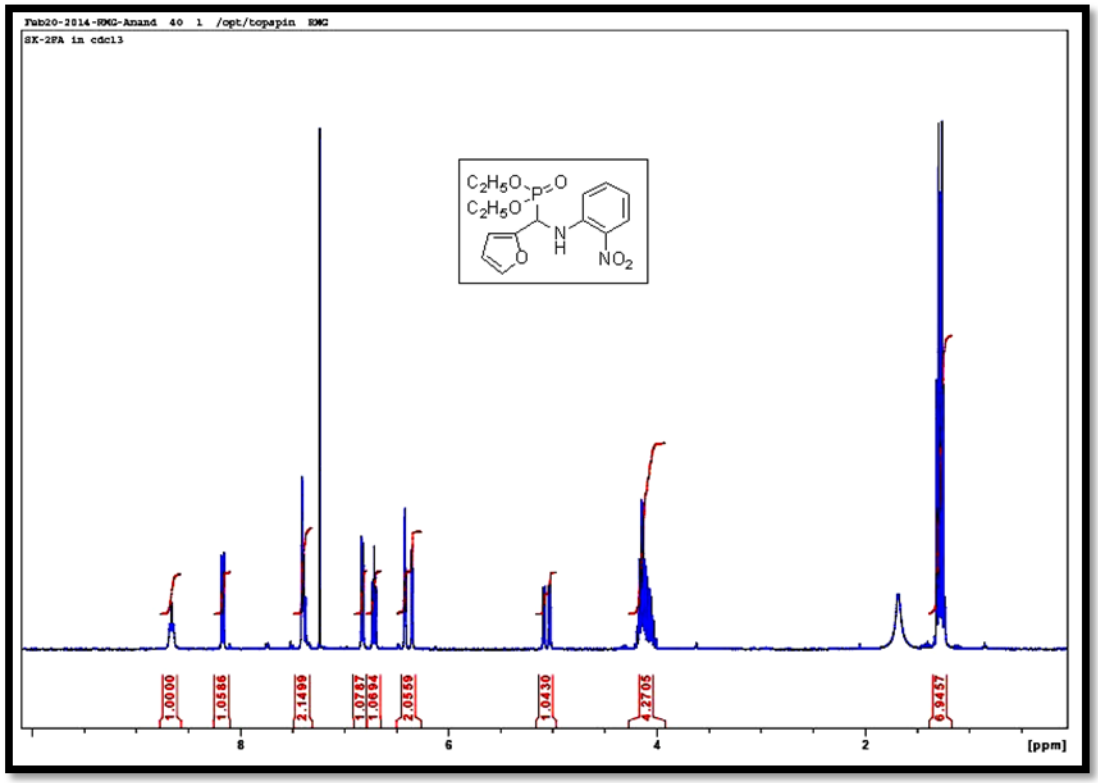

Figure. 4.42 ^{1}H-NMR spectrum of **4k**

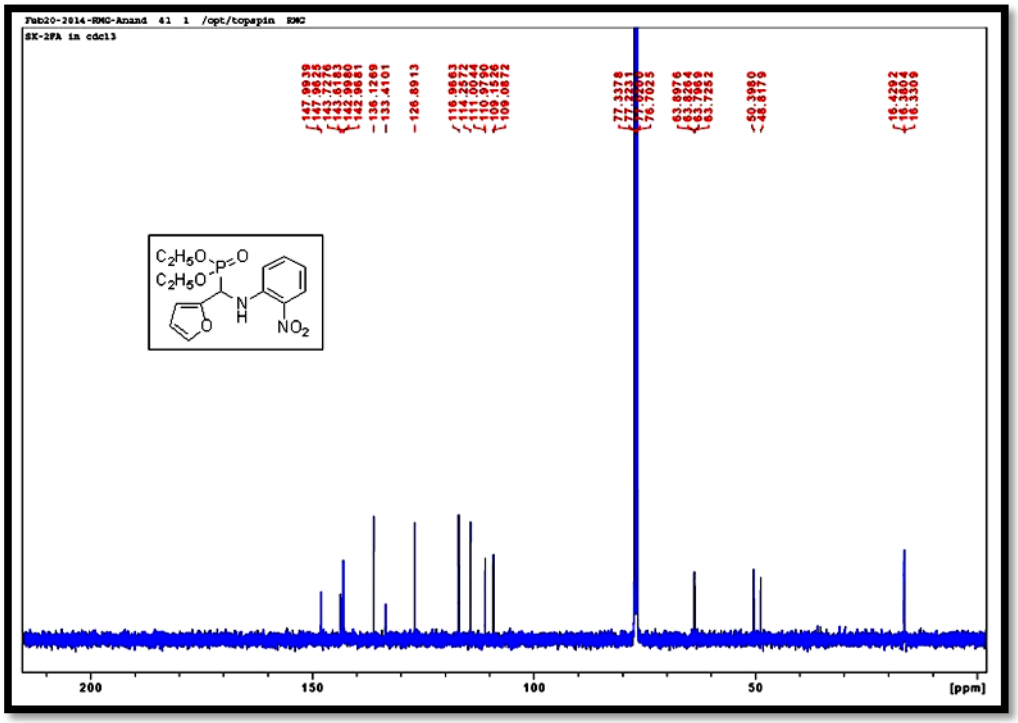

Figure. 4.43 ^{13}C-NMR spectrum of **4k**

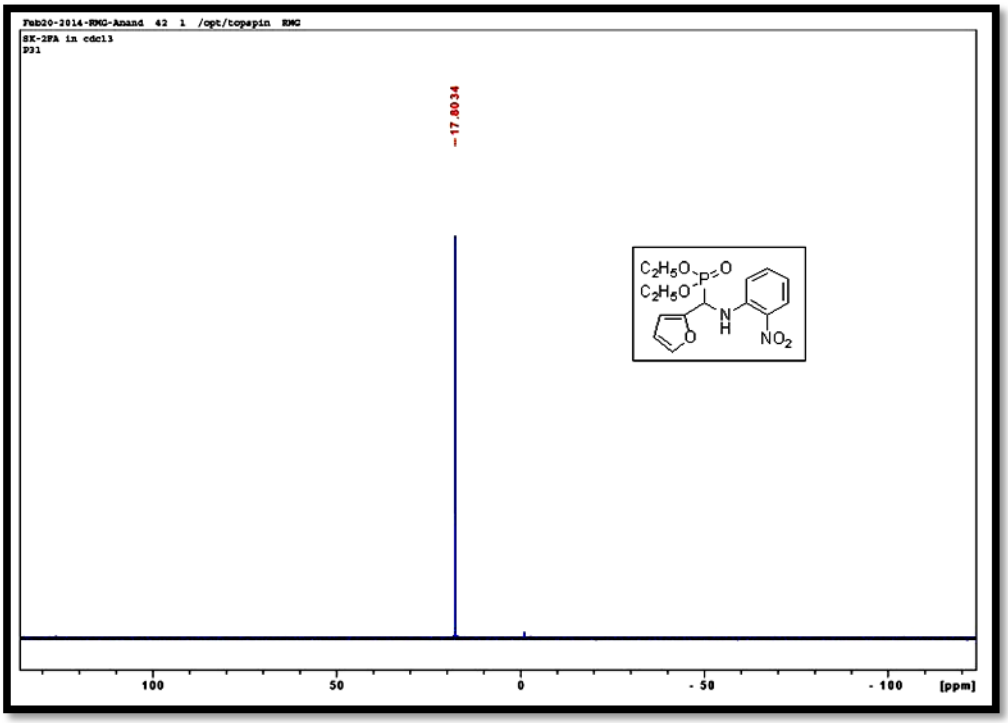

Figure. 4.44 ^{31}P-NMR spectrum of **4k**

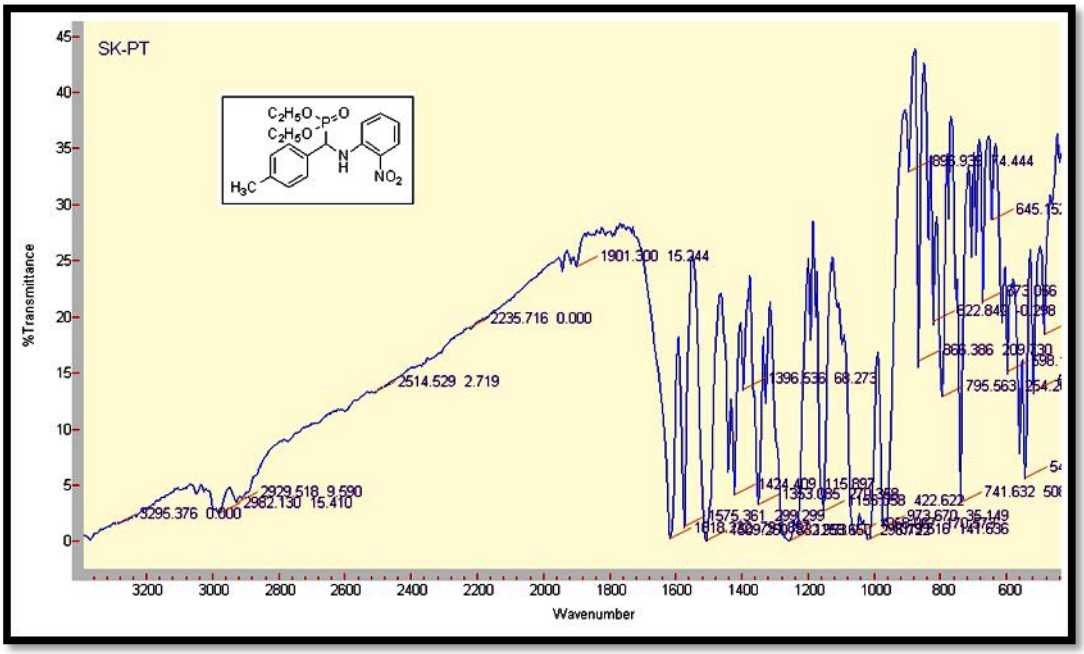

Figure. 4.45 IR Spectrum of **4l**

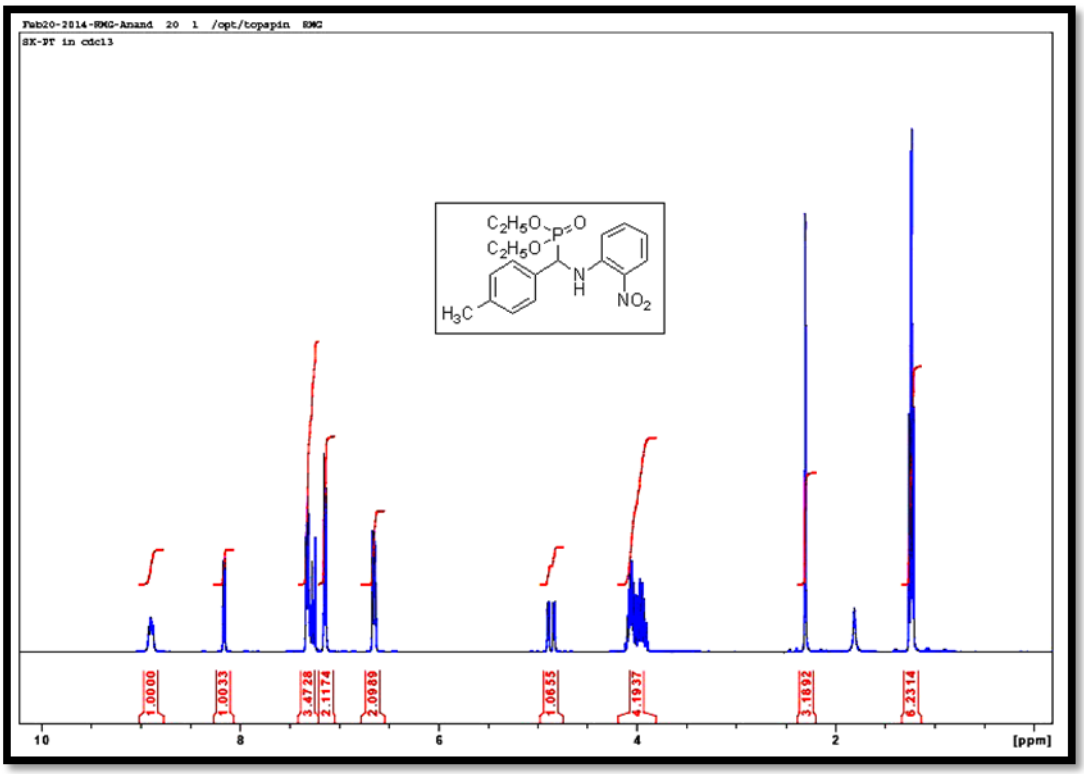

Figure. 4.46 ^{1}H-NMR spectrum of **4l**

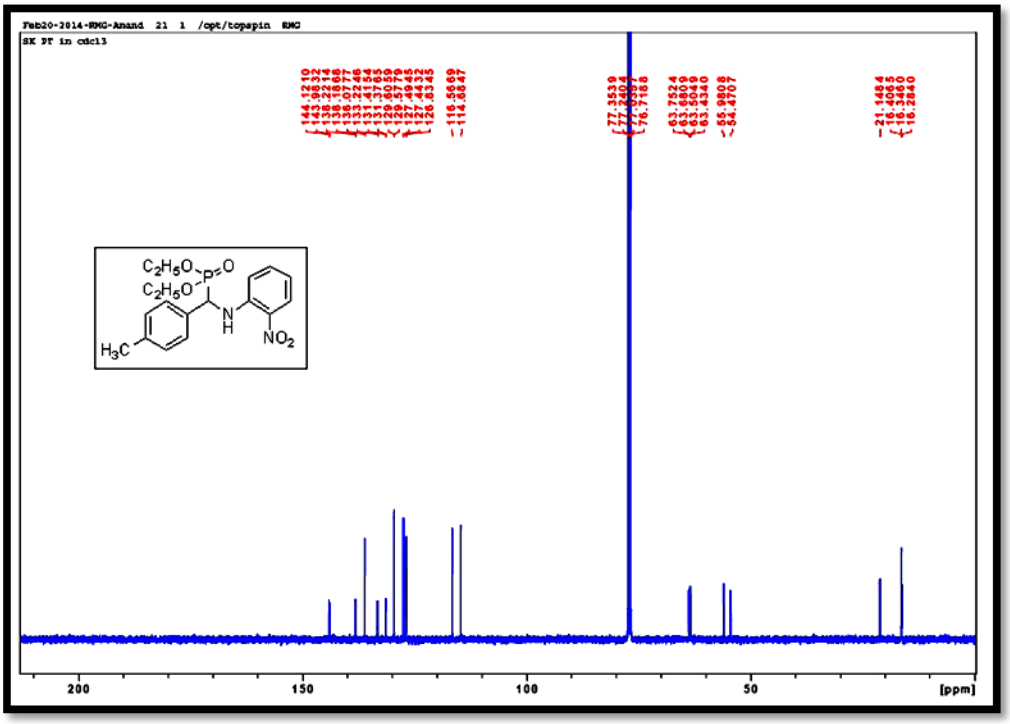

Figure. 4.47 ^{13}C-NMR spectrum of **4l**

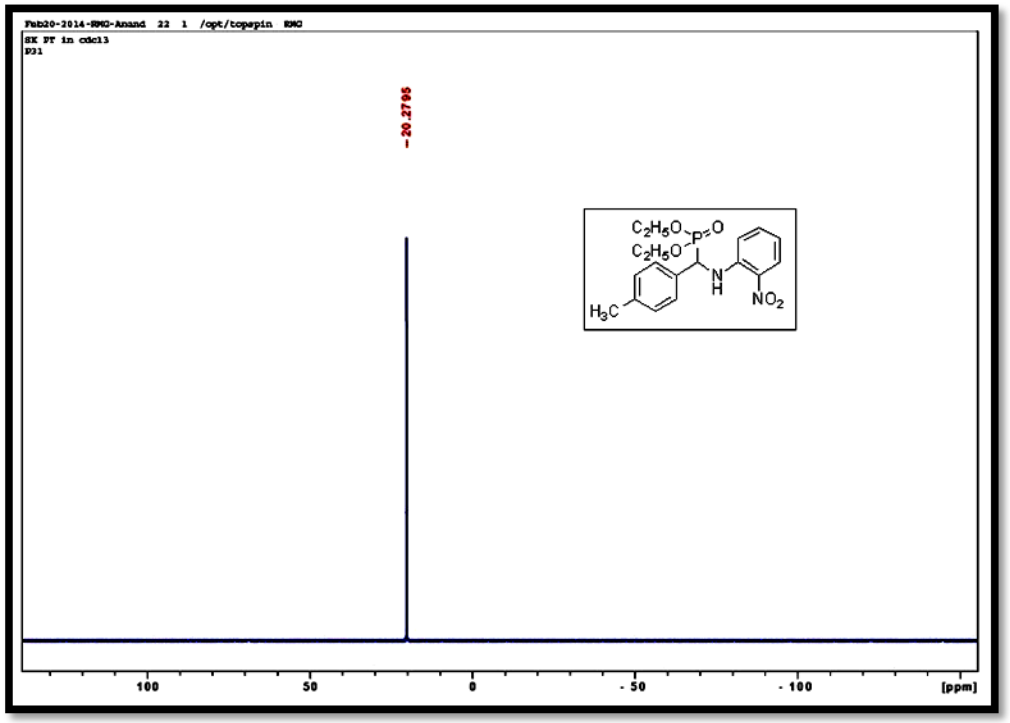

Figure. 4.48 ^{31}P-NMR spectrum of **4l**

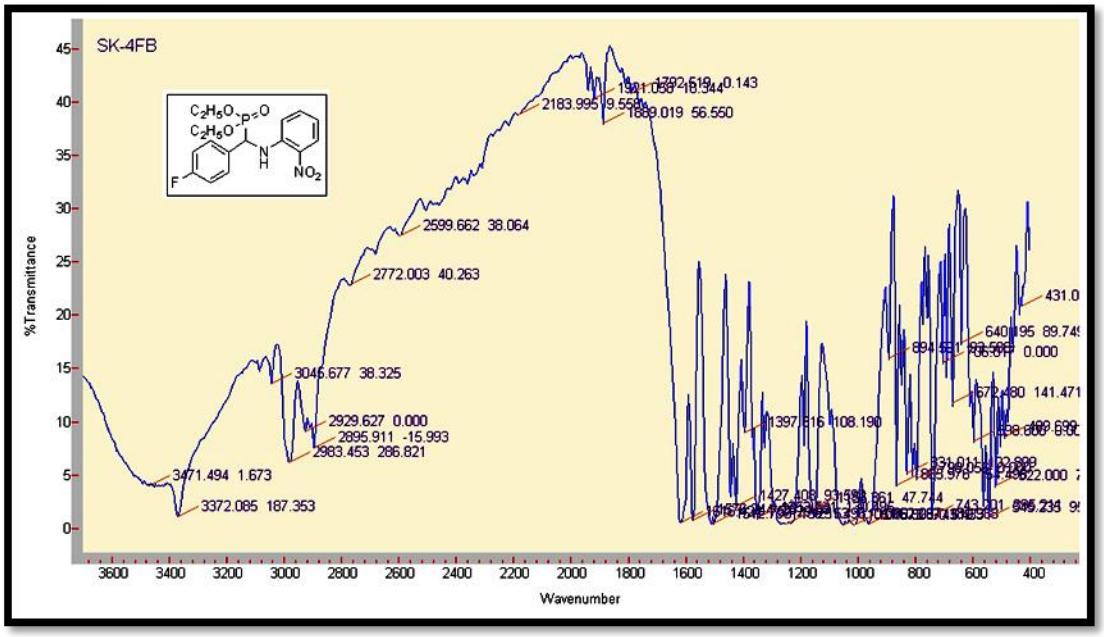

Figure. 4.49 IR Spectrum of **4m**

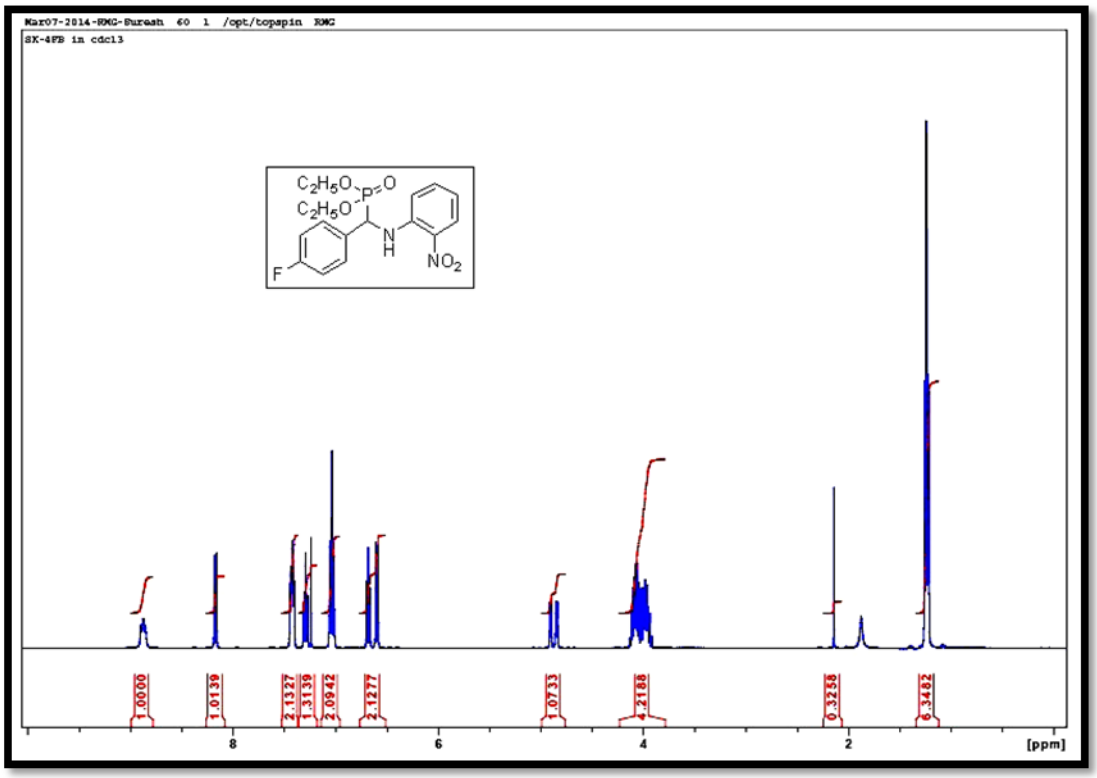

Figure. 4.50 ^{1}H-NMR spectrum of **4m**

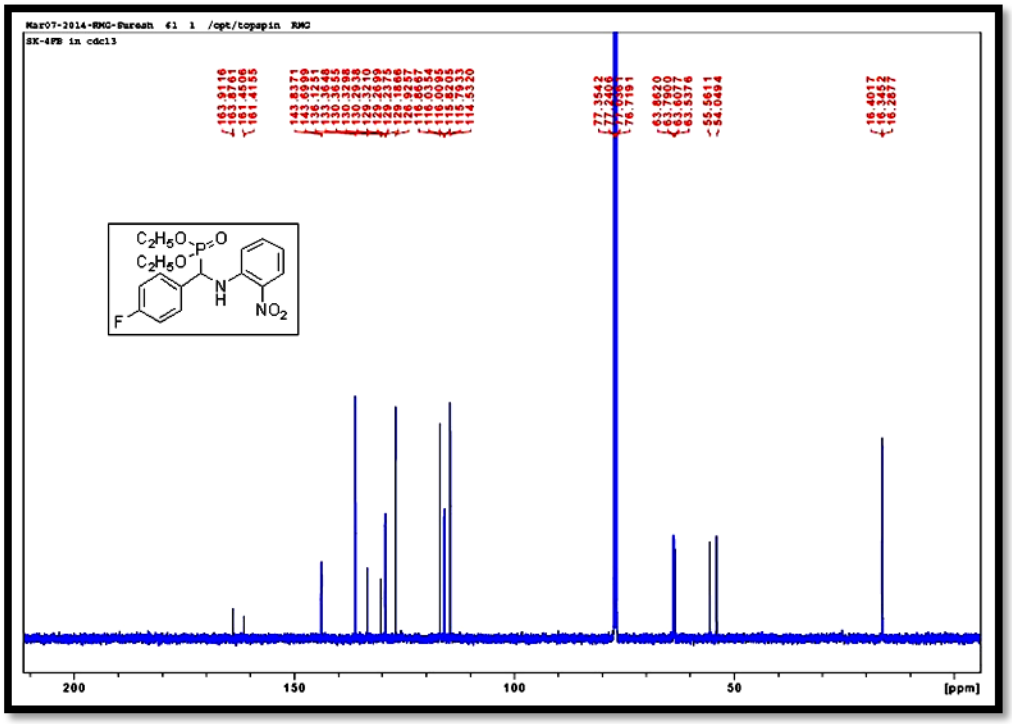

Figure. 4.51 ^{13}C-NMR spectrum of **4m**

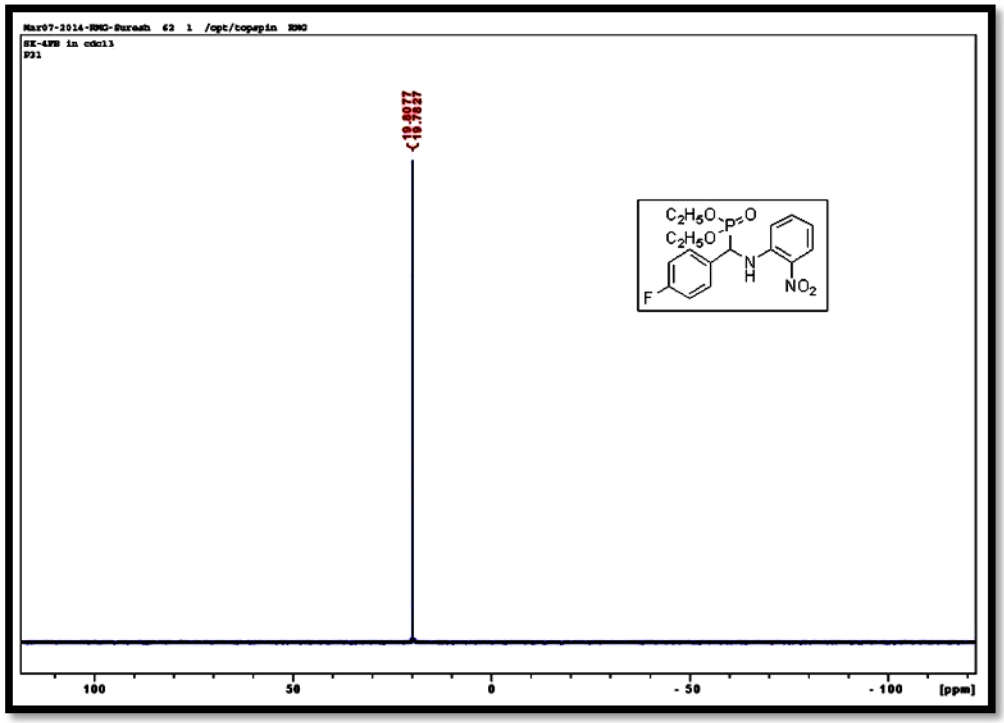

Figure. 4.52 ^{31}P-NMR spectrum of **4m**

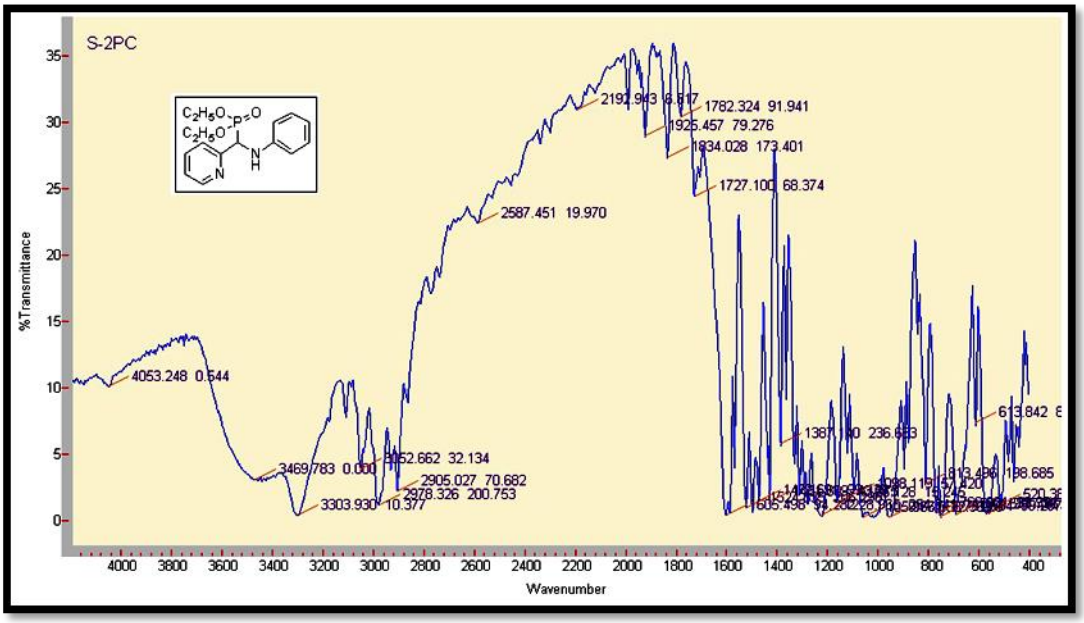

Figure. 4.53 IR Spectrum of **4n**

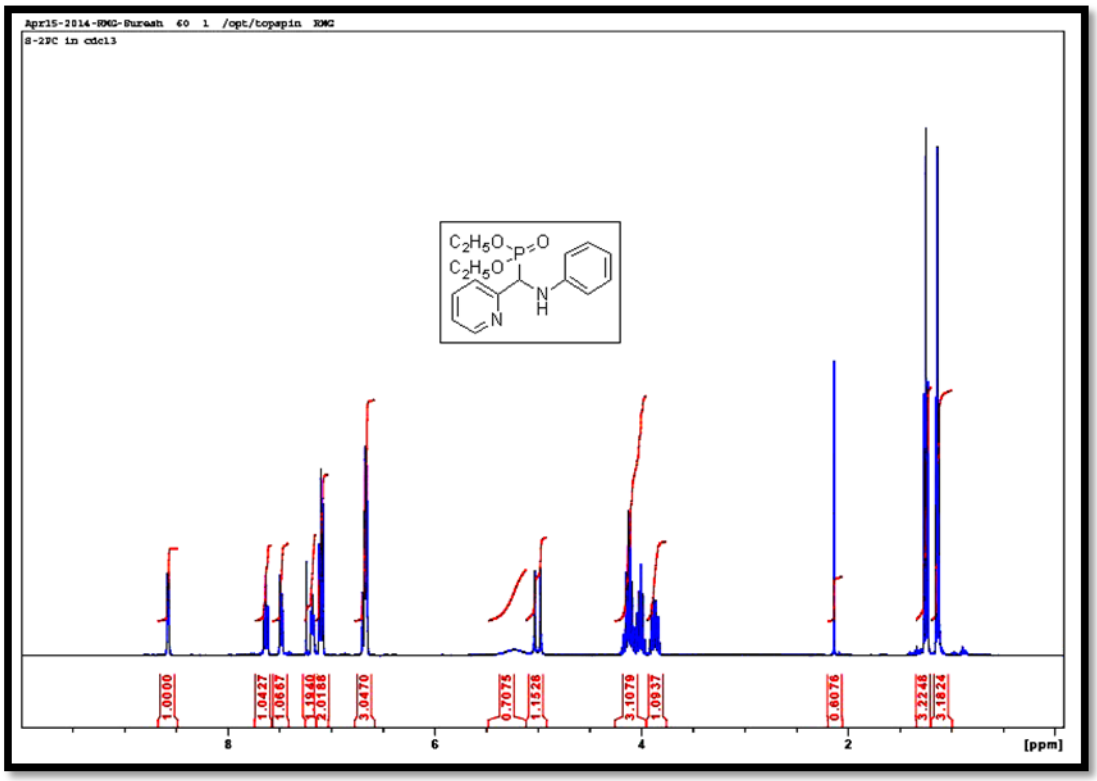

Figure. 4.54 ^{1}H-NMR spectrum of **4n**

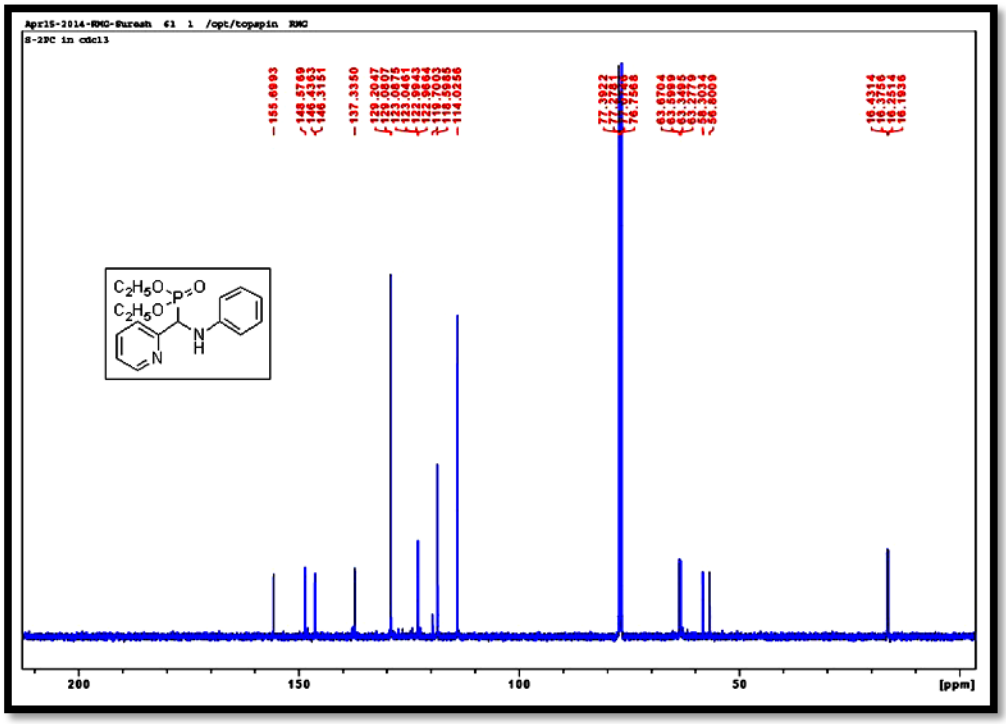

Figure. 4.55 ^{13}C-NMR spectrum of **4n**

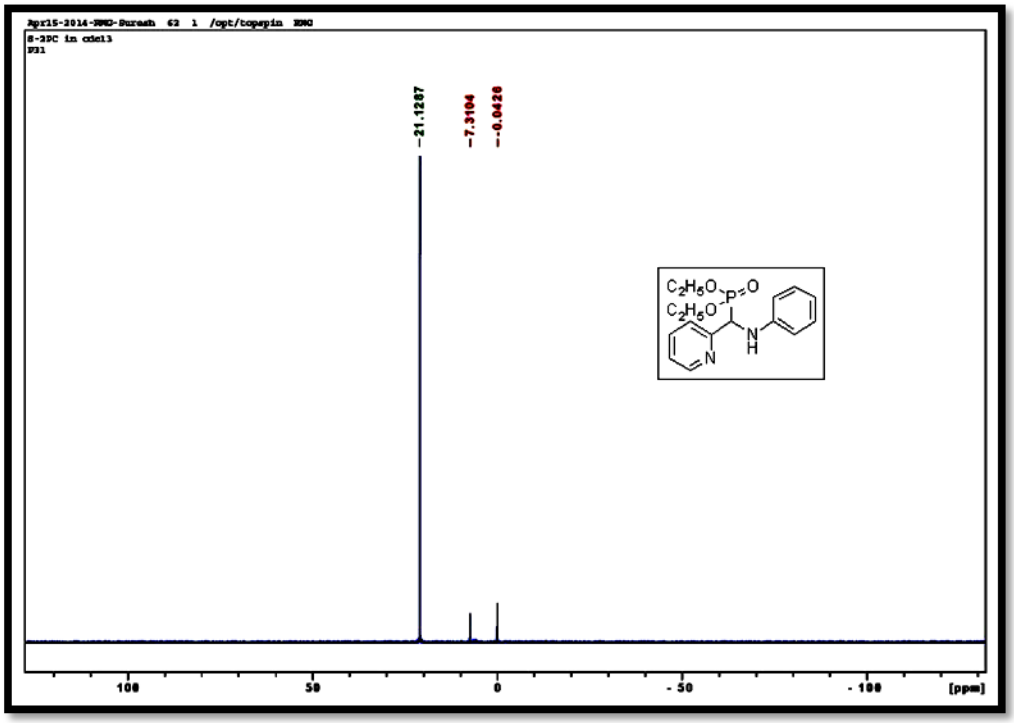

Figure. 4.56 ^{31}P-NMR spectrum of **4n**

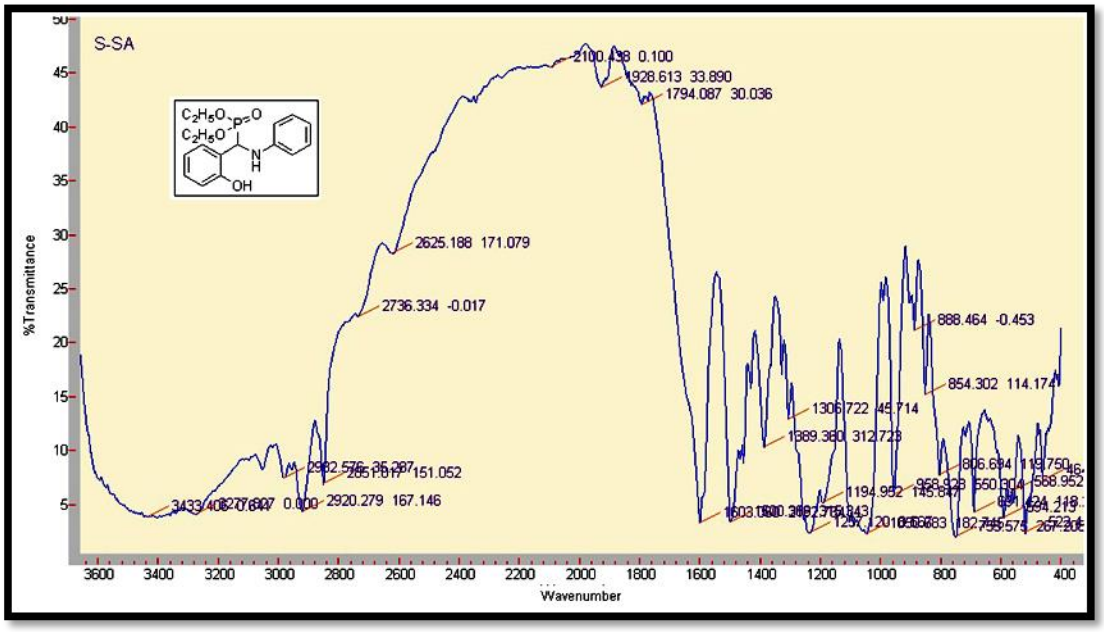

Figure. 4.57 IR Spectrum of **4o**

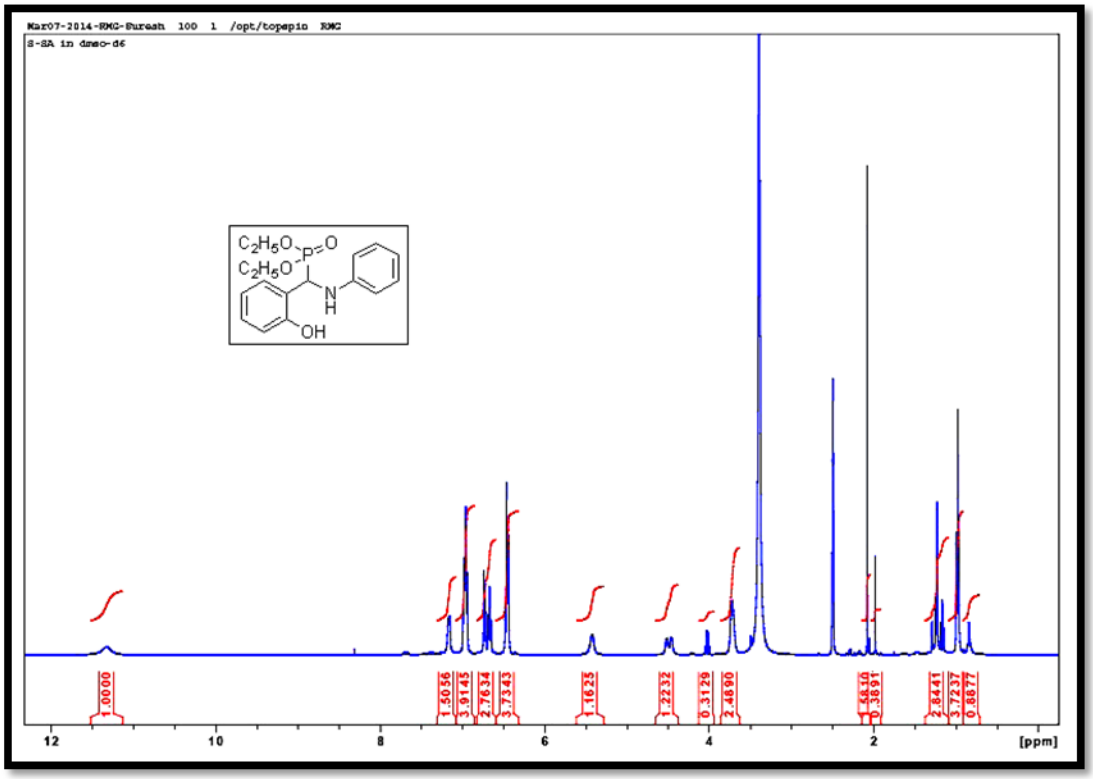

Figure. 4.58 ^{1}H-NMR spectrum of **4o**

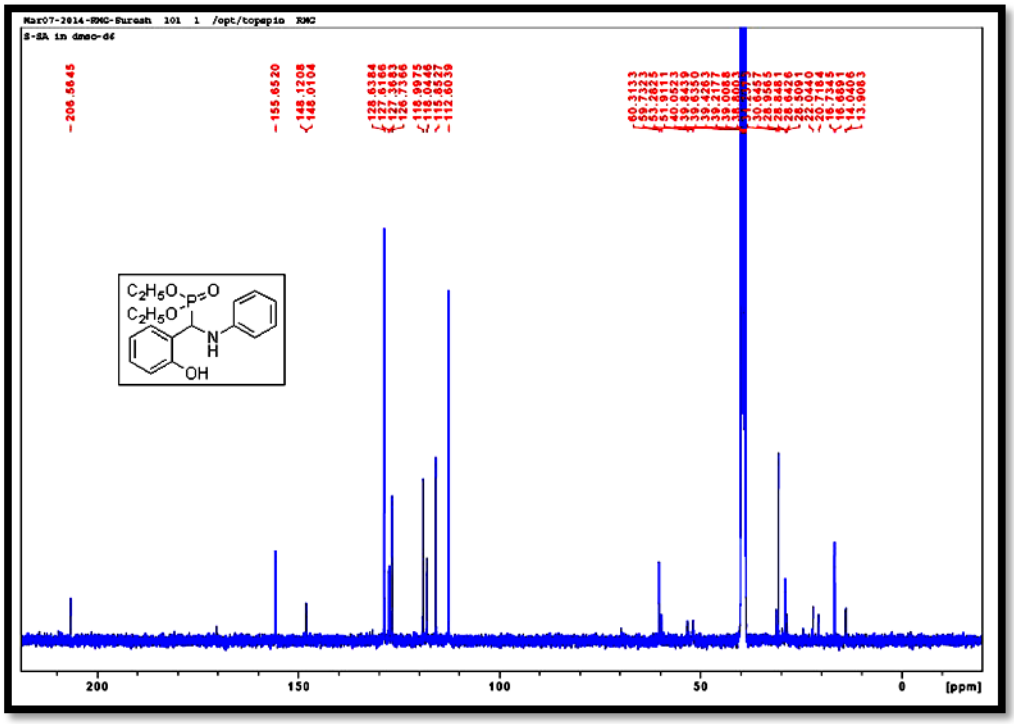

Figure. 4.59 ^{13}C-NMR spectrum of **4o**

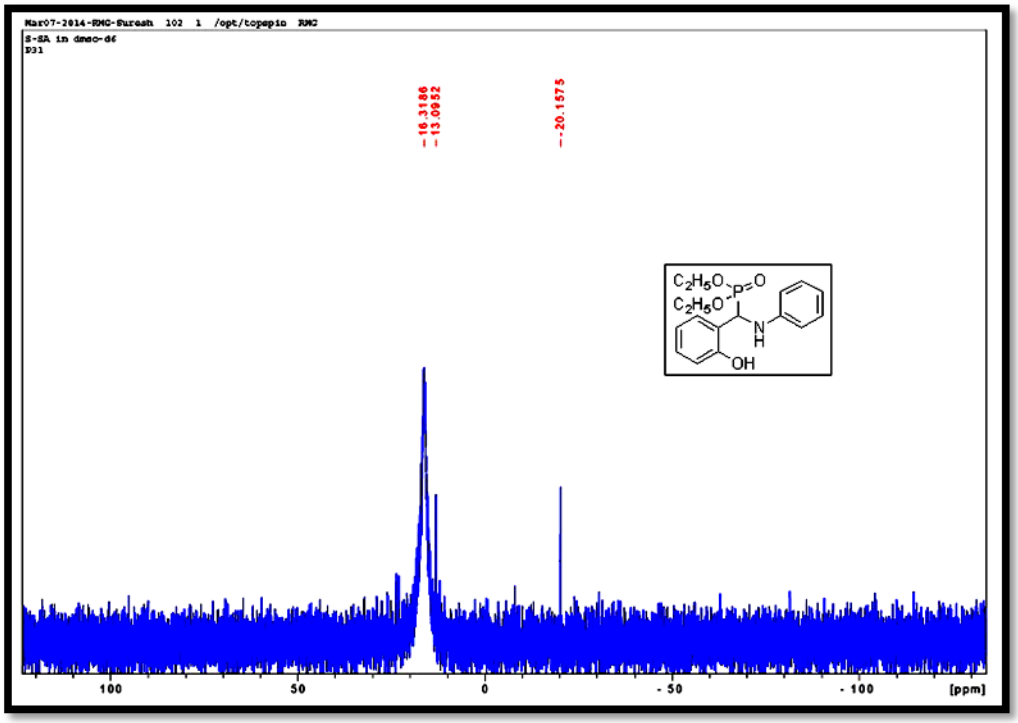

Figure. 4.60 ^{31}P-NMR spectrum of **4o**

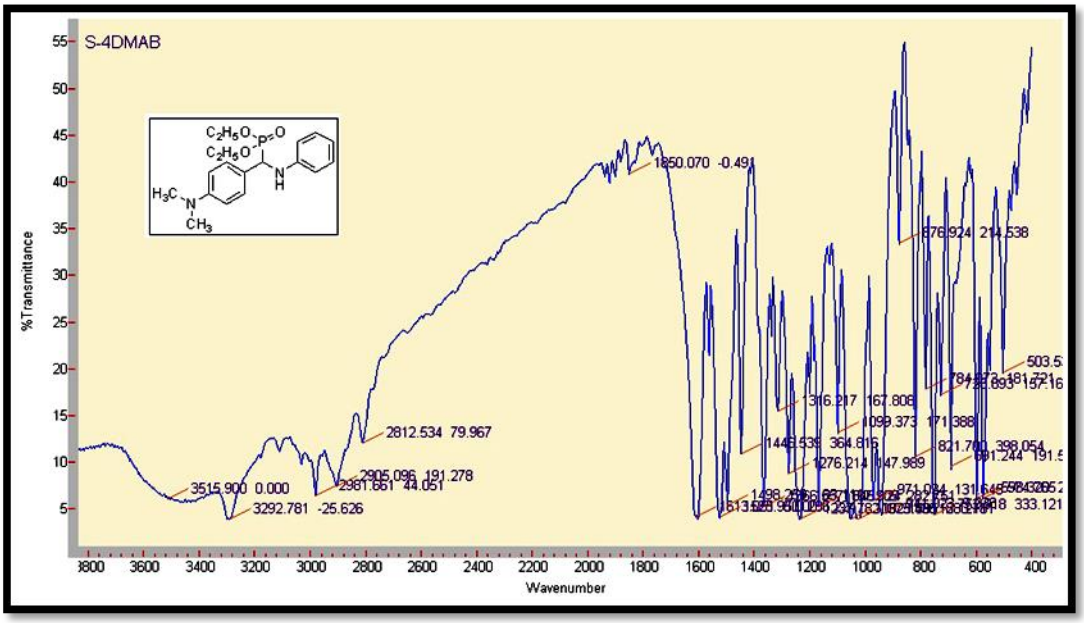

Figure. 4.61 IR Spectrum of **4p**

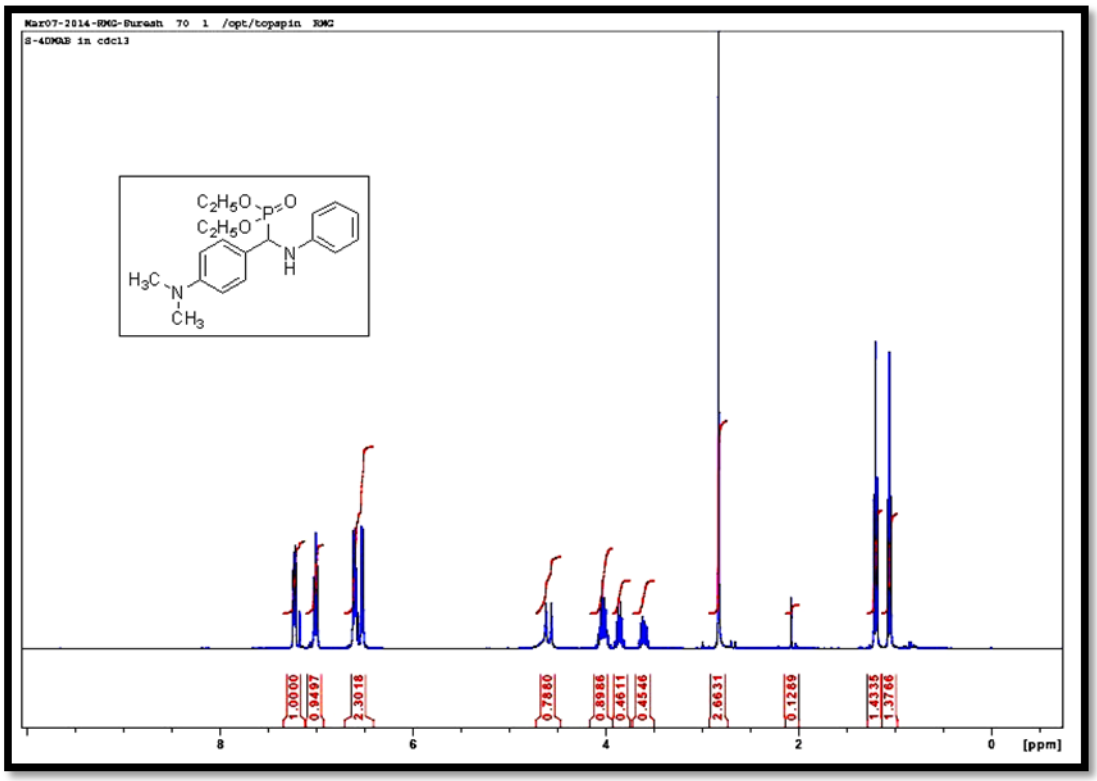

Figure. 4.62 ^{1}H-NMR spectrum of **4p**

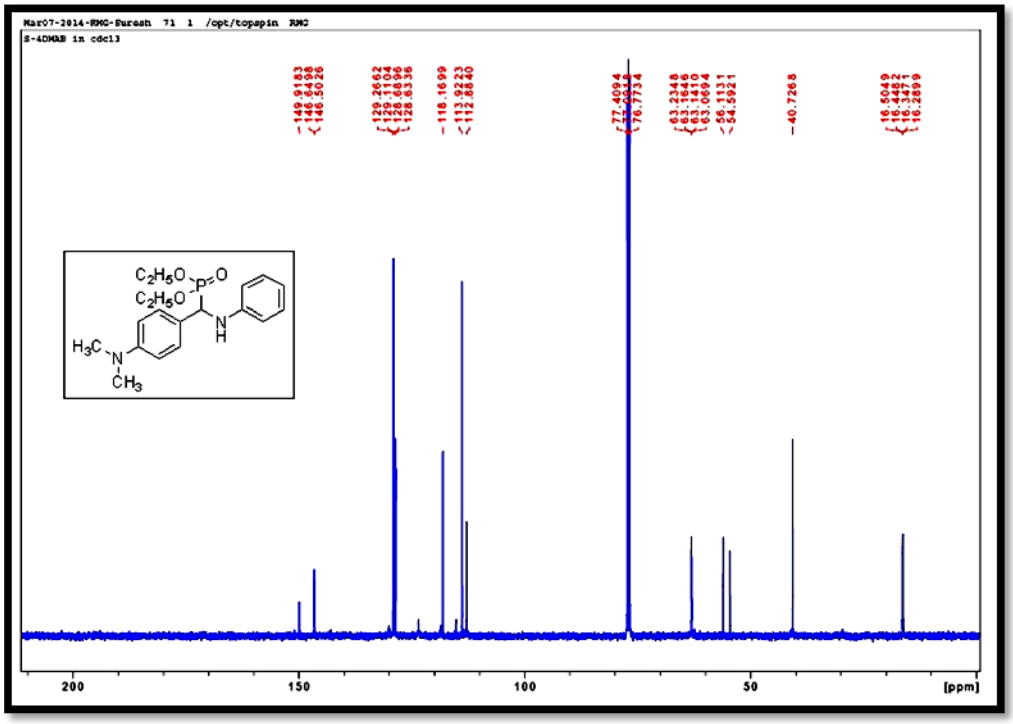

Figure. 4.63 ^{13}C-NMR spectrum of **4p**

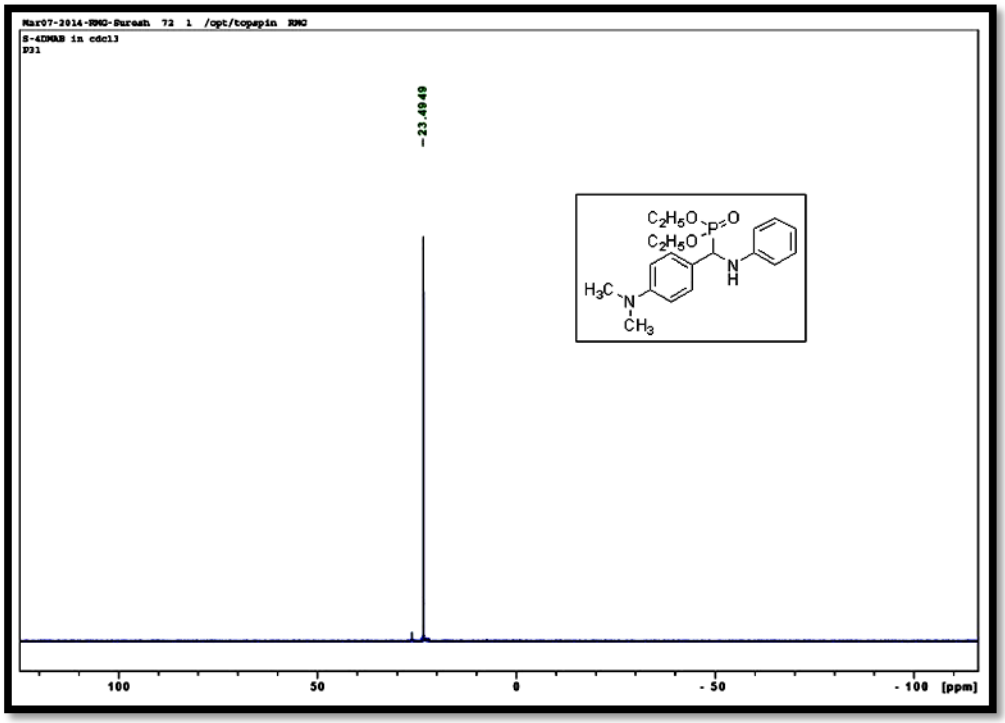

Figure. 4.64 ^{31}P-NMR spectrum of **4p**

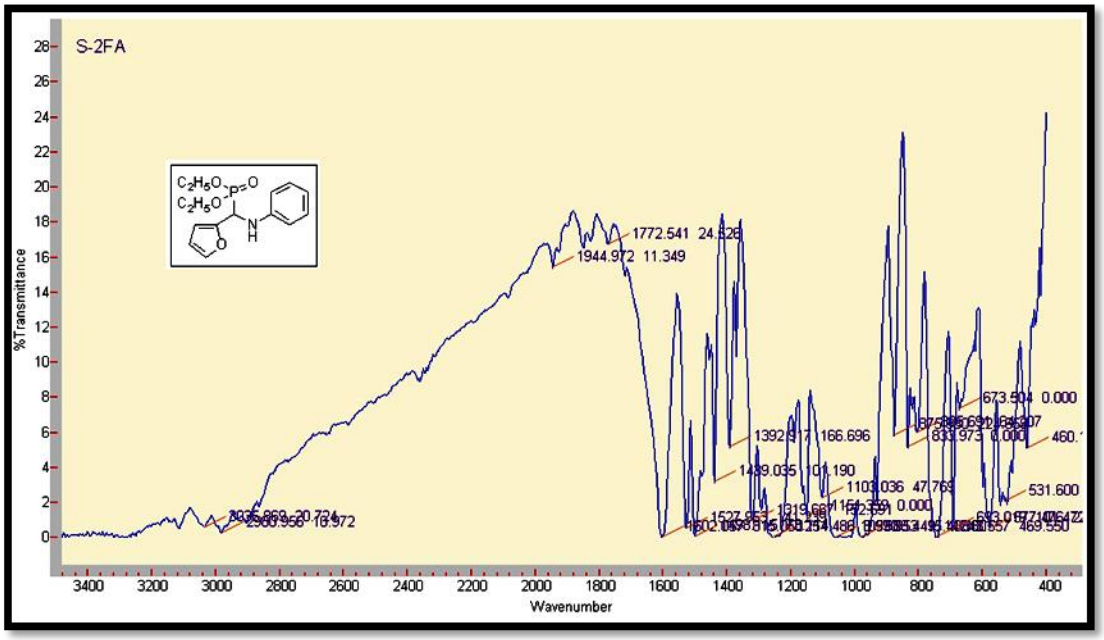

Figure. 4.65 IR Spectrum of **4q**

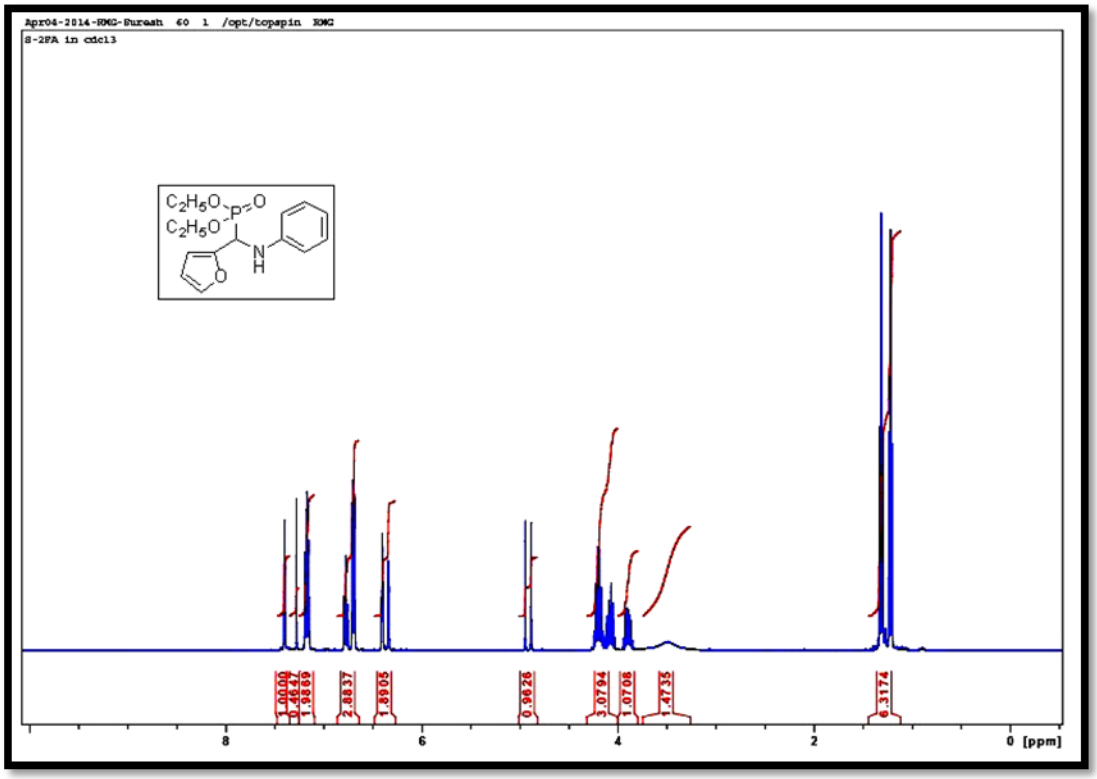

Figure. 4.66 ^{1}H-NMR spectrum of **4q**

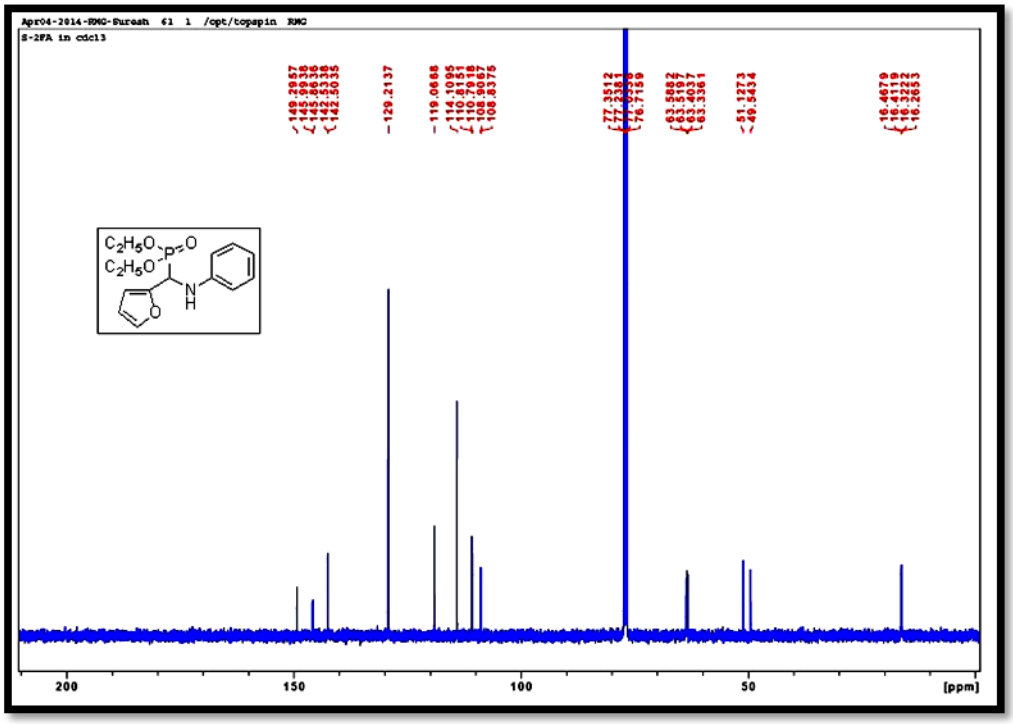

Figure. 4.67 ^{13}C-NMR spectrum of **4q**

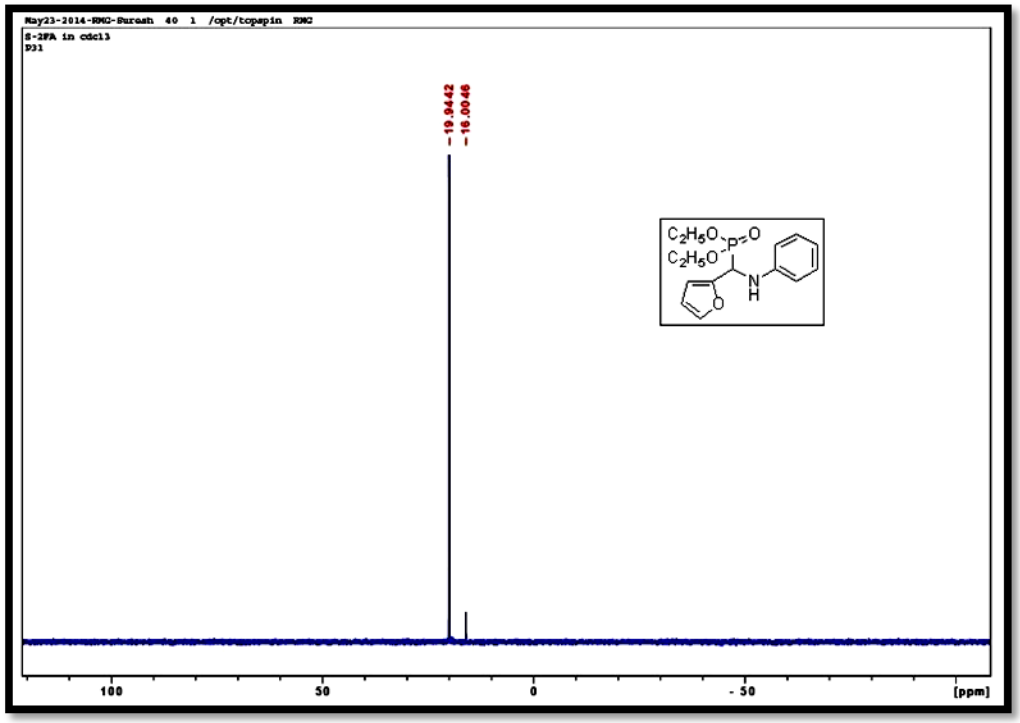

Figure. 4.68 ^{31}P-NMR spectrum of **4q**

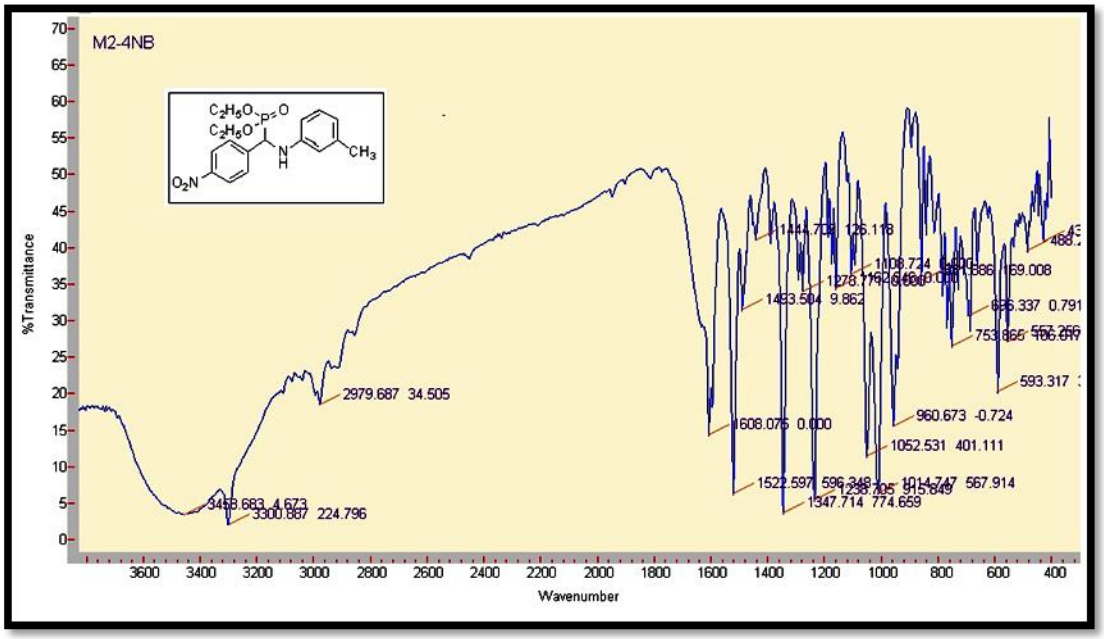

Figure. 4.69 IR Spectrum of **4r**

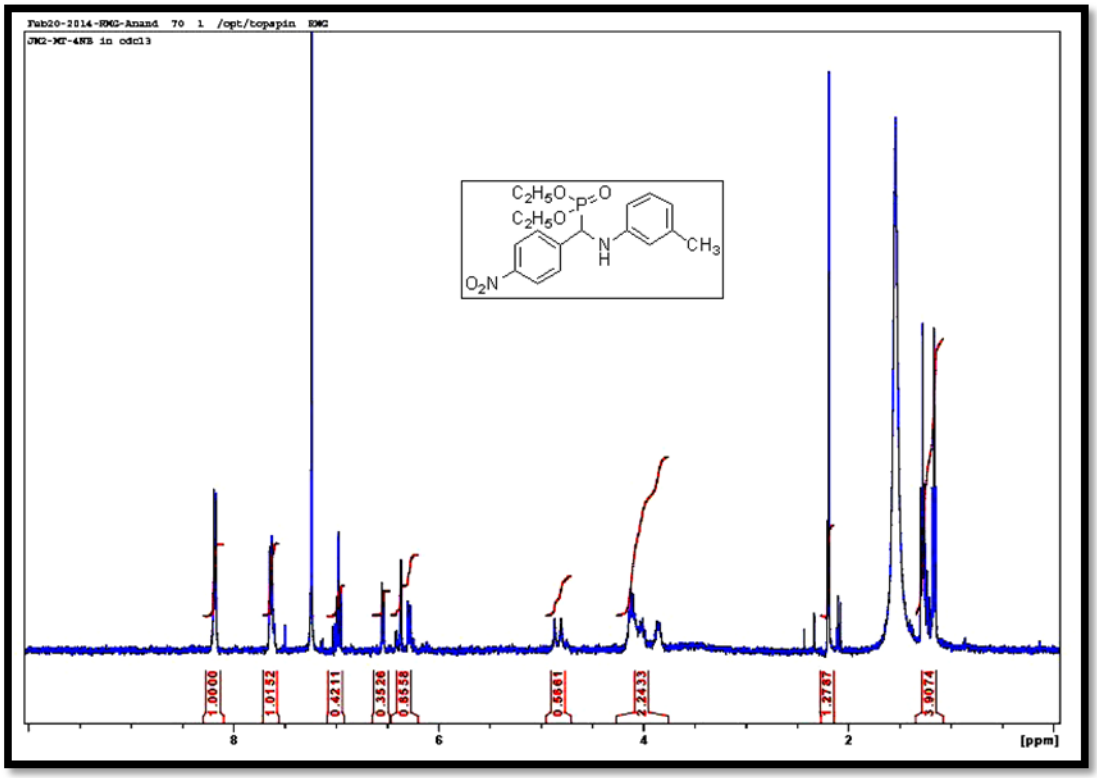

Figure. 4.70 ^{1}H-NMR spectrum of **4r**

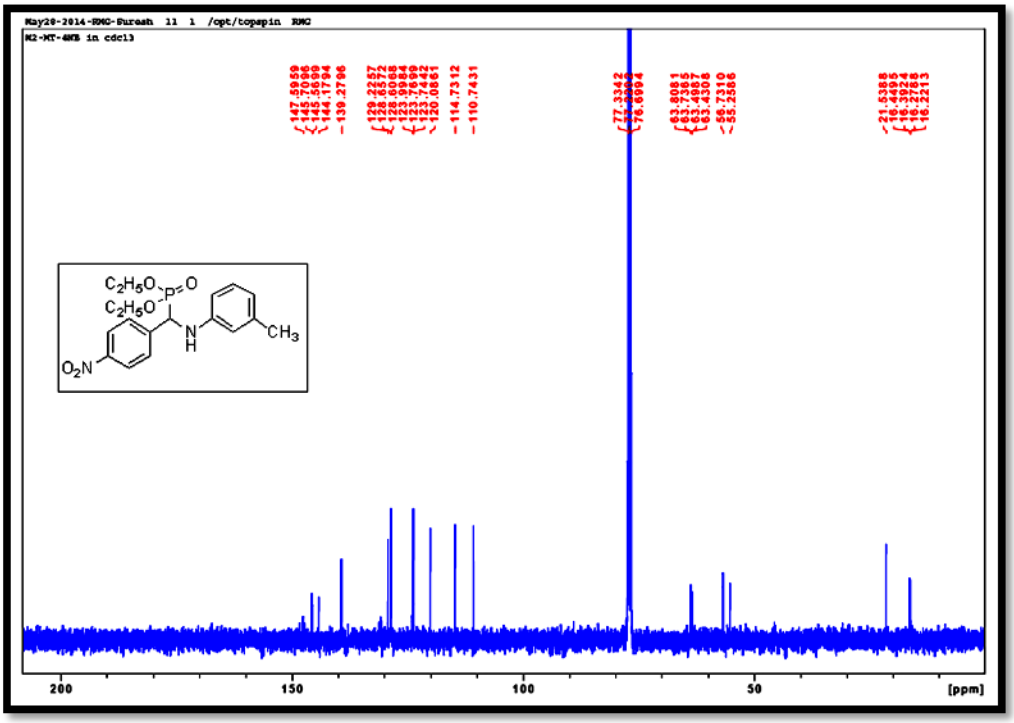

Figure. 4.71 ^{13}C-NMR spectrum of **4r**

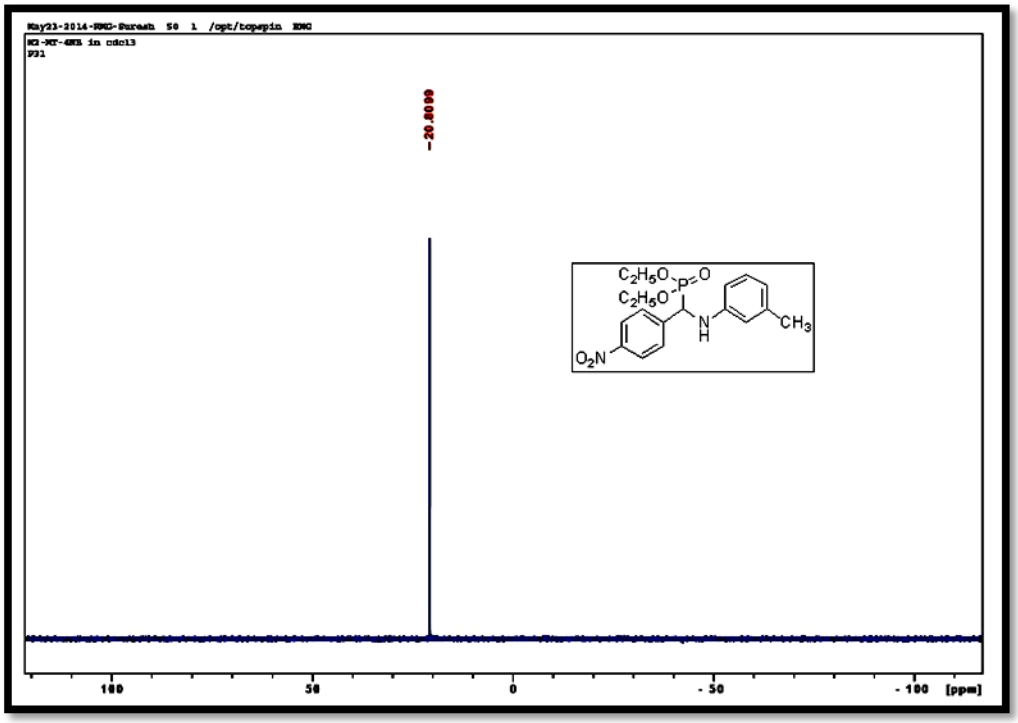

Figure. 4.72 ^{31}P-NMR spectrum of **4r**

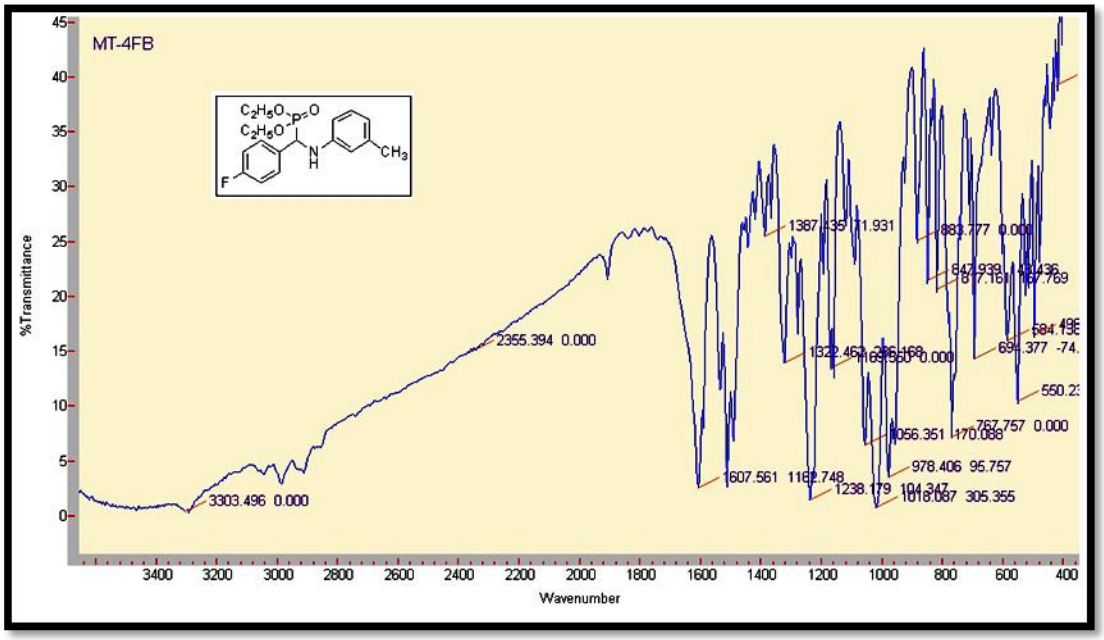

Figure. 4.73 IR Spectrum of **4s**

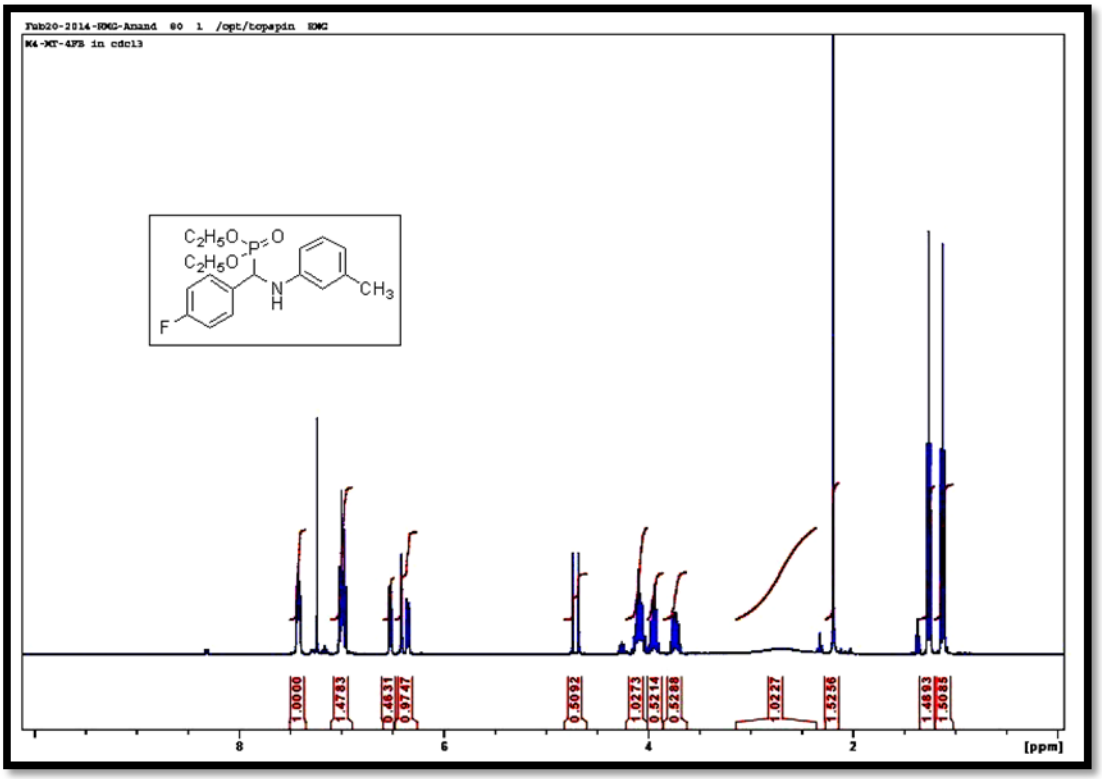

Figure. 4.74 ^{1}H-NMR spectrum of **4s**

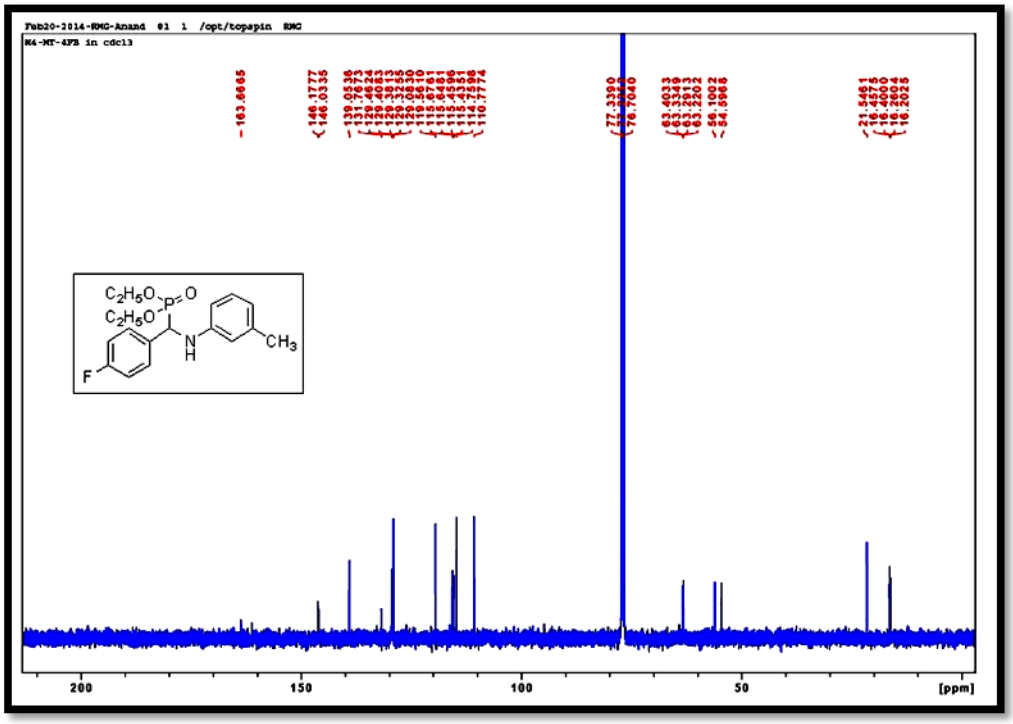

Figure. 4.75 ^{13}C-NMR spectrum of **4s**

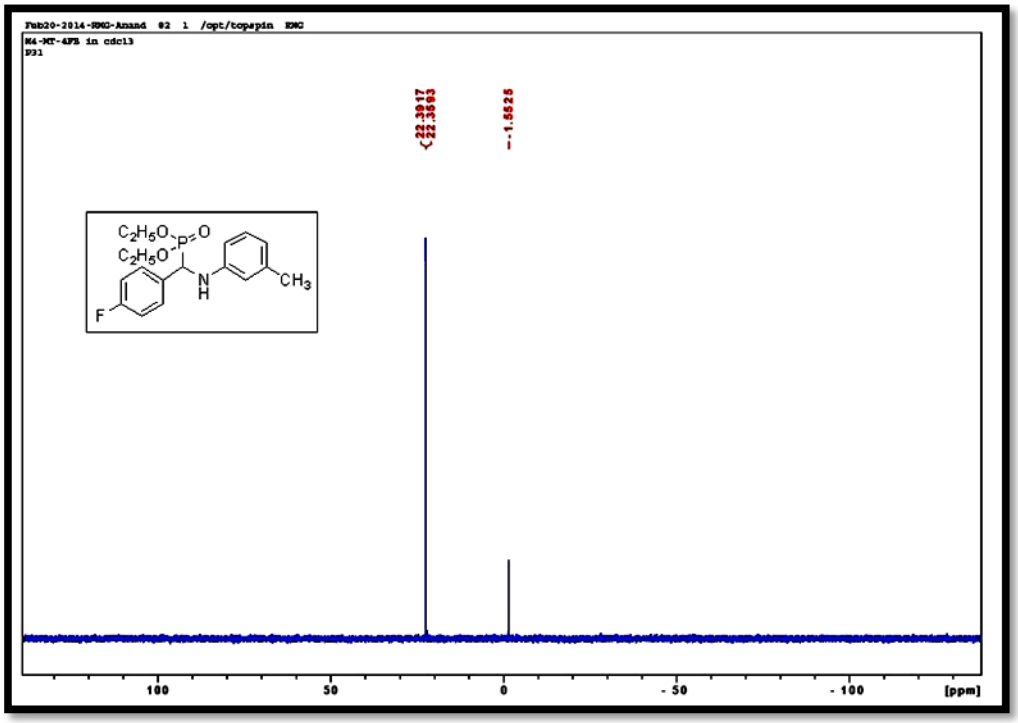

Figure. 4.76 ^{31}P-NMR spectrum of **4s**

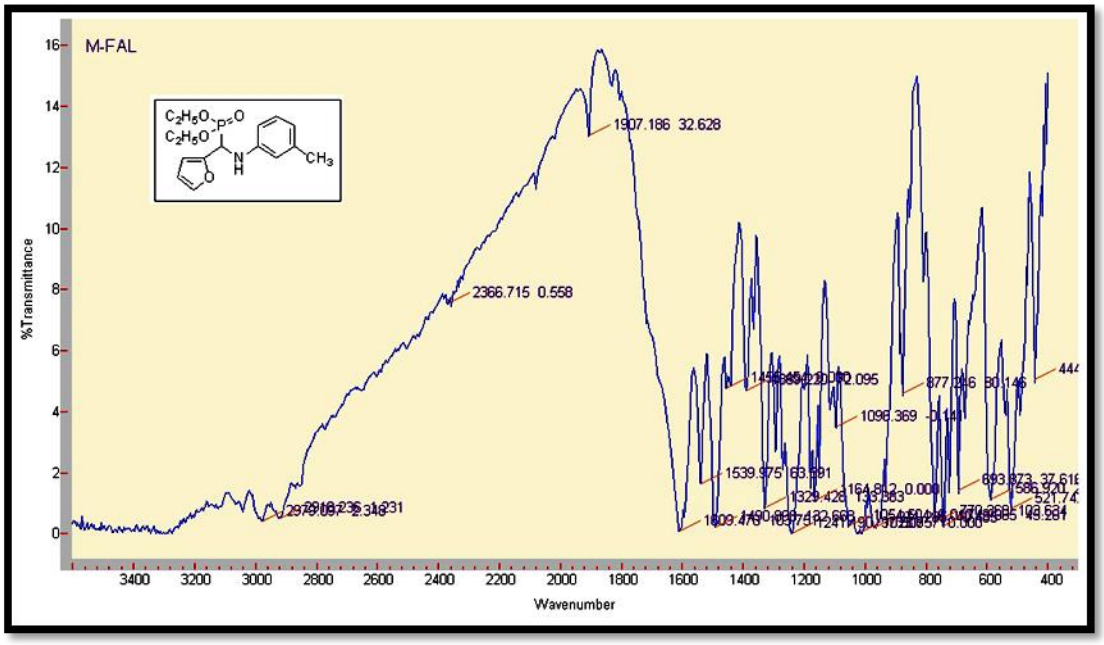

Figure. 4.77 IR Spectrum of **4t**

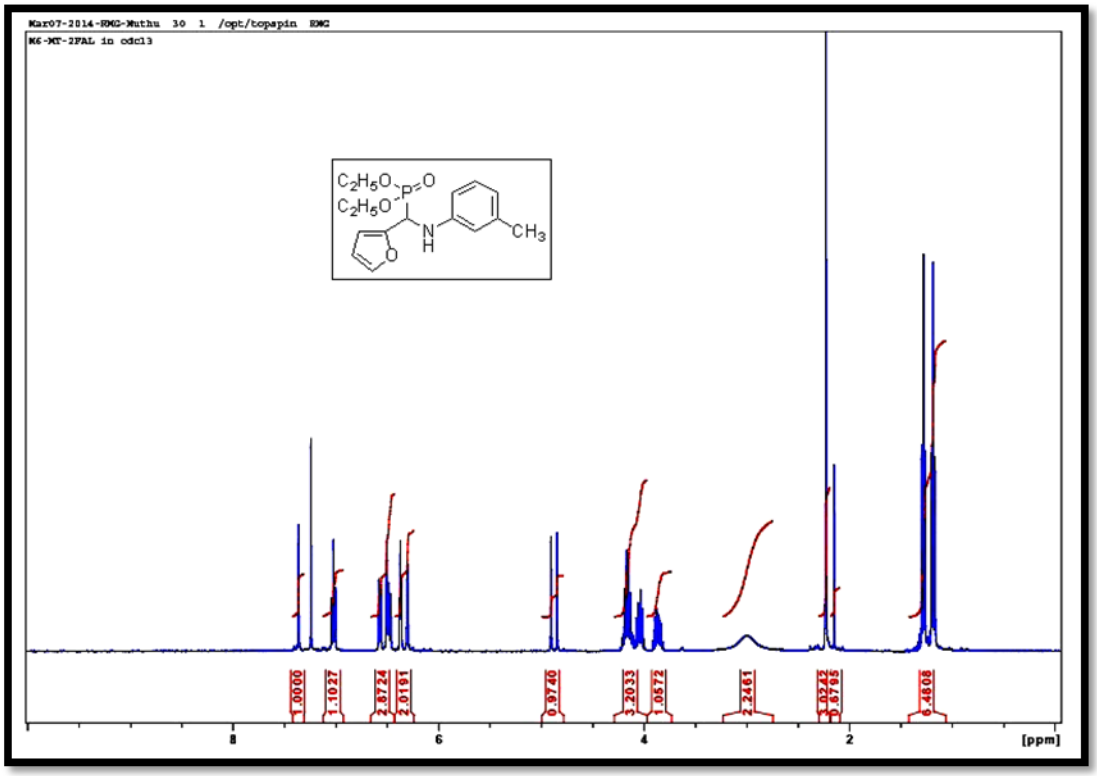

Figure. 4.78 ^{1}H-NMR spectrum of **4t**

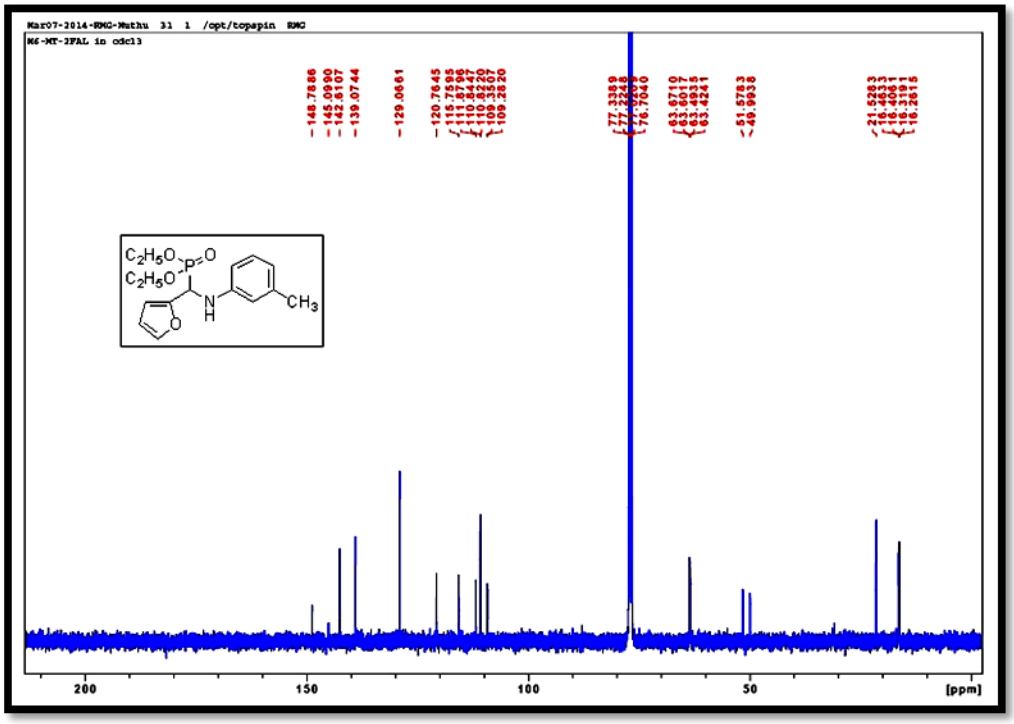

Figure. 4.79 ^{13}C-NMR spectrum of **4t**

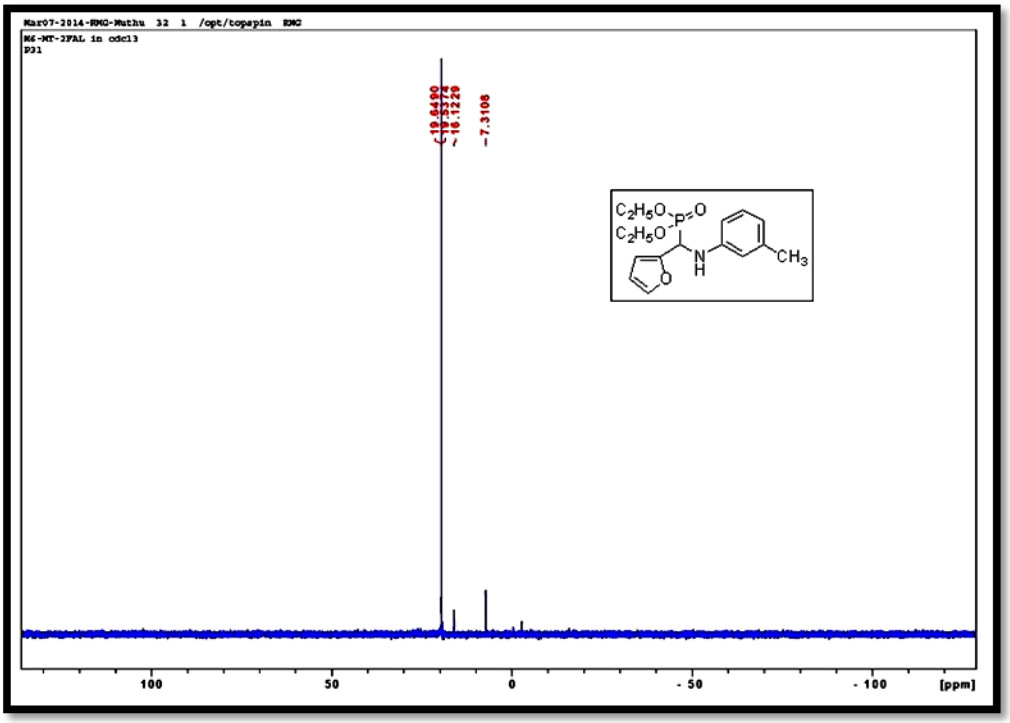

Figure. 4.80 ^{31}P-NMR spectrum of **4t**

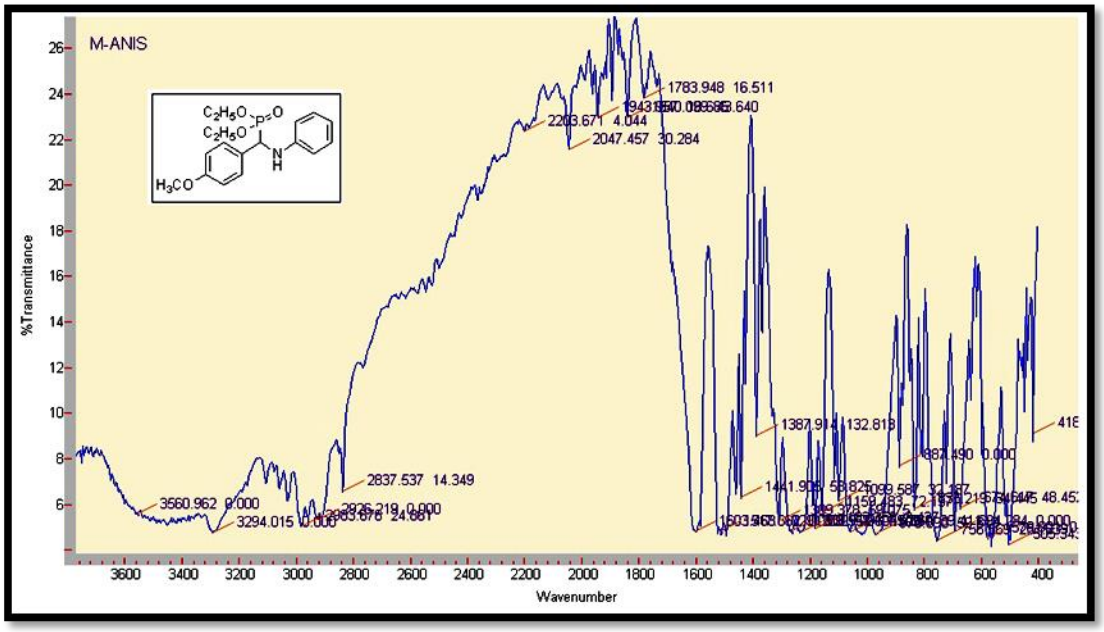

Figure. 4.81 IR Spectrum of **4u**

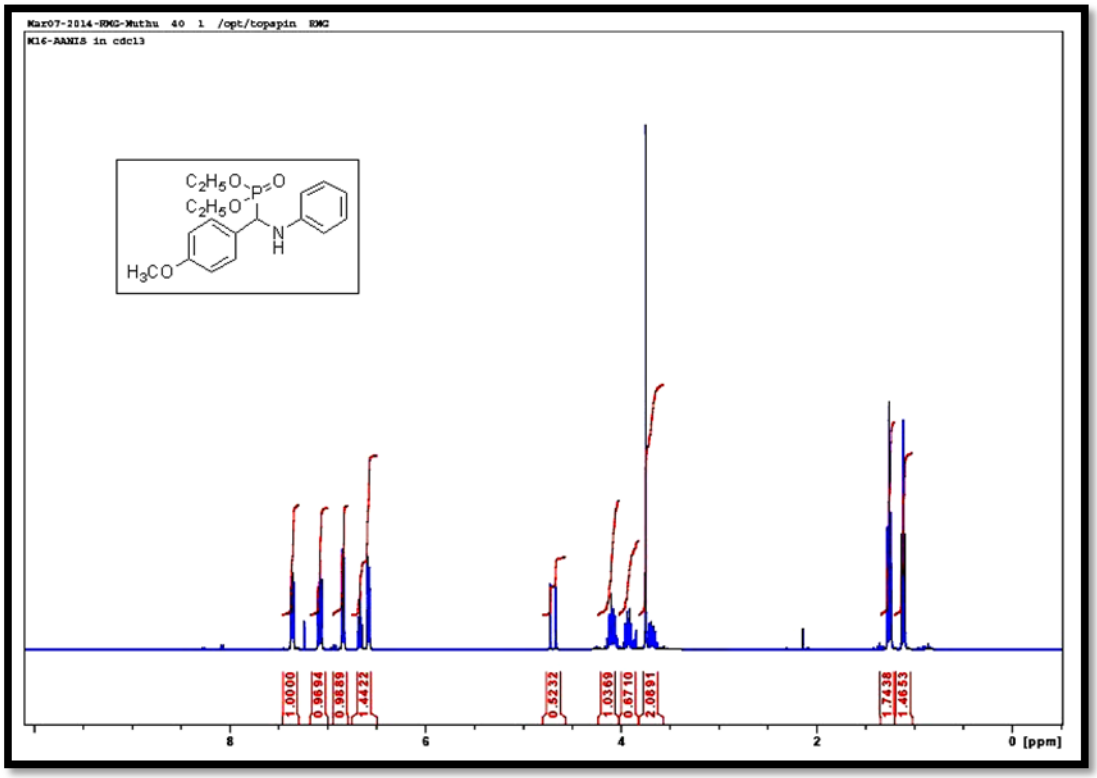

Figure. 4.82 ^{1}H-NMR spectrum of **4u**

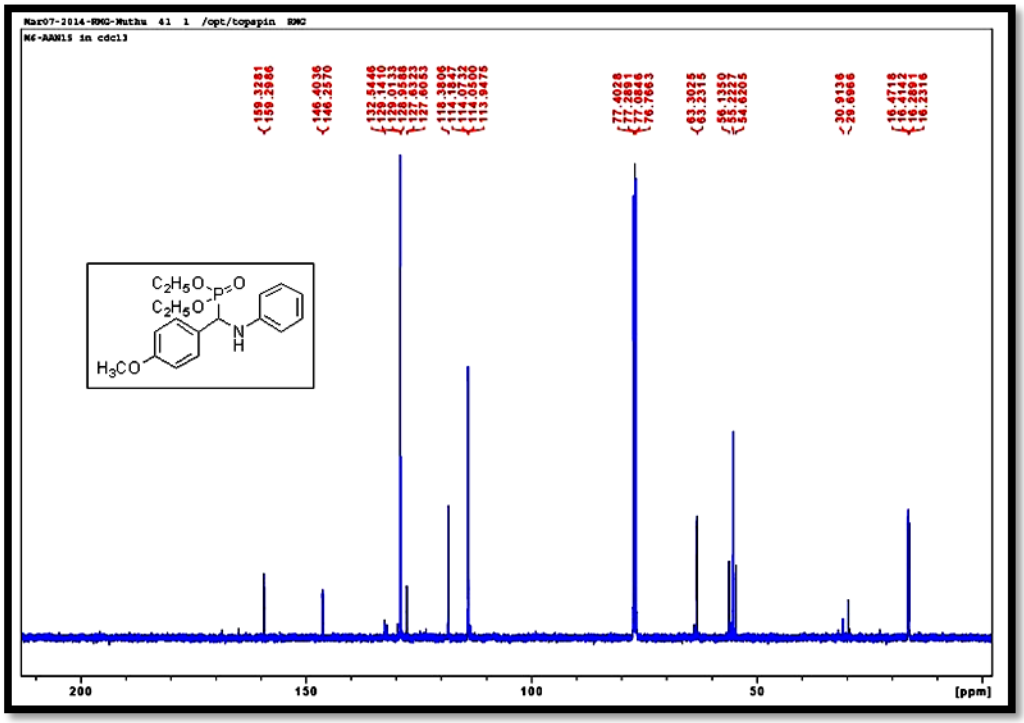

Figure. 4.83 ^{13}C-NMR spectrum of **4u**

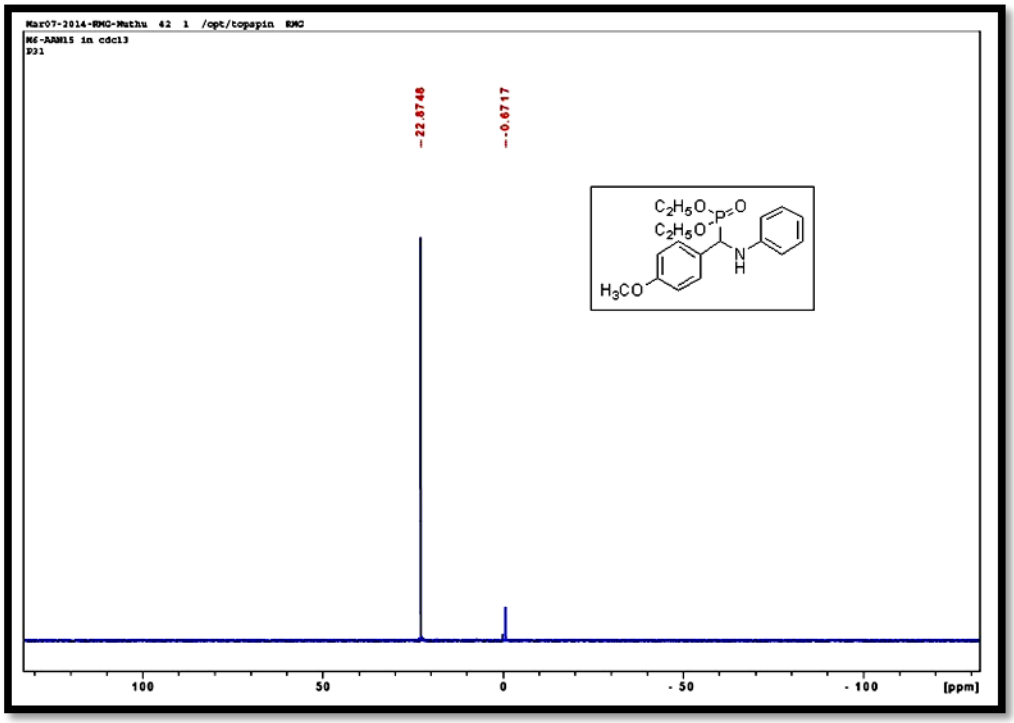

Figure. 4.84 ^{31}P-NMR spectrum of **4u**

Chapter 5

Synthesis and A549 Lung cancer cell investigation of Gold nanoparticles capped with bioactive small molecules

Introduction

Gold nanoparticles (AuNPs) have recently been explored as an attractive and excellent candidate for drug discovery. A variety of biomolecules such as proteins, DNA and drugs have been capped to AuNPs because they are biocompatible, non-toxic and can target infected cells.

This study was undertaken to synthesize two novel AuNPs capped with small molecules and determine their cytotoxicity profile in lung cancer cells.

The study is presented in two parts.

Part A

3-Amino-9-Ethylcarbazole Functionalized Gold Nanoparticles: Synthesis and Bioassay of Gold Nanoparticles

Part B

Synthesis and Bioassay of Amine-Ended Dual Thiol Ligand Functionalized Gold Nanoparticles.

CHAPTER V

PART A

3-amino-9-ethyl carbazole functionalized gold nanoparticles: synthesis and bioassay of gold nanoparticles

5A.1. Abstract

Research in nanotechnology has increased many folds in a short space of time due to its immense contribution in most spheres of life, particularly in medical field. Although several metals are used for nano synthesis, gold is a current subject of investigation in medicine because of its low toxicity in human cells. Carbazole, a model DNA intercalator, and its derivatives are of synthetic interest because of their potential biological activities.

In this study a novel carbazole thio-octanoic acid (CTN) derivative having a disulfide bond group on one terminus and a reactive functional group on the other was synthesized and subsequently capped to gold nanoparticles (AuNPs). Its cytotoxic profile was then determined with A549 lung cancer cells. A carbazole thio-octanoic acid (CTN) derivative was synthesized with carbazole, lipoic acid, HBTU and DIEA. It was characterized by IR and ^{1}H-NMR. A gold capped carbazole thio-octanoic acid (CTNAuNPs) was prepared with CTN, chloroauric acid and $NaBH_4$. Analytical techniques such as UV–vis, HRTEM, DLS and FTIR were used for characterization of CTNAu. The UV-vis spectrum showed the plasmon resonance at 552 nm. TEM images indicated that the size of AuNPs was in the range 5-50 nm. Dynamic light scattering (DLS) was used as supporting evidence to determine hydrodynamic size and zeta potential recorded as 45.87 nm and -0.172 mV, respectively. FTIR spectra suggested that AuNPs are capped with disulfide bond. The cytotoxicity of CTNAu on A549 cell lines was determined using MTT assay. The results suggested that CTN and CTNAu possessed anti-proliferative properties in the cancerous A549 cells.

5A.2. Introduction

Nanotechnology is a research field that is growing rapidly with a substantial positive contribution to human life. Although several metals are used for nano synthesis, gold is a current subject of investigation in medicine because of its low toxicity in human cells. This renaissance of gold nanoparticles has sparked an exponential increase in publications and is fostering interdisciplinary research in the field of medicine. Recently,

nanoparticles based on gold chemistry have attracted significant research and practical attention. They are versatile agents with a variety of biomedical applications including usage in highly sensitive diagnostic assays[1], thermal ablation and radiotherapy enhancement[2], as well as for drug and gene delivery since AuNPs with appropriate biomolecules are a legend which can address this issue. For biomedical applications, surface functionalization of gold nanoparticles is essential to apply them to specific disease areas and allow them to selectively interact with cells or biomolecules. Surface conjugation of antibodies and other targeting moieties is usually achieved by adsorption of the ligand to the gold surface. Surface adsorption, however, can denature the proteins or, in some cases, limit the interactions of the ligand with the target on the cell surface due to steric hinderance.

Gold nanoparticles are stabilized through capping with a wide variety of organic ligands such as amine, thiol[3-5], dithiol, etc. A number of studies have investigated the nature of bonding between the nanometal and the ligand molecules[6]. The metal–ligand interactions in the organic-capping layer plays a crucial role in the high performance materials[7]. In recent years, several studies have been focused on the sulfur–gold bonding in alkane thiol self-assembled monolayers on Au (111)[8]. However, the exact nature of the S–Au bond is still debated. In the case of dithiol ligands, it is found that gold nanoparticles are bound by both sulfur ends[9]. Nitrogen-containing heterocycles are a very important group of organic compounds because of their wide application in medicine. Among these, carbazole and indoloquinoline derivatives are of significant synthetic interest. In this study, carbazole thiooctanoic acid (CTN) moiety functionalized gold nanoparticles were synthesized. The newly synthesized carbazole conjugated gold nanoparticles were evaluated for their anti-cancer activities against A549 cells *in vitro* by the MTT assay.

5A.3. Experimental Section

5A.3.1. Materials and Methods

Gold (III) chloride trihydrate ($HAuCl_4.3H_2O$, ACS reagent), 9-ethyl-3-amino carbazole, HBTU, DIEA, lipoic acid and $NaBH_4$ were purchased from sigma aldrich (SA). All other chemicals were analytical reagent grade and were used without any further purification. All aqueous solutions were prepared using distilled water.

5A.3.2. Synthesis and Characterization of CTN capped gold nanoparticles

5A.3.2.1. Synthesis of novel carbazole thiooctanoic acid

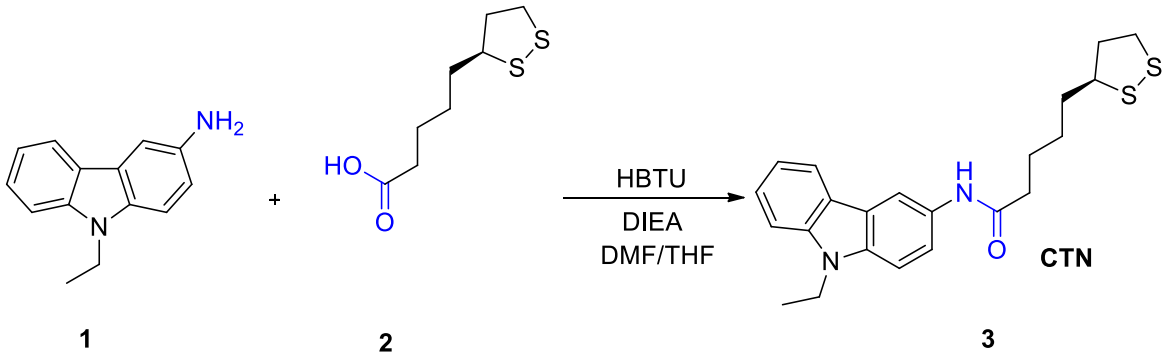

Scheme 1. Synthesis of Carbazole thiooctanoic acid (CTN)

Lipoic acid (0.55 g, 2.75 mmol) was dissolved in DMF (15 ml) and THF (5 ml) followed by addition of HBTU (1 g, 3.05 mmol), DIEA (1 ml, 6.00 mmol) and 9-ethyl-3-amino carbazole (0.56 g, 2.7 mmol). The reaction mixture was stirred at room temperature until no more starting material was detected; TLC analysis was performed. The reaction mixture was poured into 50 ml of distilled water; the mixture was then extracted thrice with ethyl acetate (25 ml). The combined extracts were dried over anhydrous sodium sulfate and then concentrated to dryness affording the crude product. This crude product was purified by column chromatography (50:50 EtOAc/Hexane) to attain the product 1.10 g (92%) as a white solid. mp: 120 °C; IR (KBr, cm^{-1}): 3462.01, 3237.92, 3058.40, 2917.84, 2513.46, 2513.46, 1900.406, 1773.85, 1736.05, 1650.38, 1587.43, 1542.65, 1485.11, 1382.07, 1277.01, 1228.44, 1152.46, 1123.774, 1085.725, 1060.128, 1020.12, 1020.128, 978.56, 888.97, 821.95; ^{1}H-NMR (400 MHz, $CDCl_3$): δ (ppm) 1.35 (m, 2H), 1.39 (s, 3H), 1.56 (q, 2H), 1.68 (m, 2H), 1.80 (m, 2H), 2.40 (t, 2H), 2.62 (m, 1H), 3.34 (m, 2H), 3.5 (t, 1H), 4.35(q, 2H), 7.0-7.1 (s, 1H), 7.16-7.19 (t, H), 7.29 (s, 1H), 7.31.(s, 1H), 7.37-7.36 (d, 1H), 7.418-7.41 (m, 1H), 8.20 (d, 1H), 8.42 (t, 1H); ^{13}C-NMR (400 MHz, $CDCl_3$,): δ (ppm) 171.00, 140.44, 137.23, 129.61, 125.85, 123.02, 122.75, 120.66, 119.49, 118.73, 112.91, 108.53, 108.45, 58.43, 40.28, 48.48, 37.39, 37.37, 34.69, 33.94, 28.93, 25.43, 24.94, 13.80.

5A.3.2.2. Synthesis of novel carbazole thiooctanoic acid capped gold nanoparticles

Gold nanoparticles were prepared by the sodium borohydride reduction method[10]. In a typical experiment, 100 ml aqueous solution of tetrachloroauric acid (10^{-4} M) was reduced by 0.01 g of $NaBH_4$ at room temperature resulting in the formation of ruby-red gold Colloidal containing gold nanoparticles with diameter about 5 nm. Gold nanoparticles thus obtain were capped by 10^{-3} M aqueous solution of CTN. The carbazole thiooctanoic acid capped gold nanoparticles formed were separated and purified by repeated centrifugation at 10000 rpm for 1 hour.

The absorption of the pink colloidal solution at pH~7, was measured using a UV-vis spectrometer (Varian Cary-50 UV spectrophotometer linked to a TCC-240A Shimadzu heating vessel temperature controlled cell holder) in the range of 200-800 nm. To obtain the particle size and shape, 1 µl of the CTNAu was placed on formvar coated grids, air dried and viewed at 100 kV to carry out transmission electron microscopy studies (JEOL 1010 TEM using a Megaview III camera and iTEM software) studies. For FTIR studies, the AuNPs colloidal solution was centrifuged at 10000 rpm for 10 min; pellets were washed three times with 20 ml of distilled water and the FTIR spectra was recorded (Varian 800 FTIR spectrophotometer). A Differential Light Scattering Malvern Zetasizer Nano ZS (Malvern Instruments Ltd, UK) Merck 2423 instrument was used to measure particle size and zeta potential.

5A.3.3. Cell culture

A549 lung cells were cultured for 6 hours (37°C, 5 % CO_2) to 90 % confluency in 25 ml flasks in complete culture media (CCM; Eagles minimum essential media, 10 % foetal bovine serum, 1 % penstrepfungizone, 1 % L-glutamine). Cells were harvested (2 x 104 cells/wells in a 96 wells microtitre plate) for the MTT analysis, ATP quantification and supernantant was stored following treatment with CCM only, 10 ug/ml and 50 ug/ml AuNPs solution for 6 hours.

Informed consent was obtained from two healthy volunteers before blood samples were taken. For the preparation of peripheral lymphocytes (PL's), buffy coats containing PL's were extracted from heparinized whole blood by differential centrifugation. Briefly, 5 ml whole blood collected from each subject was layered onto equi volume Histopaque 1077 (Sigma) in polypropylene tubes. Layered blood was then centrifuged at 4000 rpm for 30 min. Buffy coats were aspirated into new polypropylene tubes and washed twice in

phosphate buffered saline (4000 rpm, 10 min). Cell density was adjusted to 2 x 104 cells/wells using the trypan blue exclusion test.

5A.3.4. MTT assay

Following incubation with relevant treatments, cells were washed twice with PBS and each sample was supplemented with a 1:5 ratio of filter-sterilised (0.45 μm) MTT salt solution (5 mg/ml in PBS) and CCM. The plate was incubated at 37ºC for 4 hours. Following incubation, dimethyl sulphoxide (DMSO) (100 μl) was added to each well and incubated at 37ºC for a further 1 hours. Optical density of the formazan product was measured using a plate reader (Bio-tek μQuant) at 570/690 nm. Results were expressed as mean percentages of the control response.

5A.4. Results, discussion and conclusion

In the first part of the investigation, the target compound CTN **3** was synthesized by reacting lipoic acid and 3-amino-9-ethyl carbazole in the presence of HBTU and DIEA. **Mechanism 1** the base deprotonates the carboxylic acid. The resulting carboxylate anion attacks the electron deficient carbon atom of HBTU. The resulting HOBt anion reacts with the newly formed activated carboxylic acid derived intermediate to form an OBt activated ester. The amine reacts with the OBt activated ester to form the amide product CTN **3**.

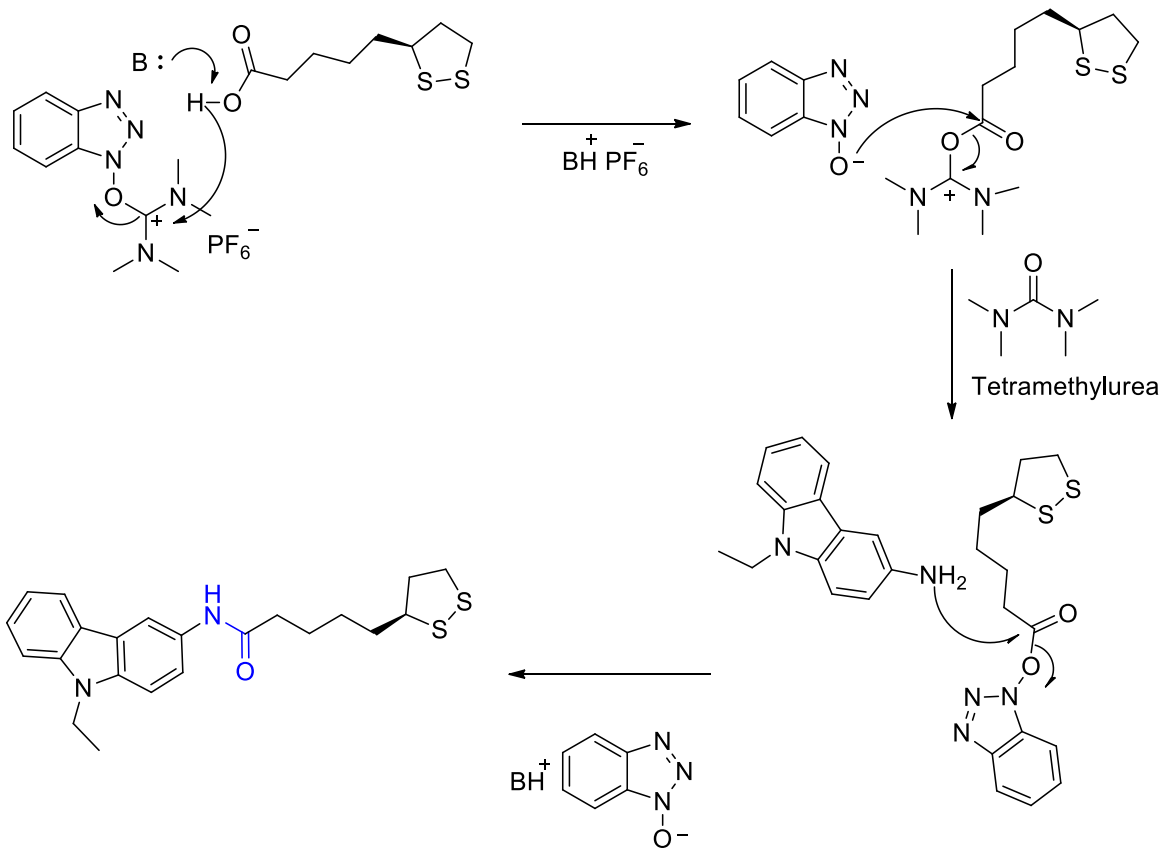

Mechanism 1. Plausible ‘’Amine to Amide’’ mechanism for the formation CTN

The IR spectrum (**Figure 5.1:** page 196) showed the NH absortion band at 3462 and C=O at 1773 cm^{-1}, respectively. The ^{1}H-NMR spectrum (**Figure 5.2:** page 196) showed amide proton a broad singlet signal near δ 7.0 (ppm) due to amide NH. In ^{13}C-NMR (**Figure 5.3**: page 197) a signal at 171.00 was due to the amide carbon, respectively.

The CTNAu was prepared by mixing an aqueous solution of CTN with a chloroauric acid solution. After stirring the solution at room temperature, $NaBH_4$ was added dropwise. **Scheme 2** shows the synthesis of CTNAu.

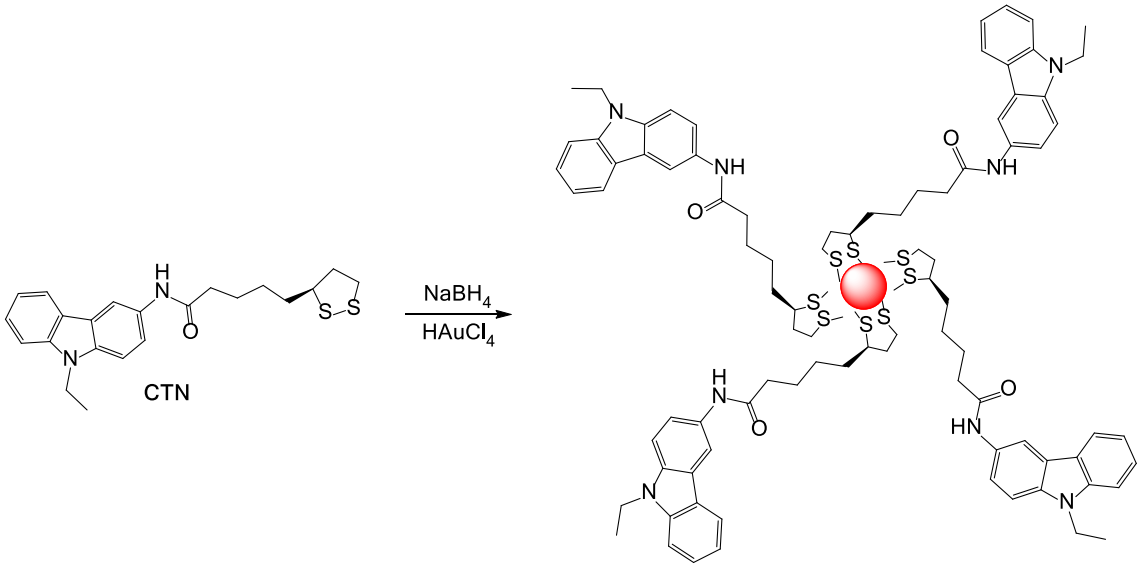

Scheme 2. The outline for the synthesis of CTNAu

The first indication of successful AuNPs formation was the appearance of a ruby red color due to the excitation of surface plasmon vibrations in gold nanoparticles. **Figure 1** shows the UV–vis spectra of CTNAu. The strong absorption in the spectra of gold nanoparticles at 530 nm (**curve a**) is the characteristic feature of gold surface plasmon resonance[11]. A red shift and broadening of the absorption band was observed in the spectra of CTNAu 552 nm (**curve b**) indicating some aggregation consequent to surface modification of gold nanoparticles. Further, a rapid colour change of the solution from ruby-red into blue by the addition of carbazole indicated the interaction of gold with carbazole.

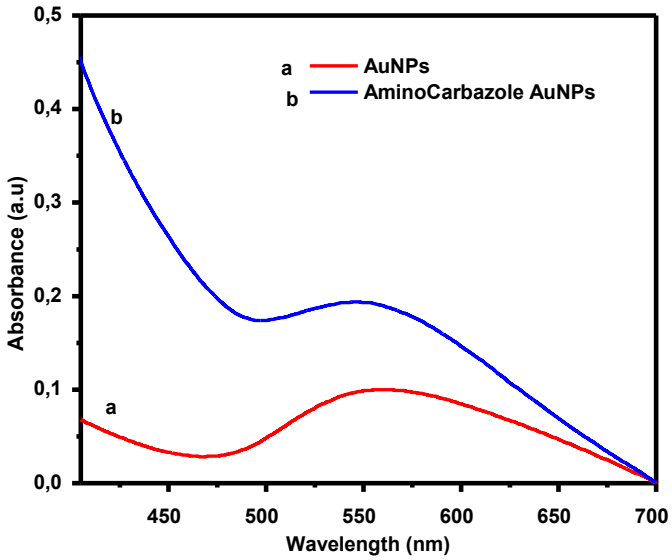

Figure 1. UV–vis spectra of gold nanoparticles line (a) (red color) and CTN capped gold nanoparticles line (b) (blue color)

The optical signature of AuNPs was determined. The distribution of sizes and shapes was conducted by transmission electron microscopy (TEM) images and supported by hydrodynamic size and zeta potential data measured by dynamic light scattering (DLS). Representative TEM images recorded from the AuNPs colloidal solution, **Figure 2** showed that most of the particles were spherical or near spherically shaped. The particles were mono-dispersed in the colloidal solution and exhibited a distribution of sizes in the range 3-5 nm and very small images of gold nanoparticles with shperical shapes were also observed.

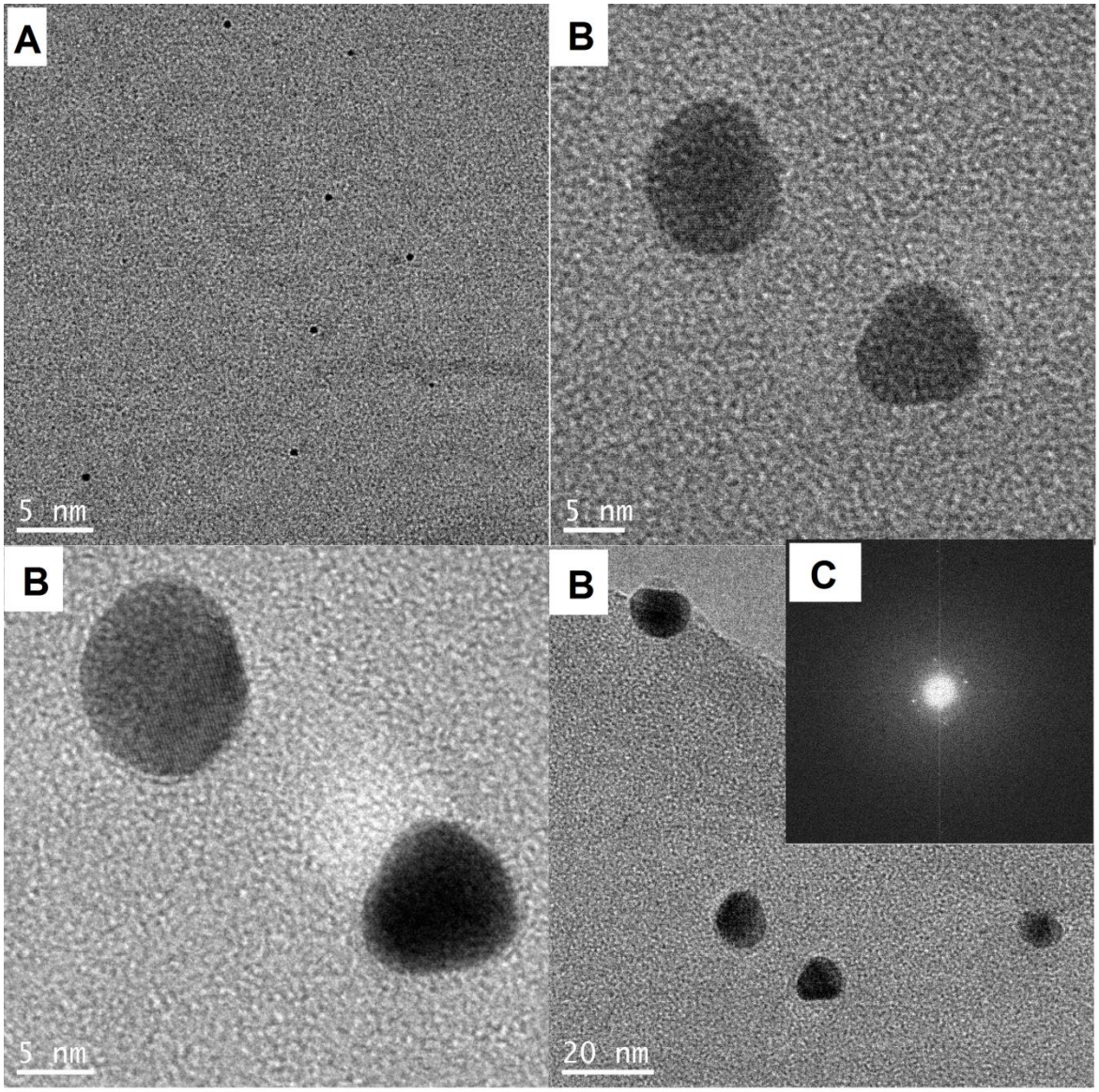

Figure 2. HRTEM images of (A) Before CTNcapped gold nanoparticles (B) After adding CTN gold nanoparticles in solution (C) HRTEM image of a part of spherical gold nanoparticle and its corresponding fast Fourier transformed image

The magnitude of the zeta potential is predictive of the colloidal stability. Nanoparticles with Zeta Potential values greater than +30 mV or less than -30 mV typically have high degrees of stability. Dispersions with a low zeta potential value will eventually aggregate due to Van Der Waals inter-particle attractions[12]. As expected, the particle size obtained from TEM and DLS scattering was marginally different due to the varying principles used for measurement. Also a stable dispersion of particles was evident from the zeta potential of -0.172 mV **Figure 3B**; a zeta potential higher than 30 mV or

lesser than 30 mV indicates a stable system. DLS size analysis showed the size distribution of particles with an average hydrodynamic size of 45 nm **Figure 3A** similar to the TEM images.

Results

		Size (d.n...	% Intensity	Width (d.n...
Z-Average (d.nm): 45.87	Peak 1:	89.57	79.9	57.34
PdI: 0.574	Peak 2:	10.72	9.1	3.715
Intercept: 0.843	Peak 3:	3669	6.1	1307

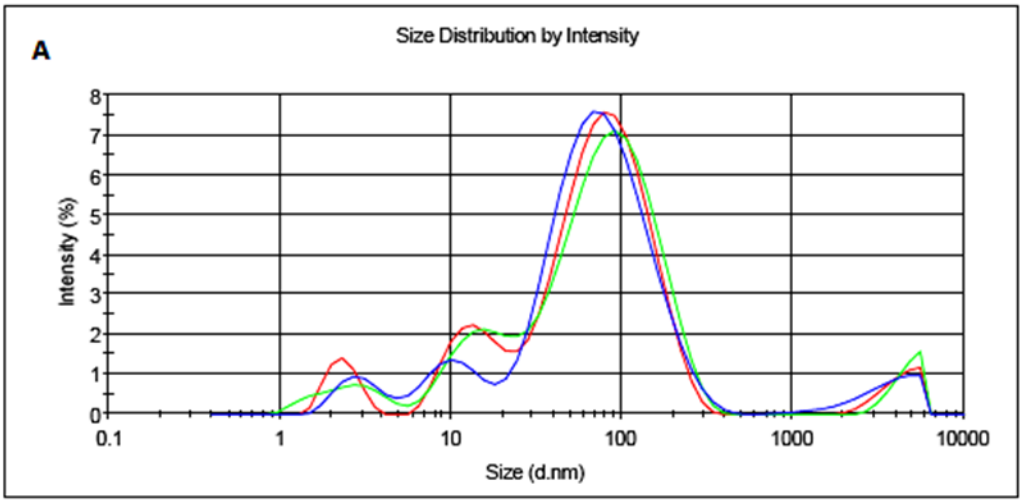

Results

		Mean (mV)	Area (%)	Width (mV)
Zeta Potential (mV): -0.172	Peak 1:	-0.172	100.0	5.33
Zeta Deviation (mV): 5.33	Peak 2:	0.00	0.0	0.00
Conductivity (mS/cm): 0.00248	Peak 3:	0.00	0.0	0.00

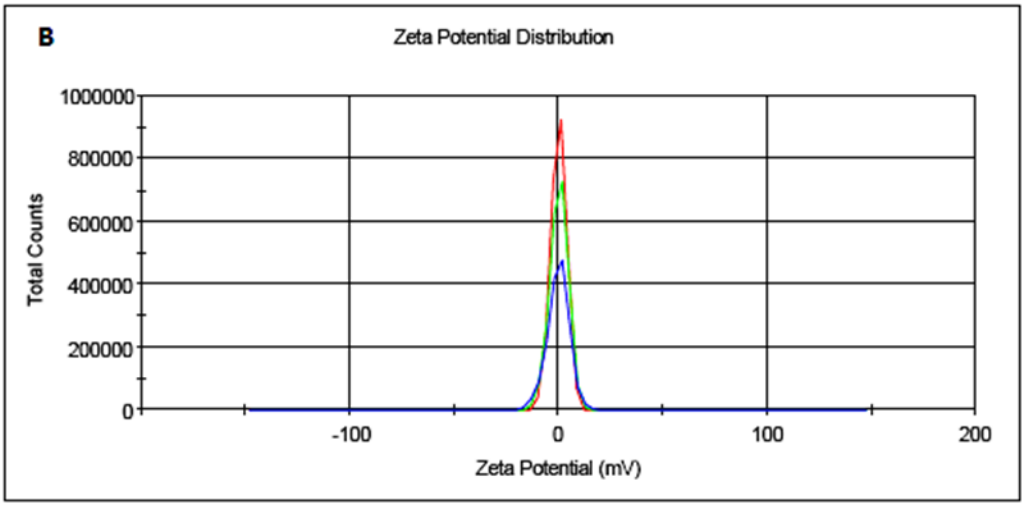

Figure 3. DLS profile: size distribution of AuNPs with maximum intensity at 45 nm **(B)** Stability of AuNPs at -0.172 mV in zeta potential analysis.

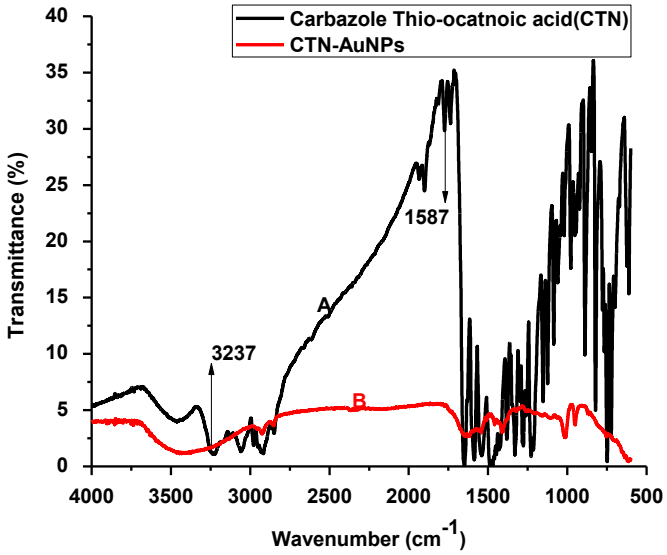

Figure 4. The FTIR Profile of CTN (line A) and CTNAu (line B)

.

Figure 4 shows the FTIR spectra which compares the spectra of CTN and CTNAu. A stretching frequency at 3237 and 1587 cm^{-1} confirmed the NH and S-S functional groups of CTN. The NH band was observed for CTNAu but it was shifted to higher values. Also the sulphur bond presenting in CTN, was absent there by containing attachment of CTN into the gold surface.

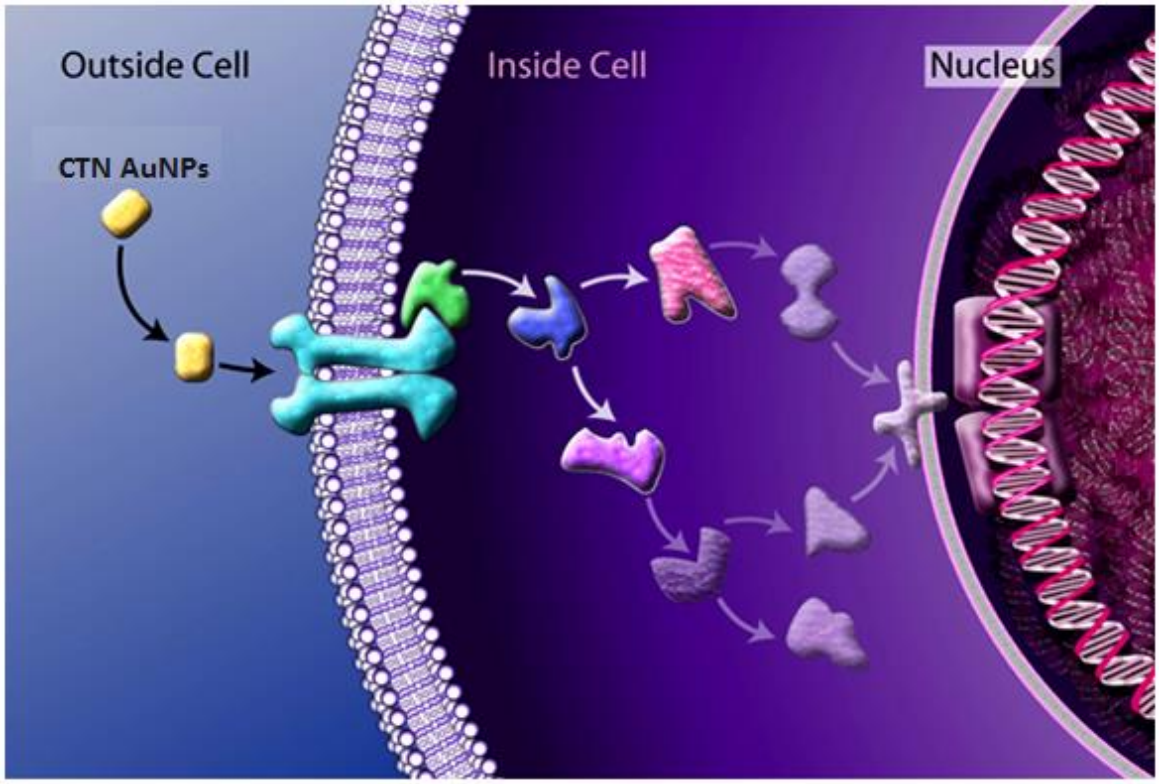

Figure 5. Graphical Picture of CTNAu interaction with cancer cells.

Toxicity of CTNAu to A549 cells was determined using the MTT assay. **Figure 5** shows a graphical representation of CTNAu interacting with cancer cells. A dose-dependent decline in cell viability was observed using CTNAu concentrations in the range 0 to 50 ug/ml for 6 hours **Table 1**. An IC50 value of 43 µg/ml was obtained and used in all subsequent assays. The novel carbazole capped gold nanoparticles were evaluated for their ability to inhibit the proliferation of the human cancer cell lines through a preliminary MTT assay[13]. Aflatoxin AFB1, the reference drug used in this study, is one of the most potent cancer agents used to produce regressions in actute leukemia, Hodgkin's disease and other lymphomas.

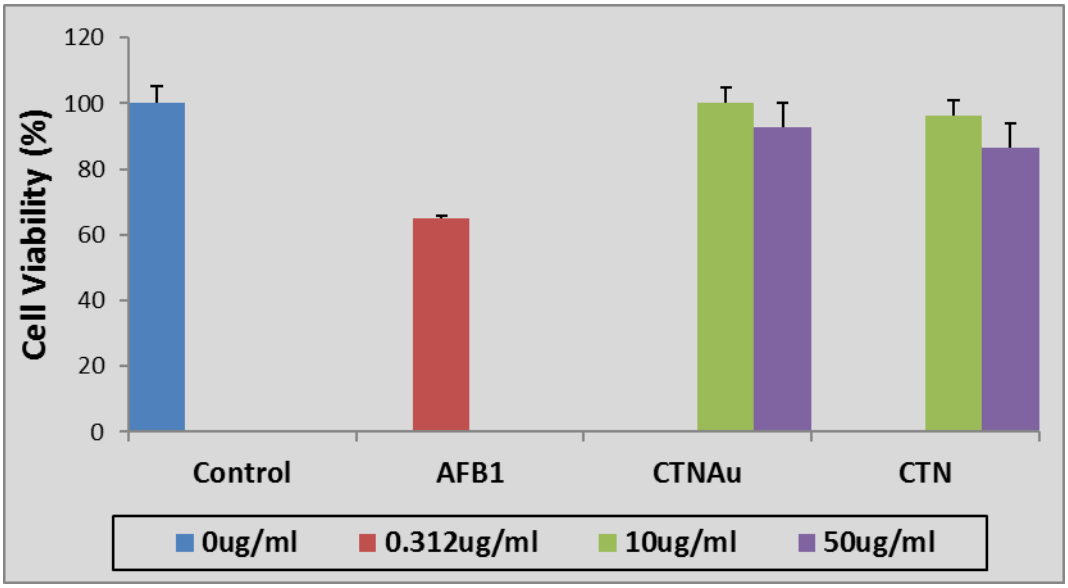

Figure 6. Cell viability of CTNAu and CTN determined against A549 cancer cell lines by MTT assay

Table 1. Cell viability of CTNAu and CTN

	6 hours		6 hours		
	0 ug/ml	0.312 ug/ml	10 ug/ml	50 ug/ml	P Value
Control	100±5.36				
AFB1		65±0.91			<0.01
CTNAu			100±4.75	96±7.44	<0.02
CTN			92±4.5	86±10.33	<0.0001

In conclusion we report the synthesis, characterization and bioassay of new gold nanoparticles CTNAu: capped with carbazole thio-octanoic acid gold nanoparticles. A primary spectroscopic investigation to identify the interaction of disulfide and AuNPs was carried out. The results showed that the disulfide moiety of carbazole lipoic acid is a very effective site to interact with gold surface at nanoscale. As a result of this interaction carbazole capped gold nanoparticles. The MTT results indicated that the dual ligands CTN induced cytotoxicity and decreased proliferation in A549 cells at various concentrations and incubation times.

Reference

(1) Goodman, C. M.; McCusker, C. D.; Yilmaz, T. *Bioconjug. Chem.* **2004**, 15, 897.

(2) Hainfeld, J. F.; Slatkin, D. N.; Smilowitz, H. M. *Phys. Med. Biol.* **2004**, 49, 309.

(3) Tshikhudo, T.R.; Demuru, D.; Wang, Z.; Brust, M.; Secchi, A.; Arduini, A.; Pochini, A. *Angew. Chem. Int. Ed.* **2005**, 44, 2913.

(4) Hasobe, T.; Imahori, H.; Kamat, P. V.; Ahn, T. K.; Kim, S. K.; Kim, D.; Fujimoto, A.; Hirakawa, T.; Fukuzumi., S. J. *Am. Chem. Soc.* **2005**, 127, 1216.

(5) Li, Z.; Jin, R.; Mirkin, C. A.; Letsinger, R. L. *Nucleic.Acids. Res.* **2002**, 30, 1558.

(6) Ding, Y.; Zhang, X.; Liu, X.; Guo, R. *Langmuir*. **2006**, 22, 2292.

(7) Schreiber, F. *J. Phys. Condens. Matter*. **2004**, 16, 881.

(8) Schreiber, F. *Prog. Surf. Sci.* **2000**, 65, 151.

(9) Garcia, B.; Salomé, M.; Lemelle, L.; Bridot, J.; Gillet, P.; Perriat, P.; Roux, S.; Tillement, O. *J. Chem. Soc., Chem. Commun.* **2005**, 369.

(10) Patil, V.; Malvankar, R.B.; Sastry, M. *Langmuir*. **1999**, 15, 8197.

(11) Link, S.; Sayed, E. *Annu Rev Phys Chem*. **2003**, 54, 331.

(12) Cho, W. S.; Thielbeer , F.; Duffin , R.; Johansson, E.; Megson, M I. L.; Bradley, W. M. K. *Nanotoxicology*. **2014**, 8, 202.

(13) Monks, A. *J. National Cancer Institute*. **1991**, 83, 757.

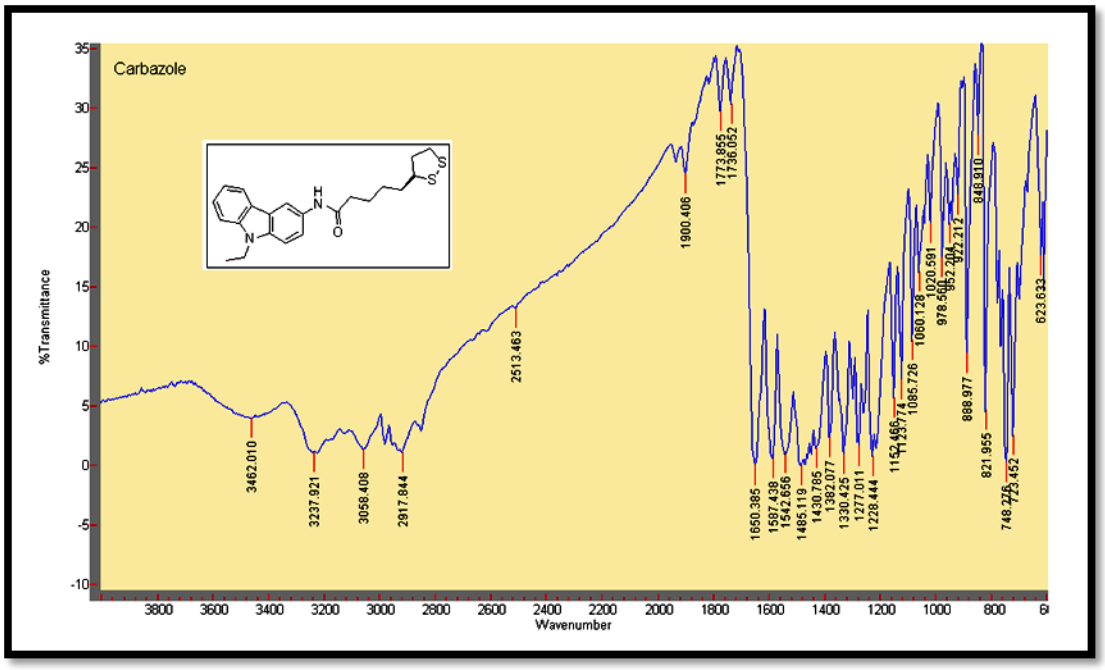

Figure. 5.1 IR Spectrum of **CTN 3**

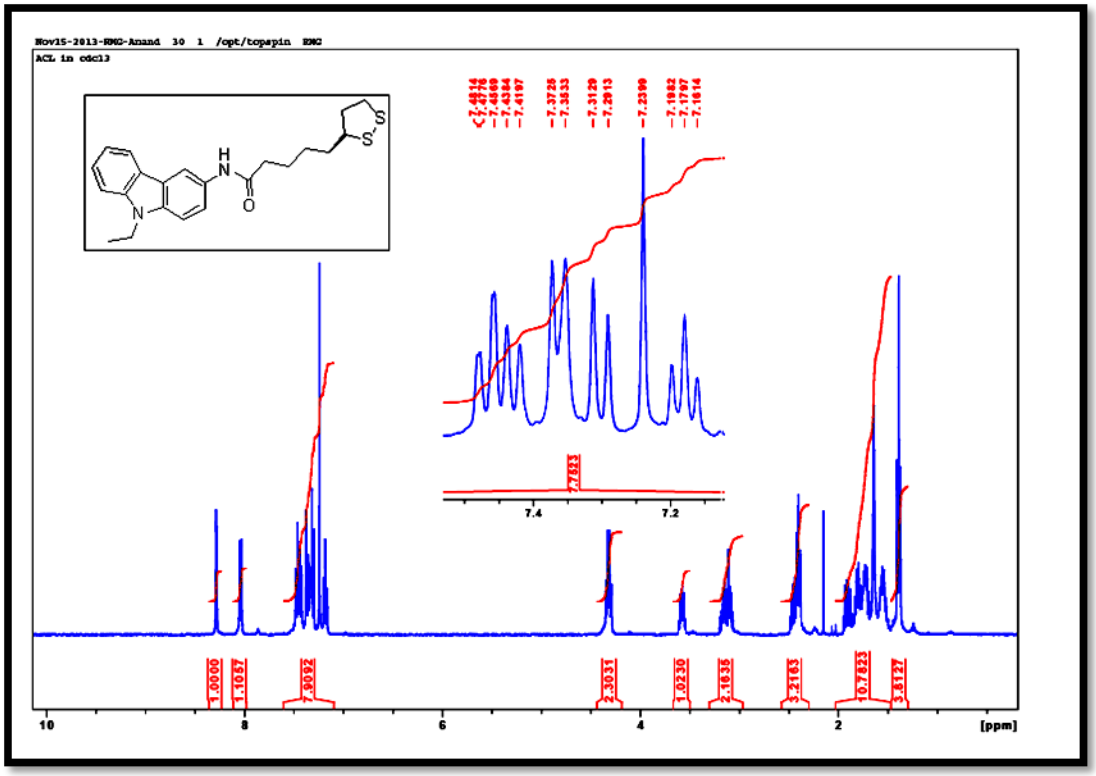

Figure. 5.2 ^{1}H Spectrum of **CTN 3**

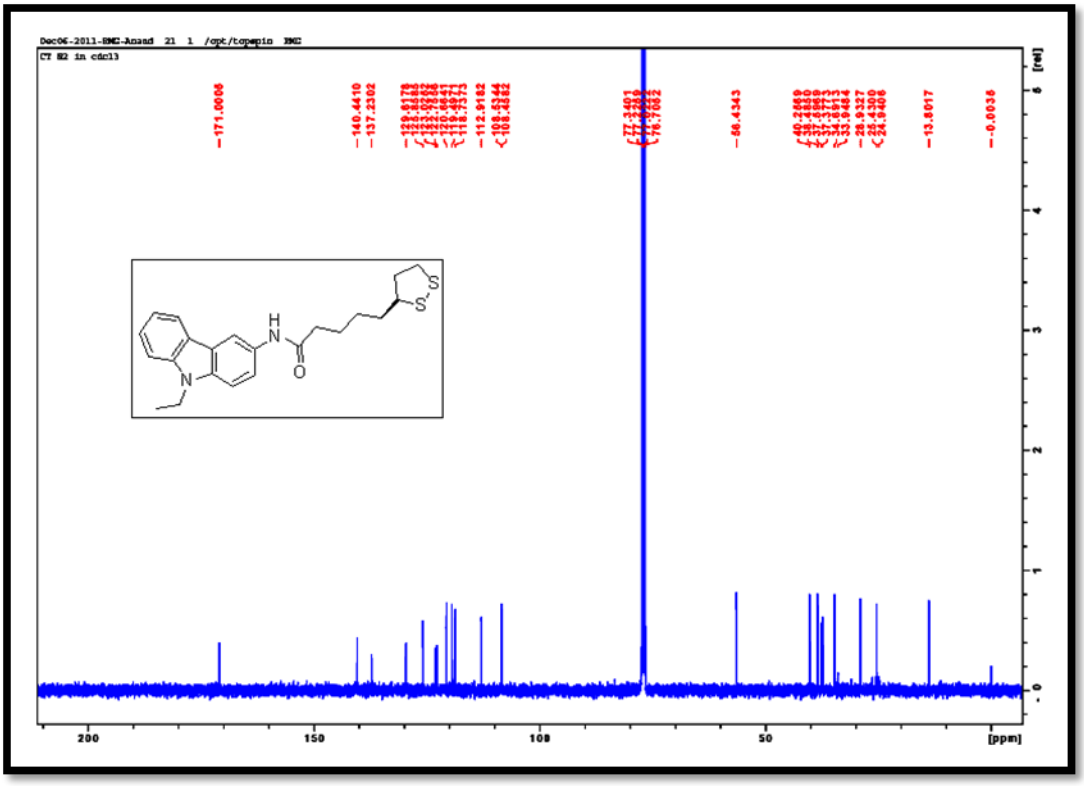

Figure. 5.3 ^{13}C Spectrum of **CTN 3**

CHAPTER V

PART B

Synthesis and bioassay of amine-ended dual thiol ligand functionalized gold nanoparticles

5B.1. Abstract

Drug delivery systems (DDS) are undergoing rapid developments for restoring health in humans; cancer is one of the epidemics that is challenging researchers world-wide. Currently, nanotechnology methods are under investigation for cancer therapy especially with gold nanoparticles (AuNPs) capped with cancer targeting molecules such as antibodies and bioactive small organic molecules. In this study, dual thiol gold nanoparticles capped with bioactive small molecules (DTAu) were synthesized and their cytotoxicity in A549 lung cancer cells were elucidated.

DTAu were synthesized with equimolar quantites of 4-aminothiophenol (4-ATP) and 5-(4-aminophenyl)-1,3, 4-oxadiazole-2-thiol (AXT) in an aqueous solution of $HAuCl_4$ and $NaBH_4$. UV-vis revealed the surface plasmon resonance at 550 nm. Transmission electron microscope (TEM) and XRD studies were used to characterize the AuNPs; the particle size was 5–50 nm. Dynamic light scattering (DLS) was used as supporting evidence to determine hydrodynamic size and zeta potential recorded as 38 nm and 0.290 mV, respectively. FTIR spectra showed the stabilization of gold nanoparticles by thiol ligands with the disappearance of SH stretching. The MTT dye reduction assay was performed on lung carcinoma cells (A549) *in vitro* to assess viability of cells treated with 10 µg/ml and 50 µg/ml of each compound for 2 and 6 hours. A significant decrease in cell viability was noted in 50 µg/ml DTAu, 4-ATP and AXT treated cells at 2 hours (85 % and 66 %) and 6 hours (83 % and 36 %) respectively, ($p < 0.01$). These results suggested that DTAu and 4-ATP possess anti-proliferative properties in the cancerous A549 cells.

5B.2. Introduction

Recently, metal and metal oxide nanoparticles have attracted much attention because of their interesting properties and a wide range of embryonic applications[1–3]. Currently, nanotechnology methods are under investigation for cancer therapy. In particular, cancer targeting molecules such as antibodies and small organic molecules are being attached to the surface of gold nanoparticles (AuNPs) to enhance cancer cell

targeting since the surface of AuNPs have strong binding affinity towards thiols and disulfides. Thiol and amine conjugated ligands are commonly used for the synthesis of stable AuNPs in aqueous media[4,5]. Synthesis of AuNPs involving inorganic gold salts and suitable stabilizing and capping ligands in both one and two phase approaches are used, however these methods are restricted to capping agents compatible with the reducing agents used. Also, these methods are limited in controlling the size and shape of AuNPs[6]. Hence multi-ligand exchange method are used to prepare stable AuNPs with different sizes and functionalities[7]. Recently, Lennox and co-workers synthesized AuNPs in organic and aqueous medium by ligand exchange method using 4-(N,N-dimethylamino)pyridine as a substrate[8]. Knoll and co-workers synthesized azobenzene disulfide capped AuNPs by ligand exchange method to avoid the direct contact of sodium borohydride with azobenzene disulfide[9]. It has been shown that when n-alkane thiol capped AuNPs were used as a precursor for ligand replacement reaction, a complete replacement of n-alkane thiols by incoming ligands was not achieved due to the covalent interaction of thiols with AuNPs[10].

The current knowledge in the synthesis of AuNPs and their toxicological profile is highly inadequate to address their potential as DDS thereby encouraging on-going investigations to understand their potential effects in the human body. However, studies show that when AuNPs are functionalised with surface moieties, they can readily enter living cells. This has encouraged research in cellular biology and therapeutic applications. The present study describes the DTAu, capped with bioactive small molecules, synthesis of AuNPs, characterization and its cytotoxic effects on the A549 human lung cancer cell line and normal healthy human peripheral lymphocytes.

5B.3. Experimental Section

5B.3.1. Materials

Gold (III) chloride trihydrate ($HAuCl_4$. $3H_2O$, ACS reagent), sodium borohydride ($NaBH_4$), 4-amino thiophenol (4-ATP) and 5-(4-aminophenyl)-1,3,4-oxadiazole-2-thiol (AXT) were purchased from Sigma-Aldrich. All aqueous solutions were prepared using distilled water. All glasswares were thoroughly cleaned with aqua regia and rinsed with double distilled water prior to use. All other chemicals used in this investigation were of analytical grade.

5B.3.2. Preparation and Characterization of goldnanoparticles

Gold nanoparticles were prepared by the sodium borohydride reduction method[11]. In a typical experiment, a mixture containing 4-ATP, dissolved in 2 ml water, (0.06 g, 0.5 mmol) and AXT, dissolved in 2 ml of 50 % aqueous ethanol, (0.09 g, 0.5 mmol) was added to 4 ml ultrapure water in a round bottom flask with constant stirring under room temperature. Then 4 ml of $NaBH_4$ (0.20 %) was added to the stirred binary mixture solution containing 4-ATP and AXT followed by the immediate addition of 100 ml of $HAuCl_4.3H_2O$ (10^{-4} M). The solution was stirred for 30 minutes to form blue colloidal solution of DTAu.

The blue colloidal solution at pH~7, was characterized using UV-vis spectrometer (Varian Cary-50 UV spectrophotometer linked to a TCC-240A Shimadzu heating vessel temperature controlled cell holder) in the range of 200-700 nm. To obtain the particle size and shape, 1 µl of the AuNPs was placed on formvar coated grids, air dried and viewed at 100 kV to carry out transmission electron microscopy (JEOL 1010 TEM using a Megaview III camera and iTEM software) studies. For FTIR studies, the AuNPs colloidal solution was centrifuged at 10000 rpm for 10 min. Pellets were washed three times with 20 ml of distilled water and the FTIR spectra recorded (Varian 800 FTIR spectrophotometer). A Differential Light Scattering Malvern Zetasizer Nano ZS (Malvern Instruments Ltd, UK) Merck 2423 instrument was used to measure particle size and zeta potential.

5B.3.3. Cell culture

A549 lung cells were cultured for 6 hours (37°C, 5% CO_2) to 90 % confluency in 25 ml flasks in complete culture media (CCM; Eagles minimum essential media, 10 % fetal bovine serum, 1 % penstrepfungizone, 1 % L-glutamine). Cells were harvested (2×10^4 cells/wells in a 96 wells microtitre plate) for the MTT analysis.

5B.3.4. MTT Assay

Following incubation with relevant treatments, cells were washed twice with PBS and each sample supplemented with a 1:5 ratio of filter-sterilised (0.45 µm) MTT salt solution (5 mg/ml in PBS) and CCM. The plate was incubated at 37°C for 4 hours. Following incubation, dimethyl sulphoxide (DMSO) (100 µl) was added to each well and incubated at 37°C for a further 1hour. Optical density of the formazan product was

measured using a plate reader (Bio-tek μQuant) at 570/690 nm. Results were expressed as mean percentages of the control response.

5B.4. Results, Discussion and Conclusion

UV–vis spectroscopy is an important tool for the characterization of colloidal AuNPs, because AuNPs show a strong surface plasmon resonance (SPR)[12] band in the visible region. The surface plasmon resonance (SPR) band will be shifted to higher or lower wavelength depending upon the size, shape and dispersity of the AuNPs. Further, the SPR band is very sensitive to the nature of the ligands capped on AuNPs.

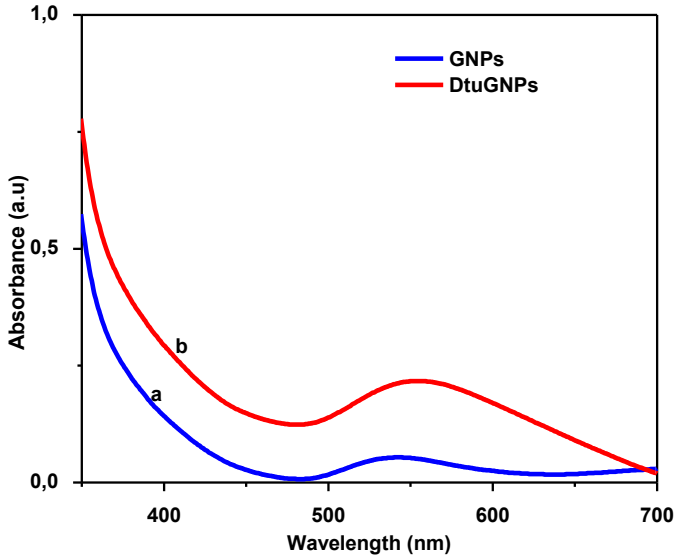

Figure 1. UV–vis spectra of pure gold nanoparticles line (a) and 4-ATP-AXT (Dual Thiol ligands) capped gold nanoparticles (DTAuNPs) line (b)

Figure 1 shows the UV–vis spectra of DTAu obtained by $NaBH_4$ reduction and Thiol/AuNPs. The strong absorption in the spectra of gold nanoparticles at 540 nm (**curve a**) is the characteristic feature of gold surface plasmon resonance (GSPR)[13]. A red shift and broadening of the above band was observed in the spectra of DTAu (**curve b**) indicating some thiol ligand interacted with AuNPs chain networks consequent to surface modification of gold nanoparticles. Further, a rapid colour change of the solution from ruby-red into blue, **Figure 2** by the addition of thiol dual ligands 4-APT and AXT indicated the interaction of gold with sulphur atom.

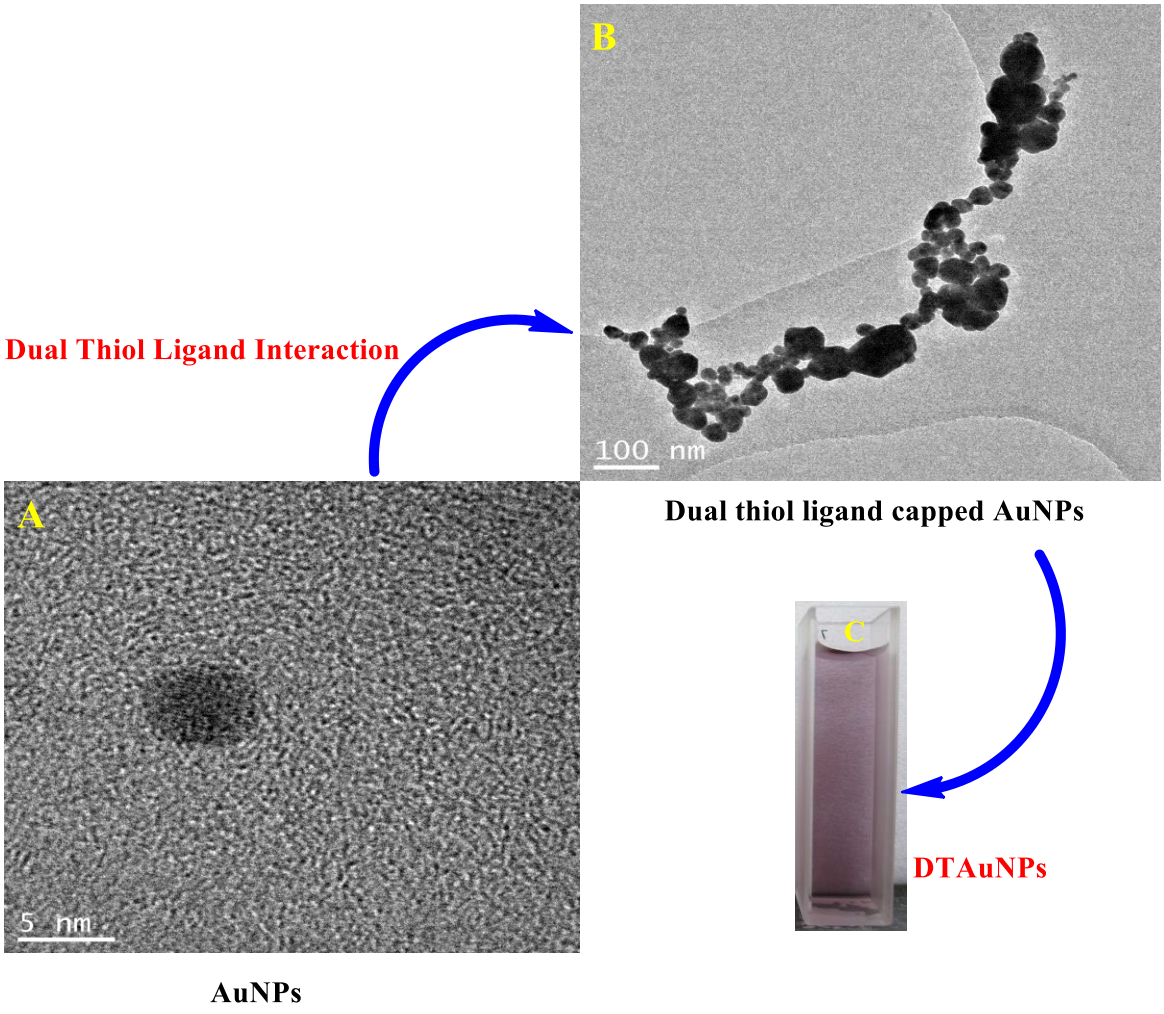

Figure 2. HRTEM images of (A) Before 4-ATP-AXT thiol ligand capped gold nanoparticles (B) After adding 4-ATP-AXT gold nanoparticles in solution and (C) colour change from ruby-red to blue (DTAu)

The optical signature of AuNPs was determined; the distribution of sizes and shapes were conducted by transmission electron microscopy (TEM) images and supported by hydrodynamic size and zeta potential data measured by dynamic light scattering (DLS). Representative TEM images recorded from the AuNPs colloidal solution **Figure 2(A)** showed that most of the particles were spherical or near spherically shaped before the addition of thiol molecules. The particles were monodispersed in the colloidal solution and exhibited a distribution of sizes in the range 3-5 nm. Very small images of gold

nanoparticles with spherical shapes were also observed. After the addition of the thiol ligands, particles grew because of intermolecular interaction between sulphur with gold surface. **Figure 2(B**) shows the particle linking with adjoining particle because the dual thiol ligands gold surface was tailored to the next particle. DTAu formed chain networks[14] instead of aggregates because, in solution, the ligands produced a uniformly distributed negative charge across the surface of the nanoparticles.

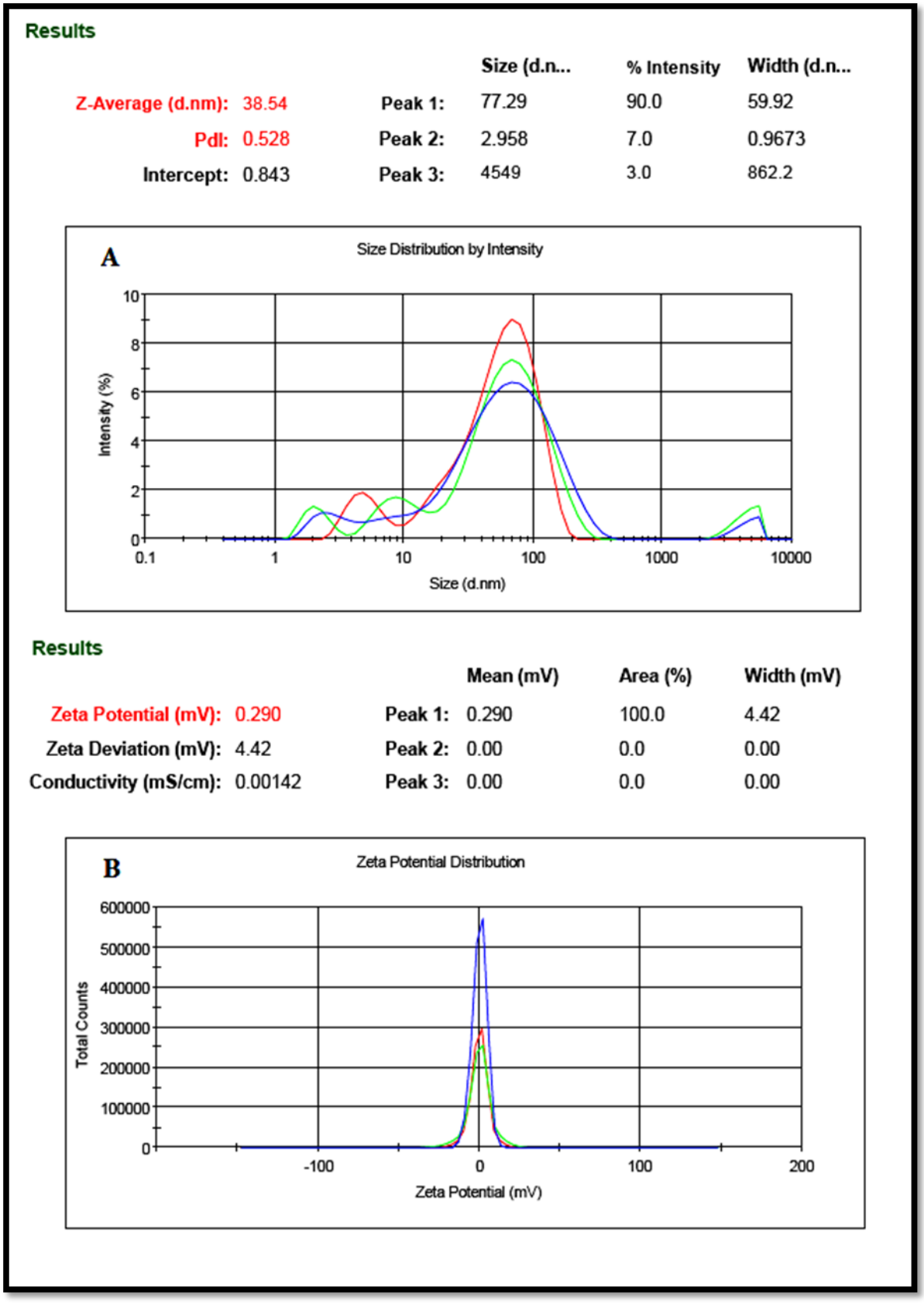

Figure 3. DLS profile size distribution of DTAu with average size of nanoparticles as 38 nm. **(B)** Stability of DTAu recorded as 0.290 mV.

The magnitude of the zeta potential is predictive of the colloidal stability. Nanoparticles with zeta potential values greater than +30 mV or less than -30 mV typically have high degrees of stability. Dispersions with a low zeta potential value will eventually aggregate due to Van Der Waals inter-particle attractions[14]. As expected, the particle size obtained from TEM and DLS scattering was marginally different due to the varying principles used for measurement. Also a stable dispersion of particles was evident from the zeta potential of 0.290 mV **Figure 3(B)** a zeta potential higher than -30 mV indicates a non stable system. DLS size analysis showed the size distribution of particles with an average hydrodynamic size of 38.54 nm **Figure 3(A)** similar to the TEM images.

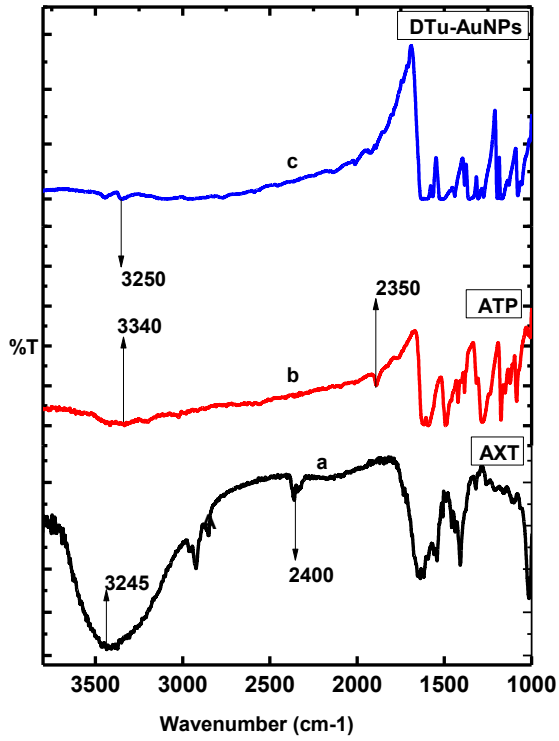

Figure 4. FTIR Profile of AXT (a) and ATP (b) and DTAu (c)

The IR spectra of the DTAu samples were compared with those of the corresponding neat substrates. It was found that the thiol (–SH) stretching frequency (2500–2600 cm^{-1}) of the bound substrates disappeared **Figure 4c**. This suggests that in all cases the bonding of the dual functional ligands to the gold surface tookplace through the thiol (-SH) end. The NH_2 group was present in the IR spectra as indicated in **Figure 4a, b**

and **c** indicating that it did not participate in any linkage or interaction with the gold surface.

Because of the propensity for inter-molecular hydrogen bonding in these dual thiol ligands, some particle aggregation and resultant broadening and red-shifting of the surface plasmon absorption peak were expected in all cases. This is most prominent in the case of DTAu. This is consistent with the TEM images shown in **Figure 2**, where we find that agglomeration in the case of DTAu particles was more severe than in the others. The particles size from TEM and DLS scattering is mariginally different due to the varying principles of measurement. Also a stable dispersion of particles chain was evident from the zeta potential value of 0.290 mV **Figure 3**. Further, the thiol bond was cleaved upon gold sulphur chemisorption[15], in agreement with the study done by Brust on the fate of sulfur-bound hydrogen during the formation of a thiol monolayer on gold.

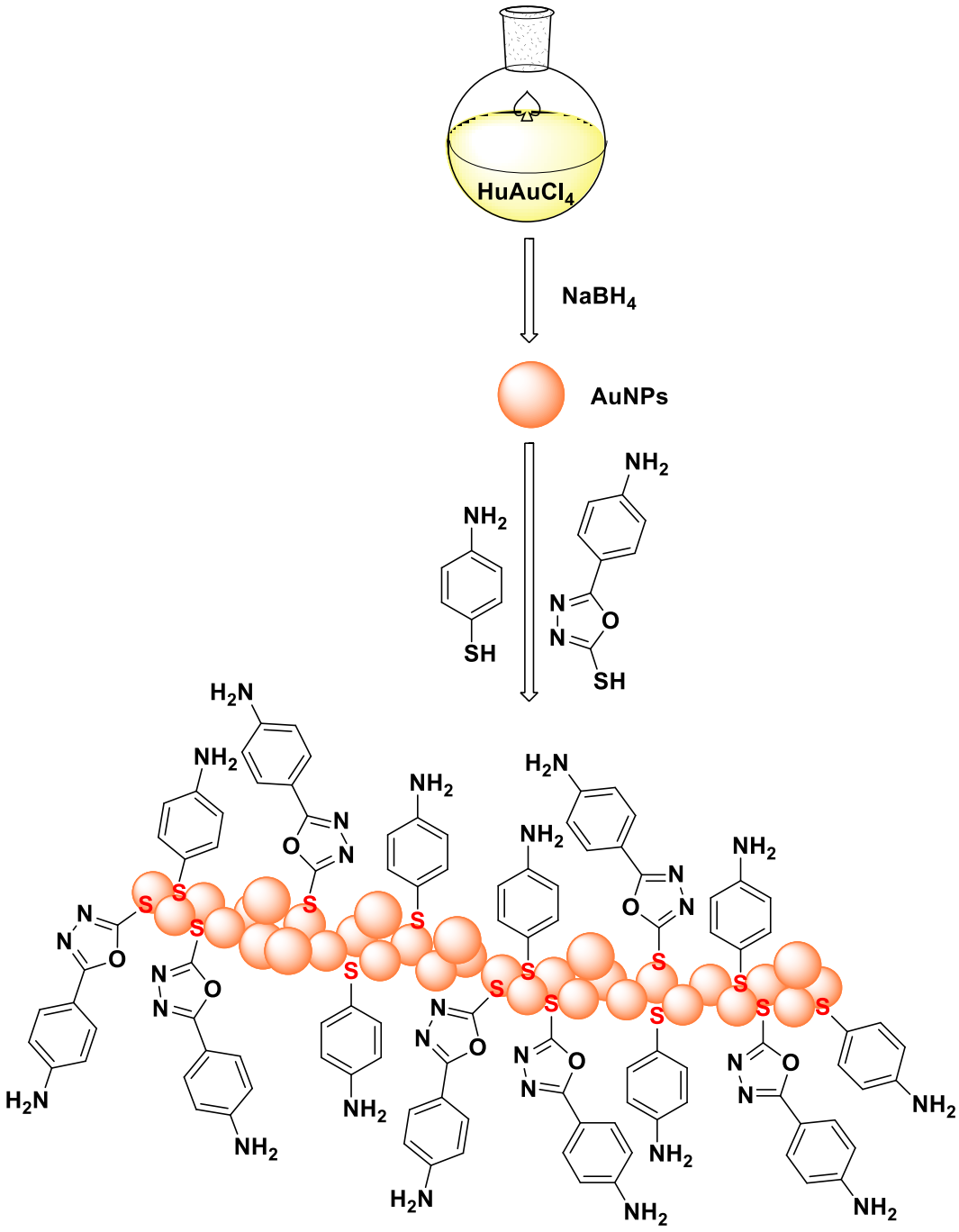

Figure 5. Schematic representation for the Amine ended dual thiol ligand (DT) used for the capping of AuNPs (a) 4-aminothiophenol (ATP) (b) 5-(4-Aminophenyl)-1,3,4-oxadiazole-2-thiol (AXT) form chain networks with AuNPs

Toxicity of DTAu in A549 cells was determined using the MTT assay[16]. A dose-dependent decline in cell viability was observed using DTAu concentrations in the range 0 to 50 ug/ml for 2 hours and 6 hours **Table 1**. A significant decrease in cell viability was noted in 50 µg/ml DTAu, 4-ATP and AXT treated cells at 2 hours (85 % and 66 %) and 6

hours (83 % and 36 %) respectively, ($p < 0.01$). These results suggest DTAu and 4-ATP possess anti-proliferative properties in the cancerous A549 cells. The encouraging results acquired from antioxidant activities prompted us to analyze the compounds against cytotoxicity. The novel DTAu capped gold nanoparticles were evaluated for their ability to inhibit the proliferation of the human cancer cell lines through a preliminary MTT assay; Aflatoxin AFB1, was used as the reference drug since it is a potent cancer agent.

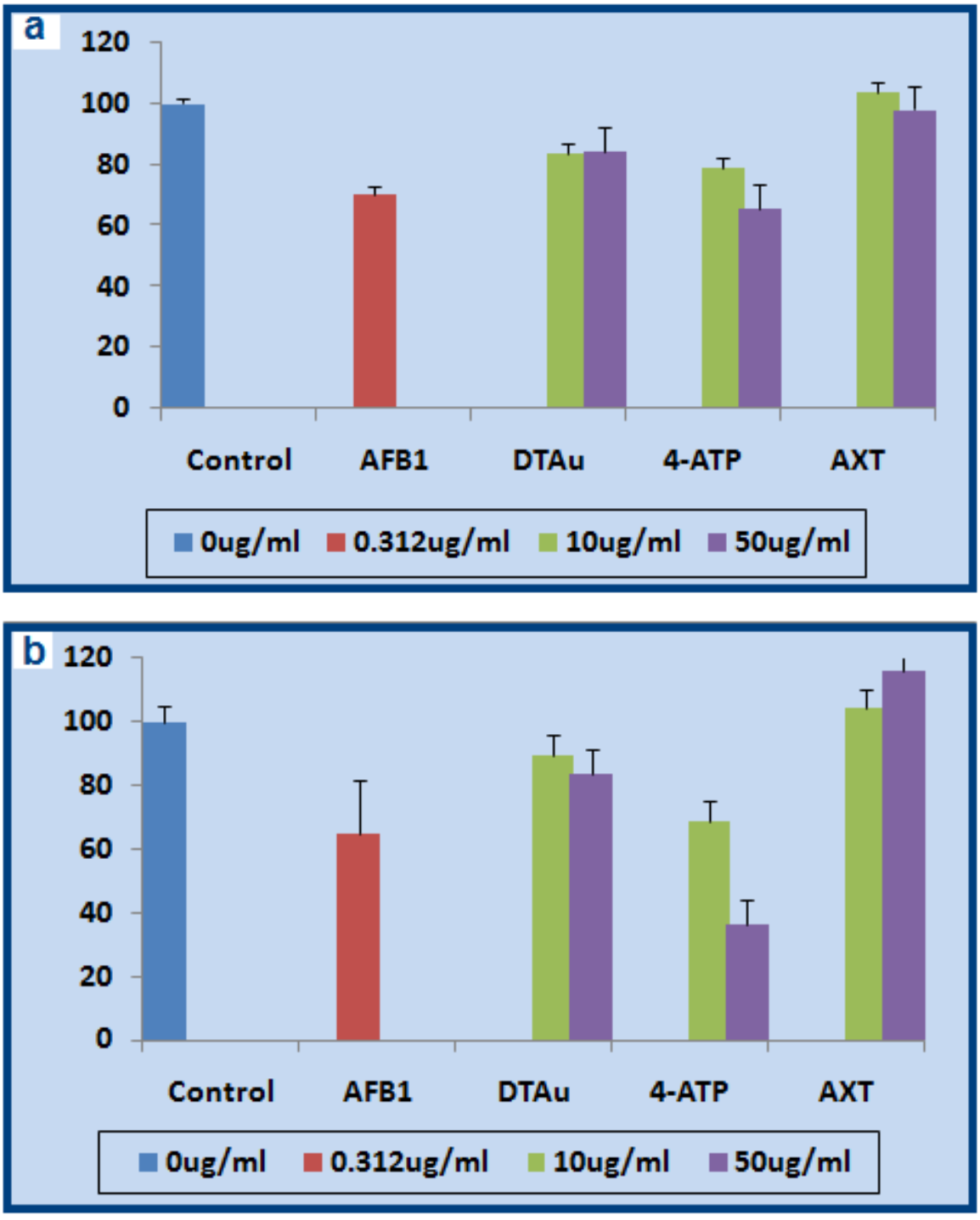

Figure 6. MTT Assay for (a) 2 hours and 6 hours

Table 1. MTT Assay for 2 hours and 6 hours

	0 ug/ml		0.312 ug/ml		
	2 hours	6 hours	2 hours	6 hours	P Value
Control	100±1.65	100±4.9			
AFB1			70±2.35	65±6.9	<0.01

	10 ug/ml		50 ug/ml		
	2 hours	6 hours	2 hours	6 hours	P Value
DTAu	84±3.82	90±11.1	85±14	83±14	<0.01
4-ATP	79±3.36	69±14.8	66±11	36±8	<0.01
AXT	104±4.84	104±6.3	98±8	116±5	>0.05

In conclusion, we reported the synthesis, characterization and bioassay of new gold nanoparticles DTAu: capped with two amine ended organic ligands viz. 4-amino thiophenol (4-ATP) and 5-(4-Aminophenyl)-1,3,4-oxadiazole-2-thiol (AXT). A primary spectroscopic investigation to identify the interaction of amino thiol and AuNPs was carried out. The results showed that the thiol moiety of amine ended ligand is a very effective site to interact with gold surface at nanoscale. As a result of this interaction non stable amine ended thiol ligand capped gold nanoparticles chain net work formed. The MTT results indicated that the dual ligands DTAu induced cytotoxicity and decreased proliferation in A549 cells at various concentrations and incubation times.

Reference

(1) *Nanotechnology in Drug Delivery*; Shah, R. B., Khan, M. A., de Villiers, M. M., Aramwit, P., Kwon, G. S. Eds.; Springer: New York, **2009**.

(2) Bangham, A. D. *Nature.* **1961**, 192, 1197.

(3) Namiki, Y.; Takahashi, T.; Ohno, T. *Gene The.* **1998,** 5, 240.

(4) Lim, C. H.; Cho, H. M.; Choo, J.; Neff, S.; Jungbauer, A.; Kumada, Y.; Katoh S.; Lee, E. K. *Biomed Microdevices.* **2009**, 663.

(5) Vibha Sing.; Santhosh, P.; Nagappan Nai.; Gopala Krishna Aradhya. *J.Nanobiotec.* **2013**, 11, 1477.

(6) Quintiliani, M.; Bassetti, M.; Pasquini, C.; Battocchio, C.; Rossi, M.; Mura, F.; Matassa, R.; Fontana, L.; Russo, M. V.; Fratoddi, I. *Mater. Chem.* **2014**, 2**,** 2517.

(7) *Nanomedicine for Cancer: Lipid-Based Nanostructures for Drug Delivery and Monitoring;* Yoshihisa N., Teruaki F., Noria T., Ryo K., Satoshi M., Yoshitaka K., Masaru N. Japan, **2011**.

(8) Uling X.; Hao H.; Vyara Z.; Matson.; Alireza J.; Wenjin X, Yunan Y.; Yin, Z.; Jonathan, W.; Engle.; Robert, J.; Nickles, M.; Weibo Cai.; Douglas, A.; Steeber.; Shaoqin Gong. Theranostics, 2012, 2 , 757.

(9) Manna, A; Chen, A; Akiyama, H; Wei, T. X; Tamada. K; Knoll. W. *Chem. Mater.* **2003**, *15*, 20.

(10) Jui-Ming Yeh.; Kuan-Yeh Huang.; Su-Yin Lin.; Yu-Yao Wu.; Chao-Chen Huang.; Shir-Joe Liou. *J. Nanotec.* **2009**, 7.

(11) Patil, V.; Malvankar, R.B.; Sastry, M. *Langmuir*, **1999**, 15, 8197.

(12) Zeng, S.; Yong, K. T.; Roy, I. D.; Xuan, Q.; Yu, X.; Luan, F. *Plasmonics*. **2011**, 6, 491.

(13) Zhu, L.; Xue, D.; Wang, Z. *Langmuir*, **2008**, 24, 11385.

(14) Cho, W. S.; Thielbeer, F.; Duffin Megson, I. L.; MacNee W.; Bradley M.;Donaldson, K. *Nanotoxicoloy.* **2014**, 8, 202.

(15) Hasan, M.; Bethell, D.; Brust, M. *J. Am. Chem. So.* **2002,** 124, 1132.

(16) Monks, A. et al. *J. National Cancer Institute.* **1991**, 83, 757.

CHAPTER 6

Synthesis of metal based nanoparticles and their anti-cancer and catalytic applications

Introduction

Nanotechnology is a relatively new, fascinating and active area of research in the field of material science. This is because nanoparticles exhibit completely new or improved properties based on specific characteristics such as size, distribution and morphology. Initially, synthesis of nanoparticles were via. various physical and chemical methods; these methods posed many new problems such as the production of toxic by-products, high costs and tedious, long and environmentally unfriendly protocols. However, with the advent of the 'green chemistry' concept, researchers in the field of nanoparticles synthesis have turned to biological systems which are close to principles of 'Nature'. At present, 100s of reports are available on the use of Algae, Fungi, Yeast and higher plants for nanoparticle synthesis.

Our aim was to synthesize metal based nanoparticles using indigenous plant parts and assesses their anti-cancer and catalytic properties.

Summarised Results

Herein, we report and attach three publications and one research paper that is accepted for publication. These are presented as follows:

Research Paper 1: R. M. Gengan, **K. Anand**, A. Phulukdaree, A. Chuturgoon, A549 lung cell line activity of biosynthesized silver nanoparticles using Albizia adianthifolia leaf, *Colloids and Surfaces B: Biointerfaces*. 105, **2013**, 87-91.

Research Paper 2: Rishalan Govender, Alisa Phulukdaree, Robert M Gengan, **Krishnan Anand** and Anil A Chuturgoon, Silver nanoparticles of Albizia adianthifolia: the induction of apoptosis in human lung carcinoma cell line, *Journal of Nanobiotechnology*. **2013**, 11:5

Research Paper 3: K. Anand, R. M. Gengan, A. Phulukdaree, A. Chuturgoon, Agroforestry waste *Moringa oleifera* petals mediated green synthesis of nanoparticles and their anti-cancer and catalytic activity, *Journal of Industrial and Engineering Chemistry*. DOI: 10.1016/j.jiec.2014.05.021

Research Paper 4: K. Anand and R. M. Gengan, Silver nanoparticles derived from *Ekebergiacapensis* leaf extract and its Catalytic degradation effect on industrial azo dyes. *Industrial Crops and Products*. Manuscript Number- **INDCRO-D-14-01217**

Research Paper 5: K. Anand, R. M. Gengan, A. Phulukdaree, A. Chuturgoon, Farm waste mediated green synthesis of palladium crystal into nanoparticles using *Moringa oleifera* and their A549 lung cell line activity and catalytic study in water. *Applied Catalysis B: Environmental.*

Conclusion

Plants were used *in situ* to synthesize silver, gold and palladium nanoparticles. These nanoparticles were characterised fully by several instrumental techniques and also assessed for their anti-cancer and catalytic potential.

and Surfaces B: Biointerfaces 105 (2013) 87–91

Contents lists available at SciVerse ScienceDirect Colloids and Surfaces B: Biointerfaces

journal homepage: www.elsevier.com/locate/colsurfb

A549 lung cell line activity of biosynthesized silver nanoparticles using *Albizia adianthifolia* leafR.M.

Gengana,*, K. Anandа, A. Phulukdareeb, A. Chuturgoonbа*Department of Chemistry, Faculty of Applied Sciences, Durban University of Technology, Durban 4001, South Africa*b*Discipline of Medical Biochemistry, School of Laboratory Medicine and Medical Sciences, Nelson R Mandela School of Medicine, University of KwaZulu-Natal, Durban 4001, South Africa*

ARTICLE INFO

Article history:
Received 17 September 2012
Accepted 28 December 2012
Available online 7 January 2013

Keywords:
Albizia adianthifolia
Biosynthesis
Silver nanoparticles
Green synthesis
A549 cells
Peripheral lymphocytesA

BSTRACT

Stable AgNPs were formed *in vitro* by reacting $AgNO_3$(aq) solution with the aqueous plant leaf extract. UV–vis revealed the surface plasmon resonance maxat 448 nm and the absorbance steadily increased in intensity as a function of reaction time. Transmission electron microscope (TEM) and XRD studies were used to characterize the AgNPs; the size was 4–35 nm. Dynamic light scattering (DLS) was used as supporting evidence to determine hydrodynamic size and zeta potential recorded as 80.27 nm and −24.7 mV, respectively. FT-IR spectra suggest that AgNPs are capped with protein molecules and other water soluble phytocompounds such as saponins and glycosides which also behave as stabilizing agents; TEM images indicate a visible layer surrounding the AgNPs. Prominent absorption bands at 3380 and 1642 $cm^{-1}$are assigned to alcohol and carbonyl groups, respectively.1H NMR of the neat aqueous plant extract indicates presence of a complex mixture of compounds; however the chemical shift at ı 6.0–8.0 and 1.0–4.0 ppm indicates the presence of few aromatic but abundant aliphatic compounds, respectively.

Toxicity of AgNPs on lung cancer cells (A549) and normal healthy peripheral lymphocytes (PLs) at 10 g/ml and 50 g/ml was assessed using the MTT, ATP and lactate dehydrogenase assays. Viability data for A549 cells showed a 21% (10 g/ml) and 73% (50 g/ml) cell viability after 6 h exposure to AgNPs compared to 117% (10 g/ml) and 109% (50 g/ml) cell viability of normal peripheral lymphocytes. Lactate dehydrogenase was only significantly altered at 50 g/ml AgNPs treated cells from 2.43 ± 0.04 units to 0.77 ± 0.04 units.

1. Introduction

The effects of global warming and dramatic climate change have sparked a worldwide awareness and effort to manage the Earth's natural resources, eliminate hazardous and toxic wastes and save our planet from unnatural ravages caused either directly or indirectly by mankind. The concept of green chemistry, in a cosmos that lives and breathes, is an important one and carries the seeds of a new and more tuneful understanding of our organic universe.

This decade has witnessed the inception of new significant technological products particularly based on nanotechnology; nanoparticle synthesis is being widely explored since they exhibit unique size and shape dependent properties for applications in optics, electronics, catalytic systems, magnetic and biomedical such as HIV inhibition, cancer cell cytotoxicity and genotoxicity [1–13]. In particular, AgNPs are becoming favorable for cancer management since it targets the mitochondrial system thereby limiting ATP altering other biological mechanistic pathways for cell survival. Recent studies have reported promising results in a variety of cell lines [14–17].

Cost effective, simple, non-hazardous and efficient methods are being sought to control the composition, size and shape of nanoparticles which can be utilized in providing improved and alternate products for the global market. Several synthetic methods for the formation of AgNPs, such as chemical reduction in solutions, sol–gel formation, hydrothermal, sonochemical, thermal decomposition of silver compounds and microwave irradiation have been utilized [18–23]. Usually synthetic methodologies are a threat to human health and the environment since toxic and hazardous reagents are used and in some instances toxic by-products are generated. Some of the toxic products which are generated *via* a redox reaction process whereby $Ag^+$is reduced to Ag tend to bond to the AgNPs surfaces and may adversely affect the property and performance of AgNPs.

Recently, microorganisms such as bacteria, virus, fungi and plants have been ascertained as possible eco-friendly nanofactories, however, the use of plants for the synthesis of AgNPs boasts several advantages such as elimination of elaborate processes of

* Corresponding author. Tel.: +27 31 3732309; fax: +27 31 2022671.
E-mail address: genganrm@dut.ac.za(R.M. Gengan).and

0927-776

– see front matter
http://dx.doi.org/10.1016/j.colsurfb.2012.12.044

cell cultures, easy scale up for large-scale synthesis and cost effectiveness. Although some reports have been presented on the synthesis of AgNPs with the aid of plant extracts, the plant kingdom still remains relatively unexplored and understudied; an infinite number of plants with an array of potential applications are available for study in a wide range of research areas [24–28].

Members of the Fabaceae family, particularly Albizia adianthifolia are easily available and grow abundantly in the east coast of South Africa. The phytochemistry of this plant has not been elucidated adequately however saponins such as prosapogenins and triterpenesaponins were identified; they display a broad range of biological and pharmacological properties [29–32]. Both bark and root extracts from *A. adianthifolia* inhibit acetylcholinestarase and cyclooxygenase acitivity [33]. These anti-inflammatory properties may be useful in the treatment of human diseases related to oxidative stress.

The present study describes the *A. adianthifolia* leaf-mediated *in vitro* one pot synthesis of AgNPs, characterization and its cytotoxic effects on the A549 human lung cancer cell line and normal healthy human peripheral lymphocytes.

2. Experimental

2.1. Materials

Silver nitrate ($AgNO_3$, 99% pure) was purchased from Sigma, South Africa. All aqueous solutions were prepared using de-ionised water. *A. adianthifolia* leaves were collected from the Steve Biko campus, Durban University of Technology, Durban, South Africa and identified at the KwaZulu-Natal Herbarium.

2.2. Preparation and characterization of silver nanoparticles

Fresh leaves were collected and washed several times with de-ionised water; 20 g of the leaves were finely cut and 200 ml of de-ionised water was added. The leaves with the water was heated to boil for 15 min, allowed to cool, filtered through a Whatman No. 1 filter paper and 1 ml of the supernatant leaf extract was added to 49 ml of 1×10^{-3}M $AgNO_3$solution at room temperature and the solution stirred.

The yellowish-brown colloidal solution, at pH 7, was characterized using UV–vis spectrometer (Varian Cary-50 UV spectrophotometer linked to a TCC-240A Shimadzu heating vessel temperature controlled cell holder) in the range of 200–800 nm. To obtain the particle size and shape, 1 l of the AgNPs was placed on Formvar coated grids, air dried and viewed at 100 kV to carry out transmission electron microscopy (JEOL 1010 TEM using a Megaview III camera and iTEM software) studies. For X-ray diffraction studies, the AgNPs colloidal suspension was centrifuged at 10,000 rpm for 10 min and the supernatant discarded. The pellets were cast onto a glass plate, air dried and subjected to X- ray diffraction analyses (Philips PW1050 diffractometer) at 1°/min with a scanning step size of 0.02°from 40°to 100°2 using monochromated CoK radiation. Data were captured (Sietronics 122D automated micro-processor linked to the diffractometer). To study the interaction between AgNPs and components in the leaf extract, the AgNPs colloidal solution was centrifuged at 10,000 rpm for 10 min; pellets were washed three times with 20 ml of de-ionized water and the FTIR spectra recorded (Varian 800 FT-IR spectrophotometer). A differential light scattering Malvern Zetasizer Nano ZS (Malvern Instruments Ltd., UK) Merck 2423 instrument was used to measure particle size and zeta potential.

2.3. Cell culture

A549 lung cells were cultured for 6 h (37°C, 5% CO_2) to 90% confluency in 25 ml flasks in complete culture media (CCM; Eagles minimum essential media, 10% fetal bovine serum, 1% penstrepfungizone, 1% L-glutamine). Cells were harvested (2×10^4cells/well in a 96 well microtitre plate) for the MTT analysis, ATP quantification and supernantant was stored following treatment with CCM only, 10 g/ml and 50 g/ml AgNPs solution for 6 h.

Ethical approval from the Biomedical Research Ethics Administration Office of the University of KwaZulu-Natal (Reference number: BE063/08) was obtained. Informed consent was obtained from two healthy volunteers before blood samples were taken. For the preparation of peripheral lymphocytes (PLs), buffy coats containing PLs were extracted from heparinized whole blood by differential centrifugation. Briefly, 5 ml whole blood collected from each subject was layered onto equivolume Histopaque 1077 (Sigma) in polypropylene tubes. Layered blood was then centrifuged at 4000 rpm for 30 min. Buffy coats were aspirated into new polypropylene tubes and washed twice in phosphate buffered saline (4000 rpm, 10 min). Cell density was adjusted to 2×10^4cells/well using the trypan blue exclusion test.

2.4. MTT assay

Following incubation with relevant treatments cells were washed twice with PBS and each sample supplemented with a 1:5 ratio of filter-sterilised (0.45 m) MTT salt solution (5 mg/ml in PBS) and CCM. The plate was incubated at 37°C for 4 h. Following incubation, dimethyl sulphoxide (DMSO) (100 l) was added to each well and incubated at 37°C for a further 1 h. Optical density of the formazan product was measured using a plate reader (Bio-tek Quant) at 570/690 nm. Results were expressed as mean percentages of the control response.

2.5. Lactate dehydrogenase (LDH) assay

The LDH cytotoxicity detection kit (Roche) was used to measure enzyme activity in cell culture medium as an indicator of cell damage/death. Supernantant (100 l) was transferred into microtitre plates in triplicate. Thereafter, substrate mixture (100 l) containing catalyst (diaphorase/NAD^+) and dye solution (INT/sodium lactate) from the kit was added to sample and allowed to react at ambient temperature for 25 min. Optical density of the resulting formazan product was measured at 500 nm with an ELISA plate reader (Bio-tek Quant).

2.6. Statistical analysis

Results are expressed as the mean plus or minus the standard deviation. Statistical significance between samples was determined using one way ANOVA Tukey Kramer Multiple Comparisons test with Dunns post-test using the GraphPad Prism Software (GraphPad Software Inc.).

3. Results and discussion

The first indication of silver nanoparticle (AgNP) formation in a plant extract is visual; this is the appearance of a yellowish-brown color in an aqueous solution due to excitation of surface plasmon vibrations in silver nanoparticles [10]. We observed a yellowish-brown colloidal solution (Fig. 1C) within the first few seconds of reaction of the silver nitrate solution with the aqueous leaf extract of *A. adianthifolia*. This validated the occurrence of a redox reaction whereby Ag^+ions are reduced to $Ag^0$by the plant components which are in turn oxidized to other species. Although

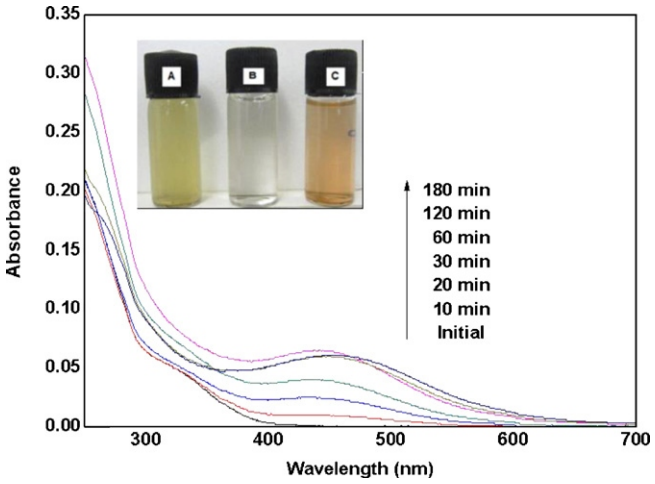

Fig. 1. (A) Aqueous leaf extracts solution. (B) $AgNO_3$solution. (C) Yellowish-brown colloidal solution of AgNPs and UV–vis spectra of AgNPs showing the surface plasmon resonance at 448 nm for the reaction at different time intervals. (For interpretation of the references to color in this figure legend, the reader is referred to the web version of this article.)the

actual mechanism is not properly understood, it is components such as phenolics, polyols, amines, flavonoids, water-soluble heterocyclic components as well as proteins, reducing sugars and other oxido-reductively labile metabolites which have the ability to act as reducing agents. Phytochemical analysis of *A. adianthifolia* revealed saponins [30,32] and glycosides [34] which could have functional groups responsible for AgNPs formation.

We used UV–vis spectroscopy to monitor the reaction medium as a function of reaction time (Fig. 1). Our system showed $_{max}$at 448 nm and the absorbance steadily increases in intensity as a function of reaction time. A change in absorbance intensity of *ca.* 0.065 a.u, in the first 3 min of reaction, was recorded; this intensity increased over longer reaction time. Since the peak wavelength did not shift during the reaction [35], we concluded that there was no change in the nanoparticle size during this time as well as the preparation is mainly composed of small spherical AgNPs as indicated by the single broad symmetrical absorption peak.

The optical signature of AgNPs was elucidated in terms of the distribution of sizes and shapes observed by transmission electron microscopy (TEM) images and supported by hydrodynamic size and zeta potential data measured by dynamic light scattering (DLS). Representative TEM images recorded from the AgNPs colloidal solution (Fig. 2A) showed that most of the particles are spherical or near spherically shaped. The particles were poly-dispersed in the colloidal solution and exhibited a distribution of sizes in the range 4–35 nm. Under careful examination, it was evident that a thin layer of materials surrounded [36] some of the particles which suggested the presence of organic-based capping agents inherent in the aqueous extract. Fig. 2B shows the pictogram of AgNPs; particle size of 10 nm is abundant. DLS analysis showed the size distribution of particles with an average hydrodynamic size of 80.27 nm (Fig. 3A) similar to the leaf extract of *Melia azedarach* [37,38]. As expected, the particle size obtained from TEM and DLS scattering is marginally different due to the varying principles used for measurement. Also a stable dispersion of particles was evident from the zeta potential of −24.7 mV (Fig. 3B); a zeta potential higher than 30 mV or lesser than −30 mV is indicative of a stable system. It was reported [36] that terpenoids, present in Neem leaf broth might be the surface active molecules stabilizing the nanoparticles and reaction of the metal ions is possibly facilitated by reducing sugars and/or terpenoids. Our study reveals organic molecules such as saponins, proteins and sugars as surface active molecules responsible

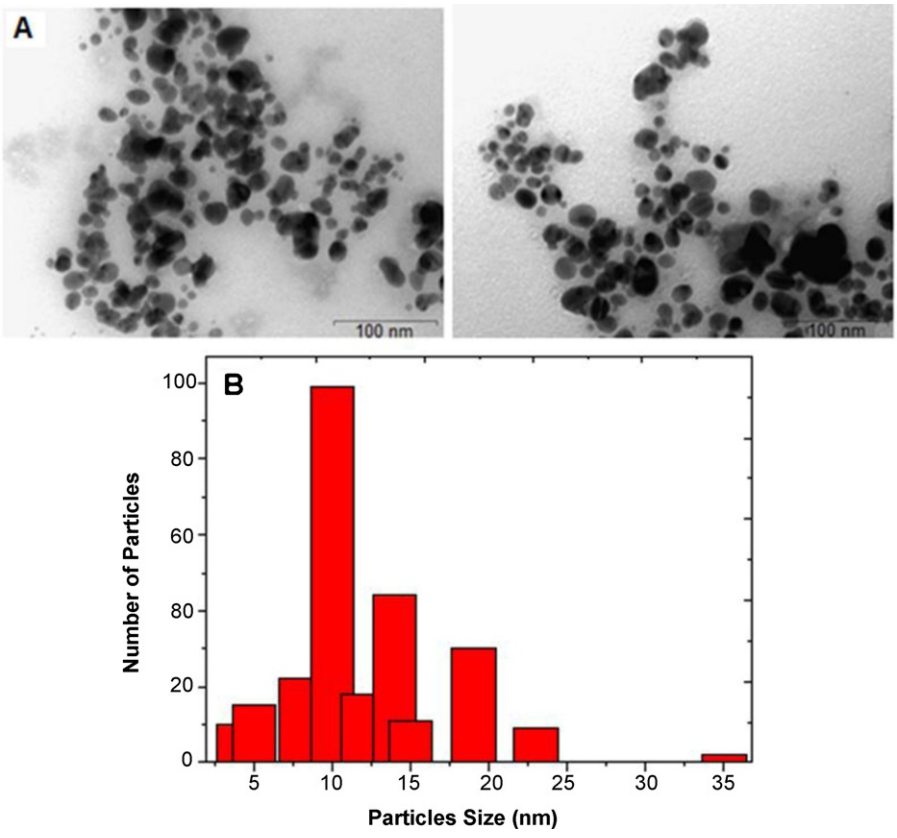

Fig. 2. (A). Representative TEM micrograph of AgNPs biosynthesized by aqueous leaf extract of *Albizia adianthifolia*. (B) Histogram representation of size distribution of AgNPs.

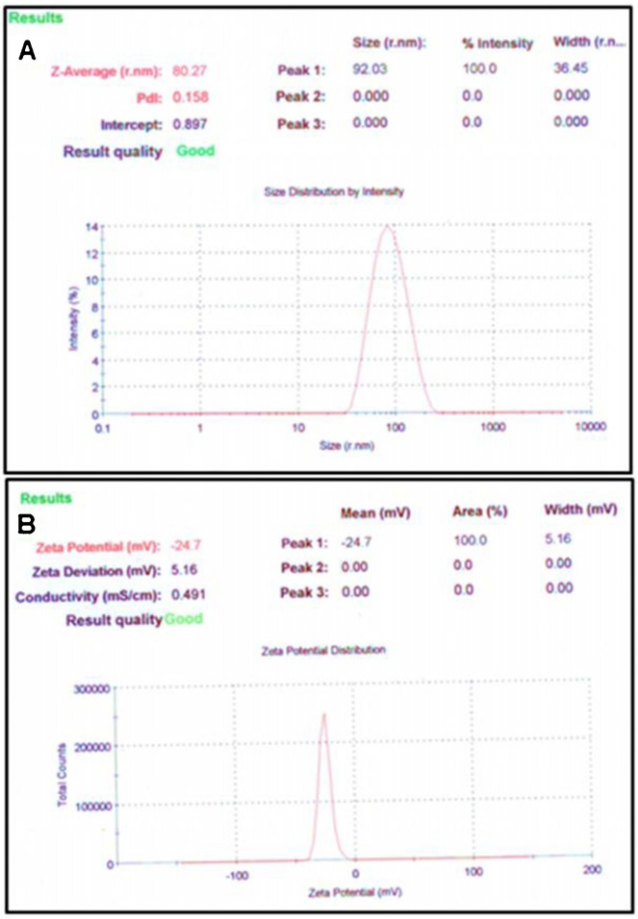

Fig. 3. DLS profile: (A) size distribution of AgNPs with maximum intensity at 80.27 nm. (B) Stable AgNPs at −24.7 mV in zeta potential analysis.for

stability and AgNPs formation; however further studies are required to elucidate the mechanism of biological AgNPs synthesis.

Fig. 4 shows the XRD pattern; the crystalline nature of the AgNPs was confirmed and the characteristic Bragg's XRD peaks at 20 of 44.8°, 52.2°, 76.8°, 93.3°and 98.8°are indexed to the (1 1 1), (2 0 0), (2 2 0), (3 1 1) and (2 2 2) crystallographic planes of the AgNPs, respectively.

FTIR analyses (Fig. 5) of the crude aqueous extract and AgNPs treated spectra showed a stretching frequency shift from 3290 to 3380 cm^{-1}suggesting an OH functional group [39,40]. Furthermore

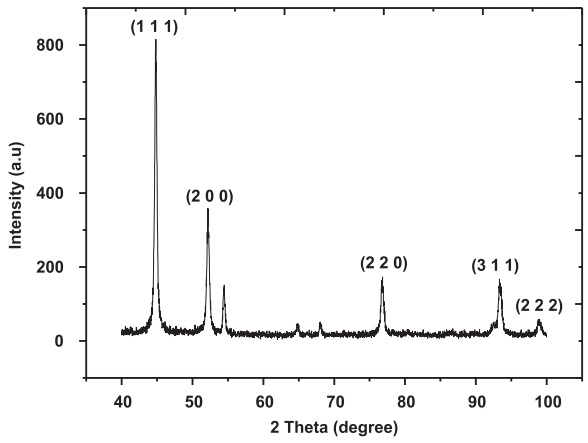

Fig. 4. XRD pattern of AgNPs exhibiting the facets of crystalline silver.

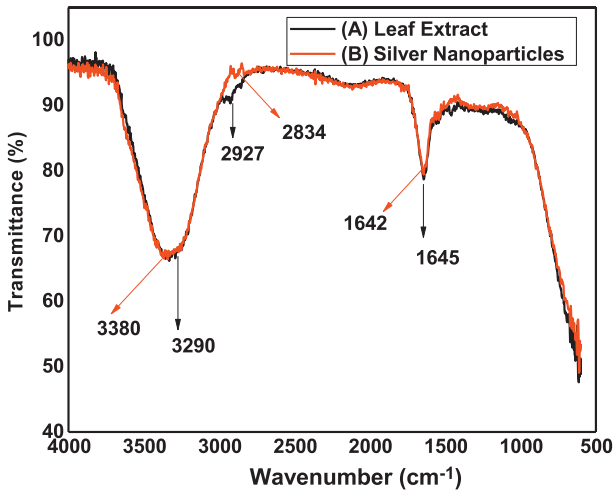

Fig. 5. The FTIR spectra of (A) aqueous leaf extract and (B) AgNPs biosynthesized by *Albizia adianthifolia* leaf extract.a

shift from 1645 to 1642 $cm^{-1}$is assigned to the C═O stretch. A significant but smaller absorption band at stretching frequency 2927 is shifted to 2834 cm^{-1}which indicates the alkyl C—H group; this suggests the presence of saturated molecules. Although saponin type compounds were identified by phytochemistry work, other biomolecules, secondary metabolites, proteins and lipids are present in the plant cell, at different concentrations, which may be responsible for the bio-reduction of Ag^{+}ions. Specifically, conversion of C═O group of biomolecules to C(O)═O group may be responsible for the reduction of $Ag^{+}$to Ag^{0}.

In order to identify the capping reagents and molecules responsible for the reduction of the silver ions, the crude aqueous plant extract of *A. adianthifolia* was investigated by GC–MS and ^{1}H NMR spectroscopy. The total ion chromatogram (TIC) indicates the presence of various organic compounds with significantly abundant peaks at retention time 17.099, 17.238, 20.671, 20.754, 20.950 and 21.040 min having molecular ions (*m*/*z*) of 578.1, 377.0, 331.1, 334.2, 355.0 and 435.8, respectively. The complex pattern of the ^{1}H NMR spectrum further supports that several compounds are present in the extract [41]. The signals at ı 6–8 and ı 1–4 ppm clearly indicate presence of trace aromatic but abundant aliphatic compounds, respectively. Further studies are required to unravel the types and role of phytocompounds in the biosynthesis of AgNPs and a detail mechanism needs to be elucidated.

Although synthetic AgNPs are being widely applied, there is limited data based on the cytotoxicity of biologically synthesized AgNPs. We used the MTT and LDH assays to determine cytotoxicity in the transformed A549 (human lung epithelial adenocarcinoma cells) and normal healthy peripheral lymphocytes. The results are presented in Table 1.

The AgNPs were significantly cytotoxic to A549 cells at both 10 g/ml and 50 g/ml, with viabilities of 79% and 27%, respectively. However, this cytotoxic effect was not observed in the normal healthy PLs at both concentrations of AgNPs, with cell viabilities of 117% and 109%, respectively. This data strongly suggests that the AgNPs may possess anti-cancer/anti-proliferative properties. The cytotoxic potential of the AgNPs was further validated by measuring LDH leakage from treated cells. The A549 cells treated with 50 g/ml showed the highest activity in the cell culture supernatant, which is indicative of cell damage and toxicity. Again, the normal healthy PLs showed no adverse effects to the AgNPs treatments at both concentrations. Plant extracts are normally rich in nutrients and phytocompounds that result in antihyperglycaemic effects. This is clearly observed in the normal healthy PLs, where

Table 1
% Cell viability (MTT assay) and % cytoxicity (LDH activity) in A549 cells and normal healthy peripheral lymphocytes after treatment with 10 and 50 g/ml AgNPs.

	MTT – cell viability (mean OD ± SD)		LDH – cytotoxicity (mean OD ± SD, %)	
	Peripheral lymphocytes	A549 cells	Peripheral lymphocytes	A549 cells
Control	0.71 ± 0.03 (100%)	1.19 ± 0.06 (100%)	2.57 ± 0.06 (100%)	2.13 ± 0.04 (100%)
10 g/ml	0.84 ± 0.05 (117%)$_a$0.93	± 0.08 (79%)	2.57 ± 0.08 (100%)	2.14 ± 0.04 (101%)
50 g/ml	0.77 ± 0.02 (109%)	0.32 ± 0.12 (27%)$_b$2.60	± 0.11 (101%)	0.77 ± 0.01 (36%)$_c$

Data represented as mean ± standard deviation (SD). Tukey Kramer Multiple Comparisons ANOVA with Dunns post-test where a, b, and c: $p < 0.05$ is considered statistically significant.the

cell viability is greater than 100%. It is noteworthy that such an effect is not observed in the cancerous A549 cells, in spite of increased glycolysis being the hall mark of cancer proliferation. We are currently investigating the mechanism of cell death by these AgNPs in the A549 cells.

4. Conclusion

A green method which is simple, quick, cost-effective and reproducible was developed to synthesise AgNPs *in vitro* using the aqueous leaf extract *of A. adianthifolia*. These nanoparticles showed characteristic UV–vis absorption peak at 448 nm.TheAgNPs were characterized by XRD, TEM and DLS; silver particles are spherical in shape, are poly-dispersed and stable. Furthermore, AgNPs causes significant cytotoxicity to A549 cells and did not induce cytotoxicity in normal healthy PLs.

Acknowledgements

We are grateful to J.W. Smith (Electron Microscope Unit, UKZN) for TEM measurements, J. Hughes (School of Environmental Sciences, UKZN) for XRD measurements and T. Govender (Department of Pharmacology, UKZN) for DLS studies. We also thank M.A. Ngwenya of the KwaZulu-Natal Herbarium for identifying the plant species. Thanks to the National Research Foundation (NRF), Durban University of Technology (DUT) and University of KwaZulu-Natal for funding this project.

Appendix A. Supplementary data

Supplementary data associated with this article can be found, in the online version, at http://dx.doi.org/10.1016/j.colsurfb.2012.12.044.

References[1]

B.R. Cuenya, Thin Solid Films 518 (2010) 3127.
[2] A. Tripathy, A.M. Raichur, N. Chandrasekaran, T.C. Prathna, A. Mukherjee, J. Nanopart. Res. 12 (2010) 237.
[3] P. Rajasekharreddy, P.U. Rani, B. Sreedhar, J. Nanopart. Res. 12 (2010) 1711.
[4] V. Kumar, S.K. Yadav, J. Chem. Technol. Biotechnol. 842 (2009) 151.
[5] N. Mude, A. Ingle, A. Gade, M. Rai, J. Plant Biochem. Biotechnol. 18 (2009) 83.
[6] J.Y. Song, B.S. Kim, Bioprocess. Biosyst. Eng. 32 (2009) 79.
[7] J.Y. Song, H.K. Jang, B.S. Kim, Process Biochem. 44 (2009) 1133.
[8] M. Rai, A. Yadav, A. Gade, Biotechnol. Adv. 27 (2009) 76.
[9] R.O. Becker, Met. Based Drugs 6 (1999) 297.
[10] S. Silver, FEMS Microbiol. Rev. 27 (2003) 341.
[11] J.L. Elechiguerra, J.L. Burt, J.R. Morones, A.C. Bragado, X. Gao, H.H. Lara, M.J. Yacaman, J. Nanobiotechnol. 3 (2005) 1.
[12] R. Sukirtha, K.M. Priyanka, J.J. Antony, S.K. lakkannan, R. Thangam, P. Gunasekaran, M.L. Krishnan, S. Achiraman, Process Biochem. 47 (2012) 273.
[13] R. Foldbjerg, D.A. Dang, H. Autrup, Arch. Toxicol. 85 (2011) 743.
[14] S.M. Hussain, K.L. Hess, J.M. Gearhart, K.T. Geiss, J.J. Schlager, Toxicol. In Vitro 19 (2005) 975.
[15] S.M. Hussain, A.K. Javorina, A.M. Schrand, H.M. Duhart, S.F. Ali, J.J. Schlager, Toxicol. Sci. 92 (2006) 456.
[16] L.B. Stolle, S. Hussain, J.J. Schlager, M.C. Hofmann, Toxicol. Sci. 88 (2005) 412.
[17] C. Carlson, S. Hussain, A.M. Schrand, L.B. Stolle, K.L. Hess, R.L. Jones, J.J. Schlager, J. Phys. Chem. B 112 (2008) 13608.
[18] H. Wang, X. Qiao, J. Chen, S. Ding, Colloids Surf. A: Physicochem. Eng. Aspects 256 (2005) 111.
[19] M. Epifani, C. Giannini, L. Tapfer, L. Vasanelli, J. Am. Ceram. Soc. 83 (2000) 2385.
[20] Z. Yang, H. Qian, H. Chen, J.N. Anker, J. Colloid Interface Sci. 352 (2010) 285.
[21] Y. Zhu, X. Wang, W. Guo, J. Wang, C. Wang, Ultrason. Sonochem. 17 (2010) 675.
[22] S. Lee, Y. Yeong, H. Oh, J. Lee, O. Lee, C. Chi, Metal Mater. Inter. 15 (2009) 631.
[23] J. Chen, J. Wang, X. Zhang, Y. Jin, Mater. Chem. Phys. 108 (2008) 421.
[24] J. Kasturi, S. Veerapandian, N. Rajendiran, Colloids Surf. B: Biointerfaces 68 (2009) 55.
[25] D. Philip, Physica E 42 (2010) 1417.
[26] M. Sathishkumar, K. Sneha, S.W. Won, C.W. Cho, S. Kim, Y.S. Yun, Colloids Surf. B: Biointerfaces 73 (2009) 332.
[27] S.C. Prathap, M. Chaudhary, R. Pasricha, A. Ahmad, M. Sastry, Biotechnol. Progr. 22 (2006) 577.
[28] A.M. Fayaz, K. Balaji, P.T. Kalaichelvan, R. Venkatesan, Colloids Surf. B: Biointerfaces 74 (2009) 123.
[29] M.A. Lacaille-Dubois, H. Wagner, Atta-Ur-Rahman (Eds.), Studies in Natural Products Chemistry, vol. 633, Elsevier, Amsterdam, 2000 (Chapter 21).
[30] M. Haddad, I.A. Khan, M.A.L. Dubois, Pharmazie 57 (2002) 705.
[31] M. Haddad, V. Laurens, M.A. Lacaille-Dubois, Bioorg. Med. Chem. 12 (2004) 4725.
[32] M. Haddad, T. Miyamoto, M.A. Lacaille-Dubois, Helv. Chim. Acta 87 (2004) 1228.
[33] I.M.S. Eldeen, E.E. Elgorashi, J.V. Staden, J. Ethnopharmacol. 102 (2005) 457.
[34] H. Mohamed, M. Tomofumi, L. Ve'ronique, D. Marie-AlethLacaille, J. Nat. Prod. 66 (2003) 372.
[35] S. Jae Yong, K. BeomSoo, Bioprocess Biosyst. Eng. 32 (2009) 79.
[36] S.S. Shankar, A. Rai, A. Ahmad, M. Sastry, J. Colloid Interface Sci. 275 (2004) 496.
[37] S. Raman, M.P. Kandula, J.A. Jacob, K. Soundararajan, T. Ramar, G. Palani, K. Muthukalingan, A. Shanmugam, Process Biochem. 47 (2012) 273.
[38] U. Suriyakalaa, J.J. Antony, S. Suganya, D. Siva, R. Sukirtha, S. Kamalakkannan, P.B.T. Pichiah, S. Achiraman, Colloids Surf. B: Biointerfaces, doi:10.1016/j.colsurfb.2012.06.039.
[39] S.P. Dubey, M. Lahtinen, M. Sillanpaa, Process Biochem. 45 (2010) 1065.
[40] S. Priyadarshini, V. Gopinath, N. MeeraPriyadharsshini, D. MubarakAli, P. Velusamy, Colloids Surf. B: Biointerfaces, doi:10.1016/j.colsurfb.2012.08.018.
[41] S.M. Roopan, A. Bharathi, R. Kumar, V.G. Khanna, A. Prabhakarn, Colloids Surf. B: Biointerfaces 92 (2012) 209.

Govender et al. Journal of Nanobiotechnology 2013, 11:5
http://www.jnanobiotechnology.com/content/11/1/5

JOURNAL OF NANOBIOTECHNOLOGY

RESEARCH Open Access

Silver nanoparticles of *Albizia adianthifolia*: the induction of apoptosis in human lung carcinoma cell line

Rishalan Govender[1], Alisa Phulukdaree[1], Robert M Gengan[2], Krishnan Anand[2] and Anil A Chuturgoon[1*]

Abstract

Background: Silver nanoparticles (AgNP), the most popular nano-compounds, possess unique properties. *Albizia adianthifolia* (AA) is a plant of the Fabaceae family that is rich in saponins. The biological properties of a novel AgNP, synthesized from an aqueous leaf extract of AA (AA_{AgNP}), were investigated on A549 lung cells. Cell viability was determined by the MTT assay. Cellular oxidative status (lipid peroxidation and glutathione (GSH) levels), ATP concentration, caspase-3/-7, -8 and −9 activities were determined. Apoptosis, mitochondrial (mt) membrane depolarization (flow cytometry) and DNA fragmentation (comet assay) were assessed. The expression of CD95 receptors, p53, bax, PARP-1 and smac/DIABLO was evaluated by flow cytometry and/or western blotting.

Results: Silver nanoparticles of AA caused a dose-dependent decrease in cell viability with a significant increase in lipid peroxidation (5-fold vs. control; $p = 0.0098$) and decreased intracellular GSH ($p = 0.1184$). A significant 2.5-fold decrease in cellular ATP was observed upon AA_{AgNP} exposure ($p = 0.0040$) with a highly significant elevation in mt depolarization (3.3-fold vs. control; $p < 0.0001$). Apoptosis was also significantly higher (1.5-fold) in AA_{AgNP} treated cells ($p < 0.0001$) with a significant decline in expression of CD95 receptors ($p = 0.0416$). Silver nanoparticles of AA caused a significant 2.5-fold reduction in caspase-8 activity ($p = 0.0024$) with contrasting increases in caspase-3/-7 (1.7-fold vs. control; $p = 0.0180$) and −9 activity (1.4-fold vs. control; $p = 0.0117$). Western blots showed increased expression of smac/DIABLO (4.1-fold) in treated cells ($p = 0.0033$). Furthermore, AA_{AgNP} significantly increased the expression of p53, bax and PARP-1 (1.2-fold; $p = 0.0498$, 1.6-fold; $p = 0.0083$ and 1.1-fold; $p = 0.0359$ respectively).

Conclusion: Data suggests that AA_{AgNP} induces cell death in the A549 lung cells via the mt mediated intrinsic apoptotic program. Further investigation is required to potentiate the use of this novel compound in cancer therapy trials.

Keywords: Nanosilver, Albizia adianthifolia, Cancer, Apoptosis, Smac/DIABLO

Introduction

Cancer is a leading cause of global morbidity and mortality [1]. In 2006 there were 4525 deaths due to lung cancer in South Africa [1]. As much as 80-90% of lung cancer cases are attributed to smoking, with the smaller proportion (10-20%) as a result of occupational exposure to heavy metals [2,3]. Much recently, an association has been found between the acquired immunodeficiency syndrome (AIDS) and the development of lung cancer [4]. This is of concern considering the crisis of AIDS in South Africa. The financial strain of anti-retroviral treatment and cancer therapy necessitates the need for alternate means of cancer treatment that is cost effective, easily accessible and safe.

Nanoparticles (NPs) are small sized (1-100 nm) compounds that are able to function as whole units. These compounds are becoming widespread for their use in consumer products and medical applications; with potential for utilization as therapeutic compounds, transfection vectors, anti-microbial agents and fluorescent labels [5]. Silver NPs are the most commercialized and prominent group of nano-compounds, attributed to their diverse applications in the health sector.

* Correspondence: chutur@ukzn.ac.za
[1]Discipline of Medical Biochemistry, School of Laboratory Medicine and Medical Sciences, University of KwaZulu-Natal, Private Bag 7, Congella, Durban 4013, South Africa
Full list of author information is available at the end of the article

Silver (Ag) possesses unique and unusual chemical, physical as well as biological properties [6]. Silver, in a colloidal form, is used for the treatment of bacterial infections in open wounds, and preparation of ointments, bandages and wound dressings [7]. Additionally, nanosilver has been used as a contraceptive, and marketed as a water disinfectant [8,9].

Silver NPs are now being exploited for the treatment of various diseases such as retinal neurovascularization [10,11] and acquired immunodeficiency syndrome as a result of human immunodeficiency virus [12]. Additionally, AgNPs are well known for their anti-microbial properties and are used as antiviral agents against hepatitis B, herpes simplex virus type 1, monkey pox virus and respiratory syncytial virus [13,14].

Concerns on environmental exposure to AgNPs have initiated toxicity studies. Silver NP-hydrogel induced DNA damage and the production of reactive oxygen species (ROS) in cultured HeLa cells [15]. A study using human lymphocytes revealed that AgNPs caused DNA damage and cell death [16]. Additionally, AgNPs induced oxidative stress and caused impairment of nuclear DNA in Swiss albino mice [16].

Recently, the use of AgNPs as anti-cancer agents has proved promising [6]. Various attempts to incorporate AgNPs into cancer treatments have been made, with positive outcomes [17]. Although the induction of oxidative stress by AgNP induced mt damage has been observed as the general mode of AgNP toxicity, mechanistic pathways remain unclear [18].

Albizia adianthifolia, a plant member of the Fabaceae family found abundantly on the east coast of South Africa, contains saponins such as prosapogenins and triterpene saponins [19,20]. Saponins are plant glycosides that were found to induce cell cycle arrest in a human breast cancer cell line and initiation of apoptosis in a leukemia cell line [21]. Additionally, certain classes of saponins can sequester serum cholesterol and modulate the immune response [22]. The individual properties of Ag and AA were considered for the synthesis of a novel AgNP using aqueous leaf extracts of the plant.

The A549 cell line (human lung carcinoma) is well characterized and extensively used in *in vitro* nanotoxocity studies [23]. A recent study postulated that the induction of ROS and alterations in mt membrane permeability were possible mechanisms by which AgNP exerted its toxic effects in A549 cells [24]. The aim of this study was to investigate the effects of AA_{AgNP} on lung cancer cells. It was hypothesized that AA_{AgNP} induced cell death by apoptosis as a result of AA_{AgNP} mediated generation of ROS. We report on a possible mechanism by which AA_{AgNP} induced apoptosis in the A549 cells.

Results

Cell viability assay

Toxicity of AA_{AgNP} to A549 cells was determined using the MTT assay. A dose-dependent decline in cell viability was observed using AA_{AgNP} concentrations in the range 0 to 75 μg/ml for 6h (95% Cl = 31.96 to 57.72) (Figure 1). An IC_{50} value of 43 μg/ml was obtained and used in all subsequent assays.

ATP analysis

Levels of ATP were assessed using luminometric assay. Silver nanoparticles of AA significantly reduced ATP levels with a 2.5-fold decrease (350,000 ± 1500RLU; 95% CL = 330,000 to 370,000) compared to the control (990,000 ± 40,000RLU; 95% Cl = 480,000 to 1,500,000; $p = 0.0040$) (Figure 2).

Oxidative status

Glutathione concentrations were measured as a marker for intracellular anti-oxidant capacity. The concentration of GSH was higher in untreated cells (15 ± 1.3 μM) compared to AA_{AgNP} treated cells (12 ± 0.24 μM, 95% Cl = −1.0 to 6.2; $p = 0.1184$) (Figure 3A). Lipid peroxidation (MDA) was significantly 5-fold higher in cells exposed to AA_{AgNP} (0.16 ± 0.023 μM) compared to controls (0.032 ± 0.016 μM, 95% Cl = −0.21 to −0.049; $p = 0.0098$) (Figure 3B).

Analysis of caspases

AA_{AgNP} significantly increased the activities of caspase-3/-7 (1.7-fold, 95% Cl = −1,000,000 to −260,000; $p = 0.0180$)

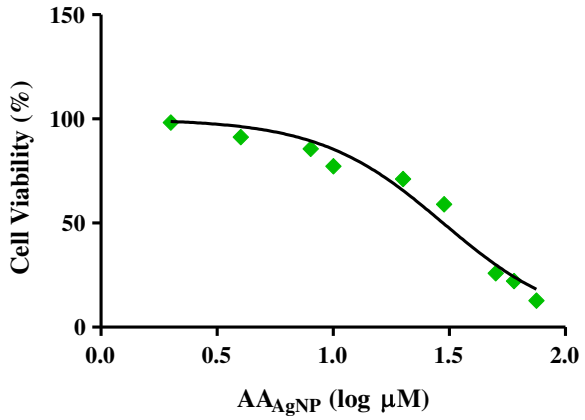

Figure 1 A dose-dependent decline in A549 cell viability after AA_{AgNP} treatment. The MTT assay was used to determine effect of AA_{AgNP} on A549 cell viability. Cells were exposed to AA_{AgNP} in the range 0-75 μg/ml for 6h, after which the formazan product was quantified spectrophotometrically. A distinct dose dependent effect was observed where AA_{AgNP} at lower concentrations induced minimal cell death. A gradual decrease in cell viability occurred with increasing AA_{AgNP} concentration (95% Cl = 31.96 to 57.72). An IC_{50} value of 43 μg/ml was obtained and used for subsequent assays.

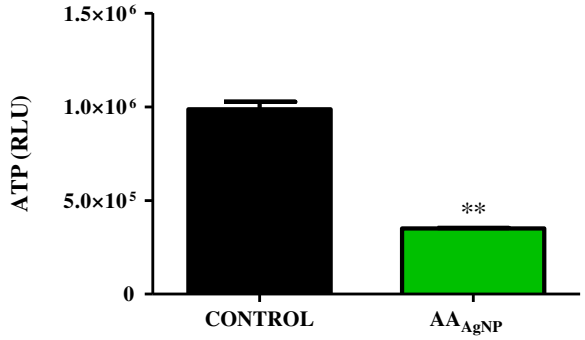

Figure 2 Levels of ATP in control and AA_{AgNP} treated A549 cells. Cellular ATP levels were detected by the ATP CellTitre Glo assay (Promega, Madison, USA). A significant decline in ATP was noted after treatment with AA_{AgNP} (350000 ± 1500RLU; 95% CL = 330000 to 370000) compared to the control cells (990000 ± 40000RLU; 95% CI = 480000 to 1500000; $p = 0.0040$). RLU: relative light units.

and −9 (1.4-fold, 95% CI = −610,000 to −220,000; $p = 0.0117$) compared to the control. The activity of caspase-8 however was significantly decreased by AA_{AgNP} compared to untreated cells (2.5-fold, 95% CI = 550,000 to 840,000; $p = 0.0024$) (Table 1).

Flow cytometry

Silver nanoparticles of AA significantly increased PS translocation A549 cell compared to the control (57 ± 0.59% vs. 10 ± 0.84%, 95% CI = −50 to −43; $p < 0.0001$) (Figure 4A). Additionally, the percentage of necrotic cells were also significantly higher in AA_{AgNP} treated cells (17 ± 0.79% vs. control: 4.6 ± 0.70%, 95% CI = −16 to −9.2; $p < 0.0001$) (Figure 4A). The apoptosis inducing potential of AA_{AgNP} was further verified in disrupting mt Δ Ψ. The treated cells had significantly higher mt depolarization compared to untreated cells (77 ± 0.88% vs. 23 ± 1.8%, 95% CI = 44 to 57; $p < 0.0001$) (Figure 4B).

The expression of CD95 was significantly down regulated (2-fold; 2.8 ± 0.58% vs. control: 5 ± 0.44%, 95% CI = 0.13 to 4.2; $p = 0.0416$) (Table 2). In contrast, AA_{AgNP} significantly increased the expression of smac/DIABLO, a pro-apoptotic protein (29 ± 0.32%) compared to the control (18 ± 0.66%, 95% CI = −13 to −8.5; $p < 0.0001$) (Table 2). Additional files contain the histograms for extra- and intracellular staining (see Additional file 1: Figure S1 and Additional file 2: Figure S2 respectively).

Comet assay

Silver nanoparticles of AA were significantly genotoxic to A549 cells as noted by the increased DNA fragmentation. Comet tail lengths were significantly longer in treated (90 ± 1.3 μm) compared to untreated cells (20 ± 0.71 μm, 95% CI = −73 to −67; $p < 0.0001$) (Figure 5).

Western blot analysis

The expression of selected apoptotic proteins and validation of flow cytometric intracellular stained smac/DIABLO was determined by western blotting. The expression of p53 was observed to be significantly higher post AA_{AgNP} exposure (1.0 ± 0.018RBI vs. control: 0.82 ± 0.045RBI, 95% CI = −0.42 to −0.00037; $p = 0.0498$). A significant increase in the 24kDa fragment of PARP-1 was noted after AA_{AgNP} treatment (3.5 ± 0.069RBI vs. control: 3.1 ± 0.0043RBI, 95% CI = −0.65 to −0.058; $p = 0.0359$). Evaluation of bax showed higher levels of the protein in cells that were treated with AA_{AgNP} (3.4 ± 0.11RBI) compared to untreated cells (2.1 ± 0.047RBI, 95% CI = −1.9 to −0.81; $p = 0.0083$). Highly significant differences were seen in the expression of smac/DIABLO between experimental and control cells. Silver nanoparticles of AA treated cells presented with a 4.1-fold greater band intensity (1.1 ± 0.045RBI vs. control: 0.27 ± 0.010RBI, 95% CI = −0.99 to −0.59; $p = 0.0033$) (Figure 6).

Discussion

Several pathological syndromes such as liver failure, stroke or heart attack are associated with abrupt death of tissue or organs as a result of apoptotic dysregulation. Conversely, the survival of abnormal cells, due to aberrant

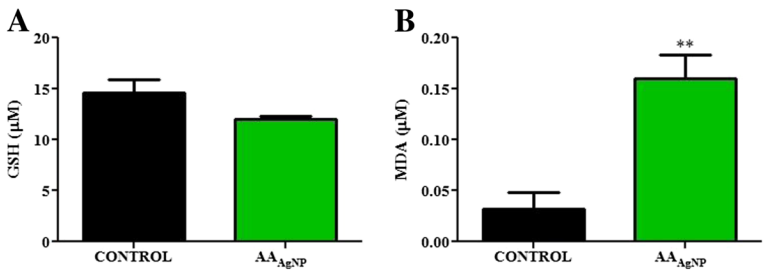

Figure 3 A) Levels of GSH and B) MDA (lipid peroxidation) in AA_{AgNP} treated and untreated cells. The oxidative status of A549 cells were assessed by quantifying GSH and MDA. Levels of the anti-oxidant GSH were measured by the GSH-Glo™ Glutatione assay (Promega, Madison, USA). AA_{AgNP} caused a decrease in GSH (12 ± 0.24 μM) compared to untreated cells (15 ± 1.3 μM, 95% CI = −1.0 to 6.2; $p = 0.1184$). The TBARS assay was utilized to quantify MDA levels as marker for lipid peroxidation induced by ROS. A significant elevation in MDA levels were found in cells exposed to AA_{AgNP} (0.16 ± 0.023 μM) compared to the control (0.032 ± 0.016 μM, 95% CI = −0.21 to −0.049; $p = 0.0098$).

Table 1 Caspase activity in AA_{AgNP} treated cells

	Control	AA_{AgNP}	
	Mean RLU ± sem	Mean RLU ± sem	*p* value
CASPASE-8	$1.2 \times 10^6 \pm 2.6 \times 10^4$	$4.6 \times 10^5 \pm 2.3 \times 10^4$	0.0024**
CASPASE-9	$9.2x10^5 \pm 3.3 \times 10^4$	$1.3x10^6 \pm 3.1 \times 10^4$	0.0117*
CASPASE-3/-7	$9.2x10^5 \pm 4 \times 10^3$	$1.6x10^6 \pm 8.6 \times 10^4$	0.0180*

RLU: relative light units.

apoptosis, may lead to tumorigenesis [25]. Apoptosis is commonly altered in cancerous cells, which have the ability to evade the apoptotic cascade.

Silver nanoparticles of AA significantly increased PS externalization, a transmembrane glycoprotein, in the treated A549 cells (Figure 4A).

The signal transduction of apoptosis involves a cascade of initiator and executioner caspases [26]. Executioner caspases-3/-7 cleave specific substrates leading to alteration changes linked with apoptosis and ultimately cell death [27]. Initiator caspses-8 and −9 are responsible for the activation of executioner caspases. Silver nanoparticles of AA significantly up regulated the activities of caspases-3/-7 and −9 (Table 1). Furthermore AA_{AgNP} increased DNA fragmentation (Figure 5)-an end stage characteristic of apoptosis. In response to this DNA damage, the nuclear enzyme PARP-1 catalyzes the transfer of NAD^+ to a specific set of nuclear substrates [28]. During apoptosis, PARP-1 is cleaved, by executioner caspases-3/-7, to a 24kDa DNA binding domain and an 89kDa fragment containing catalytic activity. Silver nanoparticles of AA was responsible for the cleavage of PARP-1 as evidenced by the significantly increased expression of 24kDa fragment compared to untreated control cells (Figure 6B).

Mitochondria play an important role in apoptosis, via the intrinsic apoptotic program. An initial step for activation of the intrinsic apoptotic pathway is the depolarization of the mt membrane. Depolarized mt is as a result of the formation of mt permeability transition (PT) pores [29]. Mitochondrial PT has been associated with various metabolic consequences such as halted functioning of the electron transport chain with associated elevation in ROS and decreased production of ATP [30]. Bax, a pro-apoptotic protein of the Bcl-2 family, translocates from the cytosol to the outer mt membrane during apoptosis where it interacts with lipids and induces mt PT pores. A significant increase in mt depolarization was observed after AA_{AgNP} treatment (Figure 4B), with an accompanying decrease in ATP concentration (Figure 2). The high levels of bax expression (Figure 6C), high mt depolarization and decreased ATP suggest that AA_{AgNP} induces cellular apoptosis in cancerous lung cells via the intrinsic apoptotic pathway.

Silver has a high affinity for thiol (−SH) groups [31]. In this study, the levels of cysteine-rich GSH were decreased whilst lipid peroxidation was significantly elevated by AA_{AgNP} (Figure 3). This oxidant/anti-oxidant imbalance has previously been documented as an apoptotic mechanism by AgNP mediated cytotoxicity [32,33].

The extrinsic apoptotic pathway is mediated by CD95 death receptor, which recruits Fas-associated protein with death domain (FADD) adapter protein. The adapter protein FADD binds to and activates caspase-8 via the formation of a death-inducing signaling complex [25]. The results of this study show that CD95 expression (Table 2) and caspase-8 activity (Table 1) was significantly decreased by AA_{AgNP}. The extracts of AA are rich in saponins, which will promote rapid entry of the AA_{AgNP} into the cells resulting in mt mediated intrinsic apoptotic pathway. A well characterized biological action of saponins is their ability to induce cell membrane permeabilization [34]. Decreased ATP concentrations and increased MDA as a result of ROS may be due to disruptions in the mt respiratory chain. Nanoparticles preferentially localize in mt and cause oxidative stress as

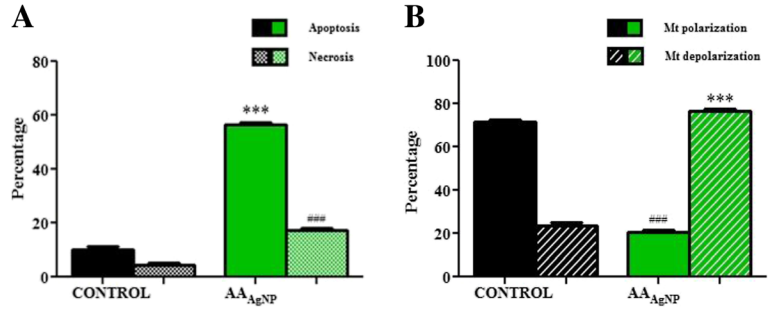

Figure 4 A) Percentages of apoptotic and necrotic cells and B) Mt depolarization after treatment with AA_{AgNP}. Flow cytometry was used to examine PS translocation (annexin-V-Fluos assay (Roche)) and mt membrane integrity (BD™ MitoScreen kit (BD Biosciences). A significant increase in apoptosis (57 ± 0.59% vs. control: 10 ± 0.84%, 95% CI = −50 to −43; $p < 0.0001$) and necrosis (17 ± 0.79% vs. control: 4.6 ± 0.70%, 95% CI = −16 to −9.2; $p < 0.0001$) following treatment was seen. Furthermore, mt membrane depolarization was significantly higher in AA_{AgNP} treated cells (77 ± 0.88% vs. control: 23 ± 1.8%, 95% CI = 44 to 57; $p < 0.0001$).

Table 2 Surface expression of CD95 and intracellular smac/DIABLO in A549 cells treated with AA_{AgNP} as determined flow cytometrically

	Control	AA_{AgNP}	
	Mean % ± sem	Mean % ± sem	*p* value
FITC + ve (CD95)	5 ± 0.44	2.8 ± 0.58	0.0416*
APC + ve (smac/DIABLO)	18 ± 0.66	29 ± 0.32	<0.0001***

well as potentiate structural damage [35,36]. Various studies have associated AgNP toxicity with mt damage [37,38].

Several pro-apoptotic molecules are released from the mt during apoptosis. In the presence of ATP, mt released cytochrome c associates with apoptotic protease-activating factor (Apaf)-1 in the cytosol inducing its oligomerization. An apoptosome is then formed with the oligomeric Apaf-1 complex and procaspase-9, inducing the activation of caspase-9, which in turn activates effector caspases-3 and −7 [26]. An interesting finding in this study was that although ATP levels were reduced post AA_{AgNP} treatment, the activity of caspase-9 was still elevated (Table 1).

A class of molecules involved in the regulation of apoptosis is the inhibitor of apoptosis (IAP) proteins. These proteins avert cell death by suppressing the activity of caspases. X-chromosome-linked inhibitor of apoptosis (XIAP) is the most well characterized member of IAPs [25]. The ability of IAPs to act as endogenous suppressors of procaspase activation is attributed to the presence of domains referred to as baculoviral IAP repeats (BIR).

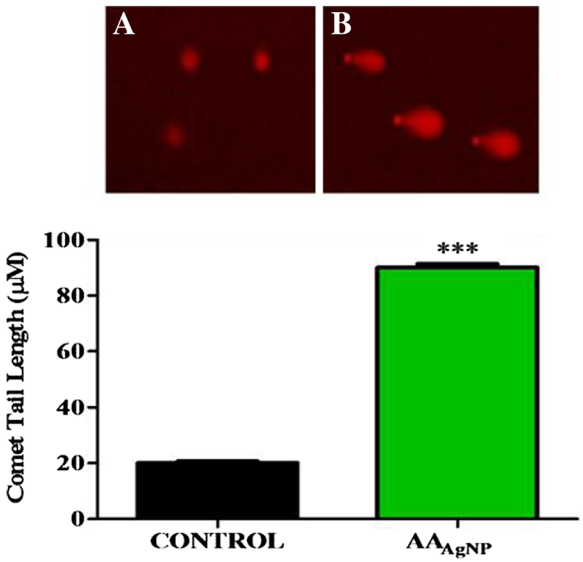

Figure 5 Fragmentation of DNA in cells exposed to AA_{AgNP} (B) and untreated control cells (A) (100x). To assess the genotoxic effects of AA_{AgNP}, the comet assay was used. Fragmentation of DNA (indicated by comet tails) was significantly induced by AA_{AgNP} treatment (90 ± 1.3 μm) compared to control cells (20 ± 0.71 μm, 95% CI = −73 to −67; $p < 0.0001$).

In particular, BIR3 and a region adjacent to BIR2 are responsible for the inhibition of caspases-9, and −3 and −7 respectively. Smac/DIABLO, a mt protein, is able to abolish the inhibitory effects of XIAP [26]. Both smac/DIABLO and caspases-3,-7 and −9 contain IAP-binding motifs that fit into the BIR domains of XIAP. Thus, smac/DIABLO is able to relieve inhibition by replacing and releasing caspases-3, -7 and −9 from the XIAP inhibitory complex [25,26]. We postulated that AA_{AgNP} released smac/DIABLO from the mt. The increased intracellular staining (Table 2) and expression of smac/DIABLO by western blotting (Figure 6D) confirmed that AA_{AgNP} induced its release from the mt.

The p53 protein mediates a range of anti-proliferative processes in response to different stress stimuli by directly activating apoptosis and promoting the release of bax [39] and inducing executioner caspase activity [40] Also, p53 interferes with mt integrity and function leading to the release of pro-apoptotic molecules and the generation of ROS [41]. This study clearly shows the increased expression of p53 after addition of AA_{AgNP} to cells (Figure 6A).

Conclusion

In conclusion, this novel AA_{AgNP} possesses potent pro-apoptotic potential. We have shown, mechanistically, that AA_{AgNP} activates the intrinsic apoptotic pathway in A549 lung carcinoma cells. The findings of this study suggest the potential for AA_{AgNP} in drug development against cancer. None the less, further studies need to be conducted to ascertain if the effects of AA_{AgNP} are consistent in other cancerous cell lines and also non-toxic to healthy systems.

Materials and methods

Materials

A549 cells were purchased from Highveld Biologicals (Johannesburg, South Africa). Cell culture reagents were purchased from Whitehead Scientific (Johannesburg, South Africa). LumiGLO® chemiluminescent substrate kit was purchased from Gaithersburg (USA) and western blot reagents were purchased from Bio-Rad (USA). All other reagents were purchased from Merck (South Africa).

Synthesis of AA_{AgNP}

Synthesis and characterization of AA_{AgNP}, described by Gengan *et al.* 2013, was conducted at the Steve Biko campus, Durban University of Technology, Durban, South Africa. A one-pot green synthesis technique was used [42]. Briefly, fresh leaves of AA were extracted with deionized water. The crude extract was filtered and the supernatant was allowed to react with silver nitrate solution at room temperature (RT). Silver nanoparticles of AA solution (pH 7) were then characterized using UV spectrometry. Particle size was determined by transmission electron microscopy. To assess the interaction between nanosilver

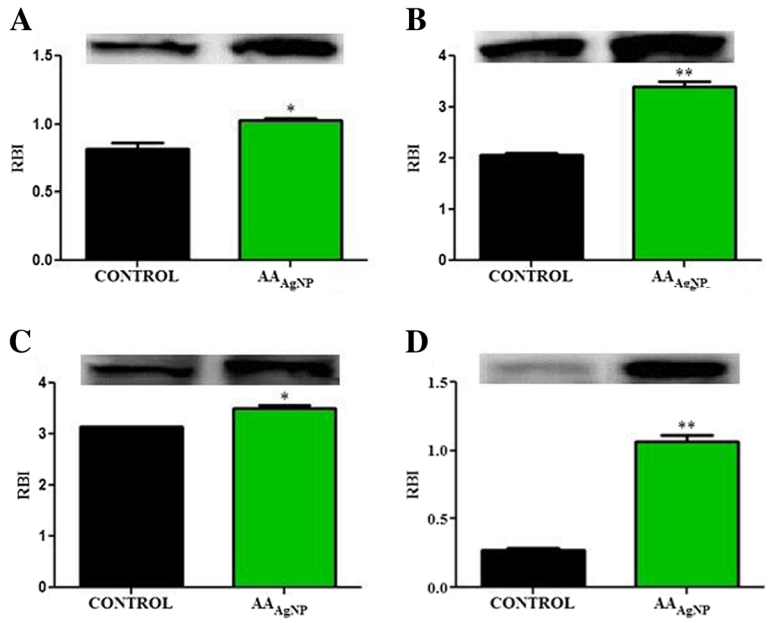

Figure 6 The expression of apoptotic proteins (A) p53, B) PARP-1, C) bax and D) smac/DIABLO) in AA_{AgNP} treated and untreated cells. Western blotting assessed the expression of selected apoptotic proteins. Levels of p53 were significantly higher post AA_{AgNP} exposure (1.0 ± 0.018RBI vs. control: 0.82 ± 0.045RBI, 95% CI = −0.42 to −0.00037; $p = 0.0498$). Cleavage of PARP-1 was distinct with significant increase in the 24kDa fragment after AA_{AgNP} treatment (3.5 ± 0.069RBI vs. control: 3.1 ± 0.0043RBI, 95% CI = −0.65 to −0.058; $p = 0.0359$). The expression of bax was significantly higher in cells that were treated with AA_{AgNP} (3.4 ± 0.11RBI) compared to untreated cells (2.1 ± 0.047RBI, 95% CI = −1.9 to −0.81; $p = 0.0083$). AA_{AgNP} treated cells presented with a 4.1-fold greater band intensity for smac/DIABLO (1.1 ± 0.045RBI vs. control: 0.27 ± 0.010RBI, 95% CI = −0.99 to −0.59; $p = 0.0033$). Protein bands were standardized against β-actin.

and compounds of the aqueous extracts of AA leaves, Fourier transform infrared spectrophotometry was employed [42]. Ethical approval from the Biomedical Research Ethics Administration Office of the University of KwaZulu-Natal (Reference number: BE050/08) was obtained.

Cell culture and exposure protocol

The A549 cells were cultured in Eagle's minimum essential medium supplemented with 1% L-glutamine, 1% penstrepfungizone and 10% fetal bovine serum. Cultures were maintained at 37°C with 5% CO_2. For the 3-(4,5-Dimethyl-2-thiazolyl)-2,5-diphenyl-2H-tetrazolium bromide (MTT) assay, cells were seeded into a 96-well microtitre plate, allowed to attach overnight and treated with AA_{AgNP} solution (0-75 μg/ml). For flow cytometry assays, caspase, ATP and lipid peroxidation assays, cells were cultured to 90% confluency in 25 cm^2 tissue flasks and treated with AA_{AgNP}. For the GSH assay, cells were plated in 96-well microtitre plates and allowed to attach overnight, followed by treatment with AA_{AgNP}. For western blot analysis and the comet assay, cells were grown to 90% confluency in 6-well culture plates and treated with AA_{AgNP}.

Cell viability assay

Cell viability was determined using the MTT assay. Approximately 20,000 cells (in six replicates) were used for exposure to AA_{AgNP} concentrations in the treatment range. After incubation with AA_{AgNP} for 6 h, cells were washed twice with 0.1M phosphate buffer saline (PBS) and incubated with MTT salt solution (5 mg/ml in 0.1M PBS) and complete culture medium (37°C, 4 h). Thereafter, 100 μl of dimethyl sulfoxide was added to each well and incubated (37°C, 1 h). Optical density of the formazan product was measured using a spectrophotometer (Bio-tek μQuant) at 570/690 nm. The results were expressed as percentage cell viability vs. concentration of AA_{AgNP}, from which the half maximal inhibitory concentration (IC_{50}) was determined.

ATP assay

Cells (20,000/well in six replicates) were aliquoted in an opaque 96-well microtitre plate to which the ATP CellTitre Glo (Promega, Madison, USA) reagent (50 μl) was added and allowed to react in the dark (30 min, RT). After incubation, the luminescent signal proportional to the cellular ATP content was detected with a Modulus™ microplate reader (Turner Biosystems, Sunnyvale, USA). The results were expressed as mean relative light units (RLU).

Glutathione assay

The GSH-Glo™ Glutatione assay (Promega, Madison, USA) was utilized to quantify intracellular GSH levels. Subsequent

to treatment of cells (10,000 cells/well in six replicates) in an opaque 96-well microtitre plate, culture medium was removed and 25 μl of 1X GSH-Glo™ reagent (prepared according to manufacturer's guidelines) was added to each well. Glutathione standards (0-5M) were serially diluted (two-fold) from a 5 mM stock in deionized water. After brief mixing on a shaker and 30 min incubation at RT, 100 μl of Luciferin detection reagent was added to the wells (15 min, RT). Luminescence was detected on a Modulus™ microplate luminometer (Turner Biosystems, Sunnyvale, USA). A calibration curve was constructed and sample GSH concentrations (μM) were calculated.

Lipid peroxidation

To investigate the AA_{AgNP}-mediated generation of reactive oxygen species (ROS), malondialdehyde (MDA-a product of lipid peroxidation) levels were measured using the thiobarbituric acid reactive substances (TBARS) assay. Briefly, the following was added to a set of test tubes: 200 μl of 2% H_3PO_4, 400 μl of 7% H_3PO_4, 400 μl of TBA/BHT solution and 200 μl of 1M HCL. Following treatment of cells (50,000 cells/well) in a 6-well plate, supernatants were recovered. For test samples, 100 μl of cell supernatant (in triplicate) was then added to each test tube. A positive control was prepared by adding 1 μl of MDA to a test tube. All tubes were incubated in a water bath (100°C, 15 min) and after cooling; butanol (1.5 ml) was added to each tube, vortexed for 10 seconds and allowed to separate into two distinct phases. Approximately 800 μl of the upper butanol phase was then transferred to 1.5 ml tubes and centrifuged (840 x g, 24°C; 6 min). To a 96-well micotitre plate, 100 μl of supernatant was transferred in six replicates and the absorbance read using a spectrophotometer (Bio-tek μQuant) at 532/600 nm. The mean absorbance was divided by the extinction co-efficient (156 mM^{-1}) and results were expressed as μM concentrations.

Assessment of caspase activity

Caspase-3/-7, -8 and -9 activities were detected with Caspase-Glo® assays (Promega, Madison, USA). As per manufacturer's protocol, Caspase-Glo®-3/-7, -8 and -9 reagents were reconstituted and added to wells (in six replicates) of an opaque 96-well microtitre plate (40 μl of reagent per 100 μl of 10,000 cells/well). Samples were mixed and incubated in the dark (30 min, RT). The luminescent signal was measured on a Modulus™ microplate luminometer (Turner Biosystems, Sunnyvale, USA). Caspase-3/-7, -8 and -9 activities were expressed as relative light units (RLU).

Annexin-V-FLUOS assay

The annexin-V-Fluos assay (Roche) was used to determine phosphatidylserine (PS) translocation. To each flow cytometry tube, 100 μl of staining buffer, 100 μl of annexin-V-Fluos labeling solution (annexin-V: propidium iodide (PI): staining buffer (1:1:50 vol/vol/vol)) and 100 μl of cell suspension was added, and incubated in the dark (15 min, RT). Samples were analyzed on a FACS Calibur (BD Biosciences) flow cytometer. Data were analyzed using CellQuest PRO v4.02 software (BD Biosciences). Cells were gated to exclude cellular debris using FlowJo v7.1 software (Tree Star, Inc). Approximately 50,000 events were analyzed for apoptotic (annexin-V + ve, PI -ve), necrotic (annexin-V + ve, PI + ve) and live cells (annexin-V -ve, PI -ve). The results were expressed as percentage of the total events.

JC-1 MitoScreen assay

Mitochondrial membrane potential (Δ Ψ) was assayed with the BD™ MitoScreen kit (BD Biosciences). JC-1, a cationic dye, is sensitive to Δ Ψ and accumulates in mt with polarized membranes. JC-1 working solution was prepared and 100 μl added to each flow cytometry tube, followed by 100 μl of cell suspension. Tubes were incubated at 37°C with 5% CO_2 for 15 min, after which 100 μl of JC-1 wash buffer was added. Approximately 50,000 events were analyzed for mt depolarization. A FACS Calibur flow cytometer was used and data were analyzed using CellQuest PRO v4.02 software. Cells were gated to exclude cellular debris using FlowJo v7.1 software. The results were expressed as percentage of the total events.

Comet assay

The comet assay was used to determine DNA fragmentation in the AA_{AgNP} treated lung cells. Briefly, three slides per sample were prepared with a first layer containing 400 μl of 1% low melting point agarose (LMPA, 37°C), a second layer of 25 μl of cells from each sample with 175 μl 0.5% LMPA (37°C) and a third layer containing 200 μl of 1% LMPA (37°C). Cover slips were removed and slides were subjected to lysis (4°C, 1 hr, protected from light) by being submerged in cells lysis buffer (2.5M NaCl, 100 mM EDTA, 1% Triton X-100, 10 mM Tris (pH 10) and 10% DMSO). The slides were equilibrated in electrophoresis buffer (300 mM NaOH, 1 mM Na_2EDTA, pH 13; 20 min) then electrophoresced (300 mA, 25V, 35 min) after which slides were washed three times (0.4M Tris, pH 7.4; 5 min) and finally stained with 40 μl ethidium bromide. Cover slips were placed onto slides and maintained overnight at 4°C. Slides were viewed using a fluorescent microscope (Olympus IXSI inverted microscope/510-560 nm excitation and 590 nm emission wavelengths). Images were captured and comet tails of 50 cells were measured using Life Science-Soft Imaging System (analySIS® v5). The results were expressed as mean tail length in μm.

CD95 (Fas) analysis

CD95 receptor expression was determined by cell surface staining on a flow cytometer. Briefly, 100 μl of 0.1M PBS and 1 μl of fluorescein isothiocyanate (FITC) conjugated mouse anti-human CD95 antibody (BD Pharmingen, 555673) was added to 100 μl of cell suspension. Reaction mixture was incubated in the dark for 15 min at RT, thereafter run on a FACS Calibur. Data were analyzed using CellQuest PRO v4.02 software. Cells were gated to exclude cellular debris using FlowJo v7.1 software. The results were expressed as a percentage.

Intracellular staining

Intracellular levels of smac/DIABLO were assessed by flow cytometry. Cells were rendered permeable by incubation in Fix and Perm medium A (Caltag) (15 min in the dark), after which they were treated with Fix and Perm medium B (Caltag) containing monoclonal anti-smac/DIABLO primary antibody (smac/DIABLO, ab110291) (1:500; 30 min, RT). After washing, cells were re-suspended in medium B containing allophycocyanin (APC) conjugated anti-mouse secondary antibody (Thermo Scientific, 31430) (1:100; 15 min, RT) protected from light. Cells were then washed, re-suspended in 0.1M PBS and run on a FACS Calibur. Data were analyzed using CellQuest PRO v4.02 software. Cells were gated to exclude cellular debris using FlowJo v7.1 software. The results were expressed as percentage.

Western blot analysis

Cytobuster™ reagent (Novagen) supplemented with protease and phosphatase inhibitors (Roche, 05892791001 and 04906837001 respectively) was used for protein isolation. Cytobuster (200 μl) was added to the cells (4°C, 10 min) and centrifuged (180 x g; 4°C, 10 min) to obtain a crude protein extract. Protein samples were quantified using the bicinchoninic assay and standardized to 1 mg/ml. Samples (25 μl) were electrophoresced on 7.5% sodium dodecyl sulfide-polyacrylamide gel electrophoresis gels and thereafter transferred to nitrocellulose membranes. Membranes were blocked with 3% bovine serum albumin (BSA) in Tris buffer saline (20 mM Tris–HCl (pH 7.4), 500 mM NaCl and 0,01% Tween 20 (TBST)) for 1 h, and incubated with primary antibody (p53, ab26; bax, ab5714; parp-1, ab110915; smac/DIABLO, ab110291 and β-actin, ab8226; 1:1,000) in 1% BSA in TBST at 4°C overnight. Membranes were then washed thrice (10 ml TBST, 15 min) and treated with horseradish peroxidase-conjugated secondary antibody (mouse, ab97046; 1:2,000) (1 h, RT). Membranes were washed again 3 times (TBST, 15 min) and immunoreactivity was detected by the LumiGLO® chemiluminescent substrate system (KPL) with the Uvitech Image Documentation System (UViTech Alliance 2.7). Protein bands were analyzed with the UViBand Advanced Image Analysis software (UViTech v12.14). The results were expressed as mean relative band intensity (RBI).

Statistical evaluation

Statistical analyses were performed using GraphPad Prism version 5.00 software package (GraphPad PRISM®). Data are expressed as mean ± standard error of the mean (sem). Comparisons were made using unpaired t tests. Statistical significance was set at 0.05.

Additional files

Additional file 1: Figure S1. Extracellular staining-flow cytometry was used to evaluate the expression of CD95 (Fas receptor). Three replicates were done for both treated (B1-B3) and untreated (A1-A3) cells. AAAgNP significantly down regulated the expression of CD95 in A549 cells compared to the control (2.8 ± 0.58% vs. 5 ± 0.44%; $p = 0.0416$; 95% CI = 0.13 to 4.2).

Additional file 2: Figure S2. Levels of smac/DIABLO, a pro-apoptotic protein, were determined flow cytometrically using an intracellular staining assay. A significantly higher expression of smac/DIABLO was observed in A549 cells after treatment with AAAgNP (B1-B3) compared to untreated cells (A1-A3) (29 ± 0.32% vs. 18 ± 0.66%; $p < 0.0001$; 95% CI = -13 to -8.5).

Competing interests

The authors declare that they have no competing interests.

Authors' contributions

The design of the study was proposed by AAC. RMG and KA were responsible for the synthesis and characterization of AA_{AgNP}. RG and AP carried out cell culture, subsequent experimental procedures as well as statistical analyses. The manuscript was drafted by RG, AP and AAC. All authors read and approved the final manuscript.

Acknowledgements

Mr R Govender acknowledges funding for this study from the College of Health Sciences, University of KwaZulu-Natal and a scholarship from the National Research Foundation (SA).

Author details

[1]Discipline of Medical Biochemistry, School of Laboratory Medicine and Medical Sciences, University of KwaZulu-Natal, Private Bag 7, Congella, Durban 4013, South Africa. [2]Department of Chemistry, Faculty of Applied Sciences, Durban University of Technology, Durban 4001, South Africa.

Received: 14 November 2012 Accepted: 30 January 2013
Published: 18 February 2013

References

1. Bello B, Fadahun O, Kielkowski D, Nelson G: **Trends in lung cancer mortality in South Africa: 1995–2006.** *BMC Public Health* 2011, **11**:209.
2. Siemiatycki J, Richardson L, Straif K, Latreille B, Lakhani R, Campbell S, Rousseau MC, Boffetta P: **Listing occupational carcinogens.** *Environ Health Perspect* 2004, **112**(15):1447–59.
3. Driscoll T, Nelson DI, Steenland K, Leigh J, Concha-Barrientos M, Fingerhut M, Pruss-Ustun A: **The global burden of disease due to occupational carcinogens.** *Am J Ind Med* 2005, **48**(6):419–31.
4. Long JL, Engels EA, Moore RD, Gebo KA: **Incidence and outcomes of malignancy in the HAART era in an urban cohort of HIV-infected individuals.** *AIDS* 2008, **22**(4):489–96.
5. Su J, Zhang J, Liu L, Huang Y, Mason RP: **Exploring feasibility of multicolored CdTe quantum dots for in vitro and in vivo fluorescent imaging.** *J Nanosci Nanotechnol* 2008, **8**(3):1174–7.
6. Moaddab S, Ahari H, Shahbazzadeh D, Motallebi AA, Anvar AA, Rahman-Nya J, Shokrgozar MR: **Toxicity Study of Nanosilver (Nanocid®) on Osteoblast Cancer Cell Line.** *Int. Nano Lett* 2011, **1**(2):6.

7. Arora S, Jain J, Rajwade JM, Paknikar KM: **Cellular responses induced by silver nanoparticles: In vitro studies.** *Toxicol Lett* 2008, **179**(2):93–100.
8. Hansen SF, Michelson ES, Kamper A, Borling P, Stuer-Lauridsen F, Baun A: **Categorization framework to aid exposure assessment of nanomaterials in consumer products.** *Ecotoxicology* 2008, **17**(5):438–47.
9. Madhumathi K, Sudheesh Kumar PT, Abhilash S, Sreeja V, Tamura H, Manzoor K, Nair SV, Jayakumar R: **Development of novel chitin/nanosilver composite scaffolds for wound dressing applications.** *J Mater Sci Mater Med* 2010, **21**(2):807–813.
10. Bhattacharya R, Mukherjee P: **Biological properties of "naked" metal nanoparticles.** *Adv Drug Deliv Rev* 2008, **60**(11):1289–306.
11. Kalishwaralal K, Barathmanikanth S, Pandian SR, Deepak V, Gurunathan S: **Silver nano - a trove for retinal therapies.** *J Control Release* 2010, **145**(2):76–90.
12. Lara HH, Ayala-Nunez NV, Ixtepan-Turrent L, Rodriguez-Padilla C: **Mode of antiviral action of silver nanoparticles against HIV-1.** *J Nanobiotechnology* 2010, **8**:1.
13. Lu L, Sun RW, Chen R, Hui CK, Ho CM, Luk JM, Lau GK, Che CM: **Silver nanoparticles inhibit hepatitis B virus replication.** *Antivir Ther* 2008, **13**(2):253–62.
14. Baram-Pinto D, Shukla S, Perkas N, Gedanken A, Sarid R: **Inhibition of herpes simplex virus type 1 infection by silver nanoparticles capped with mercaptoethane sulfonate.** *Bioconjug Chem* 2009, **20**(8):1497–502.
15. Xu L, Li X, Takemura T, Hanagata N, Wu G, Lee Chou L: **Genotoxicity and molecular response of silver nanoparticle (NP)-based hydrogel.** *Journal of Nanobiotechnology* 2012, **10**(16):1–11.
16. Ghosh M, Manivannan J Sinha S, Chakraborty A, Mallick SK, Bandyopadhyay M, Mukherjee A: **In vitro and in vivo genotoxicity of silver nanoparticles.** *Mutation Research/Genetic Toxicology and Environmental Mutagenesis* 2012, **749**:60–69.
17. Vaidyanathan R, Kalishwaralal K, Gopalram S, Gurunathan S: **Nanosilver–the burgeoning therapeutic molecule and its green synthesis.** *Biotechnol Adv* 2009, **27**(6):924–37.
18. Foldbjerg R, Dang DA, Autrup H: **Cytotoxicity and genotoxicity of silver nanoparticles in the human lung cancer cell line, A549.** *Arch Toxicol* 2011, **85**(7):743–50.
19. Lacaille-Dubois MA, Wagner H: **Bioactive saponins from plants: An update.** In *Studies in Natural Products Chemistry*. Edited by Attaur R. The Netherlands: Elsevier Science B. V.; 2000:633–687.
20. Haddad M, Laurens V, Lacaille-Dubois MA: **Induction of apoptosis in a leukemia cell line by triterpene saponins from Albizia adianthifolia.** *Bioorg Med Chem* 2004, **12**(17):4725–34.
21. Mujoo K, Haridas V, Hoffmann JJ, Wachter GA, Hutter LK, Lu Y, Blake ME, Jayatilake GS, Bailey D, Mills GB, Gutterman JU: **Triterpenoid saponins from Acacia victoriae (Bentham) decrease tumor cell proliferation and induce apoptosis.** *Cancer Res* 2001, **61**(14):5486–90.
22. Francis G, Kerem Z, Makkar HP, Becker K: **The biological action of saponins in animal systems: a review.** *Br J Nutr* 2002, **88**(6):587–605.
23. Sahu SC, Casciano DA: *Nanotoxicity, from In vivo and In vitro Models to Health Risks*. USA: John Wiley and Sons, Ltd; 2009:609.
24. Chairuangkitti P, Lawanprasert S, Roytrakul S, Aueviriyavit S, Phummiratch D, Kulthong K, Chanvorachote P, Maniratanachote R: **Silver nanoparticles induce toxicity in A549 cells via ROS-dependent and ROS-independent pathways.** *Toxicology in Vitro* 2013, **27**:330–338.
25. Fischer U, Schulze-Osthoff K: **New approaches and therapeutics targeting apoptosis in disease.** *Pharmacol Rev* 2005, **57**(2):187–215.
26. Chai J, Du C, Wu JW, Kyin S, Wang X, Shi Y: **Structural and biochemical basis of apoptotic activation by Smac/DIABLO.** *Nature* 2000, **406**(6798):855–62.
27. Kasibhatla S, Tseng B: **Why target apoptosis in cancer treatment?** *Mol Cancer Ther* 2003, **2**(6):573–80.
28. Shall S, de Murcia G: **Poly(ADP-ribose) polymerase-1: what have we learned from the deficient mouse model?** *Mutat Res* 2000, **460**(1):1–15.
29. Hirsch T, Marzo I, Kroemer G: **Role of the mitochondrial permeability transition pore in apoptosis.** *Biosci Rep* 1997, **17**(1):67–76.
30. Wang X: **The expanding role of mitochondria in apoptosis.** *Genes Dev* 2001, **15**(22):2922–33.
31. Navarro E, Piccapietra F, Wagner B, Marconi F, Kaegi R, Odzak N, Sigg L, Behra R: **Toxicity of silver nanoparticles to Chlamydomonas reinhardtii.** *Environ Sci Technol* 2008, **42**(23):8959–64.
32. Foldbjerg R, Olesen P, Hougaard M, Dang DA, Hoffmann HJ, Autrup H: **PVP-coated silver nanoparticles and silver ions induce reactive oxygen species, apoptosis and necrosis in THP-1 monocytes.** *Toxicol Lett* 2009, **190**(2):156–62.
33. Ueda S, Masutani H, Nakamura H, Tanaka T, Ueno M, Yodoi J: **Redox control of cell death.** *Antioxid Redox Signal* 2002, **4**(3):405–14.
34. Hostettmann K, Martson A: *Saponins*. Cambridge: Cambridge University Press; 1995.
35. Derfus AM, Chan WCW, Bhatia SN: **Intracellular Delivery of Quantum Dots for Live Cell Labeling and Organelle Tracking.** *Adv Mater* 2004, **16**(12):961–966.
36. Xia T, Kovochich M, Brant J, Hotze M, Sempf J, Oberley T, Sioutas C, Yeh JI, Wiesner MR, Nel AE: **Comparison of the abilities of ambient and manufactured nanoparticles to induce cellular toxicity according to an oxidative stress paradigm.** *Nano Lett* 2006, **6**(8):1794–807.
37. Carlson C, Hussain SM, Schrand AM, Braydich-Stolle LK, Hess KL, Jones RL, Schlager JJ: **Unique cellular interaction of silver nanoparticles: size-dependent generation of reactive oxygen species.** *J Phys Chem B* 2008, **112**(43):13608–19.
38. Xia T, Kovochich M, Liong M, Madler L, Gilbert B, Shi H, Yeh JI, Zink JI, Nel AE: **Comparison of the mechanism of toxicity of zinc oxide and cerium oxide nanoparticles based on dissolution and oxidative stress properties.** *ACS Nano* 2008, **2**(10):2121–34.
39. Miyashita T, Krajewski S, Krajewska M, Wang HG, Lin HK, Liebermann DA, Hoffman B, Reed JC: **Tumor suppressor p53 is a regulator of bcl-2 and bax gene expression in vitro and in vivo.** *Oncogene* 1994, **9**(6):1799–805.
40. MacLachlan TK, El-Deiry WS: **Apoptotic threshold is lowered by p53 transactivation of caspase-6.** *Proc Natl Acad Sci U S A* 2002, **99**(14):9492–7.
41. Hwang PM, Bunz F, Yu J, Rago C, Chan TA, Murphy MP, Kelso GF, Smith RA, Kinzler KW, Vogelstein B: **Ferredoxin reductase affects p53-dependent, 5-fluorouracil-induced apoptosis in colorectal cancer cells.** *Nat Med* 2001, **7**(10):1111–7.
42. Gengan RM, Anand K, Phulukdaree A, Chuturgoon A: **A549 lung cell activity of biosynthesized silver nanoparticles using Albizia adianthifolia leaf.** *Colloids and Sufaces B: Biointerfaces* 2013, doi:10.1016/j.colsurfb.2012.12.044.

doi:10.1186/1477-3155-11-5
Cite this article as: Govender *et al.*: Silver nanoparticles of *Albizia adianthifolia*: the induction of apoptosis in human lung carcinoma cell line. *Journal of Nanobiotechnology* 2013 **11**:5.

G Model
JIEC 2048 1–7

ARTICLE IN PRESS

Journal of Industrial and Engineering Chemistry xxx (2014) xxx–xxx

Contents lists available at ScienceDirect

Journal of Industrial and Engineering Chemistry

journal homepage: www.elsevier.com/locate/jiec

Agroforestry waste *Moringa oleifera* petals mediated green synthesis of gold nanoparticles and their anti-cancer and catalytic activity

Q1 K. Anand [a], R.M. Gengan [a,*], A. Phulukdaree [b], A. Chuturgoon [b]

[a] Department of Chemistry, Faculty of Applied Sciences, Durban University of Technology, Durban, South Africa
[b] Discipline of Medical Biochemistry, School of Laboratory Medicine and Medical Sciences, Nelson R Mandela School of Medicine, University of KwaZulu-Natal, Durban, South Africa

ARTICLE INFO

Article history:
Received 27 February 2014
Received in revised form 4 May 2014
Accepted 14 May 2014
Available online xxx

Keywords:
Moringa oleifera
Nitroaromatics
Gold nanoparticles
Peripheral lymphocytes
A549 cells

ABSTRACT

Stable gold nanoparticles (AuNPs) from aqueous 1 M chloroauric acid and *Moringa oleifera* flower aqueous extract. The UV–vis spectrum of AuNPs displays the surface plasmon resonance at 540 nm. The AuNPs was characterized using transmission electron microscopy, scanning electron microscopy, energy dispersive X-ray analysis and dynamic light scattering whilst Fourier transform infrared and ^{1}H-NMR spectroscopy were used to probe the type of capping agents. The AuNPs were assessed for their catalytic reduction of nitrophenol and nitroaniline by UV–vis showed a rapid reduction within 3 min thereby indicating degradation of industrial effluents. Furthermore, the AuNPs may possess good anti-cancer properties.

1. Introduction

Over the past two decades, studies in nanotechnology has expanded in various research areas such as electronics [1] catalysis [2] medicine and biomedical applications [3]. Metal nanoparticles are currently used as drug carriers [4] whilst their widespread use in cell toxicity remediation are being extensively explored [5]. Gold nanoparticles are being used in medicine because of their non-toxicity, ease of biodegradability and decreased side effects in patients. Hence studies of the synthesis of gold nanoparticles (AuNPs) and their application to the medical field is being continually persued. Nanotechnology is also playing an important role in eliminating environmental issues caused by chemical industries releasing pollutants, in wastewater, and due to accidental spillages; pollutants such as organic dyes [6], oils [7], mercury and arsenic [8] are becoming ubiquitous. A class of organic pollutant, which is causing aquatic toxicology and hence affecting life therein is benzene derivatives such as the nitro aromatic compounds. Hence catalytic reduction protocols of nitro aromatics are being studied to reduce toxicity and subsequently applied especially in industrial wastewater effluents. Traditional catalytic reduction methods are hazardous; nowadays nanotechnologists are attempting to improve and source novel method for reducing nitro compounds by using metal nanoparticles, which display less aquatic toxicity. The synthesis of AuNPs can be attained through diverse methods. Most of the nanoparticles synthesized by chemical methods involve toxic chemicals that may affect the environment and human health. Hence, biological approaches using micro-organisms and plants or plant extracts for metal nanoparticle synthesis are valuable alternatives to chemical methods [9]. The use of plants for the preparation of nanoparticles is advantageous [10] because it does not require elaborate processes such as intracellular synthesis and multiple purification steps or the maintenance of microbial cell cultures [11]. Several plants and their parts have been successfully used for the extracellular synthesis of metal nanoparticles.

Moringa oleifera Lam. (Family: Moringaceae), commonly known as drumstick or horseradish tree, is a small deciduous tree of 2.5–10 m in height. It is reported to contain various phytochemicals, viz. carotenoids, vitamins, minerals, amino acids, sterols, glycosides, alkaloids, flavonoids and phenolics [12–16]. Constituents such as leaf, flower, fruit and bark have been anecdotally used as herbal medicines in treatments for inflammation, paralysis and hypertension. Many reports describe *M. oleifera* extracts as highly potent anti-inflammatory [17], hepatoprotective [18], anti-hypertensive [19] and anti-tumor [20] agents. Although research studies

* Corresponding author. Tel.: +27 842654314/+27 31 3732309; fax: +27 866740441/+27 31 2022671.
E-mail addresses: activateanand@gmail.com, organicanand@gmail.com, genganrm@dut.ac.za (R.M. Gengan).

http://dx.doi.org/10.1016/j.jiec.2014.05.021
1226-086X/

on the synthesis of nanoparticles using different parts of the *M. oleifera* plant have been reported as well as their application in different research fields, no study has reported work on either the synthesis of AuNPs using the flower or their cancer and catalytic potential. The present study describes the *M. oleifera* flower-mediated in vitro one-step transform of AuNPs, characterization, its catalytic reduction of nitrophenol and nitroaniline and cytotoxic effects on the A549 human lung cancer cell line and normal healthy human peripheral lymphocytes.

2. Experimental

2.1. Materials and methods

Gold(III) chloride trihydrate ($HAuCl_4{\cdot}3H_2O$, ACS reagent) was purchased from Sigma-Aldrich, South Africa. All aqueous solutions were prepared using de-ionised water. *M. oleifera* flower was collected from Phoenix, Durban, South Africa and identified at the KwaZulu-Natal Herbarium.

2.2. Preparation and characterization of gold nanoparticles

Fresh flowers were collected and washed several times with de-ionised water; 20 g of the flower were finely cut and 200 ml of de-ionised water was added. The flower with the water was heated to boiled for 20 min, allowed to cool, filtered through a Whatman No.1 filter paper and 1 ml of the supernatant leaf extract was added to 49 ml of 1×10^{-3} M $HAuCl_4$ solution at room temperature and the solution stirred. The pinkish ruby red colloidal solution, at pH ~ 7, was characterized using UV–vis spectrophotometer (Varian Cary-50 UV spectrophotometer linked to a TCC-240A Shimadzu heating vessel temperature controlled cell holder) in the range of 200–800 nm. To obtain the particle size and shape, 1 μl of the AuNPs was placed on Formvar coated grids, air dried and viewed at 100 kV to carry out transmission electron microscopy (JEOL 1010 TEM using a Megaview III camera and iTEM software) studies. The nanopartilces size distribution was determined by using *ImageJ* software and the resultant data were plotted in histograms. For particles' images and elemental analysis studies, the AuNPs colloidal suspension was centrifuged at 10,000 rpm for 10 min, and the supernatant discarded. The pellets were cast onto a sample holder, air dried and subjected to Carl Zeiss Ultra Plus scanning electron microscope with EDX detector. To study the interaction between AuNPs and organic compounds in the flower extract, the AuNPs colloidal solution was centrifuged at 10,000 rpm for 10 min; pellets were washed three times with 20 ml of de-ionized water and the FTIR spectra recorded (Varian 800 FT-IR spectrophotometer). A Differential Light Scattering Malvern Zetasizer Nano *ZS* (Malvern Instruments Ltd., UK) Merck 2423 instrument was used to measure particle size and zeta potential.

2.3. Cell culture

A549 lung cells were cultured for 6 h (37 °C, 5% CO_2) to 90% confluency in 25 ml flasks in complete culture media (CCM; Eagles minimum essential media, 10% foetal bovine serum, 1% penstrep-fungizone, 1% L-glutamine). Cells were harvested (2×10^4 cells/well in a 96 well microtitre plate) for the MTT analysis, ATP quantification and supernatant was stored following treatment with CCM only, 10 μg/ml and 50 μg/ml AuNPs solution for 6 h. Ethical approval from the Biomedical Research Ethics Administration Office of the University of KwaZulu-Natal was obtained. Informed consent was obtained from two healthy volunteers before blood samples were taken. For the preparation of peripheral lymphocytes (PL's), buffy coats containing PL's were extracted from heparinized whole blood by differential centrifugation. Briefly, 5 ml whole blood collected from each subject was layered onto equivolume Histopaque 1077 (Sigma) in polypropylene tubes. Layered blood was then centrifuged at 4000 rpm for 30 min. Buffy coats were aspirated into new polypropylene tubes and washed twice in phosphate buffered saline (4000 rpm, 10 min). Cell density was adjusted to 2×10^4 cells/well using the trypan blue exclusion test.

2.4. MTT assay

Following incubation with relevant treatments, cells were washed twice with PBS and each sample supplemented with a 1:5 ratio of filter-sterilised (0.45 μm) MTT salt solution (5 mg/ml in PBS) and CCM. The plate was incubated at 37 °C for 4 h. Following incubation, dimethyl sulphoxide (DMSO) (100 ml) was added to each well and incubated at 37 °C for a further 1 h. Optical density of the formazan product was measured using a plate reader (Bio-tek μQuant) at 570/690 nm. Results were expressed as mean percentages of the control response.

2.5. Statistical analysis

Results are expressed as the mean plus or minus the standard deviation. Statistical significance between samples was determined using one way ANOVA Tukey Kramer Multiple Comparisons test with Dunns Post-test using the GraphPad Prism Software, (GraphPad Software Inc.).

2.6. Catalytic reduction of 4-nitrophenol and 4-nitroaniline

Ice cold aqueous solution of $NaBH_4$ (1 ml, 15 mM) was mixed with 4-nitrophenol (1.7 ml, 0.2 mM) in a standard quartz cuvette. The light yellow color of the 4-nitrophenol changed yellowish green due to the formation of 4-nitrophenolate ion. An aliquot of AuNPs prepared at room temperature (0.3 ml) was added to the resulting solution, and the time-dependent absorbance spectra peak were recorded with a time interval of 0.5 min in the scanning range of 200 to 700 nm at room temperature. The same procedure was followed for the catalytic study using 4-nitroaniline.

3. Results and discussion

3.1. Nanoparticle composition and size distribution

The first indication of successful AuNPs formation was the appearance of a pink color due to excitation of surface plasmon vibrations in gold nanoparticles [21]. This was a rapid reaction as indicated by the immediate colour change on mixing the aqueous gold(III) chloride trihydrate solution with the aqueous flower extract of *M. oleifera*. This colour change validated the occurrence of a redox reaction whereby Au^+ ions are reduced to Au^0 by the plant components, which are in turn oxidized to other species. Although the actual mechanism is not properly understood, its components such as phenolics, polyols, amines, flavonoids, water-soluble heterocyclic components as well as tannins, saponins, gallic acids, proteins, reducing sugars and other oxido-reductively labile metabolites, which have the ability to act as reducing agents. Previous studies [12–16] on the phytochemistry of *M. oleifera* reported many organic compounds present therein and hence suggesting water-soluble hydroxy functional group containing compounds are responsible for the reduction of Au^+ ions.

UV–vis spectroscopy (Fig. 1) was used to monitor the reactions as function of reaction time. Our system showed λ_{max} at 540 nm and the absorbance steadily increases in intensity as a function of reaction time. A change in absorbance intensity of ca. 0.48 a.u., in

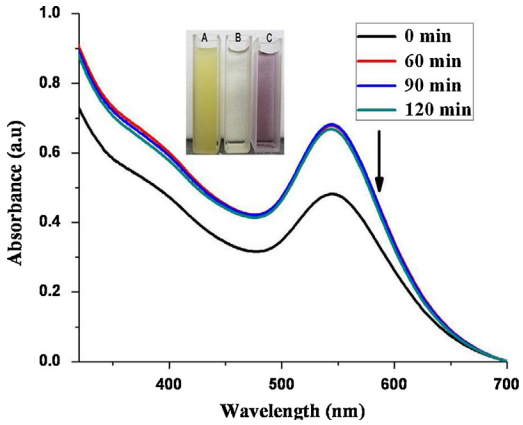

Fig. 1. UV–vis absorption spectra of AuNPs at different reaction times. (For interpretation of the references to colour in this figure legend, the reader is referred to the web version of the article.) (A) Aqueous flower Extract (B) Chloroauric acid ($HAuCl_4$) solution (C) Gold Nanoparticles.

the first 60 min of reaction, was recorded; this intensity increased over longer reaction time. Since the peak wavelength did not shift during the reaction, we concluded that there was no change in the nanoparticle size during this time as well as the preparation is mainly composed of small spherical AuNPs as indicated by the single broad symmetrical absorption peak.

The optical signature of AuNPs was determined; the distribution of sizes and shapes was conducted by transmission electron microscopy (TEM) images and supported by hydrodynamic size and zeta potential data measured by dynamic light scattering (DLS). Representative TEM images recorded from the AuNPs colloidal solution (Fig. 2A) showed that most of the particles are spherical or near spherically shaped. The particles were polydispersed in the colloidal solution and exhibited a distribution of sizes in the range 3–5 nm and some very large images of gold nanoparticles with hexagonal and triangular shapes were also observed. In addition a thin layer of materials surrounded [22] the AuNPs which indicates the possibility of organic- based capping agents inherent in the aqueous extract. Fig. 2B shows the pictogram of AuNPs; particle size of 3 nm is abundant.

DLS analysis showed the size distribution of particles with an average hydrodynamic size of 203 nm (Fig. 3A) similar to the leaf extract of *Melia azedarach* [23]. As expected, the particle size obtained from TEM and DLS scattering is marginally different due to the varying principles used for measurement. Also a stable dispersion of particles was evident from the zeta potential of −14.1 mV (Fig. 3B); a zeta potential higher than 30 mV or lesser than 30 mV indicates a stable system. Many reports have proposed that surface-active molecules can stabilize the nanoparticles and reaction of the metal ions is possibly facilitated by reducing sugars and/or terpenoids. We suggest organic molecules such as carotenoids, vitamins, minerals, amino acids, sterols, glycosides, alkaloids, flavonoids and phenolics can act as surface active

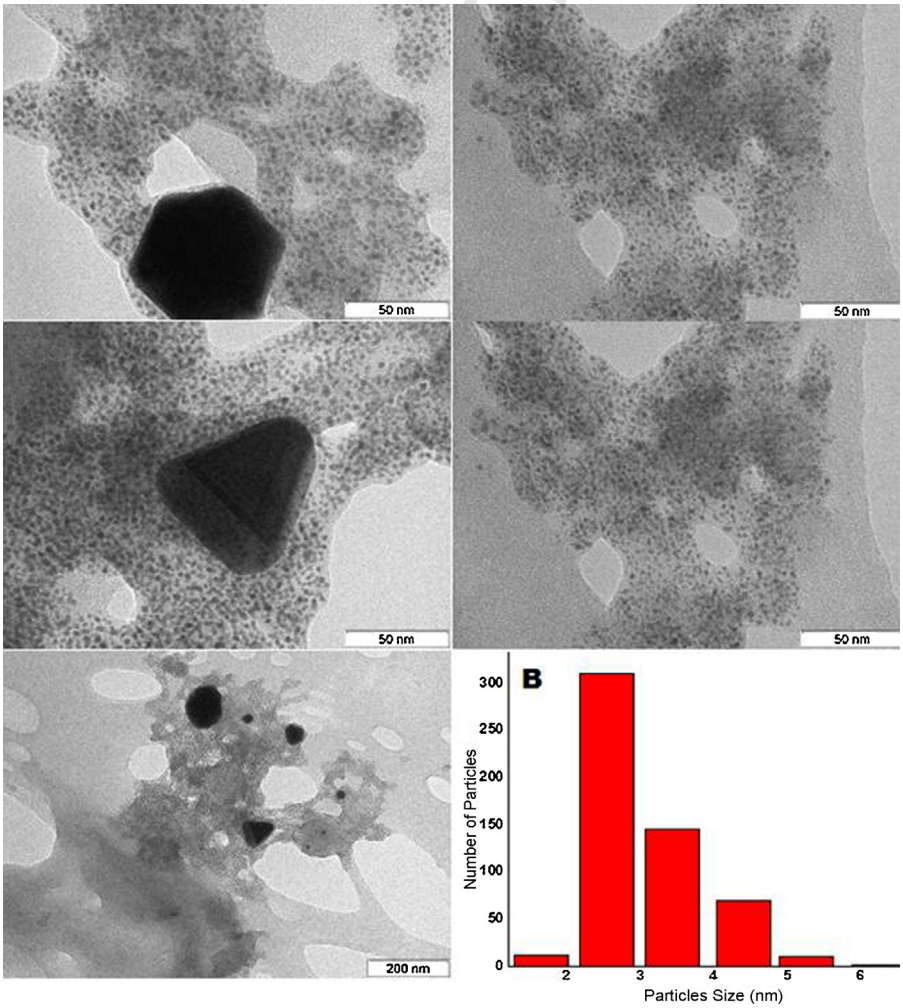

Fig. 2. (A). Representative TEM micrograph of AuNPs biosynthesized by aqueous flower extracts of *M. oleifera* (B) Histogram representation of size distribution of AuNPs.

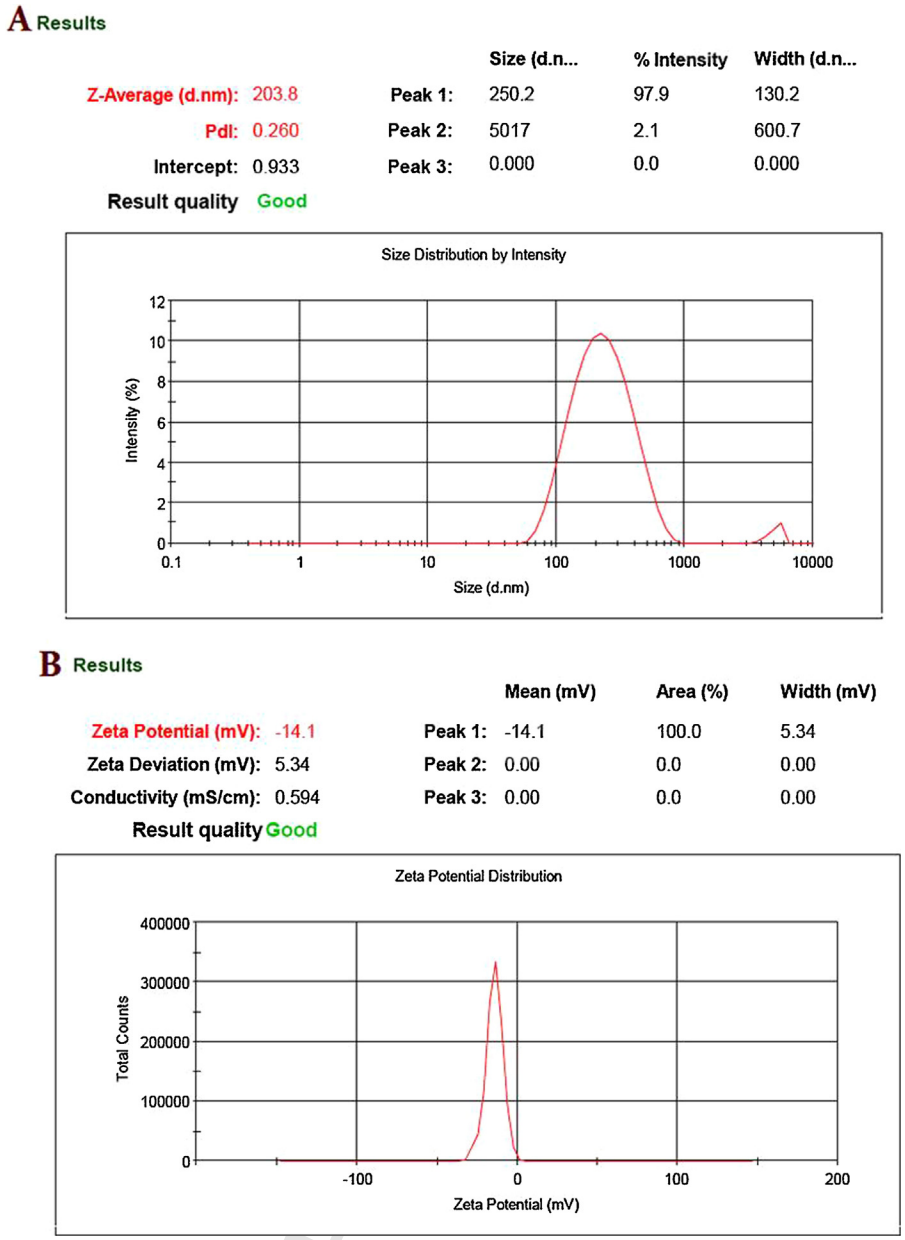

Fig. 3. DLS profile: (A) size distribution of AuNPs with maximum intensity at 203 nm. (B) Stability of AuNPs at −14.1 mV in zeta potential analysis.

molecules responsible for stability and AuNPs formation; however further studies are required to elucidate the mechanism of biological AuNPs synthesis and validate this hypothesis.

The crystalline nature of the AuNPs and nano size was confirmed by SEM and the EDX pattern (Fig. 4). The particle dimensions of nano material were observed 200 nm and 100 nm range AuNPs showed spherical morphology of particle with size 100 nm.EDS pattern for *M. oleifera* shows signals for gold nanoparticles at five different places.

FTIR analysis (Fig. 5) and comparison of the spectra of a crude aqueous flower extract and AuNPs showed a marginal stretching frequency shift from 3390 to 3378 cm^{-1} thereby indicating the possibile presence of an amide functional group. Also the AuNPs spectrum lacked the 2916 and 2848 cm^{-1} peaks which was present in the flower extract. This suggests the loss of the OH intramolecular hydrogen bond functional group [24,25] which might be responsible for the reduction of Au^{+} to Au^{0}. Furthermore, a small shift from 1641 to 1635 cm^{-1} is assigned to the C=O stretch and the 1108 cm^{-1} peak in the crude flower extract is assigned to the C–O stretch. Although carotenoids, vitamins, minerals, amino acids, sterols, glycosides, alkaloids, flavonoids and phenolics are found in *M. olifera*, other secondary metabolites, proteins and lipids are present in the plant cell, at different concentrations, which may be responsible for the bio-reduction of Au^{+} ions. Specifically, conversion of C=O group of biomolecules to C(O)=O group may be responsible for the reduction of Au^{+} to Au^{0}.

3.2. Chemistry involved in AuNPs formation

To identify the capping reagents and molecules responsible for the reduction of the gold ions, the crude aqueous flower extract of *M. oleifera* was investigated by ^{1}H-NMR spectroscopy. The complex pattern of the ^{1}H-NMR spectrum (Fig. 6) suggests that several compounds are present in the aqueous extract [26]. The strong signal observed at δ = 1.5–3.81 ppm is due single bond; δ = 4.76–4.81 ppm is due to double bond; signal at δ = 5.55 ppm could be

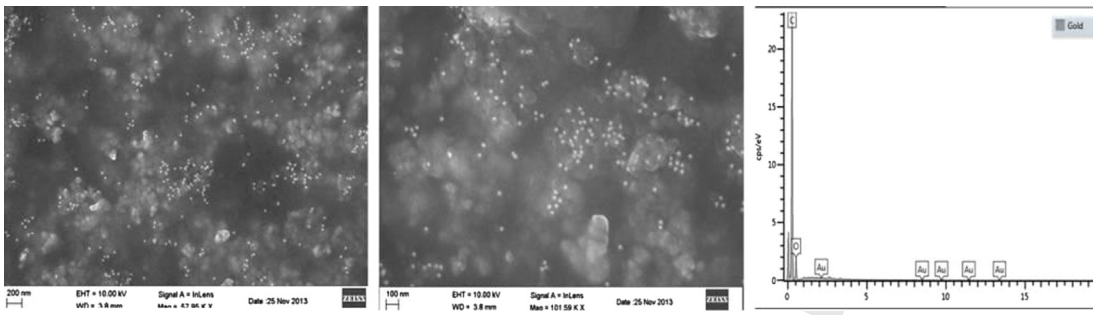

Fig. 4. SEM with EDX of (A) SEM image of AuNPs synthesized using *M. oleifera* flower extract. (B) EDX showed the presence of the elements on the surface of the AuNPs.

due to aliphatic single bond OH group, whereas the signals appearing between $\delta = 1.26–1.32$ ppm are related to aliphatic $–CH_2–$ groups. The signals at $\delta = 6–8$ and $\delta = 1–4$ ppm clearly indicates the presence of trace aromatic but abundant aliphatic compounds, respectively. Further studies are required to unravel the types of compounds present in the AuNPs surfaces.

3.3. Catalytic hydrogenation and anti-cancer study of gold nanoparticles

The catalytic reduction of 4-nitrophenol and 4-nitroaniline is perhaps the most often used reaction to test the catalytic activity of AuNPs in aqueous solution. Hence we selected two chemical reactions that qualify as model reactions i.e. the reduction of 4-nitrophenol and 4-nitroaniline by sodium borohydride [27]. This reaction was easily monitored by UV–vis spectroscopy (Fig. 6). The strong absorption of 4-nitrophenolate ions at 400 nm was initially observed however a time profile study showed significant decrease in absorption within 210 s. This appears to be a well-controlled chemical reaction that converts the nitro to the amine group in the presence of the nanoparticles without any observable side reactions or by-products. Moreover, no reaction occurred in the absence of AuNPs. A similar trend was observed for the reduction of 4-nitroaniline; there was a significant decrease in absorption, at 394 nm, within 270 s and Fig. 7 shows a schematic diagram of the catalytic hydrogenation of 4-nitrophenol and 4-nitroaniline. These reactions proceeded under mild conditions, at room temperature and in an aqueous medium thereby implying possible use in industrial toxic wastewater nitro-organic effluents also $NaBH_4$ is toxic however this effect is decreased because the reaction mechanism involves production of $NaBO_2$; sodium metaborate has low toxicity when ingested, inhaled or in contact with the skin [28]. Although synthetic AuNPs are being widely applied, there is limited data based on the cytotoxicity of biologically synthesized AuNPs. We used the MTT assays to determine cytotoxicity in the transformed A549 (human lung epithelial adenocarcinoma cells) and normal healthy peripheral lymphocytes (PLs). The results are presented in Table 1 (Fig. 8).

The AuNPs were significantly cytotoxic to A549 cells at both dilution 1:100, 1:50, 1:25, 1:10, and 1:3 with viabilities of 140%, 139%, 71%, 49%, and 12%, respectively. However, this cytotoxic effect was not observed in the normal healthy PLs treated with

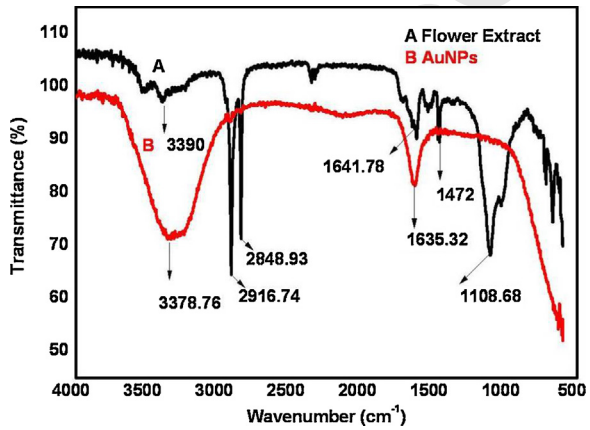

Fig. 5. FTIR spectra of (A) aqueous *Moringa oleifera* flower extract and (B) FTIR Profile of AuNPs synthesized using *Moringa oleifera* flower extract.

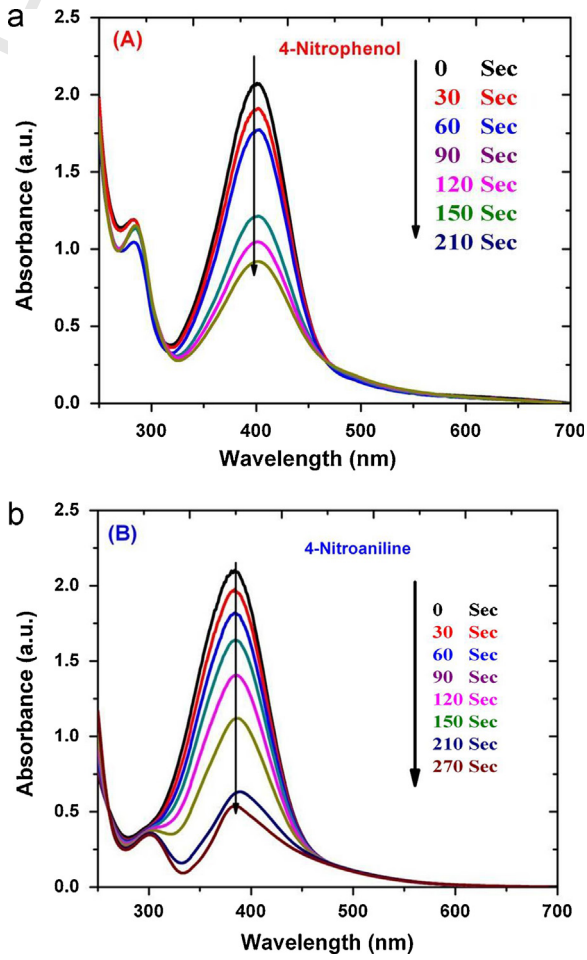

Fig. 6. A time course profile showing catalytic reduction of (A) 4-nitrophenol and (B) 4-nitroaniline by AuNPs.

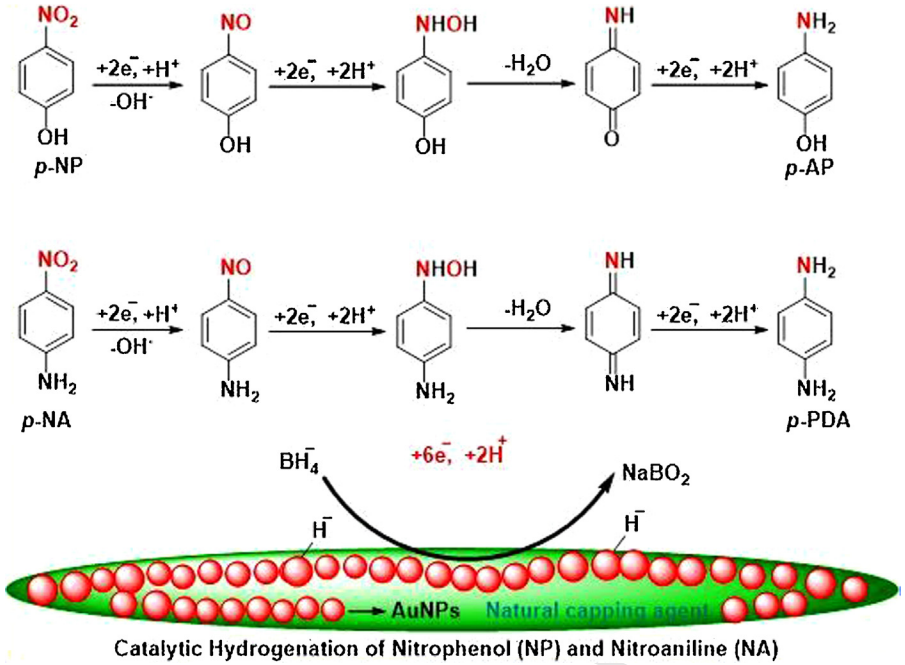

Fig. 7. This figure shows a schematic catalytic hydrogenation of 4-nitrophenol (NP) and 4-nitroaniline (NA).

AuNPs, with cell viabilities of 100%, 100%, 101%, 106%, 106% and 97%, respectively. This data and cell viability curve strongly suggests that the AuNPs may possess anti-cancer/anti-proliferative properties. Plant extracts are normally rich in nutrients and phytocompounds that result in antihyperglycemic effects. This is clearly observed in the normal healthy PLs, where the cell viability is greater than 100%. It is noteworthy that such an effect is not observed in the cancerous A549 cells, in spite of increased glycolysis being the hallmark of cancer proliferation. We are currently investigating the mechanism of cell death by these AuNPs in the A549 cells.

Table 1
Cell viability of healthy peripheral lymphocytes and lung cancer cells (A549) treated with a range of dilutions of AuNPs synthesized with an aqueous extract from flowers of *M. oleifera*. Cells were seeded (10,000 cells/well) and allowed to adhere for 24 h. Media was discarded and cells were then treated and incubated for 6 h with AuNPs.

	MTT-cell viability (mean OD ± SD)	
Dilution	Peripheral lymphocytes	A549 cells
0	0.799 ± 0.05 (100%)	1.353 ± 0.01 (100%)
1:100	0.798 ± 0.02 (100%)	1.893 ± 0.05 (140%)
1:50	0.814 ± 0.01 (101%)	1.881 ± 0.19 (139%)
1:25	0.844 ± 0.07 (106%)	0.955 ± 0.15 (71%)*
1:10	0.850 ± 0.01 (106%)	0.669 ± 0.03 (49%)**
1:3	0.773 ± 0.01 (97%)	0.168 ± 0.00 (12%)**

* $p < 0.05$, ** $p < 0.01$ significantly different compared to untreated controls using a one way analysis of variance with the Dunnets multiple comparisons test.

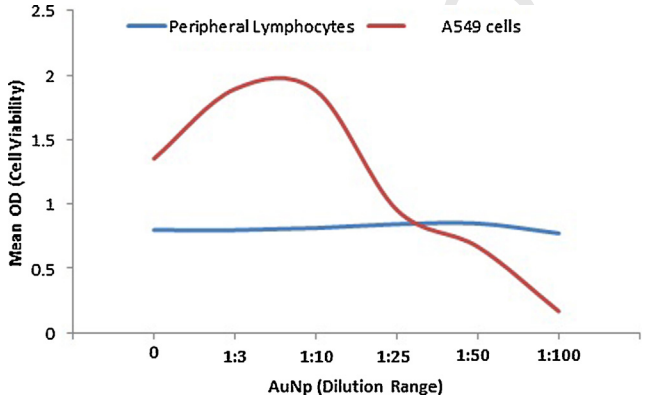

Fig. 8. Cell viability curve of healthy peripheral lymphocytes and lung cancer cells (A549).

4. Conclusion

A green method, which is simple, quick, cost-effective and reproducible was developed to synthesise AuNPs in vitro using the aqueous flower extract of *M. olifera*. These nanoparticles showed characteristic UV–vis absorption peak at 540 nm. The AuNPs were characterized by XRD, TEM and DLS whereas FTIR and ^{1}H-NMR spectroscopy was used to determine the type of natural capping agens; the AuNPs were well-dispersed triangular, hexagonal and nearly spherical AuNPs having size less than 5 nm in diameter. The AuNPs displayed catalytic activity in reducing 4-nitrophenol and 4-nitroaniline rapidly. Furthermore, AuNPs causes significant cytotoxicity to A549 cells and did not induce cytotoxicity in normal healthy PLs.

Acknowledgments

We are grateful to J.W. Smith (Electron Microscope Unit, UKZN) for TEM measurements, J. Hughes (School of Environmental Sciences, UKZN) for XRD measurements and T. Govender (Department of Pharmacology, UKZN) for DLS studies. We also thank M.A. Ngwenya of the KwaZulu-Natal Herbarium for identifying the plant species. Thanks to the National Research Foundation (NRF), Durban University of Technology (DUT) and University of KwaZulu-Natal for funding this project.

Appendix A. Supplementary data

Supplementary data associated with this article can be found, in the online version, at doi:10.1016/j.jiec.2014.05.021.

References

[1] M.A. Albrecht, C.W. Evans, C.L. Raston, Green Chem. 8 (2006) 417.
[2] (a) G. Cao (Ed.), Nanostructures & Nanomaterials: Synthesis, Properties & Applications, Imperial College Press, London, 2004, p. 273;
(b) R.N. Nageswara, M. Rohit, P.K. Bera, R. Dhodapkar, S. Bakardjieva, Z. Bastl, Metal-Organic Nano-Metal Chem. 40 (2010) 332.
[3] (a) X.J. Chen, B.L. Sanchez-Gaytan, Z.X. Qian, S.J. Park, Nanomed. Nanobiotechnol. 4 (2012) 273;
(b) M. Veerapandian, Cytotoxicity of biosynthesized nanomaterials and functionalized nanomaterials, in: D.K. Yi, G.C. Papaefthymiou (Eds.), Nanobiomaterials Development and Applications, CRC Press, 2013, p. 417.
[4] B. Duncan, C. Kim, V.M. Rotello, J. Controlled Release 148 (2010) 122.
[5] L. Zhang, F.X. Gu, J.M. Chan, A.Z. Wang, R.S. Langer, O.C. Farokhzad, Clin. Pharmacol. Ther. 83 (2008) 761.
[6] J.A. Dahl, B.L.S. Maddux, J.E. Hutchison, Chem. Rev. 107 (2007) 2228.
[7] S.R. Pezeshki, M.W. Hester, Q. Lin, J.A. Nyman, Environ. Pollut. 108 (2000) 129.
[8] D.J. Thompson, Chem. Biol. Interact. 88 (1993) 89.
[9] (a) M. Sastry, A. Ahmad, M.I. Khan, R. Kumar, C.M. Niemeyer, C.A. Mirkin (Eds.), Microbial Nanoparticle Production, Wiley-VCH, Weinheim, Germany, 2004, p. 126;
(b) A. Chakraborty, D.K. Das, M. Sinha, S. Dey, S. Bhattacharjee, J. Bionanosci. 7 (2013) 5;
(c) S. Sathya, S. Parthasarathi, V. Murugan, S. Ramesh, Y. Kyusik, Biol. Met. 25 (2012) 351;
(d) G. Rishalan, P. Alisa, R.M. Gengan, K. Anand, A.A. Chuturgoon, J. Nanobiotechnol. 11 (2013) 5.
[10] D. Bhattacharya, R. Gupta, Biotechnol. Crit. Rev. 25 (2005) 199.
[11] P. Mohanpuria, N.K. Rana, S.K. Yadav, J. Nanopart. Res. 10 (2008) 507.
[12] S. Nesamani (Ed.), Medicinal Plants, Vol. I, State Institute of Languages. Thiruvananthapuram, Kerala, India1999, p. 425.
[13] H.P.S. Makkar, K. Becker, Anim. Feed Sci. Technol. 63 (1996) 211.
[14] S. Faizi, B.S. Siddiqui, R. Saleem, F. Shaheen, A.H. Gilani, Planta Med. 64 (1998) 225.
[15] P. Siddhuraju, K. Becker, J. Agric. Food Chem. 51 (2003) 2144.
[16] F. Anwar, S. Latif, M. Ashraf, A.H. Gilani, Phytother. Res. 21 (2007) 17.
[17] (a) I.C. Ezeamuzle, A.W. Ambadederomo, F.O. Shode, S.C. Ekwebelem, Int. J. Pharmacogn. 34 (1996) 207;
(b) M.R. Sulaiman, Z.A. Zakaria, A.S. Bujarimin, M.N. Somchit, D.A. Israf, S. Moin, Pharm. Biol.V 46 (2008) 845.
[18] L. Pari, N.A. Kumar, J. Med. Food 5 (2002) 171.
[19] S. Faizi, B.S. Siddiqui, R. Saleem, S. Siddiqui, K. Aftab, A.H. Gilani, Phytochemistry 38 (1995) 957.
[20] A. Murakami, Y. Kitazono, S. Jiwajinda, K. Koshimizu, H. Ohigashi, Planta Med. 64 (1998) 319.
[21] S. Link, E. Sayed, Annu. Rev. Phys. Chem. 54 (2003) 331.
[22] S.S. Shankar, A. Rai, A. Ahmad, M.J. Sastry, Colloid Interface Sci. 275 (2004) 496.
[23] S. Raman, M.P. Kandula, J.A. Jacob, K. Soundararajan, T. Ramar, G. Palani, K. Muthukalingan, A. Shanmugam, Process Biochem. 47 (2012) 273.
[24] S.P. Dubey, M. Lahtinen, M. Sillanpaa, Process Biochem. 45 (2010) 1065.
[25] S. Priyadarshini, V. Gopinath, N.M. Priyadharsshini, A.D. Mubarak, P. Velusamy, Colloids Surf., B: Biointerfaces 102 (2013) 232.
[26] R.M. Gengan, K. Anand, A. Phulukdaree, A. Chuturgoon, Colloids Surf., B: Biointerfaces 105 (2013) 87.
[27] H. Pablo, P.L. Moise, M.L. Luis, D. Joachim, L. Yan, B. Matthias, Chem. Soc. Rev. 41 (2012) 5577.
[28] R.J. Weir, R.S. Fisher, Toxicol. Appl. Pharmacol. 23 (1972) 351.

Elsevier Editorial System(tm) for Industrial Crops and Products
Manuscript Draft

Manuscript Number: INDCRO-D-14-01217

Title: Silver nanoparticles derived from Ekebergia capensis leaf extract and its Catalytic degradation effect on industrial azo dyes

Article Type: Original Research Paper

Keywords: Ekebergiacapensis; Azo dye; Silver nanoparticles; Congo red; Allura red

Corresponding Author: Prof. Robert Moonsamy Gengan, Ph.D

Corresponding Author's Institution: Durban University of Technology

First Author: Anand Krishnan, M.Sc

Order of Authors: Anand Krishnan, M.Sc; Robert Moonsamy Gengan, Ph.D

Abstract: The integration of green chemistry principles to nanotechnology is being pursued with zeal since both are recently coined concepts. Nanoparticle synthesis is being intensively and extensively studied because their unique size and shape exhibits physical, chemical and biological properties to materials different from the bulk material. Biological methods of synthesis have paved way for greener synthesis of nanoparticles and these have proven to be better methods due to slower kinetics, better manipulation and control over crystal growth thereby providing better properties for applications in several fields of study. Herein, we report for the first time the in-vitro synthesis of silver nanoparticles (AgNPs) from an indigenous South African plant: Ekebergiacapensis. The AgNPs were characterised by UV-Vis spectroscopy, TEM, XRD, DLS and FT-IR. The effect of concentration of silver nitrate and a time course reaction profile for the synthesis of AgNPs are described. The AgNPs were applied to three azo dyes, viz., Allura red and Congo red.

Suggested Reviewers: Manikandan E Ph.D
Nano Research Centre, Dept of Physics, B.S.Abdur Rahman University, India
maniphysics@gmail.com
This researcher has good experience on catalytic investigation by using nano materilas

Ravindran Balasubramani Ph,D
Research Associate , Department Of Biology, Hongkong Baptist University, Hongkong
kalamravi@gmail.com
This researcher has expertise in the Bioremediation and biodegradation of organic pollutants using microbes and fermented waste on crop plant growth.

Rasiah Ladchumananasivam Ph,D
Professor, Department of Textile Engineering, Centre of Technology-UFRN,Campus Universitario, Brazil
rlsivam@gmail.com
This researcher is a leading investigator of plants crops products studies and Industrial applications

Murugan Veerapandian Ph,D
Assistant Professor, Department of Chemistry, Université de Montréal, Canada

momugan@gmail.com
This researcher has good experience on dye reduction investigations by using nano materials

Navaneethan Duraisamy Ph,D
Research Associate , Department of Mechatronics Engineering, Jeju National University, Republic of Korea
naveeneac@gmail.com
This researcher has expertise in the synthesis of nanostructured materials for sensors and energy applications

30 may 2014
The Editor-in-Chief:
Industrial Crops and Products
Subject: Manuscript Submission for Publication
Dear Sir/Madam
Herewith I am submitting an original manuscript:

Silver nanoparticles derived from *Ekebergia capensis* leaf extract and its Catalytic degradation effect on industrial azo dyes

with authors name as in the order:
K. Anand and R. M. Gengan

All authors were actively involved in this research. The work described in this research paper has not been published nor will be submitted to any other journals.

Scientific motivation
Most dyes are complex aromatic structures which are difficult to dispose of; in particular azo dyes are resistant to biodegradation and are of an environmental concern because of their high water solubility and persistence. The industrial disposal of untreated effluents not only mars the natural beauty of the rivers but can cause serious ecological problems; dyes significantly affect the photosynthetic activity of aquatic plants by reducing light penetration and they may be toxic to some aquatic organisms. Although there are several physical, chemical and biological methods for the degradation and removal of dyes, recent studies are reported on the efficacy of AgNPs prepared from plant extracts as a catalyst in a $NaBH_4$ reaction scheme.

This study arose because of an environmental concerns on the issue of azo dyes as pollutants in waste water. Hence the catalytic activity of novel AgNPs, which are synthesized from an indigenous plant, is studied; two food and textile based azo dyes systems were used to assess their potential degradation by AgNPs. This research presents novel AgNPs which contains *in situ* generated capping agents and these AgNPs exhibits good potential to degrade azo dyes in synthetic waste water.

General significance of the obtained results
Silver nanoparticles were synthesized for the first time from the leaf of an indigenous plant, *Ekebergia capensis* found in South Africa. These AgNPs were characterized by several known techniques. The effect of concentration of substrates and a reaction in room temperature were studied. In addition, a first time study was undertaken on

evaluating the catalytic degradation of two important azo dyes, by these novel biosynthesis of stable silver nanoparticles using dried leaves of *Ekebergia capensis*, that are commonly used by food and textile industries locally; these dyes are ubiquitous in waste water. We found that the novel AgNPs displays good potential to degrade the to azo dyes.

Funding source

This research study was funded by the National Research Foundation and the Durban University of Technology. These two bodies provided funds but were not involved with the design of the project, interpretation of data or written report.

Kindly contact me if you require any further information or details.

Thanking you and kind regards

Dr Robert. M. Gengan
Associate Professor: Department of Chemistry
Durban University of Technology
Durban, 4001, South Africa.
Email: genganrm@dut.ac.za
Tel: +27 31 3732309

Graphical Abstract

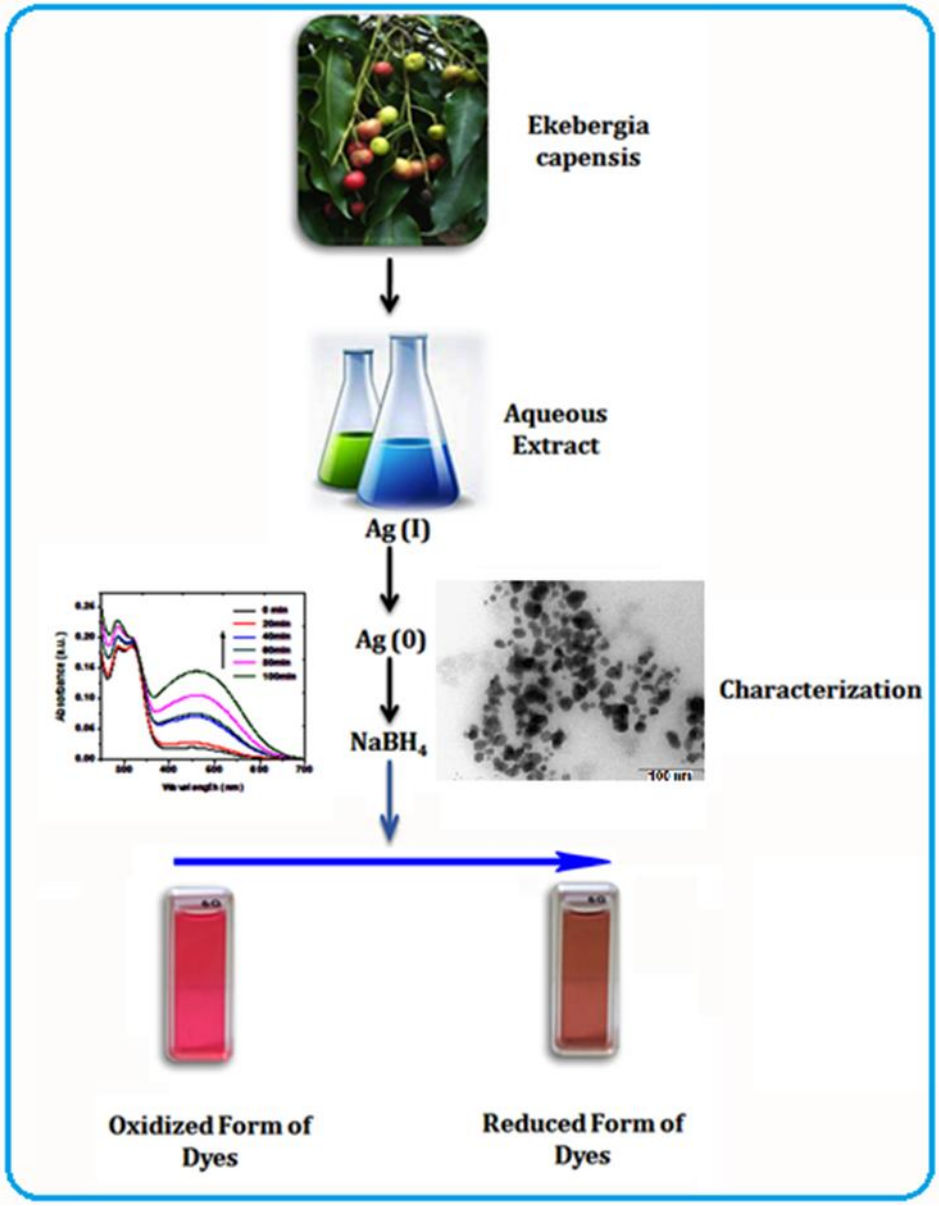

Highlights:

- This is a green synthesis of AgNPs from leaf extract of *Ekebergia capensis*
- Characterization of AgNPs is by UV–vis spectroscopy, TEM, FTIR, DLS, XRD
- The AgNPs have a catalytic effect on the degradation of industrial azo dyes

Silver nanoparticles derived from *Ekebergia capensis* leaf extract and its Catalytic degradation effect on industrial azo dyes

K. Anand and R.M. Gengan *

Department of Chemistry, Faculty of Applied Sciences, Durban University of Technology, Durban 4001, South Africa.

* Corresponding author: Tel.: +27 31 3732309; fax + 27 31 2022671.

E-mail address: genganrm@dut.ac.za

Abstract

The integration of green chemistry principles to nanotechnology is being pursued with zeal since both are recently coined concepts. Nanoparticle synthesis is being intensively and extensively studied because their unique size and shape exhibits physical, chemical and biological properties to materials different from the bulk material. Biological methods of synthesis have paved way for greener synthesis of nanoparticles and these have proven to be better methods due to slower kinetics, better manipulation and control over crystal growth thereby providing better properties for applications in several fields of study. Herein, we report for the first time the *in-vitro* synthesis of silver nanoparticles (AgNPs) from an indigenous South African plant: *Ekebergia capensis*. The AgNPs were characterised by UV–vis spectroscopy, TEM, XRD, DLS and FT-IR. The effect of concentration of silver nitrate and a time course reaction profile for the synthesis of AgNPs are described. The AgNPs were applied to two azo dyes, viz., Allura red and Congo red.

Keywords

Ekebergia capensis; Azo dye; Silver nanoparticle; Congo red; Allura red

1. Introduction

Since antiquity, man has co-evolved with plants and their derivative products. Modern life is nowbased on plant-based accompaniments to provide shelter, food and serve humanity in the curing of different ailments (Ankamwar et al., 2005). The exploration of plants for new bioactive phyto-compounds and the development of modern technology is a rapidly growing field of study. This decade has witnessed the inception of plants as a source to synthesise nanoparticles. This is a huge breakthrough in science since it is regarded as a green methodology contributing to a global attempt to save the cosmos from further damage by man-made pollutants.

Nanoparticle synthesis is being intensively and extensively studied because their unique size and shape provides better properties for applications inoptics, electronics and catalytic systems, magnetic and biomedical such as HIV inhibition, cancer cell cytotoxicity and genotoxicity (Chaudhary et al., 2005; Becker, 1999; Chandran et al., 2006; Cuenya, 2010; Dubay et al., 2009; Elechiguerra et al., 2005; Foldbjerg et al., 2011; Gengan et al., 2013; Ghosh et al., 2012; Govender et al., 2013; Gupta et al., 2011; Jaleel et al., 2009; Sethuraman

et al., 2012; Jebakumar Immanuel Edison et al., 2013). Several examples are reported of hazards of nanoparticle production via chemical protocols.However, this has been significantly reduced by using benign biological processes including fungi, algae, bacteria, cyanobacteria, actinomycetes and cell cultures. However, potential advantages of using plants as an effective template for synthesis of silver nanoparticles (AgNPs) (Kasthuri et al., 2009; Kouvaris et al., 2012; Krishnaraj et al., 2010; Kumar and Yadav, 2009; Loo et al., 2012) include elimination of elaborate processes of maintaining cell cultures, easy scale up for large-scale synthesis, simplicity and cost effectiveness. Although the universe is endowed with an abundance of plants, only recent scientific exploration has tapped plants for the synthesis of AgNPs. Studies on plants such as *Arbutus unedo*, *Acalyphaindica*, *Dioscoreabulbifera*, *Tamarind*, *Eucalyptus hybrid*, *Aloe vera*, *Hibiscus rosa sinensis*, *Emblica officianalis*, *Artemesianilagirica*, *Camellia sinensis*, *Albizia adianthifolia*, *Punicagranatum*, *Ficus panda* and *Terminalia chebula* are documented (Mabogo, 1990; Mezohegyi et al., 2007; Mude et al., 2009; Mulaudzi et al., 2011; Nishiyama et al., 1996; Philip, 2010; Philips, 2010; Rai et al., 2009; Rajan et al., 2013; Rajasekharreddy et al., 2010; Raman et al., 2012; Sathishkumar et al., 2009; Shukla et al., 2010; Silver et al., 2003). Initially, studies were solely based on synthesis and characterisation of AgNPs by plant extracts; nowadays application based studies of AgNPs is imperative especially in seeking better concoctions against infections and diseases and towards maintaining a cleaner environment.

A limited number of research investigations are documented on catalytic studies of AgNPs on dye molecule although dyes are becoming ubiquitous due to malpractices by chemical and allied industries. Most dyes are complex aromatic structures which are difficult to dispose of; in particular azo dyes are resistant to bio-degradation (Silver et al., 2003) and are of an environmental concern because of their high water solubility and persistence. The industrial dumping of untreated effluents not only mars the natural beauty of the rivers, but can cause serious ecological problems; dyes significantly affect the photosynthetic activity of aquatic plants by reducing light penetration and they are toxic to some aquatic organisms (Song, 2009). Although several physical, chemical and biological methods for the degradation and removal of dyes are documented, recent studies have reported the efficacy of AgNPs from plants as a catalyst in a $NaBH_4$ reaction scheme. The catalytic degradation of methyl orange was reported for AgNPs synthesized from metal salts (Song and Kim, 2009) whereas

methylene blue was used in studies of AgNPs from *Ficuspanda* and *Terminaliachebula* and ayurvedic medicine *Guggulutiktham Kashayam* (Shukla et al., 2010; Silver, 2003).

Motivated by the abundance of unexplored plants available in South Africa, we investigated the potential use of *Ekebergia capensis* (Meliaceae Family) in synthesising AgNPs and elucidating their catalytic properties against food based azo dyes. This plant is a fairly large tree, locally available in our area and used by traditional healers to treat venereal diseases, chronic cough, emetic, backache, headache, dysentery and skin diseases (Stephen et al 2012). Although the phytochemistry of this plant has not been exhaustively studied, compounds such as limonoids, acyclic triterpenoids, oleanoic acid, 3-epioleanolic acid, oleanolic acid, sucrose and coumarins were identified. Different levels of phenolics, flavonoids, gallotannins and condensed tannins were also detected. Plants have their own machinery, enzymes and mechanistic processes to produce a variety of organic compounds, ranging from simple to complex molecules. *Ekebergia capensis* has its own biochemical scheme with enzymes such as tannase and hence a host of compounds are produced which can provide the key feature in reducing an aqueous $AgNO_3$ solution to metallic silver in nano scale of 1 to 100 nm. During the synthesis, we avoided the use of surfactants and any polymeric stabilising agents and maintained the reaction under standard room temperature and pressure conditions thereby ensuring cost effectiveness in the event of a scale-up to an industrial scale. The AgNPs are characterized by known instrumental techniques then elucidated for its catalytic properties in the reduction of azo dyes.

2. Experimental

2.1. Materials and Methods

Silver nitrate ($AgNO_3$, ACS reagent) was purchased from Sigma-Aldrich, South Africa. All aqueous solutions were prepared using de-ionised water. Fresh leaves of *Ekebergia capensis* were collected from the ML Sultan Technikon, Durban University of Technology, Durban, South Africa and identified at the KwaZulu-Natal Herbarium.

2.2. Synthesis of silver nanoparticles

Ekebergia capensis leaves were dried for 2 days at room temperature. The plant leaf broth solution was prepared by taking 10 g of thoroughly washed and finely cut leaves in a 300 mL Erlenmeyer flask along with 100 mL of sterile distilled water and then boiling the mixture for 10 min, cooled and stored at 4 °C; this concoction was used within a week. Typically, 5 mL of leaf broth was added to 100 mL of 1 mM aqueous $AgNO_3$ solution for the reduction of

Ag^+ ions. UV-Vis spectra were recorded as a function of the reaction; the intensity steadily increased to saturation as a function of the reaction time. The $AgNO_3$ solution concentration was also varied; 1mM, 2mM and 3mM.

2.3. Characterization

X-Ray Diffraction (XRD) was conducted with a Philips PW1050 diffractometer at 1^o/min with a scanning step size of 0.02° from 40° to 100° 2θ using monochromated CoK_α radiation. Data were captured by a Sietronics 122D automated micro-processor linked to the diffractometer. Transmission Electron Microscope (TEM) was conducted with a JEOL 1010 TEM and viewed at 100 kV; the TEM images were captured using Megaview III camera and iTEM software. Fourier Transform Infra-Red Spectroscopy (FT-IR) spectra were recorded of the green aqueous leaf extract and AgNPs with Varian 800 FT-IR spectrophotometer. UV-vis (UV) spectra were recorded on a Varian Cary-50 UV spectrophotometer linked to a heating vessel temperature controlled cell holder (TCC -240A Shimadzu) in the range of 200-800 nm. A Differential Light Scattering Malvern Zetasizer Nano ZS (Malvern Instruments Ltd, UK) Merck 2423 instrument was used to measure particle size and zeta potential.

2.4. Catalytic reduction of Azo Dyes

An aqueous ice cold solution of $NaBH_4$ (1 mL, 15 mM) was mixed with aqueous stock solution of Allura red and Congo red (1.7 mL, 10^{-5} mM) in a standard quartz cuvette and AgNPs (25 µL) was added. The final volume was adjusted with Millipore water to get the final volume as 3 mL. The mixture was shaken well and the reaction was monitored with UV- vis spectrophotometer with a time interval of 1 min in the scanning range of 200 to 800 nm at room temperature.

3. Results and discussion

3.1. Nanoparticle composition and size distribution

A colour change to yellow-brown within a few seconds (see Fig. 1) of mixing the leaf extract with the $AgNO_3$ solution supported the formation of AgNPs; this is due to the excitation of surface plasmon vibrations in AgNPs. This observation validated the reduction of Ag^+ ions to Ag^0 by the plant components which are in turn oxidized to other species. Although the mechanism has not been adequately elucidated, it is components such as phenolics, polyols, amines, flavonoids, water-soluble heterocyclic components as well as other components such as proteins, reducing sugars and other oxido-reductively labile metabolites which have this ability to reduce Ag^+ ions to Ag^0.

The effect of $AgNO_3$ concentration (see Fig. 1) on formation of AgNPs indicated a clear trend on particle size; increasing the concentration of $AgNO_3$ resulted in an increase in particle size distribution observable as a wider UV band. A blue shift is also noticed thereby supporting the formation of smaller particles at low $AgNO_3$ concentrations. The effect of reaction time (see Fig.2) on formation of AgNPs was also analyzed by UV–vis spectroscopy. There is an exponential increase in UV absorption as the reaction was maintained for a longer time. The absorption band is wider however there is no indication of a distinct shift of λ_{max} thereby indicating no effect of reaction time on particle size.

The optical signature of AgNPs was characterised in terms of the distribution of sizes and shapes by Transmission Electron Microscopy (TEM) images and supported by hydrodynamic size and zeta potential data measured by dynamic light scattering (DLS). Representative TEM images (see Fig. 3A) showed that most of the particles are spherical or near spherically shaped. The particles were spherical in the colloidal solution and exhibited a distribution of sizes in the range 4–60 nm. Under careful examination, it was evident that a thin layer of materials surrounded some of the particles which suggested the presence of organic-based capping agents inherent in the aqueous extract. Fig. 3B shows the pictogram of AgNPs; particle size of 22 nm is abundant. DLS analysis showed the size distribution of particles with an average hydrodynamic size of 120 nm (see Fig. 4A). As expected, the particle size obtained from TEM and DLS scattering is marginally different; similar observations were reported for AgNPs prepared from Meliaazedarach and Albiziaadianthifolia (Raman et al., 2012). However, a less stable dispersion of particles was evident from the zeta potential of -32.1 mV (see Fig. 4B); a zeta potential higher than 30 mV or lesser than -30 mV is indicative of a stable system. It was reported (Song and Kim, 2009) that terpenoids, present in Neem leaf broth might be the surface active molecules stabilizing the nanoparticles and reaction of the metal ions is possibly facilitated by reducing sugars and/or terpenoids. The crystalline nature of the AgNPs was confirmed by XRD analysis; the characteristic Bragg's XRD peaks at 2θ of 44.8°, 52.2°, 76.8°, 93.3° and 98.8° is indexed to the (111), (200), (220), (311) and (222) crystallographic planes of the AgNPs, respectively (see Fig. 5).

3.2. Chemistry involved in AgNPs formation and azo dyes degradation

FTIR was used to identify any potential biomolecules, present in the leaf extract, which are responsible for reducing Ag^+ ions to Ag^0. FTIR spectra (see Fig. 6) of the crude aqueous extract and AgNPs showed a decrease in stretching frequency from 3390 to 3378 cm^{-1} suggesting an OH functional group. Furthermore a shift from 1698 to 1671 and 1650 to 1641

cm^{-1} is assigned to the C=O and C=C stretch, respectively. We speculate that conversion of C=O group of biomolecules to C(O)=O group may be responsible for the reduction of Ag^{+} to Ag^{0}. Although limonoids, triterpenoids, carboxylic acids, carbohydrates and coumarins were identified by phytochemistry studies (Mabogo, 1990; Mezohegyi et al., 2007; Mude et al., 2009) of *Ekebergia capensis*, other biomolecules, secondary metabolites, proteins and lipids are also present in the plant cell, at different concentration, which may be responsible for the bio-reduction of Ag^{+} ions. Further study is required to unravel the role of the biomolecules and the detail mechanism in the bio-reduction phenomena.

We investigated the catalytic property of AgNPs with two azodyes viz., Allura red and Congo red by UV-vis. Fig.7 and 8, shows λ_{max} of the untreated dye (labelled A) and the change in absorbance when AgNPs were added for different reaction time. A decrease in absorbance of the two dyes were observed. In the case of allura red and congo red, there was a huge decrease in absorbance in the first 30 seconds whereas the other two dyes yielded a gradual decrease. Since the structure of the dyes differ in the type of electron donor group at the *ortho* position, it is possible these electron donating and withdrawing groups are responsible for the rate of degradation of the dyes. These results indicated a marginal change in reaction rates accountable to the groups present in the aromatic core skeleton of the dye (see Fig. 9). It showed that aqueous extract contains compounds having the phenolics or flavonoids as a functional group in the structure (Gupta et al., 2011). Hence the reaction between broth of E. capensis aqueous leaf extract and the Ag^{+} ion might occur according to the following schematics design and the mechanistic of the dye reduction reaction by monitoring the degradation products. With respect to the potential for application of AgNPs in the treatment of waste waters from the dye industries, the implications of this study is that the reaction is very rapid and hence the AgNPs is an ideal candidate for catalysis.

4. Conclusion

In this manuscript we have tailored a biogenic synthesis of AgNPs using the aqueous leaf extract of Ekebergiacapensis at room temperature. XRD, TEM, DLS, FTIR and UV-vis techniques were used to confirm AgNPs formation. The AgNPs prepared by this protocol are relatively stable, is a green protocol which is simple, quick, cost-effective and reproducible and can be easily scaled-up to prepare AgNPs in bulk. Furthermore, the AgNPs have a catalytic effect on the degradation of azo dyes and this protocol could be manipulated by industries to tear waste water samples containing industrial azo type dyes.

5. Acknowledgements

The authors are grateful to J. W Smith of the Electron Microscope Unit, UKZN-Westville Campus for TEM measurements and J Hughes of the School of Environmental Sciences, UKZN-Pietermaritzburg Campus for XRD measurements. We thank M. A. Ngwenya of the KwaZulu-Natal Herbarium for identifying the plant species. This research was sponsored by the National Research Foundation (NRF) and the Durban University of Technology.

References

Ankamwar, B., Chinmay, D., Absar, A., Murali, S., 2005. Green synthesis and Electrochemical Characterizations of Gold Nanoparticles Using Leaf Extract of Magnolia kobus. J. Nanosci. Nanotechnol. 10, 1665-1671.

Ankamwar, B., Chaudhary, M., Murali, S., 2005. Biosynthesis of Gold and Silver Nanoparticles Using Emblica Officinalis Fruit Extract, Their Phase Transfer and Transmetallation in an Organic Solution. Synth. React. Inorg. Met. Org. Nanomet. Chem. 35, 19-26.

Becker, R.O., 1999. Silver ions in the treatment of local infections. Met. Based Drugs. 6, 297-300.

Chandran, S.P., Chaudhary, M., Pasricha, R., Ahmad, R., Sastry, M., 2006. Biosynthesis of Silver nanoparticles. Biotechnol. 22, 577-583.

Cuenya, B.R., 2010. Synthesis and catalytic properties of metal nanoparticles: Size, shape, support, composition, and oxidation state effects. Thin Solid Films. 518, 3127-3150.

Dubay, M., Bhadauria, S., Kushwah, B.S., 2009. Green synthesis of nanosilver particles from extract of Eucalyptus hybrida (Safeda) Leaf. Dig. J. Nanomater. Biostruct. 4, 537-543.

Elechiguerra, J.L., Burt, J.L., Morones, J.R., Bragado, A.C., Gao, X., Lara, H.H., Yacaman, M.J., 2005. Interaction of silver nanoparticles with HIV-1. J. Nanobiotechnol. 3, 1-6.

Foldbjerg, R., Dang, D.A., Autrup, H., 2011. Cytotoxicity and genotoxicity of silver nanoparticles in the human lung cancer cell line, A549. Arch. Toxicol. 85, 743-749.

Gengan, R.M., Anand, K., Phulukdaree, A., Chuturgoon, A., 2013. A549 lung cell line activity of biosynthesized silver nanoparticles using Albizia adianthifolia leaf. Colloids. Surfaces B: Biointerf. 105, 87- 91.

Ghosh, S., Patil, S., Ahire, M., Kitture, R., Kale, S., Pardesi, K., Cameotra, S.S., Bellare, J., Dhavale, D.D., Jabqunde, A., Chopade, B.A., 2012. Gnidia glauca flower extract mediated synthesis of gold nanoparticles and evaluation of its chemocatalytic potential. Int. J. Nanomed. 7, 483-496.

Govender, R., Phulukdaree, A., Gengan, R.M., Anand, K., Chuturgoon, A.A., 2013. Silver nanoparticles of Albizia adianthifolia: the induction of apoptosis in human lung carcinoma cell line. J. Nanobiotech. 11, 1-9.

Gupta, N., Singh, H.P., Sharma, R.K., 2011. Metal nanoparticles with high catalytic activity in degradation of methyl orange An electron relay effect. J. Mol. Catalysis A. 335, 248-252.

Jaleel, C.A., Gopi, R., Gomathinayagam, M., Panneerselvam, R., 2009. Leaf Anatomical Modifications in Catharanthus roseus as Affected by Plant Growth Promoters and Retardants. Process Biochem. 44, 205-209.

Jebakumar Immanuel Edison, T., Sethuraman, M.G., 2012. Instant green synthesis of silver nanoparticles using Terminalia chebula fruit extract and evaluation of their catalytic activity on reduction of methylene blue. Process Biochem. 47, 1351-1357.

Jebakumar Immanuel Edison, T., Sethuraman, M.G., 2013. Biogenic robust synthesis of silver nanoparticles using Punica granatum peel and its application as a green catalyst for the reduction of an anthropogenic pollutant 4-nitrophenol. Spectrochim. Acta A. 104, 262-264.

Kasthuri, J., Veerapandian, S., Rajendiran, N., 2009. Biological synthesis of silver and gold nanoparticles using apiin as reducing agent. Colloids Surf B Biointerf. 68, 55-60.

Kouvaris, P., Delimitis, A., Zaspalis, V., Papadopoulos, D., Tsipas, S.A., Michailidis, N., 2012. Green synthesis and characterization of silver nanoparticles produced using Arbutus Unedo leaf extract. Mater.Lett. 76, 18-20.

Krishnaraj, C., Jagan, E.G., Rajasekar, S., Selvakumar, P., Kalaichelvan, P.T., Mohan, N., 2010. Synthesis of silver nanoparticles using Acalypha indica leaf extracts and its antibacterial activity against water borne pathogens. Colloids Surf. B: Biointerf. 76, 50-56.

Kumar, V., Yadav, S.K., 2009. Plant-mediated synthesis of silver and gold nanoparticles and their applications. J. Chem. Technol. Biotechnol. 842, 151-157.

Loo, Y.Y., Chieng, B.W., Nishibuchi, M., Radu, S., 2012. Synthesis of silver nanoparticles by using tea leaf extract from Camellia Sinensis Int. J. Nanomed. 7, 4263-4267.

Mabogo, D.E.N., 1990. Medicinal Plants. The Ethnobotany of the Vha-Venda. M.Sc. Thesis. University of Pretoria, Pretoria, RSA.

Mezohegyi, G., Kolodkin, A., Castro, U.I., Bengoa, C., Stuber, F., Font, J., Fabregat, A., Fortuny, A., 2007. Effective anaerobic decolorization of azo dye acid orange 7 in continuous up flow packed-bed reactor using biological activated carbon system. Indus. Eng. Chem. Res. 46, 6788-6792.

Mude, N., Ingle, A., Gade, A., Rai, M., 2009. Synthesis of Silver Nanoparticles by the callus extract of Carica papaya: A first report. J. Plant Biochem. Biotechnol. 18, 83-86.

Mulaudzi, R.B., Ndhlala, A.R., Kulkarni, M.G., Finnie, J.F., Van Staden, J., 2011. Antimicrobial properties and phenolic contents of medicinal plants used by the Venda people for conditions related to venereal diseases. J. Ethnopharmacology. 135, 330-337.

Nishiyama, Y., Moriyasu, M., Ichimaru, M., Tachibana, Y., Kato, A., Mathenge, S.G., Nganga, J.N., 1996. Acyclic triterpenoids from Ekebergia capensis.Phytochemistry. 42, 803-807.

Philip, D., 2010. Green synthesis of gold and silver nanoparticles using Hibiscus rosa sinensis. Physica E. 42, 1417-1424.

Philips, D., 2010. Honey mediated green synthesis of silver nanoparticles. J. Spectrochim. Acta A. 75, 1078-1081.

Rai, M., Yadav, A., Gade, A., 2009. Silver nanoparticles as a new generation of antimicrobials. Biotechnol. Adv. 27, 76-83.

Rajan.A., Meenakumari, M., Philip, D., 2013. Shape tailored green synthesis and catalytic properties of gold nanocrystals. Spectrochimica Acta A. 118, 793-799.

Rajasekharreddy, P., Rani, P.U., Sreedhar, B., 2010. Synthesis of Plant-Mediated Silver Nanoparticles Using Dioscorea batatas Rhizome Extract and Evaluation of Their Antimicrobial Activities. J. Nanopart. Res. 12, 237-246.

Raman, S., Kandula, M.P., Jacob, J.A., Soundararajan, K., Ramar, T. Palani, G., Muthukalingan, K., Shanmugam, A., 2012. Cytotoxic effect of Green synthesized silver nanoparticles using Melia azedarach against in vitro HeLa cell lines and lymphoma mice model. Process. Biochem .47, 273-279.

Sathishkumar, M., Sneha, K., Won, S.W., Cho, C.W., Kim, S., Yun, Y.S., 2009. Cinnamon zeylanicum bark extract and powder mediated green synthesis of nano-crystalline silver particles and its bactericidal activity. Colloids Surf B; Biointerf. 73, 332-338.

Shukla, V.K., Singh, R.P., Pandey, A.C., 2010. Black pepper assisted biomimetic synthesis of silver nanoparticles. J. Alloys Compd. 507, 13-16.

Silver, S., 2003. Bacterial silver resistance, molecular biology and uses and misuses of silver compounds. FEMS. Microbiol. Rev. 27, 341-353.

Silver, S., 2003. Bacterial silver resistance: molecular biology and uses and misuses of silver compounds. FEMS Microbiol. Rev 27, 341-351.

Song, J.Y., Jang, H.K., Kim, B.S., 2009. Biological synthesis of gold nanoparticles using Magnolia kobusand Diopyros kaki leaf extracts. Process Biochem 44, 1133-1138.

Song, J.Y., Kim, B.S., 2009. Rapid biological synthesis of silver nanoparticles using plant leaf extracts. Bioprocess. Biosyst. Eng. 32, 79-84.

Stephen, O.A, Adeyemi, O.A, Mack, M and Johannes, V.S, 2012. Antioxidant and acetylcholinesterase-inhibitory properties of long-term stored medicinal plants. BMC. Comple. Alter. Medi, 12, 87

List of Figure Captions:

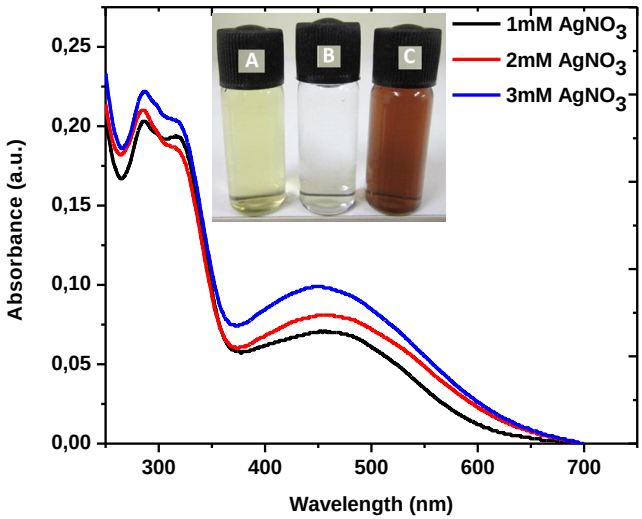

Fig.1 UV-vis absorption spectra of AgNPs at three different $AgNO_3$ concentrations. (For interpretation of the references to colour in this figure legend, the reader is referred to the web version of the article (A) Aqueous Leaf Extract (B) Silver nitrate solution (C) Silver Nanoparticles

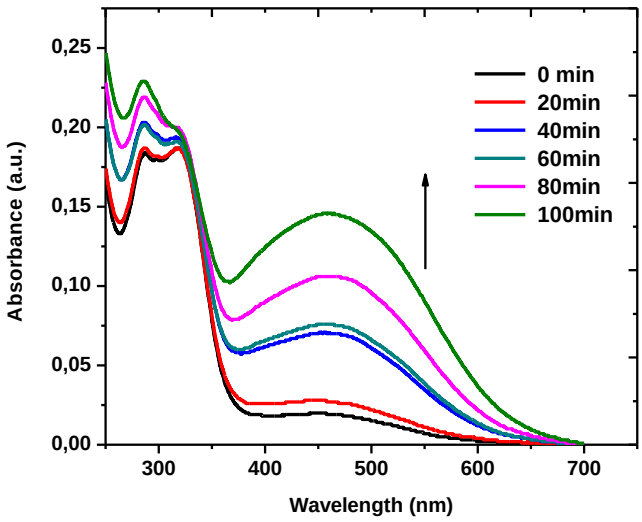

Fig.2 UV–vis absorption spectra of AgNPs at different reaction times. (For interpretation of the references to colour in this figure legend, the reader is referred to the web version of the article)

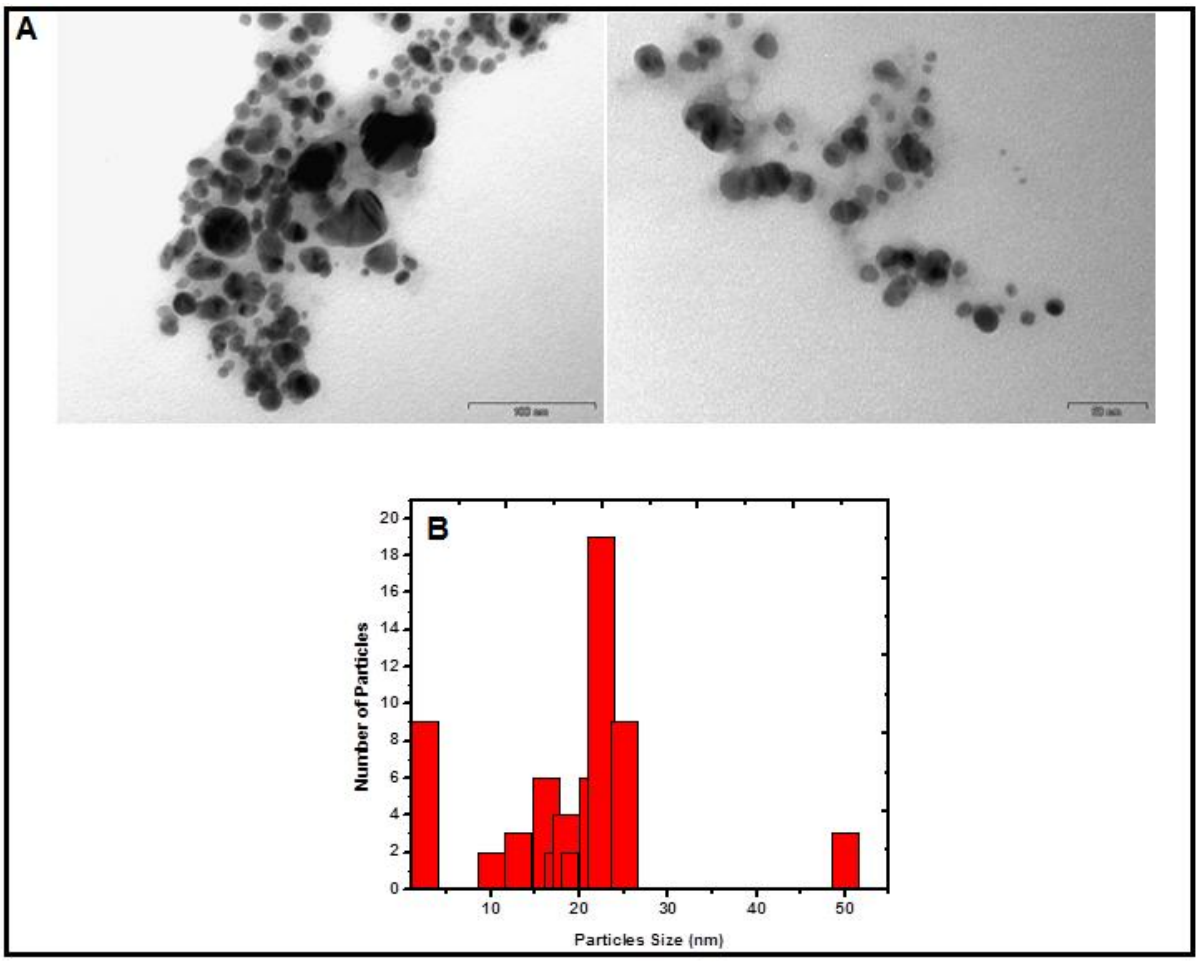

Fig.3 (A) Representative TEM micrograph of AgNPs biosynthesized by aqueous leaf extract of E.capensis (B) Histogram representation of size distribution of AgNPs

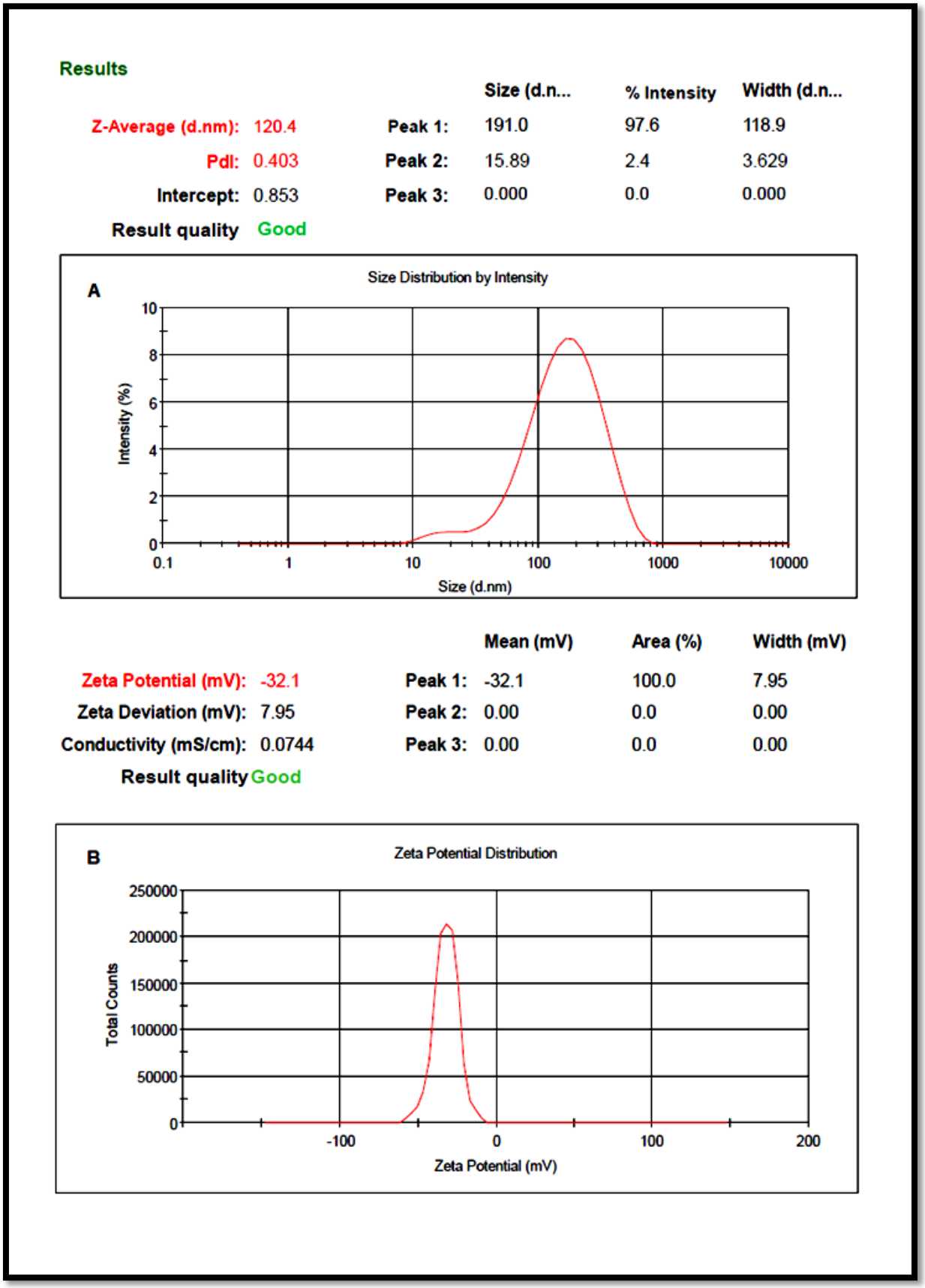

Fig.4 DLS profile: (A) size distribution of AgNPs with maximum intensity at 120 nm. (B) Stability of AgNPs at -32.1 mV in zeta potential analysis

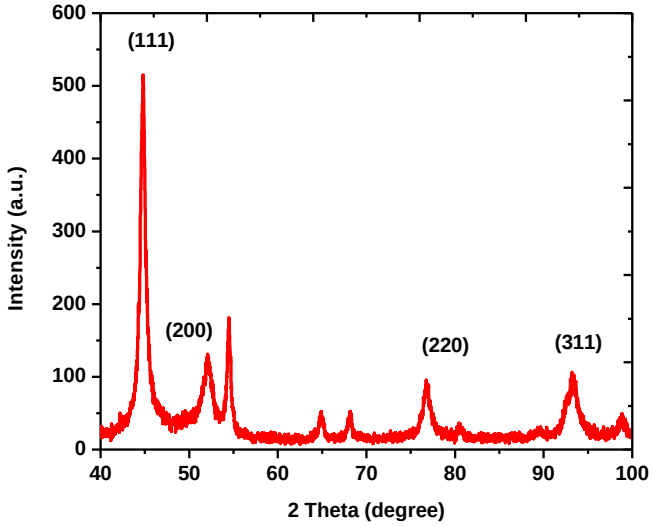

Fig.5 XRD patterns of AgNPs synthesized using *Ekebergia capensis* leaf extract

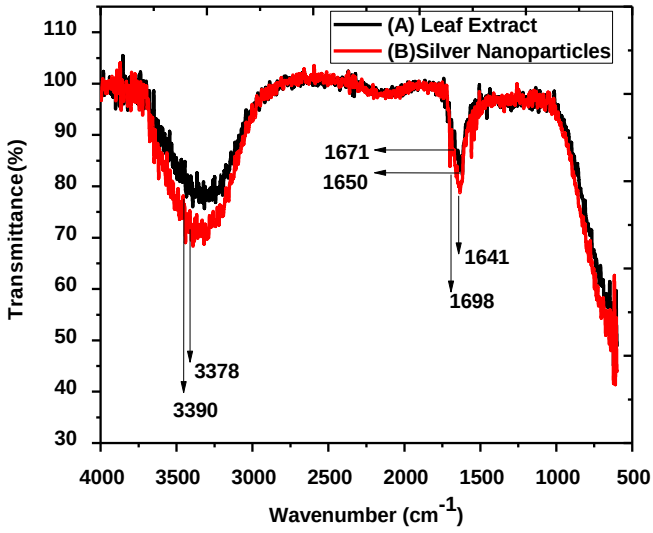

Fig.6 FTIR Profile of AgNPs synthesized using *Ekebergia capensis* leaf extract

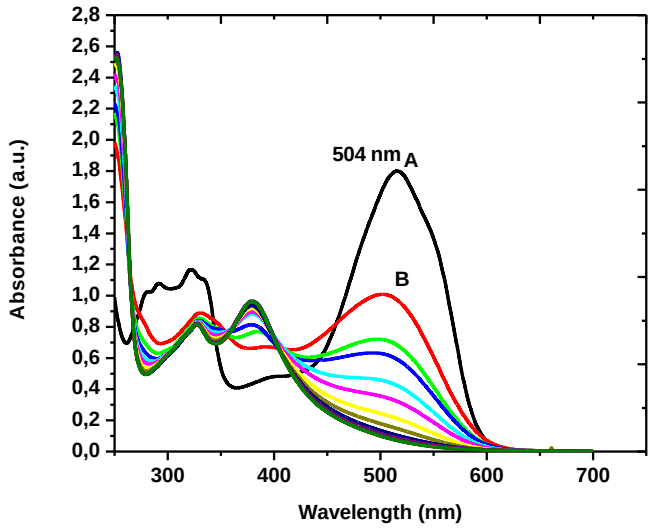

Fig.7 The UV-vis Profile of Allura Red and treated with AgNPs

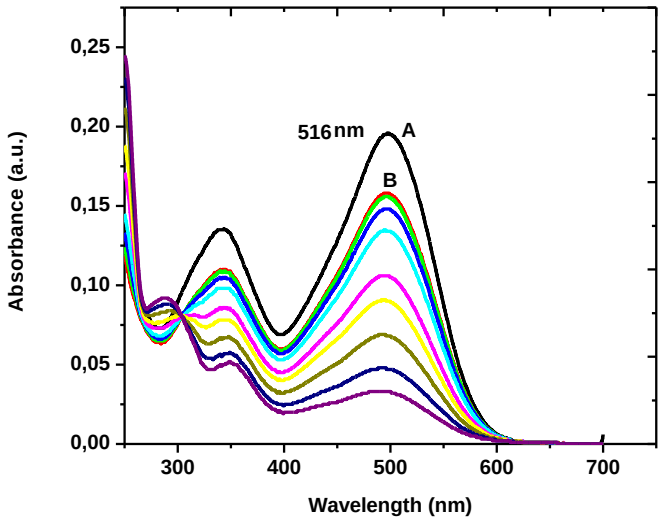

Fig.8 The UV-vis Profile of Congo Red and treated with AgNPs

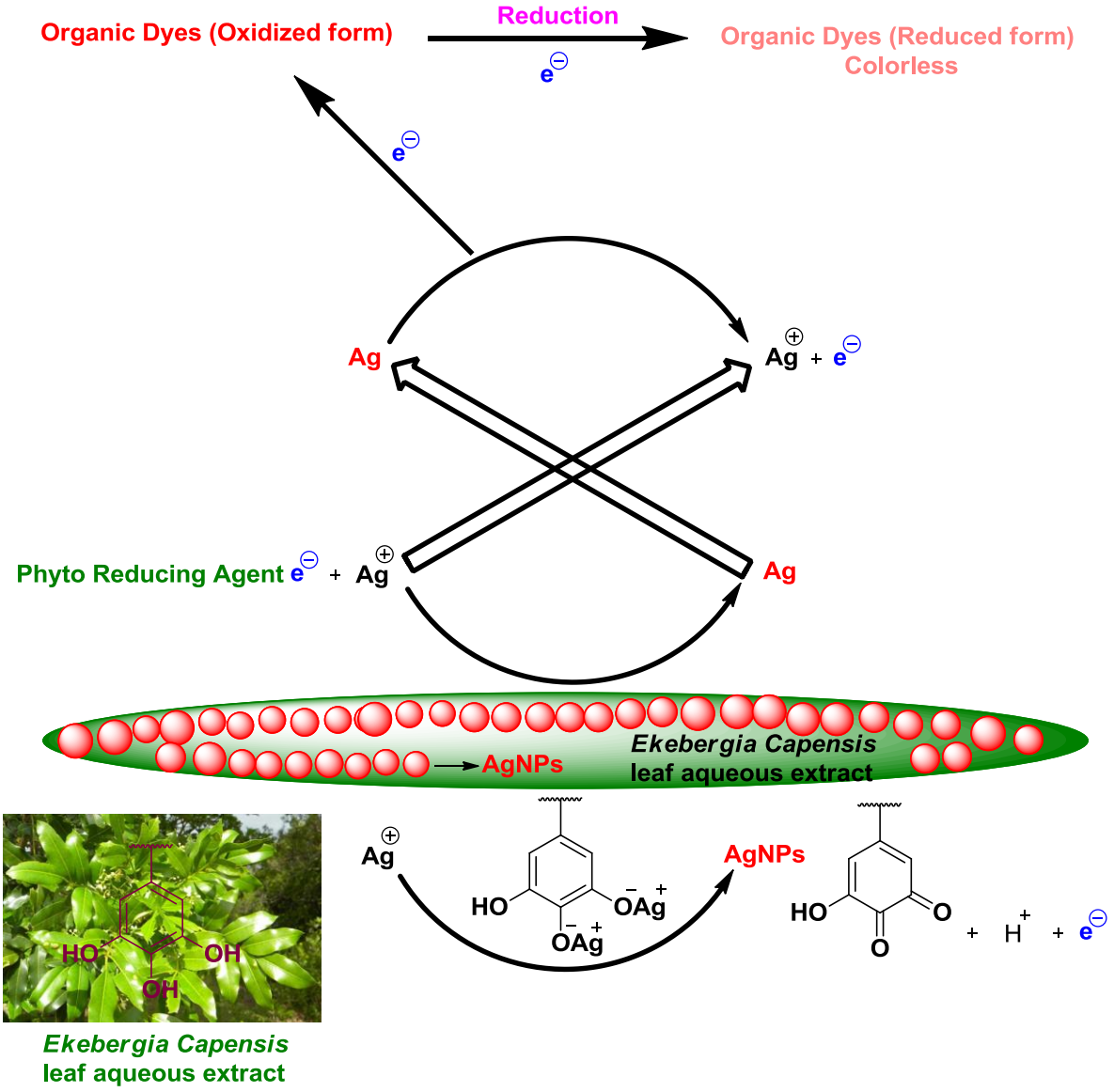

Fig.9 Mechanism involved in the formation of AgNPs and Catalytic reduction of industrial azo dyes

Elsevier Editorial System(tm) for Applied Catalysis B: Environmental
Manuscript Draft

Manuscript Number:

Title: Farm waste mediated green synthesis of crystalline palladium into nanoparticles using Moringa oleifera and their A549 lung cell line and catalytic activities

Article Type: Research Paper

Keywords: Moringa oleifera; p-Nitrophenol; Methylene blue; Suzuki coupling

Corresponding Author: Prof. Robert Moonsamy Gengan, Ph.D

Corresponding Author's Institution: Durban University of Technology

First Author: Anand Krishnan, M.Sc

Order of Authors: Anand Krishnan, M.Sc; Robert Moonsamy Gengan, Ph.D; Alisa Phulukdaree, Ph.d; Anil Chuturgoon, Ph.d

Cover Letter

The Editor
X. Verykios
Dept. of Chemical Engineering,
University of Patras,
Patras,
Greece

Dear Professor X. Verykios

We hereby submit a manuscript entitled "**Farm waste mediated green synthesis of crystalline palladium into nanoparticles using *Moringa oleifera* and their A549 lung cell line and catalytic activites**" by K. Anand, R. M. Gengan, A. Phulukdaree, A. Chuturgoon to be considered for publication as a research article in Applied Catalysis B Environmental. There are three files in all: the main manuscript file, 1 Figures file (containing 8 figures), 1 Tables file (containing 2 tables), 1 Supplementary Data file, 1 Graphical Abstract file and 1 Highlights file.

This article Palladium nanoparticles (PdNPs) were synthesized for the first time from the farm unused flower of an indigenous medicinal plant, *Moringa oleifera* found in South Africa. These PdNPs were characterized by several known techniques. The cytotoxic to normal cells and A549 cancer cells of PdNPs profile were studied. PdNPs cause significant cytotoxicity to A549 cells and did not induce cytotoxicity in normal healthy Peripheral Lymphocytes (PLs). In addition, a first time study was undertaken on evaluating the catalytic degradation of important organic dye and nitrophenol by these novel PdNPs, that are commonly used by Pharma and textile industries locally; these dyes are ubiquitous in waste water. We found that the novel PdNPs displays good potential to degrade; Suzuki coupling to form carbon- carbon in bond water as green solvent. We believe these findings will be of interest to the readers of your journal.

We declare that this manuscript is original, has not been published before and is not currently being considered for publication elsewhere.

We hope you find our manuscript suitable for publication and look forward to hearing from you.
Sincerely,

Thanking you, sincerely

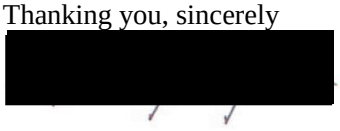

RM Gengan
Associate Professor: Department of Chemistry

Durban University of Technology

*List of Three (3) Potential Reviewers

Suggested Reviewers

Professor E. Manikandan

Nano Research Centre,

Dept of Physics,

B.S.Abdur Rahman University,

India

maniphysics@gmail.com

This researcher has good experience on catalytic investigation by using nano materials

---

Assistant Professor V. Murugan

Deapartment of chemistry

Unversity of montreal

Canada

momugan@gmail.com

This researcher has good experience on dye reduction investigations by using nano materials

---

Professor R. Ladchumananasivam

Department of Textile Engineering,

Centre of Technology-UFRN, Campus Universitario,

Brazil

rlsivam@gmail.com

This researcher is a leading investigator of plants crops products studies and Industrial applications

---

Farm waste mediated green synthesis of crystalline palladium into nanoparticles using *Moringa oleifera* and their A549 lung cell line and catalytic activities

K. Anand[1], R. M. Gengan[1]*, A. Phulukdaree[2], A. Chuturgoon[2]

[1]Department of Chemistry, Faculty of Applied Sciences, Durban University of Technology, Durban, South Africa.

[2]Discipline of Medical Biochemistry, School of Laboratory Medicine and Medical Sciences, Nelson R Mandela School of Medicine, University of KwaZulu-Natal, Durban, South Africa

*Corresponding author: Tel.: +27 31 3732309; fax + 27 31 2022671.

E-mail address: genganrm@dut.ac.za

Abstract

The present work reports a new one step method for the synthesis of palladium nanoparticles (PdNPs) from aqueous solution of crystalline palladium acetate by using farm unused petals of *Moringa oleifera*, as a natural reducing and capping agent. The formation of palladium nanoparticles was confirmed by continuous absorption in the UV region and a brown colour change. A strong surface plasmon peaks for palladium nanoparticles occurred at 460 nm. PdNPs were characterized by various analytical techniques. The analysis of small particles with elemental palladium by scanning electron microscopy (SEM) and energy dispersive X-ray (EDX) were conducted. Fourier transform infrared spectroscopy (FTIR) measurements confirmed the chemical surface structure of PdNPs. TEM images showed the monodispersed palladium spherical nanoparticles of 50 nm. The in vitro cytotoxicity evaluation of the extract capped nanoparticles was carried out using human lung carcinoma cells (A549) and peripheral lymphocytes normal cells by MTT cell viability assay. Further, the catalytic degradation effect of industrial organic toxic effluents p-nitrophenol (PNP) and methylene blue dye were investigated by PdNPs. A ligand free base mediated suzuki coupling reaction of iodobenzene and phenylboronic acid, in water occurred in the presence of PdNPs.

Keywords: *Moringa oleifera*; p-Nitrophenol; PdNPs; Methylene blue; Suzuki Coupling

1. Introduction

Agroforestry waste presents a problem for disposal and negatively impacts on the environment if left to rot or burn. Although it can be burned to produce to generate heat, it is being under utilized[1]. However using agricultural waste and forestry residuals at the nanoscale can create a new market for farmers and other independent craftsmen who possess stockpiles of agricultural waste as a by product of their trade. Farmers can generate revenue for themselves while providing a greener and sustainable form of technology. The dramatic expansion of the nanotechnology industry has prompted the need to investigate potential toxic effects of nanosized particles (NPs) on human health as well as to the environment[2]. Such knowledge is import for nanotechnology to grow in a responsible and sustainable manner. p-nitrophenol (PNP) and methylene blue (MB) are synthetic chemicals that is used as a starting material to manufacture textiles, pharmaceuticals and cosmetics products; hence it is widely distributed in the environment[3]. Since PNP is toxic and may accumulate in the food chain, it poses significant health and environmental risks, and is also regarded as a priority pollutant by the US Environmental Protection Agency[3]. Acute inhalation or ingestion of nitrophenol in humans causes headaches, drowsiness, nausea, and cyanosis. Basic dyes like MB are reported to cause allergic dermatitis, skin irritation, cancer, and mutations[4]. Contact with eyes causes irritation in humans. One of the major problems concerning textile waste water is the disposal of dye effluent[5]. Therefore, removal of dyes from the effluent is the responsibility of textile units before its final discharge.

Nanocatalysis is a recent important technology leading to the total mineralization of most organic effluents[6]. The utilization of silver, platinum, gold and palladium metal nanoparticles have numerous applications in heterogeneous and homogeneous catalysis. The development of one step green synthesis method for monodispersed palladium nanocrystals using cheap and nontoxic chemicals, environmentally benign solvents and renewable is an important green strategy. Organic reactions in water are environmentally friendly; the Suzuki coupling reaction has recently been used to synthesize compounds for industry. It is used in the synthesis of intermediates for pharmaceuticals or fine chemicals[7-11].

Moringa oleifera (Family: Moringaceae), is reported to contain various phytochemicals, viz. carotenoids, vitamins, minerals, amino acids, sterols, glycosides, alkaloids, flavonoids and phenolics[12-16]. Constituents such as leaf, flower, fruit and bark have been anecdotally

used as herbal medicines in treatments for inflammation, paralysis and hypertension. Many reports describe *Moringa oleifera* extracts as highly potent anti-inflammatory[17], hepatoprotective[18], anti-hypertensive[19] and anti-tumor[20] agents. Although research studies on the synthesis of nanoparticles using different parts of the plant have been reported as well as their application in different research fields, no study has reported on either the synthesis of palladium nanoparticles using the *Moringa oleifera* flower or their cancer and catalytic applications.

The present study describes the*Moringa oleifera* flower mediated in vitro one step facile assembly of PdNPs, characterization, its catalytic reduction of methylene blue, p-nitrophenol and Suzuki coupling reaction. Furthermore cytotoxic effects on the A549 human lung cancer cell line and normal healthy human peripheral lymphocytes are elucidated.

2. Experimental

2.1. Materials and Methods

Monoclinic crystalline palladium acetate [$Pd(OAc)_2$] was purchased from Sigma-Aldrich (South Africa). All aqueous solutions were prepared using distilled water. *Moringa oleifera* flower was collected from Phoenix agricultural farm, Durban, South Africa and identified at the KwaZulu-Natal Herbarium.

2.2. Preparation and Characterization of Palladium Nanoparticles

Fresh flowers were collected and washed several times with distilled water; 10 g of the flower were finely cut and 100 ml of distilled water was added. The flower with the water was heated to boil for 20 min, allowed to cool, filtered through a Whatman No.1 filter paper and 1 ml of the supernatant leaf extract was added to 49 ml of 1 mM palladium acetate aqueous solution at 60°C and the solution was stirred. The color of the solution gradually turned from dark brown to light yellow within 6 h, at pH~7. The PdNps was characterized using UV-vis spectrometer (Varian Cary-50 UV spectrophotometer) linked to a TCC-240A Shimadzu heating vessel temperature controlled cell holder) in the range of 200- 800 nm. To obtain the particle size and shape, 1 µl of the PdNPs was placed on formvar coated grids, air dried and viewed at 100 kV to conduct transmission electron microscopy (JEOL 1010 TEM using a Megaview III camera and iTEM software) studies. The nanoparticles' size distribution was determined by using *ImageJ* software and the resultant data were plotted in histograms. For the particles' images and elemental analysis studies, the PdNPs colloidal suspension was centrifuged at 10,000 rpm for 10 min, and the supernatant was discarded. The pellets were cast onto a sample holder; air dried and

subjected to Carl Zeiss Ultra Plus scanning electron microscope with EDX detector and the FTIR spectra recorded (Varian 800 FTIR spectrophotometer)**.** A Differential Light Scattering *Malvern Zetasizer Nano ZS* (*Malvern* Instruments Ltd., UK) Merck 2423 instrument was used to measure particle size and zeta potential.

2.3. Cell culture

A549 lung cells were cultured for 6 h (37 ^{o}C, 5% CO_2) to 90 % confluency in 25 ml flasks in complete culture media (CCM; Eagles minimum essential media, 10% foetal bovine serum, 1% penstrepfungizone, 1% L-glutamine). Cells were harvested (2 x 10^4 cells/well in a 96 wells microtitre plate) for the MTT analysis, ATP quantification and supernantant was stored following treatment with CCM only, 10 ug/ml and 50 ug/ml PdNPs solution for 6 h. Ethical approval from the Biomedical Research Ethics Administration Office of the University of KwaZulu-Natal was obtained. Informed consent was obtained from two healthy volunteers before blood samples were taken. For the preparation of peripheral lymphocytes (PL's), buffy coats containing PL's were extracted from heparinized whole blood by differential centrifugation. Briefly, 5 ml whole blood collected from each subject was layered onto equivolume Histopaque 1077 (Sigma) in polypropylene tubes. Layered blood was then centrifuged at 4000 rpm for 30 min. Buffy coats were aspirated into new polypropylene tubes and washed twice in phosphate buffered saline (4000 rpm, 10 min). Cell density was adjusted to 2×10^4 cells/well using the trypan blue exclusion test.

2.4. MTT Assay

Following incubation with relevant treatments, cells were washed twice with PBS and each sample supplemented with a 1:5 ratio of filter-sterilised (0.45 μm) MTT salt solution (5 mg/ml in PBS) and CCM. The plate was incubated at 37ºC for 4 h. Following incubation, dimethyl sulphoxide (DMSO) (100 ml) was added to each well and incubated at 37 ºC for a further 1 h. Optical density of the formazan product was measured using a plate reader (Bio-tek μ Quant) at 570/690 nm. Results were expressed as mean percentages of the control response.

2.5. Statistical Analysis

Results are expressed as the mean plus or minus the standard deviation. Statistical significance between samples was determined using One Way ANOVA Tukey Kramer

Multiple Comparisons test with Dunns Post-test using the GraphPad Prism Software, (GraphPad Software Inc.).

2.6. Catalytic Reduction of Methylene Blue (MB)

An aqueous ice cold solution of $NaBH_4$ (0.5 ml of 0.1M) was mixed with aqueous stock solution of methylene blue (2 ml, 10^{-5}M) in a standard quartz cuvette and PdNPs (25 µl) was added. The final volume was adjusted with Millipore water to get the final volume as 3 ml. The mixture was shaken well and the reaction was monitored with the help of a UV-vis spectrophotometer in the scanning range of 300 to 700 nm at room temperature.

2.7. Catalytic Reduction of P-Nitrophenol (PNP)

Ice cold aqueous solution of $NaBH_4$ (1 ml, 15 mM) was mixed with 4-nitrophenol (1.7 ml, 0.2 mM) in a standard quartz cuvette. The light yellow color of the 4-nitrophenol changed yellowish green due to the formation of 4-nitrophenolate ion. An aliquot of PdNPs prepared at room temperature (0.4 ml) was added to the resulting solution, and the time-dependent absorbance spectra peak was recorded with a time interval of 0.5 min in the scanning range of 200 nm to 700 nm at room temperature.

2.8. Suzuki Reaction in Water

To a 10 ml flask, a mixture of iodobenzene (0.6 mmol, 0.067 ml), phenylboronic acid (0.5 mmol, 0.6 g) and K_2CO_3 (1.75 mmol, 0.24 g) was added to cold water (1.5 ml) and additive PEG-400 (1.5 ml). PdNPs solution (1 ml) was added as catalyst. The mixture was stirred at room temperature for 1 h. The reaction mixture was then cooled to room temperature followed by solvent extraction with ethyl acetate. The combined organic layers were dried over anhydrous sodium sulfate. The solvent was removed by slow evaporation and the product was purified by column chromatography with (50:50) Petroleum ether: EtOAc. A white solid, Yield (90 %) was obtained.

3. Results and Discussion

3.1. Nanoparticle Composition and Size Distribution

The first indication of successful PdNPs formation was the appearance of a light yellow color due to excitation of surface plasmon resonance[21]. This was a rapid reaction as indicated by the immediate colour change on mixing the aqueous palladium (II) acetate solution with the aqueous flower extract of *Moringa oleifera*. This colour change validated

the occurrence of a redox reaction whereby Pd^{2+} ions are reduced to Pd^{0} by the flower components which are in turn oxidized to other species. Although the actual mechanism shows capping molecules responsible for the reduction of palladium ions in *Moringa oleifera* aqueous flower extract is unknown. The ^{1}H-NMR indicated that the aqueous extract contains compounds having the hydroxyl. It has components such as phenolics, polyols, amines, flavonoids, water-soluble heterocyclic components as well as tannins, saponins, gallic acids, proteins, reducing sugars and other oxido-reductively labile metabolites that have the ability to act as reducing agents. Previous studies[12-16] on the phytochemistry of *Moringa oleifera* reported many organic compounds present therein and hence suggesting water soluble hydroxy functional group containing compounds are responsible for the reduction of Pd^{+} ions. Hence the reaction between *Moringa oleifera* aqueous flower extract and the Pd(II) species might occur according to the following schematic mechanism as shown in (Fig. 8).

UV-vis spectroscopy (Fig. 1) was used to monitor the reaction as a function of reaction time. The observed peaks at 420 nm at one hour indicate the presence of the Pd^{2+} ions in reaction mixture. Over the time the absorbance represent the Pd^{2+} ions began to disappear, which indicates the formation of palladium nanoparticles. This intensity increased over longer reaction time. Since the peak wavelength did not shift during the reaction, we concluded that there was no change in the nanoparticle size during this time as well as the preparation is mainly composed of small spherical PdNPs as indicated by the single broad symmetrical absorption peak.

The optical signature of PdNPs was determined; the distribution of sizes and shapes were conducted by transmission electron microscopy (TEM) images and supported by hydrodynamic size and zeta potential data measured by dynamic light scattering (DLS). Representative TEM images recorded from the PdNPs colloidal solution showed that most of the particles are spherical or near spherically shaped and exhibited a distribution of sizes in the range 3-5 nm and some very large images of palladium nanoparticles with linked monometallic shapes were also observed. The pictogram of PdNPs shown particle size of 5 nm is abundant.

DLS analysis showed the size distribution of particles with an average hydrodynamic size of 120 nm (Fig. 3A) similar to the leaf extract of *Meliaazedarach*[19]. As expected, the particle size obtained from TEM and DLS scattering is marginally different due to the

varying principles used for measurement. Also a stable dispersion of particles was evident from the zeta potential of 0.0601 mV (Fig. 3B); a zeta potential higher than 30 mV or lower than 30 mV indicates a stable system. Many reports have proposed that surface active molecules can stabilize the nanoparticles and reaction of the metal ions is possibly facilitated by reducing sugars and or terpenoids. We suggest organic molecules such as carotenoids, vitamins, minerals, amino acids, sterols, glycosides, alkaloids, flavonoids and phenolics can act as surface active molecules responsible for stability and PdNPs formation; however further studies are required to elucidate the mechanism of biological PdNPs synthesis and validate this hypothesis.

The crystalline nature of the PdNPs and nano size was confirmed by SEM spectroscopy and the EDX pattern (Fig. 4). The particle dimensions of nano material were 200 nm PdNPs showed spherical morphology of particle with size 100 nm. EDX pattern for *Moringa oleifera* shows signals for palladium nanoparticles.

FTIR analysis (Fig. 5) and comparision of the spectra of a crude aqueous flower extract and PdNPs showed a marginal stretching frequency shift from 3492 to 3487 cm^{-1} thereby indicating the possibile presence of an amide functional group. Also the PdNPs spectrum lacked the 2926 and 2924 cm^{-1} peaks which were present in the flower extract. This suggested the loss of the OH intramolecular hydrogen bond functional group[20, 21] which might be responsible for the reduction of Pd^{2+} to Pd^{0}. Furthermore, a small shift from 1647 cm^{-1} to 1637 cm^{-1} was assigned to the C=O stretch and the peak at 1099 cm^{-1} in the crude flower extract were assigned to the C-O stretch. Although carotenoids, vitamins, minerals, amino acids, sterols, glycosides, alkaloids, flavonoids and phenolics are found in *Moringa oleifera*, other secondary metabolites, proteins and lipids are present in the plant cell, at different concentrations, and may be responsible for the bio-reduction of Pd^{2+} ions. Specifically, conversion of C=O group of biomolecules to C(O)=O group may be responsible for the reduction of Pd^{2+} to Pd^{0}.

To identify the capping reagents and molecules responsible for the reduction of the gold ions, the crude aqueous flower extract of *Moringa oleifera* was investigated by ^{1}H-NMR spectroscopy. The complex pattern of the ^{1}H-NMR spectrum suggested that several compounds were present in the aqueous extract[22]. The strong signal observed at δ = 1.5-3.81 ppm was due to single bond; δ = 4.76-4.81 ppm was due to double bond; signal at δ = 5.55 ppm could be due to aliphatic single bond OH group, whereas the signals appearing

between δ = 1.26-1.32 ppm were related to aliphatic -CH_2- groups. The signals at δ 6-8 and δ 1-4 ppm clearly indicated the presence of trace aromatics and abundant aliphatic compounds respectively. Further studies are required to unravel the types of compounds present in the PdNPs surfaces.

4. Catalytic study of Palladium nanoparticles

4.1. Catalytic degradation of Methylene blue

The catalytic effectiveness of the flower extract mediated synthesized palladium nanoparticles were tested for the reduction of methylene blue using $NaBH_4$ as a reducing agent. The reduction was carried out at room temperature and the catalytic degradation process was monitored by using a UV-vis spectrophotometer. The characteristic absorption peak occurs at 665 nm for methylene blue in the UV-vis spectrum. The degradation of dyes is indicated by the decolorisation of the solution. Methylene blue, initially blue in color in an oxidizing environment, became colorless in the presence of reducing agent ($NaBH_4$) indicating the reduction of methylene blue to Leucomethylene blue (LMB)[23].

4.2. Catalytic Hydrogenation of p-nitrophenol

The catalytic reduction of p-nitrophenol is perhaps the most often used reaction to test the catalytic activity of PdNPs in aqueous solution. The reduction of p-nitrophenol by sodium borohydride is a model reaction[24]. This reaction was easily monitored by UV-vis spectroscopy (Fig. 7). The strong absorption response of p-nitrophenolate ions at 400 nm was initially observed however a time profile study showed significant decrease in absorption within 330 minutes. This appeared to be a well-controlled chemical reaction that converted the nitro to the amine group in the presence of the nanoparticles without any observable side reactions or by-products. Moreover, no reaction occurred in the absence of PdNPs. These reactions proceeded under mild conditions, at room temperature and in an aqueous medium thereby implying possible utilization in industrial waste effluents. Besides the reaction mechanism sodium borohydride involves production of $NaBO_2$; sodium metaborate has low toxicity when ingested, inhaled or in contact with skin[25].

4.3. Biphenyl via Suzuki Coupling Reaction

The Suzuki coupling reaction is presented in scheme 1. *Moringa oleifera* derived palladium nanopartilces-catalyzed Suzuki cross-coupling of iodobenzene with phenylboronic acids were has become a general and expedient synthetic route in organic chemistry toward biphenyl. This is a facile reaction which was also efficient and rapid.

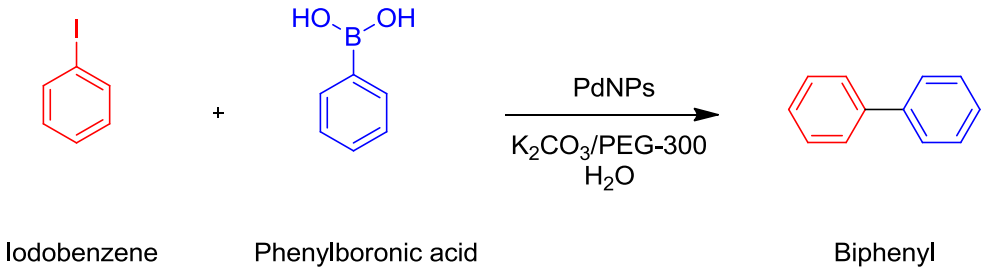

Scheme 1.Synthesis of Biphenyl

This product was a white solid produced in 94 % yield; mp: 66-67°C. IR (KBr, cm^{-1}): 1700, 1680, 1606, 839; ^{1}H-NMR (400MHz, CDCl3): δ (ppm) 7.59–7.57 (m, 4H), 7.45–7.40 (m, 4H), 7.35–7.30 (m, 2H); ^{13}C-NMR (400 MHz, CDCl3): δ (ppm) 141.24, 128.74, 127.24, 127.16, 77.32, 77.21, 76.69 (supplementary data). A highly efficient and ligand-free protocol was developed for the Suzuki coupling of aryl halides in water using green synthesis palladium nanoparticles as a catalyst and Na_2CO_3 as a base in aqueous and poly(ethylene glycol) (PEG-300) as additive. After simple workup, PdNPs–H_2O–PEG could be recycled. The biphenyl was fully characterised by ^{1}H-NMR. On comparing the new method which used PdNPs with literature (Table 1), it was found that the % yield was high (95 %). Also, the reaction (1 h) was relatively faster and the PdNPs can be regenerated by simple extraction in an organic solvent.

5. Anti-Cancer Study of Palladium Nanoparticles

The synthetic PdNPs are being widely applied, there is limited data based on the cytotoxicity of biologically synthesized PdNPs. The MTT assay was used to determine cytotoxicity in the transformed A549 cell and normal healthy peripheral lymphocytes (PLs). The results are presented in Table 2.

The PdNPs were significantly cytotoxic to A549 cells at dilution 1:100, 1:50, 1:25, 1:10, and 1:3 with viabilities of 152%, 145%, 135%, 102% and 88% respectively. However, this cytotoxic effect was not observed in PLs, treated with PdNPs, with cell viabilities of 100%, 102%, 114%, 98%, 110%, 116% and 100% respectively. This data strongly suggests that the PdNPs may possess anti-cancer/anti-proliferative properties. Plant

extracts are normally rich in nutrients and phytocompounds that result in antihyperglycaemic effects[26]. This is clearly observed in the normal healthy PLs, where the cell viability is greater than 100%. It is noteworthy that such an effect is not observed in the cancerous A549 cells, in spite of increased glycolysis being the hall mark of cancer proliferation. The mechanism of cell death by these PdNPs in the A549 cells is to be investigated.

6. Conclusion

A facile method which is simple, quick, cost-effective and reproducible was developed to synthesize PdNPs *in vitro* using the aqueous flower extract of *Moringa oleifera*. The formation of PdNPs was monitored by UV-visible spectroscopy in the 300–700 nm range. The PdNPs were characterized by TEM, SEM with EDX and DLS. ^{1}H-NMR was used to determine the structure elucidation of biphenyl and determine the type of natural capping agents. UV-visible spectroscopy proved to be useful for confirming reduction reactions. The PdNPs displayed catalytic activity in reducing 4-nitrophenol and methylene blue rapidly; Suzuki coupling to form carbon-carbon in bond water as a green solvent. Furthermore, PdNPs causes significant cytotoxicity to A549 cells and did not induce cytotoxicity in normal healthy Peripheral Lymphocytes.

7. Acknowledgements

We are grateful to J.W. Smith (Electron Microscope Unit, UKZN) for TEM measurements, J. Hughes (School of Environmental Sciences, UKZN) for XRD measurements and T. Govender (Department of Pharmacology, UKZN) for DLS studies. We also thank M.A. Ngwenya of the KwaZulu-Natal Herbarium for identifying the plant species. Thanks to the National Research Foundation (NRF), Durban University of Technology (DUT) and University of KwaZulu-Natal for funding this project.

References

(1) Albrecht, M. A.; Evans, C. W.; Raston, C. L. *Green Chem.* **2006**, 8, 417.

(2) Nanostructures and Nanomaterials: Synthesis, Properties and Applications; Cao,G., Eds.; Imperial College Press: London, **2004,** 273.

(3) Chen, X.J.; Sanchez-Gaytan, B. L.; Qian, Z.X.; Park, S. *J. Nanomed. Nanobiotechnol.* **2012**, 4273.

(4) Duncan, B.; Kim, C.; Rotello, V. M. *J. Cont. Release.* **2010**, 148, 122.

(5) Zhang, L.; Gu, F. X.; Chan, J.M.; Wang, A. Z.; Langer, R.S.; Farokhzad, O.C. *Clin Pharmacol. Ther.* **2008**, 83, 761.

(6) Dahl, J. A.; Maddux, B.L.S.; Hutchison, J. E. *Chem. Rev.* **2007**, 107, 2228.

(7) Pezeshki, S. R.; Hester, M. W.; Lin, Q.; Nyman,J. A. *Environmental. Pollution.* **2000**, 108, 129.

(8) Thompson, D. *J. Chemico Bio. Inter.* **1993**, 88, 89.

(9) Microbial nanoparticle production; Sastry, M., Ahmad, A., Khan, M.I., Kumar, R., Niemeyer,C.M., Mirkin, C.A., Eds.; Wiley-VCH: Weinheim, Germany, **2004**, 126.

(10) Bhattacharya, D.; Gupta, R. *Biotechno. Crit. Rev.* **2005**, 25, 199.

(11) Mohanpuria, P.; Rana, N. K.; Yadav, S. K. *J. Nanopart. Res.* **2008**, 10, 507.

(12) Medicinal Plants; Nesamani, S., Eds.; State Institute of Languages: Thiruvananthapuram, Kerala, India, **1999**, I, 425.

(13) Makkar, H. P. S.; Becker, K. *Anim. Feed. Sci. Technol.* **1996**,63, 211.

(14) Faizi, S.; Siddiqui, B. S.; Saleem, R.; Shaheen, F.; Gilani, A. H. *Planta. Med.* **1998**, 64, 225.

(15) Siddhuraju,P.; Becker, K. *J. Agr. Food. Chem.* **2003**, 51, 2144.

(16) Anwar, F.; Latif, S.; Ashraf, M.; Gilani, A. H. *Phytother. Res.* **2007**,21, 17.

(17) Ezeamuzle, I.C.; Ambadederomo, A.W.; Shode, F.O.; Ekwebelem, S.C. *Inter. J. Pharmacog.* **1996**, 34, 207.

(18) Pari, L.; Kumar, N.A. *J. Medi. Food.* **2002**, 5, 171.

(19) Faizi, S.; Siddiqui, B. S.; Saleem, R.; Siddiqui, S.; Aftab, K.; Gilani, A. H. *Phytochemistry.* **1995**, 38, 957.

(20) Murakami, A.; Kitazono, Y.; Jiwajinda, S.; Koshimizu, K.; Ohigashi, H. *Planta. Medica.* ***1998***, 64, 319.

(21) Link, S.; Sayed, E. *Annu, Rev. Phys. Chem.* **2003**, 54, 331.

(22) Anand, K.; Gengan, R.M.; Phulukdaree, A.; Chuturgoon, A.; *J. Indus. Eng Chem.* DOI: 10.1016/j.jiec.2014.05.021

(23) Leonard, K., Ahmmad, B., Okamura, H., Kurawaki, J. *Colloids Surf. B.* **2011**, 1, 391.

(24) Pablo, H.; Moise, P. L.; Luis, M. L.; Joachim, D.; Yan, L.; Matthias, B. *Chem. Soc. Rev.* **2012**, 41, 5577.

(25) Weir, R.J.; Fisher, R.S., *Toxicol. Appl. Pharmacol*. **1972**, 23, 351

(26) Gregersen, S; Jeppesen, P. B; Holst, J. J; Hermansen, K. *Metabolism*, **2004**, 53, 73.

(27) Kazem, K.; Mahdiyeh, G.; Nasrin, H. N. *Catalysis Communications*. **2013**, 38, 10.

(28) Rafique, U.; Witcomb, M. J.; Elmavander, L; Scurrell, M S.; Willem,V. O.; Kaushik, M.; *J. Organo. Chem*. **2011**, 696, 2206.

(29) Lyubimov, S. E.; Vasilev, A. A.; Korlyukov, A A.; Ilyin, M. M.; Pisarev, S A.; Matveev, V. V.; Chalykh, A. E.; Zlotin, S. G.; Davankov, V. A.; *React. Funct. Poly.* **2009**, 69, 755.

(30) Liang, W.; Chun, C. *J. Mole Cata A*: Chemical. **2009**, 306, 97.

(31) James, A. S.; Keith, A. F.; Holger, H.; *Catalysis Today*. **2009**, 145, 108.

(32) Debasree, S.; Kalicharan, C.; Ranu, B. C.; *Tetrahedron Lett*. **2009**, 50, 1003.

(33) Sudeshna, S.; Dipankar, S.; Piyali, D.; Rima, L.; Amitabha, S. *Tetrahedron*. **2009** 65, 4367.

Table

TABLE CAPTION

Table 1: Reaction time and percentage yield of Biphenyl in different reaction conditions compare with previous report (review of literature)

Entry	Catalyst used	Reaction condition	Reaction Time	% Yield	Reference
1	PdNPs/PS	DMF/H_2O(1:1) K_2CO_3, 100°C	12 h	94	27
2	PANI/PdNPs	Toluene, K_2CO_3, 100°C	6 h	85	28
3	Polymer-Pd resin	H_2O, K_2CO_3 100°C	4 h	74	29
4	Pd-1/FSG	H_2O,K_2CO_3,SDS, 100°C	8 h	89	30
5	MWCNT/Pd-DMAP NP	H_2O, Na_2CO_3, 100°C	10min	85	31
6	Na_2PdCl_4	H_2O,(SDS)/K_3PO_4, 100°C	5min	96	32
7	PEG-Pd	H_2O, K_2CO_3, 25°C	30min	96	33
8	Moringaoleifera/PdNPs	H_2O, K_2CO_3,PEG 25°C	1 h	95	**Present work**

Table 2. Cell viability of healthy peripheral lymphocytes and lung cancer cells (A549) treated with a range of dilutions of palladium nanoparticles synthesized with an aqueous extract from flowers of *Moringa oliefera*

	MTT- Cell Viability (mean OD ± SD)	
Dilution	Peripheral Lymphocytes	A549 cells
0	0.216 ± 0.01 (100%)	1.310 ± 0.01 (100%)
1:100	0.221 ± 0.02 (102%)	1.991 ± 0.01 (152%)
1:50	0.247 ± 0.01 (114%)	1.903 ± 0.02 (145%)
1:25	0.212 ± 0.08 (98%)	1.774 ± 0.18 (135%)
1:10	0.238 ± 0.04 (110%)	1.337 ± 0.09 (102%)
1:3	0.251 ± 0.02 (116%)	1.155 ± 0.04 (88%)*

*$p<0.05$, significantly different compared to untreated controls using a one way analysis of variance with the Dunnets Multiple Comparisons Test

List of Figure Captions

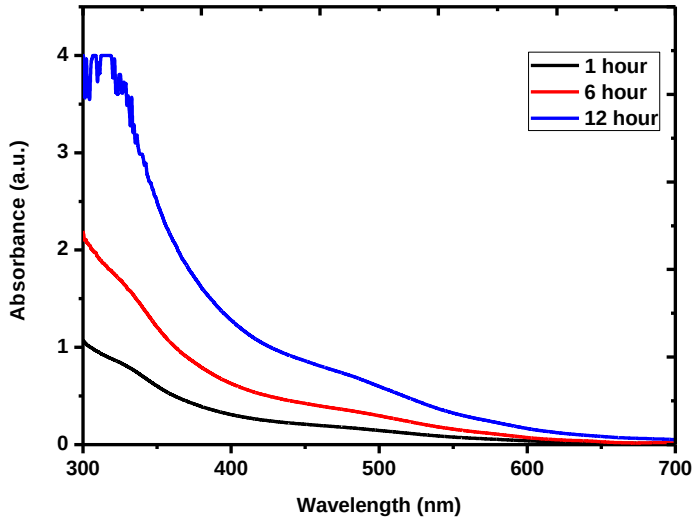

Fig. 1. UV–vis absorption spectra of PdNPs at different reaction times.

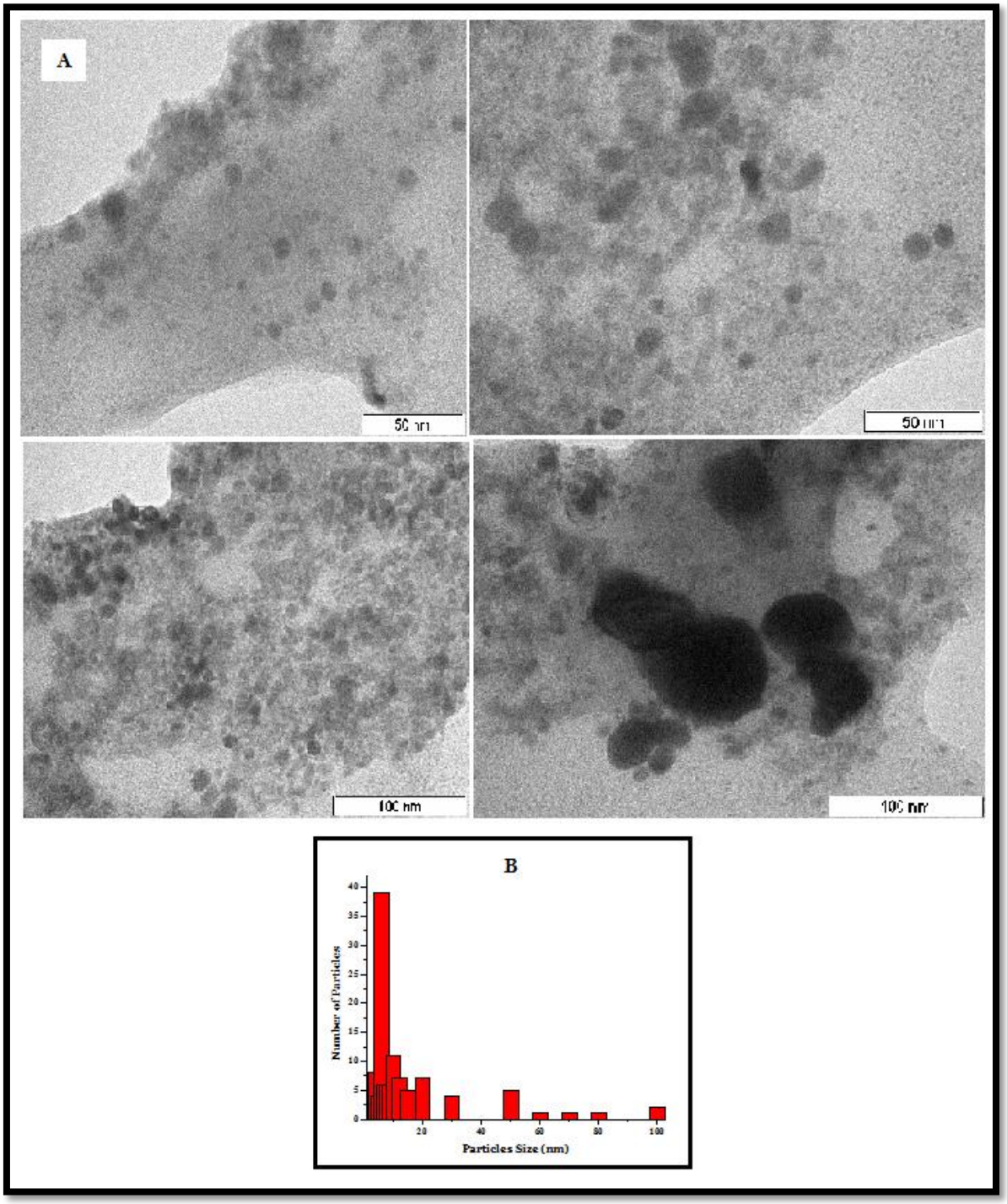

Fig. 2.(A). Representative TEM micrograph of PdNPs biosynthesized by aqueous flower extracts of *Moringa oleifera* **(B)** Histogram representation of size distribution of PdNPs.

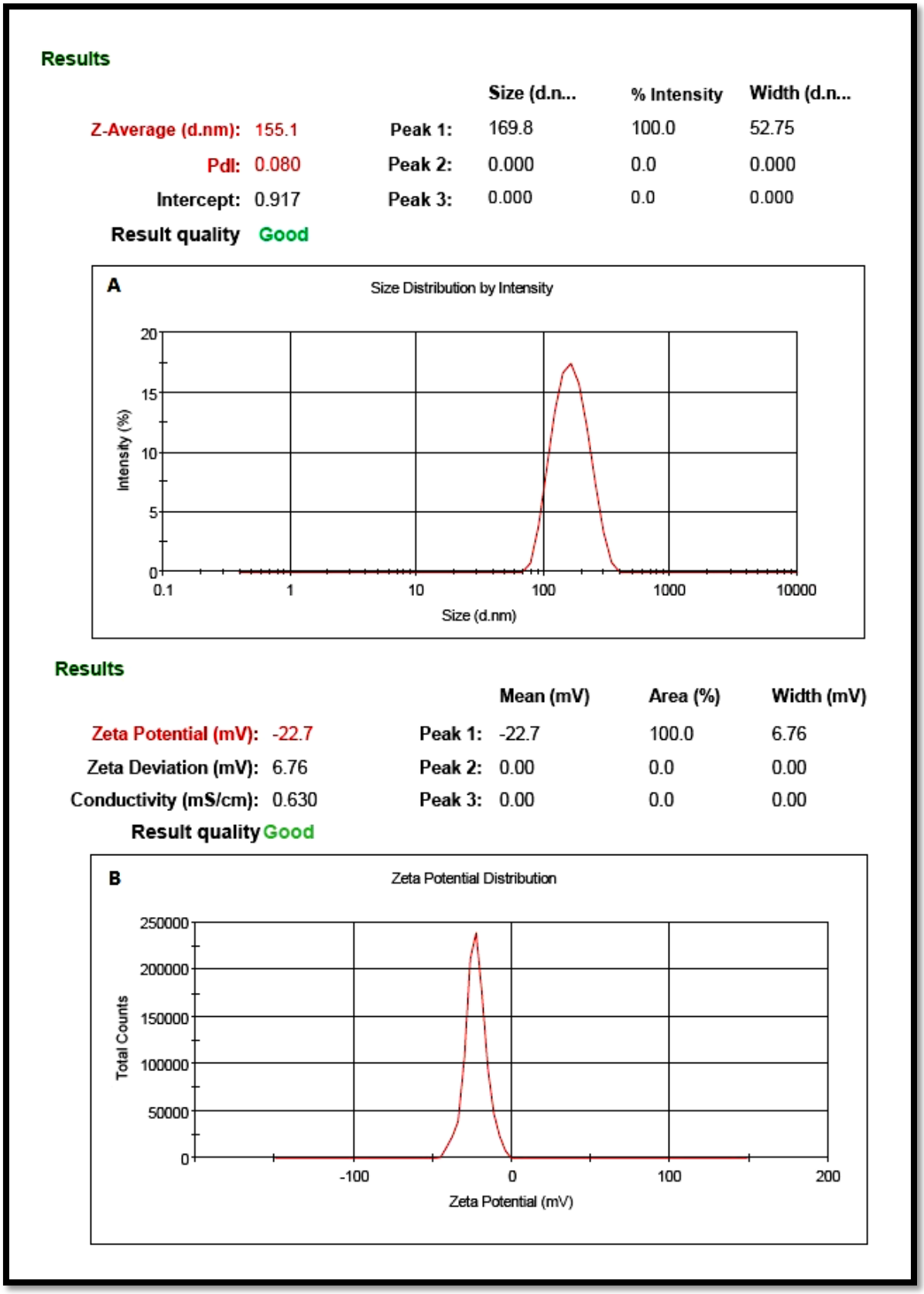

Fig. 3. DLS profile: **(A)** Size distribution of PdNPs with maximum intensity at 155 nm. **(B)** Stability of PdNPs at -22.7 mV in zeta potential analysis.

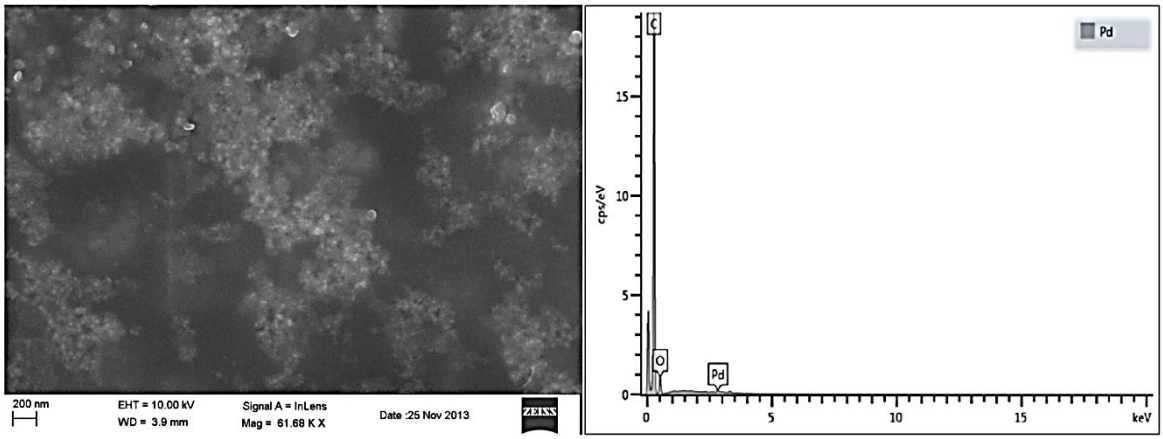

Fig. 4. SEM with EDXimage of PdNPs synthesized using *Moringa oleifera* flower extract and EDX showed the presence of the elements on the surface of the PdNPs.

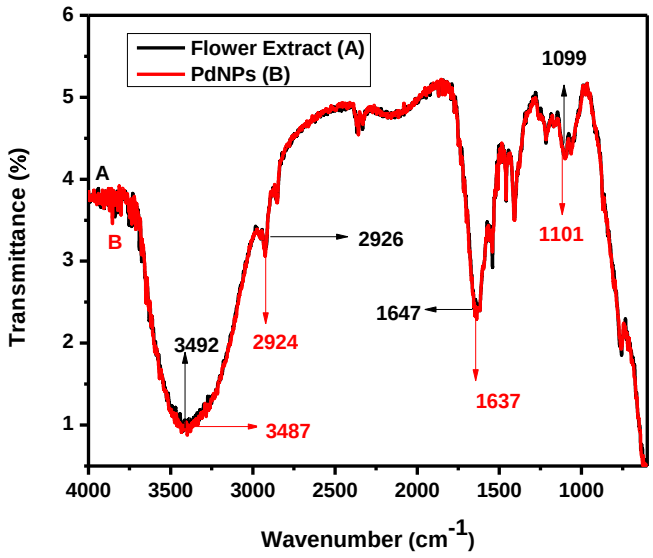

Fig. 5. FTIR spectra of **(A)** aqueous *Moringa oleifera* flower extract and **(B)** FTIR Profile of PdNPs synthesized using *Moringa oleifera* flower extract.

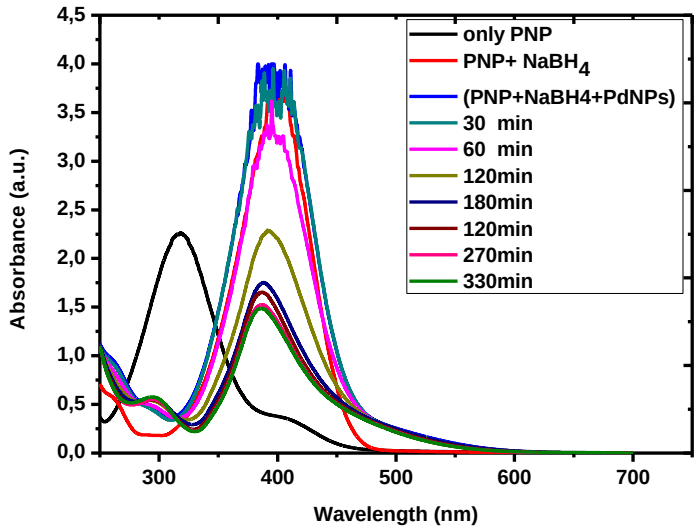

Fig. 6. A time course profile showing catalytic reduction of 4-nitrophenol by PdNPs.

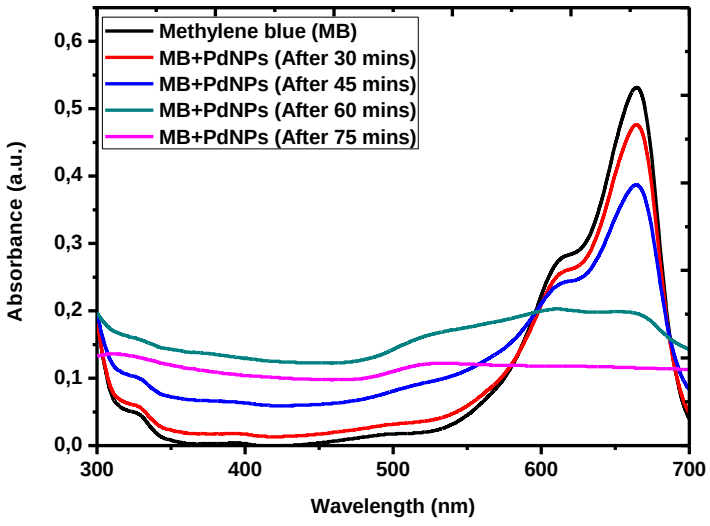

Fig. 7. A time course profile showing catalytic reduction of methylene blue by PdNPs.

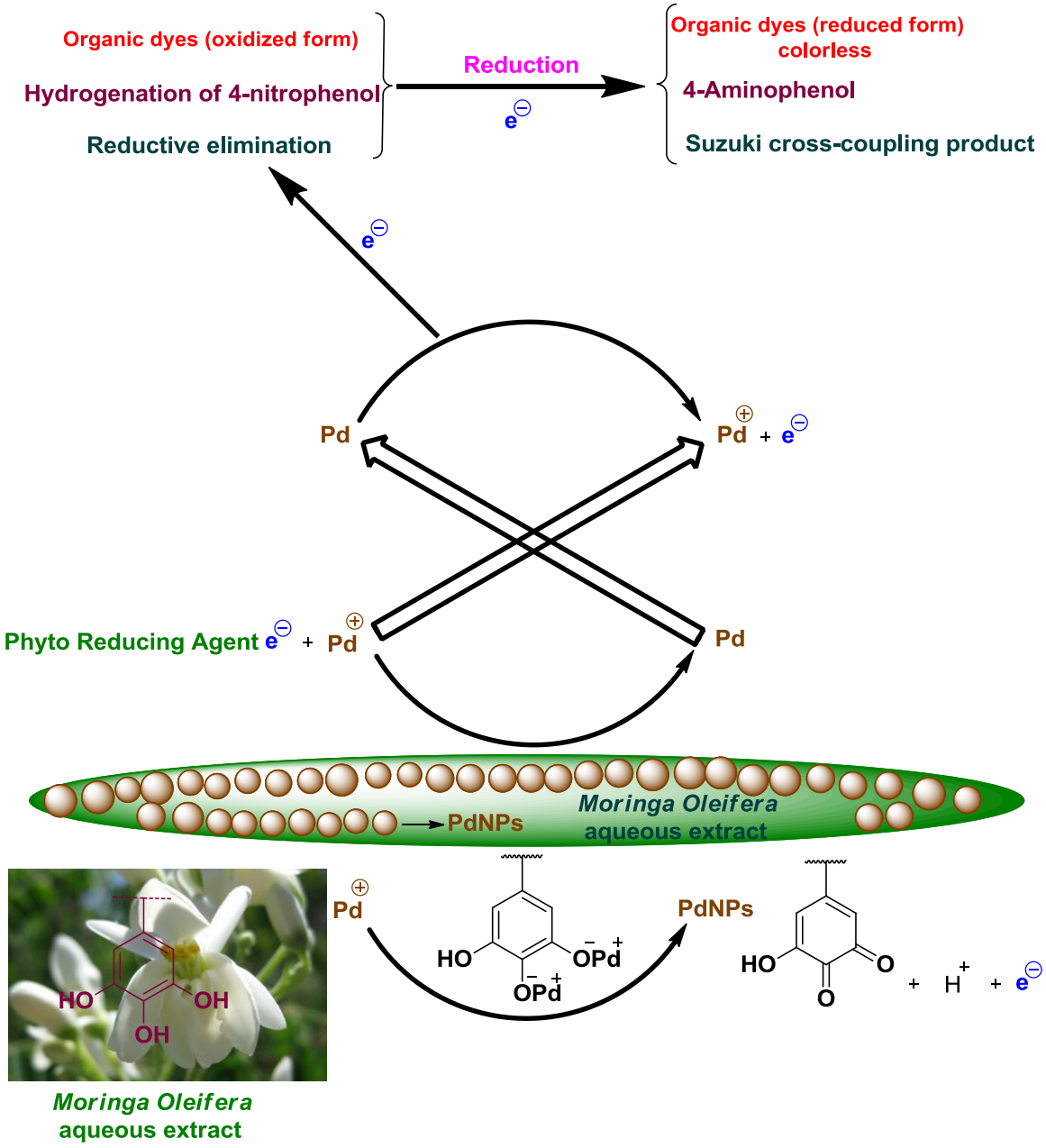

Fig. 8.Mechanism involved in the formation of PdNPs and catalytic reduction of organic dye, nitrophenol and suzuki cross coupling

Graphical Abstract

Farm waste mediated green synthesis of crystalline palladium into nanoparticles using *Moringa oleifera* and their A549 lung cell line and catalytic activities

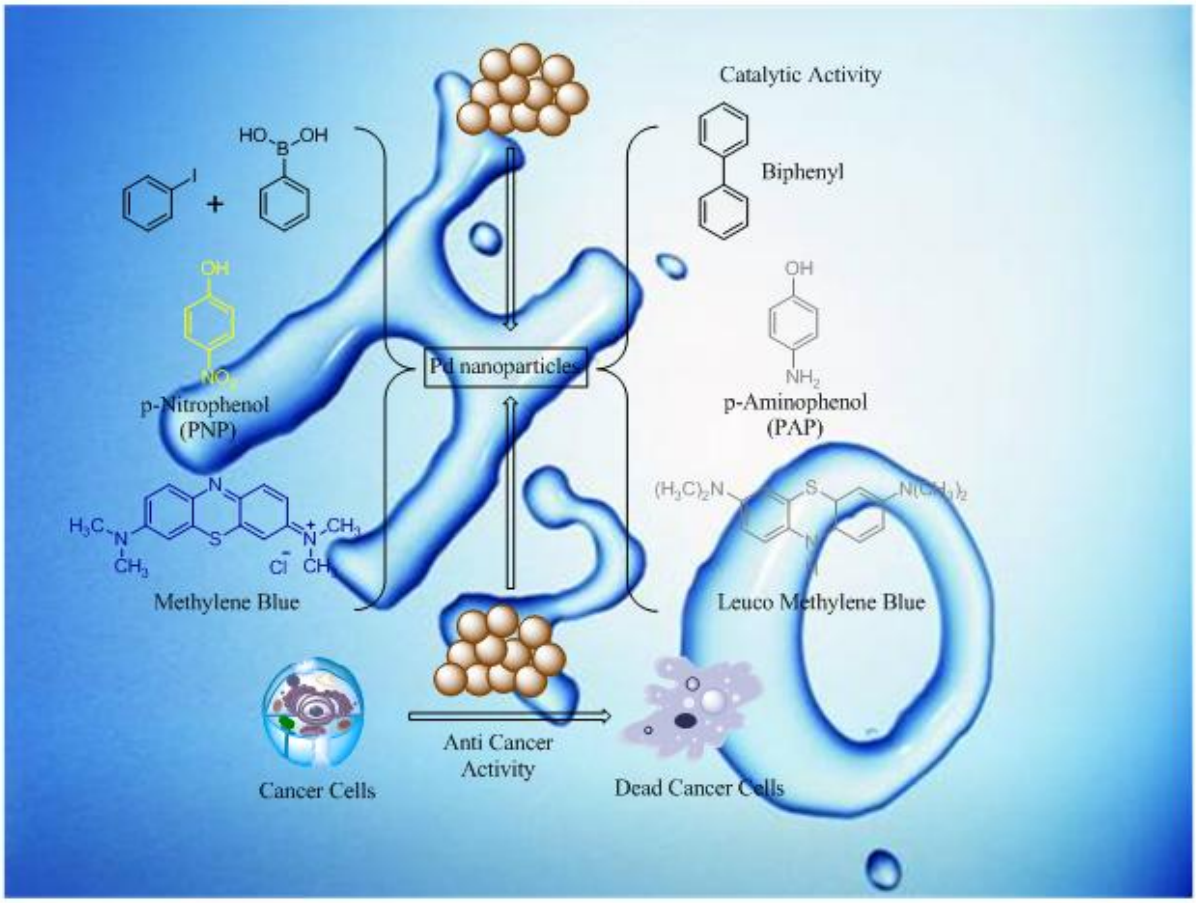

Highlights:

- Farm waste flower of *Moringa oleifera* mediated green synthesis
- Characterization of PdNPs is performed by UV–vis, TEM, FTIR, DLS and SEM with EDX
- PdNPs can reduce methylene blue (MB) and p-nitrophenol (PNP) in a $NaBH_4$ water mediated reaction system
- Suzuki Cross coupling reaction in water
- PdNPs were significant cytotoxic to A549 cells and did not induce cytotoxicity in normal healthy PLs

Supplementary Material

Click here to download Supplementary Material: Supplementary Data.docx

Summary

Chapter 1, gives the brief introduction on the synthesis and utility of nitrogen containing heterocyclic, fluorinated bioactive small molecules and ionic liquid biomolecules interaction and functionalized nanomaterials for catalytic and biological applications. Organic chemistry moves towards a multi-disciplinary environment blending biology, physics, and materials sciences.

Chapter 2, we accomplished a simple one-pot two component and three component reaction involving quinoline, 2-aminothiophenol, thiosemicarbazone and trifluoromethylbenzaldehyde. The valuable features of this method include good yields, broader substrate linked together with mild reaction conditions that makes this process attractive for the synthesis of interesting bioactive molecules. In our study we found that the benzothiazole quinoline synthesis method underwent an intramolecular aerial oxidation mechanism. Further, the rapid synthesis of fluorinated pyridine and pyran nucleus via. a one-pot three component reactions was achieved. *In vitro* anti-bacterial activity of the synthesized compounds wer investigated against a representative panel of pathogenic strains. Compounds **6**, **7**, **8**, **11** and **13** exhibited excellent anti-bacterial activity compared with first line drugs. We also found potent p53–MDM2 interaction inhibitors such as 2-thio-1,2-dihydroquinoline-3-carbaldehyde thiosemicarbazone and fluorine substituted new pyridine scaffold based on structure-based design.

Chapter 3, we described a protein-fluorinated ionic liquids interactions because of their possible technical application in the field of pharmaceuticals and biochemical reactions. The globular proteins, in particular, are frequently used as functional ingredients in healthcare and pharmaceutical products because of their ability to catalyze biochemical reactions, to be adsorbed on the surface of some substances and to bind other molecules and form molecular aggregates. One of the most widely used globular proteins for various technical applications is bovine serum albumin (BSA). In the present investigation the interaction of 1-butyl-2,3-dimethylimidazolium tetrafluoroborate ionic liquids (DMTILs) with BSA was studied by emission spectroscopy. The emission titration experiments revealed the existence of a strong interaction between BSA and 1-butyl-2,3-dimethylimidazolium tetrafluoroborate

ionic liquids. The present work will help in understanding the interactions between proteins and ILs in aqueous media. Further, we introduce a versatile isocyanide based multi-component reaction concept for where DMTILs function as reaction media as well as alternative hazardous promoters to the commonly used strong acids and base. The application of DMTILs led to excellent results in terms of both catalytic activity and selectivity.

Chapter 4, we discovered that copper-loaded boron nitride nanosheets was a robust and efficient catalyst for the preparation of α-aminophosphonates under heterogeneous conditions. This protocol avoids the use of any ligand or additive and is applied to a wide spectrum of Kabachnik–Fields reaction involving the condensation of amines, aldehydes and diethyl phosphite species. We believe this work will greatly benefit the synthesis of organic agrochemicals and potential pharmacological interest; further investivation of this heterogeneous C–P bonds formation was realized through the reaction catalyzed by copper loaded boron nitride. Cu/BN shows the best catalytic activity. Reactions of aldehydes with aromatic amines did not show remarkable difference. A phospha-Mannich imine plausible mechanism of the reaction is proposed based on these experiments. The catalytic result indicated cleaner conversion and higher yields as some of the advantages of the protocol. The catalyst could be recovered by simple filtration from the reaction mixture without further treatment and reused four times with consistent catalytic activity.

Chapter 5, we described cancer targeting molecules such as small organic sulphur molecules which are attached to the surface of gold nanopartilces to enhance cancer cell targeting since the surface of gold nanoparticles have strong binding affinity towards thiols and disulfides. The structure of the carbazole thio octanic acid (CTN) was identified by IR and NMR. CTN was attached to the gold nanoparticles surface and the capping behaviour was characterized by UV-vis spectroscopy, TEM, DLS and FTIR. The cytotoxicity of CTNAu on A549 cell lines was determined using the MTT assay. The results suggest CTN and CTNAu posses anti-proliferative properties in the cancerous A549 cells.

Furthermore this chapter includes the thiol dual ligand capped gold nanoparticle synthesis, characterization and their cytotoxic evaluation in A549 lung cancer cells. DTAu was synthesized by equimolar 4-aminothiophenol (4-ATP) and amino oxadiazole thiol (AXT). This dual ligand was attached to the gold nanoparticles surface and the capping behaviour was characterized by UV-vis spectroscopy, TEM, DLS and FTIR. The cytotoxicity of DTAu on A549 cell lines was determined using the MTT assay. The results suggest dual ligands (4-ATP, AXT) and DTAu posses anti-proliferative properties in the cancerous A549 cells

Chapter 6, described biomolecules present in plant extracts that could be used to reduce metal ions to nanoparticles in a single-step via. a green synthesis protocol. This biogenic reduction of metal ion to base metal is quite rapid, readily conducted at room temperature and pressure and easily scaled up. Also the synthesis mediated by plant extracts are environmentally benign. The reducing agents involved include various water soluble plant metabolites such as alkaloids, phenolic compounds, terpenoids and co-enzymes. Silver, gold and palladium nanoparticles were the focus of plant-based biosynthesis. These nanoparticles were elucidated for their cytotoxicity profile in A549 lung cancer cell. Catalytic reduction of organic dyes and nitrobenzene derivatives were also described. In addition, the nanoparticles were used effectively in the Suzuki coupling reaction.

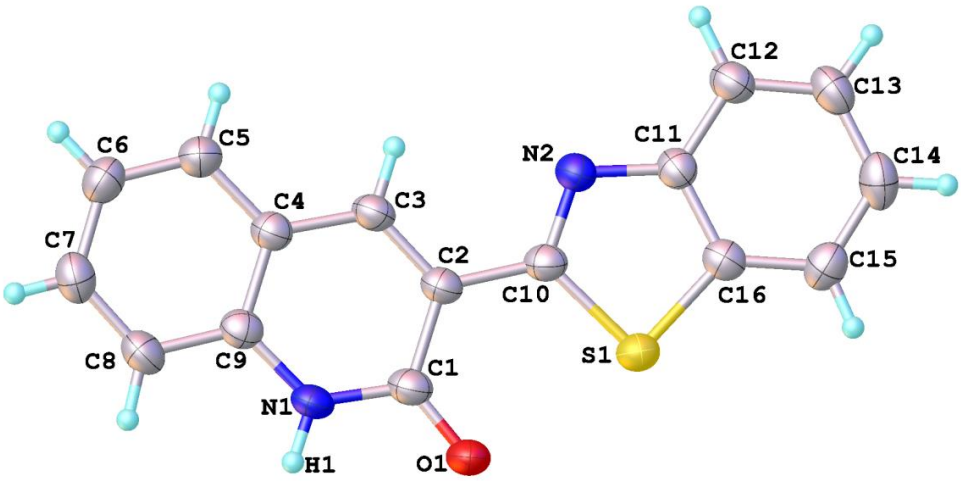

Ortep view of 3-(Benzo[d]thiazol-2-yl)quinolin-2(1H)-one **(6)**

Table 1. Crystal data and structure refinement of

3-(Benzo[d]thiazol-2-yl)quinolin-2(1H)-one **(6)**

Crystal data

$C_{16}H_{10}N_2OS$
M_r= 278.32
Monoclinic, $P2_1/c$
Hall symbol: -P 2ybc
a = 13.9176(11) Å
b = 3.9783(3) Å
c = 22.532(2) Å
α = 90.00°
β = 97.142(7)°
γ = 90.00°
V = 1237.87(19) Å^3
Z = 4
μ = 0.257 mm^{-1}
T = 293(2) K
D_x = 1.493 Mg m^{-3}
Mo $K\alpha$ radiation, λ = 0.71073Å
Cell parameters from 15350 reflections
Needle, yellowish-green
0.23 × 0.17 × 0.12 mm
$F(000)$ = 576
θ = 3.27–52.74°

Data collection

Oxford Diffraction Xcalibur Sapphire3 diffractometer with a Sapphire CCD detector
Radiation source: fine-focus sealed tube
Graphite monochromator
Detector resolution: 15.9853 pixels mm^{-1}
Rotation method data acquisition using ω scan
Absorption correction: multi-scan (*CrysAlis PRO*; Oxford Diffraction, 2009)
T_{min} = 0.9433, T_{max} = 0.9699
15350 measured reflections
2500 independent reflections
2183 reflections with $I > 2\sigma(I)$
R_{int} = 0.039
θ_{max} = 26.4°, θ_{min} = 3.3°
h = –17→17
k= –4→4
l = –28→28

Refinement

Refinement on F^2
Least-squares matrix: full
$R[F^2 > 2\sigma(F^2)]$ = 0.052
$wR(F^2)$ = 0.126
S = 1.14
221 parameters
2500 reflections
0 restraints
H-atom parameters constrained
Primary atom site location: structure-invariant direct methods
Secondary atom site location: difference Fourier map
Hydrogen site location: inferred from neighbouring sites
H-atom parameters constrained
$w = 1/[\sigma^2(F_o^2) + (0.0564P)^2 + 0.4687P]$ where $P = (F_o^2 + 2F_c^2)/3$
$(\Delta/\sigma)_{max}$< 001
$\Delta\rho_{max}$ = 0.22 Å^{-3}
$\Delta\rho_{min}$ = –0.23 Å^{-3}

Gold Bull (2012) 45:99–104
DOI 10.1007/s13404-012-0047-8

CONFERENCE REPORT

Conference report: gold highlights at the International Conference on Nanomaterials and Nanotechnology 2011 (ICNANO-2011) in Delhi, India, 18–21 December 2011

Sónia A. C. Carabineiro

Published online: 4 May 2012

Nano-biomaterials and biomedicals

The conference started with a plenary lecture from one of the conference chairs, *Anthony Turner* (Linköping University, Sweden), who spoke about 'Nanomaterials for biosensors and bioelectronics' and showed that several sensors contain gold films or gold surfaces. In fact, in surface plasmon resonance imaging, the sensor surface is almost always a thin layer of gold. Most immobilisation techniques involve the first layer of a chemical linker directly bound to the gold surface, allowing subsequent anchoring of molecules of interest [1]. Gold on glass electrodes are also starting points for the fabrication of artificial enzyme electrodes [2] and Au sputtered layers in the template synthesis of polyaniline nanostructures (Fig. 1) [3]. Turner was the winner of the Acharya Vinoca International award 2011 for his work on biosensors and bioelectronics (Fig. 2). This award is named after Vinayak Narahari Bhave, an Indian advocate of non-violence and human rights, and is given annually by the Vinova Research Institute of India, for notable and outstanding research in *Materials Science and Technology.*

Ashutosh Tiwari (from the same university) was the winner of the Nano Award 2011 (Fig. 2), for his work on gold nanobioelectronics. This award is honoured annually by the Vinova Bhave Research Institute for notable and outstanding research in the field of *Nanoscience and Nanotechnology.* Tiwari's plenary lecture dealt with the fabrication on an amperometric biosensor for the quantitative determination of urea in aqueous medium using hematein, a pH-sensitive natural dye [4]. The urease (Urs) was covalently immobilised onto an electrode made of gold nanoparticles functionalized with hyperbranched polyester-Boltron® H40 (H40–Au) coated onto an indium–tin oxide (ITO)-covered glass substrate (Fig. 3). Chitosan/gold–MPA nanocomposites for sequence-specific oligonucleotide detection were also mentioned. A 20-mer single-stranded oligodeoxyribonucleotide was covalently probed onto the nanocomposite electrode, made up of an ITO glass surface coated with chitosan, which is bonded with carboxyl functionalized thiol capped gold nanoparticles [5]. TEM micrograph of the composite electrode showed that gold nanoparticles had the diameter ranging from 4 to 16 nm.

Robert Gengan (Durban University of Technology, South Africa) spoke about the preparation of novel 3-amino-9-ethyl carboazole functionalized gold nanoparticle synthesis. The cytotoxicity of aflatoxin B_1, 3-amino-9-ethylcarboazole and gold nanoparticles on A549 cell lines was determined using a bioassay.

Soma Chattopadhyay (Illinois Institute of Technology, USA) spoke about the synthesis and EXAFS study of Au core–Ag shell nanoparticles inside unmodified horse spleen apoferritin protein, with Au core diameter smaller than 2 nm.

Alok Pandya (Gujarat University, India) talked about a water-soluble glucose biosensor based on an ultrasensitive boronic acid-calix[4]arene functionalized gold nanoprobe. This molecular receptor shows naked eye colour change from pink to blue due to aggregation, as confirmed by other techniques.

Neelam Verma (Punjab University, India) spoke about gold and silver nanoparticles used as sensors for electrochemical detection of organophosphorous pesticides. The lowest detection limit achieved for methyl parathion detection was 0.25 ppb, and for chlopyriphos, it was 1 ppt.

S. A. C. Carabineiro (✉)
Laboratory of Catalysis and Materials, Department of Chemical Engineering, Faculty of Engineering, University of Porto,
Rua Dr. Roberto Frias, s/n,
4200-465 Porto, Portugal
e-mail: scarabin@fe.up.pt

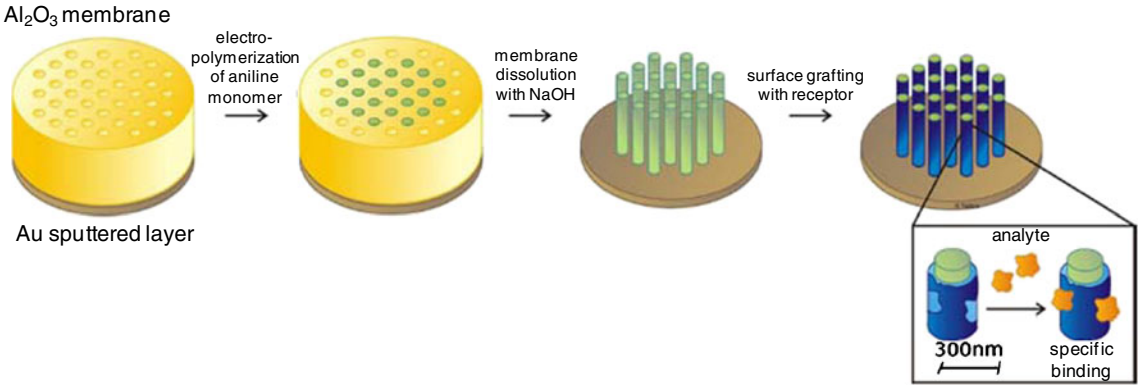

Fig. 1 Scheme of the template synthesis of polyaniline nanostructures (adapted from [3])

Minni Singh's oral presentation (from the same university) was about the enhanced response in electrochemical detection of glucose using model enzyme glucose oxidase by incorporating bimetallic Au–Pt nanoparticles in the conducting immobilisation matrix polypyrrole. The improved sensitivity of detection is particularly important for clinical diagnostics, food safety and environmental applications.

Dinesh Kumar (Banasthali University, India) spoke about core–shell (SiO_2@Ag/Au), metallic (Ag/Au) and capped metallic (Au/Ag@citrate) nanomaterials used as sensors for heavy metal ions (Cd(II), Zn(II), Fe(III) and Pb(II)) detection in water. These materials showed good performance and were simple, fast and possible to use by non-experts.

C.S. Pundir (Maharshi Dayanand University, India) talked about the immobilisation of oxalate oxidase onto gold nanoparticle–porous $CaCO_3$ microsphere hybrid encapsulated in silica sol and deposited on a Au electrode, for amperometric determination of oxalate in biological fluids (urine, plasma, fruits and vegetables). The biosensor showed to be reliable, have high sensitivity and was able to measure concentrations of oxalate as low as 1 μM.

Priyanka Sharma (Institute of Microbial Technology, India) presented a poster on the synthesis and characterisation of gold-coated iron oxide core–shell nanoparticles functionalised with receptor molecules (antibodies or proteins) to be used as functional biomaterials. They proved to be viable for exploiting the gold surface protein-binding reactivity for bioassay and the iron oxide core magnetism for magnetic bioseparation.

A. Chopra (from the same institute) presented a poster on a novel low-cost laser-ablated gold sensor modified with multiwalled carbon nanotubes using cysteamine. The presence of nanotubes on the surface of the Au electrode improved the direct transfer of glycated haemoglobin due to its intrinsic activity and a linear reproductible response was obtained. The method presented proved to be selective, sensitive, inexpensive and promising since the presently available tests for this haemoglobin are quite complicated and costly.

Deepika Bhatnaga's poster (Central Scientific Instruments Organization, India) and *N. Chauhan's* poster (Kurukshetra University, India) also reported on the use of multiwalled carbon nanotubes to modify a gold screen-printed electrode for direct electrochemistry and label-free detection of haemoglobin, and for a nanocomposite of Au nanoparticles and polyaniline for improved amperometric determination of lysine, respectively.

Prem Pandey's poster (Banaras Hindu University, India) reported on a prussian blue/gold nanoparticle nanocomposite to be used in the electrocatalytic determination of glutathione, with promising results.

Bindu Sharma's poster (Karnatak University Dharwad, India) dealt with the synthesis and optical characterization of biocompatible fluorescent gold nanoparticles, while *Krishnan Anand* (Durban University of Technology, South Africa) presented a poster on thiol-dual ligand gold nanoparticles (synthesis and bioassay).

Shobhana K. Menon (Gujarat University, India) presented a poster on a rapid detection of codeine using gold

Fig. 2 Anthony Turner (*left*) and Ashutosh Tiwari (*right*) from Linköping University, Sweden, receiving the Acharya Vinoca International Award 2011 and the Nano Award 2011, respectively, for their work on gold biosensors and bioelectronics (see text for details)

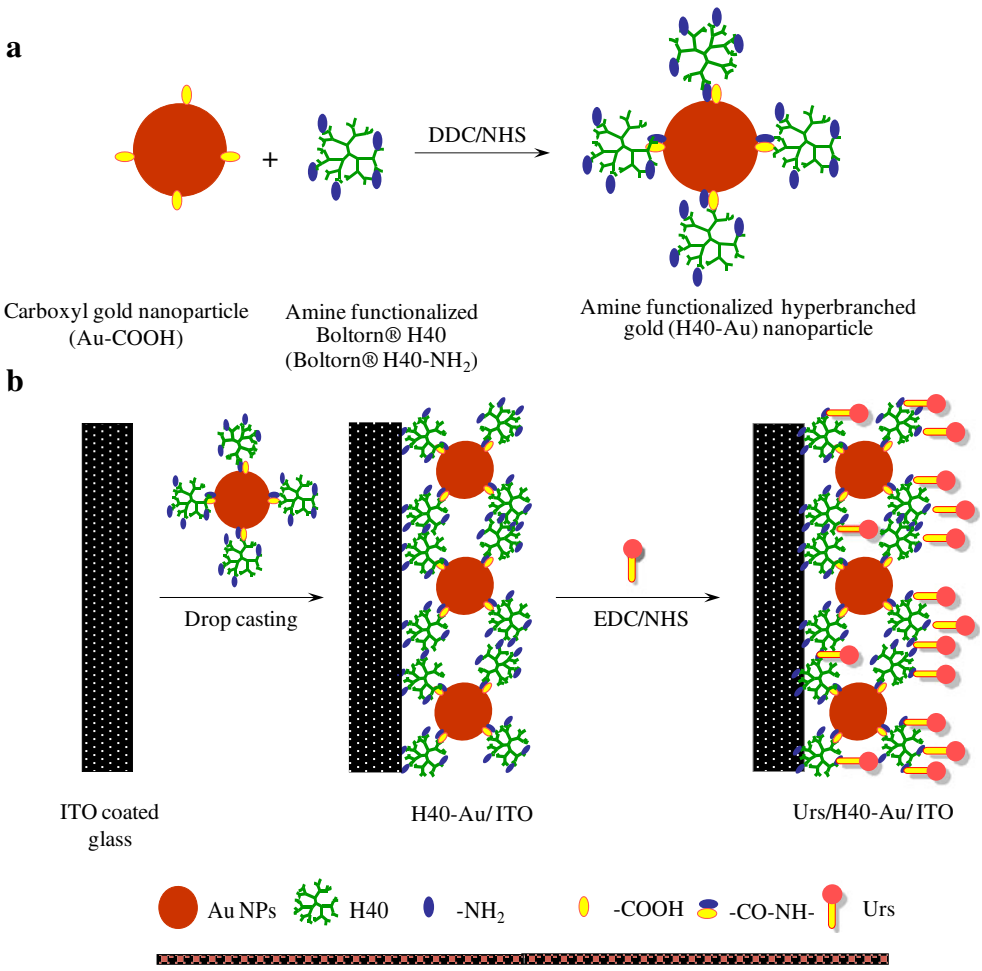

Fig. 3 **a** Preparation of hyperbranched gold (H40–Au) nanoparticles and **b** fabrication of H40–Au/ITO and Urs/H40–Au/ITO electrodes (adapted from [4])

nanoparticles as a probe. In this work, nanoparticles at nanomolar concentration can be clearly observed by the naked eye and allow sensitive detection with minimal consumption of drug samples from a crime scene. This can have interesting applications in forensic science since codeine and heroin drugs (Fig. 4, left and middle) are rapidly metabolised to morphine (Fig. 4, right) and the detection of the latter alone does not provide complete information.

Arghya Bandyopadhyay (University of Kalyani, India) presented a poster on the synthesis of nanofilm assemblies of gold protected by monodispersed iron oxide core metal shell magnetic nanoparticles. This novel nanocomposite may be used to develop a biosensor for detecting biomolecules quantitatively and qualitatively.

S. Malathi (University of Madras, India) presented a poster on the synthesis of gold nanoparticles by a green method using chitosan as a reducing/capping agent. These Au nanoparticles of ~10 nm were then used as carriers for the controlled delivery of the antituberculosis drug rifampicin and its catalytic activity was examined for gram-positive and gram-negative bacteria with promising results.

Balu A. Chopade's group (University of Pune, India) presented a poster on the use of *Dioscorea bulbifera* tuber extract (also called 'air potato', a plant with therapeutic use in Indian and Chinese traditional medicine) mediated synthesis of gold nanoparticles (gold nanotriangles, nanoprisms, nanotrapezoids and nanospheres). These bioreducted gold nanoparticles showed potent anticancer activity against three cancer cells lines, namely HL60, MCF7 and HeLa.

S.K. Pandey (Punjab University, India) presented a poster on gold nanoparticles induced chemiluminescence for VI antigen detection (a virulence factor of typhoid fever caused

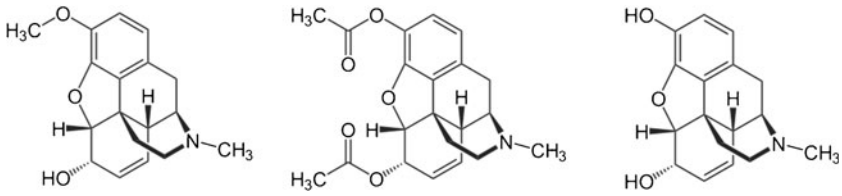

Fig. 4 Molecular structures of codeine (*left*), heroin (*middle*) and morphine (*right*) drugs

by *Salmonella enterica* serovar Typhi that is a life-threatening systemic infection and a major public health problem in developing countries). The proposed method is promising for the determination of clinically important bioactive analytes and may prove to be valuable in detecting important virulence strains of pathogens.

Saptarshi Chatterjee (University of Kalyani, India) presented a poster on the successful preparation of glutathione-functionalised gold nanoparticles used on a novel method of transformation of plasmid DNA in *Escherichia coli*. The process is less time consuming and increased the transformation efficient when compared to conventional methods. Plus, the Au nanoparticles are non-toxic making this gene delivery method suitable for biotechnological applications.

S. Lata (Maharshi Dayanand University, India) presented a poster dealing with nickel oxide nanoparticles/carboxylated multiwalled carbon nanotubes/polyaniline hybrid films electrodeposited on the surface of a gold electrode. Cytochrome c oxidised obtained from goat heart was covalently immobilised onto the hybrid film in order to construct an enzyme electrode. A biosensor was further constructed, which gave accurate and satisfactory results for the determination of cytochrome c on different serum samples.

Nano-fabrication, characterization and properties

V. N. Bhoraskar's plenary lecture (University of Pune, India) was about the synthesis and modification of Au, Ag, Cu, CdS and Ni nanoparticles by electron irradiating the respective chemical solutions with 6.5 MeV electrons and also the thin films of the respective elements by 15 keV electrons [6]. The average size of the particles could be tailored in the range of 50–130 nm for gold (Fig. 5). It was shown that Au nanoparticles could diffuse in polymers up to a depth of ~2 μm, using this method.

Habib Ullah's oral presentation (Pusan National University, Korea) concerned a work carried out in collaboration with the American International University of Bangladesh, dealing with water-soluble gold nanoparticles coordinated to poly(vinylpyrrolidone) (PVP). The final gold colloids were very stable as the PVP molecules coordinated through the C–N and C=O sites, instead of the C=O site alone.

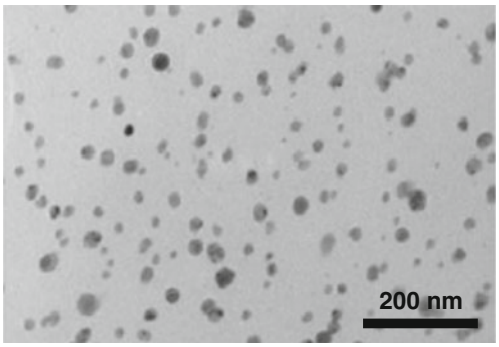

Fig. 5 TEM image of a 15 keV electron-irradiated Au coating (adapted from [6])

Ali Ayati's oral presentation (Ferdowsi University of Mashhad, Iran) concerned the synthesis of stabilised 45 nm gold nanorods generated by a green chemistry type process using $H_6[PMo_9V_3O_{40}]$, a harmless polyoxometalate (POM), under UV irradiation and in the absence of any surfactant or seed. This POM plays the role of a photocatalyst, reducing agent and efficient stabiliser.

Biswajit Chowdhury (Indian School of Mines, India) described the preparation of ceria-based mixed oxide solid solutions having nanocrystallinity, where not only the pore size but also the defect sites can be created in the mixed oxide by doping lower valent cations. The gold nanoclusters on the oxide surface can dissociate the chemisorbed oxygen which diffuses through the defect oxides, providing excellent activity towards benzyl alcohol oxidation using molecular oxygen.

Sajid Ali Ansari (Aligarh Muslim University, India) presented a poster on polyaniline silver and gold composites prepared by in situ polymerization of aniline and ammonium peroxydisulphate as oxidising agent and Ag and Au colloidal nanoparticle solutions (reduced with sodium borohydride). These composites showed to have good optical and dielectric properties.

S. Tripathi (UGC-DAE Consortium for Scientific Research, India) in a collaborative work with the Karlsruher Institut für Technologie in Germany and the Catholic University of Leuven, Belgium, presented a poster with results of structural and magnetic characterisation of Co/Au system with two different compositions where Co was grown as a discontinuous layer sandwiched between a pair of Au layers. Interesting magnetic and structural transformations of the layers were observed due to the formation of a non-magnetic phase at the interface with temperature increase.

Parul Khurana (Banasthali University, India) had a poster on the synthesis and plasmonic properties of Au–Ag core–shell nanostructures. Ag and Au nanoshells were grown on silica microspheres with diameters ranging from 50 to 60 nm. Reduction of Au and Ag precursors onto gold decorated microspheres resulted in increasing gold coverage on the silica core. The product may also have many potential applications in optical, magnetic, biochemical and biomedical fields.

Sheenam Thatai (from the same group) had a poster dealing with the detection of Cd^{2+}, Zn^{2+} and Pb^{2+} ions in water using Au@citrate and SiO_2@Au nanoparticles as highly selective and sensitive nanosensors. The presence of metal ions changes the colour of the solution, visible to the naked eye, and causes aggregation of nanoparticles.

F. Hashemi (Khayyam University, Iran) presented a poster on theoretical investigations of the substituent effect on the molecular wire, Au/guanine/Au, performed using density functional calculations by considering the influence of an external electric field. The obtained results showed that an organic molecule can be functionalised as a molecular diode.

Nano-advanced materials

Palani Barathi (Velore Institute of Technology University, India) spoke about a nickel hexcyanoferrate-modified disposable gold nail electrode for electrocatalytic response of hydrazine in neutral pH. The sodium sulphate–sodium acetate pH 7 solution showed a well-defined, reversible and stable voltammetric responses and enhanced catalytic activity towards hydrazine without any excess alkali metal cation added solution. Under optimal conditions, the modified electrode showed a linear response for hydrazine in the concentration range from 0.5 to 10 mM.

S.K. Boruah (Gauhati University, India) presented a poster dealing with green synthesis of gold nanoparticles using a simple, fast, low-cost and economical technique, using fresh leaves and buds of *Camellia sinensis* tea (Fig. 6). The polyphenols present in the young leaves of tea extract reduce $HAuCl_4$ at room temperature. The core size of gold nanoparticles decreases as the amount of tea extract increases. Particles ranging from 9 to 12 nm were obtained.

The poster of *M. Yazdani* (Shiraz University, Iran) was about the synthesis of gold nanoparticles with imidazolium-based ionic liquids, which show preferential binding affinity towards gold crystal surfaces. 1-Dodecyl-3-methyl imidazolium tryptophan (long chain) and 1-ethyl-3-mehyl imidazolium tryptophan (short chain) were used, in order to test the effect of steric repulsion on the gold nanoparticles stability, being shown that the longer chain ionic liquids produced better results. Those nanoparticles showed to have a hydrophilic nature.

Fig. 6 *C. sinensis* leaves and flower used in tea

B. Batra (Maharshi Dayanand University, India) presented a poster on immobilisation of tyramine oxidase (purified from black gram seeds) on citrate-coated silver nano particles, deposited on a Au electrode, through cysteine layer, to obtain a tyramide biosensor that showed good performance in the detection of tyramide in beer and sauce, with a detection limit of 0.01 mM. Its advantage is that it does not suffer from leaching of the enzyme and measures this compound specifically.

A. Kedia (University of Delhi, India) presented a poster describing a simple, versatile and environmentally friendly one-step room temperature chemical synthesis route for the preparation of polyvinyl pyrrolidone functionalised size/shape-controlled gold nanoparticles by in situ polymerisation of the N-vinyl pyrrolidone monometer using $HAuCl_4$ as the oxidant. Water molecules act as a nucleophile that attacks the gold–vinyl complexes.

Ida Tiwari (Banaras Hindu University, India) presented a poster dealing with the addition of gold nanoparticles to multiwalled carbon nanotubes which were used to modify a glassy carbon electrode that showed good electrocatalytic activity towards the oxidation of NADH enzyme, better adhesion properties, good stability and no leaching of nanocomposite, thus being a promising electrochemical sensor for this enzyme in the future.

A collaborative work of *Naheed Ahmad* et al. (Patna University, India) and the Universities of Magadh, India, and of Aveiro, Portugal, dealt with the rapid green synthesis of silver and gold nanoparticles from the biowaste of pomegranate fruit (*Punica granatum*) at room temperature. The extracts of all parts of the fruit have therapeutic properties and the biosynthetic products along with reduced cofactors play an important role in the reduction of the Au salt to nanoparticles of ~10 nm, which showed to be quite stable.

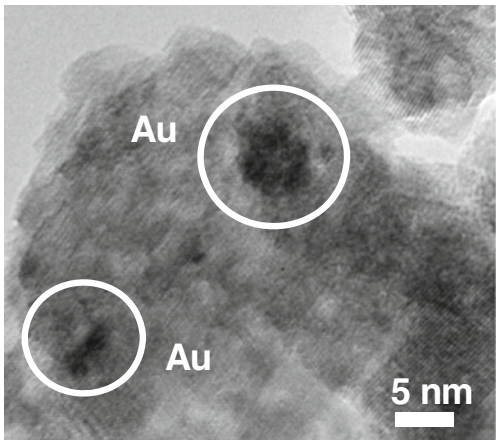

Fig. 7 HRTEM image of a Ce–Mn–O support (with a molar percentage of 30 % Mn and 70 % Ce) with gold nanoparticles (adapted from [7])

Sónia Carabineiro (University of Porto, Portugal) presented two posters dealing with gold nanoparticles supported on oxides, used for CO oxidation, namely, Ce–Mn–O composite materials. It was shown that the addition of Ce to Mn_xO_y produced supports with larger surface area, which led to smaller gold nanoparticles (Fig. 7) and consequentially improved catalytic activity. Another poster dealt with the heterogenation of organometallic complexes of several metals on carbon materials, to be used as catalysts for alkane oxidation. Heterogenised gold complexes showed promising results.

Deepshikha (Amity University, India) had a poster on the synthesis of polymer nanocomposites based on nanostructured polyaniline, gold nanoparticles and graphene nanosheets, by in situ polymerization. The nanodispersion could also be electrodeposited to produce a uniform nanofilm on an indium tin oxide surface. These composites showed good electrochemical properties and conductivity.

M. Misra's poster (Central Scientific Instruments Organization, India) also dealt with indium tin oxide, used as substrate for gold nanoparticles caped TiO_2 nanorod arrays for use in dye-sensitised solar cell technology. The Au nanoparticles on TiO_2 strongly absorb light, due to the localised surface plasmon resonance, and thereby promote light absorption of the dye.

J.P. Singha (King Saud University, Saudi Arabia) presented a poster dealing with the immobilisation of Pt, Au and Pt–Au nanoparticles on highly ordered TiO_2 nanotubes by pulse electro-deposition. The electrochemical behaviour of these composites was examined through the study of oxygen reduction.

Isha Mudahar (Khalsa College, India) presented a poster dealing with density functional calculations on pure dimers (C_{60}–C_{60}) and dimers doped with N and B ($C_{60-x}N_x$–$C_{60-x}B_x$) with gold contacts, in order to investigate the charge transfer in molecular nano junctions across C_{60} dimers. The results obtained suggest that there is a charge transfer from C to Au atoms.

Acknowledgments I am grateful to Prof. Anthony Turner for providing me the slides of his plenary lecture. Fundação para a Ciência e Tecnologia (FCT) is acknowledged for funding (CIENCIA 2007 programme and project PTDC/QUI-QUI/100682/2008, financed by FCT and FEDER in the context of Programme COMPETE).

References

1. Scarano S, Mascini M, Turner APF, Minunni M (2010) Review: surface plasmon resonance imaging for affinity-based biosensors. Biosens Bioelectron 25:957–966
2. Lakshmi D, Withcombe MJ, Davis F, Chianella I, Piletska EV, Guerreiro A, Subrahmanyam S, Brito PS, Fowler SA, Piletsky SA (2009) Chimeric polymers formed from a monomer capable of free radical, oxidative and electrochemical polymerisation. Chem Commun 9:2759–2761
3. Berti F, Todros S, Lakshmi D, Chianella I, Ferroni M, Piletsky SA, Turner APF, Marrazza G (2010) Quasi-monodimensional polyaniline nanostructures for enhanced molecularly imprinted polymer-based sensing. Biosens Bioelectron 26:497–503
4. Tiwari A, Aryal S, Pilla S, Gonga S (2009) An amperometric urea biosensor based on covalently immobilized urease on an electrode made of hyperbranched polyester functionalized gold nanoparticles. Talanta 78:1401–1407
5. Cao S, Mishra R, Pilla S, Tripathi S, Pandey MK, Shah G, Mishra AK, Prabaharan M, Mishra SB, Xin J, Pandey RR, Wu W, Pandey AC, Tiwari A (2010) Novel chitosan/gold-MPA nanocomposite for sequence-specific oligonucleotide detection. Carbohydr Polym 82:189–194
6. Mahapatra SK, Bogle KA, Dhole SD, Bhoraskar VN (2007) Synthesis of gold and silver nanoparticles by electron irradiation at 5–15 keV energy. Nanotechnology 18(13):135602
7. Carabineiro SAC, Silva AMT, Dražić G, Tavares PB, Figueiredo JL (2012) CO oxidation using gold supported on Ce-Mn-O composite materials. In: DiLoreto D, Corcoran I (eds) Carbon monoxide: sources, uses and hazards. Nova Publishers, Nova Science Pub Inc., New York

List of Conferences attended

Presentation

International & National

3-Amino-9-ethylcarbazole functionalized gold nanoparticles: synthesis and bioassay of gold clusters paper presented in an international conference on nanomaterials & nanotechnology held at Delhi, India from 18-21 December, **ICNANO 2011**

A facile one-pot synthesis of ellipticine derivatives and its effect on A549 lung cell lines paper presented in an international conference on international conference on pure and applied chemistry held at Mauritius from 2-6 July, **IUPAC 2012**

Copper loaded Boron Nitride Nanosheet as Heterogeneous Reusable Catalyst paper presented in an international conference on Composites, Biocomposites and Nanocomposites held at Durban, South Africa from 2-4 December, **ICCBN 2013**

List of Publications

(1) A549 lung cell line activity of biosynthesized silver nanoparticles using *Albizia adianthifolia* leaf. (Cited by Sigma Aldrich Chemical Company)
Gengan RM, **Anand K**, Phulukdaree A, Chuturgoon A. *Colloids and Surfaces B: Biointerfaces*, **2013**, 105, 87-91.

(2) Silver nanoparticles of *Albizia adianthifolia*: the induction of apoptosis in human lung carcinoma cell line. (Highly Accessed)
Rishalan Govender, Alisa Phulukdaree, Robert M Gengan, **Krishnan Anand**, Anil A Chuturgoon. *Journal of Nanobiotechnology*, **2013**, 11:5.

(3) Agroforestry waste *Moringa oleifera* petals mediated green synthesis of gold nanoparticles and their anti-cancer and catalytic activity.
Anand K, Gengan R M, Phulukdaree A, Chuturgoon A. *Journal of Industrial and Engineering Chemistry*, DOI: 10.1016/j.jiec.2014.05.021

(4) Silver nanoparticles derived from *Ekebergia capensis* leaf extract and its catalytic degradation effect on industrial azo dyes.
Anand K, Gengan RM. *Industrial Crops and Products* (under review)

(5) Farm waste mediated green synthesis of crystalline palladium into nanoparticles using *Moringa oleifera* and their A549 lung cell line and catalytic activities.
K. Anand, R. M. Gengan, A. Phulukdaree, A. Chuturgoon. *Applied Catalysis B: Environmental* (under review)

(6) Synthesis and bioassay of amine-ended thiol-dual ligand capped gold nanoparticles.
Anand K, Gengan R M, Phulukdaree A, Chuturgoon A. (manuscript under preparation)

(7) Aminocarbazole lipoyl moiety functionalized gold nanoparticles synthesis and bioassay of gold clusters.
Anand K, Gengan R M, Phulukdaree A, Chuturgoon A. (manuscript under preparation)

(8) Copper-loaded Boron nitride nanocatalyst for Kabachnik-Fields three-component reaction.
Anand K, Sureshkumar M, Muthu T, Gengan R M. (to be communicated)

(9) 1-Butyl-2,3-dimethylimidazolium tetrafluoroborate Ionic Liquid induced strong interaction with bovine serum albumin in aqueous media.
Arumugam Selva Sharma, Ramar Rajamanikandan, **Krishnan Anand,** Robert M Gengan, Gan G Redhi. (to be communicated)